INSECT OLFACTORY PROTEINS (FROM GENE IDENTIFICATION TO FUNCTIONAL CHARACTERIZATION), VOLUME II

EDITED BY: Peng He, Xiaojiao Guo, Yang Liu, Wei Xu, Jin Zhang, Ya-Nan Zhang and J. Joe Hull

PUBLISHED IN: Frontiers in Physiology

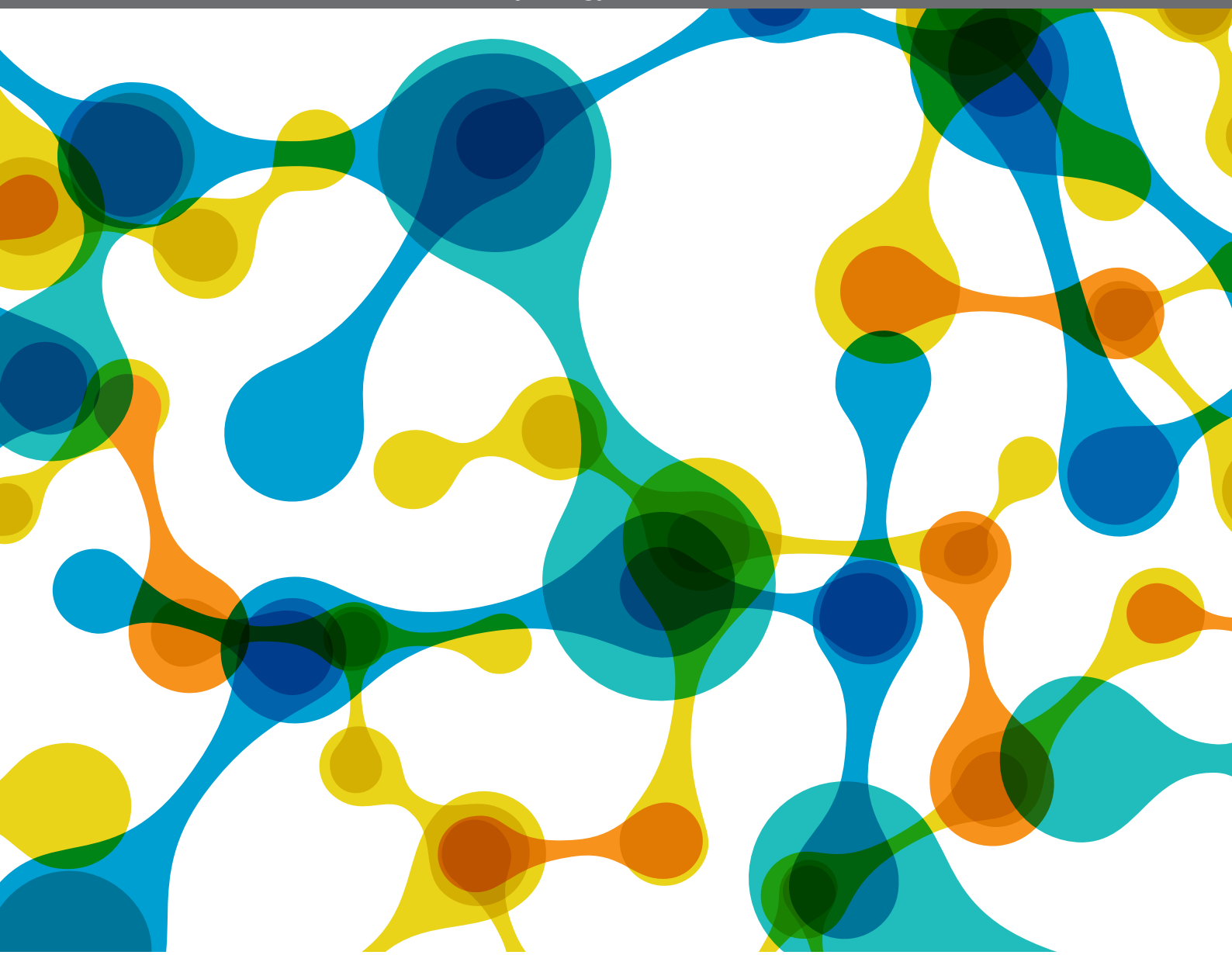

frontiers Research Topics

frontiers

ISSN 1664-8714
ISBN 978-2-88974-749-8
DOI 10.3389/978-2-88974-749-8

About Frontiers

Frontiers is more than just an open-access publisher of scholarly articles: it is a pioneering approach to the world of academia, radically improving the way scholarly research is managed. The grand vision of Frontiers is a world where all people have an equal opportunity to seek, share and generate knowledge. Frontiers provides immediate and permanent online open access to all its publications, but this alone is not enough to realize our grand goals.

Frontiers Journal Series

The Frontiers Journal Series is a multi-tier and interdisciplinary set of open-access, online journals, promising a paradigm shift from the current review, selection and dissemination processes in academic publishing. All Frontiers journals are driven by researchers for researchers; therefore, they constitute a service to the scholarly community. At the same time, the Frontiers Journal Series operates on a revolutionary invention, the tiered publishing system, initially addressing specific communities of scholars, and gradually climbing up to broader public understanding, thus serving the interests of the lay society, too.

Dedication to Quality

Each Frontiers article is a landmark of the highest quality, thanks to genuinely collaborative interactions between authors and review editors, who include some of the world's best academicians. Research must be certified by peers before entering a stream of knowledge that may eventually reach the public - and shape society; therefore, Frontiers only applies the most rigorous and unbiased reviews.
Frontiers revolutionizes research publishing by freely delivering the most outstanding research, evaluated with no bias from both the academic and social point of view. By applying the most advanced information technologies, Frontiers is catapulting scholarly publishing into a new generation.

What are Frontiers Research Topics?

Frontiers Research Topics are very popular trademarks of the Frontiers Journals Series: they are collections of at least ten articles, all centered on a particular subject. With their unique mix of varied contributions from Original Research to Review Articles, Frontiers Research Topics unify the most influential researchers, the latest key findings and historical advances in a hot research area! Find out more on how to host your own Frontiers Research Topic or contribute to one as an author by contacting the Frontiers Editorial Office: frontiersin.org/about/contact

INSECT OLFACTORY PROTEINS (FROM GENE IDENTIFICATION TO FUNCTIONAL CHARACTERIZATION), VOLUME II

Topic Editors:
Peng He, Guizhou University, China
Xiaojiao Guo, Institute of Zoology (CAS), China
Yang Liu, Institute of Plant Protection, Chinese Academy of Agricultural Sciences, China
Wei Xu, Murdoch University, Australia
Jin Zhang, Max Planck Institute for Chemical Ecology, Germany
Ya-Nan Zhang, Huaibei Normal University, China
J. Joe Hull, U.S. Arid Land Agricultural Research Center (USDA ARS), United States

Citation: He, P., Guo, X., Liu, Y., Xu, W., Zhang, J., Zhang, Y.-N., Hull, J. J., eds. (2022). Insect Olfactory Proteins (From Gene Identification to Functional Characterization), Volume II. Lausanne: Frontiers Media SA.
doi: 10.3389/978-2-88974-749-8

Table of Contents

frontiers in Physiology

EDITORIAL
published: 02 March 2022
doi: 10.3389/fphys.2022.858728

Editorial: Insect Olfactory Proteins (From Gene Identification to Functional Characterization), Volume II

Peng He[1], Yang Liu[2]*, J. Joe Hull[3]*, Ya-Nan Zhang[4]*, Jin Zhang[5]*, Xiao-Jiao Guo[6]* and Wei Xu[7]**

[1] State Key Laboratory Breeding Base of Green Pesticide and Agricultural Bioengineering, Key Laboratory of Green Pesticide and Agricultural Bioengineering, Ministry of Education, Guizhou University, Guiyang, China, [2] State Key Laboratory for Biology of Plant Diseases and Insect Pests, Institute of Plant Protection, Chinese Academy of Agricultural Sciences, Beijing, China, [3] Pest Management and Biocontrol Research Unit, US Arid Land Agricultural Research Center, USDA Agricultural Research Services, Maricopa, AZ, United States, [4] Anhui Key Laboratory of Pollutant Sensitive Materials and Environmental Remediation, College of Life Sciences, Huaibei Normal University, Huaibei, China, [5] Department of Evolutionary Neuroethology, Max Planck Institute for Chemical Ecology, Jena, Germany, [6] State Key Laboratory of Integrated Management of Pest Insects and Rodents, Institute of Zoology, Chinese Academy of Sciences, Beijing, China, [7] Agricultural Sciences, Murdoch University, Murdoch, WA, Australia

Keywords: odorant-binding proteins, chemosensory proteins, odorant receptors, ionotropic receptors, odorant-degrading enzymes

Edited and reviewed by:
Sylvia Anton,
Institut National de la Recherche Agronomique (INRA), France

****Correspondence:***
Peng He
phe1@gzu.edu.cn
Yang Liu
yangliu@ippcaas.cn
J. Joe Hull
joe.hull@usda.gov
Ya-Nan Zhang
ynzhang_insect@163.com
Jin Zhang
jinzhang@ice.mpg.de
Xiao-Jiao Guo
guoxj@ioz.ac.cn
Wei Xu
W.Xu@murdoch.edu.au

Specialty section:
This article was submitted to Invertebrate Physiology, a section of the journal Frontiers in Physiology

Received: *20 January 2022*
Accepted: *21 January 2022*
Published: *02 March 2022*

Citation:
He P, Liu Y, Hull JJ, Zhang Y-N, Zhang J, Guo X-J and Xu W (2022) Editorial: Insect Olfactory Proteins (From Gene Identification to Functional Characterization), Volume II. Front. Physiol. 13:858728. doi: 10.3389/fphys.2022.858728

Editorial on the Research Topic

Insect Olfactory Proteins (From Gene Identification to Functional Characterization), Volume II

The insect olfactory system is a highly evolved network of proteins that are essential for perception of the local environment, which includes communication with conspecific individuals and determining the location of suitable hosts and mating partners. The olfactory receptor neurons (ORNs) that comprise the detection component of the system are housed in the hair-like sensilla that line the antennae (i.e., the predominate olfactory organ). To date, a number of genes essential for differentiating key information from the complex odorant milieu of the environment have been identified. This filtering system includes: odorant carrier proteins, such as odorant-binding proteins (OBPs) and chemosensory proteins (CSPs), receptor proteins, which consist of odorant receptors (ORs) and ionotropic receptors (IRs), and odorant-degrading enzymes (ODEs) including various enzymes such as carboxylesterases, P450, oxidases, and so on. Although advances in sequencing technologies have driven a surge in the number of olfactory genes identified, our understanding of their functionality and the molecular mechanisms underlying their respective interactions remains limited. This Topic, an expansion of the Insect Olfactory Proteins (From Gene Identification to Functional Characterization) topic, seeks to address this limitation by highlighting research on a diversity of insect olfactory systems. In total, we have collected 18 papers representing species from three insect orders (8 Lepidoptera, 6 Coleoptera, and 4 Hemiptera) that impact the agricultural, forest, and medical fields.

In addition to the studies elucidating components of the first step in olfaction (i.e., detection), we have also included two studies examining the neural-based second step—perception. In the paper by Chen et al. the authors measured the electrophysiological responses of *Spodoptera frugiperda* labial palps to CO_2 and host volatiles. In the other paper, Liu J. et al. generated 3D digital reconstructions of the antennal lobe macroglomerular complex of males from two sibling

moth species (*Ectropis obliqua* and *Ectropis grisescens*) that respond to opposite sex pheromone combinations. Volumetric differences in the anterior-lateral glomerulus and posterior-ventral glomerulus of the two species suggest a possible reason for the differing biological responses to sex pheromone compounds.

TRANSCRIPTOME-BASED IDENTIFICATION AND EXPRESSION PATTERN OF NOVEL OLFACTORY-RELATED GENES

Improvements in RNA sequencing and subsequent data processing/analyses have made transcriptomes more economical, which has not only facilitated identification of olfactory-related genes but also made it feasible to assess transcript expression across a range of tissues, development stages, and conditions. In this Topic, Zhu et al. generated sex specific antennal transcriptomes for a bark beetle (*Scolytus schevyrewi*) fruit tree pest. In addition to identifying 47 ORs, 22 IRs, 22 OBPs, and 11 CSPs, their study also used RT-PCR to examine the tissue expression profile of the identified OBPs and CSPs. In a different study, Yi et al. screened adult antennal transcriptomes from another beetle pest (*Holotrichia parallela*) for a specific class of ODE, carboxylesterases (CXEs). Homologous BLAST analyses allowed the authors to identify 20 candidate CXEs, seven of which were found via RT-qPCR to exhibit antennae-biased expression. Similarly, Liu H. et al. identified 17 candidate CXE glutathione-S-transferases (GSTs) from antennal transcriptomes of the Indian meal moth (*Plodia interpunctella*), one of which *PiGSTd1* was predominantly expressed in male antennae and was shown to efficiently degrade a sex pheromone component as well as some host odorants.

Using an antenna-specific transcriptome from the greater wax moth (*Galleria mellonella*), Jiang et al. identified 102 olfactory genes, including 21 OBPs, 18 CSPs, 43 ORs, 18 IRs, and 2 SNMPs, and examined the tissue expression profile of a subset of the genes. In contrast, Zhang, X. et al. used broader transcriptomic datasets (larval heads and integuments) to identify 15 OBPs, 6 CSPs, 2 ORs, 14 IRs, and 1 SNMP in *Endoclita signifier*, a lepidopteran pest of eucalyptus trees. Elevated expression of a subset (5 OBPs, 2 CSPs, and 1 OR) of the genes in larval heads led the authors of the study to posit potential olfactory roles. In a comparative study of sibling beetle weevil (*Eucryptorrhynchus scrobiculatus* and *Eucryptorrhynchus brandti*) transcriptomes, Wang Q. et al. identified 12 CSPs and found that *CSP7*, *8*, and *9* in both species are mainly expressed in adult antennae. Additionally, EscrCSP8a and EbraCSP8 shared relatively low sequence identity and showed distinct binding affinities with (1R)-(+)-alpha-pinene, (−)-beta-caryophyllene, and beta-elemen *via* docking analysis.

OBP expression profiles are frequently differentiated by phenotypic-dependent functional roles. In support of this, Zhang S. et al. used transcriptomic datasets from the grain aphid (*Sitobion miscanthi*) to examine the temporal expression of five OBPs including three previously identified as aphid alarm pheromone (E-β-farnesene, EBF) binding proteins. Intriguingly, they found relatively stable and high expression of *OBP9* in adults of both wing morphs and that expression was upregulated in response to EBF induction suggesting this protein may be a crucial molecule for EBF recognition in aphids. In contrast, the effects of EBF on *OBP7* were limited to only winged adults and that *OBP3* was not induced in either wing type.

Wang L. et al. similarly used transcriptomic and RT-qPCR analyses across various tissues to examine OBP expression in two wing morphs of the soybean aphid (*Aphis glycines*). In this aphid species, all 15 OBPs, including three novel OBPs, exhibited varied expression profiles across tissues. The expression of seven OBPs, however, were significantly higher in winged adults than wingless adults, and *OBP6* were differentially expressed between the two wing phenotypes.

TYPICAL AND ATYPICAL FUNCTIONAL ROLES OF OBPS AND CSPS

Although the olfactory function of OBPs and CSPs is frequently indicated by elevated and/or specific expression in antennae, the role of these proteins in binding biologically relevant odorants has also been demonstrated both *in vivo* and *in vitro*. Using an *in vitro* fluorescence-binding assay, Li et al. measured the binding affinities of a subset of recombinant OBPs and CSPs from the coleopteran pest *Galeruca daurica* (Joannis) for host-derived odorants. Two OBPs (*6* and *15*) and two CSPs (*4* and *5*) were found to bind multiple host plant odorants. Furthermore, RNAi-mediated knockdown of *OBP15* and *CSP5* reduced electroantennogram (EAG) responses in female adults to a panel of host volatiles. Similarly, Wang Z. et al. show that expression of *CSP15* in the brown marmorated stink bug (*Halyomorpha halys*) is likewise antennae dominant and *in vitro* assays revealed high binding affinities for EAG-active host volatiles β-ionone, cis-3-hexen-1-yl benzoate, and methyl (2E,4E,6Z)-decatrienoate.

In addition to olfaction, OBPs and CSPs have also been implicated in gustation, vision, and insecticide responses. Guo et al. comprehensively analyzed the spatiotemporal expression profile of four silkmoth (*Bombyx mori*) OBPs—two pheromone-binding proteins (PBP) and two general odorant-binding proteins (GOBPs). Expression of the respective transcripts varied with age and all were found expressed in non-olfactory tissues including the early embryo, brain, and silk gland. Furthermore, expression in non-olfactory tissues was induced in response to abamectin exposure. Based on these results, the authors posit novel roles for OBPs in pesticide binding and suggest they have additional functions beyond antennal sex pheromone detection.

MOLECULAR AND FUNCTIONAL CHARACTERIZATION OF ORS

Functional ORs are a dimeric complex between specific, narrowly tuned ORs and Orco, a highly conserved OR co-receptor. In this Topic, Zhang, Liu, et al. cloned the *Orco* gene from the white-spotted flower chafer (*Protaetia brevitarsis*) and found that silencing the gene impaired EAG responses to an aggregation

pheromone and impeded identification of fresh food sources. In contrast, He et al. focused on characterizing a pair of a narrowly tuned ORs from the potato tuber moth (*Phthorimaea operculella*), both of which were specifically activated by two of the major sex pheromone components, suggesting that they function *in vivo* as pheromone receptors (PRs). Ji et al. similarly used an *in vitro Xenopus* expression system to examine OR ligand specificity and found that OR6 from the red palm weevil (*Rhynchophorus ferrugineus*) is narrowly tuned to α-pinene.

OVERVIEW AND CHARACTERIZATION OF ODES

Although ODEs consist of multiple enzyme families, esterases are the most well-studied to date. In their review of lepidopteran antennal ODEs, Godoy et al. highlight evolutionary relationships as well as key structural/functional features and discuss efforts to target ODEs for inhibition as a potential integrated pest management strategy. In contrast, Liu H. et al. focus on characterization of a single, highly expressed, male antennae dominant GST from the Indian meal moth (*P. interpunctella*) that efficiently degraded both acetate sex pheromones and a series of aldehyde host volatiles.

PROSPECTS, CHALLENGES, AND POTENTIAL APPLICATIONS TO PEST MANAGEMENT

Even though advances in sequencing technologies have facilitated the identification of numerous genes critical to insect olfaction, incorporation and successful implementation of this knowledge into pest management remains challenging. Liu F. et al. provide a broad overview of olfaction in hematophagous hemipterans from the current olfactory mechanism paradigm to effects on host-seeking behavior and finally chemosensation-based management possibilities. They suggest that a combination of PULL-PUSH-MASK could be the best solution based on classic chemical ecology using chemical lures, repellents, and confusants. Further investment in reverse chemical ecology will continue to offer the possibility of accurately predicting critical chemical structures based on crucial olfactory genes. However, pairing that approach with novel gene editing/knockdown methods such as CRISPR and RNAi, could lead to the development of critical breakthroughs that allow olfaction-based methods of pest management to replace current reliance on chemical pesticides.

CONCLUDING REMARKS

We truly appreciate all authors' contributions to this Topic, which illustrate the diversity of studies currently underway on insect olfactory proteins. We also thank all reviewers and editors who assisted us and provided thorough comments and invaluable suggestions, as well as the Frontiers editorial team for its support on the Topic management.

AUTHOR CONTRIBUTIONS

PH, YL, JH, Y-NZ, JZ, X-JG, and WX wrote, edited, and finalized this document. All authors contributed to the article and approved the submitted version.

FUNDING

This report was supported by the National Natural Science Foundation of China (Grant No. 31860617 for PH), the Natural Science Foundation of Guizhou Province of China [Grant No. QKH-J (2020)1Y077 for PH], the Talent Cultivation Program at Guizhou University [(2019)05 for PH], the Program of Introducing Talents of Discipline to Universities of China (111 Program, D20023), and the Frontiers Science Center for Asymmetric Synthesis and Medicinal Molecules, Department of Education, Guizhou Province [Qianjiaohe KY number (2020) 004].

Conflict of Interest: The authors declare that the research was conducted in the absence of any commercial or financial relationships that could be construed as a potential conflict of interest.

Publisher's Note: All claims expressed in this article are solely those of the authors and do not necessarily represent those of their affiliated organizations, or those of the publisher, the editors and the reviewers. Any product that may be evaluated in this article, or claim that may be made by its manufacturer, is not guaranteed or endorsed by the publisher.

frontiers in Physiology

ORIGINAL RESEARCH
published: 25 January 2021
doi: 10.3389/fphys.2020.618983

Identification and Functional Characterization of Two Putative Pheromone Receptors in the Potato Tuber Moth, *Phthorimaea operculella*

Xiaoli He[1], Yajie Cai[1], Jinglei Zhu[1,2], Mengdi Zhang[2], Yadong Zhang[1], Yang Ge[1], Zengrong Zhu[1], Wenwu Zhou[1], Guirong Wang[2]* and Yulin Gao[2]**

[1]Institute of Insect Sciences, Key Laboratory of Biology of Crop Pathogens and Insects of Zhejiang Province, Key Laboratory of Molecular Biology of Crop Pathogens and Insects, Ministry of Agriculture, State Key Laboratory of Rice Biology, Hangzhou, China, [2]State Key Laboratory for Biology of Plant Disease and Insect Pests, Institute of Plant Protection, Chinese Academy of Agricultural Sciences, Beijing, China

OPEN ACCESS

Edited by:
Peng He,
Guizhou University, China

Reviewed by:
Ya-Nan Zhang,
Huaibei Normal University, China
Dan-Dan Zhang,
Lund University, Sweden
Arthur de Fouchier,
EA4443 Laboratoire d'Éthologie Expérimentale et Comparée (LEEC), France

***Correspondence:**
Wenwu Zhou
wenwuzhzou@zju.edu.cn
Guirong Wang
wangguirong@caas.cn
Yulin Gao
gaoyulin@caas.cn

Specialty section:
This article was submitted to Invertebrate Physiology, a section of the journal Frontiers in Physiology

Received: 19 October 2020
Accepted: 18 December 2020
Published: 25 January 2021

Citation:
He X, Cai Y, Zhu J, Zhang M, Zhang Y, Ge Y, Zhu Z, Zhou W, Wang G and Gao Y (2021) Identification and Functional Characterization of Two Putative Pheromone Receptors in the Potato Tuber Moth, Phthorimaea operculella. Front. Physiol. 11:618983. doi: 10.3389/fphys.2020.618983

Pheromones are a kind of signal produced by an animal that evoke innate responses in conspecifics. In moth, pheromone components can be detected by specialized olfactory receptor neurons (OSNs) housed in long sensilla trichoids on the male antennae. The pheromone receptors (PRs) located in the dendrite membrane of OSNs are responsible for pheromone sensing in most Lepidopteran insects. The potato tuber moth *Phthorimaea operculella* is a destructive pest of Solanaceae crops. Although sex attractant is widely used in fields to monitor the population of *P. operculella*, no study has been reported on the mechanism the male moth of *P. operculella* uses to recognize sex pheromone components. In the present study, we cloned two pheromone receptor genes *PopeOR1* and *PopeOR3* in *P. operculella*. The transcripts of them were highly accumulated in the antennae of male adults. Functional analysis using the heterologous expression system of *Xenopus* oocyte demonstrated that these two PR proteins both responded to (*E*, *Z*)-4,7–13: OAc and (*E*, *Z*, *Z*)-4,7,10–13: OAc, the key sex pheromone components of *P. operculella*, whilst they responded differentially to these two ligands. Our findings for the first time characterized the function of pheromone receptors in gelechiid moth and could promote the olfactory based pest management of *P. operculella* in the field.

Keywords: *Phthorimaea operculella*, pheromone receptor, *Xenopus* oocytes, pheromone communication, sexual pheromone

INTRODUCTION

The potato tuber moth, *Phthorimaea operculella* (Lepidoptera: Gelechiidae), is one of the main pests affecting potatoes around the world (Rondon, 2020). It reduces potato production either *via* mining and damaging leaves in fields or *via* burrowing and destroying tubers in storage. The sex pheromone glands of *P. operculella* females produce a blend of odors that can influence the behavior of males. Two major pheromone components trans-4, cis-7-tridecadienyl acetate ((*E*, *Z*)-4,7–13: OAc) and tran-4, cis-7, cis-10-tridecatrienyl acetate ((*E*, *Z*, *Z*)-4,7,10–13: OAc) have been identified from this blend (Roelofs et al., 1975; Persoons et al., 1976). The structures of

these components are quite similar, with the only difference in their double bond numbers. In field trapping studies, *P. operculella* males flew to lure sources containing either single or mixed compounds, while (*E*, *Z*, *Z*)-4,7,10–13: OAc attracted more male moths than (*E*, *Z*)-4,7–13: OAc, indicating the differentiated recognition of these components in male antennae. Moreover, when both compounds were present the number of moths attracted also increased significantly. While pheromone-based technologies have been widely used as part of sustainable control strategies, it remains unclear how these two pheromones are detected by *P. operculella*.

Insects use pheromones for mate recognition, and these chemical cues are mainly perceived by olfactory sensory neurons (OSNs), which are housed in olfactory sensilla on the antenna (Laurent, 1999; Steinbrecht, 1999). Pheromone detection is mediated by the heteromeric ligand-gated ion channels in the cell membrane of OSN dendrites. These channels are formed by the combination of specific pheromone receptors (PRs) and the olfactory co-receptor (Orco; Sato et al., 2008). Previous studies indicated that PRs belong to the olfactory receptor (OR) family, and they are thought to constitute a monophyletic clade in the phylogeny of insect OR for a long time (Liu et al., 2018b). However, recent studies found that except classical clade, there are multiple PR clades that have evolved independently (Yuvaraj et al., 2018). For example, Bastin-Heline et al. (2019) found SlitOR5, a PR from the cotton leafworm *Spodoptera littoralis*, grouped with a novel PR clade. With a typical structure of seven transmembrane domains, PRs are more abundantly expressed in male antennae (He et al., 2014; Zhang and Löfstedt, 2015; Ke et al., 2017), whilst some PRs are also found in female antennae and other tissues such as the wings and ovipositor (Chang et al., 2015; Li et al., 2020).

In Lepidopteran insects, PR was first functionally characterized in *Bombyx mori* using the heterologous expression system of *Xenopus* oocyte (Sakura et al., 2004), after that more than 60 PRs have been studied in over 30 moth species across 10 families by using different systems, such as in *Xenopus* oocytes (Wang et al., 2011), HEK293 cells (Forstner et al., 2009), transgenic *Drosophila* (Montagné et al., 2012), and more recently, in specific insects *via* CRISPR/Cas techniques (An et al., 2020). These PRs are predominately identified from moths causing crop damages, such as *Manduca sexta* (Große, 2010), *Spodoptera exigua* (Liu et al., 2013a), *Spodoptera litura* (Zhang et al., 2015a), *Plutella xylostella* (Sun et al., 2013; Liu et al., 2018b), *Ostinia furnacalis* (Liu et al., 2018a), *Athetis lepigone* (Zhang et al., 2018), *Sesamia inferens* (Zhang et al., 2015b), and *Athetis dissimilis* (Liu et al., 2019; Guo et al., 2020). Based on these studies, PRs were further grouped into three types: (1) narrowly tuned to a single component of the sex pheromones; (2) tuned to one component with high specificity, but still sensitive to other components at higher doses; and (3) broadly tuned to a wide range of pheromone components (Liu et al., 2018b).

Sex pheromone components have been characterized in *P. operculella* and other gelechiid insects and widely used in the management of pests, while the molecular mechanism of sex pheromone component perception is still largely unknown (Persoons et al., 1976). In the present study, we cloned two pheromone receptor genes *PopeOR1* and *PoprOR3* in *P. operculella*. Their transcripts were highly accumulated in the antennae of male adults. Their expression patterns were measured in different tissues of male and female adults by using the quantitative real-time PCR (qPCR). The function of these two candidate PRs in the detection of the key pheromones (*E*, *Z*)-4,7–13: OAc and (*E*, *Z*, *Z*)-4,7,10–13: OAc were further characterized using the heterologous expression system of *Xenopus* oocyte. Our results provide insights into the mechanism of pheromone perception in a gelechiid insect.

MATERIALS AND METHODS

Animals

Phthorimaea operculella used for this study were collected from a suburban area in Yunnan Province in 2017 and the larvae were reared on potatoes at 26 ± 1°C on a 16:8 h (light/dark) photoperiod cycle and 70 ± 5% relative humidity at the Institute of Plant Protection, Chinese Academy of Agricultural Science (Beijing, China). The adults were fed with a 10% honey solution for three generations.

RNA Extraction and cDNA Synthesis

Total RNA was isolated from tissues using Trizol Reagent (Invitrogen) according to the manufacturer's protocol. Total RNA was dissolved in RNase-free water and gel electrophoresis was used to verify its quality. The concentration of RNA was determined by NanoDrop-2000 (Thermo Scientific, Waltham, MA, USA). cDNA was synthesized from 1 μg of total RNA using a RevertAid Frist Strand cDNA Synthesis Kit (Fermentas, Vilnius, Lithuania). The cDNA products were stored at −20°C until use.

Gene Cloning

Two candidate PR genes, *PopeOR1* and *PopeOR3*, and the *Orco* gene (*PopeOrco*) were identified from the transcriptome of *P. operculella* (unpublished data). Their full length cDNAs were cloned with specific primers (**Supplementary Table 1**) designed by primer5.0 (PREMIER Biosoft International, CA, United States). The open-reading frames (ORFs) of these three genes were predicted using the ORF Finder.[1] The PCR reaction was performed in a 50 μl system containing 25 μl of *TransStartPfu* PCR SuperMix (TransGen Biotech, Beijing, China), 22 μl of ddH_2O, 1 μl of cDNA template, and 1 μl of forward and reverse primers (10 μM). The PCR conditions were: 95°C for 2 min; 35 cycles of 98°C for 10 s, 55°C for 30 s, 72°C for 1.4 min; 72°C for 10 min. The PCR products were verified on a 1.2% agarose gel, and the band was recovered and purified by an AxyPrep™ DNA gel extraction kit (YMbio, Beijing, China). Purified fragments were cloned in the pEASY®-Blunt3 cloning vector (TransGen Biotech, Beijing, China) and then transformed into *Trans5α* chemically competent cells (TransGen Biotech, Beijing, China). The transformants were incubated on

[1]www.ncbi.nlm.nih.gov

LB-Agar plates containing 100 μg ml^{-1} of ampicillin. The target DNA products were sequenced by Novogene (Beijing, China).

Phylogenic Analysis and Sequence Analysis

To construct the phylogenic tree, OR genes from *H. virescens*, *S. littoralis* (Walker et al., 2019), *M. sexta*, and *B. mori* were used, and the MEGA7 program was used for phylogenic analysis (Tamura et al., 2011). The phylogenic tree was constructed by the neighbor-joining method with a bootstrap test using 500 replications. The Genbank accession numbers for all the OR genes used are shown in **Supplementary Table 2**, and all the *P. operculella* OR proteins used for the phylogenetic analysis are presented in **Supplementary Material**.

Transmembrane domains of the two candidate PRs were predicted by TMHMM Server Version 2.0,[2] and the amino acid sequences of PopeOR1 and PopeOR3 were aligned by the DNAMAN 8.0 software (Lynnon Biosoft, San Ramon, CA, United States).

Tissue Specific Expression Profiles of Two Candidate Pheromone Receptor Genes

To determine the tissue expression profiles of the two candidate PR genes, female antennae (FA), male antennae (MA), heads without antennae (H), thoraxes (T), abdomens (AB), legs (L), wings (W), and genitalia (G) from 3-day-old unmated adult moths were collected between the 6th and 8th hours of the dark period, and were immediately frozen in liquid nitrogen and stored at −80°C. Total RNA was extracted and cDNA was synthesized as mentioned above. The qPCR analysis was conducted using an ABI Prime 7,500 Detection System (Applied Biosystem, United States). The qPCR reaction was performed in a 20 μl system containing 10 μl of SYBR Green PCR Master Mix (Biomed, Beijing, China), 0.4 μl of each primer (10 μM), 0.4 μl of ROX Reference Dye II, 1 μl of cDNA template, and 7.8 μl of nuclease-free water. The thermal cycling parameters were: 95°C for 1 min, 40 cycles of 95°C for 10 s, 55°C for 5 s, and 72°C for 15 s. DNase were used to eliminate the DNA contamination of the RNAs samples. The actin gene was used to standardize the target gene expression (Sun et al., 2013). For each tissue, three biological replicates were measured with three technical replicates for each replicate, gene expression levels were analyzed using the $2^{-\Delta\Delta CT}$ method (Livak and Schmittgen, 2001). The sequences of the primer pairs used in this analysis are listed in **Supplementary Table 1**. The SPSS 20.0 software (IBM, Endicatt, NY, United States) was used for data analysis, the statistical comparison of the expression of the PRs was assessed using one-way ANOVA followed by Tukey's honest significant differences (HSD) test ($p < 0.05$), data were presented as mean ± SEM.

Vector Construction and cRNA Synthesis

Primers containing the Kozak consensus sequence and restriction enzyme cutting site (*Apa* I and *Not* I) were designed to amplify the open-reading frame (ORFs) of *PopeOR1*, *PopeOR3*, and *PopeOrco*. The products were then cloned into pT_7T_s vectors with the primers listed in **Supplementary Table 1** (Wang et al., 2011). The extracted plasmids were linearized by digestion with *Sam*I, and used as templates to synthesis cRNAs by using T7 polymerase of the mMESSAGE mMACHINE®T7 Kit

[2]www.cbs.dtu.dk/services/TMHMM/

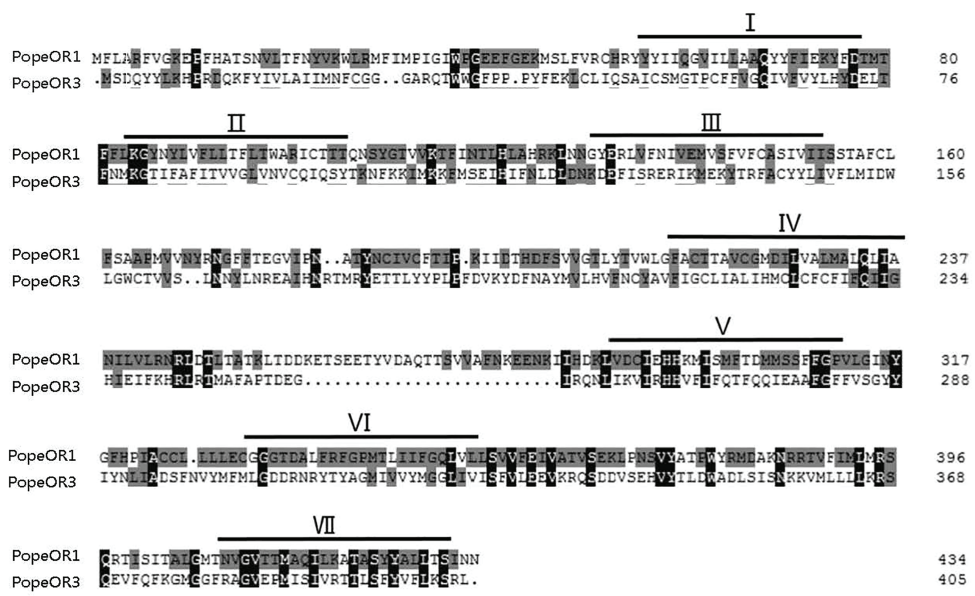

FIGURE 1 | Alignment of the amino acid sequences of the two candidate PRs in *Phthorimaea operculella*. Identical amino acids are marked with gray and black shading. Predicted seven transmembrane domains (TMD1-TMD7) are indicated by bold lines.

(Thermo Fisher Scientific, Waltham, MA, United States). The purified cRNAs were diluted with nuclease-free water at a concentration of 2 μg/μl and stored at −80°C until use.

Pheromone Components

The pheromones (*E*, *Z*)-4,7–13: OAc and (*E*, *Z*, *Z*)-4,7,10–13: OAc were purchased from Nimrod Inc. (Changzhou, China) with 95% minimum purity. The stock solution was prepared in dimethyl sulfoxide (DMSO) at 1 M concentration and stored at −20°C. Prior to the two-electrode voltage clamp electrophysiological recording experiments, the stock solutions were diluted with Ringer's buffer (96 mM of NaCl, 2 mM of KCl, 5 mM of $MgCl_2$, 0.8 mM of $CaCl_2$, and 5 mM of HEPES; pH=7.6) into the concentration of 10^{-4} M Ringer's buffer containing 0.1% DMSO was used as the negative control. All chemicals were freshly prepared for the experiments.

Receptor Expression in *Xenopus* Oocytes and Two Electrode Voltage Clamp Electrophysiological Recordings

Each of the two candidate PRs were co-expressed with the PopeOrco in *Xenopus* oocytes for 3–4 d, and the ligand sensitivity was detected using a two electrode voltage-clamp recording as previously reported (Lu et al., 2007; Wang et al., 2010). Healthy, matured *Xenopus* oocytes (stage V-VII) were treated with 2 mg/ml of collagenase in washing buffer (96 mM of NaCl, 2 mM of KCl, 5 mM of $MgCl_2$, 5 mM of HEPES; pH 7.6) for 1–2 h at room temperature. Equal amounts of PR and Orco cRNA (27.6 ng) were microinjected into the oocytes (Wang et al., 2011). The oocytes were then incubated at 18°C for 4–7 d in 1× Ringer's solution (96 mM of NaCl, 2 mM of KCl, 5 mM of $MgCl_2$, 0.8 mM of $CaCl_2$, and 5 mM of HEPES; pH=7.6) supplemented with dialyzed horse serum (5%),

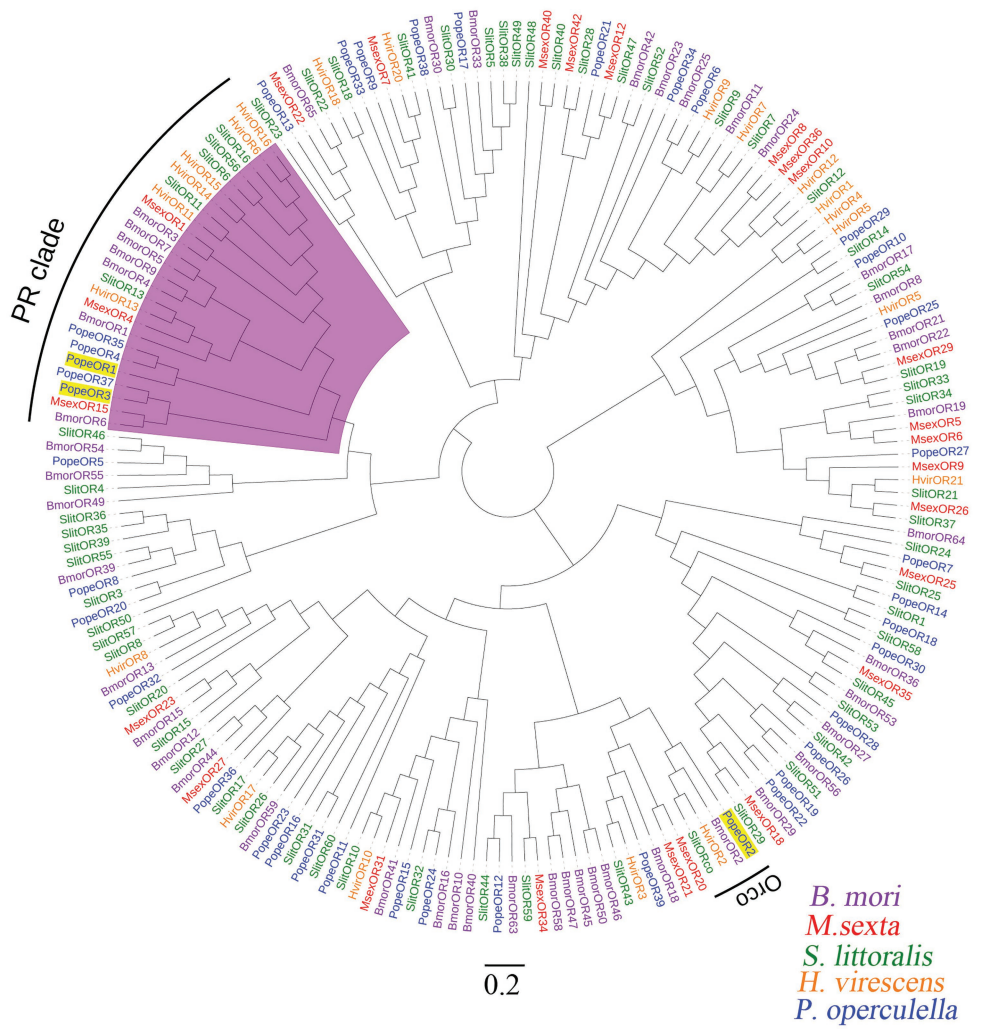

FIGURE 2 | An unrooted neighbor-joining tree of the two candidate PRs of *P. operculella* together with the ORs from four other Lepidopteran species; *B. mori*: *Bombyx mori* (purple), *M. sexta*: *Manduca sexta* (red), *S. littoralis*: *Spodoptera littoralis* (green), and *H. virescens*: *Heliothis virescens* (orange) was constructed. The clade in purple indicates the pheromone receptor clade. The two candidate PRs and Orco of *P. operculella* are marked with yellow shading.

tetracycline (50 μg/ml), streptomycin (100 μg/ml), and sodium pyruvate (550 μg/ml). Whole-cell currents were recorded from the injected *Xenopus* oocytes in an OC-725 two-electrode voltage clamp amplifier (Warner Instruments, United States) at a holding potential of −80 mV. Oocytes were exposed to a concentration series of different pheromone components from low to high with an interval between exposures that allowed the current to return to baseline. To avoid the sequential effect of two sex pheromone components on the candidate PRs, the experiment was repeated by reversing the order of component stimulation. Oocytes containing PopeOR1/Orco and PopeOR3/Orco were injected with 1× Ringer's buffer solution containing 0.1% DMSO to be used as negative control, respectively. All experiments were repeated 5 times on different oocytes. The Digidata 1440A and pCLAMP 10.2 software were used to collect and analyze the data (Axon Instruments Inc., United States). Dose-response curves were obtained and analyzed using GraphPad Prism 5 (GraphPad Software Inc., United States). A statistical comparison of the response of the oocytes to the candidate ligands was assessed using student's *t*-test with the SPSS 10.0.1 software (IBM, Endicatt, NY, United States).

RESULTS

Gene Cloning and Phylogenic Analysis

The full-length sequences of the three candidate PR genes were cloned, based on the nomenclature of ORs in other Lepidopteran insects, they were named *PopeOR1*, *PopeOR2*, and *PopeOR3*. In addition, *PopeOR2* was likely a pheromone co-receptor gene of *P. operculella*, and was further named *PopeOrco*. The lengths of the complete ORF region of *PopeOR1*, *PopeOR3*, and *PopeOrco* were 1,302, 1,215, and 1,419 bp, which encode 434, 405, and 473 amino acid residues, respectively. Consistent with other insect ORs, the predicted PopeOR1 and PopeOR3 proteins contain seven putative transmembrane domains (**Figure 1**) with a predicted extracellular C-terminus and an intracellular N-terminus. Phylogenic analysis showed that these two PRs were grouped into the same branch with PRs from other Lepidopteran species, and this branch was independent from other ORs which may mainly respond to general environmental odors. In the phylogenic tree, PopeOR1 and PopeOR3 clustered with PRs of other Lepidopteran insects including BmorOR1, BmorOR3, BmorOR6, HvirOR11, HvirOR13, and SlitOR11, SlitOR13. The PopeOrco gene (*PopeOR2*) clustered into the Lepidopteran Orco group with HvirOrco, SlitOrco, and BmorOrco (**Figure 2**).

Expression Profiles of the Candidate PR Genes

The qPCR was performed to evaluate the transcription levels of two candidate PRs in different tissues of adults (**Figure 3**). As expected, the transcripts of both PR genes were highly accumulated in the male antennae. The transcript of *PopeOR1* was not expressed in other tissues including heads (without antennae), thoraxes, abdomens, legs, wings, and genitalia. For *PopeOR3*, its transcript was also hardly detectable in heads (without antennae), thoraxes, abdomens, legs, and genitalia, but not in the wings.

Functional Characterization of the Two Candidate PRs in the *Xenopus* Oocyte System

The heterologous expression system of *Xenopus* oocyte and the voltage clamp recording technique were used to explore the function of the two candidate PRs. Both PopeOR1/PopeOrco and PopeOR3/PopeOrco were successfully activated by two pheromone components (*E*, *Z*)-4,7–13: OAc and (*E*, *Z*, *Z*)-4,7,10–13: OAc. PopeOR1/PopeOrco responded to (*E*, *Z*)-4,7–13: OAc and (*E*, *Z*, *Z*)-4,7,10–13: OAc with the responses of 313.7 ± 28.26 and 137.6 ± 19.22 nA, respectively (**Figures 4A,B**). For PopeOR3/PopeOrco, a strong response was observed when bound to (*E*, *Z*, *Z*)-4,7,10–13: OAc (155.7 ± 20.26 nA), while

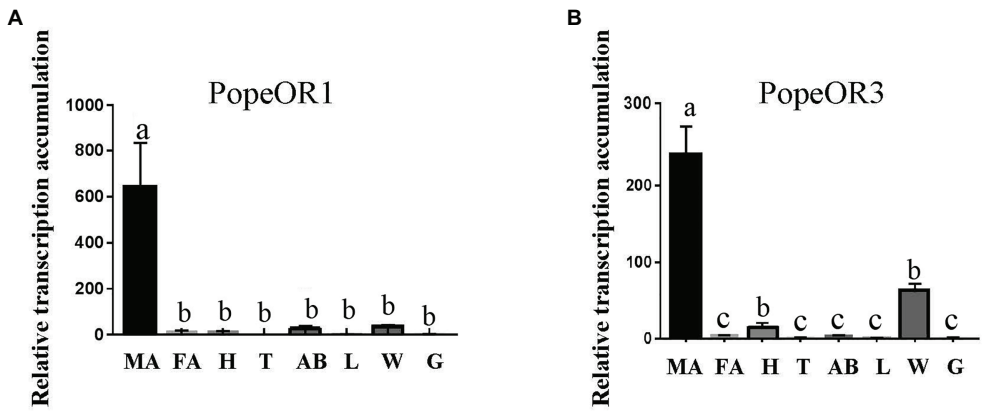

FIGURE 3 | Expression profiles of *PopeOR1* **(A)** and *PopeOR3* **(B)** genes in different tissues. MA, male antennae; FA, female antennae; H, heads (without antennae); T, thoraxes; AB, abdomens; L, legs; W, wings, G, genitalia. Error bars indicate standard error of three biological replicates. Different letters within the same figure mean that the values are significantly different under one-way ANOVA followed by Tukey's honest significant differences (HSD) test ($p < 0.05$).

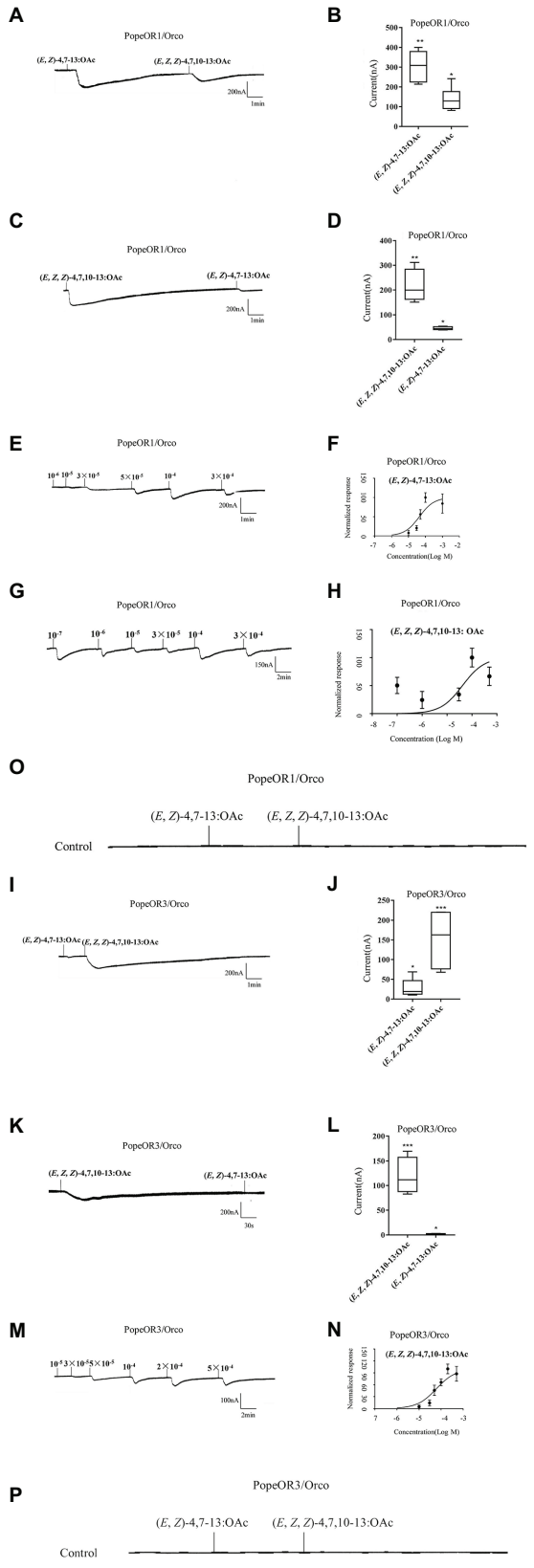

FIGURE 4 | Continued

FIGURE 4 | Functional characterization of PopeOR1 and PopeOR3 in *Xenopus* oocytes. **(A,I)** Inward current responses of PopeOR1/Orco and PopeOR3/Orco expressed *Xenopus* oocytes in response to a 10^{-4} mol/L solution of tested compounds. **(B,J)** Boxplots of tested compounds response profile of PopeOR1/Orco and PopeOR3/Orco expressed *Xenopus* oocytes. **(C,K)** Inward current responses of PopeOR1/Orco and PopeOR3/Orco expressed *Xenopus* oocytes in response to a 10^{-4} mol/L solution of tested compounds (reverse stimuli order). **(D,L)** Boxplots of tested compounds response profile of PopeOR1/Orco and PopeOR3/Orco expressed *Xenopus* oocytes (reverse stimuli order). **(E)** PopeOR1/Orco expressed *Xenopus* oocytes stimulated by a series of concentrations of (*E*, *Z*)-4,7–13: OAc. **(F)** Dose-response curves of PopeOR1/Orco expressed *Xenopus* oocytes to (*E*, *Z*)-4,7–13: OAc. Responses were normalized by setting the maximal response to 100. EC_{50} values were calculated to be 7.3×10^{-5} M. **(G)** PopeOR1/Orco expressed *Xenopus* oocytes stimulated by a serious of concentrations of (*E*, *Z*, *Z*)-4,7,10–13: OAc. **(H)** Dose-response curves of PopeOR1/Orco expressed *Xenopus* oocytes to (*E*, *Z*, *Z*)-4,7,10–13: OAc. Responses were normalized by setting the maximal response to 100. EC_{50} values were calculated to be 3.9×10^{-5} M. **(M)** PopeOR3/Orco expressed *Xenopus* oocytes stimulated by a range of concentrations of (*E*, *Z*, *Z*)-4,7, 10–13: OAc. **(N)** Dose-response curves of PopeOR3/Orco expressed *Xenopus* oocytes to (*E*, *Z*, *Z*)-4,7,10–13: OAc. Responses were normalized by setting the maximal response to 100. EC_{50} values were calculated to be 8.9×10^{-5} M. Error bars indicate SEM ($n = 6$). **(O,P)** Negative control of PopeOR1/Orco and PopeOR3/Orco expressed *Xenopus* oocytes stimulated by tested compounds. Significance is indicated by asterisk.

weak responses were found when bound to (*E*, *Z*)-4,7–13: OAc (29.41 ± 6.87 nA; **Figures 4I,J**). By reversing the order of the stimulation from the two components, the PopeOR1/Orco showed decreased responses on (*E*, *Z*)-4,7–13: OAc with a current value of 45.4 ± 3.207 nA, but enhanced responses on (*E*, *Z*, *Z*)-4,7,10–13: OAc with a current value of 215.5 ± 34.07 nA (**Figures 4C,D**), while changing the order of the supply of components had no impact on the sensitivity of PopeOR3/PopeOrco to them (**Figures 4K,L**). Oocytes injected with the buffer did not respond to any of the test compounds (**Figures 4O,P**).

In the dose-response comparison experiments, PopeOR1/PopeOrco responded to (*E*, *Z*)-4,7–13: OAc at the concentration of 10^{-6} M, and the response peak occurred at 10^{-4} M, with an EC_{50} value of 7.3×10^{-5} M (**Figures 4E,F**); PopeOR1/PopeOrco responded to (*E*, *Z*, *Z*)-4,7,10–13: OAc at the concentration of 10^{-7} M, and the response peak occurred at 10^{-4} M, with an EC_{50} value of 3.9×10^{-5} M (**Figures 4G,H**). PopeOR3/PopeOrco responded to (*E*, *Z*, *Z*)-4,7,10–13: OAc at the concentration of 10^{-6} M and the response peak occurred at 2×10^{-4} M, with the calculated EC_{50} of 8.9×10^{-5} M (**Figures 4M,N**).

DISCUSSION

Pheromone communication is widely used by Lepidopteran insects to find cognate individuals of the opposite sex (Vogt, 2005). Of all the protein families involved in pheromone perception, PRs play critical roles in determining the specificity and sensitivity of the recognition of the chemical mating signals (Liu et al., 2018b), which is considered an important basis for interspecies isolation and intraspecies choice (Groot et al., 2006). In the current study, we identified and

characterized two candidate PRs from *P. operculella*, an important pest of the Solanaceae crop.

The expression analysis suggested that both the two PR genes in *P. operculella* were almost only expressed in male antennae. The males of Lepidopteran insects are the main receivers for pheromone cues. It is therefore reasonable to see the sex-specific expression of PR genes in *P. operculella* and many other Lepidopteran species (Krieger et al., 2004; Sakura et al., 2004; Wang et al., 2011; Liu et al., 2013b, 2018a). Moreover, it is interesting to see that *PopeOR3* is also expressed in the wings of male adults. A recent study into *Helicoverpa assulta* found that an odorant receptor gene, *HassOR31* which was highly expressed in the ovipositor rather than in antennae, was related to the determination of oviposition in host plants in females. This finding reveals that some ORs located outside the antenna might also have a functional role *in vivo* (Li et al., 2020). Therefore, further studies are needed to uncover the function of *PopeOR3* in the wings of *P. operculella*.

The heterologous expression in *Xenopus* oocytes and electrophysiological recording were widely used in investigating the function of insect PRs. In the phylogenic tree, PopeOR1 and PopeOR3 clustered with the PRs from other insects, including BmorOR1, BmorOR3, HvirOR6, and SlitOR6, whose functions in pheromone detection have been confirmed (Sakura et al., 2005; Wang et al., 2011; Cheng et al., 2017), indicating their potential roles as PRs. When co-expressed with PopeOrco, both PopeOR1 and PopeOR3 showed strong responses to the (*E*, *Z*, *Z*)-4,7,10–13: OAc, whereas only PopeOR1 had strong responses to (*E*, *Z*)-4,7–13: OAc. Thus, it is likely that PopeOR1 is more sensitive to female-produced pheromones than PopeOR3. Moreover, we found that PopeOR1 had a higher affinity to (*E*, *Z*, *Z*)-4,7,10–13: OAc (with an EC_{50} value of 3.9×10^{-5} M) than to (*E*, *Z*)-4,7–13: OAc (with an EC_{50} value of 7.3×10^{-5} M). A previous field study found that sole sex pheromones can attract males, and (*E*, *Z*, *Z*)-4,7,10–13: OAc was more attractive to *P. operculella* males than (*E*, *Z*)-4,7–13: OAc (Persoons et al., 1976). Our findings may partially explain this phenomenon. Despite the fact that single sex pheromone compounds can attract males, a field study revealed that when (*E*, *Z*)-4,7–13: OAc and (*E*, *Z*, *Z*)-4,7,10–13: OAc are mixed with a ratio of 1:4, the combination showed the highest attraction (Persoons et al., 1976). This implied that in the field the two pheromone compounds should stimulate the OSN together simultaneously and that co-stimulation of the two sex pheromone components would enhance the overall response of the neurons. A previous study on the PRs of noctuid moth *Spodoptera littoralis* indicated that two different PRs can detect the same pheromone compound with a different sensitivity (de Fouchier et al., 2015). In this study, we noticed that PopeOR1 and PopeOR3 showed different affinities to the same sex pheromone compound (*E*, *Z*, *Z*)-4,7,10–13: OAc. One possible reason is that these two PRs might be located on different sites of the male antennae, which contributes to their distinct affinities to the single same sex pheromone compound. Another possibility is that these two receptors are expressed by two different types of OSNs, in which case they are able to show different affinities for the same sex pheromone compound.

Although we identified the roles of PopeOR1 and PopeOR3 in the detection of two key pheromones *in vitro*, since we only tested two pheromone compounds in the present study, we supposed that these PRs might also detect other pheromone components untested here. Further studies in testing a wider range of pheromone compounds on this insect and also the identification of other candidate PR genes in the genome of *P. operculella* could provide more information on the pheromone detection of this pest. Moreover, while the *Xenopus* oocytes system is widely used to analyze the function of PRs, recent findings suggested that PRs were more sensitive to pheromones when pheromone binding proteins were present (Chang et al., 2015). It might be interesting to see the *in vivo* biological functions of PopeOR1 and PopeOR3 by using techniques such as CRISPR/Cas in *P. operculella*.

DATA AVAILABILITY STATEMENT

The original contributions presented in the study are included in the article/**Supplementary Material**, further inquiries can be directed to the corresponding authors.

ETHICS STATEMENT

The animal study was reviewed and approved by Ethics Committee of Institute of Insect Sciences, Key Laboratory of Biology of Crop Pathogens and Insects of Zhejiang Province, Key Laboratory of Molecular Biology of Crop Pathogens and Insects, Ministry of Agriculture, State Key Laboratory of Rice Biology, Zhejiang University.

AUTHOR CONTRIBUTIONS

WZ, GW, and YuG conceived and designed the experiments. XH and JZ wrote the manuscript. XH, YC, JZ, MZ, YZ, and YaG performed the experiments. WZ, GW, and YuG provided valuable suggestions and helped to revise the manuscript. All authors discussed the results and approved the final manuscript.

FUNDING

This work was supported by the National Nature Science Foundation of China (Grant No. 31701798); the Key Research and Development Program of Zhejiang Province (Grant No. 2018C04G2011264); and the National Key Research and Development Program (Grant No. 2018YFD0200802).

SUPPLEMENTARY MATERIAL

The Supplementary Material for this article can be found online at: https://www.frontiersin.org/articles/10.3389/fphys.2020.618983/full#supplementary-material

REFERENCES

An, X. K., Khashaveh, A., Liu, D. F., Xiao, Y., Wang, Q., Wang, S. N., et al. (2020). Functional characterization of one sex pheromone receptor (AlucOR4) in *Apolygus lucorum* (Meyer-Dür). *J. Insect Physiol.* 120:103986. doi: 10.1016/j.jinsphys.2019.103986

Bastin-Heline, L., de Fouchier, A., Cao, S., Koutroumpa, F., Caballero-Vidal, G., Robakiewicz, S., et al. (2019). A novel lineage of candidate pheromone receptors for sex communication in moth. *eLife* 8:e49826. doi: 10.7554/eLife.49826

Chang, H., Liu, Y., Yang, T., Pelosi, P., Dong, S., and Wang, G. (2015). Pheromone binding proteins enhance the sensitivity of olfactory receptors to sex pheromones in *Chilo suppressalis*. *Sci. Rep.* 5:13093. doi: 10.1038/srep13093

Cheng, T., Wu, J., Wu, Y., Chilukuri, R. V., Huang, L., Yamamoto, K., et al. (2017). Genomic adaptation to polyphagy and insecticides in a major east Asian noctuid pest. *Nat. Ecol. Evol.* 1, 1747–1756. doi: 10.1038/s41559-017-0314-4

de Fouchier, A., Sun, X., Monsempes, C., Mirabeau, O., Jacquin-Joly, E., and Montagné, N. (2015). Evolution of two receptors detecting the same pheromone compound in crop pest moth of the genus *Spodoptera*. *Front. Ecol. Evol.* 3:95. doi: 10.3389/fevo.2015.00095

Forstner, M., Breer, H., and Krieger, J. (2009). A receptor and binding protein interplay in the detection of a distinct pheromone component in the silkmoth: *Antheraea polyphemus*. *Int. J. Biol. Sci.* 5, 745–757. doi: 10.7150/ijbs.5.745

Groot, A., Horovitz, J. L., Hamiton, J., Santangelo, R. G., Schal, C., and Gould, F. (2006). Experimental evidence for interspecific directional selection on moth pheromone communication. *Proc. Natl. Acad. Sci. U. S. A.* 103, 5858–5863. doi: 10.1073/pnas.0508609103

Große, W. (2010). Sex-specific odorant receptors of the tobacco hornworm, *Manduca sexta*. *Front. Cell. Neurosci.* 4:22. doi: 10.3389/fncel.2010.00022

Guo, J. M., Liu, X. L., Liu, S. R., Wei, Z. Q., Han, W. K., Guo, Y., et al. (2020). Functional characterization of sex pheromone receptors in the fall armyworm (*Spodoptera frugiperda*). *Insects* 11:193. doi: 10.3390/insects11030193

He, P., Zhang, J., Li, Z. Q., Zhang, Y. N., Yang, K., Dong, S. L., et al. (2014). Functional characterization of an antennal esterase from the noctuid moth, *Spodoptera exigua*. *Arch. Insect Biochem. Physiol.* 86, 85–99. doi: 10.1002/arch.21164

Ke, Y., Huang, L. Q., Chao, N., and Wang, C. Z. (2017). Two single-point mutations shift the ligand selectivity of a pheromone receptor between two closely related moth species. *eLife* 6:e29100. doi: 10.7554/eLife.29100

Krieger, J., Grosse, W. E., Gohl, T., Dewer, Y. M., Raming, K., and Breer, H. (2004). Genes encoding candidate pheromone receptors in a moth (*Heliothis virescens*). *Proc. Natl. Acad. Sci. U. S. A.* 101, 11845–11850. doi: 10.1073/pnas.0403052101

Laurent, G. (1999). A systems perspective on early olfactory coding. *Science* 286, 723–728. doi: 10.1126/science.286.5440.72

Li, R. T., Huang, L. Q., Dong, J. F., and Wang, C. Z. (2020). A moth odorant receptor highly expressed in the ovipositor is involved in detecting host-plant volatiles. *eLife* 9:e53706. doi: 10.7554/elife.53706.sa2

Liu, W., Jiang, X. C., Cao, S., Yang, B., and Wang, G. R. (2018a). Functional studies of sex pheromone receptors in asian corn borer, *Ostrinia furnacalis*. *Front. Physiol.* 9:591. doi: 10.3389/fphys.2018.00591

Liu, Y., Liu, Y., Jiang, X., and Wang, G. (2018b). Cloning and functional characterization of three new pheromone receptors from the diamondback moth, *Plutella xylostella*. *J. Insect Physiol.* 107, 14–22. doi: 10.1016/j.jinsphys.2018.02.005

Liu, Y., Liu, C., Lin, K., and Wang, G. (2013a). Functional specificity of sex pheromone receptors in the cotton bollworm, *Helicoverpa armigera*. *PLoS One* 8:e62094. doi: 10.1371/journal.pone.0062094

Liu, C., Liu, Y., Walker, W. B., Dong, S., and Wang, G. (2013b). Identification and functional characterization of sex pheromone receptors in beet armyworm, *Spodoptera exigua* (Hubner). *Insect Biochem. Mol. Biol.* 43, 747–754. doi: 10.1016/j.ibmb.2013.05.009

Liu, X. L., Sun, S. J., Khuhro, S. A., Elzaki, M. E. A., Yan, Q., and Dong, S. L. (2019). Functional characterization of pheromone receptors in the moth, *Athetis dissimilis* (Lepidoptera: Noctuidae). *Pestic. Biochem. Physiol.* 158, 69–76. doi: 10.1016/j.pestbp.2019.04.011

Livak, K. J., and Schmittgen, T. D. (2001). Analysis of relative gene expression data using real-time quantitative PCR and the $2^{-\Delta\Delta Ct}$ method. *Methods* 25, 402–408. doi: 10.1006/meth.2001.1262

Lu, T., Qiu, Y. T., Wang, G., Kwon, J. Y., Rutzler, M., Kwon, H. W., et al. (2007). Odor coding in the maxillary palp of the malaria vector mosquito, *Anopheles gambiae*. *Curr. Biol.* 17, 1533–1544. doi: 10.1016/j.cub.2007.07.062

Montagné, N., Chertemps, T., Brigaud, I., Francois, A., Francois, M. C., de Fouchier, A., et al. (2012). Functional characterization of a sex pheromone receptor in the pest moth *Spodoptera littoralis* by heterologous expression in *Drosophila*. *Eur. J. Neurosci.* 36, 2588–2596. doi: 10.1111/j.1460-9568.2012.08183

Persoons, C. J., Voerman, S., Verwiel, P. E. J., Ritter, F. J., Nooyen, W. J., and Minks, A. K. (1976). Sex pheromone of the potato tuberworm moth, *Phthorimaea operculella*: isolation, dentification and field evaluation. *Entomol. Exp. Appl.* 20, 289–300. doi: 10.1111/j.1570-7458.1976.tb02645.x

Roelofs, W. L., Kochansky, J. P., Carde, R. T., Kennedy, G. G., and Corbin, V. L. (1975). Sex pheromone of the potato tuberworm moth, Phthorimaea operculella. Ithaca, NY: Cornell Research Foundation, Inc. U.S. Patent No 4,010,255.

Rondon, S. I. (2020). Decoding phthorimaea operculella (*Lepidoptera: Gelechiidae*) in the new age of change. *J. Integr. Agric.* 19, 316–324. doi: 10.1016/S2095-3119(19)62740-1

Sakura, T., Nakagawa, T., Hidefumi, M., Mori, H., Endo, Y., Tanoue, S., et al. (2004). Identification and functional characterization of a sex pheromone receptor in the silkmoth, *Bombyx mori*. *Proc. Natl. Acad. Sci. U. S. A.* 101, 16653–16658. doi: 10.1073/pnas.0407596101

Sakura, T., Nakagawa, T., Mitsuno, H., Mori, H., Endo, Y., and Tanoue, S. (2005). Insect sex-pheromone signals mediated by specific combinations of olfactory receptors. *Science* 307, 1638–1642. doi: 10.1126/science.1106267

Sato, K., Pellegrino, M., Nakagawa, T., Nakagawa, T., Vosshall, L. B., and Touhara, K. (2008). Insect olfactory receptors are heteromeric ligand-gated ion channels. *Nature* 452, 1002–1009. doi: 10.1038/nature06850

Steinbrecht, S. A. (1999). *Atlas of arthropod sensory receptor-dynamic morphology in relation to function*. Tokyo: Springer, 155–176.

Sun, M., Liu, Y., Walker, W. B., Liu, C., Lin, K., Gu, S., et al. (2013). Identification and characterization of pheromone receptors and interplay between receptors and pheromone binding proteins in the diamondback moth, *Plutella xyllostella*. *PLoS One* 8:e62098. doi: 10.1371/journal.pone.0062098

Tamura, K., Peterson, D., Peterson, N., Stecher, G., Nei, M., and Kumar, S. (2011). MEGA5: molecular evolutionary genetics analysis using maximum likelihood, evolutionary distance, and maximum parsimony methods. *Mol. Biol. Evol.* 28, 2731–2739. doi: 10.1093/molbev/msr121

Vogt, R. G. (2005). Molecular basis of pheromone detection in insects. *Comp. Mol. Insect. Sci. 3,* 735–803. doi: 10.1016/B0-44-451924-6/00047-8

Walker, W. B., Roy, A., Anderson, P., Schlyter, F., and Larsson, M. C. (2019). Transcriptome analysis of gene families involved in chemosensory function in *Spodoptera littoralis* (Lepidoptera: noctuidae). *BMC Genomics* 20:428. doi: 10.1186/s12864-019-5815-x

Wang, G., Carey, A. F., Carlson, J. R., and Zwiebel, L. J. (2010). Molecular basis of odor coding in the malaria vector mosquito, *Anopheles gambiae*. *Proc. Natl. Acad. Sci. U. S. A.* 107, 4418–4423. doi: 10.1073/pnas.0913392107

Wang, G., Vásquez, G. M., Schal, C., Zwiebel, L. J., and Gould, F. (2011). Functional characterization of pheromone receptors in the tobacco budworm, *Heliothis virescens*. *Insect Mol. Biol.* 20, 125–133. doi: 10.1111/j.1365-2583.2010.01045.x

Yuvaraj, J. K., Andersson, M. N., Corcoran, J. A., Anderbrant, O., and Löfstedt, C. (2018). Functional characterization of odorant receptors from Lampronia capitella suggests a non-ditrysian origan of the lepidopteran pheromone receptor clade. *Insect Biochem. Mol. Biol.* 100, 39–47. doi: 10.1016/j.ibmb.2018.06.002

Zhang, Y., Du, L. X., Xu, J. W., Wang, B., Zhang, X. Q., Yan, Q., et al. (2018). Functional characterization of four sex pheromone receptors in the newly discovered maize pest *Athetis lepigone*. *J. Insect Physiol.* 113, 59–66. doi: 10.1016/j.jinsphys.2018.08.009

Zhang, D. D., and Löfstedt, C. (2015). Moth pheromone receptors: gene sequences, function, and evolution. *Front. Ecol. Evol.* 3:105. doi: 10.3389/fevo.2015.00105

Zhang, J., Yan, S., Liu, Y., Jacquin-Joly, E., Dong, S., and Wang, G. (2015a). Identification and functional characterization of sex pheromone receptors in the common cutworm (*Spodoptera litura*). *Chem. Senses* 40, 7–16. doi: 10.3389/fphys.2018.00591

Zhang, Y. N., Zhang, J., Yan, S. W., Chang, H. T., Liu, Y., and Wang, G. R. (2015b). Functional characterization of sex pheromone receptors in the purple stem borer, *Sesamia inferens* (walker). *Insect Mol. Biol.* 23, 611–620. doi: 10.1111/imb.12109

Conflict of Interest: The authors declare that the research was conducted in the absence of any commercial or financial relationships that could be construed as a potential conflict of interest.

frontiers in Physiology

REVIEW
published: 31 March 2021
doi: 10.3389/fphys.2021.643281

An Overview of Antennal Esterases in Lepidoptera

*Ricardo Godoy[1,2], Juan Machuca[1,2], Herbert Venthur[2], Andrés Quiroz[2] and Ana Mutis[2]**

[1]*Programa de Doctorado en Ciencias de Recursos Naturales, Universidad de La Frontera, Temuco, Chile,* [2]*Centro de Investigación Biotecnológica Aplicada al Medio Ambiente (CIBAMA), Universidad de La Frontera, Temuco, Chile*

Lepidoptera are used as a model for the study of insect olfactory proteins. Among them, odorant degrading enzymes (ODEs), that degrade odorant molecules to maintain the sensitivity of antennae, have received less attention. In particular, antennal esterases (AEs; responsible for ester degradation) are crucial for intraspecific communication in Lepidoptera. Currently, transcriptomic and genomic studies have provided AEs in several species. However, efforts in gene annotation, classification, and functional assignment are still lacking. Therefore, we propose to combine evidence at evolutionary, structural, and functional level to update ODEs as well as key information into an easier classification, particularly of AEs. Finally, the kinetic parameters for putative inhibition of ODEs are discussed in terms of its role in future integrated pest management (IPM) strategies.

Keywords: Lepidoptera, antennal esterases, transcriptomic, semiochemicals, inhibition, olfactory system

OPEN ACCESS

Edited by:
Wei Xu,
Murdoch University, Australia

Reviewed by:
Liang Sun,
Chinese Academy of Agricultural Sciences (CAAS), China
Carlos Ueira-Vieira,
Federal University of Uberlandia, Brazil

****Correspondence:***
Ana Mutis
ana.mutis@ufrontera.cl

Specialty section:
This article was submitted to Invertebrate Physiology, a section of the journal Frontiers in Physiology

Received: *17 December 2020*
Accepted: *15 March 2021*
Published: *31 March 2021*

Citation:
Godoy R, Machuca J, Venthur H, Quiroz A and Mutis A (2021) An Overview of Antennal Esterases in Lepidoptera. Front. Physiol. 12:643281. doi: 10.3389/fphys.2021.643281

INTRODUCTION

In insects, the detection and processing of chemical cues through olfaction is crucial for successful mating, avoidance of harmful compounds, and location of either oviposition sites or food sources (Choo et al., 2013; Li et al., 2018). For instance, pollinators need to find floral resources using a sophisticated system capable of detecting and distinguishing volatile organic compounds (VOCs) in a short timescale (below 500 ms; Rusch et al., 2016). Unlike other senses, such as touch, vision, or hearing, the use of VOCs by insects (e.g., aphids, beetles, flies, and moths) to communicate messages over relatively long distances is an advantage (El-Shafie and Romeno, 2017).

These volatile chemicals are called semiochemicals and mediate interactions between organisms of the same species (i.e., pheromone) and different species (i.e., allelochemicals). These chemicals are recognized through a systematic cascade of events that occur in chemosensory organs named sensilla, which can be found in maxillary palps, legs, and mainly covering the antennae (Zhou, 2010; Pelosi et al., 2017). Chemoreception is mainly related to four key protein families (**Figure 1**), such as odorant-binding proteins (OBPs), chemosensory proteins (CSPs), chemosensory receptors, and odorant degrading enzymes (ODEs; Pelosi et al., 2006, 2017; Mei et al., 2018; Song et al., 2018). Upon entry of odorants through cuticular pores, OBPs and CSPs transport these hydrophobic molecules across aqueous lymph (sensillar lymph) to odorant receptors (ORs). OBPs can be divided in three groups (Zhou, 2010): pheromone binding proteins (PBPs), general OBPs (GOBPs), and antennal binding protein x (ABPx; Krieger et al., 1996; Wang et al., 2020). The chemosensory receptors can be divided in ORs, ionotropic receptors (IRs), gustatory receptors (GRs), and sensory neuron membrane proteins (SNMPs; Klein, 1987; Pelosi and Maida, 1995; Isono and Morita, 2010; Zhou, 2010; Leal, 2013). Thus, a chemical

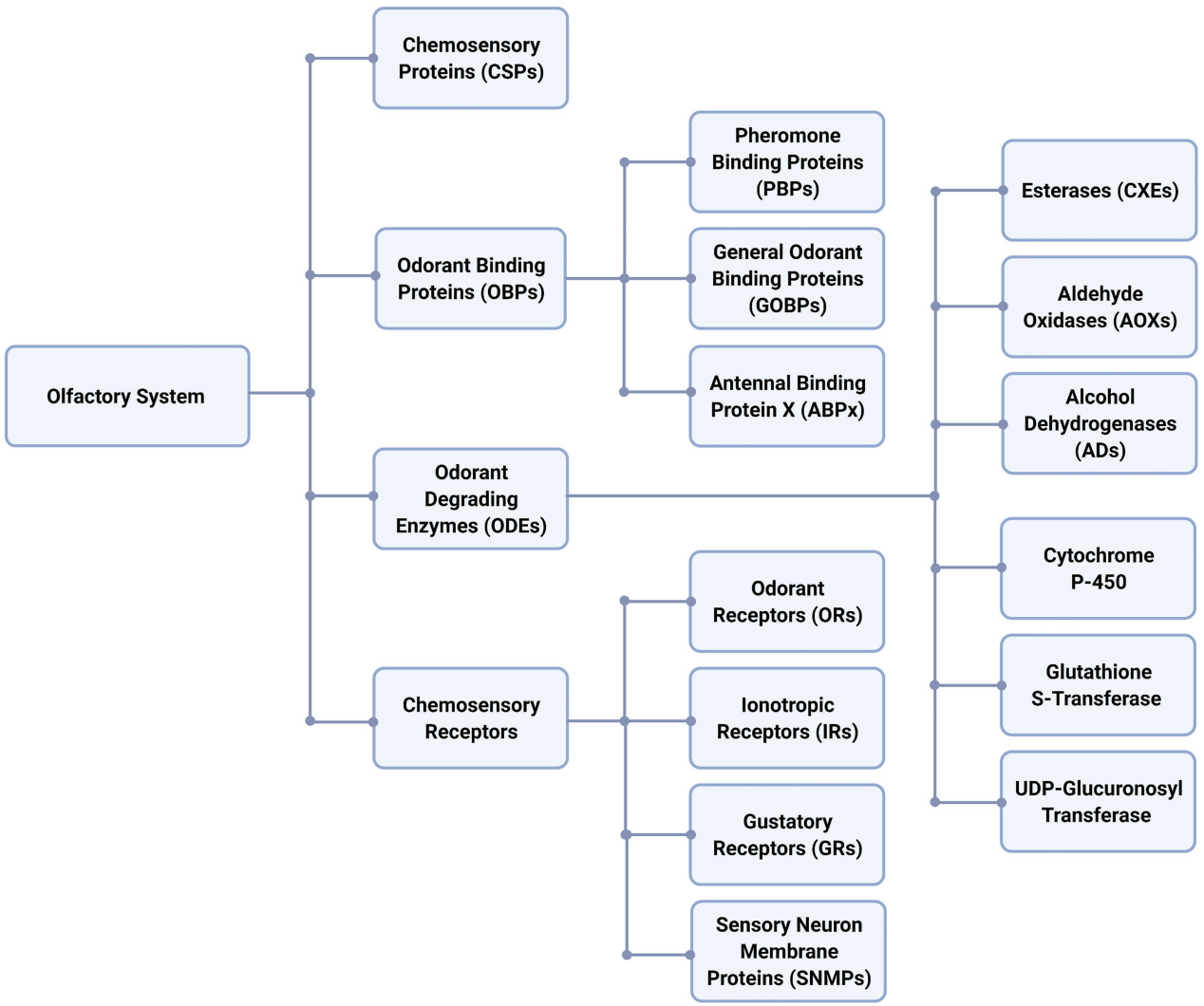

FIGURE 1 | Schematic organization of proteins present in the olfactory system of Lepidoptera. It is possible to identify the four families, chemosensory proteins (CSPs), odorant-binding proteins (OBPs), odorant degrading enzymes (ODEs), and chemosensory receptors (Vogt, 2005; Pelosi et al., 2006, 2017; Rytz et al., 2013).

signal is transduced into an electrical stimulus when ORs are activated (Sato and Touhara, 2008) leaving these semiochemicals in the sensillar lymph (**Figure 2A**).

One question that arises is the final destination of these chemicals after receptor activation: if these compounds are not degraded, then they could accumulate in the peripheral space interfering with the olfactory system in insects (Choo et al., 2013). Indeed, there are enzymes known as ODEs, which operate on the recovery of sensitivity in the olfactory system to detect new odorants (Sakurai et al., 2014; Zhang et al., 2017; Li et al., 2018).

Early studies reported the identification and isolation of an enzyme called antennae-specific esterase (ApolPDE) from the sensillar lumen of the Giant silk moth, *Antheraea polyphemus* (Vogt and Riddiford, 1981). Interestingly, through a kinetic study of ApolPDE, the authors showed that in the presence of this enzyme, the pheromone (*E,Z*)-6,11-hexadecadienyl acetate (E6,Z11-16:OAc) has an estimated half-life of 15 ms suggesting that ApolPDE is a pheromonal deactivator (Vogt et al., 1985). Ishida and Leal (2008) later supported this rapid degradation where ≈30 ms were necessary to reset the olfactory system of the Japanese beetle, *Popillia japonica*, through the study of the sex pheromone degradation using a recombinant enzyme. In this context, understanding the main actors in the inactivation of chemical signals is fundamental to the discovery of new molecules capable of disabling this mechanism (Leal, 2013). According to Vogt (2005), ODEs can be a target for behavioral inhibition because they degrade many different types of volatile compounds. Scientists have identified these enzymes as the beginning of more in-depth studies related to control and integrated pest management (IPM).

Despite the increasing amount of reported ODEs, no evolutionary analyses have been performed on these proteins

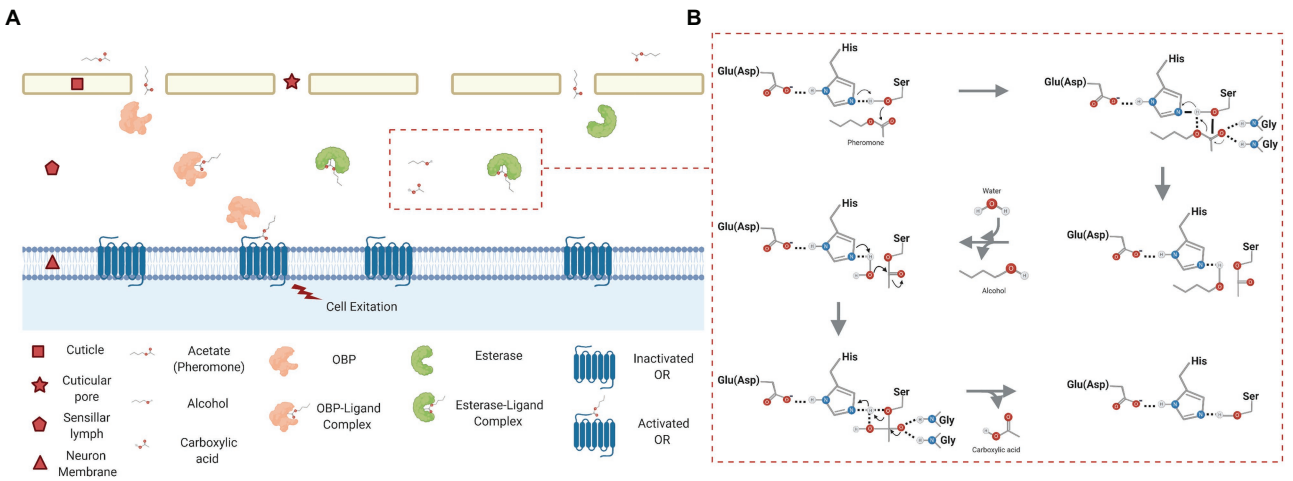

FIGURE 2 | (A) Schematic representation of the olfactory mechanism in sensilla of Lepidoptera with emphasis on esterases. Compounds from the environment pass through cuticular pores toward the sensillar lymph. Here, OBPs bind and transport these molecules to odorant receptors (ORs) located in the dendritic membrane of olfactory neurons where they are activated. After cell excitation, the molecules are degraded by the action of ODEs (esterases). These enzymes can even act when the molecules enter to the sensillar lymph (Leal, 2013). **(B)** Reaction mechanism of the esterases in Lepidoptera. The ester hydrolysis occurs in a two-step reaction plus water addition. There is first a nucleophilic attack produced by the serine hydroxyl on the carbonyl carbon of the pheromone. The reaction is then stabilized by the histidine, and this amino acid is stabilized by the glutamic acid at the same time. A molecule of alcohol is then released, and the enzyme is acetylated. Second, the water molecule has affinity with the histidine residue and then acts as a nucleophile on the acetylated enzyme. Finally, a carboxylic acid is released, and the enzyme is free to start a new reaction. Importantly, there are two conserved glycines participating in the stabilization of the transition states in the oxyanion hole (Montella et al., 2012).

among Lepidoptera. Furthermore, the structural features of the enzymes that could explain their selectivity have not yet been studied. Considering the diversity of acetate esters reported as sex pheromone compounds (463 acetate esters have been identified in the Pherobase database, https://www.pherobase.com/), the main focus of this review is the structure and evolutionary traits of antennal esterases (AEs) in Lepidoptera, which are responsible for the degradation of acetate ester-type pheromone components.

Thus, this text will offer a wider spectrum of new enzymes identified through bioinformatics techniques (i.e., transcriptomic) to attach a function through further functional studies. We propose specific guidelines that might help to clarify whether an ODE can be classified into a pheromone degrading enzyme (PDE) or not. The last step includes directed studies for this type of enzymes due to their participation in the degradation of pheromones, which in turn have a role in the behavior of organisms of the same species. In this way, new alternative and less costly pest management strategies could be implemented.

ODORANT DEGRADING ENZYMES AND THEIR ROLE IN SEXUAL COMMUNICATION

The olfactory system of insects has evolved to such an extent that it can process hundreds of compounds with different chemical structures from the environment to produce a change in behavior. Particularly, Lepidoptera emerged from a basal linage called non-Ditrysia to a new linage called Ditrysia since the Mesozoic era (over 100 million years); the species-specific pheromone components have similarly evolved. The sex pheromone that is generally emitted by females is crucial to attract a conspecific partner and achieve reproductive success. It is therefore not surprising that there are considerable structural differences in the blends of sex pheromones (Ando et al., 2004). We advise reviewing Löfstedt et al. (2016) for a complete understanding of the different types of pheromones in Lepidoptera.

Broadly, four groups of sex pheromones are described: Type 0 pheromones are structurally analogous to plant volatile compounds with short-chain ketones and alcohols. They are considered as primitive because they are also identified in non-Ditrysia species. The leaf miner moth, *Eriocrania semipurpurella*, is an example of non-Ditrysia moths and uses (2*S*, 6*Z*)-6-nonen-2-ol and (2*R*, 6*Z*)-6-nonen-2-ol as sex pheromone (Yuvaraj et al., 2017). Type I pheromones are biosynthesized *de novo* from acetate with C_{10}–C_{18} alcohols, aldehydes, and esters. Type II pheromones are biosynthesized from decarboxylation and epoxidation from dietary linolenic or linoleic acids where C_{17}–C_{25} polyunsaturated hydrocarbons are part of their structure (Millar, 2000). Type III pheromones contain one or more methyl branches in their structure with C_{17}–C_{23} saturated and unsaturated hydrocarbons. Many sex pheromone compounds have been identified especially in Lepidoptera and other orders such as Diptera and Coleoptera (El-Sayed et al., 2006) since the discovery of (*E*,*Z*)-10,12-hexadecadien-1-ol (bombykol) – the sex pheromone of the silk moth *Bombyx mori* (Butenandt et al., 1959).

Most mating disruption techniques used today for controlling and monitoring moth pests are based on these chemicals (Arn et al., 1992; Witzgall et al., 2010). For instance, *Tuta absoluta*

is a pest that attacks tomato crops, and components of its sexual pheromone [(*E*,*Z*,*Z*)-3,8,11-tetradecatrienyl acetate and (*E*,*Z*)-3,8-tetradecadienyl acetate] have been tested in greenhouses to control this insect (Cocco et al., 2012). Some studies have used inhibitors of ODEs such as trifluoromethyl ketones (TFMKs) to affect the pheromone detection and alter the behavior of moths. Malo et al. (2013) studied the male antennal response of the fall armyworm *Spodoptera frugiperda* against the inhibitor (*Z*)-9-tetradecenyl TFMK (Z9-14:TFMK) through electroantennography assay. This inhibitor is analogous to the main pheromone component (*Z*)-9-tetradecenyl acetate (Z9-14:Ac) of *S. frugiperda*, and it can significantly reduce the antennal response from 2.51 ± 0.37 mV to 1.10 ± 0.24 mV. On the other hand, Bau et al. (1999) disrupted the orientation flight of *Spodoptera littoralis* and *Sesamia nonagrioides* males in wind tunnel assays using TFMKs.

This background suggests that ODEs have an important role in the degradation of these pheromones. Consequently, one question that arises is if ODEs have evolved in order to degrade a wide range of these chemical cues or are limited to degrade a particular sex pheromone group for olfactory purposes. In this sense, transcriptomic analyses have provided the profile of ODEs that several moths could use for olfaction purposes. Acetates are the main sex pheromone components in Lepidoptera, and dozens of esterases in antennae have been reported as summarized in **Table 1**. Putative functions of ODEs have been suggested such as plant volatile and/or sex pheromone degradation though a few studies have actually addressed the functional role of some of these. In that sense, most enzymes characterized today are related to their sexual role in the degradation of pheromone components.

Transcriptomic advances have provided scientists a constantly growing database of sequences to identify ODEs including some with tissue-biased expression through reverse transcriptase polymerase chain reaction (RT-PCR) and quantitative (RT-qPCR) experiments. For example, 18 carboxylesterase (*CXE*) genes have been identified in the rice leaffolder, *Cnaphalocrocis medinalis*, through its antennal transcriptome (Zhang et al., 2017). Furthermore, the Egyptian armworm *S. littoralis* has an encoding-gene to *SlCXE7* that was 3-fold more expressed in males than females through RT-qPCR analysis (Durand et al., 2011). A greater expression of these enzymes in male antennae suggests that ODEs participate in the modulation of pheromone concentration since it is the female who produces and releases these semiochemicals to attract her conspecific mate in most species of moths.

EVOLUTIONARY TRAITS OF ODEs ACROSS LEPIDOPTERA

Insects are the most abundant and specious group of organisms. Nearly 150,000 species have been described in the Lepidoptera order alone. Considering their ecological impact, they have served as model systems to understand their mechanisms to locate mates and hosts plants as main examples. Furthermore, moths are important subjects of study within an evolutionary context due to their phenotypic plasticity, which comprises the ability of an organism (specifically a genotype) to respond to an environmental alteration with a change in its morphology, physiology, behavior, or life history (Moczek, 2010). These evolutionary processes are related to structural or regulatory mutations and change an amino acid in the coding region of a protein or affect the gene expression, respectively (Albre et al., 2012).

Genetic drift and natural selection can also contribute to the divergence of new enzymatic functions (Jones, 2017). In support of this, the cytochrome P450 enzymes (commonly involved in detoxification function) have had many mutations capable of catalyzing many chemical compounds (Bloom et al., 2007). In this sense, Lepidoptera are a clear representation of speciation where these changes are often related to their olfactory system for conspecific mate recognition. The extensive list of sex pheromone compounds identified to date (e.g., 463 acetate esters, 390 aldehydes, 331 primary alcohols, 299 secondary alcohols, and 28 tertiary alcohols reported in the Pherobase database) serves as a clue to the different types of enzymes involved in their biosynthesis. New desaturases have emerged by gene duplication and then diverged toward new functions (Roelofs et al., 2002). For instance, this has led to the evolution of castes and social organization in ants due to the expansion of the desaturase gene (Helmkampf et al., 2014). In this context, diverse enzymes are needed to degrade the large number of semiochemicals present in the environment that insects have to interact.

Odorant degrading enzymes have evolved from one gene family where catalytic and non-catalytic enzymes emerge (Oakeshott et al., 2005). Some studies have performed phylogenetic analysis for CXEs, and it is important to emphasize that the results showed a monophyletic clade where the most representative PDE (ApolPDE) was presented (He et al., 2014; Zhang et al., 2016). In **Figure 3**, we show a PDE clade (**Supplementary Figure S1**, a complete phylogenetic tree) constructed with some esterases in order to understand how these enzymes have evolved to degrade certain types of compounds. SlCXE13 from *S. littoralis* (Durand et al., 2010a); SlitCXE13 from *Spodoptera litura* (Zhang et al., 2016); SexiCXE13from *Spodoptera exigua* (He et al., 2014); SinfCXE13 from *Sesamia inferens* (Zhang et al., 2014); and ApolPDE1 from *A. polyphemus* (Ishida and Leal, 2005) belong to Ditrysia moths that use Type I sex pheromones. These enzymes are phylogenetically closer compared to EsemCXE6 from *E. semipurpurella*, a non-Ditrysia moth that use Type 0 sex pheromone. Moreover, PJAPPDE1 from *P. japonica*, and DmelEST6 from the fruit fly, *Drosophila melanogaster* were added due to their enzymes have been functionally well studied (Ishida and Leal, 2008; Younus et al., 2017). Lepidoptera, Coleoptera, and Diptera belong to the Holometabola group, but it is unknown the origin of physiological and morphological innovations in insects (Misof et al., 2014). Here, putative PDEs in Lepidoptera seem to have evolved from the ancient moth *E. semipurpurella*, as expected considering its non-Ditrysian origin. Overall, these results shed light on the evolution of these enzymes from *D. melanogaster*. It has been reported that DmelEST6 acts as an ODE with activity toward food esters, such as propyl, hexyl, heptyl, nonyl, decyl, neryl, and geranyl

TABLE 1 | Summary of esterases from Lepidoptera.

Lepidoptera species	Number of esterases	Technique of identification	Antennae-biased expression *	Sex-biased expression	Esters in sex pheromone	Reference
Antheraea polyphemus	1 CXE	Native-PAGE	ApolPDE (Ant-spe)	M	E6,Z11-16:Ac	Vogt et al., 1985; Ishida and Leal, 2005
Mamestra brassicae	1 CXE	RACE-PCR	Mbra-EST (Ant-enr)	M = F	Z11-16:Ac	Maïbèche-Coisne et al., 2004
Sesamia nonagrioides	1 CXE	Native-PAGE and RACE-PCR	SnonCXE (Ant)	M = F	Z11-16:Ac	Merlin et al., 2007
Sesamia inferens	18 CXEs	Transcriptomic and RACE-PCR	4 SinfCXEs (13,14,18, and 20; Ant-enr)	M = F	Z11-16:Ac	Zhang et al., 2014
			SinfCXE10 (Ant-spe)	M = F		
Spodoptera litura	24 CXEs	Transcriptomic	4 SlitCXEs (Ant-enr)	M = F	Z9,E11-14:Ac; Z9,E12-14:Ac; E11-14:Ac; and Z9-14:Ac	Zhang et al., 2016
			SlitCXE10 (Ant-spe)	M = F		
Spodoptera exigua	6 CXEs	Transcriptomic and RACE-PCR	3 SexiCXEs (4, 17, and 20;Ant-enr)	M = F	Z9,E12-14:Ac; Z9-14:Ac	He et al., 2014
			3 SexiCXEs (5, 18, and 31; Ant)	M = F		
Spodoptera littoralis	20 CXEs	Native-PAGE,ESTs, and RACE-PCR	17 SlCXEs (Ant)	M = F	Z9,E11-14:Ac; Z9,E12-14:Ac	Merlin et al., 2007; Durand et al., 2010a,b, 2011
			SlCXE7 (Ant-spe)	M > F		
			SlCXE8 (Ant-spe)	M = F		
			SlCXE10 (Ant-enr)	M > F		
Cnaphalocrosis medinalis	18 CXEs	Transcriptomic	CmedCXE17 (Ant-enr)	M = F	Z11-16:Ac; Z13-18:Ac	Zhang et al., 2017
			CmedCXE20 (Ant-enr)	M = F		
			CmedCXE24 (Ant-enr)	M = F		
Ostrinia furnacalis	15 CXEs	Transcriptomic	–	–	E12-14:Ac; Z12-14:Ac	Yang et al., 2015
Epiphyas postvittana	5 CXEs	ESTs, 2D gel electrophoresis and mass spectrometry	–	–	E11-14:Ac; E9,E11-14:Ac; 12:Ac	Jordan et al., 2008
Agrotis ipsilon	17 CXEs	Transcriptomic	–	–	Z11-16:Ac; Z9-14:Ac; Z7-12:Ac; Z8-12:Ac; and Z5-10:Ac	Gu et al., 2013
Plutella xylostella	5 CXEs	Transcriptomic	5 PxylCXEs (Ant-enr)	M = F	Z11-16:Ac	He et al., 2017
Ectropis obliqua	35 CXEs	Transcriptomic	EoblCXE7 (Ant-enr)	M = F	**Z3,Z9-6,7-epo-18:Hy; Z3,Z6,Z9-18:Hy	Sun et al., 2017; Guo et al., 2019
			EoblCXE10 (Ant-enr)	M > F		
			EoblCXE13 (Ant-enr)	M = F		

PAGE, polyacrylamide gel electrophoresis; ESTs, expressed sequence tags; RACE, rapid amplification of cDNA ends; PCR, polymerase chain reaction; Ant, antennae; Ant-enr, antennae enriched expressed; Ant-spe, antennae specific expressed; Ant-sli, antennae slightly expressed; M, male; F, female; and (–), no information reported.
**The antennal-related location of esterases might not exclude other organs.*
***No acetate ester-type as sex pheromone.*

acetates (Younus et al., 2017). Therefore, it is proposed that Lepidoptera PDEs might have evolved from a common ancestor (i.e., DmelEST6), changing from catalytic activity toward food esters to specific acetate-based sex pheromone components. In this context, this issue could be considered when classifying an esterase as a PDE; however, a necessary functional assay to confirm such a role is needed.

ANTENNAL ESTERASES IN LEPIDOPTERA

Among insects, esterases have been classified in three major classes: (I) as enzymes with neuro/developmental functions; (II) intracellular enzymes with dietary detoxification functions, and (III) secreted enzymes that use hormones or pheromones as substrates (Claudianos et al., 2006). The latter is related to catalytically active enzymes that belong to *CXE* gene family and the α/β hydrolase superfamily (Punta et al., 2012). Their function is to hydrolyze esters in a two-step reaction plus water addition (**Figure 2B**). First, an alcohol-type metabolite is produced from the hydrolysis of ester bonds to subsequently generate an enzyme in an acylated, carbamylated, or phosphorylated form depending on its substrate (carboxylic, carbamic, or phosphoric ester, respectively). An acid-type metabolite is then formed and released due to water molecule addition so that the enzyme goes back to its active state (Montella et al., 2012). Thus, these CXEs play important roles,

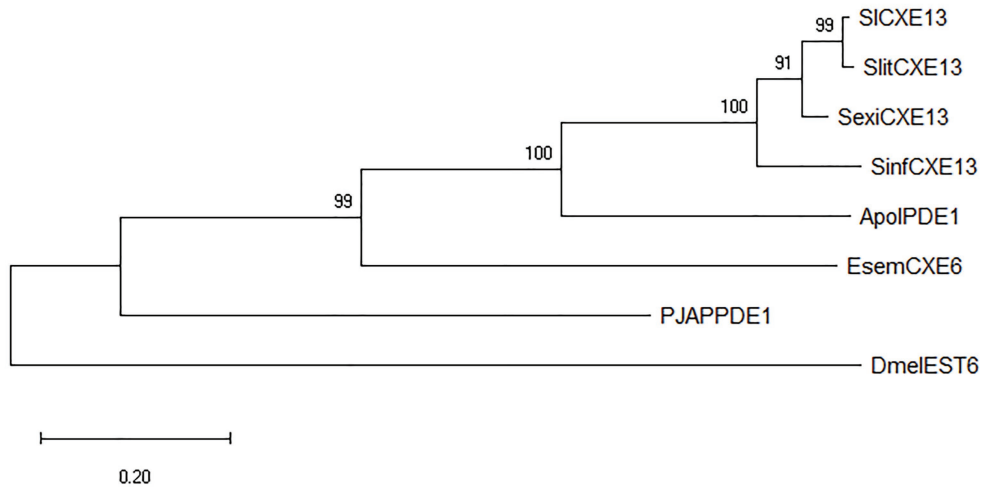

FIGURE 3 | Phylogenetic tree of esterases. SlCXE13 (*S. littoralis*), SlitCXE13 (*S. litura*), SexiCXE13 (*S. exigua*), SinfCXE13 (*S. inferens*), ApolPDE1 (*A. polyphemus*), EsemCXE6 (*Eriocrania semipurpurella*), PJAPPDE1 (*Popillia japonica*), and DmelEST6 (*Drosophila melanogaster*). Phylogenetic analyses for esterases were performed by using MAFFT sever for multiple sequence alignments and FastTree software for phylogenetic relationships based on maximum-likelihood method (Price et al., 2010).

such as neurogenesis, development regulation, xenobiotic detoxification, and pheromones (Yu et al., 2009). The first CXE related to olfaction in moths was the PDE from *A. polyphemus* (Vogt et al., 1985); more recently, the CXEs identified in the tobacco cutworm *S. litura* (Zhang et al., 2016), the light brown apple moth *Epiphyas postvittana* (Jordan et al., 2008), and the black cutworm *Agrotis ipsilon* (Gu et al., 2013) among others have been studied by RNA-seq approaches (**Table 1**).

To date, *CXE* genes have been localized in different tissues of several moth species according to RT-PCR and RT-qPCR experiments. On the other hand, native polyacrylamide gel electrophoresis (Native-PAGE) has been used to study the enzymatic activity of some esterases (He et al., 2014). The expression in a specific tissue could shed lights on the function of a CXE. For example, Zhang et al. (2014) found five CXE genes in *S. inferens* where all of them (*SinfCXE10*, *SinfCXE13*, *SinfCXE14*, *SinfCXE18*, and *SinfCXE20*) were significantly expressed in different tissues, such as pheromone glands, thoraxes, abdomens, and antennae. However, *SinfCXE10* was expressed specifically in the antennae; therefore, the authors propose that this gene could be involved in pheromone degradation particularly in (*Z*)-11-hexadecenyl acetate. Although CXEs are present in olfactory organs (e.g., antennae), it seems that their pheromone-degrading function is more related to sex-biased expression. Durand et al. (2011) confirmed that a CXE gene from *S. littoralis* (*SlCXE7*) was restricted to antennae rather than other tissues through *in situ* hybridization (ISH) technique. This was more significantly expressed in males than in females according to RT-qPCR. Depending on its sensillar location such as pheromone-sensitive sensilla (i.e., trichodea, Str I), *SlCXE7* could play a role in pheromone signal termination as well as degrading odorant background noise.

On the contrary, He et al. (2014) reported one CXE gene from the beet armyworm, *S. exigua* (*SexiCXE4*), highly expressed in antennae and proboscises but had no sex-biased expression. *SexiCXE4* presented a higher preference (70-fold) to plant volatiles [(*Z*)-3-hexenyl acetate and hexyl acetate] than pheromone compounds (*Z*,*E*)-9,12-tetradecenyl acetate and (*Z*)-9-tetradecenyl acetate *via in vitro* functional assays. This suggests a role as a general ODE (GODE). Likewise, two CXEs genes (*EoblCXE7* and *EoblCXE13*) in the tea geometrid moth *Ectropis obliqua* were localized in pheromone-related sensilla (Str I) as well as sensilla basiconica (Sba) and gustatory sensilla styloconica (Sst) using fluorescence ISH (FISH) technique (Sun et al., 2017). *EoblCXE13* showed a differential expression pattern where it was restricted to the base of Str I in males. The lack of male-biased localization in this study suggests that the CXE genes might be involved in the hydrolysis of host plant volatiles rather than pheromone components (He et al., 2014). Despite the large amount of CXE expressed in the antennae of *E. obliqua*, no acetate ester-type sex pheromone degradation role could be attributed because this insect uses unsaturated hydrocarbons and enantiomers of epoxy hydrocarbons [(*Z*,*Z*,*Z*)-3,6,9-octadecatriene and 6,7-epoxy-(*Z*,*Z*)-3,9-octadecadiene] as sex pheromone (Type II sex pheromones; Sun et al., 2017). Likely, an epoxide hydrolase could participate in the degradation of the pheromone of *E. obliqua*, by catalyzing the hydrolysis of epoxide-like compounds to diols as many epoxy hydrolases do with epoxide-containing lipids (Morisseau, 2013), but further studies are needed.

STRUCTURAL FEATURES OF ESTERASES

The ability of proteins to bind to chemical compounds strongly depends on their amino acid constitution and conformation,

such as domain arrangement, conformational dynamics, as well as the shape and amount of binding sites. Naturally, enzymes are not the exception with several enzymes as targets for the identification of substrates as well as competitive and non-competitive inhibitors or allosteric compounds in a drug-discovery approach.

A good example is the study of acetylcholinesterase (AChE) inhibitors such as organophosphorus compounds used as insecticides or toxic carbamates applied as pesticides (Čolović et al., 2013). For insects and particularly moths, evolution has provided highly specific adaptations for sexual communication that has resulted in evolved structural features. For instance, conserved structural regions have been found for ORs with seven transmembrane domains, increased sequence identity toward the C-terminal region, and, more interestingly, sequence motifs, such as LLLLECS, QQLIQ, and ILKTS in pheromone receptors (PRs; Zhang and Löfstedt, 2015; Köblös et al., 2018).

On the other hand, three and two conserved disulfide bridges play an important role giving structural stability in OBPs and CSPs, respectively (Pelosi et al., 2006). As a third player in perireceptor events, ODEs have not been structurally characterized so far from a wide viewpoint. In these cases, some enzymes appear to have preserved domains where acid (i.e., aspartic or glutamic acid) and base (i.e., histidine, arginine, or lysine) side chains of residues are part of the active sites (Jimenez-Morales et al., 2012).

After the identification of *A. polyphemus* CXE as a PDE (ApolPDE), structural investigations revealed that these enzymes share common features among moths. For instance, they have a conserved pentapeptide "G-X-S-X-G" (X represent any amino acid) motif that is characteristic of esterases (Cygler et al., 1993; Yin et al., 2011) and common catalytic triad "S-E(D)-H" that can catalyze the hydrolysis of esters – an important group of pheromone compounds with 10–18 carbon atoms and one or two unsaturated carbons (Löfstedt and Kozlov, 1997; Oakeshott et al., 1999). The absence of one of these residues causes these hydrolases to be transformed into catalytically inactive proteins (e.g., neurotactin or neuroligin); thus, they will be assigned in recognition or signal processing functions for neurodevelopment (Oakeshott et al., 2005). Moreover, CXEs bear an oxyanion hole formed with the amine group (–NH) from the "G-G-A" motif that stabilizes high-energy intermediates and the transition state through hydrogen bonding in the active site (Zhang et al., 2002, 2017). This feature is conserved in all esterase families in both vertebrates and invertebrates (Oakeshott et al., 1999).

On the other hand, some studies have found N-glycosylation sites that could help to improve resistance against proteolysis, reduce non-specific protein interactions, and increase the protein solubility and stability (Fonseca-Maldonado et al., 2013; Sun et al., 2015). The idea that CXEs are secreted into the extracellular medium is based on the presence of an N-terminal signal peptide (Oakeshott et al., 2005). This latter characteristic is relevant because they can be found in the sensillar lymph that can interact with the compounds that enter through the cuticular pores. Although CXEs do not share many similarities in the DNA sequences, they do have homology in their structure because the residues are conserved in the catalytic sites. Therefore, this family of proteins likely originated from a common ancestor (Nardini and Dijkstra, 1999).

As mentioned in the previous sections, bioinformatic techniques have appeared as an alternative in the search for new enzymes. Thus, several antennal transcriptomes have been published and are very useful because they have free access. **Figure 4** shows the modeled structures of the ApolPDE1 from *A. polyphemus*, EsemCXE6 from *E. semipurpurella* (public RNAseq raw data were downloaded from NCBI database, https://www.ncbi.nlm.nih.gov/, under the experiment SRX2627820), SinfCXE13 from *S. inferens*, and SlitCXE13 from *S. litura*. No crystallized CXEs structures have been published yet for Lepidoptera; however, three crystallized structures in Diptera with the access code 4FNM (Jackson et al., 2013), 5CH3 (Correy et al., 2016), and 5THM (Younus et al., 2017) in the protein data bank were used as templates in molecular modeling. These structures confirm the conservation of these enzymes in relation to their binding site regardless of their non-Ditrysia or Ditrysia origin.

SinfCXE13 and SlitCXE13 have been reported as enzymes expressed in the antenna, but they are not tissue-specific. Interestingly, these two are within the phylogenetic clade of enzymes secreted that use pheromones as substrates and are close to ApolPDE1 (He et al., 2014; Zhang et al., 2016). So far, putative esterase sequences from the transcriptome of *E. semipurpurella* have not been published; therefore, as a complement to this work, 17 CXEs transcripts were identified according to a phylogenetic analysis (data not included): Only EsemCXE6 was in the same clade as ApolPDE1, SinfCXE13, and SlitCXE13. Here, is possible to visualize the α-helices (red helical ribbons), β-sheets (yellow arrows), and loops (green smooth ropes) in all modeled structures (**Figures 4A–D**), which is consistent with those values reported for esterases (Montella et al., 2012). Interestingly, these characteristics are typical of α/β hydrolases and their folding gives a conformation of globular proteins. Furthermore, these sequences have a signal peptide indicating that these enzymes enter a secretory pathway, but they are not necessarily secreted to the extracellular environment (Nielsen, 2017). Despite the evolution of these moths, the antennal esterases conserved the residues in their active site that are responsible for the catalysis of chemical compounds (**Figures 4E–H**).

ANTENNAL ESTERASES INHIBITION IN INTEGRATED PEST MANAGEMENT

Antennal esterases are ubiquitous in the olfaction process and can control the levels of stimuli in the sensilla through the rapid catabolism of semiochemicals-mainly acetate-type pheromones. Therefore, inhibition of these enzymes emerges as a complement to IPM because current strategies are costly, e.g., the use of synthetic pheromones for mating disruption (Guerrero and Rosell, 2005). Several analogous compounds to sex pheromones have been tested in Lepidoptera as reported by Reddy and Guerrero (2010), where TFMKs appear to

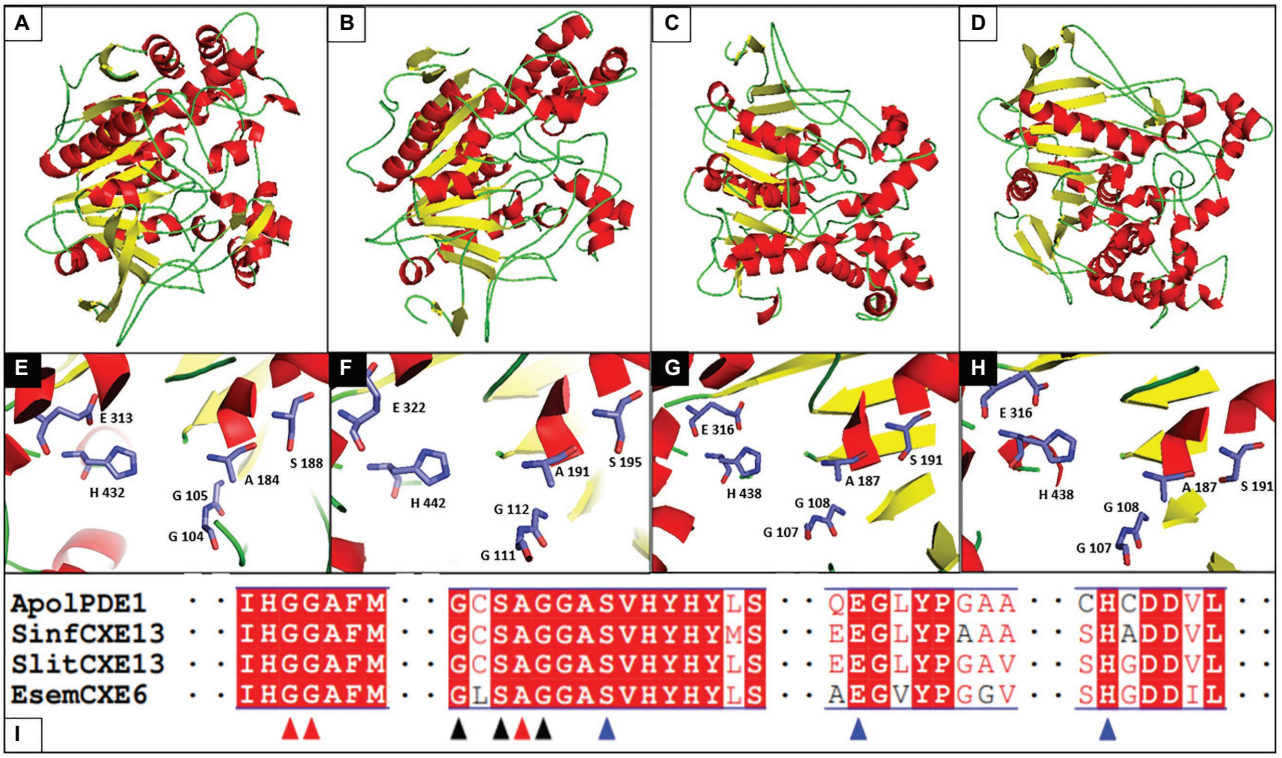

FIGURE 4 | Modeled structures of esterases in Lepidoptera and partial alignment. **(A)** ApolPDE1 from *A. polyphemus*, **(B)** EsemCXE6 from *E. semipurpurella*, **(C)** SinfCXE13 from *S. inferens*, and **(D)** SlitCXE13 from *S. litura*. **(E–H)** Active sites of ApolPDE1, EsemCXE6, SinfCXE13, and SlitCXE13, respectively. **(I)** Partial alignment of amino acids sequences. Amino acids not shown are represented by two sequential dots. Oxyanion hole (G104-G105-A184) is indicated by red arrows. G181-X-S183-X-G185 motif is indicated by black arrows. The catalytic triad [S188-E(D)313-H432] is indicated by the blue arrows. The program Modeler 9.15 (Sali and Blundell, 1993; Webb and Sali, 2016) was used to build the three-dimensional structures and 4FNM (ApolPDE1), 5CH3 (SinfCXE13 and SlitCXE13), and 5THM (EsemCXE6) as templates were used to obtain these modeled structures. Moreover, molecular dynamic (MD) simulations were performed using the NAMD 2.9 (Phillips et al., 2005) so as to achieve a refinement of the modeled structure *via* the root mean square deviation (RMSD).

be good candidates for enzyme inhibition. These molecules enter through cuticular pores (**Figure 2A**) toward the sensillar lymph where OBPs can bind these inhibitors. Indeed, Campanacci et al. (1999) showed that the (*Z*)-11-hexadecenyl TFMK was efficient in displacing the sex pheromone by binding to the recombinant PBP from *Mamestra brassicae* (MbraPBP1) through functional assays. Likewise, TFMKs can interact with ODEs inside the sensilla where it may form stable hydrates acting as transition-state analogues of pheromones. In brief, the inhibitory activity of TFMKs is due to a stable hemiacetal of tetrahedral geometry that is formed between the conserve serine residues of the antennal esterases with the highly electrophilic carbonyl (Durán et al., 1993; Wiedemann et al., 1998). Some studies have been performed with TFMKs and electrophysiological assays in *Plutella xylostella* (Prestwich and Streinz, 1988), *Thaumetopoea pityocampa* (Parrilla and Guerrero, 1994), *M. brassicae* (Renou et al., 2002), *Cydia pomonella* (Giner et al., 2009), and *S. frugiperda* (Malo et al., 2013). Moreover, TFMKs have been used with antennal extracts of different moth species, e.g., *S. littoralis* (Durán et al., 1993), *Ostrinia nubilalis* (Riba et al., 2005), and *C. pomonella* (Giner et al., 2009). All of these studies have shown that TFMKs had an effect on the catalytic activity of antennal esterases. On the other hand, behavior assays in tunnel wind with these inhibitors have shown a disruptive effect on the orientation flight in males of *S. nonagrioides*, *S. littoralis*, and *C. pomonella* (Bau et al., 1999; Giner et al., 2009). In the field, it has been reported that TFMKs are effective pheromone antagonists for several insect pests, such as *S. nonagrioides* (Riba et al., 2001), *C. pomonella* (Giner et al., 2009), *Zeuzera pyrina* (Muñoz et al., 2011), *O. nubilalis* (Solé et al., 2008), or *T. absoluta* (Dominguez et al., 2016). The reduction in damage caused by *S. nonagrioides* and *O. nubilalis* in maize fields after application of Z11-16:TFMK was particularly remarkable, i.e., this is an analogue of the pheromone of the former species at a dose of 80 g/ha (Solé et al., 2008).

Riba et al. (2001) further evaluated the biological toxicity of (*Z*)-11-hexadecenyl TFMK (Z11-16:TFMK) and 3-octylthio-1,1,1-trifluoropropan-2-one (OTFP) in mice, and the results showed low toxicity (LD_{50} 1 g/kg after the 6th day of the assay). Overall, an accurate identification and characterization of these enzymes could provide the basis for the development of putative inhibitory compounds that will be an alternative to IPM.

CONCLUDING REMARKS AND FURTHER PERSPECTIVES

The olfactory system is critical for reproductive success in many insect species. Some of these are of great economic importance in agriculture and forestry fields such as moths from the Tortricidae and Pyralidae family. Fortunately, the semiochemical compounds involved in host recognition, mating, or defense behaviors are being used to manage insect pests through environmentally friendly approaches, e.g., mating disruption and mass trapping. However, globalization has facilitated the dissemination of insect species throughout the world. How do insects adapt to these new environments? More specifically, how their olfactory system responds to these new conditions?

To answer these questions, it is important to understand the molecular basis and mechanisms involved in insect olfaction where proteins are the main players. Comprehensive studies have been performed for ORs, OBPs, and CSPs; ODEs have garnered less attention. These enzymes are novel targets for the use of species-specific chemicals in IPM. Therefore, we propose that an improved approach to classify a certain ODE into PDE would be crucial based on a highly specific sex pheromone communication. The evidence presented in this work suggests that a limited number of ODEs would actually be antennal- and pheromone-specific. Therefore, gene expression through RT-qPCR should consider comparing between sexes in antennae and then in the rest of tissues.

Phylogenetic analyses could help to filter ODEs close to already characterized PDEs (e.g., ApolPDE). Particularly, some studies (*S. inferens* and *S. littura*) found that a monophyletic clade (proposed as PDE clade) is present in moths. With this in mind, further ODEs that fall within this clade could be considered for characterization as putative PDEs. Finally, heterologous expression of the selected ODE(s) with purification and kinetic assays would be crucial for such task.

Alternatively, localization techniques such as FISH in specific sensilla could strongly support pheromone degradation function. Of note, transcriptomics has arisen as a useful tool to identify putative enzymes. Four modeled structures (ApolPDE1, SinfCXE13, SlitCXE13, and EsemCXE6) were shown to visualize their conformation and the residues of the active site, which resulted in conserved function. With the above issue addressed, the identification and characterization of these enzymes could provide the basis for the development of putative inhibitory compounds (e.g., TFMKs) that will be a complement to IMP strategies.

AUTHOR'S NOTE

All the information performed in this work is of a public nature. We created the figures and the data generated in relation to the transcripts identified from the antennal transcriptome of *E. semipurpurella.*

AUTHOR CONTRIBUTIONS

RG wrote all sections. JM developed the tables and figures. HV and AM conceived the idea for the review article. AQ supervised the project. All authors contributed to the article and approved the submitted version.

ACKNOWLEDGMENTS

We would like to thank ANID N° 21190666 scholarship.

SUPPLEMENTARY MATERIAL

The Supplementary Material for this article can be found online at: https://www.frontiersin.org/articles/10.3389/fphys.2021.643281/full#supplementary-material

REFERENCES

Albre, J., Liénard, M., Sirey, T., Schmidt, S., Tooman, L., Carraher, C., et al. (2012). Sex pheromone evolution is associated with differential regulation of the same desaturase gene in two genera of leafroller moths. *PLoS Genet.* 8:e1002489. doi: 10.1371/journal.pgen.1002489

Ando, T., Inomata, S. I., and Yamamoto, M. (2004). "Lepidopteran sex pheromones" in *The chemistry of pheromones and other semiochemicals I*. ed. S. Schulz (Berlin, Heidelberg: Springer), 51–96.

Arn, H., Tóth, M., and Priesner, E. (1992). *List of sex pheromones of Lepidoptera and related attractants. 2nd Edn*. Montfavet, France: International Organization for Biological Control.

Bau, J., Martínez, D., Renou, M., and Guerrero, A. (1999). Pheromone-triggered orientation flight of male moths can be disrupted by trifluoromethyl ketones. *Chem. Senses* 24, 473–480. doi: 10.1093/chemse/24.5.473

Bloom, J., Romero, P., Lu, Z., and Arnold, F. (2007). Neutral genetic drift can alter promiscuous protein functions, potentially aiding functional evolution. *Biol. Direct* 2:17. doi: 10.1186/1745-6150-2-17

Butenandt, A., Beckman, R., Stamm, D., and Hecker, E. (1959). Über den sexuallockstoff des seidenspinners *Bombyx mori Reindarstellung und konstitution. Z. Naturforsch. B* 14, 283–284. doi: 10.1515/bchm2.1963.333.1.114

Campanacci, V., Longhi, S., Nagnan-Le Meillour, P., Cambillau, C., and Tegoni, M. (1999). Recombinant pheromone binding protein 1 from *Mamestra brassicae* (MbraPBP1). Functional and structural characterization. *Eur. J. Biochem.* 264, 707–716. doi: 10.1046/j.1432-1327.1999.00666.x

Choo, Y. M., Pelletier, J., Atungulu, E., and Leal, W. S. (2013). Identification and characterization of an antennae-specific aldehyde oxidase from the navel orangeworm. *PLoS One* 8:e67794. doi: 10.1371/journal.pone.0067794

Claudianos, C., Ranson, H., Johnson, R. M., Biswas, S., Schuler, M. A., Berenbaum, M. R., et al. (2006). A deficit of detoxification enzymes: pesticide sensitivity and environmental response in the honeybee. *Insect Mol. Biol.* 15, 615–636. doi: 10.1111/j.1365-2583.2006.00672.x

Cocco, A., Deliperi, S., and Delrio, G. (2012). Control of *Tuta absoluta* (Meyrick) (Lepidoptera: Gelechiidae) in greenhouse tomato crops using the mating disruption technique. *J. Appl. Entomol.* 137, 16–28. doi: 10.1111/j.1439-0418.2012.01735.x

Čolović, M., Krstić, D., Lazarević-Pašti, T., Bondžic, A., and Vasić, V. (2013). Acetylcholinesterase inhibitors: pharmacology and toxicology. *Curr. Neurol.* 11, 315–335. doi: 10.2174/1570159X11311030006

Correy, G., Carr, P., Meirelles, T., Mabbitt, P., Fraser, N., Weik, M., et al. (2016). Mapping the accessible conformation landscape of an insect

carboxylesterase using conformational ensemble analysis and kinetic crystallography. *Structure* 24, 977–987. doi: 10.1016/j.str.2016.04.009

Cygler, M., Schrag, J., Sussman, J., Harel, M., Silman, I., Gentry, M. K., et al. (1993). Relationship between sequence conservation and three-dimensional structure in a large family of esterases, lipases, and related proteins. *Prot. Sci.* 2, 366–382. doi: 10.1002/pro.5560020309

Dominguez, A., Puigmartí, M., Bosch, M. P., Rosell, G., Crehuet, R., Ortiz, A., et al. (2016). Synthesis, functional assays, electrophysiological activity and field test of pheromone antagonists of the tomato leafminer *Tuta absoluta*. *J. Agric. Food Chem.* 64, 3523–3532. doi: 10.1021/acs.jafc.6b00674

Durán, I., Parrilla, A., Feixas, J., and Guerrero, A. (1993). Inhibition of antennal esterases of the Egyptian armyworm Spodoptera littoralis by trifluoromethyl ketones. *Bioorg. Med. Chem. Lett.* 3, 2593–2598. doi: 10.1016/S0960-894X(01)80722-8

Durand, N., Carot-Sans, G., Bozzolan, F., Rosell, G., Siaussat, D., Debernard, S., et al. (2011). Degradation of pheromone and plant volatile components by a same odorant-degrading enzyme in the cotton leafworm, *Spodoptera littoralis*. *PLoS One* 6:e29147. doi: 10.1371/journal.pone.0029147

Durand, N., Carot-Sans, G., Chertemps, T., Bozzolan, F., Party, V., Renou, M., et al. (2010b). Characterization of an antennal carboxylesterase from the pest moth *Spodoptera littoralis* degrading a host plant odorant. *PLoS One* 5:e15026. doi: 10.1371/journal.pone.0015026

Durand, N., Carot-Sans, G., Chertemps, T., Montagné, N., Jacquin-Joly, E., Debernard, S., et al. (2010a). A diversity of putative carboxylesterases is expressed in the antennae of the noctuid moth *Spodoptera littoralis*. *Insect Mol. Biol.* 19, 87–97. doi: 10.1111/j.1365-2583.2009.00939.x

El-Sayed, A. M., Suckling, D., Wearing, C., and Byers, J. (2006). Potential of mass trapping for long term pest management and eradication of invasive species. *J. Econ. Entomol.* 99, 1550–1564. doi: 10.1093/jee/99.5.1550

El-Shafie, H. A. F., and Romeno, J. (2017). "Semiochemicals and their potential use in pest management" in *Biological control of pest and vector insects*. ed. V. Shields (London: IntechOpen), 3–22.

Fonseca-Maldonado, R., Serradella, D., Sanchez, J., Bonneil, E., Thibault, P., and Ward, R. J. (2013). Engineering the pattern of protein glycosylation modulates the thermostability of a GH11 xylanase. *J. Biol. Chem.* 288, 25522–25534. doi: 10.1074/jbc.M113.485953

Giner, M., Sans, A., Riba, M., Bosch, D., Gago, R., Rayo, J., et al. (2009). Development and biological activity of a new antagonist of the pheromone of the codling moth *Cydia pomonella*. *J. Agric. Food Chem.* 57, 8514–8519. doi: 10.1021/jf901979k

Gu, S. H., Wu, K. M., Guo, Y. Y., Pickett, J. A., Field, L. M., Zhou, J. J., et al. (2013). Identification of genes expressed in the sex pheromone gland of the black cut worm *Agrotis ipsilon* with putative roles in sex pheromone biosynthesis and transport. *BMC Genomics* 14:636. doi: 10.1186/1471-2164-14-636

Guerrero, A., and Rosell, G. (2005). Biorational approaches for insect control by enzymatic inhibition. *Curr. Med. Chem.* 12, 461–469. doi: 10.2174/0929867053363126

Guo, F., Yu, J., and Wan, X. (2019). Response to enantiomers of (Z3Z9)-6,7-epoxy-octadecadiene, sex pheromone component of *Ectropis obliqua* Prout (Lepidoptera: Geometridae): electroantennagram test, field trapping, and *in silico* study. *Fla. Entomol.* 102, 549–554. doi: 10.1653/024.102.0318

He, P., Zhang, Y. F., Hong, D. Y., Wang, J., Wang, X. L., Zuo, L. H., et al. (2017). A reference gene set for sex pheromone biosynthesis and degradation genes from the diamondback moth, *Plutella xylostella*, based on genome and transcriptome digital gene expression analyses. *BMC Genomics* 18:219. doi: 10.1186/s12864-017-3592-y

He, P., Zhang, J., Li, Z., Zhang, Y., Yang, K., and Dong, S. (2014). Functional characterization of an antennal esterase from the noctuid moth *Spodoptera exigua*. *Arch. Insect Biochem. Physiol.* 86, 85–99. doi: 10.1002/arch.21164

Helmkampf, M., Cash, E., and Gadau, J. (2014). Evolution of the insect desaturase gene family with an emphasis on social hymenoptera. *Mol. Biol. Evol.* 32, 456–471. doi: 10.1093/molbev/msu315

Ishida, Y., and Leal, W. S. (2005). Rapid inactivation of a moth pheromone. *Proc. Natl. Acad. Sci.* 102, 14075–14079. doi: 10.1073/pnas.0505340102

Ishida, Y., and Leal, W. S. (2008). Chiral discrimination of the Japanese beetle sex pheromone and a behavioral antagonist by a pheromone-degrading enzyme. *Proc. Natl. Acad. Sci. U. S. A.* 105, 907–9080. doi: 10.1073/pnas.0802610105

Isono, K., and Morita, H. (2010). Molecular and cellular designs of insect taste receptor system. *Front. Cell. Neurosci.* 4:20. doi: 10.3389/fncel.2010.00020

Jackson, C., Liu, J. W., Carr, P., Younus, F., Coppin, C., Meirelles, T., et al. (2013). Structure and function of an insect α-carboxylesterase (α*Esterase7*) associated with insecticide resistance. *Proc. Natl. Acad. Sci. U. S. A.* 110, 10177–10182. doi: 10.1073/pnas.1304097110

Jimenez-Morales, D., Liang, J., and Eisenberg, B. (2012). Ionizable side chains at catalytic active sites of enzymes. *Eur. Biophys. J.* 41, 449–460. doi: 10.1007/s00249-012-0798-4

Jones, B. (2017). Evolution-guided Engineering of Alpha/Beta Hydrolases. PhD Thesis. University of Minnesota Digital Conservancy.

Jordan, M. D., Stanley, D., Marshall, S. D. G., De Silva, D., Crowhurst, R. N., Gleave, A. P., et al. (2008). Expressed sequence tags and proteomics of antennae from the tortricid moth, Epiphyas postvittana. *Insect Mol. Biol.* 17, 361–373. doi: 10.1111/j.1365-2583.2008.00812.x

Klein, U. (1987). Sensillum-lymph proteins from antennal olfactory hairs of the moth *Antheraea polyphemus* (Saturniidae). *Insect Biochem.* 17, 1193–1204. doi: 10.1016/0020-1790(87)90093-X

Köblös, G., François, M. C., Monsempes, C., Montagné, N., Fónagy, A., and Jacquin-Joly, E. (2018). Molecular characterization of MbraOR16, a candidate sex pheromone receptor in *Mamestra brassicae* (Lepidoptera:Noctuidae). *J. Insect Sci.* 18:5. doi: 10.1093/jisesa/iey090

Krieger, J., von Nickisch-Rosenegk, E., Mameli, M., Pelosi, P., and Breer, H. (1996). Binding proteins from the antennae of *Bombyx mori*. *Insect Biochem. Mol. Biol.* 26, 297–307. doi: 10.1016/0965-1748(95)00096-8

Leal, W. (2013). Odorant reception in insects: roles of receptors, binding proteins, and degrading enzymes. *Annu. Rev. Entomol.* 58, 373–391. doi: 10.1146/annurev-ento-120811-153635

Li, G. W., Chen, X. L., Xu, X. L., and Wu, J. X. (2018). Degradation of sex pheromone and plant volatile components by an antennal glutathione S- transferase in the oriental fruit moth, *Grapholita molesta* Busck (Lepidoptera: Tortricidae). *Arch. Insect Biochem. Physiol.* 99:e21512. doi: 10.1002/arch.21512

Löfstedt, C., and Kozlov, M. (1997). "A phylogenetic analysis of pheromone communication in primitive moths" in *Insect pheromone research-new directions*. eds. R. T. Cardé and A. K. Minks (New York: Chapman & Hall), 473–489.

Löfstedt, C., Wahlberg, N., and Millar, J. M. (2016). "Evolutionary patterns of pheromone diversity in Lepidoptera" in *Pheromone communication in moths: Evolution, behavior and application*. eds. J. D. Allison and R. T. Cardé (Berkeley: University of California Press), 43–78.

Maïbèche-Coisne, M., Merlin, C., François, M. C., Queguiner, I., Porcheron, P., and Jacquin-Joly, E. (2004). Putative odorant- degrading esterase cDNA from the moth *Mamestra brassicae*: cloning and expression patterns in male and female antennae. *Chem. Senses* 29, 381–390. doi: 10.1093/chemse/bjh039

Malo, E., Rojas, J., Gago, R., and Guerrero, A. (2013). Inhibition of the responses to sex pheromone of the fall armyworm *Spodoptera frugiperda*. *J. Insect Sci.* 13:134. doi: 10.1673/031.013.13401

Mei, T., Fu, W. B., Li, B., He, Z. B., and Chen, B. (2018). Comparative genomics of chemosensory protein genes (CSPs) in twenty-two mosquito species (Diptera: Culicidae): identification, characterization, and evolution. *PLoS One* 13:e0190412. doi: 10.1371/journal.pone.0190412

Merlin, C., Rosell, G., Carot-Sans, G., François, M. C., Bozzolan, F., Pelletier, J., et al. (2007). Antennal esterase cDNAs from two pest moths, *Sesamia nonagrioides* and *Spodoptera littoralis*, potentially involved in odorant degradation. *Insect Mol. Biol.* 16, 73–81. doi: 10.1111/j.1365-2583.2006.00702.x

Millar, J. G. (2000). Polyene hydrocarbons and epoxides: a second major class of lepidopteran sex attractant pheromones. *Annu. Rev. Entomol.* 45, 575–604. doi: 10.1146/annurev.ento.45.1.575

Misof, B., Liu, S., Meusemann, K., Peters, R., Donath, A., Mayer, C., et al. (2014). Phylogenomics resolves the timing and pattern of insect evolution. *Science* 346, 763–767. doi: 10.1126/science.1257570

Moczek, A. (2010). Phenotypic plasticity and diversity in insects. *Philos. Trans. R. Soc. Lond. B. Biol. Sci.* 365, 593–603. doi: 10.1098/rstb.2009.0263

Montella, I. R., Schama, R., and Valle, D. (2012). The classification of esterases: an important gene family involved in insecticide resistance—a review. *Mem. Inst. Oswaldo Cruz* 107, 437–449. doi: 10.1590/S0074-02762012000400001

Morisseau, C. (2013). Role of epoxide hydrolases in lipid metabolism. *Biochimie* 95, 91–95. doi: 10.1016/j.biochi.2012.06.011

Muñoz, L., Bosch, P., Batllori, L., Rosell, G., Bosch, D., Guerrero, A., et al. (2011). Synthesis of allylic trifluoromethyl ketones and activity as inhibitors of the sex pheromone of the leopard moth, *Zeuzera pyrina* L. (Lepidoptera: Cossidae). *Pest Manag. Sci.* 67, 956–964. doi: 10.1002/ps.2139

Nardini, M., and Dijkstra, B. (1999). α/β hydrolase fold enzymes: the family keeps growing. *Curr. Opin. Struct. Biol.* 9, 732–737. doi: 10.1016/S0959-440X(99)00037-8

Nielsen, H. (2017). "Predicting secretory proteins with SignalP" in *Protein function prediction. Methods in molecular biology*. *Vol. 1611*. ed. D. Kihara (New York, NY: Humana Press).

Oakeshott, J., Claudianos, C., Campbell, P., Newcomb, R., and Russell, R. (2005). "Biochemical genetics and genomics of insect esterases" in *Comprehensive molecular insect science*. eds. L. I. Gilbert, K. Iatrou and S. S. Gill (Netherlands: Elsevier), 1–73.

Oakeshott, J., Claudianos, C., Russell, R. J., and Robin, G. C. (1999). Carboxyl/cholinesterases: a case study of the evolution of a successful multigene family. *BioEssays* 21, 1031–1042. doi: 10.1002/(SICI)1521-1878(199912)22:1<1031::AID-BIES7>3.0.CO;2-J

Parrilla, A., and Guerrero, A. (1994). Trifluoromethyl ketones as inhibitors of the processionary moth sex pheromone. *Chem. Senses* 19, 1–10. doi: 10.1093/chemse/19.1.1

Pelosi, P., Iovinella, I., Zhu, J., Wang, G., and Dani, F. (2017). Beyond chemoreception: diverse tasks of soluble olfactory proteins in insects. *Biol. Rev. Camb. Philos. Soc.* 93, 184–200. doi: 10.1111/brv.12339

Pelosi, P., and Maida, R. (1995). Odorant binding proteins in insects. *Comp. Biochem. Physiol. B* 111, 503–514. doi: 10.1016/0305-0491(95)00019-5

Pelosi, P., Zhou, J. J., Ban, L. P., and Calvello, M. (2006). Soluble proteins in insect chemical communication. *Cell. Mol. Life Sci.* 63, 1658–1676. doi: 10.1007/s00018-005-5607-0

Phillips, J. C., Braun, R., Wang, W., Gumbart, J., Tajkhorshid, E., Villa, E., et al. (2005). Scalable molecular dynamics with NAMD. *J. Comput. Chem.* 26, 1781–1802. doi: 10.1002/jcc.20289

Prestwich, G. D., and Streinz, L. (1988). Haloacetate analogs of pheromones: effects on catabolism and electrophysiology in *Plutella xylostella*. *J. Chem. Ecol.* 14, 1003–1021. doi: 10.1007/BF01018789

Price, M., Dehal, P., and Arkin, A. (2010). FastTree 2–approximately maximum-likelihood treesfor large alignments. *PLoS One* 5:e9490. doi: 10.1371/journal.pone.0009490

Punta, M., Coggill, P. C., Eberhardt, R. Y., Mistry, J., Tate, J., Boursnell, C., et al. (2012). The Pfam protein families databases. *Nucleic Acids Res.* 40, D290–D301. doi: 10.1093/nar/gkr1065

Reddy, G. V. P., and Guerrero, A. (2010). New pheromones and insect control strategies. *Vitam. Horm.* 83, 493–519. doi: 10.1016/S0083-6729(10)83020-1

Renou, M., Berthier, A., and Guerrero, A. (2002). Disruption of responses to pheromone by (*Z*)-11-hexadecenyl trifluoromethyl ketone, an analogue of the pheromone, in the cabbage armyworm *Mamestra brassicae*. *Pest Manag. Sci.* 58, 839–844. doi: 10.1002/ps.534

Riba, M., Sans, A., Bau, P., Grolleau, G., Renou, M., and Guerrero, A. (2001). Pheromone response inhibitors of the corn stalk borer *Sesamia nonagrioides* biological evaluation and toxicology. *J. Chem. Ecol.* 27, 1879–1897. doi: 10.1023/a:1010468911352

Riba, M., Sans, A., Solé, J., Muñoz, L., Bosch, M. P., Rosell, G., et al. (2005). Antagonism of pheromone response of *Ostrinia nubilalis* males and implications on behavior in the laboratory and in the field. *J. Agric. Food Chem.* 53, 1158–1165. doi: 10.1021/jf048994q

Roelofs, W. L., Liu, W., Hao, G., Jiao, H., Rooney, A. P., and Linn, C. E. (2002). Evolution of moth sex pheromones via ancestral genes. *Proc. Natl. Acad. Sci.* 99, 13621–13626. doi: 10.1073/pnas.152445399

Rusch, C., Broadhead, G. T., Raguso, R. A., and Riffell, J. A. (2016). Olfaction in context—sources of nuance in plant–pollinator communication. *Curr. Opin. Insect Sci.* 15, 53–60. doi: 10.1016/j.cois.2016.03.007

Rytz, R., Croset, V., and Benton, R. (2013). Ionotropic receptors (IRs): chemosensory ionotropic glutamate receptors in *Drosophila* and beyond. *Insect Biochem. Mol. Biol.* 43, 888–897. doi: 10.1016/j.ibmb.2013.02.007

Sakurai, T., Namiki, S., and Kanzaki, R. (2014). Molecular and neural mechanisms of sex pheromone reception and processing in the silkmoth *Bombyx mori*. *Front. Physiol.* 5:125. doi: 10.3389/fphys.2014.00125

Sali, A., and Blundell, T. L. (1993). Comparative protein modelling by satisfaction of spatial restraints. *J. Mol. Biol.* 234, 779–815. doi: 10.1006/jmbi.1993.1626

Sato, K., and Touhara, K. (2008). Insect olfaction: receptors, signal transduction, and behavior. *Results Probl. Cell Differ.* 47, 203–220. doi: 10.1007/400_2008_10

Solé, J., Sans, A., Riba, M., Rosa, E., Bosch, M. P., Barrot, M., et al. (2008). Reduction of damage by the Mediterranean corn borer *Sesamia nonagrioides* and the European corn borer *Ostrinia nubilalis* in maize fields by a trifluoromethyl ketone pheromone analogue. *Entomol. Exp. Appl.* 126, 28–39. doi: 10.1111/j.1570-7458.2007.00630.x

Song, Y. Q., Sun, H. Z., and Du, J. (2018). Identification and tissue distribution of chemosensory protein and odorant binding protein genes in *Tropidothorax elegans* distant (Hemiptera: Lygaeidae). *Sci. Rep.* 8:7803. doi: 10.1038/s41598-018-26137-6

Sun, H., Qi, Y., and Lm, W. (2015). Effects of N-glycosylation on protein conformation and dynamics: protein data bank analysis and molecular dynamics simulation study. *Sci. Rep.* 5:8926. doi: 10.1038/srep08926

Sun, L., Wang, Q., Wang, Q., Zhang, Y., Tang, M., Guo, H., et al. (2017). Identification and expression patterns of putative diversified carboxylesterases in the tea geometrid *Ectropis obliqua* prout. *Front. Physiol.* 8:1085. doi: 10.3389/fphys.2017.01085

Vogt, R. G. (2005). "Molecular basis of pheromone detection in insects" in *Comprehensive insect physiology, biochemistry, pharmacology and molecular biology*. eds. L. Gilbert, K. Iatrou and S. Gill (London: Elsevier), 753–804.

Vogt, R. G., and Riddiford, L. M. (1981). Pheromone binding and inactivation by moth antennae. *Nature* 293, 161–163. doi: 10.1038/293161a0

Vogt, R. G., Riddiford, L. M., and Prestwich, G. D. (1985). Kinetic properties of a sex pheromone-degrading enzyme: the sensillar esterase of *Antheraea polyphemus*. *Proc. Natl. Acad. Sci.* 82, 8827–8831. doi: 10.1073/pnas.82.24.8827

Wang, Q., Wang, Q., Li, H., Sun, L., Zhang, D., and Zhang, Y. (2020). Sensilla localization and sex pheromone recognition of odorant binding protein OBP4 in the mirid plant bud *Adelphocoris lineolatus* (Goeze). *J. Insect Physiol.* 121:104012. doi: 10.1016/j.jinsphys.2020.104012

Webb, B., and Sali, A. (2016). Comparative protein structure modeling using MODELLER. *Curr. Protoc. Bioinformatics* 54, 5.6.1–5.6.37. doi: 10.1002/cpbi.3

Wiedemann, J., Heiner, T., Mloston, G., Prakash, G. K. S., and Olah, G. A. (1998). Direct preparation of trifluoromethyl ketones from carboxylic esters: trifluoromethylation with (trifluoromethyl) trimethylsilane. *Angew. Chem. Int. Ed.* 37, 820–821. doi: 10.1002/(SICI)1521-3773(19980403)37:6<820::AID-ANIE820>3.0.CO;2-M

Witzgall, P., Kirsch, P., and Cork, A. (2010). Sex pheromones and their impact on pest management. *J. Chem. Ecol.* 36, 80–100. doi: 10.1007/s10886-009-9737-y

Yang, B., Ozaki, K., Ishikawa, Y., and Matsuo, T. (2015). Identification of candidate odorant receptors in Asian corn borer *Ostrinia furnacalis*. *PLoS One* 10:e0121261. doi: 10.1371/journal.pone.0121261

Yin, J., Zhong, T., Wei, Z. J., Li, K. B., Cao, Y. Z., and Gou, W. (2011). Molecular characters and recombinant expression of the carboxylesterase gene of the meadow moth *Loxostege sticticalis* L. (Lepidoptera: Pyralidae). *Afr. J. Biotechnol.* 10, 1794–1801. doi: 10.5897/AJB10.1551

Younus, F., Fraser, N., Coppin, C., Liu, J. W., Correy, G., Chertemps, T., et al. (2017). Molecular basis for the behavioral effects of the odorant degrading enzyme esterase 6 in *Drosophila*. *Sci. Rep.* 7:46188. doi: 10.1038/srep46188

Yu, Q. Y., Lu, C., Li, W. L., Xiang, Z. H., and Zhang, Z. (2009). Annotation and expression of carboxylesterases in the silkworm *Bombyx mori*. *BMC Genomics* 10:553. doi: 10.1186/1471-2164-10-553

Yuvaraj, J., Corcoran, J. A., Andersson, M. N., Newcomb, R. D., Anderbrant, O., and Löfstedt, C. (2017). Characterization of odorant receptors from a non-ditrysian moth, *Eriocrania semipurpurella* sheds light on the origin of sex pheromone receptors in Lepidoptera. *Mol. Biol. Evol.* 34, 2733–2746. doi: 10.1093/molbev/msx215

Zhang, Y., Kua, J., and McCammon, A. (2002). Role of the catalytic triad and oxyanion hole in acetylcholinesterase catalysis: an ab initio QM/MM study. *J. Am. Chem. Soc.* 124, 10572–10577. doi: 10.1021/ja020243m

Zhang, Y. N., Li, J. B., He, P., Sun, L., Li, Z. Q., Fang, L. P., et al. (2016). Molecular identification and expression patterns of carboxylesterase genes based on transcriptome analysis of the common cutworm, *Spodoptera litura* (Lepidoptera: Noctuidae). *J. Asia Pac. Entomol.* 19, 989–994. doi: 10.1016/j.aspen.2016.07.020

Zhang, D. D., and Löfstedt, C. (2015). Moth pheromone receptors: gene sequences, function and evolution. *Front. Ecol. Evol.* 3:105. doi: 10.3389/fevo.2015.00105

Zhang, Y. X., Wang, W. L., Li, M. Y., Li, S. G., and Liu, S. (2017). Identification of putative carboxylesterase and aldehyde oxidase genes from the antennae of the rice leaffolder, *Cnaphalocrocis medinalis* (Lepidoptera: Pyralidae). *J. Asia Pac. Entomol.* 20, 907–913. doi: 10.1016/j.aspen.2017.06.001

Zhang, Y. N., Xia, Y. H., Zhu, J. Y., Li, S. Y., and Dong, S. L. (2014). Putative pathway of sex pheromone biosynthesis and degradation by expression patterns of genes identified from female pheromone gland and adult antenna of *Sesamia inferens* (Walker). *J. Chem. Ecol.* 40, 439–451. doi: 10.1007/s10886-014-0433-1

Zhou, J. J. (2010). *Odorant-binding proteins in insects*. *1st Edn*. Burlington, VT: Elsevier Inc.

Conflict of Interest: The authors declare that the research was conducted in the absence of any commercial or financial relationships that could be construed as a potential conflict of interest.

frontiers in Physiology

ORIGINAL RESEARCH
published: 13 April 2021
doi: 10.3389/fphys.2021.649590

Characterizing the Role of Orco Gene in Detecting Aggregation Pheromone and Food Resources in *Protaetia brevitarsis* Leiws (Coleoptera: Scarabaeidae)

Xiaofang Zhang[1,2†], Panjing Liu[1,2†], Qiuju Qin[3], Min Li[1,2], Runjie Meng[4] and Tao Zhang[1,2]*

[1] Institute of Plant Protection, Hebei Academy of Agriculture and Forestry Sciences, Integrated Pest Management Center of Hebei Province, Baoding, China, [2] Key Laboratory of IPM on Crops in Northern Region of North China, Ministry of Agriculture, Baoding, China, [3] College of Plant Protection, Hebei Agricultural University, Baoding, China, [4] Baoding Vocational and Technical College, Baoding, China

OPEN ACCESS

Edited by:
Yang Liu,
Institute of Plant Protection, (CAAS), China

Reviewed by:
William Benjamin Walker III, Agricultural Research Service, United States Department of Agriculture (USDA-ARS), United States
Feng Liu, Vanderbilt University, United States

***Correspondence:**
Tao Zhang
cauzht@163.com

[†] These authors have contributed equally to this work

Specialty section:
This article was submitted to Invertebrate Physiology, a section of the journal Frontiers in Physiology

Received: 05 January 2021
Accepted: 17 March 2021
Published: 13 April 2021

Citation:
Zhang X, Liu P, Qin Q, Li M, Meng R and Zhang T (2021) Characterizing the Role of Orco Gene in Detecting Aggregation Pheromone and Food Resources in Protaetia brevitarsis Leiws (Coleoptera: Scarabaeidae). Front. Physiol. 12:649590. doi: 10.3389/fphys.2021.649590

An accurate olfactory system for recognizing semiochemicals and environmental chemical signals plays crucial roles in survival and reproduction of insects. Among all olfaction-related proteins, olfactory receptors (ORs) contribute to the conversion of chemical stimuli to electric signals and thereby are vital in odorant recognition. Olfactory receptor co-receptor (Orco), one of the most conserved ORs, is extremely essential in recognizing odorants through forming a ligand-gated ion channel complex with conventional ligand-binding odorant receptors. We have previously identified aggregation pheromone in *Protaetia brevitarsis* (Coleoptera: Scarabaeidae), a native agricultural and horticultural pest in East-Asia. However, to our best knowledge, its olfaction recognition mechanisms are still veiled. To illustrate how *P. brevitarsis* recognize aggregation pheromone and host plants, in the present study we cloned and sequenced the full-length *Orco* gene from *P. brevitarsis* antennae (named *PbreOrco*) and found that *PbreOrco* is highly conserved and similar to Orcos from other Coleoptera insects. Our real-time quantitative PCR (qRT-PCR) results showed that *PbreOrco* is mainly expressed in antenna. We also demonstrated that silencing *PbreOrco* using RNA interference through injecting dsOrco fragment significantly inhibited *PbreOrco* expression in comparison with injecting control dsGFP and subsequently revealed using electroantennogram and behavioral bioassays that decreasing *PbreOrco* transcript abundance significantly impaired the responses of *P. brevitarsis* to intraspecific aggregation pheromone and prolonged the time of *P. brevitarsis* spending on food seeking. Overall, our results demonstrated that *PbreOrco* is crucial in mediating odorant perception in *P. brevitarsis*.

Keywords: *Protaetia brevitarsis*, olfactory recognition, semiochemicals, host seeking, RNAi

INTRODUCTION

Having a precise olfactory system is of great benefit for most insects in foraging, mating, locating oviposition sites and avoiding adverse environments (Leal, 2013; Brito et al., 2016). Olfactory recognition is a complicated and sophisticated process involving numerous receptors and signaling pathways. The odorant stimuli are firstly detected by the olfactory receptor neurons (ORNs) in insect antennae and processed to bioelectric signals, which are subsequently transmitted to the main nervous system (e.g., brain), inducing various odor-evoked behaviors (Leal, 2013; Fleischer et al., 2018). During the odorants processing in ORNs, an acceptable hypothesis infers that odorants are specifically transported by odorant binding proteins (OBPs) and chemosensory proteins (CSPs) to the olfactory receptors (ORs), which belong to a family of seven-transmembrane domain proteins on the dendrite membrane of neurons and are conceived to be essential in odorant recognition (Smart et al., 2008), and thereby recognized and converted to electric signals and subsequently degraded by odorant degrading enzymes (ODEs) (Sato and Touhara, 2008; Zhou, 2010; Leal, 2013).

To recognize chemical signals, most insect ORNs express two subclasses of ORs—a conventional odorant-specific olfactory receptors and a highly conserved olfactory receptor co-receptor (Orco) (Harini and Sowdhamini, 2012). Compared to conventional ORs, Orco is more conserved (Missbach et al., 2014; Lin et al., 2015) among a variety of arthropods including Lepidoptera, Coleoptera, Hymenoptera, Orthoptera, Hemiptera and Diptera (Krieger et al., 2003; Yang et al., 2012; Lin et al., 2015; Li et al., 2016; Wang et al., 2018). During the process of recognizing odorants, Orco couples with conventional ORs to form an Orco-ORx complex, which functions as a ligand-gated ion channel and determines the sensitivity and specificity of the ORN where it is expressed (Breer et al., 2019). In this complex, Orco is a key factor for the localization, stability and correct protein folding of ORs (Larsson et al., 2004; Stengl and Funk, 2013). Studies have shown that knockout or mutation of *Orco* gene would lead to the disablement of odorant sensing in insects (Larsson et al., 2004; Neuhaus et al., 2005). For examples, *Orco* mutations in fruit flies, locusts, mosquitoes and moths lead to loss of OR function, and impaired responses to odorants such as food volatiles and sex pheromones (Asahina et al., 2008; DeGennaro et al., 2013; Koutroumpa et al., 2016; Li et al., 2016; Yang et al., 2016; Trible et al., 2017), silencing of *Orco* through RNA interference (RNAi) in beetles (*Tenebrio molitor*, *Dendroctonus armandi*, and *Ophraella communa*) impairs their ability to locate hosts and mates (Liu et al., 2016; Zhang et al., 2016; Ma et al., 2020). In addition, Orco is also involved in other important physiological activities (such as wing differentiation, metabolism regulation, stress resistance, number of glomeruli in antennal lobes and life span extension), indicating they may also participate in more physiological functions (Libert et al., 2007; Fan et al., 2015; Trible et al., 2017).

The white-spotted flower chafer (WSFC), *Protaetia brevitarsis* Leiws (Coleoptera: Scarabaeidae), is a native agricultural and horticultural pest in East-Asia, including China, Korean Peninsula, Japan, Thailand, Mongolia and Russia (Suo et al., 2015; Liu et al., 2019). WSFC larvae, which feed on soil humus, decaying plant residues, and even fermented animal manure, are cultivated as a potential resource insect for converting herbaceous and plant residues to organic fertilizer (Li et al., 2019; Wang et al., 2019). However, WSFC adults are destructive to many important crops, such as corn, wheat, apple, peach and various vegetables (Zhao and Chen, 2008; Xu et al., 2009; Cai et al., 2020). To environmentally-friendly control and monitor WSFC, we have identified 4-methylanisole (4-MA) as an aggregation pheromone for developing efficient lures (Zhang et al., 2019). Although its candidate chemosensory receptors have been identified (Liu et al., 2019), the molecular mechanisms underlying olfactory recognition, including function of *PbreORs*, remain largely unexplored. Previously, based on transcriptome analysis, we identified a *PbreOrco*-related sequence encoding a 288aa peptide, though the 5′ terminus was suspected to be missing.

To fully explore the functions of *PbreOrco*, in this study, we firstly cloned the full-length sequence of *PbreOrco* through rapid amplification of cDNA ends (RACE), analyzed its characteristics and expression pattern. We then silenced *PbreOrco* gene using RNAi and examined its pheromone- and food-seeking function. Our results could further deepen our understanding on Orco functions and benefit subsequent development of semiochemical-based strategy to control this pest.

MATERIALS AND METHODS

Insect Rearing and Tissue Collection

White-spotted flower chafer larvae were reared on fermented wheat straw in a constant environment with temperature of 25 ± 2°C, relative humidity of 50 ± 2% and photoperiod of 14L:10D (Liu et al., 2019). Newly-emerged adults were sorted by sex and fed with fresh peach. When unmated WSFCs reached approximately 7 days old, their antennae, head without antennae, thorax, abdomen, legs and wings were excised, immediately frozen in liquid nitrogen, and stored at −80°C for future experiments.

Total RNA Extraction and cDNA Synthesis

Total RNA was extracted from 50 WSFCs of each sex using TRIzol reagent (TransGen, China) following the manufacturer's instructions. RNA quality was evaluated by 1.0% agarose gel electrophoresis and Nanodrop 2000 (OD_{260}/OD_{280} ranged from 1.80 to 2.10). The first-strand cDNA was synthesized from 1 μg of total RNA using All-in-One First-Strand cDNA Synthesis SuperMix (TransGen, China) according to the manufacturer's instructions. The synthesized cDNA was stored at −20°C prior to further analysis.

Rapid Amplification of cDNA Ends to Obtain Full-Length *PbreOrco* Gene

According to the reported incomplete *PbreOrco* sequence (MH324899), the 5′ end of mRNA was obtained using a 5′-RACE Kit (Sangon, China) with the gene-specific primers

(GSP1 and GSP2) listed in **Supplementary Table 1** following the manufacturer's protocol. Briefly, the first strand cDNA was synthesized by using specific reverse transcription primers (5′ RACE-RT Primer, **Supplementary Table 1**) and reverse transcriptase mix (RNase H-). Two rounds of touchdown PCR was performed as follows: 94°C for 1 min; 10 cycles of 94°C for 60 s, 70°C (each cycle descends 1°C) for 30 s and 72°C for 60 s; 25 cycles of 94°C for 60 s, 60°C for 30 s, and 72°C for 60 s; and a final incubation at 72°C for 10 min. The first round of PCR amplification was carried out with GSP1 as downstream primer and the first strand of cDNA as template. Then, the 5′ end cDNA of *PbreOrco* was amplified by using a universal 5′ RACE outer primer containing partial splice sequence (**Supplementary Table 1**) as the upstream primer and the GSP2 as the downstream primer. The PCR product was purified, ligated into a pEASY-Blunt vector (TransGen Biotech, China), and sequenced (Sangon Biotech, China).

Sequence Analysis

The homology of PbreORCO protein was analyzed by Blastp search in NCBI database[1]. Its transmembrane domains were identified using the TMHMM Server v. 2.0 program[2]. Its topology diagram was constructed using the TOPO2 Transmembrane Protein Display[3]. Protein sequences alignment was performed using ClustalX 1.83, and the results were presented by GeneDoc 2.7.0 software. Evolutionary analyses were conducted in MEGA7 using the Maximum Likelihood method with a bootstrap test (1000 replicates, complete deletion, NN) (Kumar et al., 2016). The evolutionary distances were computed using the Poisson correction model (Zuckerkandl and Pauling, 1965). When the number of common sites was < 100 or less than one fourth of the total number of sites, the maximum parsimony method was used; otherwise BIONJ method with MCL distance matrix was used. Finally, phylogenetic trees were viewed and edited using FigTree v.1.4.3[4]. Identity calculation of Orcos in various insects was analyzed using MegAlign (DNAStar Lasergene 12.1) with the pair distances of Untitled ClustalW (slow/accurate, identity).

Tissue Expression Profiles of *PbreOrco*

The expression of *PbreOrco* in different tissues was analyzed using real-time quantitative PCR (qRT-PCR) with an ABI 7500 Real-Time PCR System (Applied Biosystems, United States). The primers for *PbreOrco* was designed by Primer 6.0 (**Supplementary Table 1**). GADPH2 was used as reference gene according to our previous study (Liu et al., 2019). qRT-PCR reactions were performed in 20 μL reaction mixtures, each containing 10 μL TransStart Tips Green Mix (TransGen, China), 0.5 μL of each primer (10 μM), 1 μL of sample cDNA, and 8 μL of sterilized H_2O. The thermocycling conditions were as follows: 95°C for 3 min; 40 cycles at 95°C for 10 s; and an annealing temperature of 60°C for 30 s. Each test was carried out three times as technical replicates. The amplification efficiency of the primers was 92–98% according to standard curve analysis. Relative expression of *PbreOrco* were analyzed using the $2^{-\Delta\Delta CT}$ method (Livak and Schmittgen, 2001). Three independent biological repeats were conducted, and each RNA sample was extracted from 30 adults.

RNAi of *PbreOrco* Gene and qRT-PCR Validation

The fragment of *PbreOrco* was amplified using specific primers with T7 RNA polymerase promoter (**Supplementary Table 1**). A double-stranded green fluorescent protein (dsGFP) fragment amplified from the *GFP* gene (GenBank No. U50963) was used as the negative control. Double-stranded RNA (dsRNA) was synthesized using the T7 Ribomax Express RNAi System (Promega, Madison, WI, United States). The quality and concentration of dsRNA were determined by agarose gel electrophoresis and Nanodrop 2000 (Thermo, United States). The newly emerged WSFCs were separated and reared individually before dsRNA injection. To each beetle, 3 μg of dsOrco or dsGFP was injected into the conjunction between the head and thorax using a microsyringe. The antennae were collected at 1, 3, 5, 7, and 9 days of post-injection to evaluate the expression of *PbreOrco* using qRT-PCR. Three independent biological repeats were collected, and each repeat contained 30 adults.

Electroantennography

The electrophysiological responses of injected WSFCs to the aggregation pheromone 4-MA (99% purity, Aladdin Reagent Co., Ltd., Shanghai China) were monitored on an Electroantennography (EAG) apparatus (Syntech Ltd., Kirchzarten, Germany) following a reported method (Zhang et al., 2020). Briefly, the antennae of WSFCs at 6–7 days of post-injection prepared by cutting off the tips were affixed to the recording electrode with electrically conductive gel and flowed over by a constant humidified airstream (∼200 mL·min-1). After that, a pulse airstream carrying volatiles from 20 μg of 4-MA in 20 μL paraffin oil was brought to the antennae through constant airstream at 30 s intervals by an air stimulus controller (CS-55). The electric signals generated by the responses of antennae were recorded and analyzed using the Syntech EAG 2000 software (Syntech, Kirchzarten, Germany). Paraffin oil was used as parallel solvent control. The EAG responses to pheromone of each treatment were calibrated by subtracting the EAG values to solvent control. Five antennae were tested with five stimuli for each antenna.

Insect Behavioral Bioassay

The responses of female and male WSFCs at 6–7 days of post-injection to 4-MA were tested by a two-choice bioassay using a glass Y-tube olfactometer (3.0 cm inner diameter) comprised of a 25-cm stem and two 20-cm branching arms at an angle of about 60° (Ikeura et al., 2012). During the assay, charcoal-filtered and humidified air was pumped through the olfactometer at a rate of 100 ml·min-1 using an atmosphere sampling instrument (QC-1B, Beijing Municipal Institute of Labor Protection, Beijing, China)

[1]https://blast.ncbi.nlm.nih.gov/Blast.cgi

[2]http://www.cbs.dtu.dk/services/TMHMM/

[3]http://www.sacs.ucsf.edu/TOPO-run/wtopo.py

[4]http://tree.bio.ed.ac.uk/software/figtree/

and 20 μl of odor sources (0.1 μg/μL in paraffin) on strips of filter paper (1 cm × 5 cm) were put into sample bottles connected to the branching arms and an injected WSFC individual was released into the stem (Yang et al., 2017). The 4-MA in paraffin oil was placed into one arm of the Y-tube, while paraffin oil was placed into the other arm as the negative control. Y-tube was cleaned with ethanol after each test. Each experiment contained 30 injected adults and lasted for 20 min.

For food-seeking behavior, the injected WSFCs (pre-starved for 24 h) were released into the four corners of a transparent box. After the insects adapted to the environment (∼15 min), half of a fresh peach was introduced into the center of the box. The WSFCs were allowed to seek food for 20 min, during which the number of WSFCs arrived food and their foraging time were recorded. If an insect has failed in arriving the food within 20 min, it shall be judged unable to seek food (Liu et al., 2016). Three independent biological repeats were conducted, and each experiment contained 10 post-injected adults.

Statistical Analysis

To analyze the results of qRT-PCR, EAG tests, Y-tube tests and food seeking behavior, one-way analysis of variance (ANOVA) with Tukey's test was used in SPSS 19.0 software. The least significant significance was set at $P < 0.05$.

RESULTS

Identification of Full-Length PbreOrco

The full-length sequence of *PbreOrco* was obtained based on the reported sequence (MH324899) using 5′-RACE and submitted to GenBank (Access No: MW382164). The open reading frame (ORF) of *PbreOrco* was 1,431 bp and encodes a protein comprising 476 amino acids. The transmembrane prediction results indicated that *PbreOrco* has seven transmembrane domains with an intracellular N-terminus and an extracellular C-terminus, indicating it is a typical Orco protein (**Figure 1**).

Sequence Analysis of *PbreOrco*

Increasing reports demonstrate that Orco receptors are highly conserved during insect evolution. Sequence alignment of *PbreOrco* with Orco from nine other Coleoptera insects (*Holotrichia parallela*, *H. oblita*, *H. plumbea*, *Anomala corpulenta*, *Anoplophora glabripennis*, *Ambrostoma quadriimpressum*, *Rhynchophorus ferrugineus*, *Sitophilus oryzae,* and *Tenebrio molitor*) revealed a relatively high amino acid identity. *PbreOrco* was 91.19, 91.19, 91.39, 92.24, 80.71, 79.96, 80.28, 79.42, and 81.21%, respectively, homologous with *HoblOrco* (*H. oblita*), *HpluOrco* (*H. plumbea*), *HparOrco* (*H. parallela*), *AcorOrco* (*A. corpulenta*), *AglaOrco* (*A. glabripennis*), *AquaOrco* (*A. quadriimpressum*), *RferOrco* (*R. ferrugineus*), *SoryOrco* (*S. oryzae*), and *TmolOrco* (*T. molitor*). In addition, the C-terminal sequences (TM5-TM7) were highly conserved (**Figure 1**).

Thirty-seven Orco sequences from six insect orders were used to construct a phylogenetic tree. The phylogenetic analysis showed that Coleoptera, Lepidoptera, Diptera and Hymenoptera were clustered together in a large branch, while Orthoptera and Hemiptera were in another branch. Compared with other insect Orcos, *PbreOrco* presented a close relationship with Orco of Coleoptera (**Figure 2**).

Expression Profiles of *PbreOrco*

qRT-PCR was used to determine the relative expression of *PbreOrco* in different adult tissues. The results showed that the expressions of *PbreOrco* in the antennae of both male and female WSFCs were significantly higher than those in other tissues. Furthermore, there was no significant difference in the expression of Orco between male and female antennae (**Figure 3**).

RNAi Efficiency

During our experiment, the injected WSFCs were all alive. The qRT-PCR results showed that injecting dsRNA significantly decreased the expression of *PbreOrco*. Compared to the dsGFP-injected control WSFCs, the expression of *PbreOrco* was significantly inhibited at 1–9 days of post-injection dsOrco (**Figure 4**). The knockdown rates were 86.07 and 85.04% for male and female at 5 days of post-injection, and maintained at > 85% in the following several days (**Figure 4**). Consequently, WSFCs at 6–8 days of post-injection were selected for electrophysiological and behavioral bioassays.

Silencing *PbreOrco* Impairs the Response to Aggregation Pheromone

Electroantennography and olfactometer assays were performed to compare the responses of dsGFP-injected and dsOrco-injected WSFCs to aggregation pheromone. The average response values of dsOrco-injected WSFCs nearly halved in comparison with those of dsGFP-injected WSFCs (males: 2.80 mV ± 0.22 vs 1.27 mV ± 0.17 mV; females: 2.78 mV ± 0.35 vs 1.45 mV ± 0.20 mV, respectively) (**Figure 5A** and **Supplementary Figure 1**). The subsequent olfactometer assays showed that the dsOrco-injected WSFCs showed no preference to 4-MA or solvent control (Male: $F_{1,4}$ = 0.500, P = 0.519; Female: $F_{1,4}$ = 1.997, P = 0.230), while non-injected (Male: 65.56 ± 5.09%; $F_{1,4}$ = 32.00, P = 0.005; Female: 71.48 ± 5.70%; $F_{1,4}$ = 50.00, P = 0.002) and dsGFP-injected WSFCs (Male: 73.33 ± 5.77%; $F_{1,4}$ = 98.00, P = 0.001; Female: 68.96 ± 8.91%; $F_{1,4}$ = 28.016, P = 0.006) significantly moved toward 4-MA (**Figure 5B**), further confirming that RNAi-based silencing of *PbreOrco* impaired the response of both female and male WSFCs to aggregation pheromone.

Silencing *PbreOrco* Influnces Food Seeking

To further verify the function of *PbreOrco* in insect feeding behavior, we set up behavioral experiments to test the food-seeking activity in response to fresh peaches. All the tested WSFCs had been starved for 24 h prior to the bioassays. The results showed that only 48.52% (male) and 46.67% (female) insects successfully arrived food within 20 min, significantly lower than dsGFP-injected (male: 76.67%; female: 79.63%) (**Supplementary Figure 2**). Furthermore, compared with the

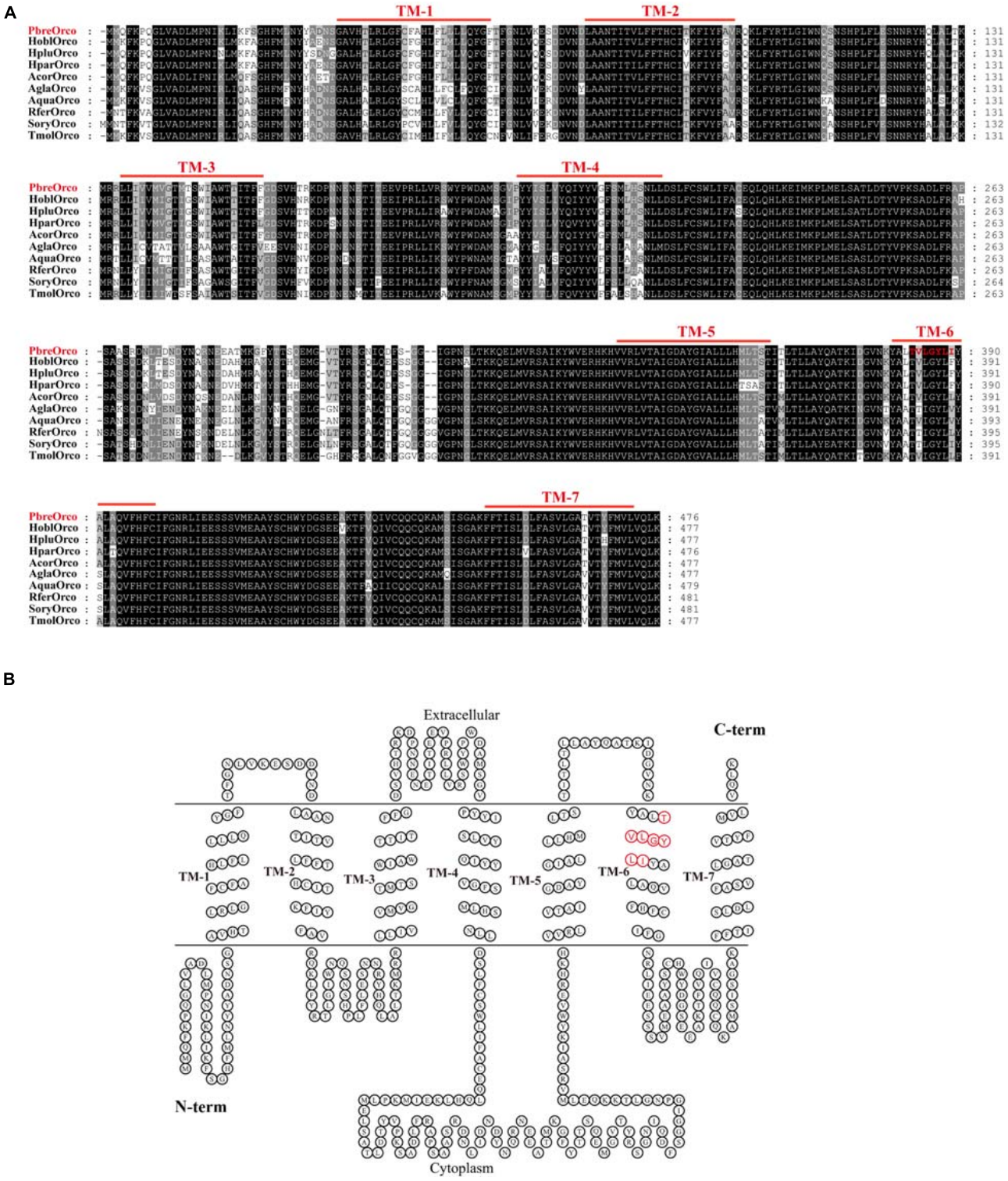

FIGURE 1 | Sequence analysis of *PbreOrco*. **(A)** Amino acid sequence alignment of *PbreOrco* with orther Orcos from Coleoptera insects. Hpar, Holotrichia parallela; Hobl, Holotrichia oblita; Hplu, Holotrichia plumbea; Acor, Anomala corpulenta; Agla, Anoplophora glabripennis; Aqua, Ambrostoma quadriimpressum; Rfer, Rhynchophorus ferrugineus; Sory, Sitophilus oryzae; Tmol, Tenebrio molitor. The sequences used in this analysis listed in **Supplementary Table 2**. **(B)** Seven-transmembrane topology of representative *PbreOrco*. The double line represents the membrane region with labeled extracellular and cytoplasmic sides. TM: transmembrane. The conserved motif (383–389: TVLGYLI) was displayed in red.

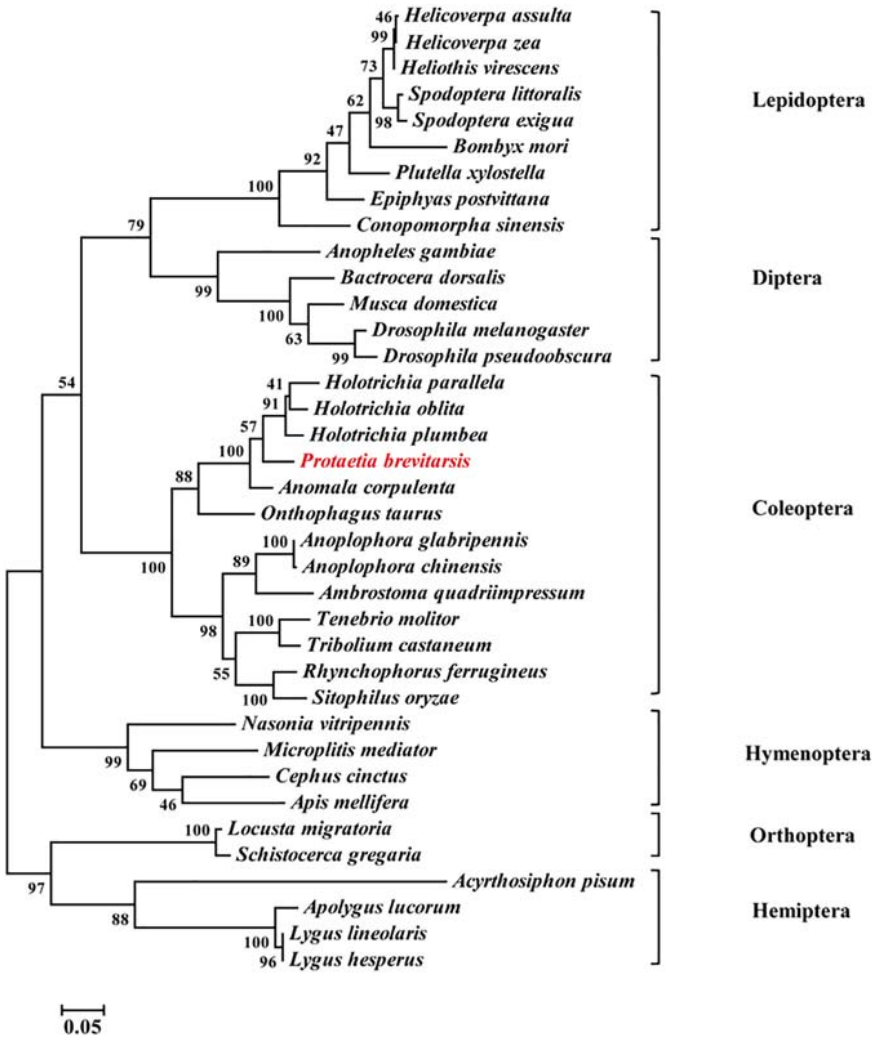

FIGURE 2 | Phylogenetic analysis of Orco orthologs from 37 insect species. The branch lengths were proportional to the percentage of sequence difference (scale: 0.05% difference). Bootstrap values expressed as percentages of 1,000 replications are shown at branch nodes. The *PbreOrco* sequence was shown in red. The sequences used in this analysis are listed in **Supplementary Table 2**.

dsGFP-injected WSFCs, the dsOrco-injected took more time to find food during the test time (male: 2.65 vs 1.43 min; female: 3.13 vs 1.46 min) (**Figure 6** and **Supplementary Video 1**).

DISCUSSION

Odorant receptors (ORs), which transform volatile stimuli to electrical signals in olfactory of insects, play important roles in recognition of various odorants (Leal, 2013). Among all ORs, Orco is the most particular and essential one: it assists the specific-ORs to bind and recognize odorants by forming a heteromeric OR-Orco complex rather than responding to odorants directly (Stengl and Funk, 2013). Thus, identification and functional study of insect Orco could provide further insights into function of ORs. In this study, we successfully cloned the full-length sequence of *PbreOrco* using the 5′RACE system from the antennae of *P. brevitarsis* and demonstrated the crucial role of *PbreOrco* in the olfactory mechanism of *P. brevitarsis*.

An abundance of reports have documented that insect Orcos are highly conserved amongst species (Krieger et al., 2003; Jones et al., 2005; Yang et al., 2012). As expected, the alignment and homology analysis showed that the sequence of *PbreOrco* is highly conserved with its orthologs in other beetles (**Figure 1A**). Especially, its C-terminus showed extremely high conservation among species. This region has been demonstrated to play an indispensable role in the functional interaction of the OR and Orco proteins (Hopf et al., 2015; Butterwick et al., 2018). Furthermore, motif TVVGYLG (393–399) located at the sixth predicted transmembrane helix of *DmelOrco* in *Drosophila melanogaster* was thought to comprise a ligand-gated selectivity filter with Val394 and Leu398 in the pores of K^+ channels (Wicher et al., 2008). In *PbreOrco* sequence, a motif (383–389: TVLGYLI) (**Figure 1**), which is also located

in the sixth transmembrane helix, is similar to the motif TVVGYLG in *DmelOrco*, indicating *PbreOrco* might function *via* the same mechanism. In addition, qRT-PCR determination showed that *PbreOrco* was mainly expressed in antennae, without significant difference in transcription level between males and females (**Figure 3**). These results are consistent with *Orcos* in *Apolygus lucorum*, *Tenebrio molitor* and *Rhodnius prolixus* (Zhou et al., 2014; Franco et al., 2016; Liu et al., 2016), strongly supporting that *PbreOrco* is essential for insect chemosensation.

Silencing the expression of a targeted gene by RNAi technology is considered as an effective method for functional verification of genes in insects (Huvenne and Smagghe, 2010). To silence a gene through RNAi, direct microinjection and artificial feeding of dsRNA are two frequently-applied approaches. Of them, microinjection is more preferred because it could easily control the precise amount of dsRNA, and induce RNAi more effectively (Franco et al., 2016; Ma et al., 2020). In this study, we also utilized direct injection of dsRNA to introduce RNAi and further study the function of Orco in WSFCs. qRT-PCR results showed that the transcription level of *PbreOrco* was reduced 86.07–90.94% in males and 85.04–87.96% in females after 5–9 days of injection (**Figure 4**), suggesting that injecting dsRNA is an ideal tool for studies on function of *PbreOrco in vivo*. Although the efficiency of silencing *PbreOrco* was determined to be satisfied within 9 days, the persistence of the silencing effect of other target genes need to be further evaluated. In addition, our results were consistent with that RNAi is a knockdown rather than a knockout method. In WSFCs, however, 9 days was long enough for us to complete the behavioral bioassays. Indeed, the results showed that the silencing of *PbreOrco* sustained for at least 9 days with an effective silencing rate. Furthermore, appropriately increasing amounts of dsRNA injected to insects could potentially prolong the silencing time (Huvenne and Smagghe, 2010; Miller et al., 2012; Joga et al., 2016). In this study, compared with smaller beetles in size (Liu et al., 2016; Zhang et al., 2016; Ma et al., 2020), we injected a relatively higher amounts of dsRNA into WSFCs (3 μg for each beetle) to ensure not only the longer silencing time, but also the silencing efficiency for such a large beetle.

Electrophysiological and behavioral bioassays are conventional approaches to evaluate the potential influences of gene silencing on injected insects (Rebijith et al., 2016; Dong et al., 2017; Bolton et al., 2019). We also employed EAG and Y-tube olfactometer to test the responses of WSFCs to

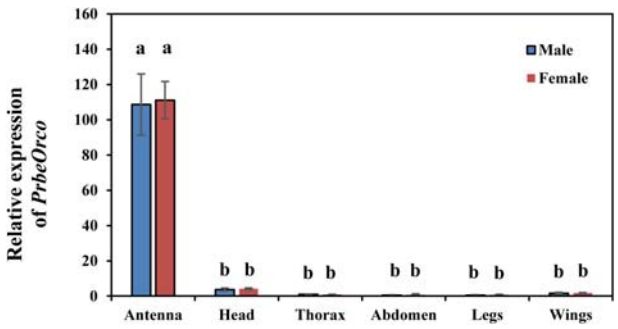

FIGURE 3 | Expression profiles of *PbreOrco* in different tissues of male and female. The head excluded antennae and maxillary palps. The relative expression levels were normalized to the GADPH2 gene, with the expression of male thorax as the calibrator. Different letters represent significant difference ($P < 0.05$).

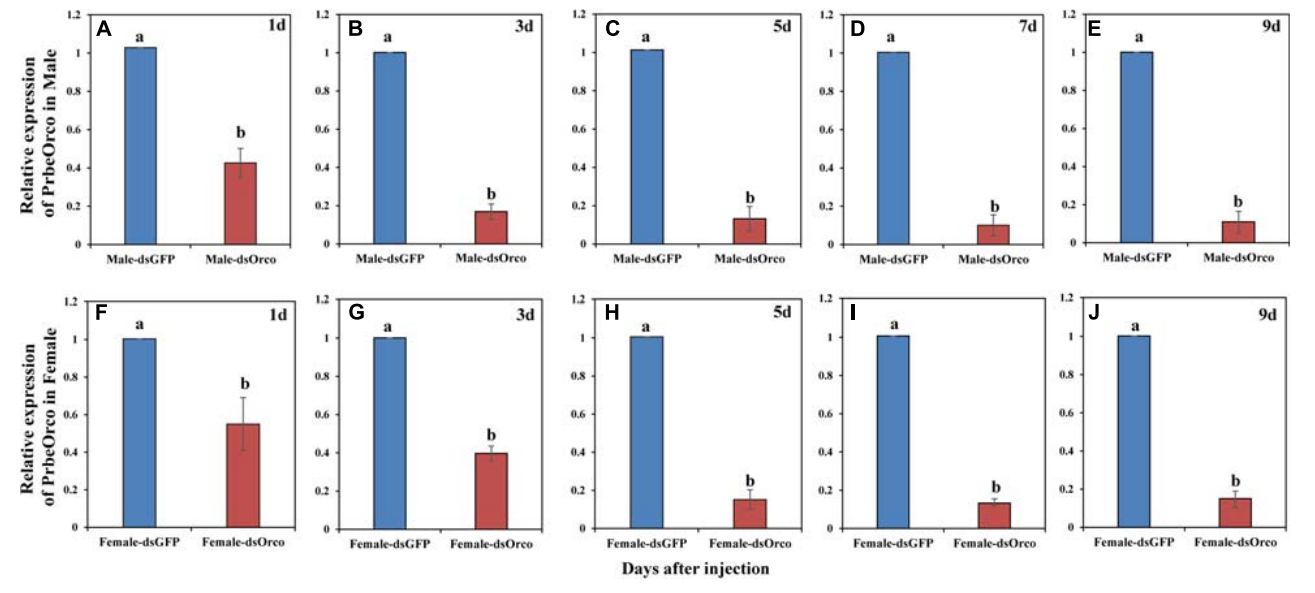

FIGURE 4 | Relative expression level of *PbreOrco* after dsRNA injection. **(A–E)** Relative expression of *PrbeOrco* in male. **(F–J)** Relative expression of *PrbeOrco* in female. The relative expression levels were normalized to the GADPH2 gene. And the expression of the corresponding dsGFP-injected as the calibrator in each image. Different letters represent significant difference ($P < 0.05$).

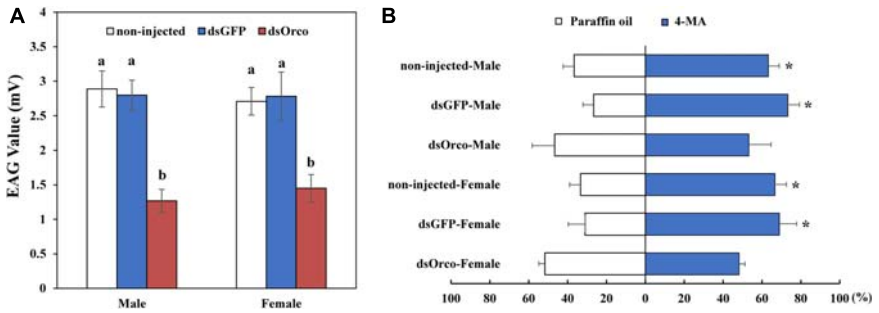

FIGURE 5 | Responses of *P. brevitarsis* to aggregation pheromone, 4-methylanisole (4-MA). **(A)** Electroantennographic (EAG) responses of dsOrco- injected dsGFP-injected and non-injected *P. brevitarsis* to 4-MA. **(B)** Behavioral response of *P. brevitarsis* to 4-MA in a Y-tube olfactometer. Different letters represent significant difference ($P < 0.05$).

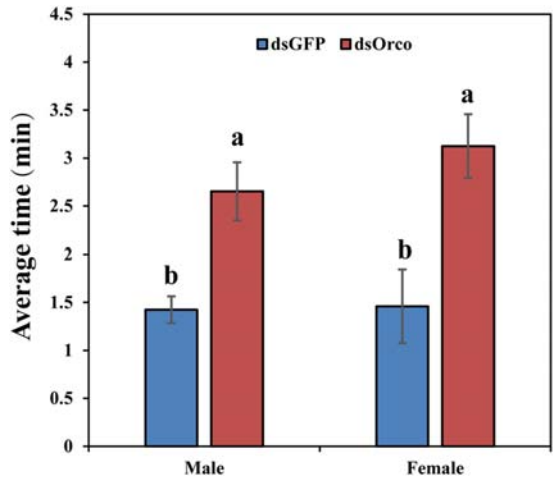

FIGURE 6 | Time required for food searching in dsGFP- and dsOrco-injected *P. brevitarsis*. Different letters represent significant difference ($P < 0.05$).

the aggregation pheromone. Compared with dsGFP-injected control, silencing *PbreOrco* almost halved the EAG responses of both female and male WSFCs to 4-methylanisole (**Figure 5A**) and significantly decreased the preference of WSFCs to 4-methylanisole in Y-tube (**Figure 5B**). Considering that *PbreOrco* expression was decreased by 90.94% (male) and 87.96% (female) at 7 days of post-injection (**Figure 4**), it was concluded that the impairment of response to the aggregation pheromone was closely related to the decrease of *PbreOrco* transcript abundance. This indicated that *PbreOrco* was involved in recognition of aggregation pheromone in WSFCs. Furthermore, we carried out cage assays to examine the influences of *PbreOrco* silencing on food-seeking abilities. The results revealed that silencing *PbreOrco* expression directly reduced the response rate and prolonged the response time, indicating that *PbreOrco* silencing significantly impaired olfactory signal-mediated host seeking behavior (**Figure 5**).

Recent studies documented that silencing Orco simultaneously deteriorated wing differentiation (Fan et al., 2015) and viability (Yang et al., 2016). These unexpected results generally occurred when dsRNA injection was performed at developmental stage (e.g., eggs, larvae, and pupae). The reasons for fewer side effects in injected WSFCs were presumably attributed to the injection at adult stage. Besides affecting olfactory-related behavior, silencing *Orco* at adult stage potentially influences the number of eggs laid, as well as oogenesis and embryogenesis (Libert et al., 2007; Trible et al., 2017; Ma et al., 2020). We did not evaluate the fecundity of injected WSFCs mainly because the life span and oviposition period are too long (>100 days in experimental condition) (Kim et al., 2018) to ensure the decrease of gene transcript abundance.

In summary, we identified the full-length sequence of *PbreOrco* in WSFCs and demonstrated that silencing *PbreOrco* would impair the abilities of WSFCs to detect pheromone and locate food. These results echo the theory about the mechanism of olfactory recognition and are beneficial to development of olfactory-based pest control strategies.

DATA AVAILABILITY STATEMENT

The original contributions presented in the study are included in the article/**Supplementary Material**, further inquiries can be directed to the corresponding author/s.

AUTHOR CONTRIBUTIONS

TZ designed the research. XZ, PL, QQ, and ML performed the experiments. QQ and RM analyzed the data. XZ, PL, and TZ wrote the manuscript. All authors have read and agreed to the published version of the manuscript.

FUNDING

This work was funded by HAAFS Agriculture Science and Technology Innovation Project (2019-1-2-2) and Hebei Province and HAAFS Research and Development Program (20326518D, 2018120304).

SUPPLEMENTARY MATERIAL

The Supplementary Material for this article can be found online at: https://www.frontiersin.org/articles/10.3389/fphys.2021.649590/full#supplementary-material

Supplementary Figure 1 | Electroantennographic (EAG) signal of injected *Protaetia brevitarsis*.

Supplementary Figure 2 | The percentage of individuals successfully find food within 20 min.

Supplementary Table 1 | Primers used in RNA interference and qRT-PCR.

Supplementary Table 2 | Sequences used in sequence alignment and phylogenetic tree.

Supplementary Video 1 | Location abilities of injected *Protaetia brevitarsis* to food.

REFERENCES

Asahina, K., Pavlenkovich, V., and Vosshall, L. B. (2008). The survival advantage of olfaction in a competitive environment. *Curr. Biol.* 18, 1153–1155. doi: 10.1016/j.cub.2008.06.075

Bolton, L. G., Piñero, J. C., and Barrett, B. A. (2019). Electrophysiological and behavioral responses of *Drosophila suzukii* (Diptera: Drosophilidae) towards the leaf volatile β-cyclocitral and selected fruit-ripening volatiles. *Environ. Entomol.* 48, 1049–1055. doi: 10.1093/ee/nvz092

Breer, H., Fleischer, J., Pregitzer, P., and Krieger, J. (2019). "Molecular mechanism of insect olfaction: olfactory receptors," in *Olfactory Concepts of Insect Control-Alternative to Insecticides*, ed. J. F. Picimbon (Cham: Springer), 93–114. doi: 10.1007/978-3-030-05165-5_4

Brito, N. F., Moreira, M. F., and Melo, A. C. (2016). A look inside odorant-binding proteins in insect chemoreception. *J. Insect Physiol.* 95, 51–65. doi: 10.1016/j.jinsphys.2016.09.008

Butterwick, J. A., Del Mármol, J., Kim, K. H., Kahlson, M. A., Rogow, J. A., Walz, T., et al. (2018). Cryo-EM structure of the insect olfactory receptor Orco. *Nature* 560, 447–452. doi: 10.1038/s41586-018-0420-8

Cai, H., Zhang, T., Su, Y., Wang, Z., Zhang, X., Wang, S., et al. (2020). Influence of trap color, type, and placement on capture efficacy for *Protaetia brevitarsis* (Coleoptera: Scarabaeidae). *J. Econ. Entomol.* 2:toaa259. doi: 10.1093/jee/toaa259

DeGennaro, M., McBride, C. S., Seeholzer, L., Nakagawa, T., Dennis, E. J., Goldman, C., et al. (2013). *orco* mutant mosquitoes lose strong preference for humans and are not repelled by volatile DEET. *Nature* 498, 487–491. doi: 10.1038/nature12206

Dong, K., Sun, L., Liu, J. T., Gu, S. H., Zhou, J. J., Yang, R. N., et al. (2017). RNAi-induced electrophysiological and behavioral changes reveal two pheromone binding proteins of *Helicoverpa armigera* involved in the perception of the main sex pheromone component Z11-16: Ald. *J. Chem. Ecol.* 43, 207–214. doi: 10.1007/s10886-016-0816-6

Fan, J., Zhang, Y., Francis, F., Cheng, D., Sun, J., and Chen, J. (2015). Orco mediates olfactory behaviors and winged morph differentiation induced by alarm pheromone in the grain aphid, *Sitobion avenae*. *Insect Biochem. Mol. Biol.* 64, 16–24. doi: 10.1016/j.ibmb.2015.07.006

Fleischer, J., Pregitzer, P., Breer, H., and Krieger, J. (2018). Access to the odor world: olfactory receptors and their role for signal transduction in insects. *Cell Mol. Life Sci.* 75, 485–508. doi: 10.1007/s00018-017-2627-5

Franco, T. A., Oliveira, D. S., Moreira, M. F., Leal, W. S., and Melo, A. C. (2016). Silencing the odorant receptor co-receptor RproOrco affects the physiology and behavior of the Chagas disease vector *Rhodnius prolixus*. *Insect Biochem. Mol. Biol.* 69, 82–90. doi: 10.1016/j.ibmb.2015.02.012

Harini, K., and Sowdhamini, R. (2012). Molecular modelling of oligomeric states of DmOR83b, an olfactory receptor in *D. Melanogaster*. *Bioinform. Biol. Insights* 6, 33–47. doi: 10.4137/BBI.S8990

Hopf, T. A., Morinaga, S., Ihara, S., Touhara, K., Marks, D. S., and Benton, R. (2015). Amino acid coevolution reveals three-dimensional structure and functional domains of insect odorant receptors. *Nat. Commun.* 6, 1–7. doi: 10.1038/ncomms70772015

Huvenne, H., and Smagghe, G. (2010). Mechanisms of dsRNA uptake in insects and potential of RNAi for pest control: a review. *J. Insect Physiol.* 56, 227–235. doi: 10.1016/j.jinsphys.2009.10.004

Ikeura, H., Murata, N., Sakura, A., Hayata, Y., and Kobayashi, F. (2012). Search for neem materials having repellent effect against green peach aphid (*Myzus persicae* Sulzer). *Acta Horticult*. 989, 97–102.

Joga, M. R., Zotti, M. J., Smagghe, G., and Christiaens, O. (2016). RNAi efficiency, systemic properties, and novel delivery methods for pest insect control: what we know so far. *Front. Physiol.* 7:553. doi: 10.3389/fphys.2016.00553

Jones, W. D., Nguyen, T. A., Kloss, B., Lee, K. J., and Vosshall, L. B. (2005). Functional conservation of an insect odorant receptor gene across 250 million years of evolution. *Curr. Biol.* 15, R119–R121. doi: 10.1016/j.cub.2005.02.007

Kim, S., Park, H. C., Kim, N., and Park, I. (2018). Effect of photoperiod and temperature on the reproductive responses of *Protaetia brevitarsis*. *Int. J. Ind. Entomol.* 37, 90–94.

Koutroumpa, F. A., Monsempes, C., François, M. C., de Cian, A., Royer, C., Concordet, J. P., et al. (2016). Heritable genome editing with CRISPR/Cas9 induces anosmia in a crop pest moth. *Sci. Rep* 6:29620. doi: 10.1038/srep29620

Krieger, J., Klink, O., Mohl, C., Raming, K., and Breer, H. (2003). A candidate olfactory receptor subtype highly conserved across different insect orders. *J. Comp. Physiol. A Neuroethol. Sens. Neural Behav. Physiol.* 189, 519–526. doi: 10.1007/s00359-003-0427-x

Kumar, S., Stecher, G., and Tamura, K. (2016). MEGA7: molecular evolutionary genetics analysis version 7.0 for bigger datasets. *Mol. Biol. Evol.* 33, 1870–1874. doi: 10.1093/molbev/msw054

Larsson, M. C., Domingos, A. I., Jones, W. D., Chiappe, M. E., Amrein, H., and Vosshall, L. B. (2004). Or83b encodes a broadly expressed odorant receptor essential for *Drosophila* olfaction. *Neuron* 43, 703–714. doi: 10.1016/j.neuron.2004.08.019

Leal, W. S. (2013). Odorant reception in insects: roles of receptors, binding proteins, and degrading enzymes. *Annu. Rev. Entomol.* 58, 373–391. doi: 10.1146/annurev-ento-120811-153635

Li, Y., Fu, T., Geng, L., Shi, Y., Chu, H., Liu, F., et al. (2019). *Protaetia brevitarsis* larvae can efficiently convert herbaceous and ligneous plant residues to humic acids. *Waste Manag.* 83, 79–82. doi: 10.1016/j.wasman.2018.11.010

Li, Y., Zhang, J., Chen, D., Yang, P. C., Jiang, F., Wang, X. H., et al. (2016). CRISPR/Cas9 in locusts: successful establishment of an olfactory deficiency line by targeting the mutagenesis of an odorant receptor co-receptor (Orco). *Insect Biochem. Mol. Biol.* 79, 27–35. doi: 10.1016/j.ibmb.2016.10.003

Libert, S., Zwiener, J., Chu, X., Vanvoorhies, W., Roman, G., and Pletcher, S. D. (2007). Regulation of *Drosophila* life span by olfaction and food-derived odors. *Science* 315, 1133–1137. doi: 10.1126/science.1136610

Lin, W., Yu, Y., Zhou, P., Zhang, J., Dou, L., Hao, Q., et al. (2015). Identification and knockdown of the olfactory receptor (OrCo) in Gypsy moth, *Lymantria dispar*. *Int. J. Biol. Sci.* 11, 772–780. doi: 10.7150/ijbs.11898

Liu, H., Zhang, X., Liu, C., Liu, Y., Mei, X., and Zhang, T. (2019). Identification and expression of candidate chemosensory receptors in the white-spotted flower chafer, *Protaetia brevitarsis*. *Sci. Rep.* 9:3339. doi: 10.1038/s41598-019-38896-x

Liu, X. M., Zhang, B. X., Li, S. G., Rao, X. J., Wang, D. M., Hu, X. X., et al. (2016). Knockdown of the olfactory co-receptor Orco impairs mate recognition in *Tenebrio molitor* (Coleoptera: Tenebrionidae). *J. Asia Pac. Entomol.* 19, 503–508. doi: 10.1016/j.aspen.2016.05.005

Livak, K. J., and Schmittgen, T. D. (2001). Analysis of relative gene expression data using real-time quantitative PCR and the $2-\Delta\Delta CT$ method. *Methods* 25, 402–408. doi: 10.1006/meth.2001.1262

Ma, C., Cui, S., Bai, Q., Tian, Z., Zhang, Y., Chen, G., et al. (2020). Olfactory co-receptor is involved in host recognition and oviposition in *Ophraella communa* (Coleoptera: Chrysomelidae). *Insect Mol. Biol.* 29, 381–390. doi: 10.1111/imb.12643

Miller, S. C., Miyata, K., Brown, S. J., and Tomoyasu, Y. (2012). Dissecting systemic RNA interference in the red flour beetle *Tribolium castaneum*: parameters affecting the efficiency of RNAi. *PLoS One* 7:e47431. doi: 10.1371/journal.pone.0047431

Missbach, C., Dweck, H. K., Vogel, H., Vilcinskas, A., Stensmyr, M. C., Hansson, B. S., et al. (2014). Evolution of insect olfactory receptors. *Elife* 3:e02115. doi: 10.7554/eLife.02115

Neuhaus, E. M., Gisselmann, G., Zhang, W., Dooley, R., Störtkuhl, K., and Hatt, H. (2005). Odorant receptor heterodimerization in the olfactory system of *Drosophila melanogaster*. *Nat. Neurosci.* 8, 15–17. doi: 10.1038/nn1371

Rebijith, K. B., Asokan, R., Hande, H. R., Kumar, N. K., Krishna, V., Vinutha, J., et al. (2016). RNA interference of odorant-binding protein 2 (OBP2) of the cotton aphid, *Aphis gossypii* (Glover), resulted in altered electrophysiological responses. *Appl. Biochem. Biotechnol.* 178, 251–266. doi: 10.1007/s12010-015-1869-7

Sato, K., and Touhara, K. (2008). "Insect olfaction: receptors, signal transduction, and behavior," in *Chemosensory Systems in Mammals, Fishes, and Insects*, eds M. Wolfgang and K. Sigrun (Berlin: Springer), 203–220. doi: 10.1007/400_2008_10

Smart, R., Kiely, A., Beale, M., Vargas, E., Carraher, C., Kralicek, A. V., et al. (2008). *Drosophila* odorant receptors are novel seven transmembrane domain proteins that can signal independently of heterotrimeric G proteins. *Insect Biochem. Mol. Biol.* 38, 770–780. doi: 10.1016/j.ibmb.2008.05.002

Stengl, M., and Funk, N. W. (2013). The role of the coreceptor Orco in insect olfactory transduction. *J. Comp. Physiol. A Neuroethol. Sens. Neural Behav. Physiol.* 199, 897–909. doi: 10.1007/s00359-013-0837-3

Suo, Z., Bai, M., Li, S., Yang, H., Li, T., and Ma, D. (2015). A geometric morphometric analysis of the morphological variations among Chinese populations of *Protaetia brevitarsis* (Coleoptera: Scarabaeidae) with an inference of the invading source of its Xinjiang populations. *Acta Entomol. Sin.* 58, 408–418.

Trible, W., Olivos-Cisneros, L., McKenzie, S. K., Saragosti, J., Chang, N. C., Matthews, B. J., et al. (2017). *Orco* mutagenesis causes loss of antennal lobe glomeruli and impaired social behavior in ants. *Cell* 170, 727–735.e10. doi: 10.1016/j.cell.2017.07.001

Wang, K., Li, P., Gao, Y., Liu, C., Wang, Q., Yin, J., et al. (2019). De novo genome assembly of the white-spotted flower chafer (*Protaetia brevitarsis*). *Gigascience* 8:giz019. doi: 10.1093/gigascience/giz019

Wang, Q., Wang, Q., Zhou, Y. L., Shan, S., Cui, H. H., Xiao, Y., et al. (2018). Characterization and comparative analysis of olfactory receptor co-receptor Orco orthologs among five Mirid bug species. *Front. Physiol.* 9:158. doi: 10.3389/fphys.2018.00158

Wicher, D., Schäfer, R., Bauernfeind, R., Stensmyr, M. C., Heller, R., Heinemann, S. H., et al. (2008). *Drosophila* odorant receptors are both ligand-gated and cyclic-nucleotide-activated cation channels. *Nature* 452, 1007–1011. doi: 10.1038/nature06861

Xu, J., Yuan, Z., Liu, Z., Liu, H., Guo, W., Tuersun, A., et al. (2009). A study on host, distribution and occurrence pattern of *Protaetia brevitarsis* Lewis in Xinjiang. *Xinjiang Agric. Sci.* 46, 1042–1046.

Yang, B., Fujii, T., Ishikawa, Y., and Matsuo, T. (2016). Targeted mutagenesis of an odorant receptor co-receptor using TALEN in *Ostrinia furnacalis*. *Insect Biochem. Mol. Biol.* 70, 53–59. doi: 10.1016/j.ibmb.2015.12.003

Yang, S., Mei, X. D., Zhang, X. F., Li, Y. F., She, D., Zhang, T., et al. (2017). Attraction of coffee bean weevil, *Araecerus fasciculatus*, to volatiles from the industrial yeast *Kluyveromyces lactis*. *J. Chem. Ecol.* 43, 180–187. doi: 10.1007/s10886-016-0809-5

Yang, Y., Krieger, J., Zhang, L., and Breer, H. (2012). The olfactory co-receptor Orco from the migratory locust (*Locusta migratoria*) and the desert locust (*Schistocerca gregaria*): identification and expression pattern. *Int. J. Biol. Sci.* 8, 159–170. doi: 10.7150/ijbs.8.159

Zhang, R., Gao, G., and Chen, H. (2016). Silencing of the olfactory co-receptor gene in *Dendroctonus armandi* leads to EAG response declining to major host volatiles. *Sci. Rep.* 6:23136. doi: 10.1038/srep23136

Zhang, T., Mei, X., Zhang, X., Lu, Y., Ning, J., and Wu, K. (2020). Identification and field evaluation of the sex pheromone of *Apolygus lucorum* (Hemiptera: Miridae) in China. *Pest. Manag. Sci.* 76, 1847–1855. doi: 10.1002/ps.5714

Zhang, T., Zhang, X. F., Liu, P. J., Liu, Y. Q., Mei, X. D., and Wang, Z. Y. (2019). *The Aggregation Pheromone of Protaetia Brevitaris and its Application*. Chinese Patent. CN 201910806317.7.

Zhao, R. G., and Chen, R. Z. (2008). General characteristics of white-spotted flower chafer, *Protaetia brevitaris* in China. *China Plant Prot*. 28, 10–20.

Zhou, J. J. (2010). "Odorant-binding proteins in insects," in *Vitamins & Hormones*, Vol. 83, ed. G. Litwack (Cambridge, MA: Academic Press), 241–272. doi: 10.1016/S0083-6729(10)83010-9

Zhou, Y. L., Zhu, X. Q., Gu, S. H., Cui, H. H., Guo, Y. Y., Zhou, J. J., et al. (2014). Silencing in *Apolygus lucorum* of the olfactory coreceptor Orco gene by RNA interference induces EAG response declining to two putative semiochemicals. *J. Insect Physiol.* 60, 31–39. doi: 10.1016/j.jinsphys.2013.10.006

Zuckerkandl, E., and Pauling, L. (1965). "Evolutionary divergence and convergence in proteins," in *Evolving Genes and Proteins*, eds V. Bryson and H. J. Vogel (New York, NY: Academic Press), 97–166. doi: 10.1016/B978-1-4832-2734-4.50017-6

Conflict of Interest: The authors declare that the research was conducted in the absence of any commercial or financial relationships that could be construed as a potential conflict of interest.

frontiers in Physiology

ORIGINAL RESEARCH
published: 20 April 2021
doi: 10.3389/fphys.2021.661310

Comparison and Functional Analysis of Chemosensory Protein Genes From *Eucryptorrhynchus scrobiculatus* Motschulsky and *Eucryptorrhynchus brandti* Harold

*Qian Wang, Xiaojian Wen, Yi Lu and Junbao Wen**

Beijing Key Laboratory for Forest Pests Control, College of Forestry, Beijing Forestry University, Beijing, China

The tree-of-heaven root weevil (*Eucryptorrhynchus scrobiculatus*) and the tree-of-heaven trunk weevil (*Eucryptorrhynchus brandti*) are closely related species that monophagously feed on the same host plant, the *Ailanthus altissima* (Mill) Swingle, at different locations. However, the mechanisms of how they select different parts of the host tree are unclear. As chemosensory systems play important roles in host location and oviposition, we screened candidate chemosensory protein genes from the transcriptomes of the two weevils at different developmental stages. In this study, we identified 12 candidate chemosensory proteins (CSPs) of *E. scrobiculatus* and *E. brandti*, three EscrCSPs, and one EbraCSPs, respectively, were newly identified. The qRT-PCR results showed that EscrCSP7/8a/9 and EbraCSP7/8/9 were significantly expressed in adult antennae, while EscrCSP8a and EbraCSP8 shared low sequence identity, suggesting that they may respond to different odorant molecule binding. Additionally, EbraCSP6 and EscrCSP6 were mainly expressed in antennae and proboscises and likely participate in the process of chemoreception. The binding simulation of nine volatile compounds of the host plant to EscrCSP8a and EbraCSP8 indicated that (1R)-(+)-alpha-pinene, (–)-beta-caryophyllene, and beta-elemen have higher binding affinities with EscrCSP8a and lower affinities with EbraCSP8. In addition, there were seven, two, and one EbraCSPs mainly expressed in pupae, larvae, and eggs, respectively, indicating possible developmental-related roles in *E. brandti*. We screened out several olfactory-related possible CSP genes in *E. brandti* and *E. scrobiculatus* and simulated the binding model of CSPs with different compounds, providing a basis for explaining the niche differentiation of the two weevils.

Keywords: *Eucryptorrhynchus scrobiculatus*, *Eucryptorrhynchus brandti*, transcriptome, chemosensory proteins, structure modeling, binding simulation

OPEN ACCESS

Edited by:
Xiaojiao Guo,
Institute of Zoology (CAS), China

Reviewed by:
Sufang Zhang,
Environment and Protection Chinese Academy of Forestry, China
Huahua Sun,
Duke University, United States

****Correspondence:***
Junbao Wen
wenjb@bjfu.edu.cn

Specialty section:
This article was submitted to Invertebrate Physiology, a section of the journal Frontiers in Physiology

Received: *30 January 2021*
Accepted: *15 March 2021*
Published: *20 April 2021*

Citation:
Wang Q, Wen X, Lu Y and Wen J (2021) Comparison and Functional Analysis of Chemosensory Protein Genes From Eucryptorrhynchus scrobiculatus Motschulsky and Eucryptorrhynchus brandti Harold. Front. Physiol. 12:661310. doi: 10.3389/fphys.2021.661310

INTRODUCTION

Most animals are strongly dependent on their chemosensory systems, which play an important role in detecting and receiving signals from the external environment to orient the animal in space. For insects, there are two chemosensory systems: olfaction and gustation (Stocker, 1994). The chemical signals, such as pheromones secreted by other insect individuals and plant volatiles,

are accepted by insects for regulating behavioral and physiological activities. There are several kinds of chemosensory genes participating in this process in insects: odorant-binding proteins (OBPs), chemosensory proteins (CSPs), odorant receptors (ORs), gustatory receptors (GRs), ionotropic receptors (IRs), sensory neuron membrane proteins (SNMPs), and odorant-degrading enzymes (ODEs) (Sanchez-Gracia et al., 2009; Leal, 2013).

OBPs and CSPs are both acidic, soluble proteins with a similar structure that binds to small organic compounds (Angeli et al., 1999; Pelosi et al., 2006), which is considered an important feature for odorant molecule binding. Relatively, the evolution of CSPs is more conservative and ancient than OBPs (Picimbon et al., 2000; Sanchez-Gracia et al., 2009). Since being detected in the regenerating legs of *Periplaneta americana* as the p10 protein (Nomura et al., 1992), members of the CSP family have been discovered in *Drosophila melanogaster* antennae (Mckenna et al., 1994) and *Cactoblastis cactorum* (Maleszka and Stange, 1997). They were later given the name chemosensory proteins because of the detection in antennal chemosensilla of *Schistocerca gregaria* (Angeli et al., 1999). As more CSPs were identified in different insects, their different functions were proven in various aspects. In addition to the role CSPs play in chemoreception, they also possess other functions in development (Maleszka et al., 2007), transport of pheromones from the cytoplasm to peripheral cell membranes (Emmanuelle et al., 2001), oviposition (Zhou et al., 2013), and elimination of xenobiotics (Xuan et al., 2015). Emmanuelle et al. (2001) suggested that CSPs may bind various hydrophobic small molecules in a non-specific manner. However, the mechanisms of the molecular functions of CSPs are still not clear, and there were only three 3-D structures of CSPs that have been identified (Lartigue et al., 2002; Tomaselli et al., 2006; Jansen et al., 2007). Despite the functional diversity of CSPs, most attention has focused on the function of chemoreception. Additionally, many CSPs have been shown to have high expression levels in the chemosensilla of various insect species, binding to specific plant volatiles and pheromones (Dani et al., 2011; Qiao et al., 2013; Younas et al., 2018; Ali et al., 2019; Waris et al., 2019; Fu et al., 2020), and indicating the importance of CSPs in chemoreception. For a more comprehensive discussion, the chemoreception role of CSPs should be considered when investigating the chemosensory process of insects.

In consideration of the importance of chemosensory systems for insect host location and oviposition, we aimed to investigate the differences in CSPs between two closely related species, the tree-of-heaven root weevil (TRW; *Eucryptorrhynchus scrobiculatus* Motschulsky) and tree-of-heaven trunk weevil (TTW; *E. brandti* Harold; Coleoptera: Curculionidae) to provide a basis for their feeding location differences. The two weevils are important forestry pests that monophagously feed on *Ailanthus altissima* (Mill) Swingle and its variants, weakening trees and even causing death when infestation persists (Sun et al., 1990). Notably, while feeding on the same host plants, the feeding and oviposition locations differ between the two weevils. TTW adults lay eggs in the trunk of the host tree, and the larvae subsequently complete their whole development in the trunk, feeding on the phloem and xylem. In contrast, TRW lay eggs around the roots at the surface of the soil, and the larvae feed on the host roots. Additionally, TTW adults feed on stems, while TRW feed on the twigs, buds, and petioles (Yugong et al., 1994; Yu, 2013; Ji et al., 2017). However, there are few studies on the biochemical mechanisms of how the weevils find their host plants and the differences in their foraging behavior.

Wen et al. (2018) identified some putative chemosensory genes from the antennal transcriptome of TTW and TRW, but without verification of the CSP expression levels in different tissues and developmental stages. Since there is functional diversity and wide CSP expression in different tissues, as well as the existence of chemosensilla in many parts of insects, the screening of CSPs should be more comprehensive, rather than limited to antennae, to distinguish different functional CSPs. In this study, we screened candidate CSPs from the transcriptomes of eggs, larvae, pupae, and adults of both species to preliminarily distinguish the developmental stage- and tissue-specific CSP genes and identify the potential CSPs playing roles in chemoreception. The results may reveal chemosensing-related CSPs and the differences between the two species, which may provide a basis for explaining the niche differentiation in the two weevils.

MATERIALS AND METHODS

Insect Collection and RNA Extraction

The transcriptome of different stages of TRW (accession number: PRJNA689057) were already sequenced by Wu et al. (2016), so we prepared samples for the RNA sequencing of TTW in this study. TTW adults, larvae, pupae, and TRW adults were collected from the Pingluo County, Ningxia Autonomous Region, China. About 100 of the TTW adults were being reared at the Forest Protection Laboratory of Beijing Forestry University for oviposition. Each pair of adults (a male and female) was fed with *A. altissima* sticks in a plastic box with a diameter of 3.5 cm at $25 \pm 1^{\circ}$C and $75 \pm 1\%$ relative humidity. Two-day-old eggs of TTW were removed with a fine brush and placed on a Petri dish lined with soaked filter paper, in preparation for RNA extraction. The fifth-instar larvae were selected for RNA extraction because of their strong foraging ability. Total RNA of a single adult, single 4-day pupa, single fifth-instar larva, and 40 eggs was extracted with the RNApure Total RNA Kit (Aidlab, Beijing, China). The total RNA of 40 pairs of antennae, 40 proboscises, 10 heads (without antennae and proboscises), two groups of legs (one included a pair of forelegs, midlegs, and hindlegs), and one abdomen (without thorax) was extracted with the methods above. Three biological repetitions were used for all RNA extractions.

cDNA Library Construction and Sequencing

RNA concentration and purification were assessed by a Nanodrop 8000 spectrophotometer (Thermo, Waltham, MA, USA) and Agilent 2100 Bioanalyzer System (Agilent Technologies, USA). mRNAs were enriched using oligo (dT) magnetic beads and then cut into short fragments as templates for first-strand cDNA synthesis. Subsequently, second-strand

cDNA was synthesized with dNTPs and DNA polymerase I based on first-strand cDNA. After purification with AMPure XP beads, cDNA libraries were enriched by PCR. The quantity and quality of the cDNA library components were detected by Qubit2.0, Agilent2100, and Q-PCR methods.

Assembly and Unigene Annotation

High-quality cDNA libraries were sequenced on an Illumina HiSeq X-Ten platform. Clean reads were obtained by removing linker sequences and low-quality fragments from raw data. The clean reads were assembled into unigenes by Trinity software (Grabherr et al., 2013).

Unigene annotation was performed by BLAST software (Altschul et al., 1997) searching against NR (NCBI Non-Redundant), Swiss-Prot (M. Kanehisa et al., 2004), GO (Gene Ontology) (Sherlock, 2009), COG/KOG (Cluster of Orthologous Groups/euKaryotic Ortholog Groups) (Tatusov et al., 2000), and KEGG (Kyoto Encyclopedia of Genes and Genomes) (Kanehisa et al., 2004) databases. The orthologs of unigenes were obtained using KOBAS 2.0 (Xie et al., 2011) against the KEGG database. Annotation with the Pfam (Finn et al., 2016) database was obtained after predicting the complete amino acid sequences of unigenes.

Candidate Chemosensory Protein Gene Identification and Phylogenetic Analysis

For CSPs belonging to the OS-D family, we downloaded the Hidden Markov model of the conservative domain of this family (Pfam: 03392) from the Pfam database, comparing the protein sequences files of transcriptomes with screen proteins that contained this domain. The candidate CSP genes were then verified using BLASTx and BLASTn programs with the NR database of the National Center for Biotechnology Information (NCBI) with a cutoff E-value of 1e−5. The open reading frames (ORFs) of candidate EbraCSPs and EscrCSPs were identified using the ORF Finder (https://www.ncbi.nlm.nih.gov/orffinder/) and confirmed by the BLASTp program of NCBI. The putative N-terminal signal peptides of candidate CSPs were predicted using the SignalP 4.1 server version (http://www.cbs.dtu.dk/services/SignalP-4.1/) with default parameters.

The alignment of candidate EbraCSPs and EscrCSPs was detected by online BLASTp (https://blast.ncbi.nlm.nih.gov/Blast.cgi) to define the sequence identities of CSP genes between the two weevils, as well as between the antennae and whole body. A neighbor-joining phylogenetic tree of these genes was constructed using MEGA 6.0 software with default settings and 1,000 bootstrap replicates. The iTOL online server (Letunic and Bork, 2019) was used to modify the appearance of the tree. The protein sequences contained in the phylogenetic tree are shown in **Supplementary Table 1**.

Expression Analysis by qRT-PCR

Five tissues (antennae, head without antennae and proboscises, proboscis, legs, and abdomen without thorax) of male and female adults were separately dissected on ice, and the RNA was extracted immediately using the RNApure Total RNA Kit (Aidlab, Beijing, China). The RNA of eggs, fifth-instar larvae, and pupae was extracted as previously described, and the instar of the larvae was distinguished as described by Luo et al. (2016). Due to the difficulty in obtaining larvae and pupae samples of TRW, only the expression of CSPs in different developmental stages of TTW was detected. The cDNA was synthesized using the TRUEscript 1st Strand cDNA synthesis Kit (Aidlab, Beijing, China). Primer3Plus online software (http://www.bioinformatics.nl/cgi-bin/primer3plus/primer3plus.cgi) was employed to design the gene-specific primers. RPS11 and UBC were both used as reference genes between different stages of TTW, while RPS11 and α-Tublin was used as a reference gene in different tissues of TTW and TRW adults, respectively. Primer sequences are shown in **Supplementary Table 2**. The qRT-PCR reactions were performed on a CFX96 Real-Time PCR Detection System with TB Green Premix Ex Taq II (Takara, Beijing, China). Cycling parameters were 95°C for 30 s, followed by 40 cycles of 95°C for 5 s and 60°C for 30 s. The relative expression levels of CSP genes were calculated using the $2^{-\Delta\Delta Ct}$ method (Pfaffl, 2001) and analyzed using GraphPad Prism 5.0 (GraphPad Software, La Jolla, CA, United States) with a one-way analysis of variance (ANOVA), followed by Duncan's test ($\alpha = 0.05$).

Structure Modeling and Secondary Structure Prediction

Until now, only three 3-D structures of CSPs had been identified, so we aligned the ORFs of EbraCSP8 and EscrCSP8a to the three gene sequences to define their homology, for selecting the best modeling template. The secondary structure of the two genes were predicted on ESPript 3.0 (Robert and Gouet, 2014) after alignment. To obtain the best model, the homology modeling of EbraCSP8 and EscrCSP8 was performed using the Swiss-Model (https://swissmodel.expasy.org) and ModWeb (https://modbase.compbio.ucsf.edu/modweb/), respectively. *Schistocerca gregaria* CSPsg4 (PDB: 2GVS) was used as a template for EbraCSP8, while *Mamestra brassicae* CSPMbraA6 (PDB: 1N8V) was used for EscrCSP8a because of the high sequence similarities (**Supplementary Table 3**). The generated models were verified separately by Procheck (Laskowski et al., 1992), Verify-3D (Bowie et al., 1991), and Errat (Colovos and Yeates, 1993). The UCSF Chimera (Pettersen et al., 2004) software was used to adjust the coordinate and torsion angle of residues to meet the detection standards of these platforms. The alignment of corrected structures and root mean square deviation (RMSD) of aligned residues were calculated on the PyMOL software.

Binding Site Prediction and Molecular Docking of the Ligand

Because of the differences in feeding preference of the two weevils, we selected the volatiles from different locations on *Ailanthus altissima* (Mill) Swingle according to Wen (2019). The nine compounds used for docking simulation were 1-hexanol (CAS number: 111-27-3), cis-3-hexen-1-ol (CAS number: 928-96-1), hexenyl acetate (CAS number: 3681-71-8), 2-tert-butyloxirane (CAS number: 2245-30-9), 2,5-diethylphenol (CAS number: 876-20-0), alpha-farnesene (CAS

number: 502-61-4), (1R)-(+)-alpha-pinene (CAS number: 7785-70-8), (−)-beta-caryophyllene (CAS number: 87-44-5), and beta-elemen (CAS number: 515-13-9). The 3-D compound structures were downloaded from the PubChem platform (https://pubchem.ncbi.nlm.nih.gov). The binding pockets were calculated using the online sever of DoGSiteScorer (https://proteins.plus) considering both the pocket properties and druggability. Molecular docking of EbraCSP8 and EscrCSP8a with different compounds was performed using Autodock 4.2 software. Hydrogens were added, while water was deleted for macromolecules and ligands before docking. Combining the parameters of binding sites of template proteins, as well as the calculated pockets of the online sever, the grid box was set at the pocket EbraCSP8_P2 (**Supplementary Figure 1A**) of EbraCSP8 and EscrCSP8a_P1 (**Supplementary Figure 1B**) of EscrCSP8a. Before docking simulation, the structures were energy minimized on the UCSF Chimera software using default parameters. The grid Nice Level was set to 20, and the default search parameters and docking parameters were used for docking. Furthermore, the ligands were combined with CSPsg4 and CSPMbraA6 in previous studies (Campanacci et al., 2003; Tomaselli et al., 2006), named oleamide and 12-bromo-1-dodecanol, and were docked with EbraCSP8 and EscrCSP8a, respectively, under the same parameters as a control. Finally, the hydrophobic contacts and hydrogen bonds were analyzed using LigPlot+ software (Laskowski and Swindells, 2011), and the contacts were drawn with PyMOL software.

RESULTS

Sequencing and Assembly of the Tree-of-Heaven Trunk Weevil Transcriptome

In this study, we extracted the total RNA from the eggs, larvae, pupae, and adults of TTW, and three repetitions were performed on each stage. Twelve cDNA libraries were constructed using the Illumina HiSeq X-Ten sequencing platform. After linkers and low-quality fragments were removed from the raw reads, we obtained 22.37 (adults), 21.91 (pupae), 21.2 (larvae), and 21.94 (eggs) million clean reads from TTW, and the percentages of clean reads were 97.03% (adults), 97.05% (pupae), 96.41% (larvae), and 95.59% (eggs). The GC content, Q20 (%), Q30 (%), and alignment ratio of all groups are given in **Supplementary Table 4**. All these clean reads were assembled into 119,489 unigenes with an average length of 587 bp, 36.97% GC content, and a 927-bp N50 value. Additionally, 14,178 transcripts were obtained with an average length of 701 bp, a GC content of 37.20%, and an N50 of 1,544 bp (**Table 1**). The datasets of the transcriptomes in this study were uploaded to the Sequence Read Archive (SRA) (accession number: PRJNA688600).

TABLE 1 | An overview of the transcriptome sequencing and assembly of *Eucryptorrhynchus brandti* at different developmental stages.

	Unigenes	Transcripts
Total Seq Num	119,489	140,178
Total Seq Len	70,154,969	98,340,633
Max Len	30,241	30,241
Min Len	201	201
Average Len	587	701
GC (%)	36.97	37.20
N50	927	1,544

Identification of Chemosensory Protein Genes in Tree-of-Heaven Trunk Weevil and Tree-of-Heaven Root Weevil

BLASTn and BLASTx analyses revealed 12 candidate CSPs in TTW and TRW. According to the sequence identities of CSPs from antennae and whole-body transcriptomes of the two weevils, we found three more candidate EscrCSPs (EscrCSP8a, EscrCSP10a, and EscrCSP13) and one more EbraCSPs (EbraCSP13) than those reported by Wen et al. (2018). All candidate CSP sequences included full-length ORFs and shared high identities (50–90%) with CSPs of other Coleopteran insects (**Supplementary Table 5**).

The alignment of candidate EbraCSPs and EscrCSPs of the whole-body transcriptome revealed that 11 orthologous pairs shared high amino acid identities (≥88.39%) between TTW and TRW, respectively, except EbraCSP8 and EscrCSP8a (identity = 46.83%) (**Supplementary Table 6**). From the phylogenetic analysis, EbraCSPs and EscrCSPs were distributed in different clades; thus, no TTW- and TRW-specific CSPs were found (**Figure 1**), except that the sequences with high identities appeared in pairs. Furthermore, the genetic distance of CSPs in the phylogenetic tree indicated their low divergence among different insect species, which is consistent with the highly conserved characteristics of CSPs.

Relative Expression of EbraCSPs and EscrCSPs by qRT-PCR

All 12 potential EbraCSPs identified from the transcriptome of TTW were differentially expressed in the four stages. There were four EbraCSPs (EbraCSP4, 6, 7, and 8) that showed high expression levels in adults, and seven EbraCSPs (EbraCSP1, 3, 4, 9, 10, 11, and 12) were mainly expressed in pupae. One (EbraCSP5) was highly expressed in larvae, and one (EbraCSP13) had a higher expression level in eggs than other stages. The relative expression profiles of EbraCSPs in different developmental stages were consistent with the fragments per kilobase of transcript per million mapped read (FPKM) values of transcriptomes (**Figure 2**).

According to the relative expression profiles of EbraCSPs and EscrCSPs in different tissues of male and female adults by qRT-PCR, we found three EbraCSPs (EbraCSP7, 8, and 9) and EscrCSPs (EscrCSP7, 8a, and 9) that were specifically expressed in antennae. EscrCSP7, EbraCSP8, and Ebra/EscrCSP9 had significantly higher expression levels in male antennae than female, and EbraCSP7 had a higher expression level in female antennae. EscrCSP6 showed a high expression level in the proboscis, while EbraCSP6 was higher in the antennae, proboscises, and legs. Additionally, Ebra/EscrCSP5

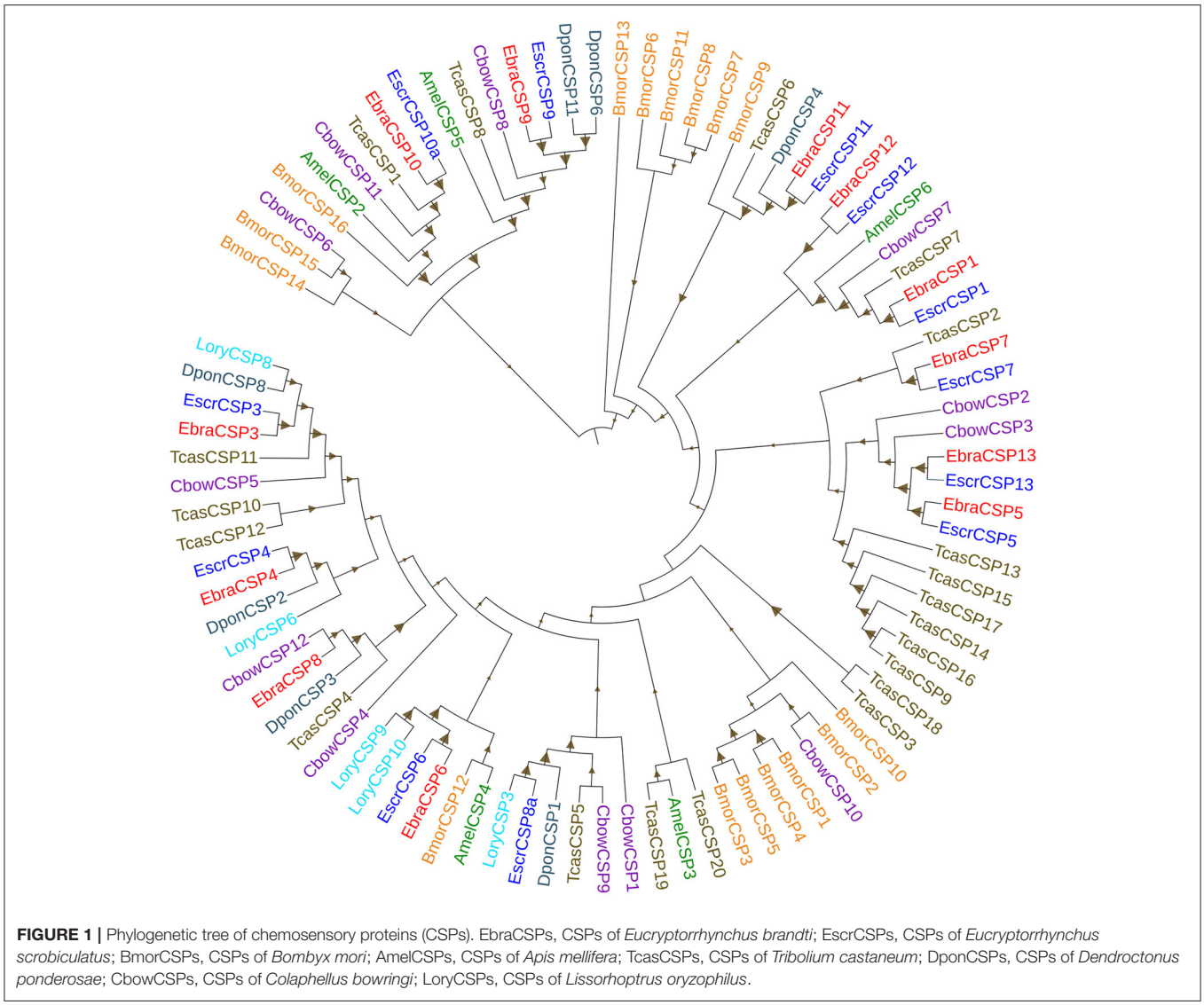

FIGURE 1 | Phylogenetic tree of chemosensory proteins (CSPs). EbraCSPs, CSPs of *Eucryptorrhynchus brandti*; EscrCSPs, CSPs of *Eucryptorrhynchus scrobiculatus*; BmorCSPs, CSPs of *Bombyx mori*; AmelCSPs, CSPs of *Apis mellifera*; TcasCSPs, CSPs of *Tribolium castaneum*; DponCSPs, CSPs of *Dendroctonus ponderosae*; CbowCSPs, CSPs of *Colaphellus bowringi*; LoryCSPs, CSPs of *Lissorhoptrus oryzophilus*.

and Ebra/EscrCSP12 were more highly expressed in the adult abdomen than other tissues (**Figures 3**, **4**). Notably, EbraCSP7/8/9 possessed a low expression level in adults but a high level in adult antennae, which may have been caused by a technical issue in which one pair of antennae of a single adult was not enough to extract sufficient amounts of RNA.

Structure Modeling and Secondary Structure Prediction

Notably, EbraCSP8 and EscrCSP8a were both specifically expressed in antennae but with low sequence identity, indicating different affinities with different volatile compounds. Therefore, we clarified the binding features of the EbraCSP8 and EscrCSP8a. Both the ORFs of EbraCSP8 and EscrCSP8a contained 137 amino acid residues with a signal peptide at the N-terminal region from 1 to 17 residues. The generated model of EbraCSP8 was consist with residues 23–126 (104 aa), while that of EscrCSP8a was consistent with residues 27–129 (103 aa). The qualities of the two models met the detection standards of Procheck, Verify-3D, and Errat. There were six α-helices in both the predicted 2D and 3D structures of the two genes shown as α1 (Ile13-His18 of EbraCSP8, Val13-Ala18 of EscrCSP8), α2 (Asp20-Leu31 of EbraCSP8, Asn20-Leu30 of EscrCSP8), α3 (Gly42-Ala54 of EbraCSP8, Thr38-Thr53 of EscrCSP8), α4 (Asp62-Asn78 of EbraCSP8, Ala60-Arg76 of EscrCSP8), α5 (Pro80-Tyr90 of EbraCSP8, Arg78-Tyr88 of EscrCSP8), and α6 (Gln98-Leu101 of EbraCSP8, Gln95-Asp102 of EscrCSP8) (**Figure 5**). However, the presence of a proline at position 50 caused a distortion in helix α3 (Gly42-Ala54) of EbraCSP8, which also occurred in the template *Schistocerca gregaria CSPsg4* (Tomaselli et al., 2006). Similar to template 1N8V and 2GVS, there were two V-shaped motifs in EbraCSP8 and EscrCSP8a, formed by the helix α1 with α2 and helix α4 with α5, respectively, while α3 ran across the two Vs, and α6 covered at the external surface. The root mean squared error (RMSD) between structures of EbraCSP8 and EscrCSP8a was 2.622 based on the 96 aligned atoms.

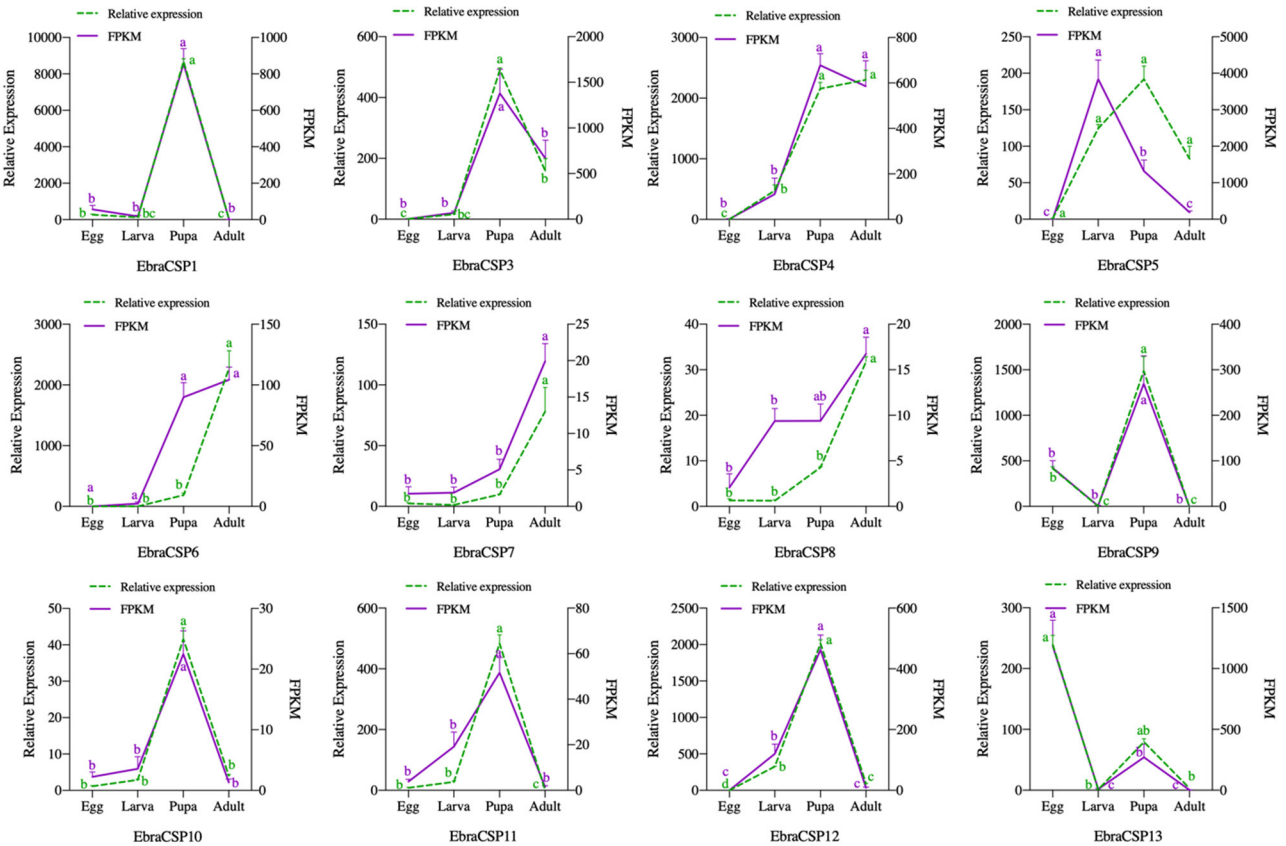

FIGURE 2 | Relative expression levels and fragments per kilobase of transcript per million mapped reads (FPKM) values of EbraCSPs in different developmental stages. Relative expression was calculated using the $2^{-\Delta\Delta Ct}$ method in the RT-qPCR experiment. FPKM values were obtained from fragments per kilobase of transcript per million mapped reads. The bar represents the standard error, and the small letters (a–d) above each bar indicate significant differences ($P < 0.05$).

Binding Sites and Molecular Docking of Ligands

The pocket parameters of EbraCSP8 and EscrCSP8 calculated by the DoGSiteScorer platform, are provided in **Supplementary Table 7**. There were six predicted pockets in the 3-D structure of EbraCSP8, and all pockets were extended to the protein surface. Notably, the second largest pocket (EbCSP8_P2, **Figure 6A**) with a volume of 306.82 Å^3 showed site similarity with the conserved cavity of the template *Schistocerca gregaria* CSPsg4 (Tomaselli et al., 2006). In contrast, the conserved cavity of CSPsg4 was internally closed, but the pocket of EbraCSP8 was partly extended to the protein surface. Additionally, other predicted pockets had little reference significance for docking because of their deviation from the cavity enclosed by the six helices. The grid box was set at the site of the pocket EbCSP8_P2 for ligand binding of EbraCSP8. The nine compounds selected above docked at the preset site with different binding energy (**Figure 7**). 1-Hexanol, cis-3-hexen-1-ol, hexenyl acetate, 2-tert-butyloxirane, 2,5-diethylphenol, and alpha-farnesene docked to EbraCSP8 with binding energy values of −4.87 to −2.85 kcal/mol. However, the binding energy of (1R)-(+)-alpha-pinene, (−)-beta-caryophyllene, and beta-elemen to EbraCSP8 was higher with values from −0.08 to 10.35 kcal/mol. The oleamide, which was the main endogenous ligand of *Locusta migratoria* was used as a ligand to analyze the key residues for the binding of CSPsg4 and showed a binding energy value of 4.23 kcal/mol with EbraCSP8. CSPs of different species can have different functions; therefore, the ligands of CSPsg4 may not combine well with EbraCSP8. As higher energy intimates a more difficult binding process of ligands to proteins, the other compounds may combine with EbraCSP8 easier than the three alkenes. Furthermore, the compounds that may combine with EbraCSP8 mainly rely on the hydrophobic contacts and hydrogen bonds, while 1-hexanol, cis-3-hexen-1-ol, and 2,5-diethylphenol formed a hydrogen bond with Tyr101 (**Figure 8**), and all the nine compounds formed hydrophobic contacts with residues Leu94 and Trp102 (**Supplementary Figure 1**).

Two pockets of EscrCSP8a were predicted by the DoGSiteScorer platform. The larger pocket (EsCSP8a_P1, **Figure 6B**) possessed a volume of 1191.23 Å^3, which resembled the binding site of the template *Mamestra brassicae* CSPMbraA6. The smaller pocket (EsCSP8a_P2) was out of consideration for its exposed structure surface, so the grid box was set at the pocket EsCSP8a_P1. Among the nine compounds, the

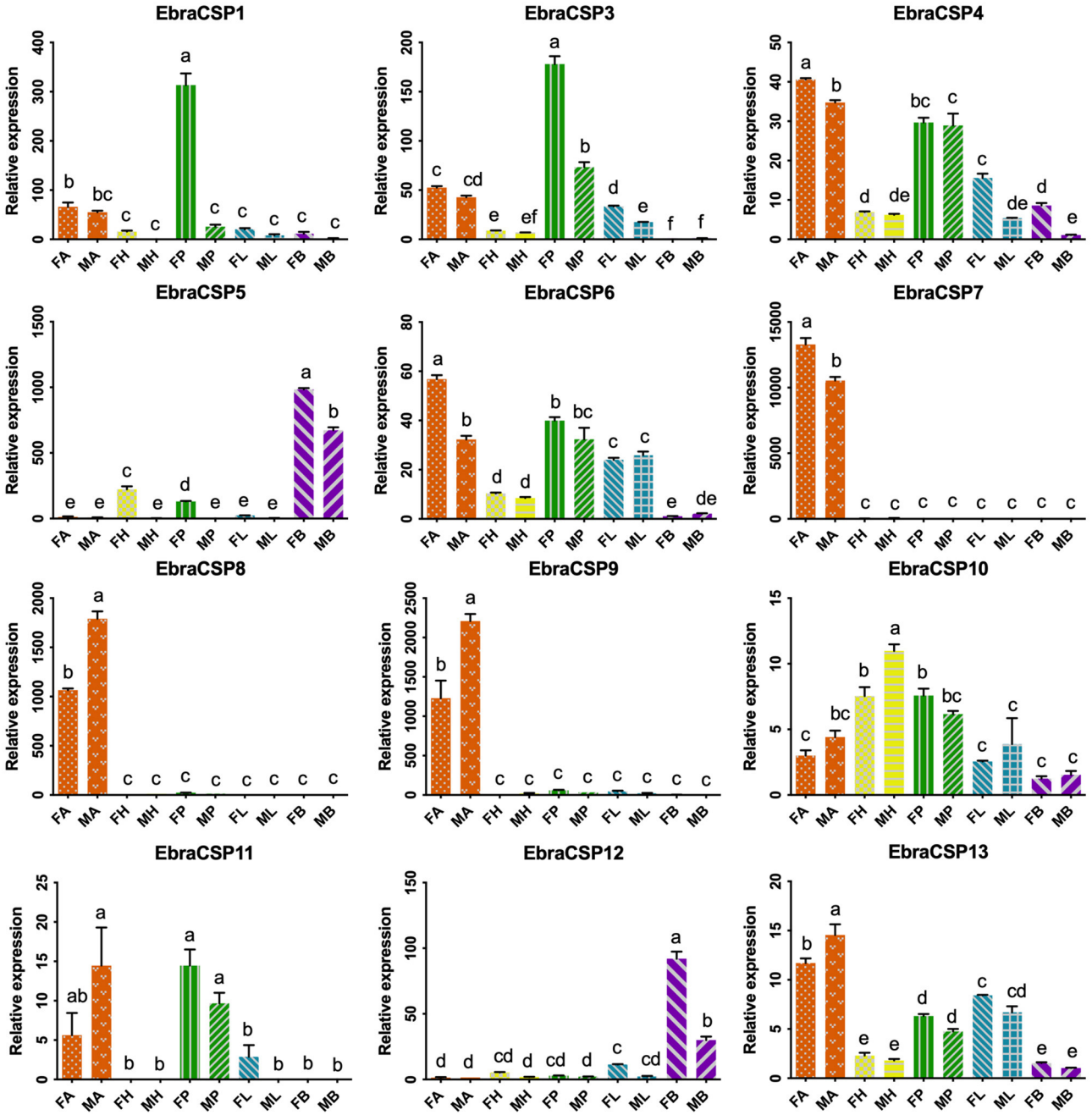

FIGURE 3 | Relative expression levels of EbraCSPs in different tissues of adults. FA, female antennae; MA, male antennae; FH, female head (without antennae); MH, male head (without antennae); FP, female proboscises; MP, male proboscises; FL, female legs; ML, male legs; FB, female abdomen; MB, male abdomen. The bar represents the standard error, and the different small letters (a–f) above each bar indicate significant differences ($P < 0.05$).

four alkenes (alpha-farnesene, (1R)-(+)-alpha-pinene, (−)-beta-caryophyllene, and beta-elemen) showed a lower binding energy of −7 to −6.43 kcal/mol with EscrCSP8a (**Figure 7**), indicating more stable binding to EscrCSP8a. Furthermore, compound 12-bromo-1-dodecanol, which was found in the natural complex CSPMbraA6 as a ligand, possessed a binding energy of −5.26 kcal/mol with EscrCSP8a. However, in pocket EsCSP8a_P1, the nine compounds mainly combined at two different binding sites, which is consistent with the phenomenon that there is more than one binding site in template MbraCSPA6 (Campanacci et al., 2003). At site 1, 1-hexanol, cis-3-hexen-1-ol, hexenyl acetate, 2-tert-butyloxirane, alpha-farnesene, and (1R)-(+)-alpha-pinene formed hydrophobic contacts with Ile77 and Tyr124 (**Supplementary Figure 2**). Additionally, 1-hexanol,

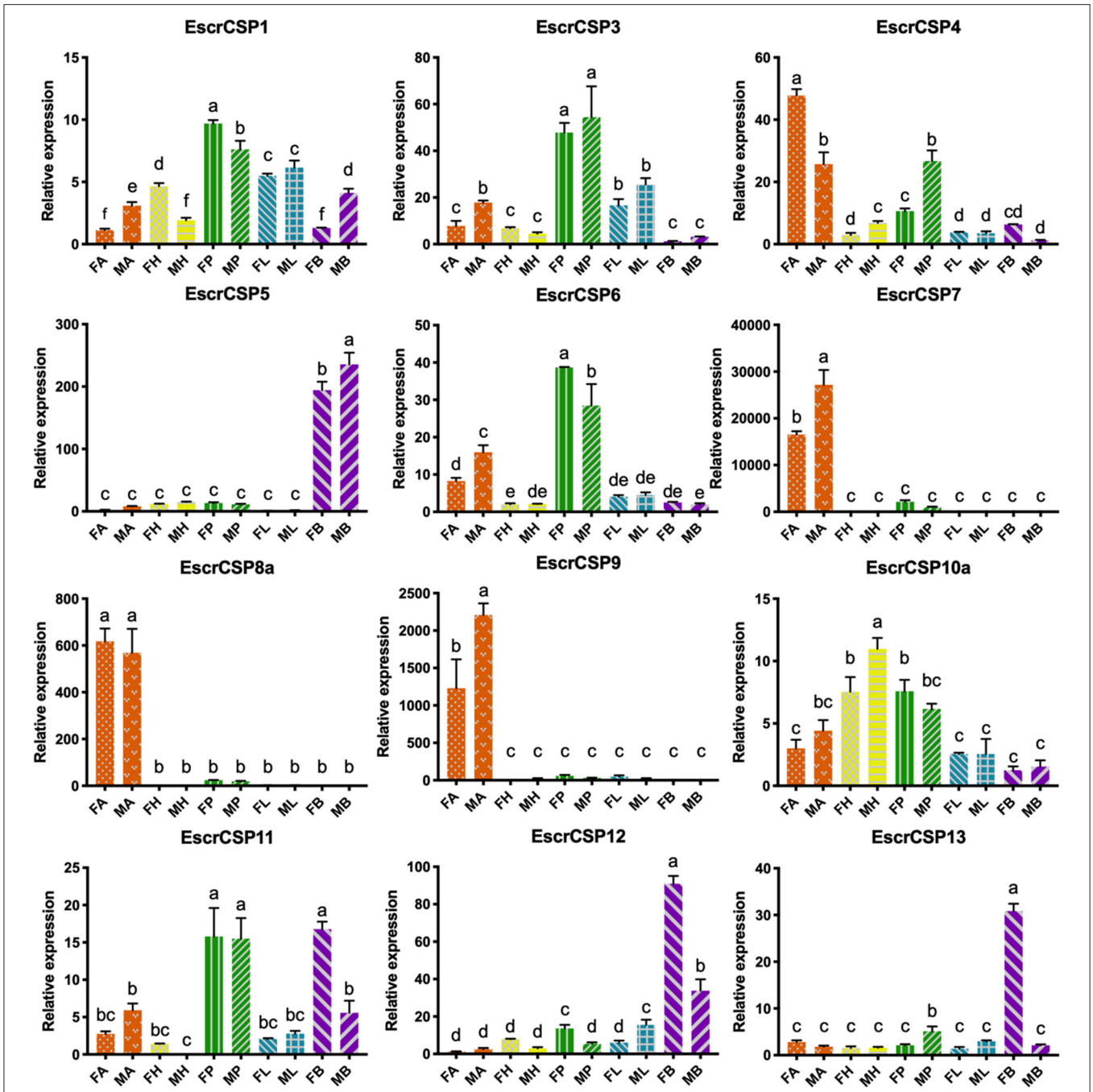

FIGURE 4 | Relative expression levels of EscrCSPs in different tissues of adults. FA, female antennae; MA, male antennae; FH, female head (without antennae); MH, male head (without antennae); FP, female proboscises; MP, male proboscises; FL, female legs; ML, male legs; FB, female abdomen; MB, male abdomen. The bar represents the standard error, and the different small letters (a–f) above each bar indicate significant differences ($P < 0.05$).

cis-3-hexen-1-ol, hexenyl acetate, and 2-tert-butyloxirane formed hydrogen bonds with Tyr124 (**Figures 9A–D**). At site 2, 2,5-diethylphenol, (–)-beta-caryophyllene, and beta-elemen formed hydrophobic contacts with Leu49, Tyr52, Val53, Leu56, and Val95 (**Supplementary Figure 2**), while 2,5-diethylphenol formed a hydrogen bond with Leu49 (**Figure 9E**).

DISCUSSION

Insect sensilla play important roles in semiochemical detection and perception both in adult and larvae stages (Sato and Touhara, 2009; Liu et al., 2011), and the chemosensory protein genes that express at the sensilla are considered to be related to

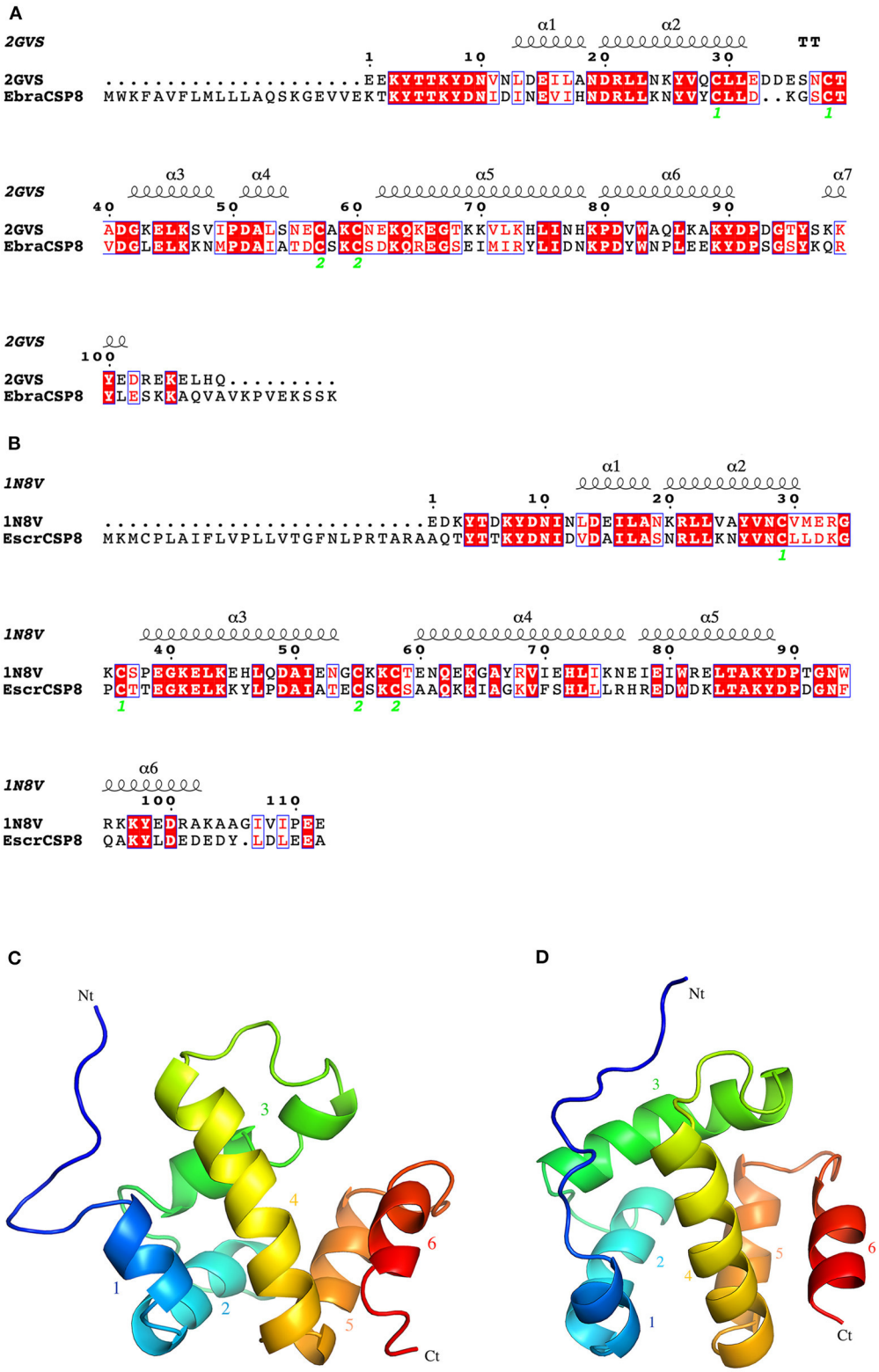

FIGURE 5 | 2D and 3D structures of EbraCSP8 and EscrCSP8a. **(A)** 2D structure of EbraCSP8; **(B)** 2D structure of EscrCSP8a; **(C)** 3D structure of EbraCSP8; **(D)** 3D structure of EscrCSP8a.

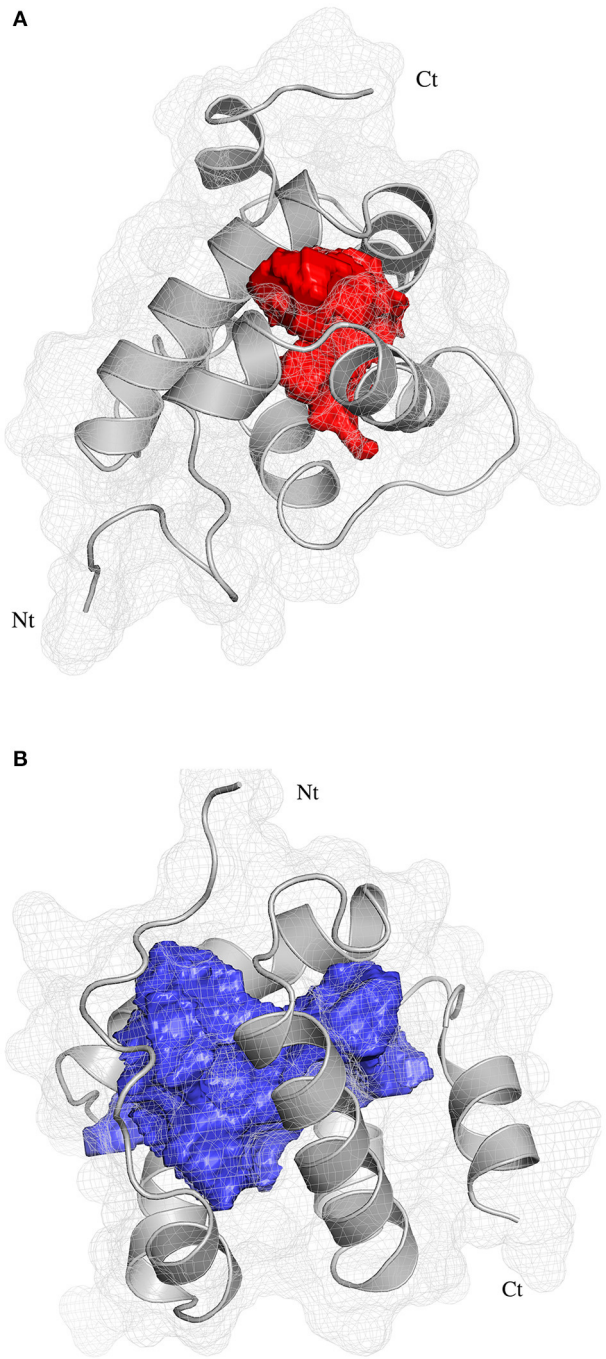

FIGURE 6 | Position of binding pockets in EbraCSP8 and EscrCSP8a. **(A)** Position of binding pockets in EbraCSP8; **(B)** Position of binding pockets in EscrCSP8a.

this process (Sanchez-Gracia et al., 2009). As insect sensilla distribute at different tissues and stages, performing the functions of smell, taste, and touch (Rees, 1970; Hu et al., 2009; Yang et al., 2017), CSP genes that express at these sensilla may be involved in the regulation of insect foraging and oviposition behavior. We screened CSPs-encoding transcripts in different developmental stages using an RNA-seq approach to complete the expression profiles of TRW and TTW CSP genes. From the transcriptome of TRW and TTW developmental stages, we identified 12 putative CSPs in TTW and TRW. There were three more candidate EscrCSPs (EscrCSP8a, EscrCSP10a, and EscrCSP13) than those reported in antennae (Wen et al., 2018), while there was one additional EbraCSP (EbraCSP13). The results proved that CSPs were distributed extensively across different tissues and developmental stages instead of being limited to antennae. All the candidate CSPs found in TTW and TRW had complete ORFs with characteristic four-cysteine signature motifs.

Phylogenetic analysis revealed the intraspecific and interspecific homology relationships of CSPs in different insect species. This may predict gene functions of some CSPs according to the closely related evolutionary relationships on the phylogenetic tree. All candidate EbraCSPs and EscrCSPs showed extremely high homology in pairs, except EbraCSP8 and EscrCSP8a. EscrCSP8a was clustered together with *L. oryzophilus* CSP3 and *D. ponderosae* CSP1 with a high homology coefficient, and *L. oryzophilus* CSP3 was significantly expressed in *L. oryzophilus* antennae (Xin et al., 2016). Considering the specific expression in antennae and the close evolutionary relationship of EscrCSP8a and LoryCSP3, we speculated that they may be involved in the chemoreception process. Conversely, EbraCSP8 was clustered on the same clade with *C. bowringi* CSP12, showing high homology with *D. ponderosae* CSP3 and *T. castaneum* CSP4. The difference between EscrCSP8a and EbraCSP8 indicated that they may bind to different volatiles in the two weevils, related to the divergence of host location. Furthermore, EbraCSP9 was phylogenetically close to *A. mellifera* CSP5 on the phylogenetic tree. Maleszka et al. (2007) speculated that AmelCSP5 is involved in the formation of the embryonic epidermis, according to ds-RNA interference. Therefore, EbraCSP9 may play a similar role in egg and pupae development, but the specific functions of this protein need to be investigated further. In addition, EscrCSP11 and EbraCSP11 were clustered into the same clade with BmorCSP9, while EbraCSP11 and BmorCSP9 were both significantly expressed in larvae. However, the treatment by RNAi of BmorCSP9 did not affect either the development of larvae or the spawning of adults (Jing, 2014). Thus, the functions of EscrCSP11 and EbraCSP11 could not be confirmed. Furthermore, there was no species-specific clade of EscrCSPs and EbraCSPs, with the exception of EbraCSP2, EbraCSP5, EscrCSP2, and EscrCSP5, which were clustered on the same clade. The dispersion of distribution of EbraCSPs and EscrCSPs indicated that chemosensory proteins are conserved among species.

The qRT-PCR results showed that EbraCSPs and EscrCSPs were widely expressed in various tissues and stages of TRW and TTW. From the candidate CSPs, we found three specifically expressed in TTW (EbraCSP7/8/9) and TRW (EscrCSP7/8a/9) adult antennae. They could be considered chemical signal molecule transporters in antennal sensilla; however, this may not be true of EbraCSP9 because of its high expression level in pupae and eggs. For the pupae of TTW staying in a state of inactivity, the proteins highly expressed in this stage may not perform the function of chemoreception. EbraCSP6

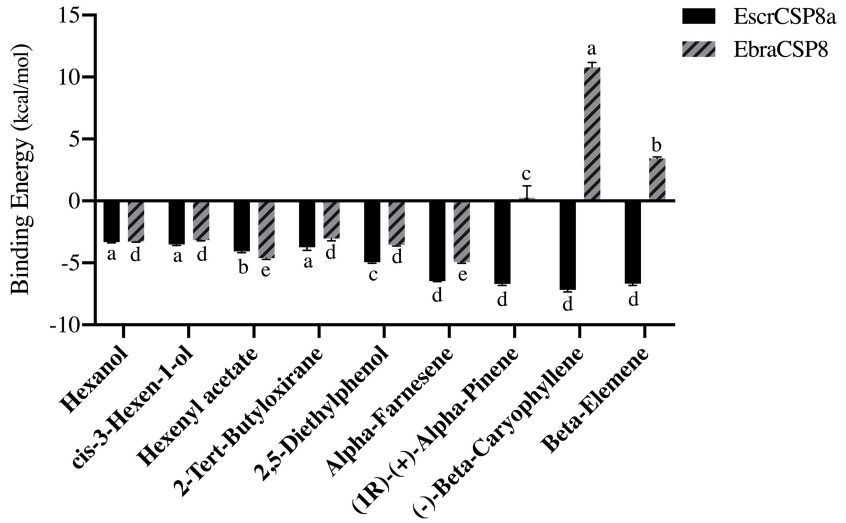

FIGURE 7 | Binding energy of different compounds docking to EbraCSP8 and EscrCSP8a. The bar represents the standard error, and the different small letters (a–e) above each bar indicate significant differences ($P < 0.05$).

and EscrCSP6 were mainly expressed in proboscises, antennae, and legs, which possess a number of sensilla; therefore, they could participate in the process of chemoreception. In contrast, EscrCSP2, EscrCSP5, EscrCSP12, EbraCSP5, and EbraCSP12 were significantly expressed in adult abdomens, among which EbraCSP5 and EbraCSP12 were also highly expressed in pupae, and EbraCSP2 was highly expressed in eggs. Accordingly, we speculated that these proteins may play roles in the process of growth and development. The extensive expression profiles of EbraCPSs and EscrCSPs revealed that although these proteins participated in a variety of biological processes, there were still some members that contributed to the chemoreception process.

In this study, the antennae-specific CSPs, EbraCSP8, and EscrCSP8a, were given special attention for binding simulations with different volatile compounds. The binding energy indicated the binding preferences of the EbraCSP8 and EscrCSP8a. The alkenes [(1R)-(+)-alpha-pinene, (–)-beta-caryophyllene, and beta-elemen] combined more easily with EscrCSP8a than EbraCSP8. However, acetate compounds seemed to have a better affinity with template MbraCSPA6 (Campanacci et al., 2003), while aromatic compounds had a better affinity with template CSPsg4 (Tomaselli et al., 2006). Although the 3-D structures of EbraCSP8, EscrCSP8a, and template proteins had a high visual similarity, their binding affinities differed with different compounds. This suggests that the functions of similar CSPs from different species are diverse, which may be determined by the host volatiles of the species. In contrast, the differences in residues on the chains may also affect the binding affinity. Relative to template 2GVS (CSPsg4), 1N8V (MbraCSPA6) is a complex combined with three 12-bromo-1-dodecanol compounds, showing a 3-fold larger cavity than the 1:1 structure (Lartigue et al., 2002). Therefore, the binding process of CSPs could rely on not only the fluidity of the internal side chain but also the flexibility of the backbone (Campanacci et al., 2003), indicating the conformations would also change dramatically in the practical binding process of EbraCSP8 and EscrCSP8a with different compounds. As several residues were involved in the hydrophobic contacts with different compounds, such as Leu94 and Trp102 of EbraCSP8 and Leu49, Tyr52, Val53, Leu56 Ile77, Val95, and Tyr124 of EscrCSP8a, they may be considered as the key residues for ligand binding of the two proteins, which may provide some basis for the follow-up research.

The various functions of CSPs have been verified in different species, and their importance in chemoreception is controversial. To date, there have been few functional studies on CSPs of the coleopteran, while none have been performed on Curculionoidea. *Monochamus alternatus* CSP5 is mainly expressed in male and female antennae with strong binding abilities to myrcene, (+)-β-pinene, and (–)-isolongifolene, suggesting the important role of chemoreception with host plant volatiles (Ali et al., 2019). *Holotrichia oblita* CSP1 and CSP2 were detected in sensillum basiconicum and sensillum placodeum with strong binding abilities with β-ionone (Guan, 2012). Sun reported that *Agrilus mali* CSP1 and CSP4 did not bind to the host plant volatiles, while CSP5 and CSP8 strongly bound with pear ester (Sun, 2018). These studies focus on the CSPs that were significantly expressed in antennae, confirming the chemoreception functions of CSPs in coleopteran. However, the structural and functional studies on CSPs of coleopteran are still deficient. Despite the diversification of functions of CSPs, the chemosensory roles should be considered in conjunction with OBPs. Other physiological and developmental functions could be explored when they exhibit physiological importance. Further studies need to confirm the binding properties to more volatiles of EbraCSP8 and EscrCSP8a, and the role of the key residues, by the fluorescence competition binding experiment, and their influences on feeding selection in TRW and TTW when EbraCSP8 and EscrCSP8a are silenced. To explore the chemosensory mechanism of feeding niche differences between TRW and TTW, chemosensory receptors

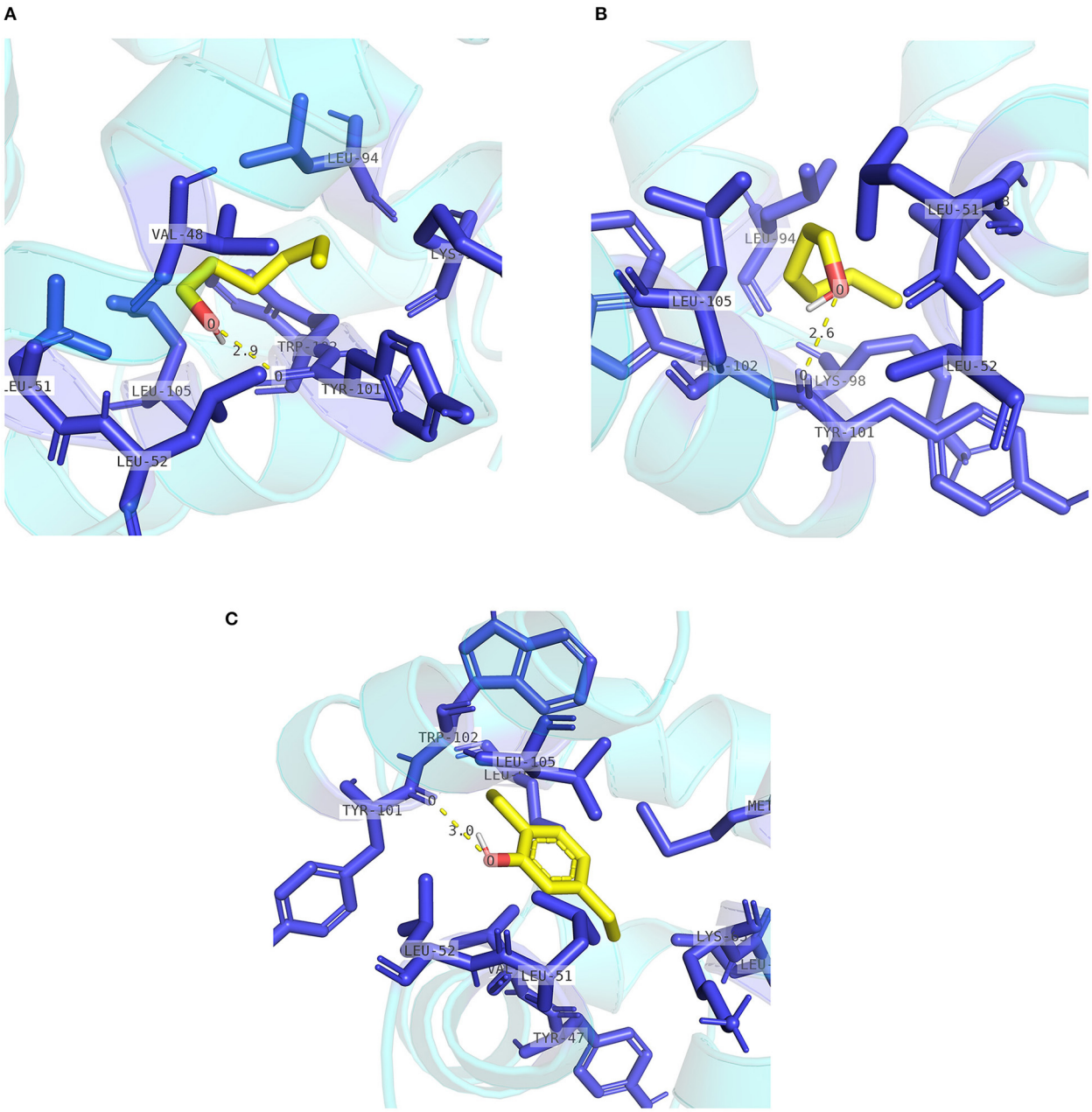

FIGURE 8 | Internal contacts of ligands with EbraCSP8 residues. Blue sticks represent non-ligand residues involved in hydrophobic contacts; yellow dotted line represent hydrogen bond and its length. **(A)** Internal contacts of 1-hexanol with EbraCSP8 residues. **(B)** Internal contacts of cis-3-hexen-1-ol with EbraCSP8 residues. **(C)** Internal contacts of 2,5-diethylphenol with EbraCSP8 residues.

and the synergism of GRs and detoxification genes should also be considered.

CONCLUSION

In this study, we found that candidate EbraCSPs and EscrCSPs were widely expressed in different stages and adult tissues. Both putative chemosensory- and development-related CSPs were screened according to phylogenetic and qRT-PCR analysis. The antennae-specific expression and differences of binding affinities of EbraCSP8 and EscrCSP8a indicated the functional importance in feeding selection of TRW and TTW adults. The more specific functions of EbraCSP8 and EscrCSP8a require further verification. This study provided a basis for explaining the niche differentiation between the two weevils, and the further research should confirm the immunolocalization and fluorescence competitive binding of the chemosensory genes of interest, as well as the synergism of GRs and detoxification genes.

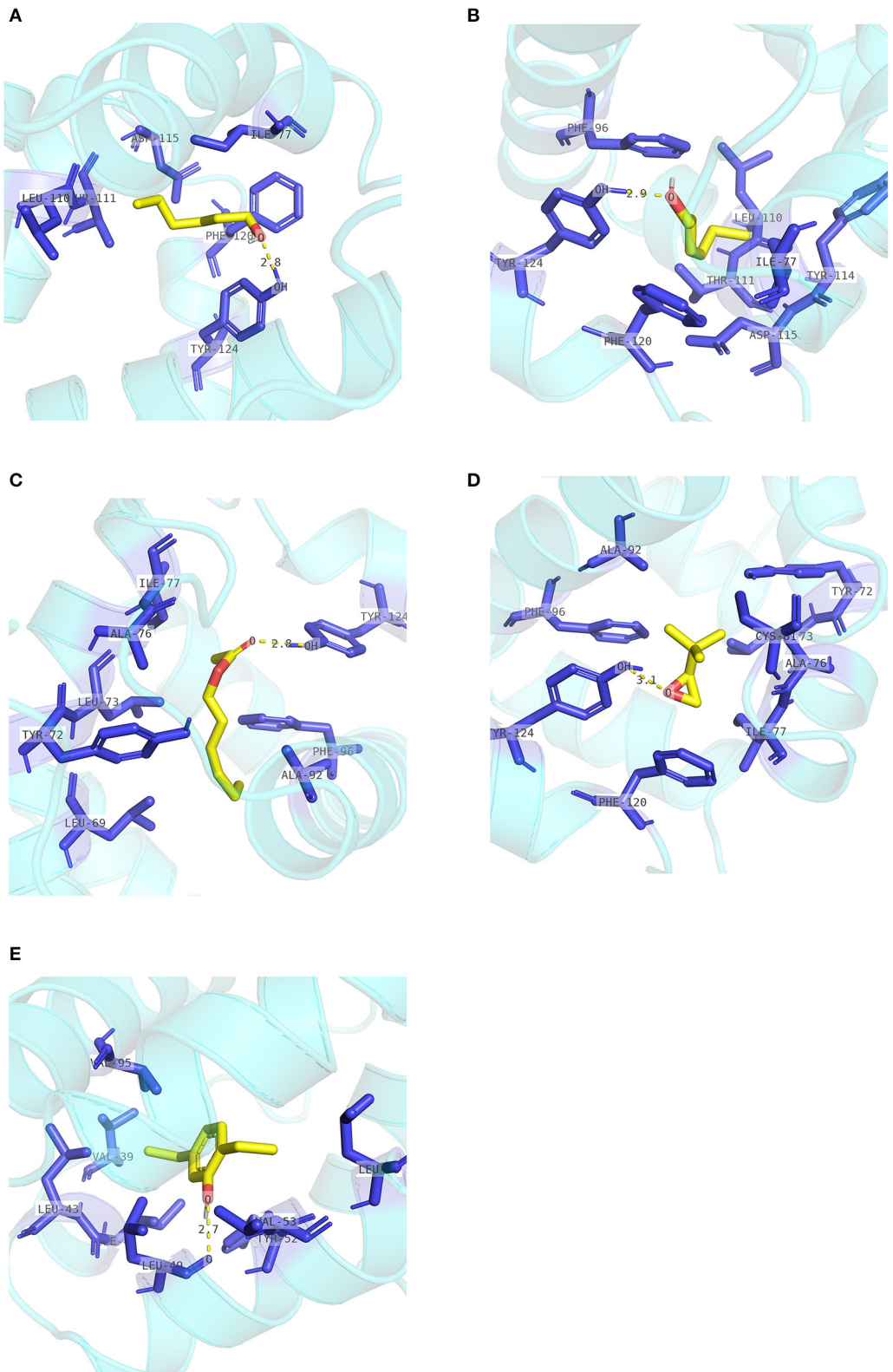

FIGURE 9 | Internal contacts of ligands with EscrCSP8a residues. Blue sticks represent non-ligand residues involved in hydrophobic contacts; yellow dotted line represent hydrogen bond and its length. **(A)** Internal contacts of 1-hexanol and with EscrCSP8a residues. **(B)** Internal contacts of cis-3-hexen-1-ol with EscrCSP8a residues. **(C)** Internal contacts of hexenyl acetate with EscrCSP8a residues. **(D)** Internal contacts of 2-tert-butyloxirane with EscrCSP8a residues. **(E)** Internal contacts of 2,5-diethylphenol with EscrCSP8a residues.

AUTHOR CONTRIBUTIONS

QW and JW conceived and designed the experiments. QW, XW, and YL performed the experiments. QW and XW analyzed the data. QW wrote the manuscript. All authors reviewed the final manuscript and approved the submitted version.

FUNDING

This work was supported by the National Key R&D Program of China (2018YFC1200400) and the National Natural Sciences Foundation of China (Grant no. 31770691).

ACKNOWLEDGMENTS

We thank Guo Wenjuan and Li Hongyu (Beijing Forestry University, China) for help with collecting samples, and Hao Enhua (Beijing Forestry University, China) for the guidance with the docking simulations. We thank LetPub (www.letpub.com) for its linguistic assistance during the preparation of this manuscript.

SUPPLEMENTARY MATERIAL

The Supplementary Material for this article can be found online at: https://www.frontiersin.org/articles/10.3389/fphys.2021.661310/full#supplementary-material

REFERENCES

Ali, S., Ahmed, M., Li, N., Ali, S., and Wang, M. (2019). Functional characteristics of chemosensory proteins in the sawyer beetle *Monochamus alternatus* Hope. *Bull. Entomol. Res.* 109, 34–42. doi: 10.1017/S0007485318000123

Altschul, S. F., Madden, T. L., Schäffer, A. A., Zhang, J., Zhang, Z., and Miller, W. et al. (1997). Gapped BLAST and PSI-BLAST: a new generation of protein database search programs. *Nucleic Acids Res.* 25, 3389–3402. doi: 10.1093/nar/25.17.3389

Angeli, S., Ceron, F., Scaloni, A., Monti, M., Monteforti, G., Minnocci, A., et al. (1999). Purification, structural characterization, cloning and immunocytochemical localization of chemoreception proteins from *Schistocerca gregaria*. *Eur. J. Biochem.* 262, 745–754. doi: 10.1046/j.1432-1327.1999.00438.x

Bowie, J. U., Lüthy, R., and Eisenberg, D. (1991). A method to identify protein sequences that fold into a known three-dimensional structure. *Science* 253, 164–170. doi: 10.1126/science.1853201

Campanacci, V., Lartigue, A., Hallberg, B. M., Jones, T. A., Giudici-Orticoni, M. T., Tegoni, M., et al. (2003). Moth chemosensory protein exhibits drastic conformational changes and cooperativity on ligand binding. *Proc. Natl. Acad. Sci. U.S.A.* 100, 5069–5074. doi: 10.1073/pnas.0836654100

Colovos, C., and Yeates, T. O. (1993). Verification of protein structures: patterns of nonbonded atomic interactions. *Prorein Sci.* 2, 1511–1519. doi: 10.1002/pro.5560020916

Dani, F. R., Michelucci, E., Francese, S., Mastrobuoni, G., Cappellozza, S., Marca, G. L., et al. (2011). Odorant-binding proteins and chemosensory proteins in pheromone detection and release in the silkmoth *Bombyx mori*. *Chem. Senses* 36, 335–344. doi: 10.1093/chemse/bjq137

Emmanuelle, J. J., Vogt, R. G., Marie-Christine, F., and Patricia, N. L. M. (2001). Functional and expression pattern analysis of chemosensory proteins expressed in antennae and pheromonal gland of *Mamestra brassicae*. *Chem. Senses* 26, 833–844. doi: 10.1093/chemse/26.7.833

Finn, R. D., Coggill, P., Eberhardt, R. Y., Eddy, S. R., Mistry, J., Mitchell, A. L., et al. (2016). The Pfam protein families database: towards a more sustainable future. *Nucleic Acids Res.* 44, D279–D285. doi: 10.1093/nar/gkv1344

Fu, S., Li, F., Yan, X., and Hao, C. (2020). Expression profiles and binding properties of the chemosensory protein PxylCSP11 from the diamondback moth, *Plutella xylostella* (*Lepidoptera*: *Plutellidae*). *J. Insect Sci.* 20, 1–11. doi: 10.1093/jisesa/ieaa107

Grabherr, M. G., Haas, B. J., Yassour, M., Levin, J. Z., and Amit, I. (2013). Trinity: reconstructing a full-length transcriptome without a genome from RNA-Seq data. *Nat. Biotechnol.* 29, 644–652. doi: 10.1038/nbt.1883

Guan, L. (2012). *Functional Analysis of Chemosensory Proteins in Holotrichia oblita Faldermann (Coleoptera: Scarabaeida)*. Master, Jilin University.

Hu, F., Zhang, G. N., and Wang, J. J. (2009). Scanning electron microscopy studies of antennal sensilla of bruchid beetles, Callosobruchus chinensis (L.) and Callosobruchus maculatus (F.) (*Coleoptera*: Bruchidae). *Micron* 40, 320–326. doi: 10.1016/j.micron.2008.11.001

Jansen, S., Chmelík, J., Žídek, L., Padrta, P., Novák, P., Zdráhal, Z., et al. (2007). Structure of Bombyx mori chemosensory protein 1 in solution. *Arch. Insect Biochem. Physiol.* 66, 135–145. doi: 10.1002/arch.20205

Ji, Y. C., Gao, P., Zhang, G. Y., Wen, C., Wen, J. B., and JBS Technology (2017). Micro-habitat niche differentiation contributing to coexistence of *Eucryptorrhynchus scrobiculatus* Motschulsky and *Eucryptorrhynchus brandti* (Harold)*. *Biocontrol Sci. Technol.* 27, 1–15. doi: 10.1080/09583157.2017.1390069

Jing, X. (2014). *Expression Analysis of BmorCSP9 in Larvae and Pupae of Silkworm, Bombyx mori*. Master, Henan Agricultural University.

Kanehisa, M., Goto, S., Kawashima, S., Okuno, Y., and Hattori, M. (2004). The KEGG resource for deciphering the genome. *Nucleic Acids Res.* 32, D277–280. doi: 10.1093/nar/gkh063

Lartigue, A., Campanacci, V., Roussel, A., and Larsson, A. M. (2002). X-ray structure and ligand binding study of a moth chemosensory protein. *J. Biol. Chem.* 277, 32094–32098. doi: 10.1074/jbc.M204371200

Laskowski, R. A., Macarthur, M. W., Moss, D. S., and Thornton, J. M. J. (1992). PROCHECK: a program to check the stereochemicai quality of protein structures. *J. Appl. Crystallogr.* 26, 283–291. doi: 10.1107/S0021889892009944

Laskowski, R. A., and Swindells, M. B. (2011). LigPlot^{+}: multiple ligand-protein interaction diagrams for drug discovery. *J. Chem. Inf. Model* 51, 2778–2786. doi: 10.1021/ci200227u

Leal, W. S. (2013). Odorant reception in insects: roles of receptors, binding proteins, and degrading enzymes. *Annu. Rev. Entomol.* 58, 373–391. doi: 10.1146/annurev-ento-120811-153635

Letunic, I., and Bork, P. (2019). Interactive tree of life (iTOL) v4: recent updates and new developments. *Nucleic Acids Res.* 47, W256–W259. doi: 10.1093/nar/gkz239

Liu, Z., Hua, B. Z., and Liu, L. (2011). Ultrastructure of the sensilla on larval antennae and mouthparts in the peach fruit moth, *Carposina sasakii* Matsumura (*Lepidoptera*: *Carposinidae*). *Micron* 42, 478–483. doi: 10.1016/j.micron.2011.01.006

Luo, W., Ji, Y.-C., and Wen, J.-B. (2016). Application of a frequency distribution method for determining instars of Eucryptorrhynchus brandti (Coleoptera: curculionidae) from several morphological variables. *Biocontrol Sci and Techn.* 26, 1329–1336. doi: 10.1080/09583157.2016.1193845

Maleszka, J., Foret, S., Saint, R., and Maleszka, R. (2007). RNAi-induced phenotypes suggest a novel role for a chemosensory protein CSP5 in the development of embryonic integument in the honeybee (*Apis mellifera*). *Dev. Genes Evol.* 217, 189–196. doi: 10.1007/s00427-006-0127-y

Maleszka, R., and Stange, G. (1997). Molecular cloning, by a novel approach, of a cDNA encoding a putative olfactory protein in the labial palps of the moth *Cactoblastis cactorum*. *Gene* 202, 39–43. doi: 10.1016/S0378-1119(97)00448-4

Mckenna, M. P., Hekmat-Scafe, D. S., Gaines, P., and Carlson, J. R. (1994). Putative Drosophila pheromone-binding proteins expressed in a subregion of the olfactory system. *J. Biol. Chem.* 269, 16340–16347. doi: 10.1016/S0021-9258(17)34013-9

Nomura, A., Kawasaki, K., Kubo, T., and Natori, S. (1992). Purification and localization of p10, a novel protein that increases in nymphal regenerating legs of Periplaneta americana (American cockroach). *Int. J. Dev. Biol.* 36, 391–398.

Pelosi, P., Zhou, J. J., Ban, L. P., and Calvello, M. (2006). Soluble proteins in insect chemical communication. *Cell. Mol. Life Sci.* 63, 1658–1676. doi: 10.1007/s00018-005-5607-0

Pettersen, E. F., Goddard, T. D., Huang, C. C., Couch, G. S., Greenblatt, D. M., Meng, E. C., et al. (2004). UCSF Chimera–a visualization system for exploratory research and analysis. *J. Comput. Chem.* 25, 1605–1612. doi: 10.1002/jcc.20084

Pfaffl, M. W. (2001). A new mathematical model for relative quantification in real-time RT–PCR. *Nucleic Acids Res.* 29:e45. doi: 10.1093/nar/29.9.e45

Picimbon, J. F., Dietrich, K., Breer, H., and Krieger, J. (2000). Chemosensory proteins of Locusta migratoria (*Orthoptera*: *Acrididae*). *Insect Biochem. Mol. Biol.* 30, 233–241. doi: 10.1016/S0965-1748(99)00121-6

Qiao, H. L., Deng, P. Y., Li, D. D., Chen, M., Jiao, Z. J., Liu, Z. C., et al. (2013). Expression analysis and binding experiments of chemosensory proteins indicate multiple roles in Bombyx mori. *J. Insect Physiol.* 59, 667–675. doi: 10.1016/j.jinsphys.2013.04.004

Rees, C. J. (1970). Age dependency of response in an insect chemoreceptor sensillum. *Nature* 227, 740–742. doi: 10.1038/227740a0

Robert, X., and Gouet, P. (2014). Deciphering key features in protein structures with the new ENDscript server. *Nucleic Acids Res.* 42, W320–324. doi: 10.1093/nar/gku316

Sanchez-Gracia, A., Vieira, F. G., and Rozas, J. (2009). Molecular evolution of the major chemosensory gene families in insects. *Heredity* 103, 208–216. doi: 10.1038/hdy.2009.55

Sato, K., and Touhara, K. (2009). Insect olfaction: receptors, signal transduction, and behavior. *Results Probl. Cell Differ.* 47, 121–138. doi: 10.1007/400_2008_10

Sherlock, G. (2009). Gene Ontology: tool for the unification of biology. *Can. Inst. Food Sci. Technol. J.* 25, 25–29. doi: 10.1038/75556

Stocker, R. F. (1994). The organization of the chemosensory system in *Drosophila melanogaster*: a rewiew. *Cell Tissue Res.* 275, 3–26. doi: 10.1007/BF00305372

Sun, C., Zhao, H., and Li, P. (1990). Investigation on main characteristics and afforestation of *Ailanthus altissima*. *Ningxia Agric. For. Sci. Technol.* 1, 26–28.

Sun, K. (2018). *Cloning, Expression and Functional Analysis of Genes Encoding Chemosensory Proteins in Agrilus Mali (Matsumura)*. Master, Northwest A&F University.

Tatusov, R. L., Galperin, M. Y., Natale, D. A., and Koonin, E. V. (2000). The COG database: a tool for genome-scale analysis of protein functions and evolution. *Nuclc Acids Res.* 28, 33–36. doi: 10.1093/nar/28.1.33

Tomaselli, S., Crescenzi, O., Sanfelice, D., Ab, E., Wechselberger, R., Angeli, S., et al. (2006). Solution structure of a chemosensory protein from the desert locust *Schistocerca gregaria*. *Biochemistry* 45, 10606–10613. doi: 10.1021/bi060998w

Waris, M. I., Younas, A., Adeel, M. M., Duan, S. G., Quershi, S. R., Kaleem Ullah, R. M., et al. (2019). The role of chemosensory protein 10 in the detection of behaviorally active compounds in brown planthopper, Nilaparvata lugens. *Insect Sci.* 27, 533–544. doi: 10.1111/1744-7917.12659

Wen, X. (2019). *Feeding Preference of Adult Eucryptorrhynchus scrobiculatus and E. brandti* (*Coleoptera*: *Curculionidae*). Doctor, Beijing Forestry University.

Wen, X., Wang, Q., Gao, P., and Wen, J. (2018). Identification and comparison of chemosensory genes in the antennal transcriptomes of *Eucryptorrhynchus scrobiculatus* and *E. brandti* Fed on *Ailanthus altissima*. *Front. Physiol.* 9:1652. doi: 10.3389/fphys.2018.01652

Wu, Z. M., Gao, P., and Wen, J. B. (2016). Characteristic analysis of microsatellite in *Eucryptorrhynchus chinensis* transcriptome. *J. Environ. Entomol.* 38, 979–983. doi: 10.3969/j.issn.1674-0858.2016.05.15

Xie, C., Mao, X., Huang, J., Ding, Y., Wu, J., Dong, S., et al. (2011). KOBAS 2.0: a web server for annotation and identification of enriched pathways and diseases. *Nucleic Acids Res.* 39, W316–322. doi: 10.1093/nar/gkr483

Xin, Y., Yan-Dong, J., Gui-Yao, W., Hang, Y., Wen-Wu, Z., Su, L., et al. (2016). Odorant-binding proteins and chemosensory proteins from an invasive pest *Lissorhoptrus oryzophilus* (*Coleoptera*: *Curculionidae*). *Environ. Entomol.* 45, 1276–1286. doi: 10.1093/ee/nvw111

Xuan, N., Guo, X., Xie, H. Y., Lou, Q. N., Lu, X. B., Liu, G. X., et al. (2015). Increased expression of CSP and CYP genes in adult silkworm females exposed to avermectins. *Insect Sci.* 22, 203–219. doi: 10.1111/1744-7917.12116

Yang, Y., Ren, L., Wang, T., Xu, L., and Zong, S. (2017). Comparative morphology of sensilla on antenna, maxillary palp and labial palp of larvae of *Eucryptorrhynchus scrobiculatus* (Olivier) and *E. brandti* (Harold) (*Coleoptera*: *Curculionidae*). *Acta Zool.* 98, 400–411. doi: 10.1111/azo.12185

Younas, A., Waris, M. I., Tahir Ul Qamar, M., Shaaban, M., Prager, S. M., and Wang, M. Q. (2018). Functional analysis of the chemosensory protein MsepCSP8 from the oriental armyworm *Mythimna separata*. *Front. Physiol.* 9:872. doi: 10.3389/fphys.2018.00872

Yu, Q. (2013). *Biological Characteristics and Artificial Feeding of Eucryptorrhynchus scrobiculatus Motschulsky*. Master, Beijing Forestry University.

Yugong, S., Anmin, W., Xiuzhen, S., and Xiwu, G. (1994). Occurrence and prevention measures of *Eucryptorrhynchus scrobiculatus* Motschulsky. *China Plant Prot.* 1, 15–15.

Zhou, X. H., Ban, L. P., Iovinella, I., Zhao, L. J., Gao, Q., Felicioli, A., et al. (2013). Diversity, abundance, and sex-specific expression of chemosensory proteins in the reproductive organs of the locust Locusta migratoria manilensis. *Biol. Chem.* 394, 43–54. doi: 10.1515/hsz-2012-0114

Conflict of Interest: The authors declare that the research was conducted in the absence of any commercial or financial relationships that could be construed as a potential conflict of interest.

frontiers in Physiology

ORIGINAL RESEARCH
published: 19 May 2021
doi: 10.3389/fphys.2021.663040

Identification of Olfactory Genes From the Greater Wax Moth by Antennal Transcriptome Analysis

Xing-Chuan Jiang[1†], Su Liu[1†], Xiu-Yun Jiang[1], Zheng-Wei Wang[2], Jin-Jing Xiao[1], Quan Gao[1], Cheng-Wang Sheng[1], Teng-Fei Shi[1], Hua-Rui Zeng[1], Lin-Sheng Yu[1] and Hai-Qun Cao[1]*

[1] Anhui Provincial Key Laboratory of Integrated Pest Management on Crops, School of Plant Protection, Anhui Agricultural University, Hefei, China, [2] CAS Key Laboratory of Tropical Forest Ecology, Xishuangbanna Tropical Botanical Garden, Chinese Academy of Sciences, Kunming, China

OPEN ACCESS

Edited by:
Ya-Nan Zhang,
Huaibei Normal University, China

Reviewed by:
Tiantao Zhang,
Chinese Academy of Agricultural Sciences (CAAS), China
Lu Xu,
Jiangsu Academy of Agricultural Sciences (JAAS), China
Qian Wang,
Zhejiang Agriculture and Forestry University, China

***Correspondence:**
Hai-Qun Cao
haiquncao@163.com

[†] These authors have contributed equally to this work

Specialty section:
This article was submitted to Invertebrate Physiology, a section of the journal Frontiers in Physiology

Received: 02 February 2021
Accepted: 22 April 2021
Published: 19 May 2021

Citation:
Jiang X-C, Liu S, Jiang X-Y, Wang Z-W, Xiao J-J, Gao Q, Sheng C-W, Shi T-F, Zeng H-R, Yu L-S and Cao H-Q (2021) Identification of Olfactory Genes From the Greater Wax Moth by Antennal Transcriptome Analysis. Front. Physiol. 12:663040. doi: 10.3389/fphys.2021.663040

The olfactory system is used by insects to find hosts, mates, and oviposition sites. Insects have different types of olfactory proteins, including odorant-binding proteins (OBPs), chemosensory proteins (CSPs), odorant receptors (ORs), ionotropic receptors (IRs), and sensory neuron membrane proteins (SNMPs) to perceive chemical cues from the environment. The greater wax moth, *Galleria mellonella*, is an important lepidopteran pest of apiculture. However, the molecular mechanism underlying odorant perception in this species is unclear. In this study, we performed transcriptome sequencing of *G. mellonella* antennae to identify genes involved in olfaction. A total of 42,544 unigenes were obtained by assembling the transcriptome. Functional classification of these unigenes was determined by searching against the Gene Ontology (GO), eukaryotic orthologous groups (KOG), and the Kyoto Encyclopedia of Genes and Genomes (KEGG) databases. We identified a total of 102 olfactory-related genes: 21 *OBP*s, 18 *CSP*s, 43 *OR*s, 18 *IR*s, and 2 *SNMP*s. Results from BLASTX best hit and phylogenetic analyses showed that most of the genes had a close relationship with orthologs from other Lepidoptera species. A large number of *OBP*s and *CSP*s were tandemly arrayed in the genomic scaffolds and formed gene clusters. Reverse transcription-quantitative PCR results showed that *GmelOBP19* and *GmelOR47* are mainly expressed in male antennae. This work provides a transcriptome resource for olfactory genes in *G. mellonella*, and the findings pave the way for studying the function of these genes.

Keywords: *Galleria mellonella*, antenna, transcriptome, olfactory genes, expression pattern, genomic distribution

INTRODUCTION

Olfaction is essential for insect activities such as food seeking, mate recognition, and oviposition. For efficient detection of chemical cues, insects have evolved an olfaction system that consists of many olfactory proteins, including odorant-binding proteins (OBPs), chemosensory proteins (CSPs), odorant receptors (ORs), ionotropic receptors (IRs), and sensory neuron membrane proteins (SNMPs) (Leal, 2013; Robertson, 2019).

OBPs are small, water soluble proteins enriched in the sensillar lymph of insect antennae (Pelosi et al., 2018). OBPs in the pores of the antennal sensillae can bind odorant compounds

and deliver them to active ORs (Sun et al., 2018). OBPs typically have six positionally conserved cysteine residues. These cysteine residues form three disulfide bridges, which are necessary for maintaining protein stability (Brito et al., 2016). In Lepidoptera, there are two special subgroups of OBP: general odorant-binding protein (GOBP) and pheromone-binding protein (PBP) (Vogt et al., 2015). GOBPs recognize "general" odorants such as volatiles from host plants, whereas PBPs perceive sex pheromone constituents. However, many studies have demonstrated that GOBPs can bind sex pheromones and PBPs can have strong affinities for plant volatiles (Gong et al., 2009b; Khuhro et al., 2017; Sun et al., 2019a). CSPs are carrier proteins enriched in the sensillar lymph with a function similar to OBPs (Pelosi et al., 2018). CSPs contain four positionally conserved cysteines that form two disulfide bridges (Pelosi et al., 2014). Some CSPs are specifically expressed in the antenna and can bind to plant volatiles and sex pheromone constituents (Zhang et al., 2014; Li et al., 2015; Duan et al., 2019). Other CSPs are highly concentrated in non-olfaction organs, such as pheromone glands and legs, suggesting they may be involved in other physiological processes besides being carriers of odorants (Zhang et al., 2016; Sun et al., 2017).

Insect ORs are located on the dendrite membrane of olfactory sensory neurons (OSNs) (Touhara and Vosshall, 2009). ORs can recognize the odorants transferred by OBPs and CSPs, and convert these chemical signals into electrical signals (Wicher, 2018). Although most insect ORs have a seven-transmembrane domain, they are not G-protein-coupled receptors (GPCRs) because they have a different type of topology (Fleischer et al., 2018). In insects, a functional OR unit comprised of one copy of poorly conserved, conventional OR along with one copy of a highly conserved, non-conventional olfactory co-receptor (Orco) (Touhara and Vosshall, 2009). The OR/Orco complex forms heteromeric ligand gated ion channels that allow insects to rapidly perceive chemical signals (Butterwick et al., 2018). IRs are also key receptors involved in the perception of odorants, such as phenylacetaldehyde, amines and acids (Rytz et al., 2013; Zhang et al., 2019). IRs are transmembrane proteins with an extracellular N-terminus, a bipartite ligand-binding domain (two lobes separated by an ion channel domain), and a short cytoplasmic C-terminus, which have a structural similarity with ionotropic glutamate receptors (iGluRs) (Benton et al., 2009). However, IRs and iGluRs diverge from each other according to their sequence characteristics and phylogenetics (Croset et al., 2010).

Insect SNMPs have homology with the human fatty acid transporter CD36 and are divided into two subfamilies: SNMP1 and SNMP2 (Vogt et al., 2009). SNMP1s are co-expressed with pheromone receptors (PRs) accumulating on the membrane of pheromone-sensitive OSNs, whereas SNMP2s are expressed in the cells surrounding the pheromone-sensitive OSNs (Forstner et al., 2008; Sun et al., 2019b). SNMPs may have the ability to transfer lipophilic sex pheromones to ORs; in fruit fly and several moth species, SNMP1s are crucial for the detection of pheromones (Jin et al., 2008; Zhang et al., 2020).

Identification of olfactory genes will help us understand the molecular mechanism of insect olfaction. This would be useful in developing novel environmentally friendly methods for pest management (Venthur and Zhou, 2018). For example, OBPs, CSPs, and ORs can be used to screen bioactive attractants and repellents and antagonists of Orco could inhibit insect olfactory behavior (Leal et al., 2008; Kepchia et al., 2017; Choo et al., 2018; Zeng et al., 2018). Knockdown and knockout of particular genes by RNA interference and CRISPR techniques, respectively, can effectively block the communication between pest insects and their hosts (Pelletier et al., 2010; Dong et al., 2017; Garczynski et al., 2017; Zhu et al., 2019).

The greater wax moth, *Galleria mellonella*, is a major pest of honeybees throughout the world (Kwadha et al., 2017). Female *G. mellonella* lay eggs within the beehive, and the larvae feed on the wax comb and honey. They cause heavy losses in the beekeeping industry (Zhu et al., 2016). Traditional methods for controlling *G. mellonella* are based on chemical insecticides, but these may cause pesticide contamination of honey products. Adult *G. mellonella* detect host volatiles and sex pheromone using olfactory adaptations (Payne and Finn, 1977; Li et al., 2019). The molecular mechanisms of olfaction are therefore important for identifying the key genes mediating chemical signal perception and developing RNAi-based management strategies. Zhao et al. (2019) analyzed the antennal transcriptome of *G. mellonella* and identified a number of chemosensory genes, including 22 OBPs, 20 CSPs, 46 ORs, 17 IRs, and 2 SNMPs. However, these numbers are fewer than the numbers found in other Lepidoptera species and suggest the existence of other, unidentified, genes.

In this study, we performed transcriptome sequencing of the *G. mellonella* antennae. We identified 102 olfactory-related genes, including 11 novel genes, from the transcriptome dataset. We analyzed the sequence characteristics, phylogeny, genomic distribution, and exon–intron organization of these genes. We also determined the expression profiles of the newly identified genes using reverse transcription-quantitative PCR (RT-qPCR).

MATERIALS AND METHODS

Insects

The *G. mellonella* used in this study originated from a colony collected from infested beehives on a bee farm in Hefei, China. The larvae were reared on an artificial diet and the adults were fed on a 10% (v/v) honey solution. Insects were reared at 27°C ± 1°C, 65 ± 5% relative humidity and a photoperiod of 14:10 h (L:D).

Sample Collection and RNA Extraction

Adult males and females (2-day-old, unmated) were sampled and different tissues were dissected. These included 300 male antennae, 300 female antennae, 60 heads (without antennae; 30 males and 30 females, pooled), 60 abdomens (30 males and 30 females, pooled), and 300 legs (150 males and 150 females, pooled). Total RNA was isolated using Trizol reagent (Life Technologies, Carlsbad, CA, United States) following manufacturer protocol. The integrity and concentration of the RNA was determined using agarose gel electrophoresis and spectrophotometry, respectively.

cDNA Library Construction

Total RNA (20 μg) from male and female antennae were used to create cDNA libraries. In brief, poly(A)+ mRNA was purified from total RNA using oligo(dT) magnetic beads and was digested to short fragments in a fragmentation buffer. The fragmented mRNA was used to generate first-strand cDNA using a random hexamer primer and MMLV reverse transcriptase, and second-strand cDNA was subsequently synthetized in a mixture of DNA polymerase I, dNTPs and RNaseH. The double-stranded cDNA was treated with T4 DNA polymerase for end-repair and T4 polynucleotide kinase for dA-tailing. After ligation of the sequencing adapters with T4 DNA ligase, these fragments were used as templates for PCR amplification. Finally, the PCR product was heat-denatured and the single-stranded cDNA was cyclized by splint oligonucleotide and DNA ligase to generate the library.

Transcriptome Assembly and Functional Annotation

The cDNA libraries from male and female antennae were sequenced on a BGISEQ-500 system using a paired-end sequencing method according to manufacturer instructions at the Beijing Genomics Institute (BGI-Wuhan, Wuhan, China). Before *de novo* assembly, the adapters and low-quality reads were filtered, and removed, from the raw data. Clean reads from males and females were assembled into a single assembly using Trinity software (v2.0.6; Grabherr et al., 2011). Reads were combined to form contigs, from which scaffolds were extended by paired-end joining and gap-filling. If a scaffold could not be extended on either end, it was defined as a unigene. Functional annotation of each unigene was performed using the BLASTX program against the NCBI non-redundant (NR) database, Gene Ontology (GO), and eukaryotic orthologous groups (KOG) with a cut-off *e*-value of 10^{-5}. The Kyoto Encyclopedia of Genes and Genomes (KEGG) pathways annotations were performed using the KEGG automatic annotation server (Yoshizawa et al., 2007).

Identification of Olfactory Genes

Candidate olfactory genes were identified by retrieving the transcriptome dataset with the TBLASTN program (Altschul et al., 1997). The annotated protein sequences of OBPs, CSPs, ORs, IRs, and SNMPs from other Lepidoptera species, including *Bombyx mori*, *Plutella xylostella*, *Manduca sexta*, *Helicoverpa armigera*, *Spodoptera litura*, *Chilo suppressalis*, *Cnaphalocrocis medinalis*, and *Ostrinia furnacalis*, were used as queries. The cut-off *e*-value was set as 10^{-5}. The output was manually checked, and overlapping variants were eliminated. Finally, all the candidates were confirmed by searching against the NCBI NR database using the BLASTX online program[1](cut-off *e*-value: 10^{-5}). In addition, all the candidate genes were compared with those reported by Zhao et al. (2019) using BLASTN program (cut-off *e*-value: 10^{-5}; Altschul et al., 1997), in order to find novel olfactory genes in *G. mellonella*.

[1]https://blast.ncbi.nlm.nih.gov/Blast.cgi

Bioinformatic Analyses

The open reading frame (ORF) was predicted using ORF Finder[2]. The theoretical molecular weight (Mw) and isoelectric point (pI) were obtained using an ExPASy tool[3]. Putative signal peptide and the transmembrane domain were predicted with SignalP[4] and TMHMM[5], respectively. The Clustal Omega program[6] was used to align deduced protein sequences. The phylogenetic trees were constructed with MEGA7 software using the neighbor-joining method with 1,000-fold bootstrap resampling (Kumar et al., 2016). The trees were viewed and edited using FigTree software[7]. The GenBank accession numbers of sequences used in the phylogenetic analyses are listed in **Supplementary Table 1**. Motif pattern analysis was performed using the MEME program[8]; insect OBPs and CSPs used in the analysis are listed in **Supplementary Table 2**. The genomic distribution of each gene was determined by mapping the cDNA with the *G. mellonella* genomic DNA (Lange et al., 2018) using the Splign program[9].

RT-qPCR

Total RNA from different adult tissues (see "Sample Collection and RNA Extraction" section) was reverse transcribed to generate first-strand cDNA using ReverTra Ace qPCR RT Master Mix with gDNA Remover (Toyobo, Osaka, Japan). Each cDNA sample was diluted to 10 ng/μL using nuclease-free water. RT-qPCR was performed in a 20 μL reaction mixture containing 10 μL SYBR Green Real-time PCR Master Mix (Toyobo, Osaka, Japan), 1 μL (10 ng) cDNA template, 0.4 μL (0.2 μM) of forward primer, 0.4 μL (0.2 μM) of reverse primer, and 8.2 μL nuclease-free water. Primers for RT-qPCR are listed in **Supplementary Table 3**, and the glyceraldehyde-3-phosphate dehydrogenase (*GAPDH*) gene was used as an internal reference to normalize target gene expression. RT-qPCR reactions were conducted in 96-well plates and run on a CFX96 Real-time System (Bio-Rad, Hercules, CA, United States). The thermal cycle parameters were one cycle of 95°C for 2 min, 40 cycles of 95°C for 5 s, and 60°C for 20 s. At the end of each thermal cycle, the PCR products were analyzed using a heat-dissociation protocol to confirm that only one single gene was amplified. A no-template control and a no-reverse transcriptase control were both included in each reaction plate to detect possible contamination. The experiment was biologically repeated three times (each with four technical replicates). Relative expression levels were calculated by using the $2^{-\Delta\Delta Ct}$ method (Livak and Schmittgen, 2001).

Statistics

Data were analyzed using Data Processing System (DPS) software version 9.5 (Tang and Zhang, 2013). One-way analysis of variance (ANOVA) with Tukey's *post hoc* test was performed to analyze

[2]http://www.ncbi.nlm.nih.gov/gorf/gorf.html
[3]http://web.expasy.org/compute_pi/
[4]http://www.cbs.dtu.dk/services/SignalP
[5]http://www.cbs.dtu.dk/services/TMHMM/
[6]http://www.ebi.ac.uk/tools/msa/clustalo/
[7]http://tree.bio.ed.ac.uk/software/figtree/
[8]http://meme-suite.org/tools/meme
[9]https://www.ncbi.nlm.nih.gov/sutils/splign/splign.cgi

differences of gene expression levels among multiple samples. Comparisons were considered significant at a $p < 0.05$.

RESULTS

Transcriptome Sequencing and Unigene Assembly

In total, 73.8 and 73.9 Mb raw reads were generated from the transcriptomes of male and female antennae, respectively (**Table 1**). These data have been deposited into the NCBI Sequence Read Archive (SRA) database under accession numbers SRR8307568 (male antennae) and SRR8307567 (female antennae). After data filtration, 70.3 Mb (male antennae) and 70.6 Mb (female antennae) clean reads were obtained. Clean reads from the two transcriptomes were assembled into 42,544 unigenes (**Table 1**). The size distribution analysis showed that the lengths of 18,844 unigenes (44.3% of all unigenes) were greater than 1,000 bp (**Figure 1A**).

Functional Annotation

We annotated the *G. mellonella* unigenes by searching against the NCBI NR database. A total of 14,481 (34%) of the 42,544 unigenes resulted from the search (**Figure 1B**). For species distribution, the *G. mellonella* unigenes were best matched to those from other species of Lepidoptera, including *B. mori* (40.6%), *P. xylostella* (23.7%), and *Danaus plexippus* (23.2%) (**Figure 1B**). Next, we performed a GO analysis to better classify the functions of the *G. mellonella* unigenes. The results indicated that 8,887 (20.9%) of the unigenes could be annotated to at least one GO term (**Figure 1C**). Among the GO categories, the *G. mellonella* unigenes were mostly enriched in "binding" and "catalytic activity" categories in the "molecular function" level, followed by "cell" and "membrane part" categories in the "cellular component" level, and "cellular process" category in the "biological process" level (**Figure 1C**). We also performed the functional classification for the unigenes by searching against KOG and KEGG databases, and the results are shown in **Supplementary Figures 1, 2**, respectively.

TABLE 1 | Information of the *G. mellonella* antennal transcriptome.

	Male antennae	Female antennae
Total size	7.0 Gb	7.0 Gb
Total number of raw reads	73.8 Mb	73.9 Mb
Total number of clean reads	70.3 Mb	70.6 Mb
Q20 (%)	97.4	97.4
Total number of unigenes	42,544	
Total length of unigenes	60.4 Mb	
Maximum length of unigenes	21,594 bp	
Mean length of unigenes	1,420 bp	
Minimum length of unigenes	297 bp	
N50	2,617 bp	
GC (%)	38.4	

Identification of *OBPs*

Zhao et al. (2019) identified 22 *OBP*s from *G. mellonella* antennae, including 2 *GOBP*s, 3 *PBP*s, and 17 *OBP*s. In the present study, we screened the antennal transcriptome dataset and identified 21 genes (**Supplementary Table 4**). Of these, four (*GmelOBP18* to *GmelOBP21*) are novel genes. A comprehensive list of *G. mellonella* OBPs is shown in **Supplementary Figure 3**, and the nucleotide and amino acid sequences of genes identified are listed in **Supplementary Table 5**. We found at least 26 *OBP*s expressed in the antennae of *G. mellonella*. Of the identified OBPs, 16 sequences had complete ORFs, while *GmelOBP4, GmelOBP20,* and *GmelOBP21* lacked the 5′- and/or 3′-terminus (**Supplementary Table 4**). Most of the *OBP*s shared ≥51% amino acid identities with orthologs from other Lepidoptera species, whereas three OBPs, *GmelOBP8*, *GmelOBP13,* and *GmelOBP18*, shared 28, 47, and 38% amino acid identities, respectively, with their respective orthologs (**Supplementary Table 4**).

The multiple sequence alignment result showed that six positionally conserved cysteine residues were presented in all OBP proteins except for GmelOBP14, which only had four cysteine residues (**Supplementary Figure 4**). A phylogenetic tree was constructed and the results indicated that the *G. mellonella* OBPs were well-segregated from each other with high bootstrap support; most of them were clustered with at least one lepidopteran ortholog (**Figure 2**). We used the MEME program to investigate the motif patterns in the identified OBPs and found eight conserved motifs (**Figure 3A**). GmelGOBP1, GmelPBP2, and GmelPBP3 have the same motif pattern 4-3-1-5-6-2-8; GmelGOBP2 is similar to GmelGOBP1 but lacks the seventh and eighth motifs at its C-terminus, whereas GmelPBP1 lacks the first motif at the N-terminus (**Figure 3B**). The most conserved motif pattern (4-1-2) was observed in nine OBPs (GmelOBP1/2/3/8/13/16/18/20/21), whereas GmelOBP7 and GmelOBP17 only had the fourth motif (**Figure 3B**).

Identification of *CSPs*

A total of 18 *CSP* genes were retrieved from the transcriptome dataset (**Supplementary Tables 4, 5**). All of these *CSP*s had complete ORFs and the length of the deduced proteins ranged from 97 to 131 amino acids (**Supplementary Table 4**). BLASTX best hit results showed that three *CSP*s (*GmelCSP9*, *GmelCSP12,* and *GmelCSP13*) had low amino acid identities (33–42%) to other known *CSP*s, whereas the other 15 CSPs had high amino acid identities (61–85%) to their lepidopteran orthologs (**Supplementary Table 4**).

Multiple sequence alignment showed that all the deduced GmelCSP proteins had four positionally conversed cysteines (**Supplementary Figure 5**). Phylogenetic analysis showed that, like GmelOBPs, most GmelCSPs were spread across different branches and that they were clustered with at least one lepidopteran ortholog (**Figure 4**). The MEME program revealed that the motif pattern 8-3-5-1-6-2-7-4 is most conserved, which existed in 10 (GmelCSP1/2/3/4/5/8/10/16/18/20) of the 20 CSPs (**Figure 5**). GmelCSP7 and GmelCSP11 had the motif pattern 8-3-5-1-6-2-4, and GmelCSP13 and GmelCSP15 had the pattern 8-3-1-6-2-4. Other GmelOBPs had distinct patterns (**Figure 5**).

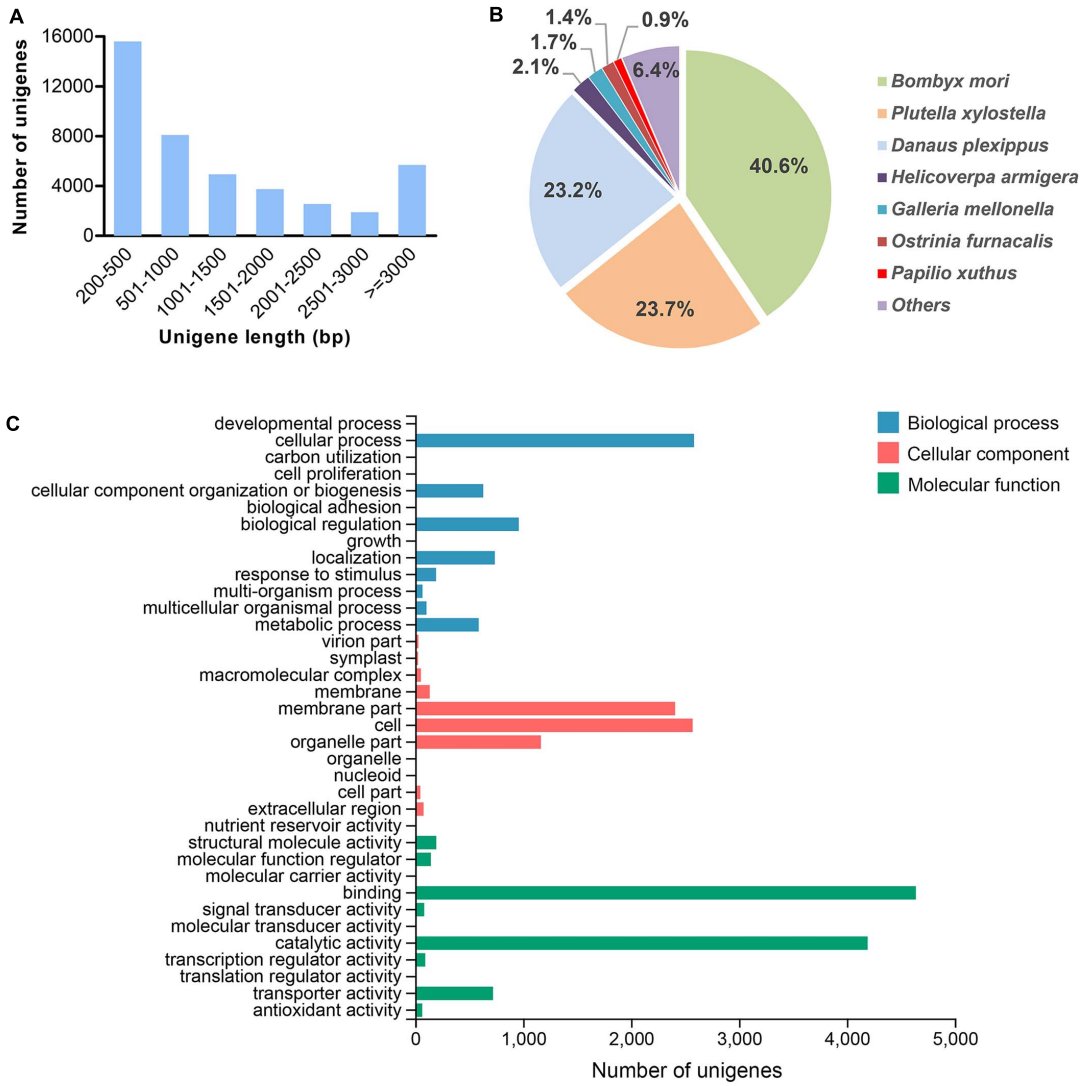

FIGURE 1 | Summary of the *G. mellonella* unigene assembly. **(A)** Size distribution of unigenes. **(B)** Species distribution of unigenes based on homology searching against the NCBI NR database. **(C)** GO classification of unigenes.

Identification of *ORs*

We identified 43 putative *ORs* from the transcriptome (**Supplementary Tables 4, 5**). Of these, five (*GmelOR46* to *GmelOR50*) were novel genes, and other sequences were previously identified by Zhao et al. (2019) (**Supplementary Figure 3**). The total number of *GmelORs* is expected to reach 51. Of the *ORs*, 27 sequences had complete ORFs, whereas other sequences had truncations in the 5′- and/or 3′-ternimus (**Supplementary Table 4**). The length of the deduced OR proteins ranged from 163 to 474 amino acids, and the transmembrane domains were predicted in all the OR proteins (**Supplementary Table 4**). BLASTX best hit results showed that all the *GmelORs* had orthologs in other species of Lepidoptera, including *O. furnacalis*, *Amyelois transitella*, *H. armigera*, and *B. mori* (**Supplementary Table 4**). In the phylogenetic analysis, GmelORs were well-segregated from each other with high bootstrap support, and most of them were clustered with at least one lepidopteran ortholog (**Figure 6**). As expected, the olfactory co-receptor, *GmelOrco*, was clustered into a branch with *Orcos* from *C. suppressalis*, *O. furnacalis*, *P. xylostella*, and *B. mori* (**Figure 6**). Additionally, *GmelOR13* and *GmelOR50* fell into the "Lepidopteran pheromone receptors (PRs)" clade with PRs from other Lepidoptera species, e.g., BmorOR1 and BmorOR3 from *B. mori*; PxylOR1 and PxylOR4 from *P. xylostella* (**Figure 6**).

Identification of *IRs* and *SNMPs*

We identified 18 putative *IRs*, including two novel genes (**Supplementary Tables 4, 5**). Together with the results of Zhao et al., the expected number of *IRs* in *G. mellonella* antennae is at least 19 (**Supplementary Figure 3**). Of these, 15 *IRs* had complete ORFs and the length of the deduced proteins ranged from 451 to 931 amino acid residues. All of

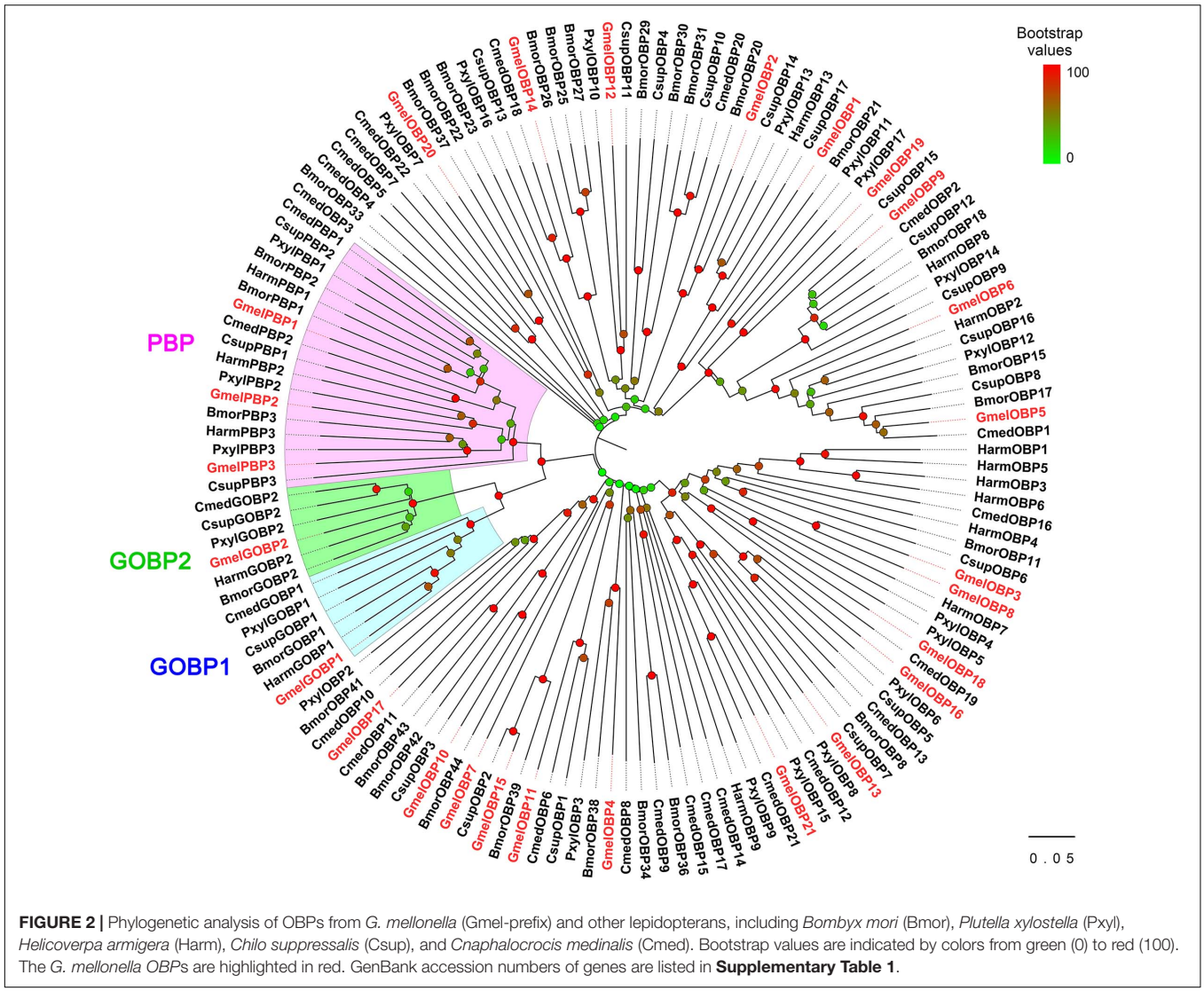

FIGURE 2 | Phylogenetic analysis of OBPs from *G. mellonella* (Gmel-prefix) and other lepidopterans, including *Bombyx mori* (Bmor), *Plutella xylostella* (Pxyl), *Helicoverpa armigera* (Harm), *Chilo suppressalis* (Csup), and *Cnaphalocrocis medinalis* (Cmed). Bootstrap values are indicated by colors from green (0) to red (100). The *G. mellonella OBP*s are highlighted in red. GenBank accession numbers of genes are listed in **Supplementary Table 1**.

the GmelIRs were transmembrane proteins which contained 2–4 transmembrane domains (**Supplementary Table 4**). Most of the GmelIRs shared ≥52% amino acid identities with their respective orthologs from other lepidopterans except for GmelIR7d and GmelIR75q1, which shared 45 and 48% amino acid identities, respectively, with other insect IRs (**Supplementary Table 4**). Phylogenetic analysis showed that most of the GmelIRs were segregated from each other, and that most GmelIRs were located on branches with other lepidopteran IRs (**Figure 7**). In addition, two putative co-receptors, GmelIR8a and GmelIR25a, were also identified (**Supplementary Table 4** and **Figure 7**).

We identified two *SNMP*s in *G. mellonella*, namely, *GmelSNMP1* and *GmelSNMP2*. *GmelSNMP1* shared 71% amino acid identity with *SNMP1* in *Eogystia hippophaecolus*, while *GmelSNMP2* was more similar to the *O. nubilalis* SNMP2 (66% amino acid identity) (**Supplementary Table 4**). The two deduced GmelSNMP proteins both had two transmembrane domains, and had five positionally conserved cysteine residues (**Supplementary Figure 6**). Phylogenetic analysis showed that *GmelSNMP1* and *GmelSNMP2* had a close relationship with their lepidopteran orthologs (**Figure 8**).

Genomic Localization of Olfactory Genes

We determined the genomic distribution of the olfactory genes identified from *G. mellonella* by mapping the cDNA sequences to genome scaffolds. We successfully matched the 118 genes (containing 16 genes identified by Zhao et al., 2019) to 61 scaffolds (**Supplementary Table 6**). Of the 26 *OBP*s, 2 *GmelGOBP*s, and 3 *GmelPBP*s were located on scaffold53, while another 10 *OBP*s (*GmelOBP3/5/6/8/9/13/16/18/19/21*) were tandemly arrayed on scaffold145 (**Figure 9A** and **Supplementary Table 6**). Of the 20 *CSP*s, 17 were found to be clustered within a 123 kb genomic region on scaffold11 (**Figure 9B** and **Supplementary Table 6**).

For *OR*s, we found that most of the scaffolds contained only one or two *OR* genes; the exceptions were scaffold2, scaffold42, scaffold43, scaffold611, and scaffold681, each of which contained three *GmelOR*s (**Supplementary Table 6**). For *IR*s

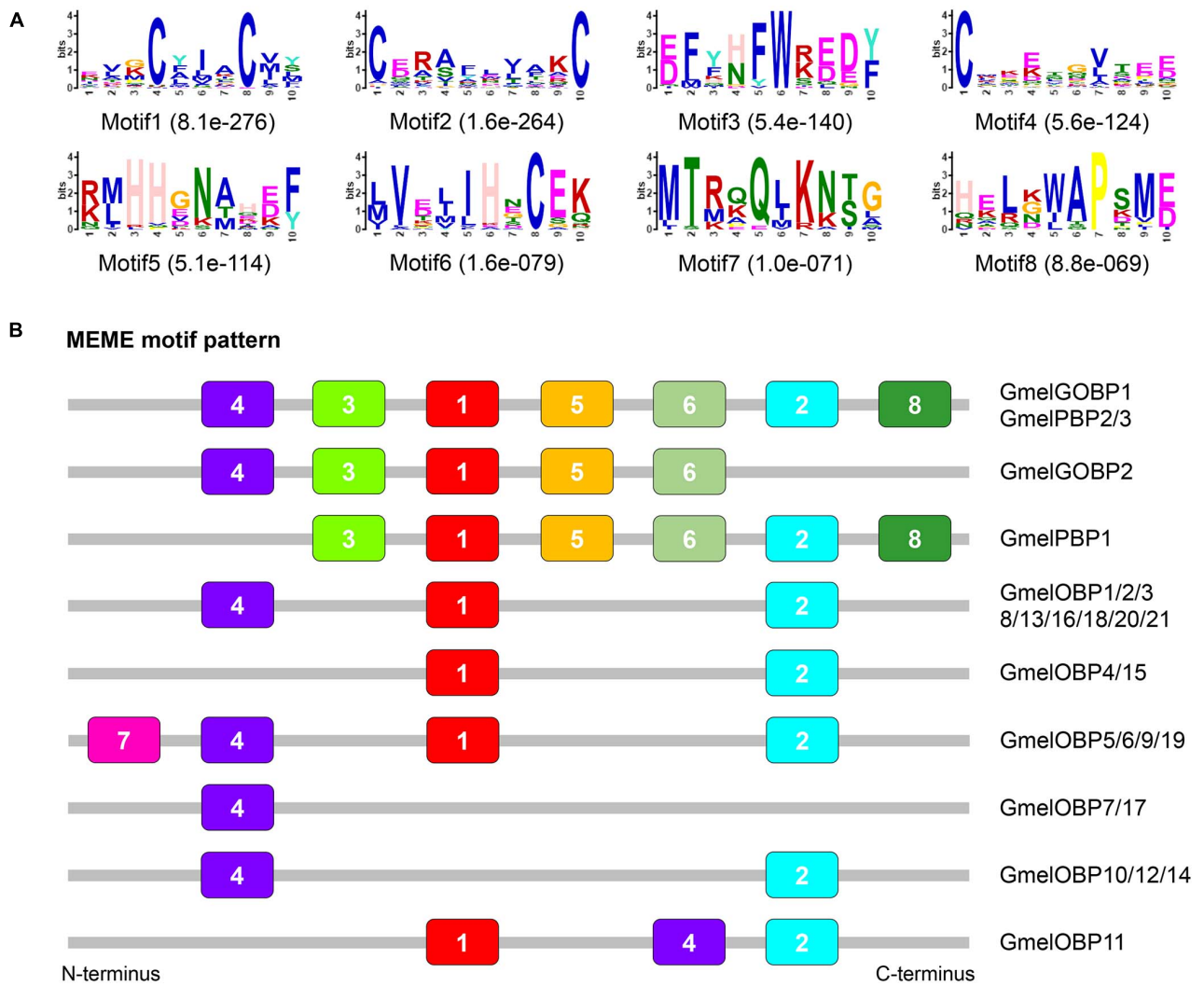

FIGURE 3 | Motif pattern analysis of *G. mellonella* OBPs. **(A)** The discovered eight motifs (motif1–8) in GmelOBP proteins and their homologs from other lepidopterans. The number in the parentheses indicated the expect-value (*e*-value) of each motif calculated by MEME program. **(B)** Locations of each motif in the protein sequences. The numbers in the colored boxes correspond to the numbered motifs in **(A)**. The protein sequences of the OBPs used are listed in **Supplementary Table 2**.

and *SNMP*s, we mapped *GmelIR75p1* and *GmelIR75p2* on scaffold319, and *GmelIR75q1* and *GmelIR75q2* on scaffold172 (**Supplementary Table 6**). The remaining *IR*s, as well as the *SNMP*s, were located individually on a single scaffold (**Supplementary Table 6**).

Expression Profiles of Olfactory Genes

The tissue- and sex-biased expression profiles of the newly identified genes (four *OBP*s, five *OR*s, and two *IR*s) were investigated using RT-qPCR. All the tested genes were predominantly or highly expressed in the antennae (**Figure 10**). Of these, the transcripts of *GmelOBP19* and *GmelOR47* were enriched in male antennae, with expression levels 1.8-fold (*GmelOBP19*) and 2.7-fold (*GmelOR47*) higher in males than in females, respectively (**Figure 10**). Other genes were expressed at equal or near-equal amounts in the antennae of both sexes (**Figure 10**).

DISCUSSION

We constructed a transcriptome dataset from the *G. mellonella* antennae. Zhao et al. (2019) previously identified 22 *OBP*s, 20 *CSP*s, 46 *OR*s, 17 *IR*s, and 2 *SNMP*s in *G. mellonella* antennae. Here, we discovered 102 olfactory-related genes, including 11 novel genes. Our findings, together with the results of Zhao et al. (2019), provide a comprehensive data resource for the olfactory genes in *G. mellonella*.

We identified 21 *OBP*s, including four novel genes, in *G. mellonella* antennae. Therefore, the total number of *OBP*s in the *G. mellonella* antennae is at least 26. Although this number

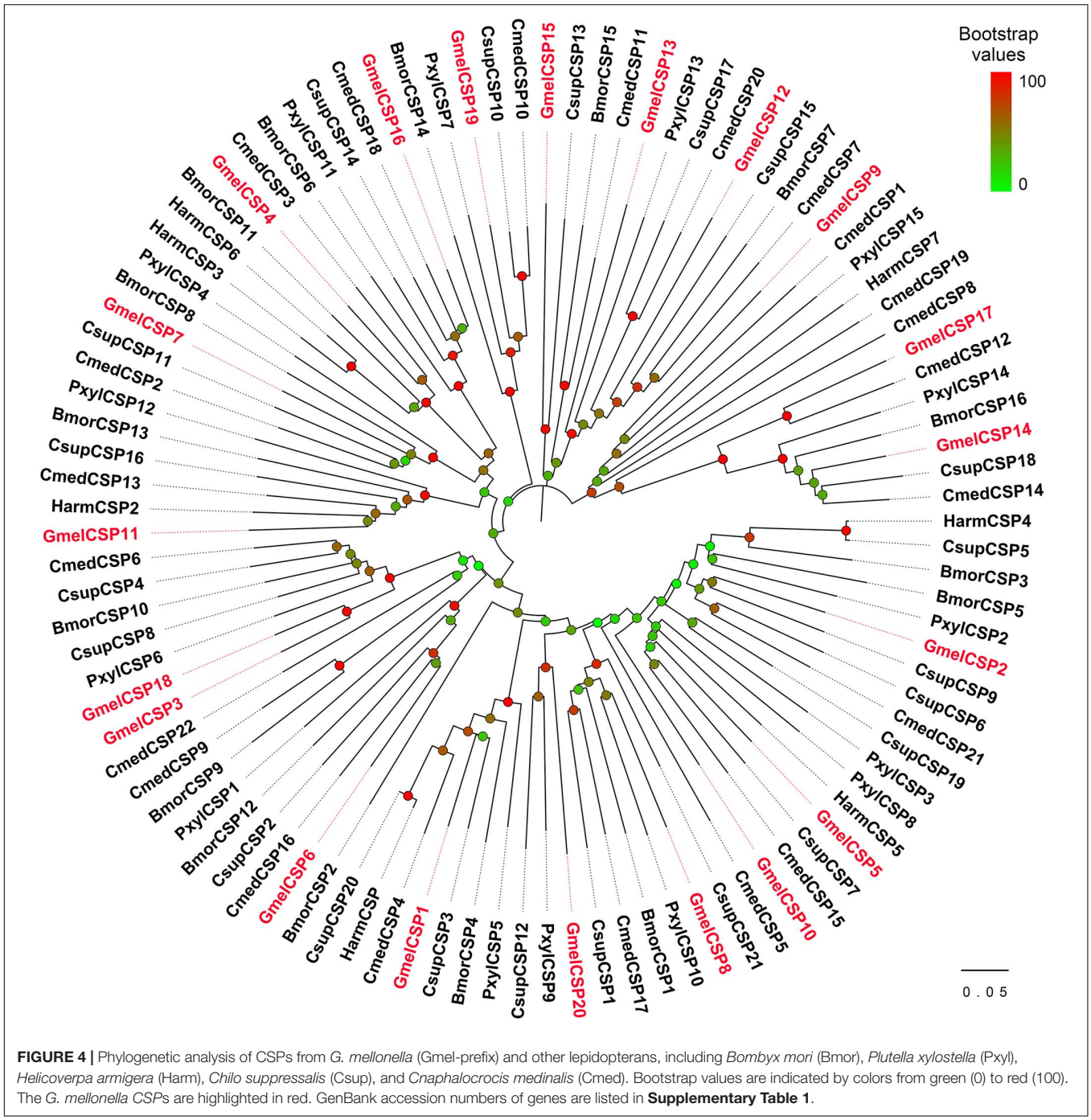

FIGURE 4 | Phylogenetic analysis of CSPs from *G. mellonella* (Gmel-prefix) and other lepidopterans, including *Bombyx mori* (Bmor), *Plutella xylostella* (Pxyl), *Helicoverpa armigera* (Harm), *Chilo suppressalis* (Csup), and *Cnaphalocrocis medinalis* (Cmed). Bootstrap values are indicated by colors from green (0) to red (100). The *G. mellonella CSP*s are highlighted in red. GenBank accession numbers of genes are listed in **Supplementary Table 1**.

is lower than the number in *Drosophila melanogaster* (52 genes), *M. sexta* (49 genes), *Spodoptera littoralis* (49 genes), and *B. mori* (46 genes) (Gong et al., 2009a; Vieira and Rozas, 2011; Vogt et al., 2015; Walker et al., 2019), it is comparable to those from other Lepidoptera, such as *O. furnacalis* (23 genes), *S. exigua* (24 genes); *P. xylostella* (24 genes), *S. frugiperda* (25 genes), and *C. suppressalis* (26 genes) (Cao et al., 2014; Zhang et al., 2015, 2018; Yang et al., 2017; Qiu et al., 2020). A number of *OBP* genes are specifically expressed in non-olfactory tissues such as abdomen and legs, as well as in larval stages of other insect species (Hull et al., 2014; Vogt et al., 2015). Since we only sequenced the antennal transcriptome of *G. mellonella*, some *OBP* genes might have been missed in the present research. Further studies examining additional tissues and developmental stages are needed.

The number of *CSP* genes in insect genomes appears to be highly variable. For instance, 34 and 33 *CSP*s were found in lepidopterans *D. plexippus* and *Heliconius melpomene*, respectively, whereas only four were discovered in the dipteran *D. melanogaster* (Vieira and Rozas, 2011;

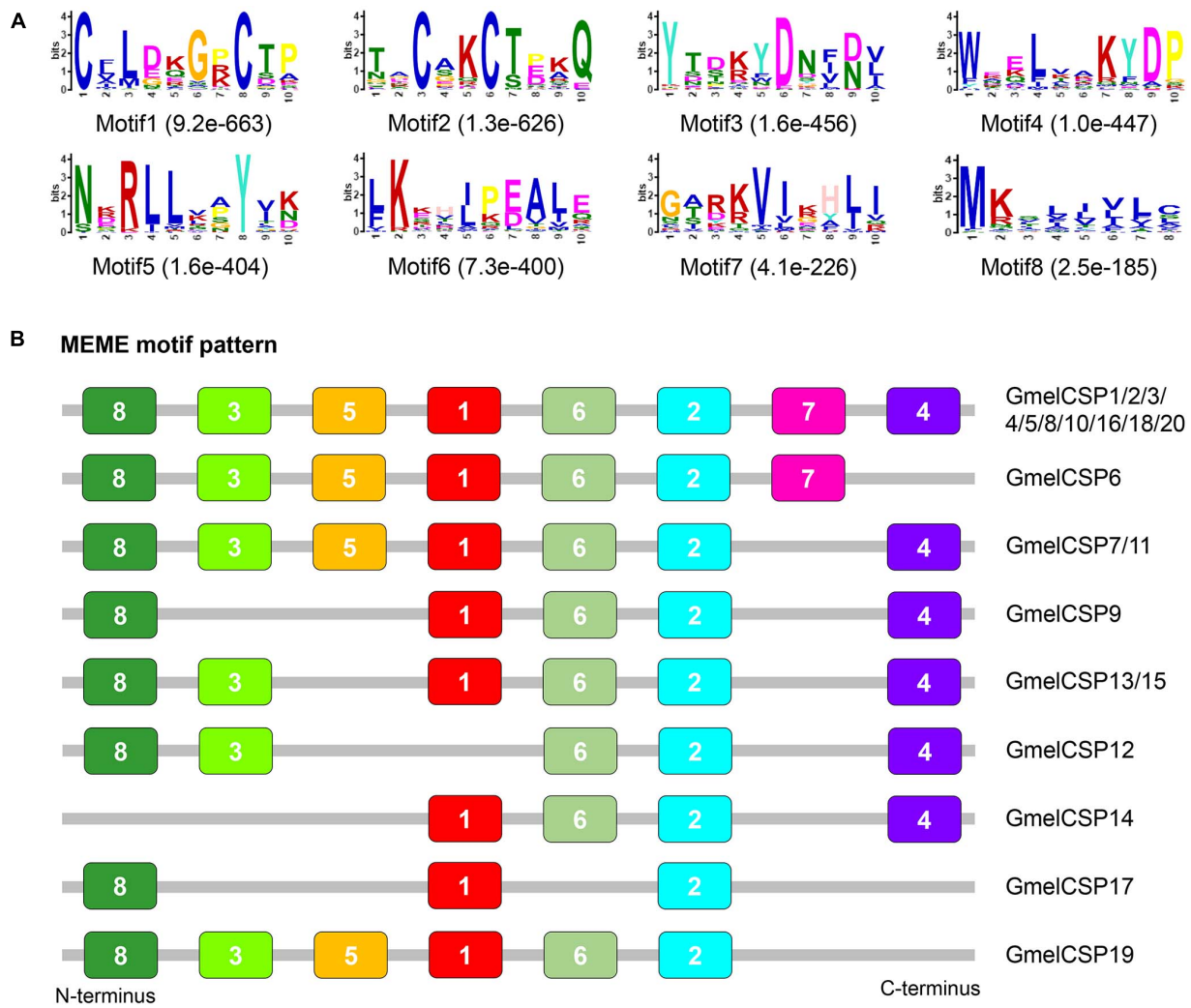

FIGURE 5 | Motif pattern analysis of *G. mellonella* CSPs. **(A)** Eight motifs (motif 1–8) discovered in GmelCSP proteins and their lepidopteran homologs. The number in the parentheses indicated the expect-value (*e*-value) calculated by MEME program. **(B)** Locations of each motif in the protein sequences. The numbers in the colored boxes correspond to the numbered motifs in **(A)**. The CSP protein sequences used are listed in **Supplementary Table 2**.

The Heliconius Genome Consortium, 2012). In this study, we identified 18 *CSP*s in *G. mellonella* antennae. The number of *GmelCSP*s is expected to reach 20 when combined with the genes discovered by Zhao et al. (2019). This number is less than the number in *D. plexippus* (34 genes) and *H. melpomene* (33 genes), but comparable to those identified in other lepidopterans, including *S. exigua* (19 genes; Zhang et al., 2018), *Plodia interpunctella* (15 genes; Jia et al., 2018), and *Streltzoviella insularis* (12 genes; Yang et al., 2019).

The motif pattern varies in different OBP and CSP proteins in insects (Zhang et al., 2016; Sun et al., 2017). Within *G. mellonella* OBPs, the most conserved pattern is 4-1-2, whereas 8-3-5-1-6-2-7-4 is most conserved in CSPs. This result implies a conserved function of the two protein families in odor recognition. We found that two GmelGOBPs and three GmelPBPs displayed different motif patterns: GmelGOBP2 lost the seventh and eighth motifs, and GmelPBP1 lacks the first motif, when compared with those in GmelGOBP1, GmelPBP2, and GmelPBP3 (**Figure 3B**). This difference suggests a possible functional differentiation. Indeed, a number of studies have indicated that lepidopteran GOBPs and PBPs display different affinities to odorants (Liu et al., 2015; Zhang et al., 2017).

We identified 43 *OR*s from *G. mellonella*, including 5 novel genes. The total number (51 genes) of *OR*s in *G. mellonella* is less than the 66 and 73 genes identified, respectively, in the genomes of *B. mori* and *S. litura*, two model lepidopteran insect species (Tanaka et al., 2009; Cheng et al., 2017), but comparable to those in *P. xylostella* (54 genes; Yang et al., 2017), *O. furnacalis* (52 genes; Yang et al., 2015), and *M. sexta* (48 genes; Grosse-Wilde et al., 2011). Numerous studies have reported that a subset of *OR* genes in insects have higher transcription levels in non-olfactory tissues than in antennae (Fleischer et al., 2018). Thus, our sequencing of the antennae limits our ability to identify potential *OR* genes enriched in other non-olfactory

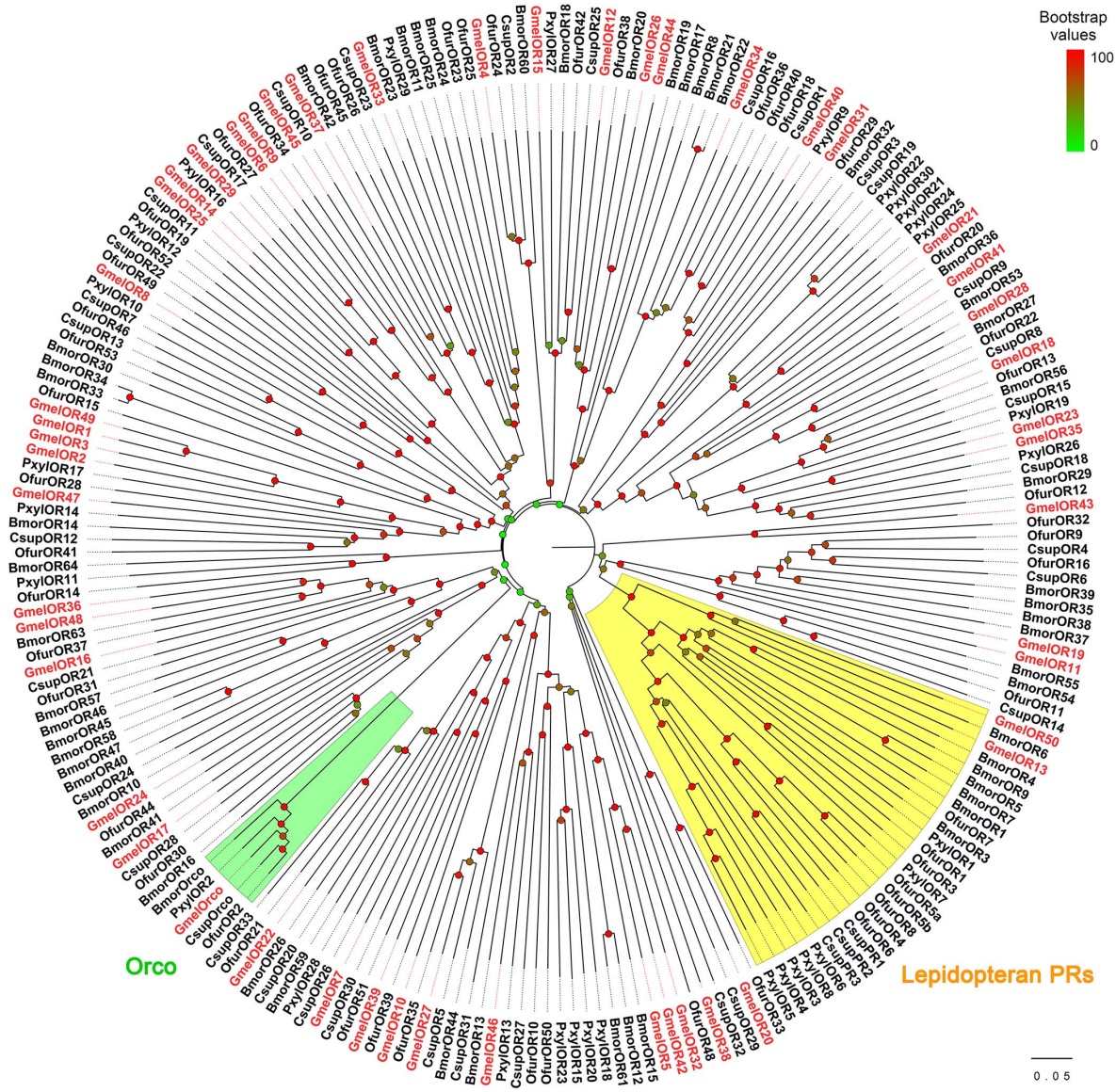

FIGURE 6 | Phylogenetic relationships of lepidopteran ORs. Gmel: *Galleria mellonella*; Bmor: *Bombyx mori*; Ofur: *Ostrinia furnacalis*; Csup: *Chilo suppressalis*; Pxyl: *Plutella xylostella*. Bootstrap values are indicated by colors from green (0) to red (100). The *G. mellonella ORs* are highlighted in red. GmelOR30 was not used for the analysis due to its short length. GenBank accession numbers of ORs used are listed in **Supplementary Table 1**.

organs. We also identified *GmelOrco*, the olfactory co-receptor, from *G. mellonella*. Insect Orco is an essential component for forming a functional OR unit (Leal, 2013). Therefore, the identification of *GmelOrco* greatly benefits the development of synthetic inhibitors or genome-editing approaches to control this insect pest (Koutroumpa et al., 2016; Kepchia et al., 2017; Liu et al., 2017a).

Apart from *ORs*, 18 *IRs* were identified in our transcriptome search. In Lepidoptera, 17, 18, 21, and 21 *IRs* were found in the antennae of *S. littoralis*, *B. mori*, *H. armigera*, and *O. furnacalis*, respectively (Croset et al., 2010; Poivet et al., 2013; Liu et al., 2014; Yang et al., 2015). Thus, the *IR* gene number in *G. mellonella* antennae is comparable to those in other Lepidoptera. We also identified the orthologs (*GmelIR8a* and *GmelIR25a*) of the highly conserved co-receptors *IR8a* and *IR25a*. The two genes are expected to encode functional proteins and play a central role in forming a functional IR receptor complex (Abuin et al., 2011, 2019). The *M. sexta* IR8a is required for acid detection and is involved in the avoidance of acids from caterpillar feces (Zhang et al., 2019).

We identified two *SNMPs* (*GmelSNMP1* and *GmelSNMP2*) in *G. mellonella*. Previous research on *Heliothis virescens* and *Antheraea polyphemus* demonstrated that *SNMP1s* are co-expressed with *PRs* in the pheromone-responsive neurons, whereas *SNMP2s* are expressed in the supporting cells around the neurons (Forstner et al., 2008). Two *SNMPs* have distinct

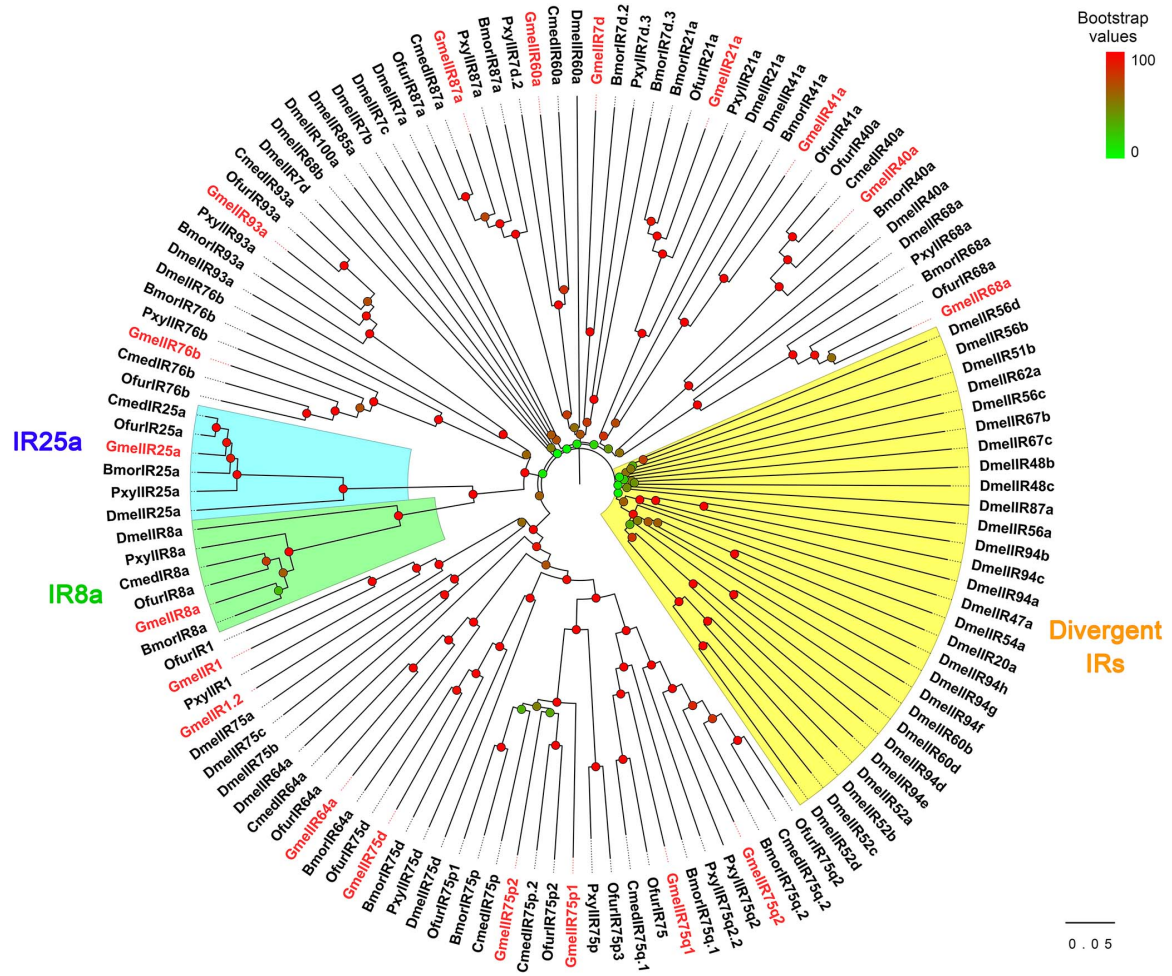

FIGURE 7 | Phylogenetic relationships of insect IRs. Dmel: *Drosophila melanogaster*; Bmor: *Bombyx mori*; Ofur: *Ostrinia furnacalis*; Pxyl: *Plutella xylostella*; Cmed: *Cnaphalocrocis medinalis*. Bootstrap values are indicated by colors from green (0) to red (100). The *G. mellonella* IRs are highlighted in red. GenBank accession numbers of IRs used are listed in **Supplementary Table 1**.

expression patterns in the antennal sensilla of *Ectropis obliqua* (Sun et al., 2019b), suggesting a functional diversification between the two genes. In *D. melanogaster*, *H. virescens*, and *B. mori*, SNMP1s play critical roles in pheromone signaling (Jin et al., 2008; Pregitzer et al., 2014; Zhang et al., 2020). The two *GmelSNMP*s identified here showed very high identities with orthologs in other insect species, indicating functional conservation among these proteins.

We analyzed the genomic distribution of olfactory genes in *G. mellonella* and found that a large number of *OBP*s and *CSP*s were located on the same scaffolds and formed gene clusters. Two or more *OBP* or *CSP* loci located on the same scaffold implies that they were derived through duplication events during evolution (Vieira and Rozas, 2011; Vogt et al., 2015). It is possible that the *G. mellonella OBP* and *CSP* families evolved through gene duplication. Clusters of *OBP* and *CSP* genes on the same scaffold have also been found in the genomes of many other insect species including *D. melanogaster*, *Apis mellifera*, *Anopheles gambiae*, and *B. mori* (Hekmat-Scafe et al., 2002; Forêt and Maleszka, 2006; Gong et al., 2009a). Further analysis of *OBP* or *CSP* gene duplication events in *G. mellonella* is needed and will extend our knowledge of gene evolution. *G. mellonella* adults display a unique pair-forming behavior in which the sex pheromone is produced by males and perceived by conspecific females (Kwadha et al., 2017). Hence, olfactory genes that are primarily expressed in female antennae might be involved in recognizing sex pheromone constituents. Previously, Zhao et al. (2019) identified several female antennae-biased genes and hypothesized that they may contribute to pheromone detection. In this study, we analyzed the expression profiles of the newly identified genes. However, we were unable to identify female antennae-biased genes in *G. mellonella*; we only found two genes (*GmelOBP19* and *GmelOR47*) that were mainly expressed in the male antennae. The male antennae-biased expression suggests that these genes may play a role in the recognition of volatiles from females and/or beehives. In other insect species, including *E. obliqua*, *O. furnacalis*, *Cotesia vestalis*, *Laodelphax striatellus*, *Leptocorisa acuta*, *Histia rhodope*, *Phthorimaea operculella*, and

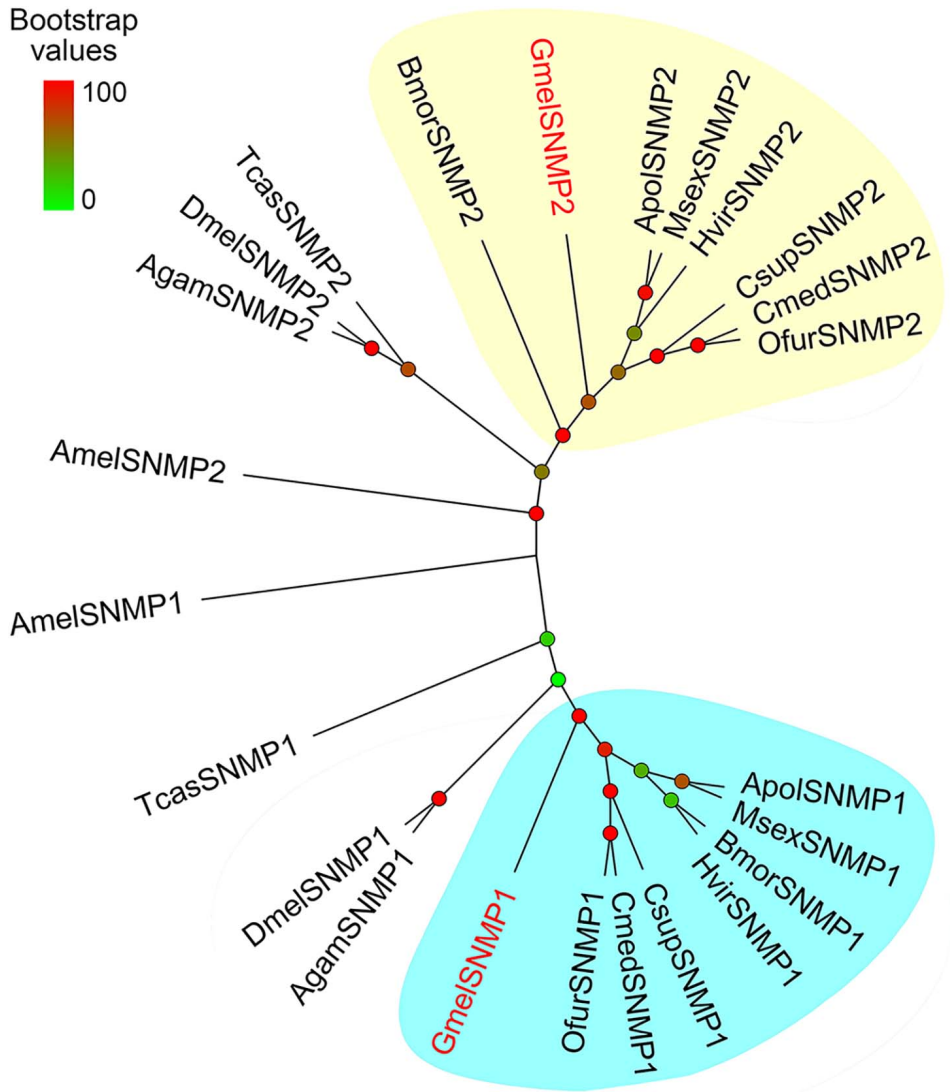

FIGURE 8 | Phylogenetic relationships of insect SNMPs. Gmel: *Galleria mellonella*; Apol: *Antheraea polyphemus*; Bmor: *Bombyx mori*; Csup: *Chilo suppressalis*; Cmed: *Cnaphalocrocis medinalis*; Hvir: *Heliothis virescens*; Msex: *Manduca sexta*; Ofur: *Ostrinia furnacalis*; Agam: *Anopheles gambiae*; Amel: *Apis mellifera*; Dmel: *Drosophila melanogaster*; Tcas: *Tribolium castaneum*. Bootstrap values are indicated by colors from green (0) to red (100). The *G. mellonella* SNMPs are highlighted in red. GenBank accession numbers of genes used are listed in **Supplementary Table 1**.

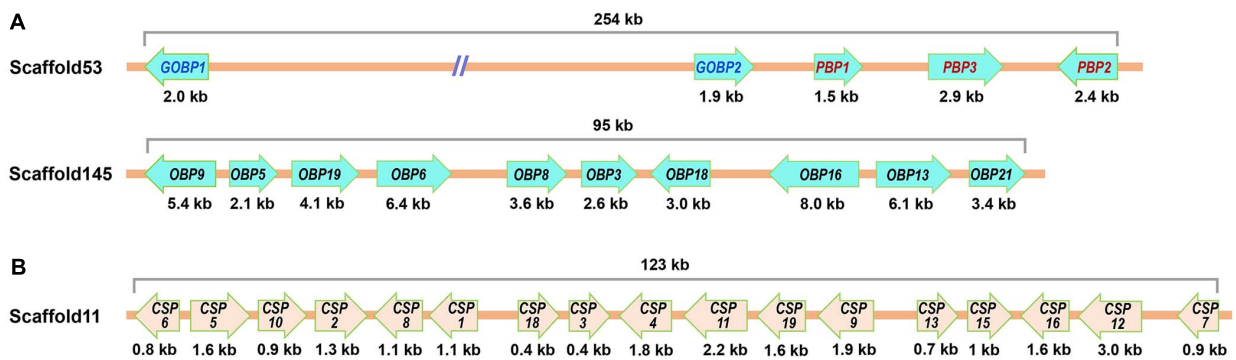

FIGURE 9 | Genomic location of *OBPs* **(A)** and *CSPs* **(B)** in *G. mellonella*.

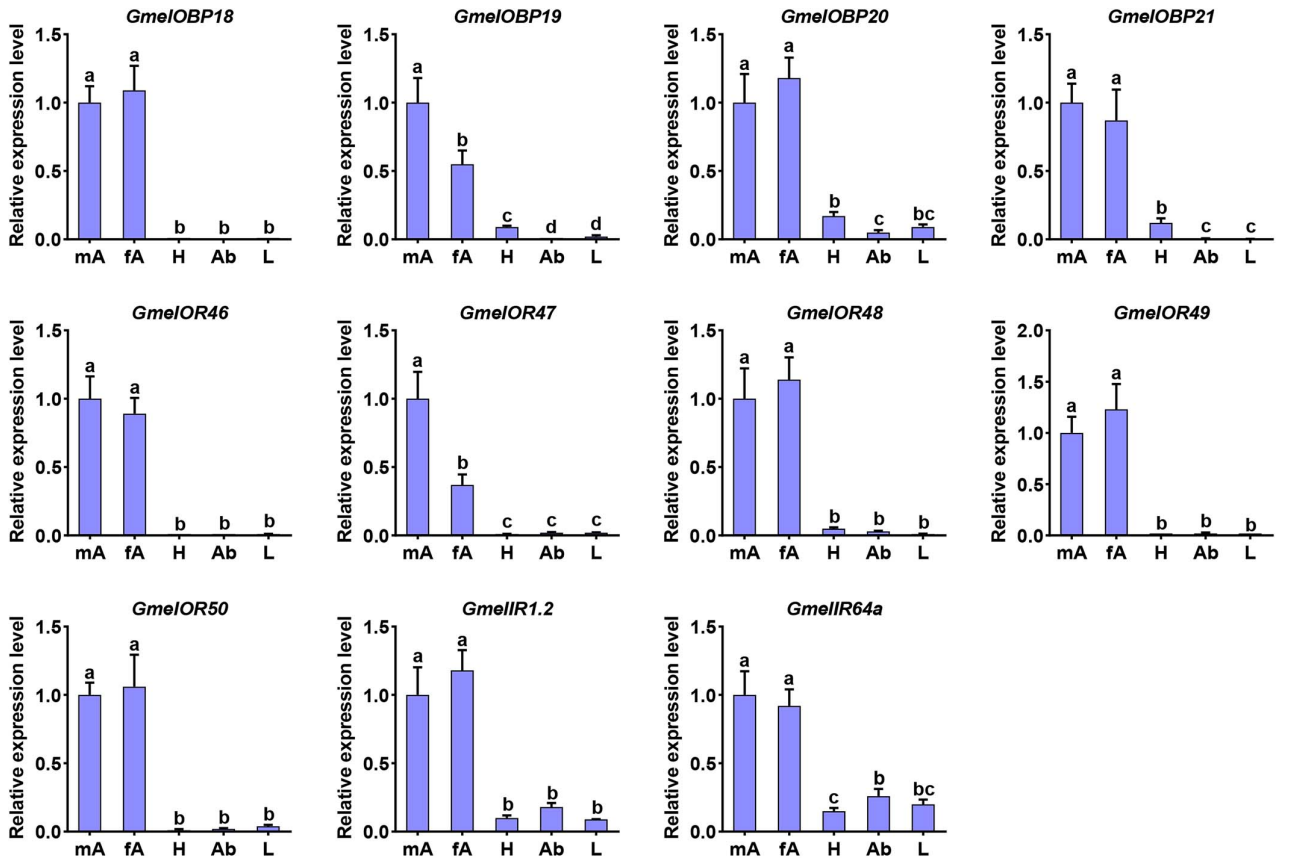

FIGURE 10 | Expression profiles of olfactory genes in different adult tissues. mA: male antennae, fA: female antennae, H: head (without antennae), Ab: abdomen, L: legs. Gene expression levels in various tissues were normalized relative to that in male antennae (set as onefold). Data are presented as mean ($n = 3$) ± SE. Different lowercase letters indicate significant differences ($p < 0.05$, one-way ANOVA with Tukey's test).

C. medinalis, a number of olfactory genes were also mainly expressed in male antennae (Zhang et al., 2015; Liu et al., 2017b, 2020; Sun et al., 2017; Li et al., 2020; Qu et al., 2020; Yang et al., 2020; He et al., 2021).

CONCLUSION

In conclusion, this study generated a transcriptome dataset of *G. mellonella* antennae. From the dataset, we identified numerous olfactory genes, including 21 *OBP*s, 18 *CSP*s, 43 *OR*s, 18 *IR*s, and 2 *SNMP*s. Several genes displayed tissue- and sex-biased expression patterns, suggesting they may play a role in olfactory processes. These results, together with the data of Zhao et al. (2019) provide a resource for olfactory genes in *G. mellonella*. Future functional studies on these genes will provide greater understanding of the molecular mechanisms underlying *G. mellonella* olfaction.

DATA AVAILABILITY STATEMENT

The datasets presented in this study can be found in online repositories. The names of the repository/repositories and accession number(s) can be found below: https://www.ncbi.nlm.nih.gov/, SRR8307567 and SRR8307568.

AUTHOR CONTRIBUTIONS

X-CJ, SL, X-YJ, Z-WW, L-SY, and H-QC conceived and designed the experimental plan. X-CJ, SL, X-YJ, Z-WW, J-JX, QG, C-WS, T-FS, and H-RZ performed the experiments. X-CJ, SL, L-SY, and H-QC analyzed the data. X-CJ and SL drafted the manuscript. L-SY and H-QC refined and approved the final manuscript. All authors contributed to the article and approved the submitted version.

FUNDING

This work was supported by the National Natural Science Foundation of China (Grant No. 31801806), the Major Science and Technology Project of Anhui Province (Grant No. 201903a06020027), the National Key Research and Development Program of China (Grant No. 2017YFD0200902), and the

National Undergraduate Training Program for Innovation and Entrepreneurship (Grant No. 201910364078).

SUPPLEMENTARY MATERIAL

The Supplementary Material for this article can be found online at: https://www.frontiersin.org/articles/10.3389/fphys.2021.663040/full#supplementary-material

Supplementary Figure 1 | KOG classification of the *Galleria mellonella* unigenes.

Supplementary Figure 2 | KEGG classification of the *G. mellonella* unigenes.

Supplementary Figure 3 | A comprehensive list of *G. mellonella OBP*, *CSP*, *OR,* and *IR* genes.

Supplementary Figure 4 | Partial alignment of the protein sequences of *G. mellonella* OBPs.

Supplementary Figure 5 | Alignment of the deduced protein sequences of *G. mellonella* CSPs.

Supplementary Figure 6 | Alignment of deduced *G. mellonella* SNMP protein sequences with orthologs from other insect species.

Supplementary Table 1 | Accession numbers of OBPs, CSPs, ORs, IRs, and SNMPs used in phylogenetic analyses.

Supplementary Table 2 | Amino acid sequences of OBPs and CSPs used in motif pattern analyses.

Supplementary Table 3 | Primers used in this study.

Supplementary Table 4 | Details of the olfactory genes identified in the *G. mellonella* antennal transcriptome.

Supplementary Table 5 | Nucleotide and amino acid sequences of chemosensory genes identified in *G. mellonella*.

Supplementary Table 6 | Details of the genomic distribution of the *G. mellonella* olfactory genes.

REFERENCES

Abuin, L., Bargeton, B., Ulbrich, M. H., Isacoff, E. Y., Kellenberger, S., and Benton, R. (2011). Functional architecture of olfactory ionotropic glutamate receptors. *Neuron* 69, 44–60. doi: 10.1016/j.neuron.2010.11.042

Abuin, L., Prieto-Godino, L. L., Pan, H., Gutierrez, C., Huang, L., Jin, R., et al. (2019). *In vivo* assembly and trafficking of olfactory ionotropic receptors. *BMC Biol.* 17:34. doi: 10.1186/s12915-019-0651-7

Altschul, S. F., Madden, T. L., Schäffer, A. A., Zhang, J., Zhang, Z., Miller, W., et al. (1997). Gapped BLAST and PSI-BLAST: a new generation of protein database search programs. *Nucleic Acids Res.* 25, 3389–3402. doi: 10.1093/nar/25.17.3389

Benton, R., Vannice, K. S., Gomez-Diaz, C., and Vosshall, L. B. (2009). Variant ionotropic glutamate receptors as chemosensory receptors in *Drosophila*. *Cell* 136, 149–162. doi: 10.1016/j.cell.2008.12.001

Brito, N. F., Moreira, M. F., and Melo, A. C. A. (2016). A look inside odorant-binding proteins in insect chemoreception. *J. Insect Physiol.* 95, 51–65. doi: 10.1016/j.jinsphys.2016.09.008

Butterwick, J. A., del Mármol, J., Kim, K. H., Kahlson, M. A., Rogow, J. A., Walz, T., et al. (2018). Cryo-EM structure of the insect olfactory receptor Orco. *Nature* 560, 447–452. doi: 10.1038/s41586-018-0420-8

Cao, D., Liu, Y., Wei, J., Liao, X., Walker, W. B., Li, J., et al. (2014). Identification of candidate olfactory genes in Chilo suppressalis by antennal transcriptome analysis. *Int. J. Biol. Sci.* 10, 846–860. doi: 10.7150/ijbs.9297

Cheng, T., Wu, J., Wu, Y., Chilukuri, R. V., Huang, L., Yamamoto, K., et al. (2017). Genomic adaptation to polyphagy and insecticides in a major East Asian noctuid pest. *Nat. Ecol. Evol.* 1, 1747–1756. doi: 10.1038/s41559-017-0314-4

Choo, Y.-M., Xu, P., Hwang, J. K., Zeng, F., Tan, K., Bhagavathy, G., et al. (2018). Reverse chemical ecology approach for the identification of an oviposition attractant for Culex quinquefasciatus. *P. Natl. Acad. Sci. U.S.A.* 115, 714–719. doi: 10.1073/pnas.1718284115

Croset, V., Rytz, R., Cummins, S. F., Budd, A., Brawand, D., Kaessmann, H., et al. (2010). Ancient protostome origin of chemosensory ionotropic glutamate receptors and the evolution of insect taste and olfaction. *PLoS Genet.* 6:e1001064. doi: 10.1371/journal.pgen.1001064

Dong, K., Sun, L., Liu, J.-T., Gu, S.-H., Zhou, J.-J., Yang, R.-N., et al. (2017). RNAi-induced electrophysiological and behavioral changes reveal two pheromone binding proteins of Helicoverpa armigera involved in the perception of the main sex pheromone component Z11–16:Ald. *J. Chem. Ecol.* 43, 207–214. doi: 10.1007/s10886-016-0816-6

Duan, S.-G., Li, D.-Z., and Wang, M.-Q. (2019). Chemosensory proteins used as target for screening behaviourally active compounds in the rice pest Cnaphalocrocis medinalis (Lepidoptera: Pyralidae). *Insect Mol. Biol.* 28, 123–135. doi: 10.1111/imb.12532

Fleischer, J., Pregitzer, P., Breer, H., and Krieger, J. (2018). Access to the odor world: olfactory receptors and their role for signal transduction in insects. *Cell. Mol. Life Sci.* 75, 485–508. doi: 10.1007/s00018-017-2627-5

Forêt, S., and Maleszka, R. (2006). Function and evolution of a gene family encoding odorant binding-like proteins in a social insect, the honey bee (*Apis mellifera*). *Genome Res.* 16, 1404–1413. doi: 10.1101/gr.5075706

Forstner, M., Gohl, T., Gondesen, I., Raming, K., Breer, H., and Krieger, J. (2008). Differential expression of SNMP-1 and SNMP-2 proteins in pheromone-sensitive hairs of moths. *Chem. Senses* 33, 291–299. doi: 10.1093/chemse/bjm087

Garczynski, S. F., Martin, J. A., Griset, M., Willett, L. S., Cooper, W. R., Swisher, K. D., et al. (2017). CRISPR/Cas9 editing of the codling moth (Lepidoptera: Tortricidae) CpomOR1 gene affects egg production and viability. *J. Econ. Entomol.* 110, 1847–1855. doi: 10.1093/jee/tox166

Gong, D.-P., Zhang, H.-J., Zhao, P., Xia, Q.-Y., and Xiang, Z.-H. (2009a). The odorant binding protein gene family from the genome of silkworm. Bombyx mori. *BMC Genomics* 10:332. doi: 10.1186/1471-2164-10-332

Gong, Z. J., Zhou, W. W., Yu, H. Z., Mao, C. G., Zhang, C. X., Cheng, J. A., et al. (2009b). Cloning, expression and functional analysis of a general odorant-binding protein 2 gene of the rice striped stem borer, Chilo suppressalis (Walker) (Lepidoptera: Pyralidae). *Insect Mol. Biol.* 18, 405–417. doi: 10.1111/j.1365-2583.2009.00886.x

Grabherr, M. G., Haas, B. J., Yassour, M., Levin, J. Z., Thompson, D. A., Amit, I., et al. (2011). Full-length transcriptome assembly from RNA-Seq data without a reference genome. *Nat. Biotechnol.* 29, 644–652. doi: 10.1038/nbt.1883

Grosse-Wilde, E., Kuebler, L. S., Bucks, S., Vogel, H., Wicher, D., and Hansson, B. S. (2011). Antennal transcriptome of Manduca sexta. *P. Natl. Acad. Sci. U.S.A.* 108, 7449–7454. doi: 10.1073/pnas.1017963108

He, X., Cai, Y., Zhu, J., Zhang, M., Zhang, Y., Ge, Y., et al. (2021). Identification and functional characterization of two putative pheromone receptors in the potato tuber moth, Phthorimaea operculella. *Front. Physiol.* 11:618983. doi: 10.3389/fphys.2020.618983

Hekmat-Scafe, D. S., Scafe, C. R., McKinney, A. J., and Tanouye, M. A. (2002). Genome-wide analysis of the odorant-binding protein gene family in *Drosophila* melanogaster. *Genome Res.* 12, 1357–1369. doi: 10.1101/gr.239402

Hull, J. J., Perera, O. P., and Snodgrass, G. L. (2014). Cloning and expression profiling of odorant-binding proteins in the tarnished plant bug. Lygus lineolaris. *Insect Mol. Biol.* 23, 78–97. doi: 10.1111/imb.12064

Jia, X., Zhang, X., Liu, H., Wang, R., and Zhang, T. (2018). Identification of chemosensory genes from the antennal transcriptome of Indian meal moth Plodia interpunctella. *PLoS ONE* 13:e0189889. doi: 10.1371/journal.pone.0189889

Jin, X., Ha, T. S., and Smith, D. P. (2008). SNMP is a signaling component required for pheromone sensitivity in Drosophila. *Proc. Natl. Acad. Sci. U.S.A.* 105, 10996–11001. doi: 10.1073/pnas.0803309105

Kepchia, D., Moliver, S., Chohan, K., Phillips, C., and Luetje, C. W. (2017). Inhibition of insect olfactory behavior by an airborne antagonist of the insect

odorant receptor co-receptor subunit. *PLoS ONE* 12:e0177454. doi: 10.1371/journal.pone.0177454

Khuhro, S. A., Liao, H., Dong, X.-T., Yu, Q., Yan, Q., and Dong, S.-L. (2017). Two general odorant binding proteins display high bindings to both host plant volatiles and sex pheromones in a pyralid moth Chilo suppressalis (Lepidoptera: Pyralidae). *J. Asia Pac. Entomol.* 20, 521–528. doi: 10.1016/j.aspen.2017.02.015

Koutroumpa, F. A., Monsempes, C., François, M.-C., de Cian, A., Royer, C., Concordet, J.-P., et al. (2016). Heritable genome editing with CRISPR/Cas9 induces anosmia in a crop pest moth. *Sci. Rep.* 6:29620. doi: 10.1038/srep29620

Kumar, S., Stecher, G., and Tamura, K. (2016). MEGA7: molecular evolutionary genetics analysis version 7.0 for bigger datasets. *Mol. Biol. Evol.* 33, 1870–1874. doi: 10.1093/molbev/msw054

Kwadha, C. A., Ong'amo, G. O., Ndegwa, P. N., Raina, S. K., and Fombong, A. T. (2017). The biology and control of the greater wax moth, Galleria mellonella. *Insects* 8:61. doi: 10.3390/insects8020061

Lange, A., Beier, S., Huson, D. H., Parusel, R., Iglauer, F., and Frick, J.-S. (2018). Genome sequence of Galleria mellonella (greater wax moth). *Genome Announc.* 6:e01220. doi: 10.1128/genomeA.01220-17

Leal, W. S. (2013). Odorant reception in insects: roles of receptors, binding proteins, and degrading enzymes. *Annu. Rev. Entomol.* 58, 373–391. doi: 10.1146/annurev-ento-120811-153635

Leal, W. S., Barbosa, R. M. R., Xu, W., Ishida, Y., Syed, Z., Latte, N., et al. (2008). Reverse and conventional chemical ecology approaches for the development of oviposition attractants for Culex mosquitoes. *PLoS One* 3:e3045. doi: 10.1371/journal.pone.0003045

Li, Y., Hu, J., Xiang, Y., Zhang, Y., Chen, D., and Liu, F. (2020). Identification and comparative expression profiles of chemosensory genes in major chemoreception organs of a notorious pests, Laodelphax striatellus. *Comp. Biochem. Physiol. D* 33:100646. doi: 10.1016/j.cbd.2019.100646

Li, Y., Jiang, X., Wang, Z., Zhang, J., Klett, K., Mehmood, S., et al. (2019). Losing the arms race: greater wax moths sense but ignore bee alarm pheromones. *Insects* 10:81. doi: 10.3390/insects10030081

Li, Z.-Q., Zhang, S., Luo, J.-Y., Zhu, J., Cui, J.-J., and Dong, S.-L. (2015). Expression analysis and binding assays in the chemosensory protein gene family indicate multiple roles in Helicoverpa armigera. *J. Chem. Ecol.* 41, 473–485. doi: 10.1007/s10886-015-0574-x

Liu, N.-Y., Xu, W., Papanicolaou, A., Dong, S.-L., and Anderson, A. (2014). Identification and characterization of three chemosensory receptor families in the cotton bollworm Helicoverpa armigera. *BMC Genomics* 15:597. doi: 10.1186/1471-2164-15-597

Liu, N.-Y., Yang, K., Liu, Y., Xu, W., Anderson, A., and Dong, S.-L. (2015). Two general-odorant binding proteins in Spodoptera litura are differentially tuned to sex pheromones and plant odorants. *Comp. Biochem. Physiol. A* 180, 23–31. doi: 10.1016/j.cbpa.2014.11.005

Liu, Q., Liu, W., Zeng, B., Wang, G., Hao, D., and Huang, Y. (2017a). Deletion of the Bombyx mori odorant receptor co-receptor (BmOrco) impairs olfactory sensitivity in silkworms. *Insect Biochem. Molec.* 86, 58–67. doi: 10.1016/j.ibmb.2017.05.007

Liu, S., Wang, W.-L., Zhang, Y.-X., Zhang, B.-X., Rao, X.-J., Liu, X.-M., et al. (2017b). Transcriptome sequencing reveals abundant olfactory genes in the antennae of the rice leaffolder, Cnaphalocrocis medinalis (Lepidoptera: Pyralidae). *Entomol. Sci.* 20, 177–188. doi: 10.1111/ens.12253

Liu, Y., Du, L., Zhu, Y., Yang, S., Zhou, Q., Wang, G., et al. (2020). Identification and sex-biased profiles of candidate olfactory genes in the antennal transcriptome of the parasitoid wasp Cotesia vestalis. *Comp. Biochem. Physiol. D* 34:100657. doi: 10.1016/j.cbd.2020.100657

Livak, K. J., and Schmittgen, T. D. (2001). Analysis of relative gene expression data using real-time quantitative PCR and the $2-\Delta\Delta CT$ method. *Methods* 25, 402–408. doi: 10.1006/meth.2001.1262

Payne, T. L., and Finn, W. E. (1977). Pheromone receptor system in the females of the greater wax moth Galleria mellonella. *J. Insect Physiol.* 23, 879–881. doi: 10.1016/0022-1910(77)90014-2

Pelletier, J., Guidolin, A., Syed, Z., Cornel, A. J., and Leal, W. S. (2010). Knockdown of a mosquito odorant-binding protein involved in the sensitive detection of oviposition attractants. *J. Chem. Ecol.* 36, 245–248. doi: 10.1007/s10886-010-9762-x

Pelosi, P., Iovinella, I., Felicioli, A., and Dani, F. R. (2014). Soluble proteins of chemical communication: an overview across arthropods. *Front. Physiol.* 5:320. doi: 10.3389/fphys.2014.00320

Pelosi, P., Iovinella, I., Zhu, J., Wang, G., and Dani, F. R. (2018). Beyond chemoreception: diverse tasks of soluble olfactory proteins in insects. *Biol. Rev.* 93, 184–200. doi: 10.1111/brv.12339

Poivet, E., Gallot, A., Montagné, N., Glaser, N., Legeai, F., and Jacquin-Joly, E. (2013). A comparison of the olfactory gene repertoires of adults and larvae in the noctuid moth Spodoptera littoralis. *PLoS One* 8:e60263. doi: 10.1371/journal.pone.0060263

Pregitzer, P., Greschista, M., Breer, H., and Krieger, J. (2014). The sensory neurone membrane protein SNMP1 contributes to the sensitivity of a pheromone detection system. *Insect Mol. Biol.* 23, 733–742. doi: 10.1111/imb.12119

Qiu, L., He, L., Tan, X., Zhang, Z., Wang, Y., Li, X., et al. (2020). Identification and phylogenetics of Spodoptera frugiperda chemosensory proteins based on antennal transcriptome data. *Comp. Biochem. Physiol. D* 34:100680. doi: 10.1016/j.cbd.2020.100680

Qu, M.-Q., Cui, Y., Zou, Y., Wu, Z.-Z., and Lin, J.-T. (2020). Identification and expression analysis of odorant binding proteins and chemosensory proteins from dissected antennae and mouthparts of the rice bug Leptocorisa acuta. *Comp. Biochem. Physiol. D* 33:100631. doi: 10.1016/j.cbd.2019.100631

Robertson, H. M. (2019). Molecular evolution of the major arthropod chemoreceptor gene families. *Annu. Rev. Entomol.* 64, 227–242. doi: 10.1146/annurev-ento-020117-043322

Rytz, R., Croset, V., and Benton, R. (2013). Ionotropic receptors (IRs): chemosensory ionotropic glutamate receptors in *Drosophila* and beyond. *Insect Biochem. Molec.* 43, 888–897. doi: 10.1016/j.ibmb.2013.02.007

Sun, J. S., Xiao, S., and Carlson, J. R. (2018). The diverse small proteins called odorant-binding proteins. *Open Biol.* 8:180208. doi: 10.1098/rsob.180208

Sun, L., Mao, T.-F., Zhang, Y.-X., Wu, J.-J., Bai, J.-H., Zhang, Y.-N., et al. (2017). Characterization of candidate odorant-binding proteins and chemosensory proteins in the tea geometrid Ectropis obliqua Prout (Lepidoptera: Geometridae). *Arch. Insect Biochem.* 94:e21383. doi: 10.1002/arch.21383

Sun, L., Wang, Q., Zhang, Y., Tu, X., Yan, Y., Wang, Q., et al. (2019a). The sensilla trichodea-biased EoblPBP1 binds sex pheromones and green leaf volatiles in Ectropis obliqua Prout, a geometrid moth pest that uses Type-II sex pheromones. *J. Insect Physiol.* 116, 17–24. doi: 10.1016/j.jinsphys.2019.04.005

Sun, L., Wang, Q., Zhang, Y., Yan, Y., Guo, H., Xiao, Q., et al. (2019b). Expression patterns and co-localization of two sensory neuron membrane proteins in Ectropis obliqua Prout, a geometrid moth pest that uses Type-II sex pheromones. *Insect Mol. Biol.* 28, 342–354. doi: 10.1111/imb.12555

Tanaka, K., Uda, Y., Ono, Y., Nakagawa, T., Suwa, M., Yamaoka, R., et al. (2009). Highly selective tuning of a silkworm olfactory receptor to a key mulberry leaf volatile. *Curr. Biol.* 19, 881–890. doi: 10.1016/j.cub.2009.04.035

Tang, Q.-Y., and Zhang, C.-X. (2013). Data processing system (DPS) software with experimental design, statistical analysis and data mining developed for use in entomological research. *Insect Sci.* 20, 254–260. doi: 10.1111/j.1744-7917.2012.01519.x

The Heliconius Genome Consortium. (2012). Butterfly genome reveals promiscuous exchange of mimicry adaptations among species. *Nature* 487, 94–98. doi: 10.1038/nature11041

Touhara, K., and Vosshall, L. B. (2009). Sensing odorants and pheromones with chemosensory receptors. *Annu. Rev. Physiol.* 71, 307–332. doi: 10.1146/annurev.physiol.010908.163209

Venthur, H., and Zhou, J.-J. (2018). Odorant receptors and odorant-binding proteins as insect pest control targets: a comparative analysis. *Front. Physiol.* 9:1163. doi: 10.3389/fphys.2018.01163

Vieira, F. G., and Rozas, J. (2011). Comparative genomics of the odorant-binding and chemosensory protein gene families across the Arthropoda: origin and evolutionary history of the chemosensory system. *Genome Biol. Evol.* 3, 476–490. doi: 10.1093/gbe/evr033

Vogt, R. G., Große-Wilde, E., and Zhou, J.-J. (2015). The Lepidoptera odorant binding protein gene family: gene gain and loss within the GOBP/PBP complex of moths and butterflies. *Insect Biochem. Molec.* 62, 142–153. doi: 10.1016/j.ibmb.2015.03.003

Vogt, R. G., Miller, N. E., Litvack, R., Fandino, R. A., Sparks, J., Staples, J., et al. (2009). The insect SNMP gene family. *Insect Biochem. Molec.* 39, 448–456. doi: 10.1016/j.ibmb.2009.03.007

Walker, W. B., Roy, A., Anderson, P., Schlyter, F., Hansson, B. S., and Larsson, M. C. (2019). Transcriptome analysis of gene families involved in chemosensory function in Spodoptera littoralis (Lepidoptera: Noctuidae). *BMC Genomics* 20:428. doi: 10.1186/s12864-019-5815-x

Wicher, D. (2018). Tuning insect odorant receptors. *Front. Cell. Neurosci.* 12:94. doi: 10.3389/fncel.2018.00094

Yang, B., Ozaki, K., Ishikawa, Y., and Matsuo, T. (2015). Identification of candidate odorant receptors in Asian corn borer Ostrinia furnacalis. *PLoS One* 10:e0121261. doi: 10.1371/journal.pone.0121261

Yang, H., Dong, J., Sun, Y., Hu, Z., Lv, Q., and Li, D. (2020). Antennal transcriptome analysis and expression profiles of putative chemosensory soluble proteins in Histia rhodope Cramer (Lepidoptera: Zygaenidae). *Comp. Biochem. Physiol. D* 33:100654. doi: 10.1016/j.cbd.2020.100654

Yang, S., Cao, D., Wang, G., and Liu, Y. (2017). Identification of genes involved in chemoreception in Plutella xyllostella by antennal transcriptome analysis. *Sci. Rep.* 7:11941. doi: 10.1038/s41598-017-11646-7

Yang, Y., Li, W., Tao, J., and Zong, S. (2019). Antennal transcriptome analyses and olfactory protein identification in an important wood-boring moth pest, Streltzoviella insularis (Lepidoptera: Cossidae). *Sci. Rep.* 9:17951. doi: 10.1038/s41598-019-54455-w

Yoshizawa, A. C., Itoh, M., Okuda, S., Moriya, Y., and Kanehisa, M. (2007). KAAS: an automatic genome annotation and pathway reconstruction server. *Nucleic Acids Res.* 35, W182–W185. doi: 10.1093/nar/gkm321

Zeng, F.-F., Liu, H., Zhang, A., Lu, Z.-X., Leal, W. S., Abdelnabby, H., et al. (2018). Three chemosensory proteins from the rice leaf folder Cnaphalocrocis medinalis involved in host volatile and sex pheromone reception. *Insect Mol. Biol.* 27, 710–723. doi: 10.1111/imb.12503

Zhang, H.-J., Xu, W., Chen, Q.-m, Sun, L.-N., Anderson, A., Xia, Q.-Y., et al. (2020). A phylogenomics approach to characterizing sensory neuron membrane proteins (SNMPs) in Lepidoptera. *Insect Biochem. Molec.* 118:103313. doi: 10.1016/j.ibmb.2020.103313

Zhang, J., Bisch-Knaden, S., Fandino, R. A., Yan, S., Obiero, G. F., Grosse-Wilde, E., et al. (2019). The olfactory coreceptor IR8a governs larval feces-mediated competition avoidance in a hawkmoth. *Proc. Natl. Acad. Sci. U.S.A.* 116, 21828–21833. doi: 10.1073/pnas.1913485116

Zhang, L.-W., Kang, K., Jiang, S.-C., Zhang, Y.-N., Wang, T.-T., Zhang, J., et al. (2016). Analysis of the antennal transcriptome and insights into olfactory genes in Hyphantria cunea (Drury). *PLoS One* 11:e0164729. doi: 10.1371/journal.pone.0164729

Zhang, T., Coates, B. S., Ge, X., Bai, S., He, K., and Wang, Z. (2015). Male- and female-biased gene expression of olfactory-related genes in the antennae of Asian corn borer, Ostrinia furnacalis (Guenée) (Lepidoptera: Crambidae). *PLoS One* 10:e0128550. doi: 10.1371/journal.pone.0128550

Zhang, T., Sun, Y., Wanner, K. W., Coates, B. S., He, K., and Wang, Z. (2017). Binding affinity of five PBPs to Ostrinia sex pheromones. *BMC Mol. Biol.* 18:4. doi: 10.1186/s12867-017-0079-y

Zhang, Y.-N., Qian, J.-L., Xu, J.-W., Zhu, X.-Y., Li, M.-Y., Xu, X.-X., et al. (2018). Identification of chemosensory genes based on the transcriptomic analysis of six different chemosensory organs in Spodoptera exigua. *Front. Physiol.* 9:432. doi: 10.3389/fphys.2018.00432

Zhang, Y.-N., Ye, Z.-F., Yang, K., and Dong, S.-L. (2014). Antenna-predominant and male-biased CSP19 of Sesamia inferens is able to bind the female sex pheromones and host plant volatiles. *Gene* 536, 279–286. doi: 10.1016/j.gene.2013.12.011

Zhao, H.-X., Xiao, W.-Y., Ji, C.-H., Ren, Q., Xia, X.-S., Zhang, X.-F., et al. (2019). Candidate chemosensory genes identified from the greater wax moth, Galleria mellonella, through a transcriptomic analysis. *Sci. Rep.* 9:10032. doi: 10.1038/s41598-019-46532-x

Zhu, G.-H., Zheng, M.-Y., Sun, J.-B., Khuhro, S. A., Yan, Q., Huang, Y., et al. (2019). CRISPR/Cas9 mediated gene knockout reveals a more important role of PBP1 than PBP2 in the perception of female sex pheromone components in Spodoptera litura. *Insect Biochem. Molec.* 115:103244. doi: 10.1016/j.ibmb.2019.103244

Zhu, X. J., Zhou, S. J., Xu, X. J., Lan, H. H., and Zhou, B. F. (2016). Freezing combs as a method for the greater wax moth (Galleria mellonella) control. *J. Apicult. Res.* 55, 351–352. doi: 10.1080/00218839.2016.1231457

Conflict of Interest: The authors declare that the research was conducted in the absence of any commercial or financial relationships that could be construed as a potential conflict of interest.

frontiers in Physiology

ORIGINAL RESEARCH
published: 09 June 2021
doi: 10.3389/fphys.2021.678698

Functional Characterization of Olfactory Proteins Involved in Chemoreception of *Galeruca daurica*

*Ling Li[1], Wen-Bing Zhang[1], Yan-Min Shan[2], Zhuo-Ran Zhang[2] and Bao-Ping Pang[1]**

[1] Research Center for Grassland Entomology, Inner Mongolia Agricultural University, Hohhot, China, [2] Inner Mongolia Forestry and Grassland Pest Control and Quarantine Station, Hohhot, China

Odorant-binding proteins (OBPs) and chemosensory proteins (CSPs) play a fundamental role in insect olfaction. *Galeruca daurica* (Joannis) is a new pest with outbreak status in the Inner Mongolia grasslands, northern China. In this study, six olfactory protein genes (*GdauOBP1*, *GdauOBP6*, *GdauOBP10*, *GdauOBP15*, *GdauCSP4*, and *GdauCSP5*) were cloned by RACE and expressed by constructing a prokaryotic expression system. Their binding affinities to 13 compounds from host volatiles (*Allium mongolicum*) were determined by fluorescence-binding assay. In order to further explore the olfactory functions of *GdauOBP15* and *GdauCSP5*, RNA interference (RNAi) and electroantennogram (EAG) experiments were conducted. Ligand-binding assays showed that the binding properties of the six recombinant proteins to the tested volatiles were different. GdauOBP6, GdauOBP15, GdauCSP4, and GdauCSP5 could bind several tested ligands of host plants. It was suspected that GdauOBP6, GdauOBP15, GdauCSP4, and GdauCSP5 were related to the host location in *G. daurica.* We also found that there were different EAG responses between males and females when the *GdauOBP15* and *GdauCSP5* genes were silenced by RNAi. The EAG response of *G. daurica* females to 2-hexenal was significantly decreased in dsRNA-OBP15-injected treatment compared to the control, and the dsRNA-CSP5-treated females significantly reduced EAG response to eight tested host volatiles (1,3-dithiane, 2-hexenal, methyl benzoate, dimethyl trisulfide, myrcene, hexanal, 1,3,5-cycloheptatriene, and p-xylene). However, the EAG response had no significant difference in males. Both GdauOBP15 and GdauCSP5 may have different functions between males and females in *G. daurica* and may play more important roles in females searching for host plants.

Keywords: *Galeruca daurica*, odorant-binding protein, chemosensory protein, fluorescence binding assay, RNA interference, electroantennogram

OPEN ACCESS

Edited by:
Yang Liu,
Institute of Plant Protection, Chinese Academy of Agricultural Sciences, China

Reviewed by:
Liang Sun,
Tea Research Institute, Chinese Academy of Agricultural Sciences (CAAS), China
Tiantao Zhang,
Chinese Academy of Agricultural Sciences (CAAS), China

***Correspondence:**
Bao-Ping Pang
pangbp@imau.edu.cn

Specialty section:
This article was submitted to Invertebrate Physiology, a section of the journal Frontiers in Physiology

Received: *10 March 2021*
Accepted: *29 April 2021*
Published: *09 June 2021*

Citation:
Li L, Zhang W-B, Shan Y-M, Zhang Z-R and Pang B-P (2021) Functional Characterization of Olfactory Proteins Involved in Chemoreception of Galeruca daurica. Front. Physiol. 12:678698. doi: 10.3389/fphys.2021.678698

INTRODUCTION

Insects depend critically on olfactory systems to perceive various chemical signals in their environment (Forêt et al., 2007; Leal, 2013). As the primary sensory organs of insects, antennae are distributed with lots of sensilla hairs (Zacharuk, 1980). When the neurons in these sensilla are activated, they trigger a series of behavioral responses related to host recognition, oviposition, and

mating (Martin et al., 2011; Hull et al., 2014). Odorant-binding proteins (OBPs) and chemosensory proteins (CSPs) have been identified in the lymph of chemosensilla (Vogt and Riddiford, 1981; McKenna et al., 1994). Both of them are small, hydrosoluble proteins that are expressed in the auxiliary cells of chemosensilla and secreted into the aqueous fluid around the olfactory neurons (Qiao et al., 2013). OBPs and CSPs are originally thought to be able to recognize and transport volatiles and lipophilic semiochemicals to the specific olfactory receptors (ORs) in the neuronal membrane across the aqueous sensillar lymph (Vogt et al., 2002; Leal, 2005; Pelosi et al., 2006). Many OBP and CSP genes have been identified so far; most of them were found in different tissues of insect, and some were even expressed in non-chemosensory organs (Gong et al., 2007; Dippel et al., 2014). They have also been implicated in embryonic development (Maleszka et al., 2007), larval ecdysis (Cheng et al., 2015), limb regeneration (Nomura et al., 1992), hematopoiesis, wound healing (Benoit et al., 2017), and humidity detection (Sun et al., 2018). Therefore, OBPs and CSPs conduct various tasks ranging from behavioral to multiple physiological and biological processes (Pelosi et al., 2017).

Fluorescence-binding assay is an efficient technique to study the binding properties of OBPs or CSPs to putative ligands and provide essential evidence for understanding their physiological function (Nathália et al., 2016). For example, fluorescence-binding assays showed that OasiCSP4, OasiCSP11, and OasiCSP12 of *Oedaleus asiaticus* showed a broad range of binding affinities to their host plant volatiles, fecal volatiles, and live body volatiles (Zhou et al., 2020). Wu et al. (2019) reported that CSP4 plays an important role during the process of transporting pheromones in *Apis mellifera* larva. The binding ability of AlinOBP11 in *Adelphocoris lineolatus* to non-volatile host plant secondary metabolites was preferential than that to volatile compounds, suggesting that AlinOBP11 could act as a carrier in the gustatory system (Sun et al., 2016). Recent studies have shown that the involvement of genes in olfactory functions can be ultimately impaired by silencing individual CSP or OBP genes to influence odor preference (Rebijith et al., 2016; Dong et al., 2017; Waris et al., 2018; Zhou et al., 2020). In addition, knowledge about the olfactory responses of insects to plant volatiles can provide strategies for pest management by identifying chemical signals (Das et al., 2013).

Galeruca daurica (Joannis) (Coleoptera: Chrysomelidae) is an oligophagous pest found in the Inner Mongolian grasslands of China in recent years (Yang et al., 2010; Hao et al., 2014). This pest has been reported to feed on the species of *Allium* plants, including *A. mongolicum*, *A. polyrhizum*, and *A. ramosum*, among which *A. mongolicum* is its favorite host (Hao et al., 2014, 2015). Extensive outbreaks of this pest have caused great losses to pasture in the Inner Mongolian grasslands since 2009, and the damage continues to increase (Zhou et al., 2019). This leaf beetle forages only *Allium* plants, implying an important role of olfaction in searching for specific host plants. However, little is known about the chemosensory mechanisms of this pest. Li et al. (2019) cloned *GdauOBP20* of *G. daurica* and clarified the binding property of the recombinant protein to main host plant volatiles. In this study, we selected *GdauOBP1*, *GdauOBP6*, *GdauOBP10*, *GdauOBP15*, *GdauCSP4*, and *GdauCSP5* (accession numbers: KX900453, KX900458, KX900462, KX900467, KY885474, and KY885475) for functional evaluation due to the fact that they were specifically highly expressed in antennae or in heads, and their expression levels were significantly different between males and females (Li et al., 2017, 2018). To clarify the function of these genes, the binding properties of four OBPs and two CSPs were analyzed using a number of ligands in competitive binding assays. Then, RNA interference (RNAi) was also used to reduce the expression levels of *GdauOBP15* and *GdauCSP5* in vivo, and the electroantennogram (EAG) response was recorded. Our present research aims to discover the molecular mechanisms of olfactory recognition and will provide a reference for pest management strategies.

MATERIALS AND METHODS

Insects Rearing and Sample Collection

The larvae of *G. daurica* were collected from Xilinhot, Inner Mongolia, China (43°54′53′′N, 115°39′13′′E) in 2018, and reared at 26 ± 1°C, 60–80% relative humidity under a 16 h light: 8 h dark period.

Cloning and Sequencing of Full-Length cDNA

Total RNA was extracted from the antennae of 3-day-old adults using the TaKaRa MiniBEST Universal RNA Extraction Kit (TaKaRa, Dalian, China). cDNA was synthesized using the PrimeScript™ 1st Strand cDNA Synthesis Kit (TaKaRa, Dalian, China). Specific primers (**Supplementary Table 1**) were designed to the coding sequences of GdauOBP1, GdauOBP6, GdauOBP10, GdauOBP15, GdauCSP4, and GdauCSP5 in Primer Premier 5.0 based on the transcriptome database of *G. daurica* assembled in our laboratory. PCR amplifications were performed as 94°C for 3 min, followed by 30 cycles of 94°C for 30 s, 56°C for 30 s (each primer used a different annealing temperature), and 72°C for 1 min. Finally, it was extended for 10 min at 72°C. The amplified product was eluted (Gel DNA Mini Purification Kit, Tiangen, China) and cloned into the pMD19-T vector. Four positive transformants per individual were selected for plasmid isolation using MiniBEST Plasmid Purification Kit (TaKaRa, Dalian, China) and sent to the Beijing Liuhe Huada Gene Technology Company for sequencing in both forward and reverse directions.

The primers were designed for 5′ and 3′ RACE (**Supplementary Table 2**) based on obtained sequence fragments. 5′- and 3′-end amplifications were performed using SMARTer® RACE 5′/3′ Kit (TaKaRa, Dalian, China) following the manufacturers' protocol. Touchdown PCR (5 cycles of 94°C for 30 s, 72°C for 3 min followed by 5 cycles of 94°C for 30 s, 70°C for 30 s, 72°C for 3 min, and 25 cycles of 94°C for 30 s, 68°C for 30 s, 72°C for 2 min) and nested PCR (25 cycles of 94°C for 30 s, 68°C for 30 s, 72°C for 2 min) were conducted to enhance the amplification specificity of the 5′-UTR and 3′-UTR sequences. The amplified product was eluted and cloned as described in the previous section.

The sequence fragments and RACE sequence were assembled in DNAMAN 6.0 to obtain the full-length cDNA sequences. Open reading frames (ORFs) were obtained in ORF Finder[1].

Prokaryotic Expression and Purification of Recombinant Proteins

Gene-specific primers (containing restriction sites) (**Supplementary Table 3**) were designed to clone the coding regions of *GdauOBP1*, *GdauOBP6*, *GdauOBP10*, *GdauOBP15*, *GdauCSP4*, and *GdauCSP5*. The purified PCR products were cloned into the pMD19-T vector and transformed into *Escherichia coli* DH5α-competent cells. The validated plasmids were double-digested with the restriction enzymes and then ligated to the pET-28a (+) vector by T4 DNA ligase (New England BioLabs, NEB). The recombinant plasmids were transformed into *E. coli* BL21 Star (DE3)-competent cells. The positive clones were selected for mass culture at 37°C overnight. The recombinant proteins were induced with 1 mM isopropyl β-D-thiogalactoside (IPTG) and cultured for 4 h at 37°C.

After bacterial cells were centrifuged at 7,800 × *g* for 15 min, the precipitant was suspended in lysis buffer (50 mM NaH_2PO_4, 300 mM NaCl, 10 mM imidazole, pH 8.0). The cells were sonicated for 30 min on ice and centrifuged. The proteins were collected from the supernatant and precipitant, then detected by SDS-PAGE electrophoresis. The supernatant was filtered through a 0.45-μm filter and pumped into a Ni-NTA Agarose column (Qiagen, Germany). The eluted protein solution was dialyzed in a dialysis bag with a cutoff of 3,500 Da. The protein solutions were concentrated in ultrafiltration tubes with a cutoff of 10,000 Da. The concentration of the purified recombinant protein was measured using the BCA Assay Kit (Beyotime, Shanghai, China). The purified proteins were stored at −80°C until use.

[1]https://www.ncbi.nlm.nih.gov/orffinder/

Fluorescence-Binding Assays

Fluorescence-binding assays were performed using a 970CRT spectrofluorophotometer (Hitachi, Japan). Instrument parameters were set as follows: Excitation slit of 10 nm, emission slit of 10 nm, sensitivity of 2 s, excitation wavelength of 337 nm, and scanning emission wavelength range of 350–700 nm. In order to measure the affinity of the fluorescent ligand 1-NPN (N-phenyl-1-naphthylamine) with the six recombinant proteins, the recombinant proteins were diluted to 2 μM in 50 mM Tris–HCl (pH 7.4) and added into a 1-cm light path quartz cuvette. Fluorescence values were recorded after the 1-NPN solution was added successively. The dissociation constant K_{1-NPN} was calculated using GraphPad Prism 7.0 software.

Thirteen main volatiles of the host plant (*A. mongolicum*) were selected as competing ligands for the fluorescence competitive binding assays (**Table 1**). All ligands were purchased from Sigma-Aldrich (St. Louis, MO, United States). These ligands were dissolved in methanol (HPLC grade) to make stock solutions of 1 mM, which were added into a 2-μM protein

TABLE 1 | List of odor samples.

Compound name	Molecular formula	Formula	CAS number	Purity (%)
Diallyl sulfide	$C_6H_{10}S$	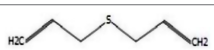	592-88-1	97
1,3-dithiane	$C_4H_8S_2$		505-23-7	97
Dimethyl trisulfide	$C_2H_6S_3$	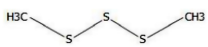	3658-80-8	98
Diallyl disulfide	$C_6H_{10}S_2$	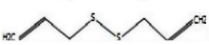	2179-57-9	98
Diallyl trisulfide	$C_6H_{10}S_3$	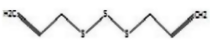	2050-87-5	98
Dimethyl disulfide	$C_2H_6S_2$	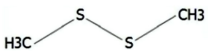	624-92-0	99
(Z)-2-Hexen-1-ol	$C_6H_{12}O$	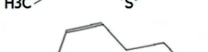	928-95-0	96
Myrcene	$C_{10}H_{16}$		123-35-3	95
2-Hexenal	$C_6H_{10}O$	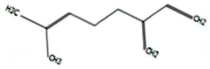	6728-26-3	97
Methyl benzoate	$C_8H_8O_2$		93-58-3	96
Hexanal	$C_6H_{12}O$	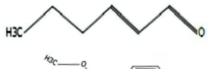	66-25-1	98
1,3,5-Cycloheptatriene	C_7H_8		544-25-2	95
p-Xylene	C_8H_{10}	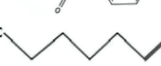	106-42-3	99

solution with 1-NPN saturated. The decrease in fluorescence intensity indicated that the bound 1-NPN was replaced by the ligands. Three duplications were used in the binding experiment. The curves were fitted using Scatchard plots. The dissociation constants (*Ki*) of the competitive ligands were calculated based on the equation: $K_i = \mathrm{IC50}/(1 + [1 - \mathrm{NPN}]/\mathrm{K1} - \mathrm{NPN})$, where IC_{50} is the concentration of a competitor that results in a 50% reduction of the initial fluorescence intensity, and [1-NPN] and K_{1-NPN} are the free concentration of 1-NPN and the dissociation constant of the recombinant protein/1-NPN complex, respectively (Campanacci et al., 2001).

RNA Interference of *GdauOBP15* and *GdauCSP5*

GdauOBP15 and *GdauCSP5* were amplified by RT-PCR using specific primers containing the T7 promoter at the 5′ end (**Supplementary Table 4**). The purified PCR products of the two genes were subcloned into the pGEM-T vector and transformed into *E. coli* DH5α-competent cells. The plasmids verified by sequencing were used as templates to amplify the target sequence. The double-stranded RNAs (dsRNA) were synthesized using the T7 RiboMAX^{TM} Express RNAi System (Promega, United States) following the manufacturer's instructions. The concentration of dsRNA was determined by NanoPhotometer^{TM} P-Class (Implen, Germany). The integrity was analyzed by 1.5% agarose gel electrophoresis. Finally, the dsRNA was diluted to 1,000 μg/μL in enzyme-free water and stored at −80°C. The double-stranded RNA of green fluorescent protein (GFP) was synthesized as control.

Two microliters of dsRNA (1,000 μg/μL) was injected into the intersegmental membrane between the fourth and fifth abdominal segments of 3-day-old adult females and males using a microinjector (Shimadzu, Japan). All the treated insects, including dsRNA-OBP15-injected, dsRNA-CSP5-injected, and dsRNA-GFP-injected, were reared under natural temperature conditions in the lab. Samples were taken 48 h later for interference efficiency measurement and electroantennogram analysis.

Quantitative Real-Time PCR (qRT-PCR) Measurement

Antenna samples were collected after the treated insects were recovered for 48 h. Each treatment was performed with three biological replicates and 20 individuals per replicate. qRT-PCR was conducted using the FTC-3000P Real-Time Quantitative Thermal Cycler (Funglyn Biotech, Canada). BRYT® Green dye (GoTaq® qPCR Master Mix, Promega, United States) was used as the fluorescence reporter for each elongation cycle. qRT-PCR was conducted in a 10-μL reaction system with three technical replicates for each sample. All reactions were performed under the following conditions: denaturation at 95°C for 10 min, 45 cycles of 95°C for 15 s, and 60°C for 1 min, and finally a dissociation curve was analyzed. The succinate dehydrogenase complex (*SDHA*) gene of *G. daurica* was used as a reference gene (Tan et al., 2016). The relative expression levels of each gene were estimated by the $2^{-\Delta\Delta CT}$ method (Livak and Schmittgen, 2001).

Electroantennogram Analysis

Electroantennograms were conducted to record the antennal responses of dsRNA-OBP15-injected, dsRNA-CSP5-injected, and dsRNA-GFP-injected to 12 plant volatiles. These odorants were dissolved in dichloromethane (HPLC grade) to make stock solutions of 1 mol/L, and dichloromethane alone served as solvent control. The antennae were cut off at the base, and the ends were removed then attached to the electrode with electrode gel. Filter paper strips (1 cm × 0.5 cm) were loaded with 10 μL of each chemical solution and then inserted into a Pasteur pipette. The tube was connected to an air stimulus controller (CS-55; SynTech). The signals were detected by a high-impedance amplifier (IDAC-2; SynTech) and analyzed using SynTech software (GC-EAD 2014 v1.2.5). The pulse duration time was 0.2 s with a stimulation interval of 30 s, and each compound was tested three times for each antenna. It was taken as the absolute value of the difference value between the maximum amplitude achieved by the odor stimulus and the baseline level. Each antenna was stimulated three times. All EAG results are presented as the mean EAG values from six female or male antennae.

Statistical Analysis

The binding assay curve was fitted by GraphPad Prism 7.0, using the least squares (ordinary) fit of the second-order polynomial. Data from qPCR and EAG assays were analyzed using SPSS Statistics 17.0. *T*-test ($P < 0.05$) was used to analyze the differences among the groups.

RESULTS

Gene Cloning

Four OBP genes (*GdauOBP1*, *GdauOBP6*, *GdauOBP10*, and *GdauOBP15*) and two CSP genes (*GdauCSP4* and *GdauCSP5*) were cloned from *G. daurica* using RT-PCR and RACE-PCR strategies. Nucleotide and amino acid sequences are shown in **Figure 1**. The full-length *GdauOBP1* complementary DNA (cDNA) consisted of 503 bp with an ORF of 396 bp. The lengths of *GdauOBP6* and *GdauOBP10* were 557 bp with an ORF of 360 and 593 bp with an ORF of 441 bp, respectively. The 5′-end cDNA cloning of *GdauOBP15* failed, and the ORF was 360 bp in length. The lengths of *GdauCSP4* and *GdauCSP4* were 460 bp with an ORF of 375 and 540 bp with an ORF of 405 bp, respectively.

Protein Expression and Purification

The calculated molecular weights of GdauOBP1, GdauOBP6, GdauOBP10, GdauOBP15, GdauCSP4, and GdauCSP5 were 15.19, 12.93, 16.64, 16.33, 14.55, and 15.32 kDa, respectively (Li et al., 2017, 2018). The recombinant proteins were successfully expressed in the *E. coli* expression system. The SDS-PAGE analysis indicated that GdauCSP4 and GdauCSP5 were mainly detected in the medium supernatant, while GdauOBP1, GdauOBP6, GdauOBP10, and GdauOBP15 were mainly detected in the precipitate (**Figure 2**). Since all

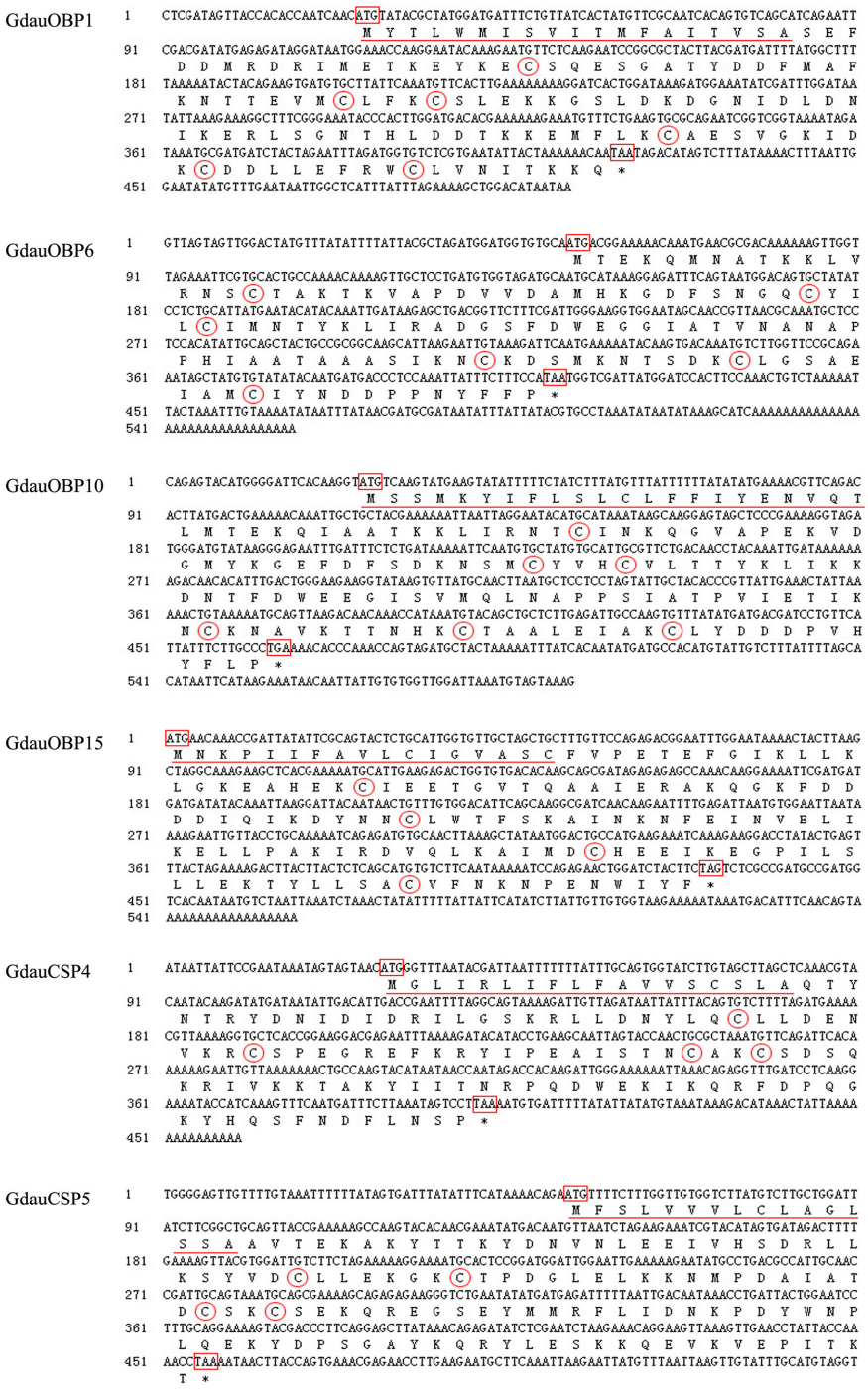

FIGURE 1 | Nucleotide and amino acid sequences of *GdauOBP1*, *GdauOBP6*, *GdauOBP10*, *GdauOBP15*, *GdauCSP4*, and *GdauCSP5*. The start and stop codons are boxed, signal peptide is underlined, conversed cysteine residues are circled, and asterisks indicate the termination of translation.

four GdauOBPs were mainly expressed in inclusion bodies, urea was added to solubilize and denature the recombinant proteins, followed by extensive dialysis to renature them, as described previously (Calvello et al., 2003; Zhang et al., 2012). The concentrations of the purified proteins were 1.02, 0.14, 0.19, 0.43, 0.58, and 0.74 mg/mL for GdauOBP1, GdauOBP6, GdauOBP10, GdauOBP15, GdauCSP4, and GdauCSP5, respectively.

Ligand-Binding Assays

The dissociation constants of six recombinant proteins with 1-NPN were measured, with GdauOBP1, GdauOBP6, GdauOBP10,

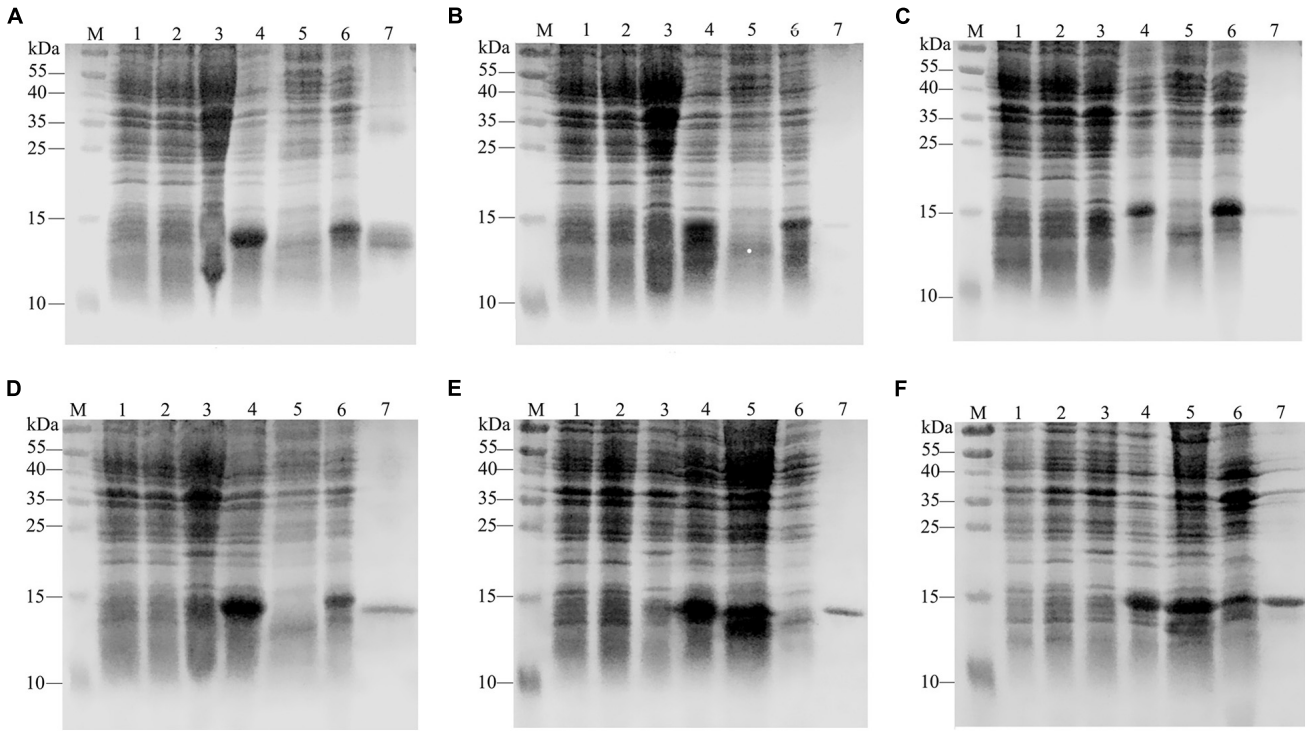

FIGURE 2 | SDS-PAGE analyses showing the expression and purification of four recombinant GdauOBPs and two GdauCSP proteins. **(A)** GdauOBP1; **(B)** GdauOBP6; **(C)** GdauOBP10; **(D)** GdauOBP15; **(E)** GdauCSP4; **(F)** GdauCSP5; M, Protein molecular weight marker; 1, non-induced pET-28a (+); 2, induced pET-28a (+); 3, non-induced recombinant proteins; 4, induced recombinant proteins; 5, supernatant after sonication; 6, inclusion body after sonication; 7, purified recombinant protein.

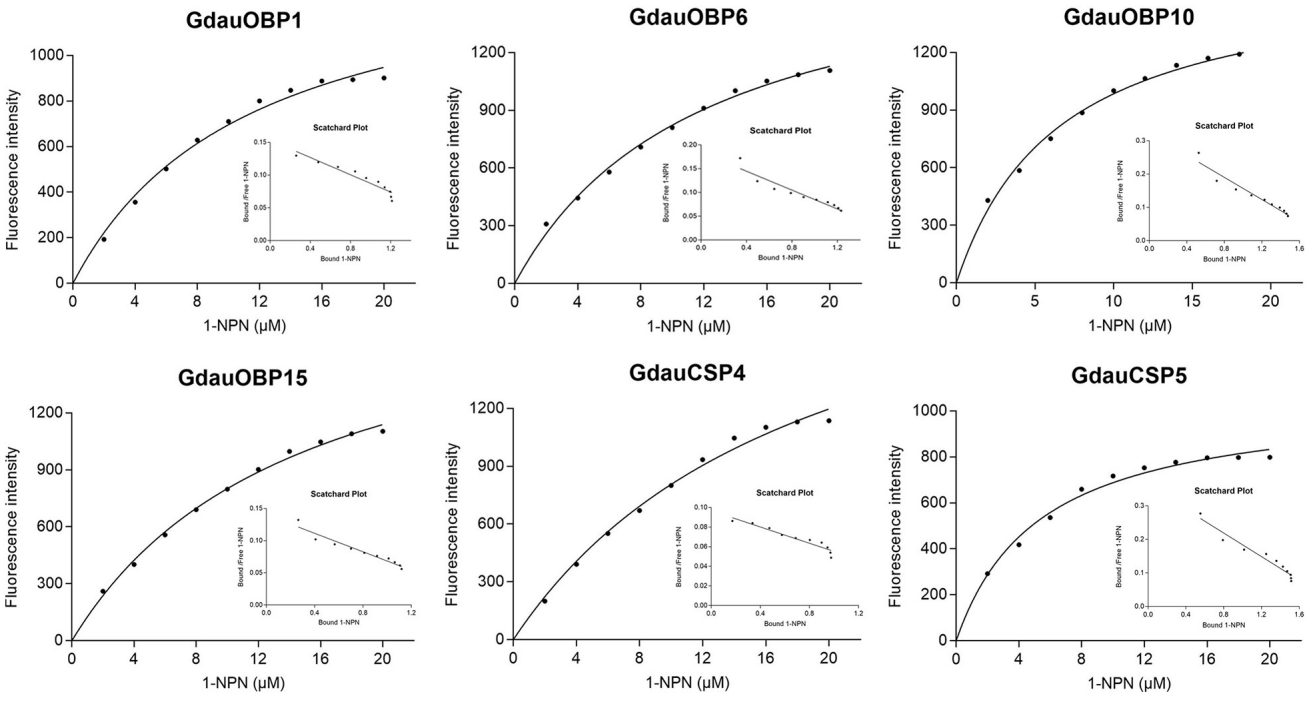

FIGURE 3 | Binding curves and Scatchard plot analysis of 1-NPN to GdauOBP1, GdauOBP6, GdauOBP10, GdauOBP15, GdauCSP4, and GdauCSP5 at pH 7.4.

TABLE 2 | Fluorescence competitive binding affinities of four recombinant GdauOBPs and two GdauCSP proteins with different ligands.

	GdauOBP1		GdauOBP6		GdauOBP10		GdauOBP15		GdauCSP4		GdauCSP5	
Ligand name	**IC_{50}**	***Ki***	**IC_{50}**	***Ki***	**IC_{50}**	***Ki***	**IC_{50}**	***Ki***	**IC_{50}**	***Ki***	**IC_{50}**	***Ki***
Diallyl sulfide	–	–	55.03	47.29	77.82	60.13	48.07	42.41	43.79	39.69	72.23	53.09
1,3-dithiane	70.65	60.34	36.66	31.50	59.45	45.93	57.18	50.46	18.46	16.73	49.99	36.74
Dimethyl trisulfide	63.20	53.98	44.45	38.19	67.40	52.07	56.69	50.03	16.58	15.03	53.71	39.47
Diallyl disulfide	97.08	82.91	72.13	61.98	–	–	42.30	37.32	23.52	21.32	61.57	45.25
Diallyl trisulfide	–	–	–	–	–	–	–	–	–	–	–	–
Dimethyl disulfide	64.87	55.41	29.85	25.65	61.87	47.80	26.17	23.09	23.12	20.96	36.02	26.47
(Z)-2-hexen-1-ol	86.39	73.78	33.02	28.37	95.58	73.84	76.04	67.10	49.96	45.29	–	73.49
Myrcene	82.62	70.56	68.71	59.04	–	–	–	–	–	–	84.17	61.86
2-hexenal	95.89	81.89	33.86	29.09	85.47	66.03	41.74	36.83	17.55	15.91	34.40	25.28
Methyl benzoate	65.37	55.83	36.44	31.31	73.92	57.11	35.87	31.65	13.30	12.06	44.30	32.56
Hexanal	70.78	60.45	32.26	27.72	52.01	40.18	68.77	60.69	15.41	13.97	61.44	45.15
1,3,5-cycloheptatriene	63.02	53.82	80.51	69.17	59.85	46.24	51.66	45.59	23.41	21.22	45.51	33.45
p-xylene	84.67	72.32	72.51	62.30	58.03	44.83	49.90	44.03	19.74	17.90	55.71	40.94

"–" no binding.

GdauOBP15, GdauCSP4, and GdauCSP5 of 11.36, 11.83, 6.54, 14.59, 18.87, and 5.34 μM, respectively, suggesting that 1-NPN is an appropriate reporter to these proteins. The binding curves and Scatchard plots are shown in **Figure 3**. 1-NPN was used as the fluorescent reporter to measure the affinity of six recombinant proteins with 13 host plant volatiles in competitive binding assays. The results are shown in **Table 2** and **Figure 4**. GdauOBP1 and GdauOBP10 had weak or no binding affinity to all tested compounds ($Ki > 30$ μM). GdauOBP6 showed strong binding affinity to dimethyl disulfide, hexanal, 2-hexenal, and (Z)-2-hexen-1-ol, with *Ki* values of 25.65, 27.72, 28.37, and 29.29 μM, respectively. GdauOBP15 bound to dimethyl disulfide specifically with the *Ki* value of 23.09 μM. The binding affinities of the two CSPs to the host plant volatiles varied greatly. GdauCSP4 showed a broad binding profile with nine compounds (methyl benzoate, hexanal, dimethyl trisulfide, 2-hexenal, 1,3-dithiane, p-xylene, dimethyl disulfide, 1,3,5-cycloheptatriene, and diallyl disulfide) with *Ki* values between 12.06 and 21.32 μM, among which the ligand with the strongest binding ability was methyl benzoate, followed by hexanal. However, GdauCSP5 could only bind dimethyl disulfide and 2-hexenal with the *Ki* values of 26.47 μM and 25.28 μM, respectively.

Efficiency Analysis of RNAi on Expression Levels of *GdauOBP15* and *GdauCSP5*

The *GdauOBP15* and *GdauCSP5* genes were silenced by RNAi to elucidate their biological functions in vivo. The efficiency of gene silencing at 48 h with 2,000 μg/μL was investigated by qRT-PCR. The results revealed that the injection of dsRNA-OBP15 and dsRNA-CSP5 significantly reduced the expression levels of *OBP15* and *CSP5* in both male and female antenna, compared with non-target control groups ($P < 0.01$) within 48 h in *G. daurica* (**Figure 5**). RNAi reduced the expression levels of *GdauOBP15* to 28.65% and 10.74% in females and males, and the expression levels of *GdauCSP5* were reduced to 2.93 and 3.31% in females and males, respectively.

Effect of RNAi on Electroantennogram Recording to *G. daurica*

We examined the responses of non-target control and dsRNA-treated (*GdauOBP15* and *GdauCSP5*) *G. daurica* adults to host plant volatiles. It was found that there were different EAG responses between males and females when the *GdauOBP15* and *GdauCSP5* genes were silenced by RNAi. The electrophysiological responses of *G. daurica* to all tested volatiles were decreased in dsRNA-OBP15-injected females compared to the control, and the response to 2-hexenal was reduced significantly ($P < 0.01$) among them (**Figure 6A**), whereas it increased in the injected males but not significantly ($P > 0.05$) (**Figure 6B**). Antennae of dsRNA-CSP5-injected females showed significantly lower electrophysiological responses to eight volatiles, 1,3-dithiane, 2-hexenal, methyl benzoate ($P < 0.01$), dimethyl trisulfide, myrcene, hexanal, 1,3,5-cycloheptatriene, and p-xylene ($0.01 < P < 0.05$) (**Figure 6C**). The EAG values of dsRNA-CSP5-injected males to most volatiles were increased but not significantly ($P > 0.05$) (**Figure 6D**).

DISCUSSION

In this study, four OBP genes (*GdauOBP1*, *GdauOBP6*, *GdauOBP10*, and *GdauOBP15*) and two CSP genes (*GdauCSP4* and *GdauCSP5*) were cloned from *G. daurica* using RT-PCR and RACE-PCR strategies. The results of ORF sequences were consistent with those identified in the transcriptome (Li et al., 2017, 2018). This experiment has laid a reliable foundation for subsequent experiments.

G. daurica feeds only on *Allium* plants, implying an important role of olfaction in searching for specific host plants. *A. mongolicum* is its favorite food (Hao et al., 2014, 2015). Therefore, 13 main representative components were selected from the *A. mongolicum* volatiles for this study. Fluorescence-binding assays showed that GdauOBP1 and GdauOBP10 had weak or no binding affinity to all tested compounds. It is

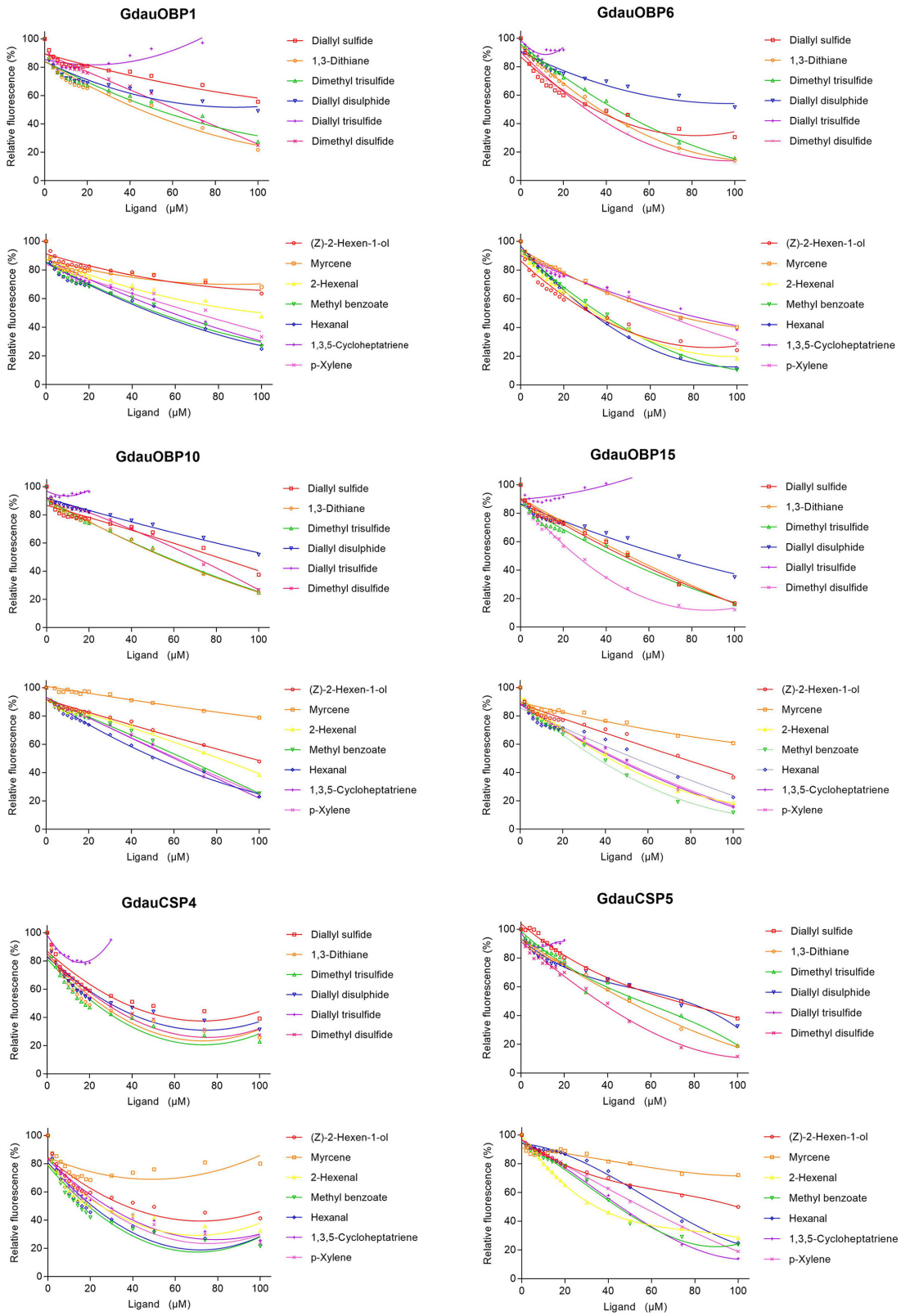

FIGURE 4 | Competitive binding curves of GdauOBP1, GdauOBP6, GdauOBP10, GdauOBP15, GdauCSP4, and GdauCSP5 with thirteen ligands from the host plant volatiles.

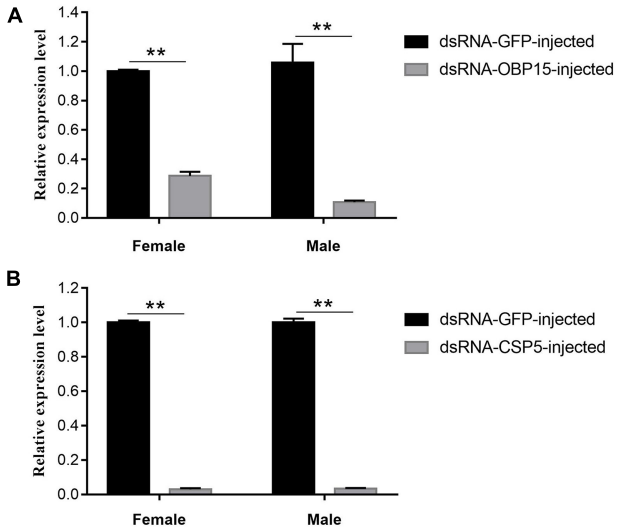

FIGURE 5 | Relative expression levels of *GdauOBP15* **(A)** and *GdauCSP5* **(B)** at 48 h after dsRNA injection in *G. daurica* antennae measured by qRT-PCR (*t*-test; $^{**}P < 0.01$). Columns indicate the mean ± standard error of three independent experiments.

necessary to expand the testing range of ligands in order to obtain the ligands with high affinity, such as sex pheromones and aggregation pheromones. For instance, GmolGOBP2 could not effectively bind host plant volatiles but showed a specific binding affinity for dodecanol, a minor sex pheromone component of *Grapholita molesta* (Li et al., 2016). PxylGOBP1 and PxylGOBP2 showed binding affinities to the sex pheromone of *Plutella xylostella* (Cai et al., 2020). There was another possibility that the structures and functions of the proteins might be affected by the expression and purification methods. GdauOBP6, GdauOBP15, GdauCSP4, and GdauCSP5 could bind several tested ligands of host plants. Among them, dimethyl disulfide, diallyl disulfide, 1,3-dithiane, and dimethyl trisulfide are sulfocompounds with a strong pungent odor, which are the symbolic components of *Allium* plants in Liliaceae such as onion and garlic (He et al., 2004; Wuren, 2011; Cheng et al., 2014; Li et al., 2015). The olfactory neurons of the basiconica sensilla on locust mouthpart could be directly activated by 2-hexenal and hexanal. In addition, hexanal could also enhance the transmission of nerve signals and regulate the ability of locusts to recognize odors (Zhang et al., 2017). Combined with our previous studies that these four genes were highly expressed in antenna (Li et al., 2017, 2018), the proteins coded by these genes could selectively bind to host volatiles,

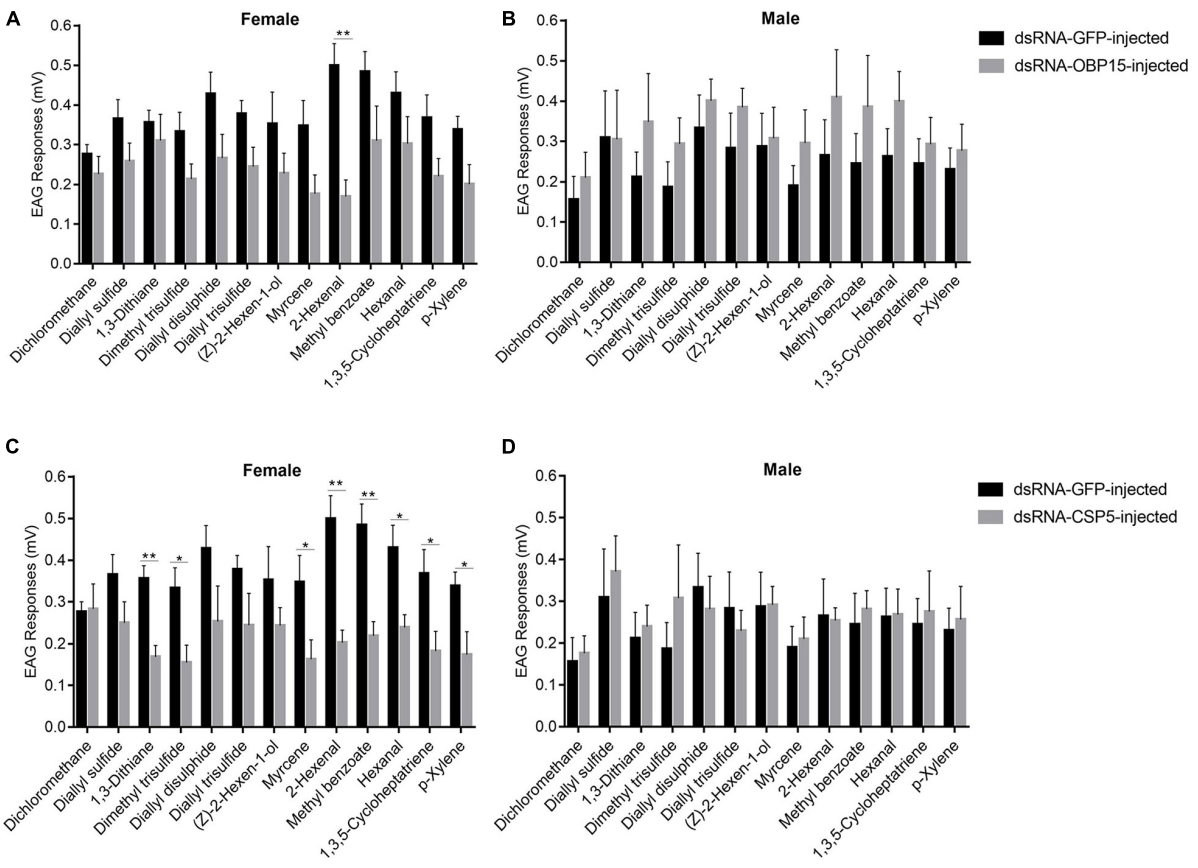

FIGURE 6 | EAG responses of dsRNA-GdauOBP15-injected **(A,B)** and dsRNA-GdauCSP5-injected **(C,D)** in *G. daurica* female and male to various compounds (*t*-test; $^{*}P < 0.05$; $^{**}P < 0.01$). Columns indicate the mean ± standard error of six independent experiments.

suggesting that they may be involved in host plant localization. For example, the *MaltCSP5* gene of *Monochamus alternatus* was mainly expressed in male and female antenna, and the binding affinity of recombinant CSP5 showed very strong binding abilities to pine plant volatiles (Ali et al., 2019). Zeng et al. (2018) found that CmedCSP1 and CmedCSP2 were localized in basiconica sensilla and showed strong binding affinities with a wide range of host-related semiochemicals. Injecting target dsRNAs resulted in a significant decrease in EAG responses evoked by the host volatiles of *Cnaphalocrocis medinalis*.

The importance of GdauOBP15 and GdauCSP5 in binding to major volatiles was further confirmed by our RNAi experiment. The injection of dsRNA-OBP15 and dsRNA-CSP5 significantly decreased the *GdauOBP15* and *GdauCSP5* expression levels. The electrophysiological response of *G. daurica* females to 2-hexenal was significantly decreased in dsRNA-OBP15-injected treatment compared to the control, and antennae of dsRNA-CSP5-treated females significantly reduced EAG response to eight tested host volatiles (1,3-dithiane, 2-hexenal, methyl benzoate, dimethyl trisulfide, myrcene, hexanal, 1,3,5-cycloheptatriene, and p-xylene). Our results corresponded with previous studies that silencing CSP or OBP genes can affect odor preferences (Rebijith et al., 2016; Dong et al., 2017; Waris et al., 2018; Zhou et al., 2019). Zhang et al. (2016) reported that silencing *AlinOBP4* by RNAi induced declining electrophysiological responses of *Adelphocoris lineolatus* to sex pheromone components and some host plant volatiles. Further study showed that the binding property of the recombinant AlinOBP4 protein was consistent with the results of RNAi (Wang et al., 2020). However, our results of EAG response after RNAi were inconsistent with the fluorescence-binding assays. GdauOBP15 had weak binding affinity to 2-hexenal, and GdauCSP5 could only bind dimethyl disulfide and 2-hexenal. The reason might be that they cooperate with multiple binding proteins to transport numerous compounds. For example, in *Anopheles gambiae*, OBP1 and OBP4 were co-expressed and formed heterodimers in the sensillum lymph, which showed different binding properties from the individual proteins (Qiao et al., 2011). In *A. lineolatus*, a mixture of AlinCSP5 and AlinCSP6 enhanced the binding affinity to terpenoids which did not bind with individuals (Sun et al., 2015). There was no significant change in the males' electrophysiological responses to host plant volatiles after RNAi. Our previous study showed that there were significant differences in the expression levels of *GdauOBP15* and *GdauCSP5* in male and female antennae (Li et al., 2018). This implies that GdauOBP15 and GdauCSP5 may have different functions in odor perception between males and females in *G. daurica*, and they play more important roles in females searching for host plants, but this needs further study for confirmation.

In this study, we tried to combine molecular and electrophysiological methods to clarify the functions of several GdauOBPs and GdauCSPs in *G. daurica*. We hypothesize that GdauOBP6, GdauOBP15, GdauCSP4, and GdauCSP5 may be involved in host recognition in the adult chemosensory system. The reduction in *GdauOBP15* and *GdauCSP5* transcript abundance leads to a decrease in the female electrophysiological responses to host plant volatiles. These discoveries provided important clues for revealing the molecular mechanism of host selection of *G. daurica* and will facilitate the development of effective volatile attractants, which provide the possibility for pest monitoring and biological control.

DATA AVAILABILITY STATEMENT

The raw data supporting the conclusions of this article will be made available by the authors, without undue reservation.

ETHICS STATEMENT

The animal subject used in this study is a leaf beetle in grasslands, which is an invertebrate and exempt from this requirement. No specific permits were required for the beetle's collection from the field and for maintenance in laboratory. This study did not involve any endangered species, protected species, or protected areas.

AUTHOR CONTRIBUTIONS

LL and B-PP conceived and designed the experiments. LL wrote the manuscript. LL, W-BZ, Y-MS, and Z-RZ performed the experiments. B-PP provided valuable suggestions and helped to revise the manuscript. All authors discussed the results and approved the final manuscript.

FUNDING

This work was supported by the National Natural Science Foundation of China (Grant No. 32001397).

SUPPLEMENTARY MATERIAL

The Supplementary Material for this article can be found online at: https://www.frontiersin.org/articles/10.3389/fphys.2021.678698/full#supplementary-material

REFERENCES

Ali, S., Ahmed, M. Z., Li, N., Ali, S. A. I., and Wang, M. Q. (2019). Functional characteristics of chemosensory proteins in the sawyer beetle *Monochamus alternatus* Hope. *Bull. Entomol. Res.* 109, 34–42. doi: 10.1017/s0007485318000123

Benoit, J. B., Vigneron, A., Broderick, N. A., Wu, Y., Sun, J. S., and Carlson, J. R. (2017). Symbiont-induced odorant binding proteins mediate insect host hematopoiesis. *eLife* 6:e19535.

Cai, L., Cheng, X., Qin, J., Qin, J., and You, M. (2020). Expression, purification and characterization of three odorant binding proteins from the diamondback moth *Plutella xylostella*. *Insect Mol. Biol.* 29, 531–544. doi: 10.1111/imb.12664

Calvello, M., Guerra, N., Brandazza, A., Ambrosio, C. D., Scaloni, A., Dani, F. R., et al. (2003). Soluble proteins of chemical communication in the social wasp *Polistes dominulus*. *Cell. Mol. Life Sci.* 60, 1933–1943. doi: 10.1007/s00018-003-3186-5

Campanacci, V., Krieger, J., Bette, S., Sturgis, J. N., Lartigue, A., Cambillau, C., et al. (2001). Revisiting the specificity of *Mamestra brassicae* and *Antheraea polyphemus* pheromone-binding proteins with a fluorescence binding assay. *J. Biol. Chem.* 276, 20078–20084. doi: 10.1074/jbc.m100713200

Cheng, D., Lu, Y., Zeng, L., Liang, G., and He, X. (2015). Si-CSP9 regulates the integument and moulting process of larvae in the red imported fire ant *Solenopsis invicta*. *Sci. Rep.* 5:9245.

Cheng, L., Luo, J., Li, P., Yu, H., Huang, J. F., and Luo, L. X. (2014). Microbial diversity and flavor formation in onion fermentation. *Food Funct.* 5, 2338–2347. doi: 10.1039/c4fo00196f

Das, A., Lee, S. H., Hyun, T. K., Kim, S. W., and Kim, J. Y. (2013). Plant volatiles as method of communication. *Plant Biotech. Rep.* 7, 9–26. doi: 10.1007/s11816-012-0236-1

Dippel, S., Oberhofer, G., Kahnt, J., Gerischer, L., Opitz, L., and Schachtner, J. (2014). Tissue-specific transcriptomics, chromosomal localization, and phylogeny of chemosensory and odorant binding proteins from the red flour beetle *Tribolium castaneum* reveal subgroup specificities for olfaction or more general functions. *BMC Genomics* 15:1141. doi: 10.1186/1471-2164-15-1141

Dong, K., Sun, L., Liu, J. T., Gu, S. H., Zhou, J. J., Yang, R. N., et al. (2017). RNAi-induced electrophysiological and behavioral changes reveal two pheromone binding proteins of *Helicoverpa armigera* involved in the perception of the main sex pheromone component. *J. Chem. Ecol.* 43, 207–214. doi: 10.1007/s10886-016-0816-6

Forêt, S., Wanner, K. W., and Maleszka, R. (2007). Chemosensory proteins in the honey bee: insights from the annotated genome, comparative analyses and expressional profiling. *Insect Biochem. Mol. Biol.* 37, 19–28. doi: 10.1016/j.ibmb.2006.09.009

Gong, D. P., Zhang, H. J., Zhao, P., Lin, Y., Xia, Q. Y., and Xiang, Z. H. (2007). Identification and expression pattern of the chemosensory protein gene family in the silkworm *Bombyx mori*. *Insect Biochem. Mol. Biol.* 37, 266–277. doi: 10.1016/j.ibmb.2006.11.012

Hao, X., Zhou, X. R., Pang, B. P., Zhang, Z. R., and Bao, X. (2015). Morphological and biological characteristics of *Galeruca daurica* Joannis. *Acta Agrest. Sin.* 23, 1106–1108.

Hao, X., Zhou, X. R., Pang, B. P., Zhang, Z. R., and Ma, C. Y. (2014). Effects of host plants on feeding amount, growth and development of *Galeruca daurica* (Joannis) larvae (Coleoptera: Chrysomelidae). *Acta Agrest. Sin.* 22, 854–858.

He, H. J., Wang, X. L., and Zhang, J. L. (2004). Analysis of volatile components of shallots by GC-MS. *J. Instr. Anal.* 23(Suppl.), 98–100.

Hull, J. J., Perera, O. P., and Snodgrass, G. L. (2014). Cloning and expression profiling of odorant-binding proteins in the tarnished plant bug *Lygus lineolaris*. *Insect Mol. Biol.* 23, 78–97. doi: 10.1111/imb.12064

Leal, W. S. (2005). Pheromone reception. *Topics Curr. Chem.* 240, 1–36.

Leal, W. S. (2013). Odorant reception in insects: roles of receptors, binding proteins, and degrading enzymes. *Annu. Rev. Entomol.* 58, 373–391. doi: 10.1146/annurev-ento-120811-153635

Li, G. W., Chen, X. L., Li, B. L., Zhang, G. H., Li, Y. P., and Wu, J. X. (2016). Binding properties of general odorant binding proteins from the Oriental Fruit Moth, *Grapholita molesta* (Busck) (Lepidoptera: Tortricidae). *PLoS One* 11:5. doi: 10.1371/journal.pone.0155096

Li, L., Tan, Y., Zhou, X. R., and Pang, B. P. (2019). Molecular cloning, prokaryotic expression and binding characterization of odorant binding protein GdauOBP20 in *Galeruca daurica*. *Sci. Agric. Sin.* 52, 3705–3712.

Li, L., Zhou, Y. T., Tan, Y., Zhou, X. R., and Pang, B. P. (2017). Identification of odorant-binding protein genes in *Galeruca daurica* (Coleoptera: Chrysomelidae) and analysis of their expression profiles. *Bull. Entomol. Res.* 107, 550–561. doi: 10.1017/s0007485317000402

Li, L., Zhou, Y. T., Tan, Y., Zhou, X. R., and Pang, B. P. (2018). Identification and expression profiling of chemosensory protein genes in *Galeruca daurica* (Coleoptera: Chrysomelidae). *Acta Entomol. Sin.* 61, 646–656.

Li, M. F., Li, T., Li, W., and Yang, L. D. (2015). Changes in antioxidant capacity, levels of soluble sugar, total polyphenol, organosulfur compound and constituents in garlic clove during storage. *Ind. Crops Prod.* 69, 137–142. doi: 10.1016/j.indcrop.2015.02.021

Livak, K. J., and Schmittgen, T. D. (2001). Analysis of relative gene expression data using real-time quantitative PCR and the $2-\Delta\Delta CT$ method. *Methods* 25, 402–408. doi: 10.1006/meth.2001.1262

Maleszka, J., Forêt, S., Saint, R., and Maleszka, R. (2007). RNAi-induced phenotypes suggest a novel role for a chemosensory protein CSP5 in the development of embryonic integument in the honeybee (Apis mellifera). *Dev. Genes Evol.* 217, 189–196. doi: 10.1007/s00427-006-0127-y

Martin, J. P., Beyerlein, A., Dacks, A. M., Reisenman, C. E., Riffell, J. A., Lei, H., et al. (2011). The neurobiology of insect olfaction: sensory processing in a comparative context. *Prog. Neurobiol.* 95, 427–447. doi: 10.1016/j.pneurobio.2011.09.007

McKenna, M. P., Hekmat-Scafe, D. S., Gaines, P., and Carlson, J. R. (1994). Putative *Drosophila* pheromone-binding proteins expressed in a subregion of the olfactory system. *J. Biol. Chem.* 269, 16340–16347. doi: 10.1016/s0021-9258(17)34013-9

Nathália, F. B., Monica, F. M., and Ana, C. A. M. (2016). A look inside odorant-binding proteins in insect chemoreception. *J. Insect Physiol.* 95, 51–65. doi: 10.1016/j.jinsphys.2016.09.008

Nomura, A., Kawasaki, K., Kubo, T., and Natori, S. (1992). Purification and localization of p10, a novel protein that increases in nymphal regenerating legs of *Periplaneta americana* American cockroach. *Int. J. Devel. Biol.* 36, 391–398.

Pelosi, P., Iovinella, I., Zhu, J., Wang, G., and Dani, F. R. (2017). Beyond chemoreception: diverse tasks of soluble olfactory proteins in insects. *Biol. Rev. Camb. Phil. Soc.* 93, 184–200. doi: 10.1111/brv.12339

Pelosi, P., Zhou, J. J., Ban, L. P., and Calvello, M. (2006). Soluble proteins in insect chemical communication. *Cell Mol. Life Sci.* 63, 1658–1676. doi: 10.1007/s00018-005-5607-0

Qiao, H., He, X., Schymura, D., Ban, L., Field, L., Dani, F. R., et al. (2011). Cooperative interactions between odorant-binding proteins of *Anopheles gambiae*. *Cell. Mol. Life Sci.* 68, 1799–1813. doi: 10.1007/s00018-010-0539-8

Qiao, H. L., Deng, P. Y., Li, D. D., Chen, M., Jiao, Z. J., Liu, Z. C., et al. (2013). Expression analysis and binding experiments of chemosensory proteins indicate multiple roles in *Bombyx mori*. *J. Insect Physiol.* 59, 667–675. doi: 10.1016/j.jinsphys.2013.04.004

Rebijith, K. B., Asokan, R., Ranjitha Hande, H., Krishna Kumar, N. K., Krishna, V., Vinutha, J., et al. (2016). RNA interference of odorant-binding protein 2 (OBP2) of the cotton Aphid, *Aphis gossypii* (Glover), resulted in altered electrophysiological responses. *Appl. Biochem. Biotechnol.* 178, 251–266. doi: 10.1007/s12010-015-1869-7

Sun, J. S., Larter, N. K., Chahda, J. S., Rioux, D., Gumaste, A., and Carlson, J. R. (2018). Humidity response depends on the small soluble protein Obp59a in *Drosophila*. *eLife* 7:e39249.

Sun, L., Wei, Y., Zhang, D. D., Ma, X. Y., Xiao, Y., Zhang, Y. N., et al. (2016). The mouthparts enriched odorant binding protein 11 of the alfalfa plant bug *Adelphocoris lineolatus* displays a preferential binding behavior to host plant secondary metabolites. *Front. Physiol.* 7:201. doi: 10.3389/fphys.2016.00201

Sun, L., Zhou, J. J., Gu, S. H., Xiao, H. J., Guo, Y. Y., Liu, Z. W., et al. (2015). Chemosensillum immunolocalization and ligand specificity of chemosensory proteins in the alfalfa plant bug *Adelphocoris lineolatus* (Goeze). *Sci. Rep.* 5:8073. doi: 10.1038/srep08073

Tan, Y., Zhou, X. R., and Pang, B. P. (2016). Reference gene selection and evaluation for expression analysis using qRT-PCR in *Galeruca daurica* (Joannis). *Bull. Entomol. Res.* 107, 359–368. doi: 10.1017/S0007485316000948

Vogt, R. G., and Riddiford, L. M. (1981). Pheromone binding and inactivation by moth antennae. *Nature* 293, 161–163. doi: 10.1038/293161a0

Vogt, R. G., Rogers, M. E., Franco, M. D., and Sun, M. (2002). A comparative study of odorant binding protein genes: differential expression of the PBP1-GOBP2 gene cluster in *Manduca sexta* (Lepidoptera) and the organization of OBP genes in *Drosophila melanogaster* (Diptera). *J. Exp. Biol.* 205, 719–744. doi: 10.1242/jeb.205.6.719

Wang, Q., Wang, Q., Li, H., Sun, L., Zhang, D., and Zhang, Y. (2020). Sensilla localization and sex pheromone recognition of odorant binding protein OBP4 in the mirid plant bug *Adelphocoris lineolatus* (Goeze). *J. Insect Physiol.* 121, 104012. doi: 10.1016/j.jinsphys.2020.104012

Waris, M. I, Younas, A., Ul Qamar, M. T., Hao, L., Ameen, A., Ali, S., et al. (2018). Silencing of chemosensory protein gene NlugCSP8 by RNAi induces declining behavioral responses of *Nilaparvata lugens*. *Front. Physiol* 9:379. doi: 10.3389/fphys.2018.00379

Wu, F., Feng, Y., Han, B., Hu, H., Feng, M., Meng, L., et al. (2019). Mechanistic insight into binding interaction between chemosensory protein 4 and volatile larval pheromones in honeybees (*Apis mellifera*). *Int. J. Biol. Macromol.* 141, 553–563. doi: 10.1016/j.ijbiomac.2019.09.041

Wuren, Z. G. (2011). *Studies on Extraction process, Chemical Composition and Bacteriostatic Action of Essential oils From Allium Mongolicum Regel[D]*. Huhhot: Inner Mongolia Agricultural University.

Yang, X. K., Huang, D. C., Ge, S. Q., Bai, M., and Zhang, R. Z. (2010). One million mu of meadow in Inner Mongolia suffer from the harm of breaking out of *Galeruca daurica* (Joannis). *Chin. Bull. Entomol.* 47:812.

Zacharuk, R. Y. (1980). Ultrastructure and function of insect chemosensilla. *Annu. Rev. Entomol.* 25, 27–47. doi: 10.1146/annurev.en.25.010180.000331

Zeng, F. F., Liu, H., Zhang, A., Lu, Z. X., Leal, W. S., Abdelnabby, H., et al. (2018). Three chemosensory proteins from the rice leaf folder *Cnaphalocrocis medinalis* involved in host volatile and sex pheromone reception. *Insect Mol. Biol.* 27, 710–723. doi: 10.1111/imb.12503

Zhang, L. W., Li, H. W., and Zhang, L. (2017). Two olfactory pathways to detect aldehydes on locust mouthpart. *Int. J. Biol. Sci.* 13, 759–771. doi: 10.7150/ijbs.19820

Zhang, T. T., Mei, X. D., Feng, J. N., Berg, B. G., Zhang, Y. J., and Guo, Y. Y. (2012). Characterization of three pheromone-binding proteins (PBPs) of *Helicoverpa armigera* (Hubner) and their binding properties. *J. Insect Physiol.* 58, 941–948. doi: 10.1016/j.jinsphys.2012.04.010

Zhang, X. Y., Zhu, X. Q., Gu, S. H., Zhou, Y. L., Wang, S. Y., Zhang, Y. J., et al. (2016). Silencing of odorant binding protein gene AlinOBP4 by RNAi induces declining electrophysiological responses of *Adelphocoris* lineolatus to six semiochemicals. *Insect Sci.* 24, 789–797. doi: 10.1111/1744-7917.12365

Zhou, X. R., Shan, Y. M., Tan, Y., Zhang, Z. R., and Pang, B. P. (2019). Comparative analysis of transcriptome responses to cold stress in *Galeruca daurica* (Coleoptera: Chrysomelidae). *J. Insect Sci.* 19, 1–6.

Zhou, Y. T., Li, L., Zhou, X. R., Tan, Y., and Pang, B. P. (2020). Three chemosensory proteins involved in chemoreception of *Oedaleus asiaticus* (Orthopera: Acridoidea). *J. Chem. Ecol.* 46, 138–149. doi: 10.1007/s10886-019-01138-5

Conflict of Interest: The authors declare that the research was conducted in the absence of any commercial or financial relationships that could be construed as a potential conflict of interest.

frontiers in Physiology

ORIGINAL RESEARCH
published: 19 July 2021
doi: 10.3389/fphys.2021.682537

Olfactory Proteins and Their Expression Profiles in the *Eucalyptus* Pest *Endoclita signifier* Larvae

Xiaoyu Zhang[1,2], *Zhende Yang*[1], *Xiuhao Yang*[3], *Hongxuan Ma*[4], *Xiumei Liu*[4] *and Ping Hu*[1,2]*

[1] Forestry College, Guangxi University, Nanning, China, [2] Forestry College, Central South University of Forestry and Technology, Changsha, China, [3] Guangxi Academy of Forestry, Nanning, China, [4] GuangxiGaofeng National Forest Farm, Nanning, China

Endoclita signifier Walker (Lepidoptera: Hepialidae), a polyphagous insect, has become a new wood-boring pest in Eucalyptus plantations in southern China since 2007, which represents a typical example of native insect adaptation to an exotic host. After the third instar, larvae move from soil to standing trees and damage the plants with a wormhole. Although females disperse to lay eggs, larvae can accurately find eucalyptus in a mingled forest of eight species, which leads us to hypothesize that the larval olfactory system contributes to its host selection. Herein, we investigated the transcriptomes of the head and tegument of *E. signifer* larvae and explored the expression profiles of olfactory proteins. We identified 15 odorant-binding proteins (OBPs), including seven general OBPs (GOPBs), six chemosensory proteins (CSPs), two odorant receptors (ORs), one gustatory receptor (GR), 14 ionotropic receptors (IRs), and one sensory neuron membrane protein (SNMP). Expression profiles indicated that all olfactory proteins, except for EsigCSP1, were expressed in the head, and most were also detected in non-olfactory tissues, especially thorax tegument. Furthermore, EsigOBP2, EsigOBP8, EsigGOBP1, EsigGOBP2, EsigGOBP5, EsigCSP3, EsigCSP5, and EsigOR1 were expressed most strongly in the head; moreover, EsigCSP3 expressed abundantly in the head. EsigGR1 exhibited the highest expression among all tissues. Besides phylogenetic analysis shows that EsigGOBP7 probably is the pheromone-binding protein (PBP) of *E. signifier*. This study provides the molecular basis for future study of chemosensation in *E. signifier* larvae. EsigCSP3 and EsigGR1, which have unique expression patterns, might be factors that govern the host choice of larvae and worth further exploration.

Keywords: expression profiles, chemosensory proteins, transcriptome, odorant binding protein, *Endoclita signifier*

OPEN ACCESS

Edited by:
Jin Zhang,
Max Planck Institute for Chemical Ecology, Germany

Reviewed by:
Ahmed Najar,
University of Alberta, Canada
Ali R. Bandani,
University of Tehran, Iran

***Correspondence:**
Ping Hu
hupingcs@163.com

Specialty section:
This article was submitted to Invertebrate Physiology, a section of the journal Frontiers in Physiology

Received: *18 March 2021*
Accepted: *09 June 2021*
Published: *19 July 2021*

Citation:
Zhang XY, Yang YD, Yang XH, Ma HX, Liu XM and Hu P (2021) Olfactory Proteins and Their Expression Profiles in the Eucalyptus Pest Endoclita signifier Larvae. Front. Physiol. 12:682537. doi: 10.3389/fphys.2021.682537

INTRODUCTION

The ghost moth *Endoclita signifer* Walker (Lepidoptera, Hepialidae) is a native polyphagous insect pest that is widely distributed in Japan, Korea, India, Thailand, Myanmar, and central, south, and southwest China (Yang et al., 2021). After *Eucalyptus* was planted in the south of China, *E. signifer* was discovered to have infested *Eucalyptus* in Guangxi in 2007.

This is an example of a native insect adapting to an exotic host, and it has resulted in great economic losses and major ecological impacts (Yang et al., 2016). In 2020, an infestation of *E. signifier* was found in 17.1% of the counties in Guangxi, where host plants included 51 species in 40 genera and 30 families (Yang et al., 2021). In Guangxi, *E. signifer* usually produces one generation a year and occasionally two. The adults eclose from mid-March through April and then mate and oviposit. Larvae hatch within 1 month and live in the soil. After the third instar stage, from July through August, the larvae move from soil to standing trees, where they feed on bark, bore into the stem, and weave wood pieces and silk over the hole entrance, constructing a home in which they reside until the following January before pupating in February (**Figure 1**). Some larvae spend two years in the tree, until January of the third year (Yang, 2013). Although female oviposition proceeds in a dispersed manner, larvae were shown to damage eight *Eucalyptus* species in mixed forests (Yang, 2017). Besides, the sensillum of *E. signifier* larva shows that only 16 sensilla in antennae, but a large number of sensilla in thoracic and abdominal tegument (Hu et al., 2021). Therefore, we hypothesized that the thoracic and abdominal tegument may have an olfactory function and help larvae to find their host.

In most insects, especially stem borers, females select the host. Olfaction plays a minor role in larvae. The small number of neurons in the *Drosophila* olfactory system makes it a very convenient system for olfactory studies (Bose et al., 2015), enabling the exploration of sensory coding at all stages of nervous system development (Bose et al., 2015). In *Drosophila* larvae, the epidermal growth factor receptor (Rahn et al., 2013) and serotonin signaling (Annina et al., 2017) are necessary for learning and memory. However, sub-circuits allow *Drosophila* larvae to integrate present sensory input into the context of past experience and elicit an appropriate behavioral response (Rahn et al., 2013). The responsiveness of larval sensilla to female-emitted sex pheromones is based on the same molecular machinery as that functioning in the antennae of adult males (Zielonka et al., 2016). Olfactory proteins that bind, transport, and degrade odor molecules play important roles in chemo-sensing in larvae and include odorant-binding proteins (OBPs), chemosensory proteins (CSPs), sensory neuron membrane proteins (SNMPs), odorant receptors (ORs), gustatory receptors (GRs), ionotropic receptors (IRs), and odor-degrading enzymes (ODEs) (Zhou, 2010). Behavior, physiology, and molecular result indicated olfactory proteins of larvae play a role in pheromone or volatile recognition. For example, four CSPs in *Chilo auricilius* larvae (Yi et al., 2019) were significantly regulated by α-pinene treatment. Pre-exposure larvae to single volatile organic compounds can upregulate ORs in *Spodoptera exigua* larvae strongly and non-specifically (Llopis-Gimenez et al., 2020). *S. exigua* larval OBP can bind to a major female sex pheromone component (Jin et al., 2015), whereas OBP8 of *Melipona scutellaris* is expressed and functioned in the larval mandible (Carvalho et al., 2017).

This study investigated the transcriptomes in the head and tegument of *E. signifer* larvae to determine the expression profiles of olfactory proteins in *E. signifer* larvae and evaluated the phylogenetic relationships between *E. signifer* OBPs and CSPs with those expressed in the larvae and adults of other species. This work illuminates the olfactory system in *E. signifer* larvae and provides a theoretical basis for further studies to explore ecologically relevant larval behaviors.

MATERIALS AND METHODS

Ethics Statement

The ghost moth *E. signifier* is a forestry pest in China, which were collected with the direct permission of the Guangxi forestry bureau. It is not included in the "list of endangered and protected animals in China." All operations were performed according to ethical guidelines in order to minimize pain and discomfort to the insects.

Insect and Tissue Collection

E. signifier larvae were collected from damaging *Eucalyptus* plantation by cutting the tree during December 2019 to January 2020 and September to November 2020 in the Gaofeng forest station, Guangxi, China. Six 12th larvae and 18 5th larvae were taken indoors and stored at −80°C. Larval thoracic and abdominal tegument were obtained by using surgical scissors to cut open the larvae abdomen through the midline and using

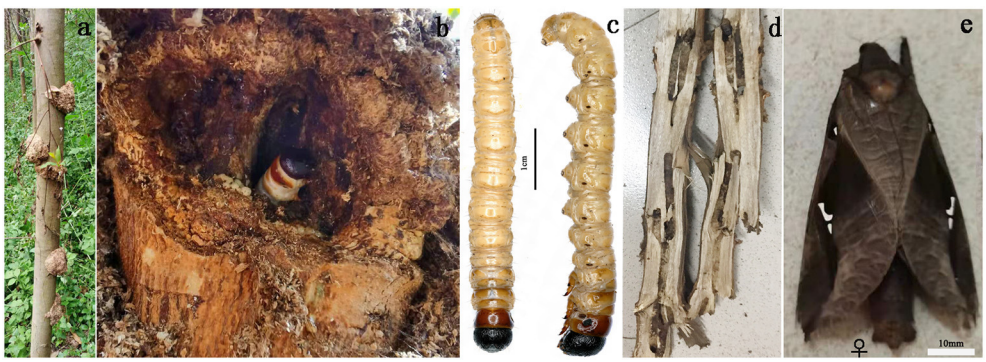

FIGURE 1 | (a,b,d) Damage caused by *E. signifer*. **(c)** Larvae and **(e)** adults of *E. signifer*.

tweezers to remove from the rest of the body (intestinal canal and fat body), and the teguments were cleaned in RNA-free ddH_2O.

cDNA Library Construction and Illumina Sequencing

Total RNA was extracted from six 12th larval head, thoracic, and abdominal tegument using TRIzol reagent (Ambion) and the RNeasy Plus Mini Kit (No. 74134; Qiagen, Hilden, Germany), following the instructions of the manufacturer, respectively. RNA quantity was detected using the NanoDrop 8000 (Thermo, Waltham, MA, USA). There is one replication, each replication with six larvae. RNA of 12th larval heads and thoracic and abdominal tegument were used to construct the cDNA libraries. cDNA library construction and Illumina sequencing of samples were performed at MajorBioCorporation (Shanghai, China). mRNA samples were purified and fragmented using the TruSeq RNA Sample Preparation Kit v2-Set A (No. RS-122-2001; Illumina, San Diego, CA, USA). Random hexamer primers were used to synthesize the first-strand cDNA, followed by synthesis of the second-strand cDNA using a buffer, dNTPs, RNase H, and DNA polymerase I at 16°C for 1 h. After end repair, A-tailing, and the ligation of adaptors, the products were amplified by PCR and quantified precisely using the Qubit DNA Br Assay Kit (Q10211; *Invitrogen*, Carlsbad, CA, USA). They were then purified using the MinElute Gel Extraction Kit (Qiagen, Cat No. 28604) to obtain a cDNA library. The cDNA library was sequenced on the HiSeq2500 platform.

Assembly and Functional Annotation

All raw reads were processed to remove low-quality and adaptor sequences by Trimmomatic (http://www.usadellab.org/cms/index.php?page=trimmomatic). Clean reads assembly was carried out with the short-read assembly program Trinity (Version: r2020-01-13), with the default parameters, after combining the heads and thoracic and abdominal tegument clean reads. The largest alternative splicing variants in the Trinity results were called "unigenes." The annotation of unigenes was performed by NCBI BLASTx searches against the Nr protein database, with an E-value threshold of 1e-5. The blast results were then imported into the Blast2GO pipeline for GO annotation. The longest ORF for each unigene was determined by the NCBI ORF Finder tool (http://www.ncbi.nlm.nih.gov/gorf/gorf.html). Expression levels were expressed in terms of FPKM values (Mortazavi et al., 2008), which were calculated by RSEM (RNA-Seq by Expectation-Maximization) (Version: v1.2.6) with default parameters (Li and Dewey, 2011).

Identification of Chemosensory Genes

With BLASTx, the available sequences of OBPs, CSPs, ORs, GRs, IRs, and SNMPs proteins from insect species were used as queries to identify candidate unigenes involved in olfaction in *E. signifier* from the Nr database. All candidate OBPs, CSPs, ORs, GRs, IRs, and SNMPs were manually checked by tBLASTn in NCBI online by assessing the BLASTx results. The nucleic acid sequences encoded by all chemosensory genes that were identified from the *E. signifier* larval head and thorax and abdomen tegument transcriptome are listed in **Supplementary Material 1**.

Sequence and Phylogenetic Analysis

The candidate OBPs were searched for the presence of N-terminal signal peptides using SignalP4.0 (http://www.cbs.dtu.dk/services/SignalP/). Amino acid sequence alignment was performed using the muscle method implemented in the Mega v6.0 software package (Tamura et al., 2011). The phylogenetic tree was constructed using the neighbor-joining (NJ) method (Saitou and Nei, 1987) with the P-distances model and a pairwise deletion of gaps performed in the Mega v6.0 software package. The reliability of the tree structure and node support was evaluated by bootstrap analysis with 1,000 replicates. The phylogenetic trees were colored and arranged in FigTree (Version 1.4.2). The phylogenetic analyses of *OBPs* were based on *Dastarcus helophoroides* (Li et al., 2020), *Chrysomya megacephala* (Wang et al., 2015), *Plutella xylostella* (Zhu et al., 2016), *S. exigua* (Liu et al., 2015; Llopis-Gimenez et al., 2020), *Helicoverpa armigera* (Chang et al., 2017), and *E. signifier*. The CSPs tree was based on *D. helophoroides* (Li et al., 2020), *C. megacephala* (Wang et al., 2015), *S. exigua* (Llopis-Gimenez et al., 2020), *H. armigera* (Chang et al., 2017), and *E. signifier*. The gene name and the Genbank number of *P. xylostella* and *H. armigera* are listed in **Supplementary Material 2**; other genes sequences are available in the reference article.

Expression Analysis by Fluorescence Quantitative Real-Time PCR

Fluorescence quantitative real-time PCR was performed to verify the expression of candidate chemosensory genes. The total RNA of the 18 fifth instar larval head, thoracic, and abdominal teguments was extracted following the methods described above. NanoDrop 2008 and agarose gel electrophoresis examined the density and quality of the RNA. cDNA was synthesized from the total RNA, using the PrimeScriptRT Reagent Kit with gDNA Eraser to remove gDNA (No. RR047A; TaKaRa, Shiga, Japan). Gene-specific primers were designed using Primer 3 (http://bioinfo.ut.ee/primer3-0.4.0/) (**Supplementary Material 3**). Eighteen SRNAs were identified, evaluated, and selected as a reference gene for qPCR (Chen and Hu, in press). A PCR analysis was conducted using the Roche LIGHT CYCLE 480II (USA). SYBRPremixExTaq^{TM} II (No. RR820A; TaKaRa) was used for the PCR reaction under three-step amplification. Each PCR reaction was conducted in a 25-μl reaction mixture containing 12.5 μl of SYBR Premix Ex Taq II, 1 μl of each primer (10 mM), 2 μl of sample cDNA, and 8.5 μl of dH2O. The RT-qPCR cycling parameters were as follows: 95°C for 30 s, followed by 40 cycles of 95°C for 5 s, 60°C for 30 s, and 65°C to 95°C in increments of 0.5°C for 5 s to generate the melting curves. To examine reproducibility, each qPCR reaction for each tissue was performed in three biological replicates (each replicate with six larvae) and three technical replicates. Negative controls without either template were included in each experiment. RocheLIGHT CYCLE 480II was used to normalize the expression based on ΔΔCq values, with GOBP3 in the head as control samples, and the $2^{-\Delta\Delta CT}$ method was used (Livak and Schmittgen, 2001). Before comparative analyses, the normal distribution and equal variance tests were examined, and all

taken logarithm data followed a normal distribution and with equal variances. The comparative analyses for every gene among six tissue types were assessed by a one-way nested analysis of variance (ANOVA), followed by Tukey's honestly significance difference (HSD) tests implemented in SPSS Statistics 18.0. Values are presented as means ± SE.

RESULTS

Transcriptome Sequencing and Sequence Assembly

We generated 53 million raw reads from a cDNA library derived from the tegument of *E. signifer* larvae, with q20 and q30 scores for 97.84% and 93.74% of the reads severally. The larval head transcriptome yielded 51 million raw reads, with q20 and q30 scores for 97.83% and 93.65% of the reads, respectively. After trimming the adapters, removing low-quality raw sequences, using Trimmomatic, blending the head and tegument sequences, splicing, and assembly (using Trinity), we obtained 44,104 transcripts, with an N_{50} of 1,707 bp, an average length of 986 bp, and a maximum length of 56,111 bp (**Figure 2A**). The *E. signifer* raw reads have been deposited in the NCBI Sequence Read Archive database under GenBank accession number PRJNA713545.

Homology Analysis and Gene Ontology Annotation

For 41.17% of the transcripts, we obtained matches with entries in the NCBI non-redundant protein database, using BLASTx with an E-value cutoff of $1e^{-5}$. The most frequent sequence matches were with *Eumeta japonica* (6.06%), followed by *Ostrinia furnacalis* (5.77%) and *Hyposmocoma kahamanoa* (5.60%) (**Figure 2B**). We used gene ontology (GO) annotations to classify the 10,177 transcripts into functional groups with BLAST2GO, with *p*-values calculated from the hypergeometric distribution test and an E-value threshold of $< 1 \times 10^{-5}$. In the *E. signifer* transcriptome, molecular functions accounted for 36.75% of the GO annotations, followed by cellular components (33.96%) and biological processes (29.29%). In the molecular function category, the terms binding, catalytic activity, and transporter activity had the highest representation. In the biological process category, the terms cellular process, metabolic process, and biological regulation were most frequent. Membrane part, cell part, and organelle were the most common cellular component terms (**Figure 3**).

Olfactory Proteins

We identified 15 transcripts-encoding putative OBPs in *E. signifer*, of which six were general OBPs (GOBPs). According to the FPKM value of the unigenes, EsigGOBP3 and EsigOBP7 were expressed less strongly in the head, and ten OBPs were not expressed in the tegument (**Table 1**). We identified six transcript-encoding putative CSPs, of which four were expressed more strongly in the head, whereas CSP1 and CSP2 were expressed more strongly in the tegument (**Table 1**). One transcript encoded a putative SNMP and was strongly expressed in the tegument (**Table 1**). Two identified ORs were strongly expressed in the tegument (**Table 1**). One transcript encoding a putative GR was strongly expressed in the head. We identified 14 IRs, of which EsigIR1, EsigIR75p-1, EsigIR40a-1, EsigIR93a-1, and EsigIR5 were more strongly expressed in the tegument, whereas the others were expressed in the head (**Supplementary Material 4**).

Olfactory Protein Expression Profiles

We characterized the expression profiles of all the OBPs, CSPs, ORs, GRs, and SNMPs in the head, thoracic, and abdominal tegument of fifth *E. signifier* larvae. Of the OBPs, EsigOBP5 was the most strongly expressed OBPs in all larval tissues (10- to 1000-fold higher values). EsigOBP2, EsigOBP8, EsigGOBP1, EsigGOBP2, and EsigGOBP5 were most strongly expressed in the head, and EsigOBP8 and EsigGOBP5 were expressed at significantly lower levels in the thorax than in the head. EsigGOBP2 exhibited significant head-biased expression. In non-olfactory tissues, EsigOBP3, EsigOBP5, EsigOBP6, EsigGOBP3, and EsigGOBP7 were most highly expressed in the thoracic tegument, with a significant thorax-biased expression of EsigGOBP3. EsigGOBP7 was expressed at significantly higher levels in the thorax and abdomen than in the head. EsigOBP1, EsigOBP7, EsigGOBP4, and EsigGOBP6 were most strongly expressed in the abdominal tegument, especially EsigOBP7. Significantly, more EsigGOBP6 was expressed in the head and abdomen than in the thorax (**Figure 4**). Of the CSPs, EsigCSP3 and EsigCSP6 were the most strongly expressed CSPs, with levels 100- to 1,000-fold of other CSPs, and EsigCSP3 was only expressed in the head, but EsigCSP6 was strongly expressed in all larval tissues. EsigCSP5 and EsigCSP3 were most strongly expressed in the head, especially EsigCSP5. The expression of EsigCSP2, EsigCSP4, and EsigCSP6 was highest in the abdomen, especially for EsigCSP2 and EsigCSP4. EsigCSP4 expression differed significantly from the others in the three tissues, and EsigCSP1 was highly expressed in the thorax (**Figure 4**). EsigGR1 was expressed most strongly in the abdomen (**Figure 4**). EsigOR1 was expressed only in the head, whereas, significantly, more EsigOR2 was expressed in the abdomen than in other tissues. We also detected significantly higher EsigSNMP1 expression in the abdomen compared with the other tissues (**Figure 4**).

Phylogenetic Analysis of OBPs and CSPs

In the phylogenetic tree of OBPs (**Figure 5**), the no-expression clade (blue) included EsigGOBP3, EsigOBP6, EsigGOBP2, EsigGOBP7, EsigOBP1, EsigOBP3, EsigOBP4, and EsigOBP8. The OBPs not expressed in larvae included SexiOBP3, SexiOBP7, SexiOBP9, SexiOBP17, SexiOBP36, SexiOBP39, SexiOBP42, -] SexiOBP46, SexiOBP47, SexiPBP1, SexiPBP2, SexiPBP4, DhelOBP1, and DhelOBP9. The expression clade (green) included EsigGOBP6, EsigGOBP5, EsigOBP2, EsigGOBP4, EsigOBP5, EsigOBP7, with SexiOBP8, SexiOBP21, SexiOBP24, SexiOBP25, SexiOBP26, SexiOBP27, SexiOBP28, SexiOBP29, SexiOBP31, SexiOBP32, SexiOBP33, and SexiOBP6 expressed only in larvae. The PBP clade (red circle) contained EsigGOBP7; four PBPs of *S. exigua*; PBP1, GOBP1, and GOBP2 of *P. xylostella*; and HarmGOBP2 (**Figure 5**). In the phylogenetic tree with CSPs, the no-larval-expression clade (blue) included EsigCSP1, EsigCSP2, and SexiCSP4, SexiCSP23, and SexiCSP24 (**Figure 6**).

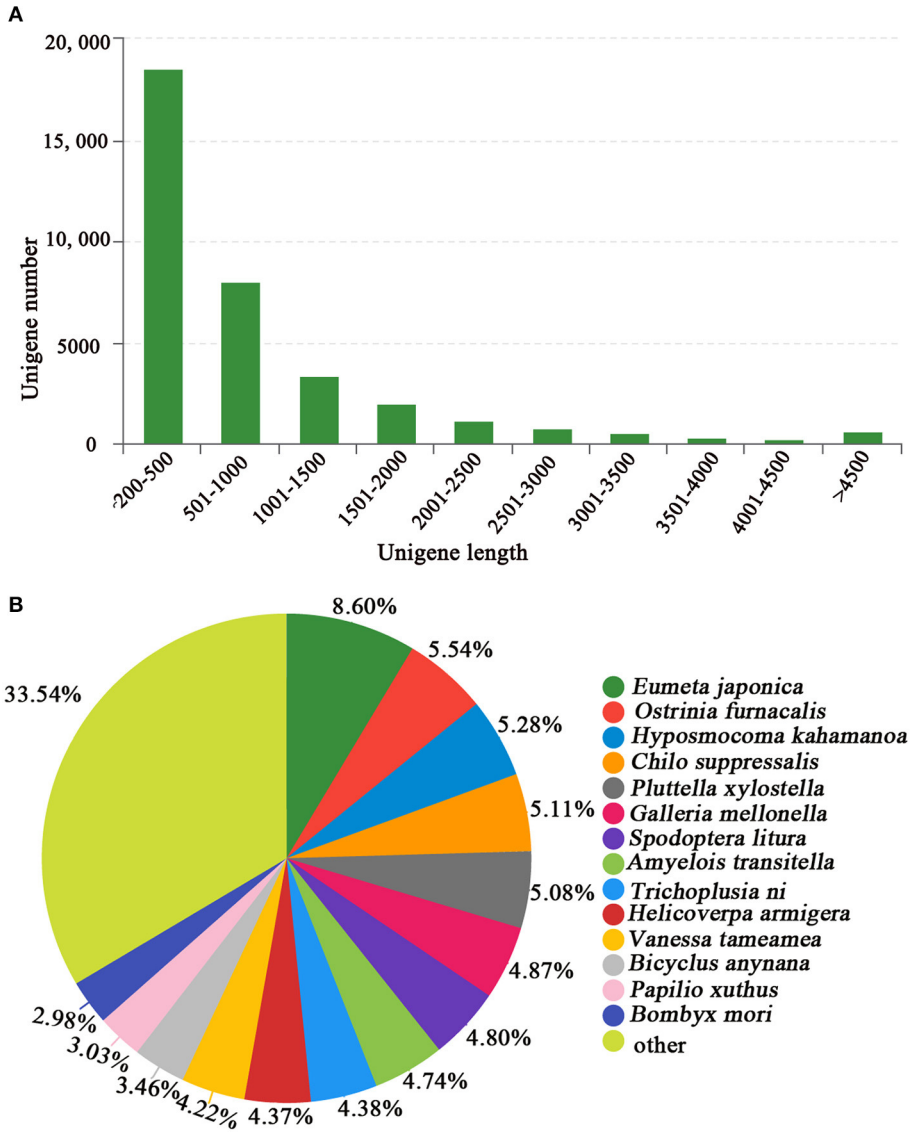

FIGURE 2 | (A) Length distribution of *E. signifer* unigenes and **(B)** BLASTx comparison of unigenes in the *E. signifer* transcriptome with those of other species.

DISCUSSION

Larval survival contributes to its host selection. From the head and tegument transcriptomes, we identified 39 olfactory proteins, including 15 OBPs, 6 CSPs, 2 ORs, 1 e GR, 1 SNMP, and 14 IRs. This is the first report of the separate larval head and tegument transcriptomes in Hepialidae. The number of olfactory proteins identified in *E. signifer* is less than that reported for most adult antennae transcriptomes, such as *Conogethe spinicolalis* (Jing et al., 2020). Additionally, larvae tend to have a shorter squirm range and a less complicated survival environment than adults and may consequently express a smaller set of olfactory genes than adults, as observed for *Spodoptera littoralis* (Poivet et al., 2013). The number of olfactory proteins in *E. signifier* is considerably fewer than the 26 OBPs and 21 CSPs identified in the transcriptomes of *H. armigera* larval antennae and mouthparts (Chang et al., 2017); the 20 OBPs, 11 CSPs, 9 ORs, 11 IRs, 7 GRs, and 4 SNMPs in the transcriptomes of newly hatched *Dastarcushelophoroides* larvae (Li et al., 2020); and the 58 ORs, 20 GRs, and 21 IRs in the transcriptomes of the antennae of males and females and the head tissue of neonates of *Cydia pomonella* (Walker et al., 2016). This reflects the scarcity of olfactory proteins of the original Lepidoptera group in the NCBI database, such as Hepialidae, resulting in less annotation of olfactory proteins in *E. signifer*.

According to the OBP expression profiles in larvae, distinct no-larval-expression or larval-specific-expression clades were apparent in the neighbor-joining tree based on OBPs, with

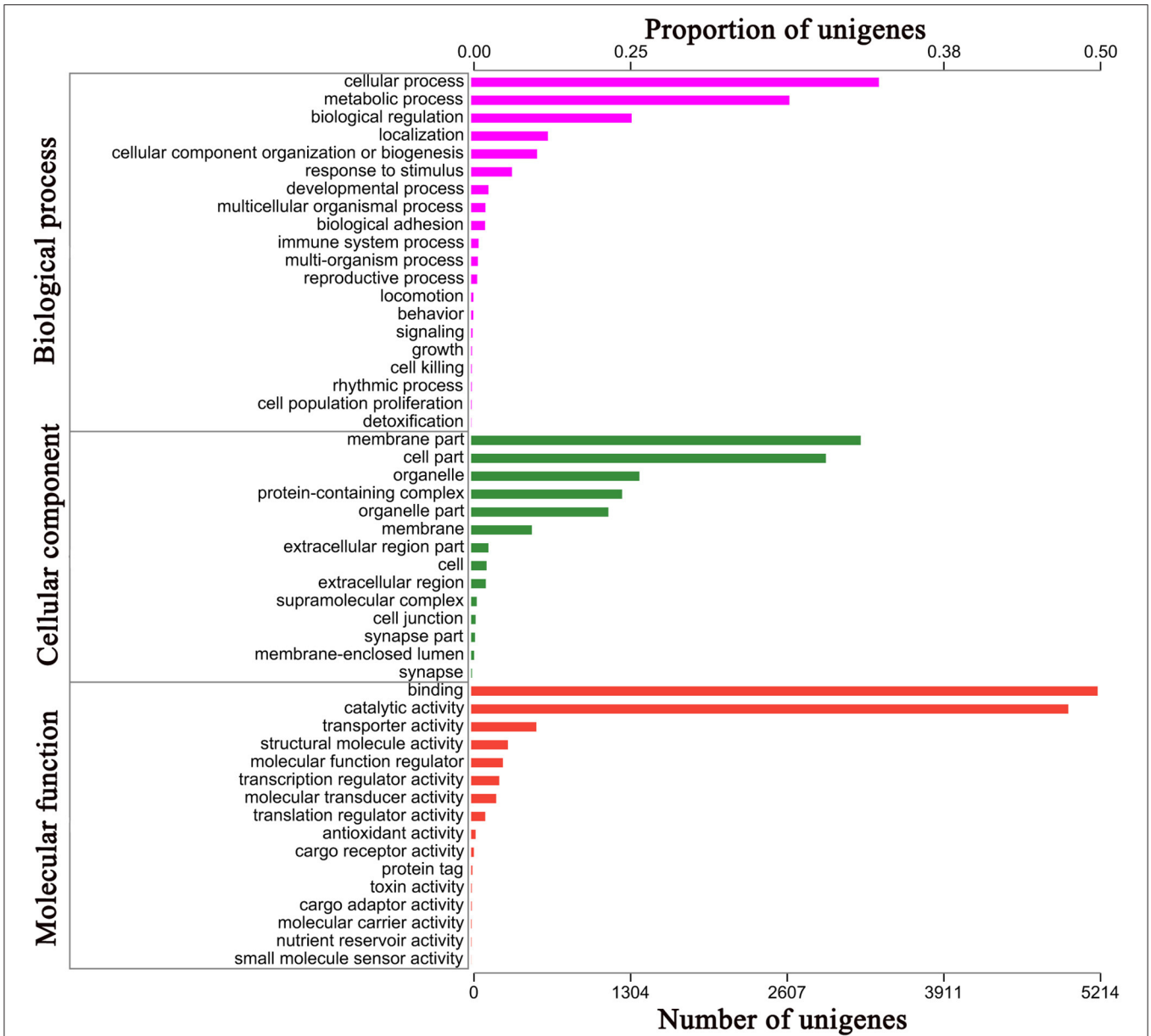

FIGURE 3 | Gene Ontology (GO) annotation results GO analysis of 10,177 genes in *E. signifier* transcriptome, according to their involvement in biological processes, cellular component and molecular function.

EsigGOBP3, EsigOBP6, EsigGOBP2, EsigGOBP7, EsigOBP1, EsigOBP3, EsigOBP4, and EsigOBP8 placed in the no-larval-expression clade. EsigCSP1 and EsigCSP2 belonged to the no-larval-expression clade in the CSP phylogenetic tree, and EsigCSP1 was not expressed in the larval head. However, EsigGOBP4, EsigGOBP5, EsigGOBP6, EsigOBP2, EsigOBP5, and EsigOBP7 were placed in the larva-specific-expression clade, and EsigOBP5 and EsigOBP7 were highly expressed in larvae compared with the other genes. The small number of proteins known to be specifically expressed in larvae may cause false positives in the larva-specific clade. EsigGOBP7 was placed in the PBP clade, suggesting that it is an *E. signifer* PBP and that PBPs expressed in larvae function as sex pheromones binding (Zielonka et al., 2016).

The expression profile of olfactory proteins in *E. signifer* larvae showed that all were expressed in at least one tissue, verifying the olfactory proteins identified in the head and tegument transcriptomes. EsigCSP6, EsigOBP5, EsigGOBP1, EsigOBP6, EsigOBP7, and EsigGR1 were highly expressed in all tissues of the fifth instar larvae, and the high expression of olfactory proteins indicates that *E. signifer* larvae require many olfactory proteins to support olfactory recognition, especially the transfer from soil to standing trees. Additionally, we observed the expression in all tissues, except the head, thorax, and abdomen

TABLE 1 | Best blastx hits for odorant-binding proteins (OBPs), chemosensory proteins (CSPs), odorant receptors (ORs), gustatory receptors (GRs), and sensory neuron membrane proteins (SNMPs) of *Endoclita signifier*.

Name	Nr description	Species	Acc. NO.	Tegument FPKM	Head FPKM	Tegument vs. Head
EsigOBP1	Odorant binding protein LOC100307012 precursor	*Bombyx mori*	NP_001159621.1	0	1.39	Down
EsigOBP2	Odorant binding protein 7	*Grapholita molesta*	AVZ44706.1	0	4.32	Down
EsigOBP3	Odorant binding protein LOC100307012 precursor	*Bombyx mori*	NP_001159621.1	0	8	Down
EsigOBP4	Odorant binding protein LOC100307012 precursor	*Bombyx mori*	NP_001159621.1	0	4.04	Down
EsigOBP5	Odorant binding protein	*Eogystia hippophaecolus*	AOG12872.1	0	2.97	Down
EsigGOBP1	General odorant-binding protein 70-like	*Amyelois transitella*	XP_013201142.1	0	2.97	Down
EsigGOBP2	General odorant-binding protein 56d-like	*Hyposmocoma kahamanoa*	XP_026319368.1	0.45	4.87	Down
EsigGOBP3	General odorant-binding protein 83a-like	*Plutella xylostella*	XP_011554700.1	1.48	0.39	Up
EsigGOBP4	General odorant-binding protein 19d-like	*Papilio xuthus*	XP_013173035.1	0	4.47	Down
EsigGOBP5	General odorant-binding protein 19d	*Eumeta japonica*	GBP31818.1	0	4.98	Down
EsigGOBP6	General odorant-binding protein 28a-like	*Hyposmocoma kahamanoa*	XP_026330999.1	0	3.07	Down
EsigOBP6	Odorant-binding protein 16	*Ectropis obliqua*	ALS03864.1	18.31	107.65	Down
EsigOBP7	Putative odorant-binding protein A10 isoform X2	*Zeugodacus cucurbitae*	XP_011177223.1	101.91	98.21	Down
EsigOBP8	Odorant binding preotein	*Conogethes punctiferalis*	APG32543.1	0.07	30.95	Down
EsigGOBP7	General odorant-binding protein 1	*Athetis dissimilis*	ALJ93806.1	0	13.48	Down
EsigCSP1	Chemosensory protein 10	*Carposina sasakii*	AYD42214.1	1.82	0.52	Up
EsigCSP2	Chemosensory protein 24	*Cnaphalocrocis medinalis*	ALT31606.1	181.82	2.78	Up
EsigCSP3	Chemosensory protein 5	*Agrotis ipsilon*	AGR39575.1	9.65	10.58	Down
EsigCSP4	Chemosensory protein CSP14	*Lobesia botrana*	AXF48711.1	3.16	9.35	Down
EsigCSP5	Chemosensory protein 5	*Empoasca onukii*	AWC68022.1	0	71.07	Down
EsigCSP6	Chemosensory protein	*Cnaphalocrocis medinalis*	AIX97837.1	10.33	218.45	Down
EsigOR1	Odorant receptor 28, partial	*Locusta migratoria*	ALD51442.1	4.17	0	Up
EsigOR2	Odorant receptor OR4	*Rhyacophila nubila*	AYN64394.1	0.98	0.94	Up
EsigGR1	Gustatory receptor	*Eogystia hippophaecolus*	AOG12970.1	17.74	76.58	Down
EsigSNMP1	Sensory neuron membrane protein 2 isoform X1	*Neodiprion lecontei*	XP_015517411.1	1.87	0.16	Up

of borers, for some proteins with olfactory functions, while some olfactory proteins with no olfactory functions, such as OcomCSP12 of *Ophraella communa*, are expressed in female ovaries, and silencing of OcomCSP12 results in significantly reduced ovipositing by females (Ma et al., 2019). Eating is the main behavior in larvae, which may explain why EsigGR1 exhibited the highest expression among all tissues, and EsigGR1 may correlate with the feeding habits of *E. signifer* larvae and reflect gustatory preferences.

The head is the center of sensation. EsigCSP3 was strongly expressed only in the head, and CSPs are known to contribute to mediating responses to plant volatility in *Mythimna separata* (Younas et al., 2018) and *Nilaparvata lugens* (Waris et al., 2020). EsigCSP3 might play key roles in the process of sensing *Eucalyptus*-derived compounds in *E. signifer* larvae. Importantly, eight genes were expressed most strongly in the head (EsigOBP2, EsigOBP8, EsigGOBP1, EsigGOBP2, EsigGOBP5, EsigCSP3, EsigCSP5, and EsigOR1), with the expression of EsigGOBP2, EsigCSP5, and EsigOR1 biased to the larval head, consistent with the observation of 50 *S. exigua* ORs expressed in larval heads (Llopis-Gimenez et al., 2020) and larvae (Liu et al., 2015). For *S. exigua* OBPs, expression levels are higher in the larval head than in the larval body (Liu et al., 2015). In the larval head, many *S. littoralis* OBPs and CSPs exhibit organ-specific transcription in caterpillar antennae and maxillary palps, suggesting the complementary involvement of these two organs in larval chemosensory detection (Poivet et al., 2013). Moreover, *H. armigera* expressed more OBPs and CSPs in the larval antennae than in the mouthparts (Chang et al., 2017). Therefore, it is necessary to examine the expression of the eight most strongly expressed olfactory genes in the antennae and mouthparts of *E. signifer* to determine their roles in smelling and tasting the odors of the host plant (Jin et al., 2015; Di et al., 2017; Waris et al., 2020).

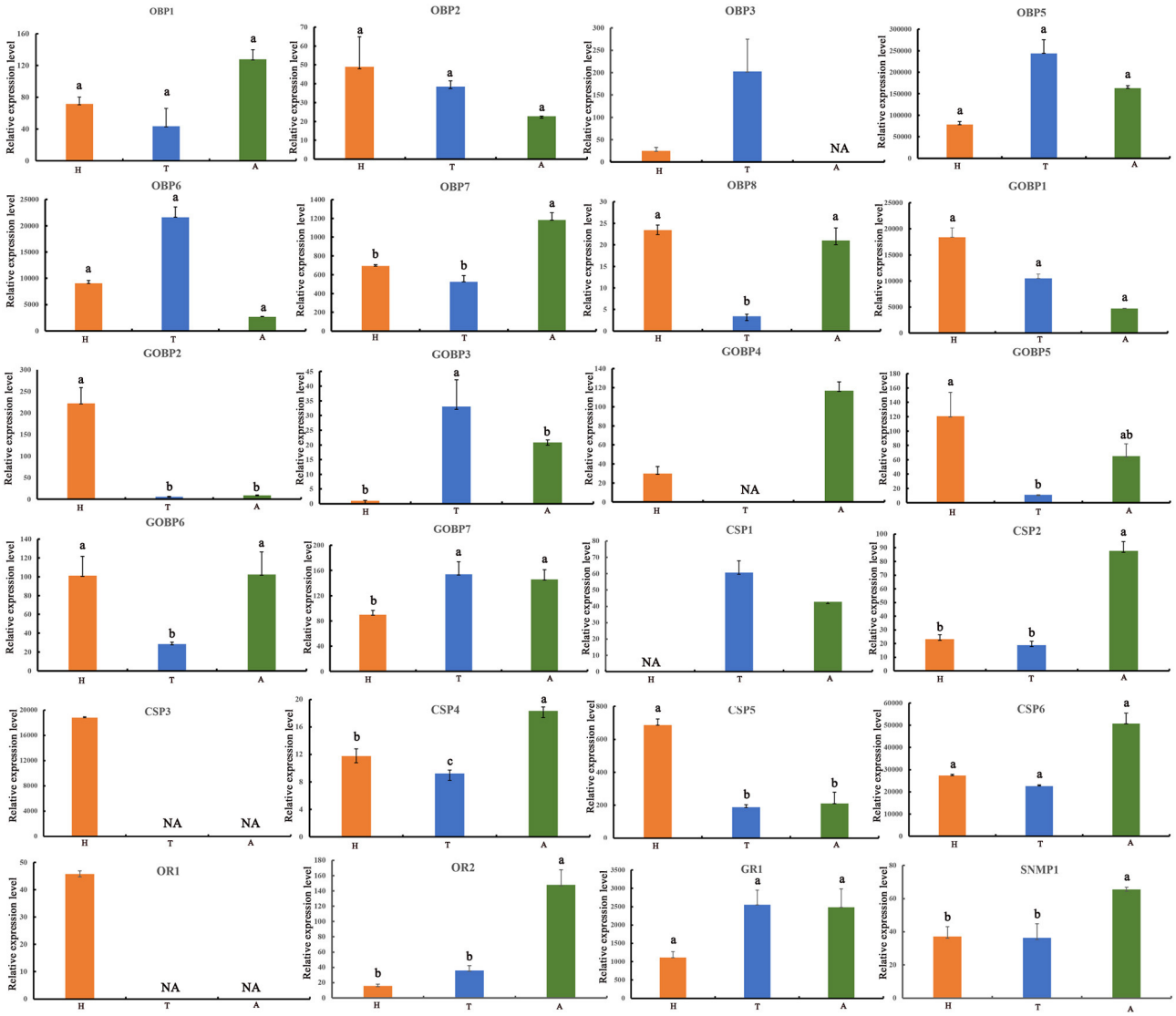

FIGURE 4 | Expression profiles of *E. signifer* olfactory proteins in three tissues. H, head; T, thoracic cuticle; A, abdominal cuticle, 18S was used as the reference gene to normalize target gene expression. The standard errors are represented by the error bars, different lowercase letters (a,b,c) above the bars denote significant differences at $p < 0.05$.

Furthermore, the expression profiles of olfactory proteins in *S. exigua* larvae indicated that they are also expressed in non-olfactory tissues, such as the larval body (Liu et al., 2015; Llopis-Gimenez et al., 2020). In *E. signifer* larvae, most olfactory proteins were highly expressed in thoracic and abdominal tegument, consistent with the large number of sensilla on the thorax and abdomen (Hu et al., 2021). This establishes the molecular basis for the head and the other main sensor tissues. Borers need to use non-olfactory tissues, such as the thorax and abdomen, to sense the wood hole environment and adapt to wood hole survival. It is necessary to explore the functions of olfactory proteins that are highly expressed in non-olfactory tissues, such as EsigGOBP3, EsigOBP7, EsigCSP2, EsigOR2, and EsigSNMP1. The patterns of olfactory protein expression during larval development have also been studied. For example, an OBP (Cmeg33593_c0) in *C. megacephala* is increasingly expressed from the first to the third instar larval stages, and the larval olfactory protein expression profile indicates that some proteins are expressed only in larvae (Wang et al., 2015). Two binding proteins appear to be larva specific in *S. littoralis* (Poivet et al., 2013) and green SexiOBPs in the OBP phylogenetic tree (Llopis-Gimenez et al., 2020), as well as six OBPs and four CSPs are larval tissue specific in *H. armigera* (Chang et al., 2017). More larval olfactory proteins are expressed in both larvae and adults of other species, as demonstrated for several *C. pomonella* ORs that exhibit sex-biased expression in adults, as well as larva-enriched transcription (Walker et al., 2016). Based on these results, the expression profile of *E. signifer* olfactory proteins should be

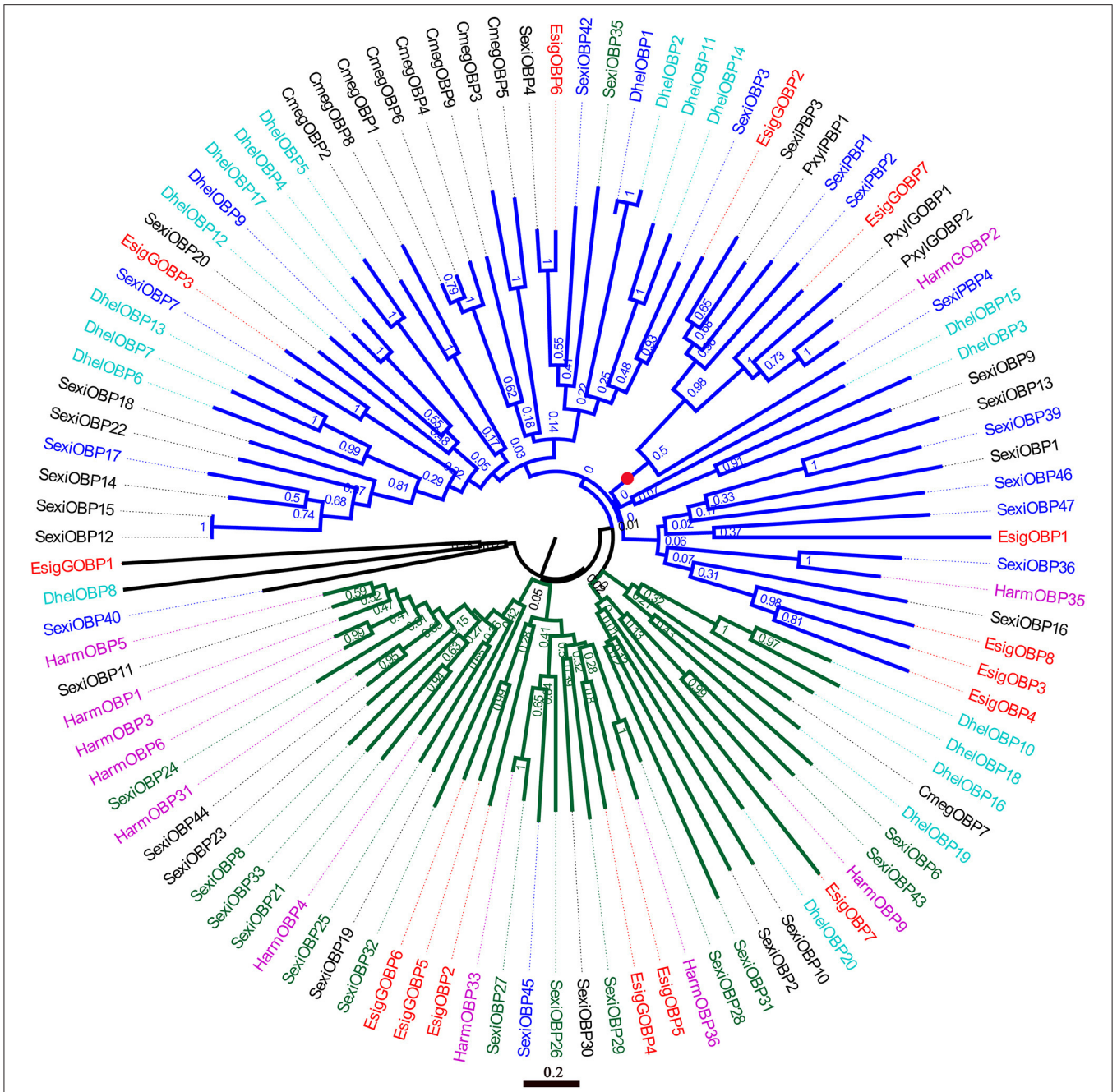

FIGURE 5 | Neighbor-joining phylogenetic tree of odorant-binding proteins (OBPs). The NJ phylogenetic analysis of OBPs of *E. signifier* (EsigOBP, red) was performed with reference OBPs of *D. helophoroides* (indigo blue), *C. megacephala* (black), *P. xylostella* (black), *S. exigua* (blue), *H. armigera* (purple). Green OBPs/GOBPs of *P. xylostella* showed only larvae expression. The stability of the nodes was assessed by bootstrap analysis with 1,000 replications. The scale bar represents 0.2 substitutions per site.

further explored in the antennae and mouthparts and at various developmental stages.

CONCLUSION

We identified 39 olfactory proteins in *E. signifer* larvae, with EsigOBP2, EsigOBP8, EsigGOBP1, EsigGOBP2, EsigGOBP5, EsigCSP3, EsigCSP5, and EsigOR1 expressed most strongly in the head. CSP3 was expressed only in the head, where it plays key roles in sensing *Eucalyptus*-derived compounds, whereas EsigGOBP2, EsigCSP5, and EsigOR1 exhibited biased expression. EsigGR1 exhibited the highest expression among all tissues, which may correlate with the feeding habits of *E. signifer* larvae based on gustatory preferences. The functions of EsigGR1 and EsigCSP3 in larval olfactory

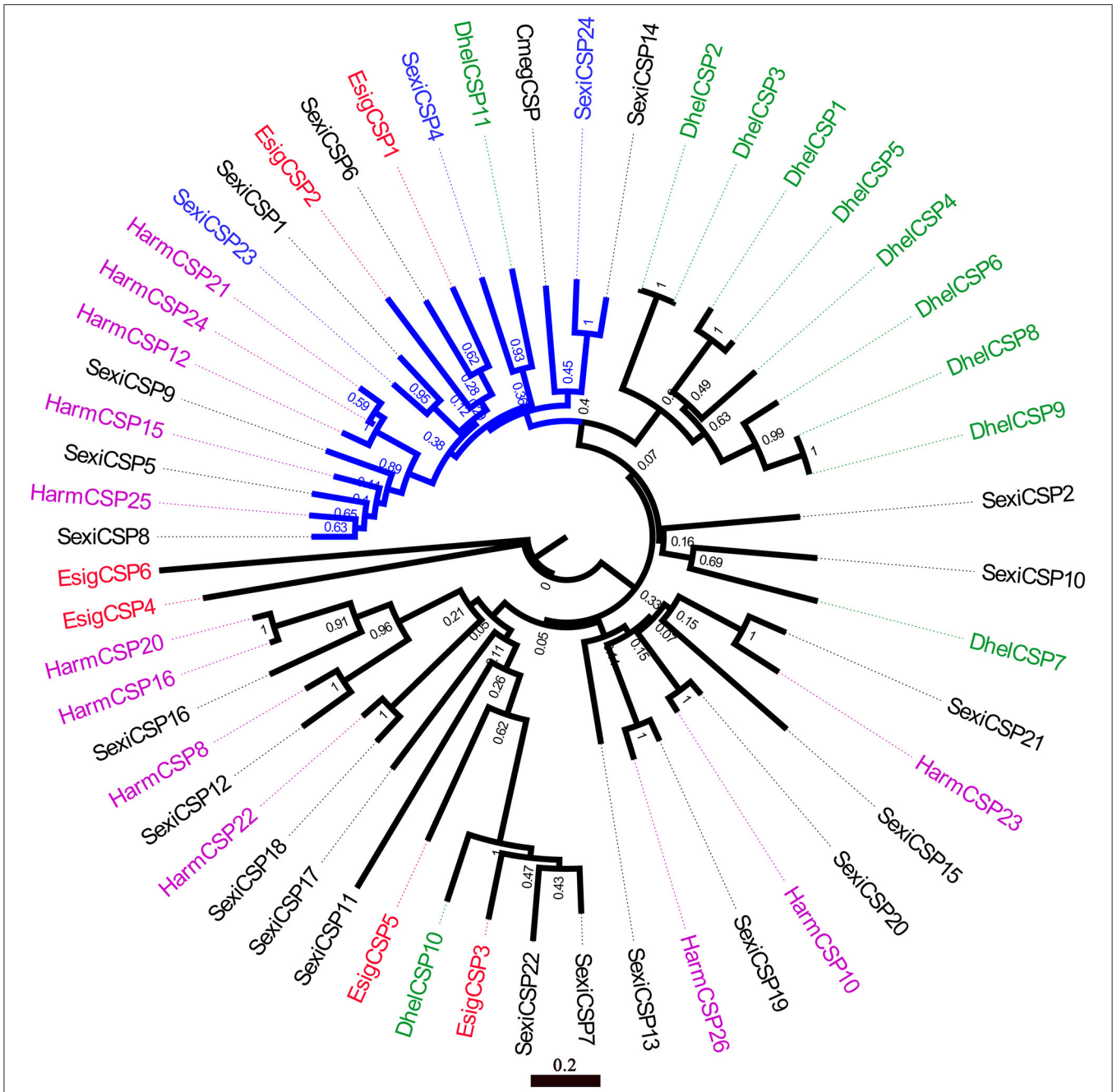

FIGURE 6 | Neighbor-joining phylogenetic tree of chemosensory proteins (CSPs). The NJ phylogenetic analysis of CSPs of *E. signifier* (EsigCSP, red) was performed with reference CSPs of *D. helophoroides* (green), *C. megacephala* (black), *S. exigua* (black), *H. armigera* (purple) and *E. signifier*. Blue CSPs of *P. xylostella* showed no larval expression. The stability of the nodes was assessed by bootstrap analysis with 1,000 replications, and only bootstrap values ≥0.6 are shown at the corresponding nodes. The scale bar represents 0.2 substitutions per site.

and gustatory recognition should be explored further. Most olfactory proteins were highly expressed in thoracic and abdominal teguments, establishing the molecular basis for the head as the center of sensation and explaining how borers use the thorax and abdomen to sense the wood hole environment.

DATA AVAILABILITY STATEMENT

The datasets presented in this study can be found in online repositories. The names of the repository/repositories and accession number(s) can be found below: https://www.ncbi.nlm.nih.gov/, PRJNA713545.

AUTHOR CONTRIBUTIONS

XYZ carried out the molecular genetic studies, performed the sequence alignment, experiments and drafted the manuscript. XHY, HXM, and XML collected all samples and participated in some experiments. PH and ZDY designed and conceived of the study. PH also helped to draft the manuscript. All authors read and approved the final manuscript.

FUNDING

This work was supported by the National Natural Science Foundation of China (Grant No. 32001321), the Guangxi Natural Science Foundationunder (Grant No. 2020JJA130068), the Special Fund for Science and Technology Bases and Talents of Guangxi Zhuang Autonomous Region (Grant No. 2020AC19057).

ACKNOWLEDGMENTS

We thank Yao Shan and Changxiong Wu for insect collection.

SUPPLEMENTARY MATERIAL

The Supplementary Material for this article can be found online at: https://www.frontiersin.org/articles/10.3389/fphys.2021.682537/full#supplementary-material

REFERENCES

Annina, H., Melanie, E., Nazli, G., Collins, K. a. N., Kathrin, B. P., Lyubov, P., et al. (2017). Anatomy and behavioral function of serotonin receptors in *Drosophila melanogaster* larvae. *PLoS ONE* 12:e0181865. doi: 10.1371/journal.pone.0181865

Bose, C., Basu, S., Das, N., and Khurana, S. (2015). Chemosensory apparatus of *Drosophila* larvae. *Bioinformation* 11, 185–188. doi: 10.6026/97320630011185

Carvalho, W. J., Fujimura, P. T., Bonetti, A. M., Goulart, L. R., Cloonan, K., Da Silva, N. M., et al. (2017). Characterization of antennal sensilla, larvae morphology and olfactory genes of *Melipona scutellaris* stingless bee. *PLoS ONE* 12:e0174857. doi: 10.1371/journal.pone.0174857

Chang, H., Ai, D., Zhang, J., Dong, S., Liu, Y., and Wang, G. (2017). Candidate odorant binding proteins and chemosensory proteins in the larval chemosensory tissues of two closely related noctuidae moths, *Helicoverpa armigera* and *H. assulta*. *PLoS ONE* 12:e0179243. doi: 10.1371/journal.pone.0179243

Chen, X., and Hu, P. (in press). Reference gene for tissue and instar of Endoclita signifier larvae. *Chin. J. Appl. Entomol.* 1–7. doi: 10.19688/j.cnki.issn1671-0886.20210008

Di, C., Ning, C., Huang, L. Q., and Wang, C. Z. (2017). Design of larval chemical attractants based on odorant response spectra of odorant receptors in the cotton bollworm. *Insect. Biochem. Molec.* 84, 48–62. doi: 10.1016/j.ibmb.2017.03.007

Hu, P., Yang, X. H., and Yang, Z. D. (2021). Morphology and distribution of sensillum in antennae, thoracic and abdominal tegument of Endoclita signifier larva. *J. Beijing Forestry Univ.* in press.

Jin, R., Liu, N.-Y., Liu, Y., and Dong, S.-L. (2015). A larval specific OBP able to bind the major female sex pheromone component in *Spodoptera exigua* (Hübner). *J. Integ. Agr.* 14, 1356–1366. doi: 10.1016/S2095-3119(14)60849-2

Jing, D., Zhang, T., Bai, S., He, K., Prabu, S., Luan, J., et al. (2020). Sexual-biased gene expression of olfactory-related genes in the antennae of *Conogethes pinicolalis* (Lepidoptera: Crambidae). *BMC Genomics* 21:244. doi: 10.1186/s12864-020-6648-3

Li, B., and Dewey, C. N. (2011). RSEM: accurate transcript quantification from RNA-Seq data with or without a reference genome. *BMC Bioinformatics* 12, 93–99. doi: 10.1186/1471-2105-12-323

Li, X., Dong, G., Fang, J., Liu, H., Guo, W., and Yin, H. (2020). Identification of putative olfactory genes in newly hatched larvae of a Coleopteran ectoparasitoid *Dastarcus helophoroides* (Fairmaire) (Coleoptera: Bothrideridae) by transcriptome analysis. *Entomol Res* 50, 329–342. doi: 10.1111/1748-5967.12436

Liu, N. Y., Zhang, T., Ye, Z. F., Li, F., and Dong, S. L. (2015). Identification and characterization of candidate chemosensory gene families from *Spodoptera exigua* developmental transcriptomes. *Int. J. Biol. Sci.* 11, 1036–1048. doi: 10.7150/ijbs.12020

Livak, K. J., and Schmittgen, T. D. (2001). Analysis of relative gene expression data using real-time quantitative PCR and the $2^{-\Delta\Delta CT}$ method. *Methods* 25, 402–408. doi: 10.1006/meth.2001.1262

Llopis-Gimenez, A., Carrasco-Oltra, T., Jacquin-Joly, E., Herrero, S., and Crava, C. M. (2020). Coupling transcriptomics and behaviour to unveil the olfactory system of *Spodoptera exigua* larvae. *J. Chem. Ecol.* 46, 1017–1031. doi: 10.1007/s10886-020-01224-z

Ma, C., Cui, S., Tian, Z., Zhang, Y., Chen, G., Gao, X., et al. (2019). *OcomCSP12*, a chemosensory protein expressed specifically by ovary, mediates reproduction in *Ophraella communa* (Coleoptera: Chrysomelidae). *Front. Physiol.* 10:1290. doi: 10.3389/fphys.2019.01290

Mortazavi, A., Williams, B. A., Mccue, K., Schaeffer, L., and Wold, B. (2008). Mapping and quantifying mammalian transcriptomes by RNA-Seq. *Nat. Methods* 5, 621–628. doi: 10.1038/nmeth.1226

Poivet, E., Gallot, A., Montagne, N., Glaser, N., Legeai, F., and Jacquin-Joly, E. (2013). A comparison of the olfactory gene repertoires of adults and larvae in the noctuid moth *Spodoptera littoralis*. *PLoS ONE* 8:e60263. doi: 10.1371/journal.pone.0060263

Rahn, T., Leippe, M., Roeder, T., and Fedders, H. (2013). EGFR signaling in the brain is necessary for olfactory learning in *Drosophila* larvae. *Learn Mem.* 20:194–200. doi: 10.1101/lm.029934.112

Saitou, N., and Nei, M. (1987). The neighbor-joining method: a new method for reconstructing phylogenetic trees. *Mol Biol Evol* 4, 406–425.

Tamura, K., Peterson, D., Peterson, N., Stecher, G., Nei, M., and Kumar, S. (2011). MEGA5: molecular evolutionary genetics analysis using maximum likelihood, evolutionary distance, and maximum parsimony methods. *Mol. Biol. Evol.* 28, 2731–2739. doi: 10.1093/molbev/msr121

Walker, W. B. 3rd, Gonzalez, F., Garczynski, S. F., and Witzgall, P. (2016). The chemosensory receptors of codling moth *Cydia pomonella* expression in larvae and adults. *Sci. Rep.* 6:23518. doi: 10.1038/srep23518

Wang, X., Xiong, M., Lei, C., and Zhu, F. (2015). The developmental transcriptome of the synanthropic fly *Chrysomya megacephala* and insights into olfactory proteins. *BMC Genomics* 16:20. doi: 10.1186/s12864-014-1200-y

Waris, M. I., Younas, A., Ameen, A., Rasool, F., and Wang, M. Q. (2020). Expression profiles and biochemical analysis of chemosensory protein 3 from *Nilaparvata lugens* (Hemiptera: Delphacidae). *J. Chem. Ecol.* 46, 363–377. doi: 10.1007/s10886-020-01166-6

Yang, X., Luo, Y., Wu, Y., Zou, D., Hu, P., and Wang, J. (2021). Distribution and damage of endoclita signifer walker, as an important wood borer pest insect on forest. *Forest Pest Dis* 1–7.

Yang, X., Yang, X., Xue, D., and Han, H. (2016). The complete mitochondrial genome of *Endoclita signifer* (Lepidoptera, Hepialidae). *Mitochondrial DNA A DNA Mapp. Seq. Anal.* 27, 4620–4621. doi: 10.3109/19401736.2015.1101585

Yang, X. H. (2013). *Studies on the Biological and Ecological Characteristics of Endoclita signifier*. Beijing: Beijing Forestry University.

Yang, X. H. (2017). *Biological Ecology and Control Techniques of Endoclita signifier, an Important Pest of Eucalyptus*. Beijing: China Forestry Publishing House

Yi, X., Shi, S., Wang, P., Chen, Y., Lu, Q., Wang, T., et al. (2019). Characterizing potential repelling volatiles for "push-pull" strategy against stem borer: a case study in *Chilo auricilius*. *BMC Genomics* 20:751. doi: 10.1186/s12864-019-6112-4

Younas, A., Waris, M. I., Tahir ul Qamar, M., Shaaban, M., Prager, S. M., and Wang, M. Q. (2018). Functional analysis of the chemosensory protein MsepCSP8 from the oriental armyworm *Mythimna separata*. *Front. Physiol.* 9:872. doi: 10.3389/fphys.2018.00872

Zhou, J.-J. (2010). Chapter ten-odorant-binding proteins in insects. *Vitam Horm.* 83, 241–272. doi: 10.1016/S0083-6729(10)83010-9

Zhu, J., Ban, L., Song, L. M., Liu, Y., Pelosi, P., and Wang, G. (2016). General odorant-binding proteins and sex pheromone guide larvae of *Plutella xylostella* to better food. *Insect. Biochem. Mol. Biol.* 72, 10–19. doi: 10.1016/j.ibmb.2016.03.005

Zielonka, M., Gehrke, P., Badeke, E., Sachse, S., Breer, H., and Krieger, J. (2016). Larval sensilla of the moth *Heliothis virescens* respond to sex pheromone components. *Insect. Mol. Biol.* 25, 666–678. doi: 10.1111/imb.12253

Conflict of Interest: The authors declare that the research was conducted in the absence of any commercial or financial relationships that could be construed as a potential conflict of interest.

frontiers in Physiology

ORIGINAL RESEARCH
published: 28 July 2021
doi: 10.3389/fphys.2021.702973

A Detailed Spatial Expression Analysis of Wing Phenotypes Reveals Novel Patterns of Odorant Binding Proteins in the Soybean Aphid, *Aphis glycines*

Ling Wang[1†], Hang Yin[2†], Zhiguo Zhu[3], Shuai Yang[1] and Jia Fan[2*]*

[1] College of Agronomy and Biotechnology, Hebei Normal University of Science and Technology, Qinhuangdao, China, [2] State Key Laboratory for Biology of Plant Diseases and Insect Pests, Institute of Plant Protection, Chinese Academy of Agricultural Sciences, Beijing, China, [3] Wuhu Institute of Technology, Wuhu, China

OPEN ACCESS

Edited by:
Peng He,
Guizhou University, China

Reviewed by:
Feng Shang,
Southwest University, China
Fengqi Li,
Beijing Academy of Agriculture and Forestry Sciences, China
Dingze Mang,
Tokyo University of Agriculture and Technology, Japan
Herbert Venthur,
University of La Frontera, Chile

***Correspondence:**
Shuai Yang
yangshuai20000@163.com
Jia Fan
jfan@ippcaas.cn

[†] These authors have contributed equally to this work

Specialty section:
This article was submitted to Invertebrate Physiology, a section of the journal Frontiers in Physiology

Received: *30 April 2021*
Accepted: *16 June 2021*
Published: *28 July 2021*

Citation:
Wang L, Yin H, Zhu Z, Yang S and Fan J (2021) A Detailed Spatial Expression Analysis of Wing Phenotypes Reveals Novel Patterns of Odorant Binding Proteins in the Soybean Aphid, Aphis glycines. Front. Physiol. 12:702973. doi: 10.3389/fphys.2021.702973

The wide range of insect niches has led to a rapid expansion of chemosensory gene families as well as their relatively independent evolution and a high variation. Previous studies have revealed some functions for odorant-binding proteins (OBPs) in processes beyond olfaction, such as gustation and reproduction. In this study, a comparative transcriptomic analysis strategy was applied for the soybean aphid, *Aphis glycines*, focusing on various functional tissues and organs of winged aphids, including the antenna, head, leg, wing, thorax, cauda, and cornicle. Detailed spatial OBP expression patterns in winged and wingless parthenogenetic aphids were detected by RT-qPCR. Twelve OBPs were identified, and three new *OBP*s in *A. glycines* are first reported. All *OBP*s showed comparatively higher expression in sensory organs and tissues, such as the antenna, head, or leg. Additionally, we found some novel expression patterns for aphid OBPs (Beckendorf et al., 2008). Five OBPs exhibited high-expression levels in the cauda and four in the cornicle (Biasio et al., 2015). Three genes (*OBP2/3/15*) were highly expressed in the wing (Calvello et al., 2003). Two (*OBP3/15*) were significantly more highly expressed in the wingless thorax than in the winged thorax with the wings removed, and these transcripts were significantly enriched in the removed wings. More details regarding OBP spatial expression were revealed under our strategy. These findings supported the existence of carrier transport functions other than for foreign chemicals and therefore broader ligand ranges of aphid OBPs. It is important for understanding how insect OBPs function in chemical perception as well as their other potential physiological functions.

Keywords: odorant binding protein, wing phenotype, *Aphis glycines*, expression pattern analysis, cauda, cornicle, antenna, wing

INTRODUCTION

The olfactory system plays an important role in directing insect behaviors, such as foraging, mating, oviposition, and predation. Similar to other insects, aphids, especially those with a migratory phenotype (winged morph), rely heavily on chemical signals, including plant volatiles and species-specific pheromones, to locate hosts, find mates, and avoid natural enemies (Pickett, 2009). In general, odorant-binding proteins (OBPs) are involved in the first step of olfactory recognition

(e.g., Pelosi et al., 2018). They bind and transport external odors through the hemolymph to activate corresponding olfactory receptors, which are responsible for transmitting environmental chemicals into electrophysiological signals. As one of the most important groups of chemo-reception proteins in insects, OBPs have been studied since 1981 (Vogt and Riddiford, 1981). Regarding aphids, OBPs have been widely reported for *Acyrthosiphon pisum* (Ji et al., 2016) genes encoding complete OBPs with a signal peptide, Zhou et al., 2010), *Myzus persicae* (Ji et al., 2016), *Megoura viciae* (Iovinella et al., 2011; Daniele et al., 2018), *Sitobion avenae* (Kim et al., 2013; Xue et al., 2016), *Aphis gossypii* (Grabherr et al., 2011; Gu et al., 2013), and *Aphis glycines* (Grabherr et al., 2011; Wang et al., 2019). Consistent with the simple facultative parasitic lifestyle of aphids, the aphid OBP family has few members, and they are generally more highly conserved than in other insects. The spatial expression profiles of these proteins have also been broadly investigated. OBP expression is not limited to the chemosensory system (e.g., Xue et al., 2016; Gao et al., 2018; Wang et al., 2019), but also occurs in non-sensory tissues and organs, such as the wings (Calvello et al., 2003; Pelosi et al., 2005; Wang et al., 2020), reproductive organs (Li et al., 2008; Sun Y. F. et al., 2012), mandibular glands (Iovinella et al., 2011), and salivary glands (Zhang et al., 2017).

The soybean aphid, *A. glycines*, is an important phytophagous pest that feeds on plants by sucking sap from leaves, stems, and pods, significantly reducing soybean yield and quality (Wang et al., 1996; Beckendorf et al., 2008; Wu et al., 2009). Moreover, in soybean plants heavily infested with aphids, sugary excretions ("honeydew") produced by aphids indirectly damage plants by reducing photosynthesis (Sun et al., 2015). Plant viruses can be transmitted during aphid infestations (Clark and Perry, 2002). Accordingly, *A. glycines* is now used as a model for studying the evolution of biotypic virulence (Wenger et al., 2017). In a recent study, we attempted to identify the OBP family of soybean aphids based on a homologous cloning strategy (Wang et al., 2019). In this study, a more detailed comparative transcriptomic analysis strategy focusing on various functional tissues and organs of winged aphids, including the antenna, head, leg, wing, thorax, cauda, and cornicle, was successfully applied to *A. glycines*. In addition to identifying more OBPs, detailed spatial expression patterns of both winged and wingless parthenogenetic aphids were analyzed by RT-qPCR and the findings were discussed.

MATERIALS AND METHODS

Insects and Sampling

Aphis glycines was reared from parthenogenetic aphids initially collected on soybean plants at the Minzhu Experimental Station, Heilongjiang Academy of Agricultural Sciences, China, and cultured in an air-conditioned insectary [24 ± 1°C, 75 ± 5% relative humidity (RH), 16-h light:8-h dark photoperiod]. Newborn aphids (0–12 h) were transferred to new plants for synchronization of developmental stages. The insects were reared for 7 days at different densities (20 aphids/plant and 100 aphis/plant) and winged and wingless aphids were separately collected in the last developmental stage (adult). For transcriptome sequencing, antenna (500), head (200), wing (500), leg (500), thorax (200), cornicle (200), and cauda (500) specimens of winged aphids were carefully dissected under the microscope. For RT-qPCR analysis, the same tissues or organs of adult wingless and winged morphs were collected. Each experiment was carried out in biological triplicate. Samples were flash-frozen in liquid nitrogen and stored at −80°C until RNA extraction.

Total RNA Extraction and Illumina HiSeq 4000 Sequencing

Total RNA was isolated from the above samples using TRIzol (Invitrogen, Carlsbad, CA, United States), and DNA fragments were removed with RNase-free DNase I (Takara, Shiga, Japan). An Agilent 2100 Bioanalyzer (Agilent Technologies, Carlsbad, CA, United States) was used to determine the concentrations, integrity, and 28S/18S values of the RNA samples, and a NanoDrop 2000 spectrophotometer (NanoDrop products, Wilmington, DE, United States) was used to access purity. mRNA was then enriched using oligo (dT) beads (Agilent Technologies) and fragmented using fragmentation buffer (Agilent Technologies) and then used for the synthesis of first-strand cDNA. After purification and the repair of cohesive ends, the DNA samples were ligated to adapters, and fragment selection and PCR amplification were conducted. The final quality assessment was performed using an Agilent 2100 Bioanalyzer (Agilent Technologies). Three DNA libraries were examined using the Illumina HiSeq 4000 sequencing platform.

Fragmentation involved the use of divalent cations under elevated temperature in NEBNext and first-strand synthesis reaction buffer (5×). Single-stranded (ss) cDNA was synthesized using a random hexamer primer, M-MuLV reverse transcriptase, DNA polymerase I, and RNase H (NEB, United States). After the adenylation of the 3′ ends of the fragments, NEBNext adaptors with a hairpin loop structure were ligated for hybridization. The library fragments were purified using the AMPure XP system (Beckman Coulter, United States), selecting cDNA fragments 150–200 bp long. Then, 3 mL of USER enzyme (NEB, United States) was applied to the size-selected, adaptor-ligated cDNA, and the reaction was incubated at 37°C for 15 min, followed by 5 min at 95°C before PCR. PCR was then performed using Phusion high-fidelity DNA polymerase, universal PCR primers, and an index (X) primer. The products were purified (AMPure XP system), and library quality was assessed using an Agilent Bioanalyzer 2100 system (Agilent Technologies, United States). Clustering of the index-coded samples was performed with a cBot cluster generation system using TruSeq PE Cluster Kit v3-cBot-HS (Illumina, China) according to the manufacturer's instructions. The library preparations were sequenced on the Illumina HiSeq 4000 platform, and paired-end reads (PE125 sequencing strategy) were generated after cluster generation.

RNA-Seq Data Generation and *de novo* Transcriptome Assembly

After sequencing, the raw reads were processed by NGS-QC to remove low-quality sequences (≥ 15% bases with Q ≤ 19),

excess adaptors (≥ 5 bp adaptor bases in reads), and reads with a high content of unknown bases (≥ 5%; CASAVA FASTQ files). The clean reads were then assembled into unigenes using Trinity r20140413p1 with min_kmer_cov:2 and the other parameters set to the default values (Langmead and Salzberg, 2012). Gene expression levels in each sample were estimated by RSEM (Li and Dewey, 2011): (I) Clean data were mapped to the transcript sequence, and (II) the read count for each gene and isoform was obtained from the mapping results. The fragments per kilo base per million (FPKM)-mapped reads value of each gene was calculated based on gene length and the mapped read number using HTSeq v0.5.4p3 and Cufflinks v2.2.1 (Mortazavi et al., 2008).

Differentially Expressed Genes and Annotation of OBP-Encoding Transcripts

Reads for the *A. glycines* transcriptomes from seven different tissues (antennae, head, wing, leg, thorax, cornicle, and cauda), with three replications for each tissue, were produced based on next-generation sequencing (NGS) results. Expression analysis was performed using TopHat and Cufflinks (Trapnell et al., 2012; Kim et al., 2013). Differential expression analyses comparing each tissue to the antenna were separately performed using the DESeq R package (version 1.10.1), which provides statistical routines for determining differential expression using a model based on the negative binomial distribution. To control the false discovery rate, the resulting *p*-values were adjusted using Benjamini and Hochberg's approach. Genes with a fold change (FC) > 2 and an adjusted *p*-value < 0.05 according to DESeq analysis were considered DEGs. The log2 (fold change) values and *p* values are shown in a volcano plot.

We used the BLASTx program of the National Center for Biotechnology Information (NCBI,[1]) to predict genes-encoding OBPs.

The basis of the annotation was a hand-curated database of OBPs containing known aphid candidate OBP sequences. The assembled sequences were compared with the reference dataset using BLASTx. All sequences that generated a hit were further analyzed by a motif search program based on a 5–6 conserved OBP cysteine pattern consisting of C1-X_{15-39}-C_2-X_3-C_3-X_{21-44}- C_4-X_{7-12}-C_5-X_8-C_6 for OBPs (Zhou et al., 2008).

Functional Annotation Enrichment Analysis

According to the DEG results, Venn diagrams of the differentially expressed olfaction genes in group 1 (antennae/head), group 2 (antennae/leg), group 3 (antennae/wing), group 4 (antennae/thorax), group 5 (antennae/cornicle), and group 6 (antennae/cauda) were constructed using "Venn Diagram"[2]. The mean FPKM values for each gene in the different tissues (antenna, head, leg, wing, thorax, cornicle, and cauda) were then log-transformed ["log2 (FPKM + 1)"] and subjected to hierarchical clustering using the minimum spanning tree; a heatmap was generated using Heml1.0 (Deng et al., 2014). Antenna-specific genes were defined as DEGs identified in tissues other than antennae with FPKM ≤ 0.3 (e.g., Sánchez-Sevilla et al., 2017; Tao et al., 2017).

Real-Time Quantitative PCR

Real-time quantitative PCR (RT-qPCR) experiments were carried out using a 7,500 Fast Real-Time PCR System (Applied Biosystems- Life Technologies, Carlsbad, CA, United States) and the cDNA samples prepared from winged and wingless aphid antennae, heads, legs, cornicles, caudae, and wings (only for winged morphs). Two reference genes, 18S *rRNA* and GAPDH dehydrogenase, were used for normalizing target gene expression and correction for sample-to-sample variation (Wang et al., 2019). Specific primers were designed for each *A. glycines* OBP gene and for the two reference genes using Primer Premier v5.0 software; the primer information is listed in **Supplementary Data 1**. PCR amplification was conducted in a volume of 20 μL containing 10 μL of 2 × SYBR Mix, 1 μL of diluted cDNA template, 7.8 μL of PCR-grade water, and 0.6 μL of each primer at 10 μM. The PCR conditions were as follows: 95°C for 30 s, 40 cycles of 95°C for 15 s, 60°C for 30 s, and 72°C for 45 s. The OBP expression status was calculated using the $2^{-\Delta\Delta Ct}$ comparative CT method (Livak and Schmittgen, 2001), and a CT value greater than 35 was considered no expression. The fold changes of *OBP*s in the tissues of both winged and wingless morphs are reported relative to the antennal transcript levels of *OBP3* in the wingless morph (wingless antennal *OBP3*). Means and standard deviations were calculated using data from experiments performed in triplicate, and the results were presented as *n*-fold differences in expression. Differences in transcriptional characteristics among various *OBP*s in different tissues were analyzed using SPSS 16.0. Statistical significance was determined using one-way ANOVA and *post hoc* Duncan multiple range tests. Significance was established at $p < 0.05$. External reference genes were randomly chosen from among *OBP*s to first perform a preliminary assessment, after which, we defined those with broader expression profiles, such as wingless *OBP2* and *OBP3*, as candidate external genes. Wingless *OBP*3 was ultimately chosen as the external gene.

RESULTS

Overview of Transcriptomes

To identify and differentiate *OBP*s transcripts among antennae, heads, legs, wings, thoraxes, cornicles, and caudae, 18 mRNA samples from the 7 different tissues (each analyzed in triplicate) were subjected to 2 × 125 paired-end sequencing using the HiSeq 4000 platform, yielding 167,359,594 bases. A total of 154,717 distinct transcripts (mean length = 1,082 bp) and 110,897 unigenes (mean length = 629 bp) were assembled (**Supplementary Data 2**).

Gene expression analysis showed the following numbers of DEGs with a log2-fold change ≥ 2 (p_{adj} value ≤ 0.05) in each paired comparison group. Compared with the antenna, the thorax showed the 14,430 significantly differentially

[1] http://blast.ncbi.nlm.nih.gov/Blast.cgi

[2] http://bioinformatics.psb.ugent.be/webtools/Venn/

expressed genes (antenna/thorax, 2,565 upregulated and 11,865 downregulated). The antenna/leg value was 14,979 (5,781 upregulated and 9,198 downregulated), the antenna/head value 13,040 (2,757 upregulated and 10,283 downregulated), the antenna/cauda value 12,549 (3,797 upregulated and 8,752 downregulated), the antenna/cornicle value 11,537 (3,801 upregulated and 11,456 downregulated), and antenna/wing value 12,719 (1,267 upregulated and 10,912 downregulated) (**Figure 1** and **Supplementary Data 3**).

Differential Expression Analysis

First, antenna-specific genes were compared among different groups and further analyzed using Venn diagrams. Although genes were found to exhibit antenna specific expression, there were no *OBP*s (**Figure 2A**; gene lists see **Supplementary Data 3**). Next, genes specifically expressed in each tissue were screened by the same strategy, and the numbers showing specific expression in the heads, legs, wings, thoraxes, caudae, and cornicles were 226, 2,005, 580, 1,735, 1,667, and 1,741, respectively, also with no *OBP*s included (**Figure 2B**, see **Supplementary Data 3** for gene lists).

OBP Prediction and Functional Enrichment

Odorant-binding proteins genes were predicted by homology comparison, the relative expression levels (FPKM) of target genes in different tissues were visualized by a heat map, and the tissue or organ specificity of expression was preliminarily analyzed.

Similar to peach aphids (Ji et al., 2016), *OBP1* was neither predicted nor identified in *A. glycines*. Twelve OBPs

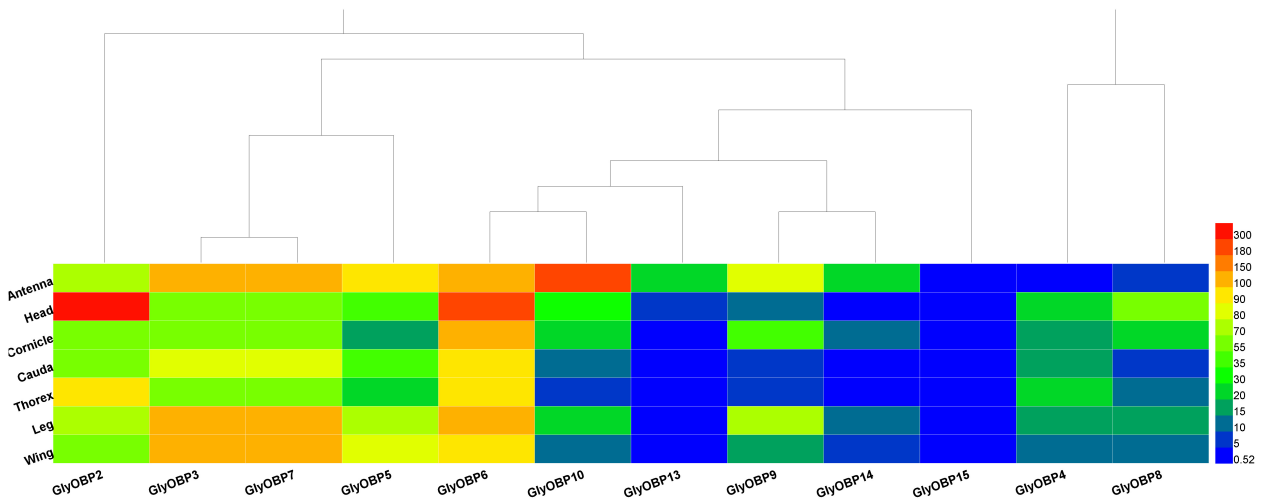

FIGURE 1 | Volcano plots for differentially expressed genes between antennae and each of the other six tissues (heads, legs, caudae, cornicles, thoraxes, and wings).

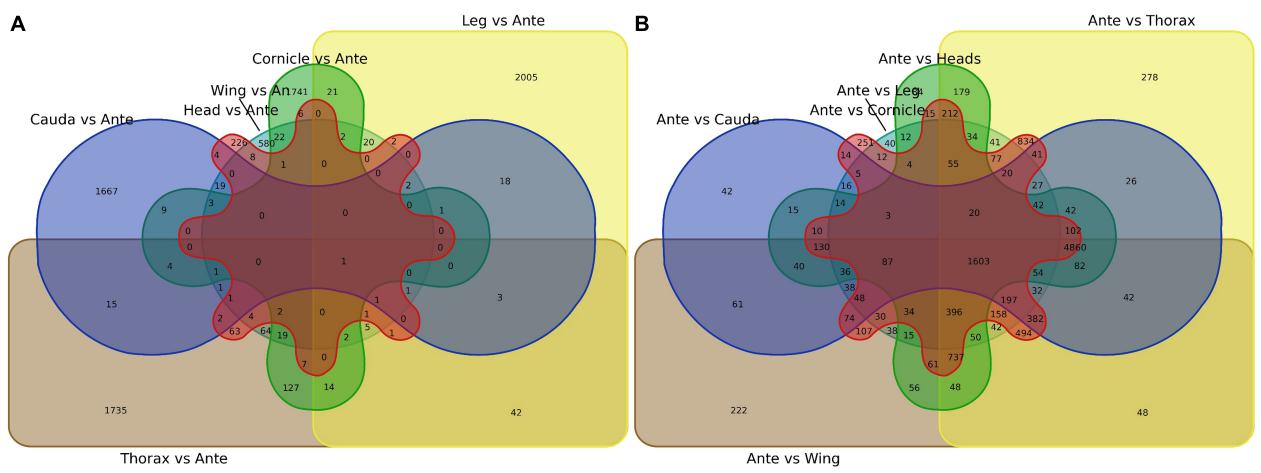

FIGURE 2 | Venn diagram of specially expressed transcripts between antennae and six other tissues (heads, legs, caudae, cornicles, thoraxes, and wings). **(A)** Specially expressed transcript numbers for six tissues compared with antennae. **(B)** Specially expressed transcript numbers for antennae compared with each of the other six tissues. An or Ante, Antenna.

were identified (GenBank accession numbers MW924836-MW924846, and MW930727) using the NCBI BLASTX program and named according to their ortholog names in other aphids, including three newly reported *OBP*s: *OBP13*, *OBP14*, and *OBP15*. The *OBP*s included in the heatmap and the sequences of these genes are listed in **Supplementary Data 4**; their FKPM values are provided in **Supplementary Data 5**. The heat map in **Figure 3** illustrates that most of the *OBP*s, such as *OBP2*-OBP10, *OBP13*, and *OBP14*, were found to mainly be expressed in sensory organs and tissues (i.e., antennae, heads and legs) but that OBP15 showed relatively low expression in all specimen types. Our results showed that *OBP*s are also expressed in organs such as caudae and cornicles, which are not chemical sensory organs. As *OBP3* and *OBP7* were assembled into one transcript (DN1170_c0_g1_i8, **Supplementary Data 4**) following the TRINITY instructions (Grabherr et al., 2011), their gene expression values were ultimately quantified as equal and then were corrected by RT-qPCR.

Detailed Spatial Expression Analysis Between Morphs by RT-qPCR

To investigate tissue expression specificity and further verify any phenotypic correlations, the spatial expression profiles of OBPs in both winged and wingless aphids were detected by RT-qPCR.

According to this analysis (**Figure 4**), 12 *OBP*s are highly expressed in sensory organs such as the antenna, head, and leg. Among these *OBP*s, six *OBP*s (OBP2/6/7/9/10/14) showed the highest transcript levels in antennae (**Figure 4A**, $p < 0.05$, $N = 3$). Moreover, *OBP4/8/13* exhibited comparatively higher expression in antennae than in other tissues (**Figures 5C,G,J**, $p < 0.05$, $N = 3$), although the levels were relatively low. In summary, nine *OBP*s (*OBP2/4/6/7/8/9/10/13/14*) were more highly expressed in antennae than in other tissues. Furthermore, seven (*OBP2/6/7/8/10/13/14*) of the nine OBPs mentioned above were significantly more highly expressed in the antennae of winged aphids than in wingless aphids; in contrast, *OBP4* showed wingless antenna-specific expression, and *OBP9* was highly expressed, but without a difference between winged and wingless antennae (**Figure 5**, $p < 0.05$, $N = 3$).

In addition to its remarkably higher expression in winged antennae, *OBP2* was found to be systemically expressed in all tissues of both morphs, including the antenna, head, leg, wing, thorax, cornicle, and cauda (**Figure 5A**). *OBP3* was also systemically expressed, with significantly higher expression in the wingless head, thorax, and cauda, and therefore showed a winged aphid-specific expression pattern in those tissues (**Figure 5B**, $p < 0.05$, $N = 3$). *OBP4* was expressed at quite a low level but still showed a phenotypic correlation with wingless aphids, with comparatively high expression in the antenna, leg, and cauda. *OBP5* was leg specific in both morphs, whereas *OBP15* was highly expressed in the wings and legs of both winged and wingless morphs (**Figure 5**).

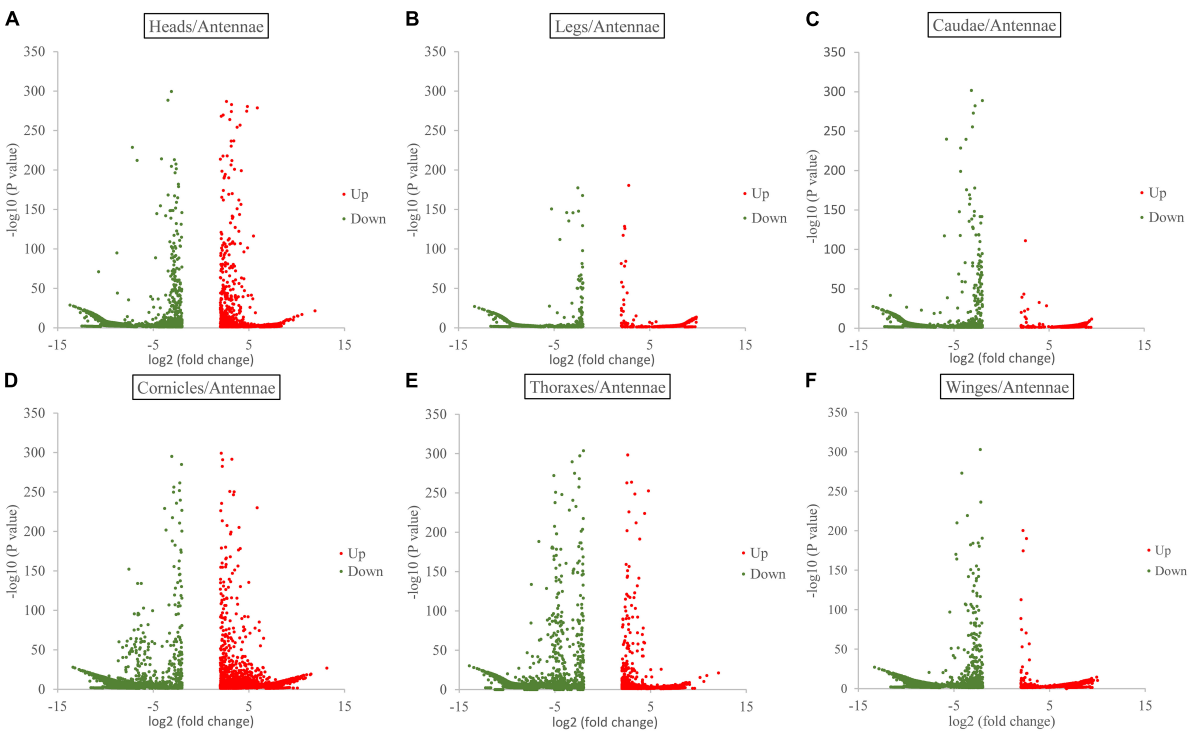

FIGURE 3 | Heatmap of 12 *OBP*s (*OBP2-10*, *OBP13-15*) FPKM values from the transcriptomes of 7 tissues and organs (antennae, heads, wings, legs, thoraxes, caudae, and cornicles). **(A–F)** were the heatmap result of 12 *OBP*s FPKM values in heads, legs, caudae, cornicles, thoraxes, and wings, respectively.

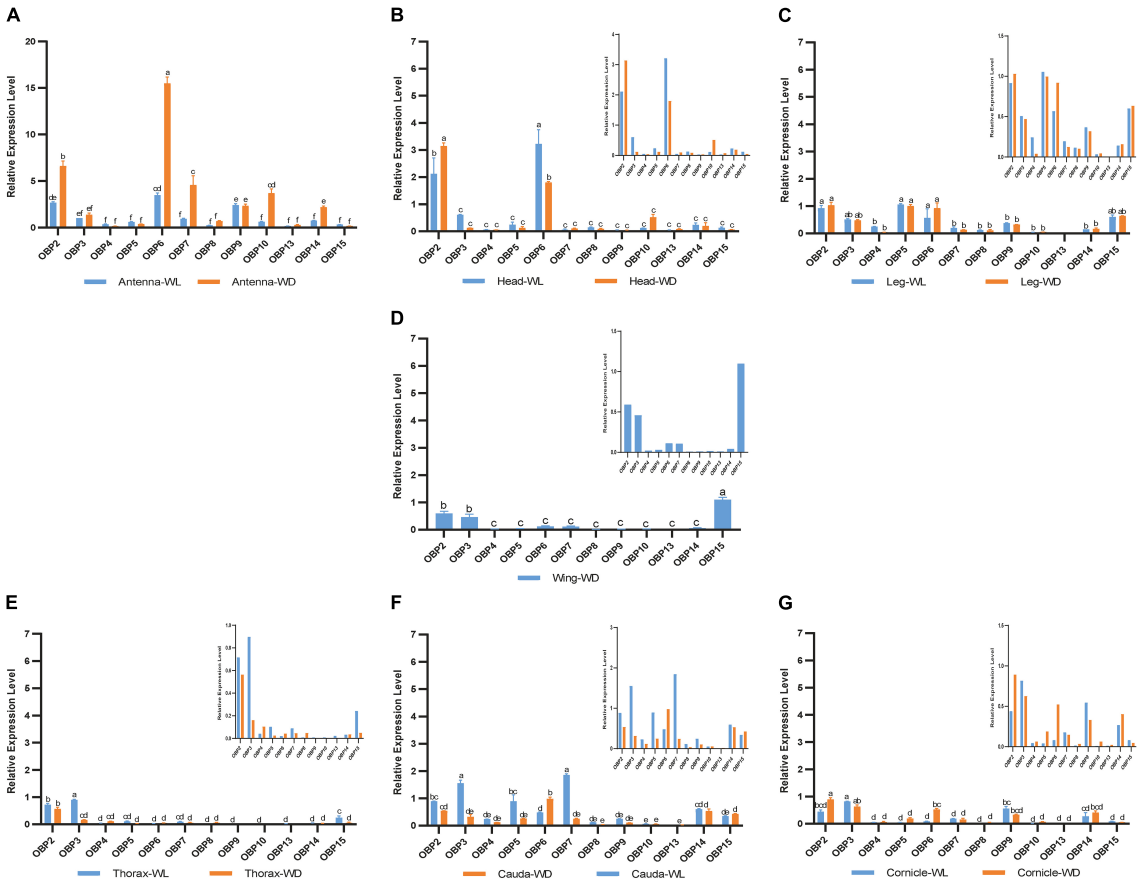

FIGURE 4 | RT-qPCR detection of 12 OBP expression patterns at the mRNA level in each tissue. WL, wingless; WD, winged; bars represent the standard deviation of the mean for three independent experiments. **(A–G)** are the results of 12 OBP expression patterns in antennae, heads, legs, wings, thoraxes, caudae, and cornicles, respectively. The letters above bars (a–f) are the result of a multicomparison, which indicated significant differences from other samples with different letters ($p < 0.05$).

In addition to *OBP2*, *OBP6* maintained high expression levels in the head of winged and wingless aphids (**Figure 4B**). Specifically, *OBP2* was more highly expressed in the winged aphids head and *OBP6* in the wingless aphid head.

Similar to *OBP3*, *OBP15* was more highly expressed in the wingless aphids thorax. *OBP2* was highly expressed in both winged and wingless morphs.

In the leg, the expression of most OBPs was quite low and showed no phenotypic correlation. Among them, *OBP2/5/6* displayed comparatively high expression, with *OBP5* being significantly more highly expressed in the leg than in other tissues (**Figure 4C**).

Surprisingly, we found that three *OBP*s, *OBP2*, *OBP3*, and *OBP15*, were expressed at much higher levels in the wing than other OBPs (**Figure 4D**).

The results for the cornicle indicated that five OBPs (*OBP2/3/6/9/14*) were highly expressed; among them, *OBP2/6* showed differential expression between morphs, though they all presented significantly elevated expression in the winged morph. Nevertheless, the expression of the other three OBPs (*OBP3/9/14*) did not differ between morphs. In addition to *OBP3* and *OBP9*, the gene coding the other EBF-binding protein, *OBP7*, was expressed in the cornicle at relatively low expression levels, with no significant difference between winged and wingless morphs.

OBP3/5/7 generally appeared to be specific to the wingless morph cauda. *OBP6* was highly expressed in wingless aphids; *OBP2* was also highly expressed, but with no significant difference between winged and wingless aphids.

DISCUSSION

In this study, three newly reported OBPs were identified based on TRINITY, which has been demonstrated to recover more full-length transcripts across a broad range of expression levels, with a sensitivity similar to the methods that rely on genome alignments (Grabherr et al., 2011). Our differential expression analysis (**Figure 1**) and enrichment results (**Figure 3**) showed that OBPs are widely expressed in the soybean aphid, although none was found to be antenna specific or specific to any of seven organs/tissues (**Figure 2**). The results derived from the aforesaid transcriptome data prompted us to further carry out a detailed

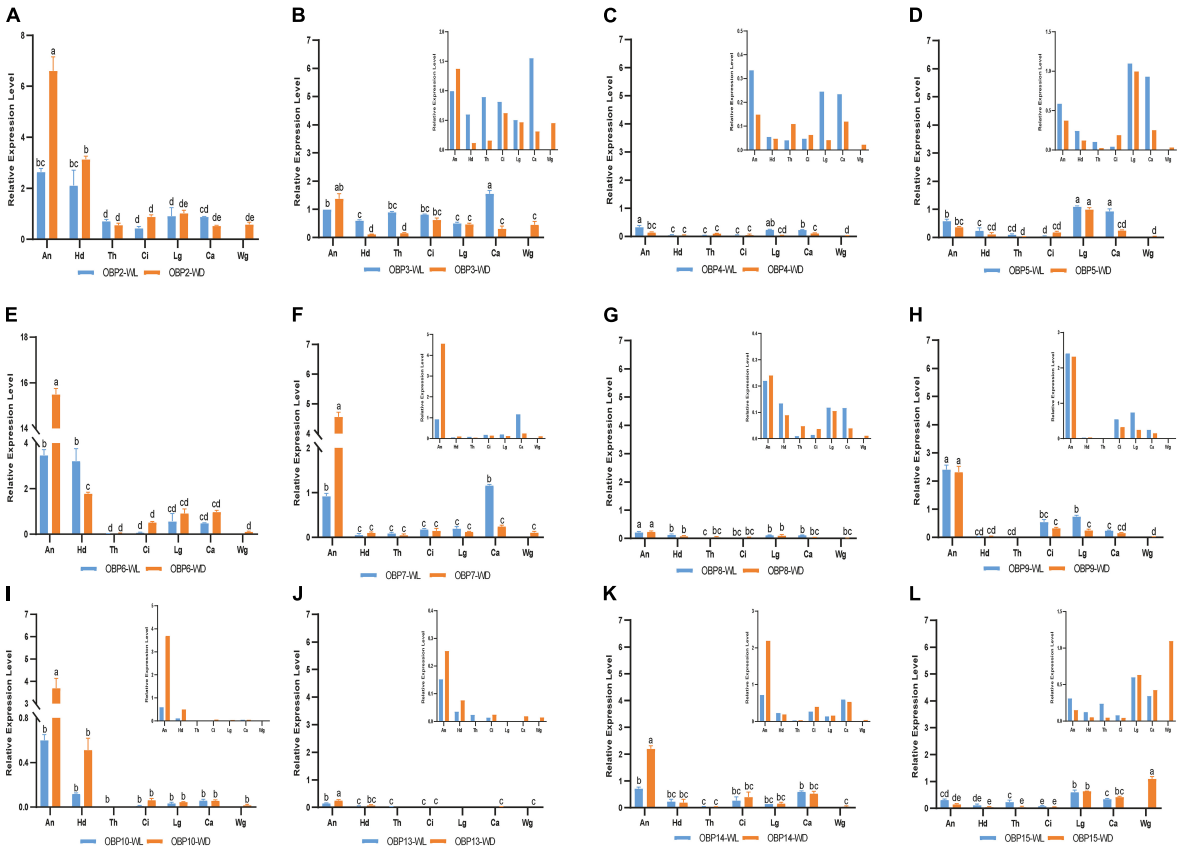

FIGURE 5 | RT-qPCR detection of each OBP expression pattern in seven tissues; WL, wingless; WD, winged; An, antennae; Hd, head; Th, thorax; Ci, cornicle; Lg, leg; Ca, cauda; Wg, wing. Bars represent the standard deviation of the mean for three independent experiments. **(A–L)** are the detection results of each OBP expression pattern in seven tissues and the sequence is from OBP2 to OBP10 and OBP13 to OBP15, respectively. The letters above bars (a–e) are the result of a multicomparison, which indicated significant differences from other samples with different letters ($p < 0.05$).

investigation and analysis of *OBP* expression levels among different wing phenotypes and different tissue parts based on RT-qPCR technology. The qPCR results show that relatively high expression of most OBPs in antennae, the main olfaction organ of aphids, of both phenotypes, and further, higher expression in the winged phenotype (**Figure 4**) are consistent with the fact that winged aphids have more developed olfaction (Pickett, 2009) and support that OBPs play key roles in aphids' olfaction.

Our work provides insight into the potential functions of OBPs correlating with their spatial expression among seven body parts, including various functional organs and tissues, including the antenna, head, leg, thorax, wing, cauda, and cornicle. We further report the breakthrough of the acquisition of aphid cauda and cornicle transcriptomes and their publication. The insect OBP family is believed to participate in chemosensory perception due to their high abundance in chemosensory organs, such as antennae, heads, and legs (e.g., Vogt and Riddiford, 1981; Sun et al., 2013). Without exception, all 12 OBPs identified in this study exhibited relatively high expression in the antenna, head, or leg of both *A. glycine* wing morphs. Most *OBPs* showed relatively high expression in the antennae, the main olfaction organ of aphids, in both phenotypes, with higher expression in the winged phenotype (**Figure 4**), consistent with the fact that winged aphids have more developed olfaction (Pickett, 2009).

OBP3 (Qiao et al., 2009), OBP7 (Sun Y. L. et al., 2012; Zhong et al., 2012; Fan et al., 2017), and OBP9 (Qin et al., 2020) in aphids are known for their high affinities for E-β-farnesene, the key component of the aphid alarm pheromone. In this study, the genes encoding the three EBF-binding proteins (*OBP3/7/9*) showed different antennal expression patterns from each other (**Figure 5**), providing a new perspective for understanding relationships among them. *OBP7* was significantly highly expressed in the antenna of both phenotypes, with higher levels in winged aphids. In contrast, there was no difference in the expression of *OBP3* or *OBP9* between the two phenotypes. Further analysis showed that *OBP3* was systemically expressed; significantly higher expression in the head, thorax, and cauda of wingless aphids was detected. However, *OBP9* presented with high expression in the antenna, leg, and cornicle. The higher expression level of *OBP7* in the antennae of winged aphids suggests that it may contribute more to the EBF sensitivity of winged aphids. Notably, the genes encoding these three reported EBF-binding proteins were all expressed in the cornicle (**Figure 4G**). Cornicles comprising a pair of tubular tissues

involved are the alarm pheromone (E-β-farnesene, EBF) storage and release organ, and *OBP3*, *OBP7*, and *OBP9* may be involved in alarm pheromone activity preservation, release or biosynthesis, and metabolism by binding to and releasing EBF.

Insect OBPs have been reported to act as carrier proteins in the male reproductive apparatus of mosquitoes (Li et al., 2008). After matting, the OBP expressed by male moths is found on the surface of fertilized eggs, which helped the larvae to avoid cannibalistic behaviors (Sun Y. L. et al., 2012). In this study, caudae were dissected with dorsal segments of the distal and abdominal segments, anus, and gonapophysis. Therefore, the high expression of OBPs observed in this tissue suggests potential functions in reproduction or excretion. In addition, carrier proteins function in the binding of or transfer of foreign chemicals or signal ligands.

Odor-binding proteins have also been found to be expressed in wings, such as in *Polistes dominula* (Calvello et al., 2003), *Vespa crabro* (Pelosi et al., 2005), and *Helicoverpa armigera* (Wang et al., 2020). Wang et al. further demonstrated lipid binding by OBPs indicating roles beyond their typical functions in the olfactory system to support insect flight activity. In this study, two *OBP*s (*OBP3* and *OBP15*) were found to be expressed in the thorax of the wingless phenotype and were significantly downregulated in the winged thorax with wings removed ($p < 0.05$, **Figures 4D,E**, **5B,L**). In addition, the removed wings expressed significantly high levels of both. Hence, there is a possibility that *OBP3* and *OBP15* were enriched from the thorax to the wings and that they may also function in other ways, such as lipid-binding proteins in the energy supply of flight or carrier proteins which we discussed above in the section on caudae.

Although *OBP3/7/9* all exhibit an affinity for EBF, they showed differential expression patterns in this study. *OBP3* was extensively expressed throughout the aphid body, *OBP7* was antenna-specifically expressed, and *OBP9* was highly expressed in the antenna, leg, and cauda. As the cornicle is the alarm pheromone (E-β-farnesene, EBF) storage and release organ, it was not surprising to find that all previously reported EBF-binding proteins were expressed in the cauda (*OBP3*, *OBP9*, and low expression of *OBP7*).

SaveOBP2, *SaveOBP4*, and *SaveOBP5* have been reported to have a limited affinity for wheat volatile benzaldehyde (Zhong et al., 2012). However, no potential ligand has yet been reported for *OBP6*, one of the most highly expressed OBPs, which suggests that the ligand spectrum for insect OBPs may be far greater than our expectations.

More details regarding OBP spatial expression were revealed under our strategy. These findings supported the existence of carrier transport functions other than for foreign chemicals and therefore broader ligand ranges of aphid OBPs. It is important for understanding how insect OBPs function in chemical perception as well as other physiological functions of OBPs.

DATA AVAILABILITY STATEMENT

The transcriptomic datasets presented in this study can be found in online repositories (http://www.ncbi.nlm.nih.gov/bioproject/744282) with temporary submission ID: SUB9958208.

AUTHOR CONTRIBUTIONS

LW and JF conceived and designed the study. LW and SY performed the experiments. HY and JF assembled and analyzed the transcriptome data. SY analyzed the RT-qPCR data analysis. JF, SY, and LW wrote the original manuscript. All the other authors contributed on polishing and revising the article.

FUNDING

This study was supported by the National Natural Science Foundation of China (31871966), the Postdoctoral Scientific Research Development Fund of Heilongjiang Province (LBHQ20175), and Collaborative Innovation Center of Internet & Modern Agricultural Application Technology (Kjcxpt202007).

SUPPLEMENTARY MATERIAL

The Supplementary Material for this article can be found online at: https://www.frontiersin.org/articles/10.3389/fphys.2021.702973/full#supplementary-material

Supplementary Data 1 | RT-qPCR primer list.

Supplementary Data 2 | Transcriptome data information.

Supplementary Data 3 | Differential expression transcript list.

Supplementary Data 4 | GlyOBP sequences.

Supplementary Data 5 | GlyOBP FPKM value.

REFERENCES

Beckendorf, E. A., Catangui, M. A., and Riedell, W. E. (2008). Soybean aphid feeding injury and soybean yield, yield components, and seed composition. *Agron. J.* 100, 237–246. doi: 10.2134/agrojnl2007.0207

Biasio, F. D., Riviello, L., Bruno, D., Annalisa, G., Congiu, T., Sun, Y. F., et al. (2015). Expression pattern analysis of odorant-binding proteins in the pea aphid *Acyrthosiphon pisum*. *Insect Sci.* 22, 220–234.

Calvello, M., Guerra, N., Brandazza, A., D'Ambrosio, C., Scaloni, A., Dani, F. R., et al. (2003). Soluble proteins of chemical communication in the social wasp Polistes dominulus. *Cell. Mol. Life Sci.* 60, 1933–1943. doi: 10.1007/s00018-003-3186-5

Clark, A., and Perry, K. L. (2002). Transmissibility of field isolates of soybean viruses by *Aphis glycines*. *Plant Dis.* 86, 1219–1222. doi: 10.1094/PDIS.2002.86.11.1219

Daniele, B., Gerarda, G., Rosanna, S., Andrea, S., Donatella, F., Annalisa, G., et al. (2018). Sensilla morphology and complex expression pattern of odorant binding proteins in the vetch aphid *Megoura viciae* (hemiptera: aphididae). *Front. Physiol.* 9:777. doi: 10.3389/fphys.2018.00777

Deng, W., Wang, Y., Liu, Z., Cheng, H., and Xue, Y. (2014). HemI: a toolkit for illustrating heatmaps. *PLoS One* 9:e111988. doi: 10.1371/journal.pone.0111988

Fan, J., Xue, W., Duan, H., Jiang, X., Zhang, Y., Yu, W., et al. (2017). Identification of an intraspecific alarm pheromone and two conserved odorant-binding

proteins associated with (E)-β-farnesene perception in aphid *Rhopalosiphum padi*. *J. Insect Physiol.* 101, 151–160.

Gao, K. X., Zhang, S., Luo, J. Y., Wang, C. Y., Li-Min, L., Zhang, L. J., et al. (2018). Molecular characterization and ligand-binding properties of six odorant binding proteins (OBPs) from Aphis gossypii. *J. Asia Pac. Entomol.* 21, 914–925. doi: 10.1016/j.aspen.2018.07.004

Grabherr, M. G., Haas, B. J., Yassour, M., Levin, J. Z., Thompson, D. A., Amit, I., et al. (2011). Full-length transcriptome assembly from RNA-Seq data without a reference genome. *Nat. Biotechnol.* 29, 644–652. doi: 10.1038/nbt.1883

Gu, S. H., Wu, K. M., Guo, Y. Y., Field, L. M., Pickett, J. A., Zhang, Y. J., et al. (2013). Identification and expression profiling of odorant binding proteins and chemosensory proteins between two wingless morphs and a winged morph of the cotton aphid *Aphis gossypii* glover. *PLoS One* 8:e73524. doi: 10.1371/journal.pone.0073524

Iovinella, I., Dani, F. R., Niccolini, A., Sagona, S., Michelucci, E., Gazzano, A., et al. (2011). Differential expression of odorant-binding proteins in the mandibular glands of the honey bee according to caste and age. *J. Proteome Res.* 10, 3439–3449. doi: 10.1021/pr2000754

Ji, R., Wang, Y., Cheng, Y., Zhang, M., Zhang, H. B., Zhu, L., et al. (2016). Transcriptome analysis of green peach aphid (*Myzus persicae*): insight into developmental regulation and inter-species divergence. *Front. Plant Sci.* 7:1562. doi: 10.3389/fpls.2016.01562

Kim, D., Pertea, G., Trapnell, C., Pimentel, H., Kelley, R., and Salzberg, S. L. (2013). TopHat2: accurate alignment of transcriptomes in the presence of insertions, deletions and gene fusions. *Genome Biol.* 14:R36. doi: 10.1186/gb-2013-14-4-r36

Langmead, B., and Salzberg, S. L. (2012). Fast gapped-read alignment with Bowtie 2. *Nat. Methods* 9, 357–359. doi: 10.1038/nmeth.1923

Li, B., and Dewey, C. N. (2011). RSEM: accurate transcript quantification from RNA-Seq data with or without a reference genome. *BMC Bioinform.* 12:323. doi: 10.1186/1471-2105-12-323

Li, S., Picimbon, J. F., Ji, S., Kan, Y., and Pelosi, P. (2008). Multiple functions of an odorant-binding protein in the mosquito *Aedes aegypti*. *Biochem. Biophys. Res. Commun.* 372, 464–468. doi: 10.1016/j.bbrc.2008.05.064

Livak, K. J., and Schmittgen, T. D. (2001). Analysis of temporal gene expression data using real-time quantitative PCR and the 2 (-Delta Delta C (T)) method. *Methods* 25, 402–408. doi: 10.1006/meth.2001

Mortazavi, A., Williams, B. A., Mccue, K., Schaeffer, L., and Wold, B. (2008). Mapping and quantifying mammalian transcriptomes by RNA-Seq. *Nat. Methods* 5, 621–628. doi: 10.1038/nmeth.1226

Pelosi, P., Iovinella, I., Zhu, J., Wang, G., and Dani, F. R. (2018). Beyond chemoreception: diverse tasks of soluble olfactory proteins in insects. *Biol. Rev.* 93, 184–200. doi: 10.1111/brv.12339

Pelosi, P., Mariantonietta, C., and Ban, L. (2005). Diversity of odorant-binding proteins and chemosensory proteins in insects. *Chem. Senses* 30:i291. doi: 10.1093/chemse/bjh229

Pickett, J. A. (2009). High-throughput ESI-MS analysis of binding between the *Bombyx mori* pheromone-binding protein BmorPBP1, its pheromone components and some analogues. *Chem. Commun.* 38, 5725–5727. doi: 10.1039/b914294k

Qiao, H. L., Tuccori, E., He, X. L., Gazzano, A., Field, L., Zhou, J. J., et al. (2009). Discrimination of alarm pheromone (E)–β-farnesene by aphid odorant-binding proteins. *Insect Biochem. Mol. Biol.* 39, 414–419.

Qin, Y. G., Yang, Z. K., Song, D. L., Wang, Q., Gu, S. H., Li, W. H., et al. (2020). Bioactivities of synthetic salicylate-substituted carboxyl (E)-β-Farnesene derivatives as ecofriendly agrochemicals and their binding mechanism with potential targets in aphid olfactory system. *Soc. Chem. Ind.* 76, 2465–2472. doi: 10.1002/ps.5787

Sánchez-Sevilla, J. F., Vallarino, J. G., Osorio, S., Bombarely, A., Posé, D., Merchante, C., et al. (2017). Gene expression atlas of fruit ripening and transcriptome assembly from RNA-seq data in octoploid strawberry (Fragaria × ananassa). *Sci. Rep.* 7:13737. doi: 10.1038/s41598-017-14239-6

Sun, W. P., Hu, Z. F., Han, L. L., Sanda, N. B., Xuan, Y. H., and Zhao, K. J. (2015). Discovery of a transitional host of the soybean aphid, *Aphis glycines* (Hemiptera: Aphididae), in northeastern China. *Appl. Entomol. Zool.* 50, 361–369. doi: 10.1007/s13355-015-0343-x

Sun, Y. F., De Biasio, F., Qiao, H. L., Iovinella, I., Yang, S. X., Ling, Y., et al. (2012). Two odorant-binding proteins mediate the behavioural response of aphids to the alarm pheromone (E)-β-farnesene and structural analogues. *PLoS One* 7:e32759. doi: 10.1371/journal.pone.0032759

Sun, Y. L., Huang, L. Q., Pelosi, P., and Wang, C. Z. (2012). Expression in antennae and reproductive organs suggests a dual role of an odorant-binding protein in two sibling *Helicoverpa* Species. *PLoS One* 7:e30040. doi: 10.1371/journal.pone.0030040

Sun, Y. P., Zhao, L. J., Sun, L., Zhang, S. G., and Ban, L. P. (2013). Immunolocalization of odorant-binding proteins on antennal chemosensilla of the peach aphid *Myzus persicae* (Sulzer). *Chem. Senses* 38, 129–136. doi: 10.1093/chemse/bjs093

Tao, S. Q., Cao, B., Tian, C. M., and Liang, Y. M. (2017). Comparative transcriptome analysis and identification of candidate effectors in two related rust species (*Gymnosporangium yamadae* and *Gymnosporangium asiaticum*). *BMC Genomics* 18:651. doi: 10.1186/s12864-017-4059-x

Trapnell, C., Roberts, A., Goff, L., Pertea, G., Kim, D., and Kelley, D. R. (2012). Differential gene and transcript expression analysis of RNA-seq experiments with TopHat and Cufflinks. *Nat. Protoc.* 7, 562–578. doi: 10.1038/nprot.2012.016

Vogt, R. G., and Riddiford, L. M. (1981). Pheromone binding and inactivation by moth antennae. *Nature* 293, 161–163. doi: 10.1038/293161a0

Wang, L., Bi, Y., Liu, M., Li, W., Liu, M., Di, S. F., et al. (2019). Identification and expression profiles analysis of odorant-binding proteins in soybean aphid, *Aphis glycines* (hemiptera: aphididae). *Insect Sci.* 27, 1019–1030. doi: 10.1111/1744-7917.12709

Wang, S., Minter, M., Homem, R. A., Michaelson, L. V., Venthur, H., Lim, K. S., et al. (2020). Odorant binding proteins promote flight activity in the migratory insect, *Helicoverpa armigera*. *Mol. Ecol.* 29, 3795–3808. doi: 10.1111/mec.15556

Wang, S. Y., Bao, X. Z., Sun, Y. J., Chen, R. L., and Zhai, B. P. (1996). Study on the effect of population dynamics of soybean aphid (*Aphis glycines*) on both growth and yield of soybean. *Soybean Sci. (China)* 15, 243–247.

Wenger, J. A., Cassone, B. J., Legeai, F., Johnston, J. S., Bansal, R., Yates, A. D., et al. (2017). Whole genome sequence of the soybean aphid, *Aphis glycines*. *Insect Biochem. Mol. Biol.* 123:102917. doi: 10.1016/j.ibmb.2017.01.005

Wu, T. L., Ma, X. H., Yao, L. M., and Wang, B. (2009). Identification of Soybean resources of resistance to aphids. *Agric. Sci. China* 8, 979–984. doi: 10.1016/S1671-2927(08)60303-X

Xue, W., Jia, F., Zhang, Y., Xu, Q., Han, Z., Sun, J., et al. (2016). Identification and expression analysis of candidate odorant-binding protein and chemosensory protein genes by antennal transcriptome of *Sitobion avenae*. *PLoS One* 11:e0161839. doi: 10.1371/journal.pone.0161839

Zhang, Y., Fan, J., Sun, J., Francis, F., and Chen, J. (2017). Transcriptome analysis of the salivary glands of the grain aphid, *Sitobion avenae*. *Sci. Rep.* 7:15911. doi: 10.1038/s41598-017-16092-z

Zhong, T., Yin, J., Deng, S., Li, K., and Cao, Y. (2012). Fluorescence competition assay for the assessment of green leaf volatiles and trans-β-farnesene bound to three odorant-binding proteins in the wheat aphid *Sitobion avenae* (Fabricius). *J. Insect Physiol.* 58, 771–781. doi: 10.1016/j.jinsphys.2012.01.011

Zhou, J. J., He, X. L., Pickett, J. A., and Field, L. M. (2008). Identification of odorant-binding proteins of the yellow fever mosquito *Aedesa egypti*: genome annotation and comparative analyses. *Insect Mol. Biol.* 17, 147–163. doi: 10.1111/j.1365-2583.2007.00789.x

Zhou, J. J., Vieira, F. G., He, X. L., Smadja, C., Liu, R., Rozas, J., et al. (2010). Genome annotation and comparative analyses of the odorant-binding proteins and chemosensory proteins in the pea aphid *Acyrthosiphon pisum*. *Insect Mol. Biol.* 19, 113–122.

Conflict of Interest: The authors declare that the research was conducted in the absence of any commercial or financial relationships that could be construed as a potential conflict of interest.

Publisher's Note: All claims expressed in this article are solely those of the authors and do not necessarily represent those of their affiliated organizations, or those of the publisher, the editors and the reviewers. Any product that may be evaluated in this article, or claim that may be made by its manufacturer, is not guaranteed or endorsed by the publisher.

frontiers in Physiology

ORIGINAL RESEARCH
published: 03 August 2021
doi: 10.3389/fphys.2021.680697

Fine Structure and Olfactory Reception of the Labial Palps of *Spodoptera frugiperda*

*Qiuyan Chen[1,2], Xiaolan Liu[1], Song Cao[1,3], Baiwei Ma[1], Mengbo Guo[1,3], Jie Shen[2] and Guirong Wang[1,3]**

[1]State Key Laboratory for Biology of Plant Diseases and Insect Pests, Institute of Plant Protection, Chinese Academy of Agricultural Sciences, Beijing, China, [2]Department of Entomology and MOA Key Laboratory for Monitory and Green Control of Crop Pest, China Agricultural University, Beijing, China, [3]Shenzhen Branch, Guangdong Laboratory for Lingnan Modern Agriculture, Genome Analysis Laboratory of the Ministry of Agriculture and Rural Affairs, Agricultural Genomics Institute at Shenzhen, Chinese Academy of Agricultural Sciences, Shenzhen, China

OPEN ACCESS

Edited by:
Peng He,
Guizhou University,
China

Reviewed by:
Hongbo Jiang,
Southwest University,
China
Zhao-Qun Li,
Chinese Academy of Agricultural Sciences (CAAS), China
Feng Liu,
Michigan State University,
United States

***Correspondence:**
Guirong Wang
grwang@ippcaas.cn

Specialty section:
This article was submitted to Invertebrate Physiology, a section of the journal Frontiers in Physiology

Received: 15 March 2021
Accepted: 24 May 2021
Published: 03 August 2021

Citation:
Chen Q, Liu X, Cao S, Ma B, Guo M, Shen J and Wang G (2021) Fine Structure and Olfactory Reception of the Labial Palps of Spodoptera frugiperda. Front. Physiol. 12:680697. doi: 10.3389/fphys.2021.680697

The olfactory system of insects is essential in many crucial behaviors, such as host seeking, mate recognition, and locating oviposition sites. Lepidopteran moths possess two main olfactory organs, including antennae and labial palps. Compared to antennae, the labial palps are relatively specific and worthy of further investigation due to the labial-palp pit organ (LPO), which contains a large number of sensilla located on the tip segment. The fall armyworm, *Spodoptera frugiperda*, is a worldwide lepidopteran pest, which can damage more than 350 plants and cause significant economic losses. In this study, we surveyed the structure of the labial palps and LPO of *S. frugiperda* using a super-high magnification lens zoom 3D microscope. Then, the distribution and fine structure of sensilla located in the LPO of *S. frugiperda* were investigated using scanning electron microscopy. Subsequently, the electrophysiological responses of labial palps to CO_2 and 29 plant volatiles were recorded by using electrolabialpalpography. Our results showed the fine structure of labial palps, the LPO, and the sensilla located in the LPO of *S. frugiperda*. Moreover, we demonstrated that the labial palps are olfactory organs that respond to both CO_2 and other volatile compounds. Our work established a foundation for further study of the roles of labial palps in insect olfactory related behaviors. Further investigations on the function of labial palps and their biological roles together with CO_2 and volatile compound responses in *S. frugiperda* are necessary, as they may provide better insect behavioral regulators for controlling this pest.

Keywords: *Spodoptera frugiperda*, olfactory, labial-palp pit organ, CO_2, volatiles

INTRODUCTION

The sophisticated olfactory sensing organs of most insects have important roles in detecting host volatiles, recognizing mates, and locating oviposition sites. These organs are mainly distributed in the head, including antennae and mouthpart appendages. As the primary olfactory sensory organs, insect antennae bear abundant of sensilla that are sensitive to plant volatiles,

sex pheromones, and other volatile components. Additionally, some olfactory sensilla are also found on mouthpart appendages, such as maxillary palps (Syed and Leal, 2007; Bohbot et al., 2014) and labial palps (Stange and Stowe, 1999; Galizia and Rossler, 2010). As an important sensory organ, the well-developed labial palps are located on each side of the proboscis in adult Lepidoptera. The labial-palp pit organ (LPO) is a unique structure of lepidopteran species that is located on the apex of labial palps, within which the sensilla lie.

The labial palps are densely covered with scales and usually contain three segments. If the scales are removed, a bottle-shaped LPO situated on the tip of the third segment of the labial palp can be observed. Detailed electron microscopical analyses have been performed on the structure of the LPO in many lepidopteran species (Stange and Stowe, 1999; Faucheux, 2008; Zhao et al., 2013; Dong et al., 2014; Barcaba and Krenn, 2015; Chen and Hua, 2016; Yan et al., 2019), which not only showed large numbers of olfactory sensilla in the LPO but also provided descriptions of the fine structure of LPO and LPO sensilla. The morphological characteristics of LPO and LPO sensilla in adult Lepidoptera are somewhat variable. Usually, the LPO of moths is about 100–300 μm deep and 30–80 μm wide. LPO sensilla can be divided into one to three morphological types. The number of LPO sensilla varies from 80 (Lee et al., 1985) to 1,750 (Kent et al., 1986) in different lepidopteran species.

Compared to antennae, the function of labial palps is largely unknown. At present, the most important function of labial palps in adult Lepidoptera that has been reported is detecting carbon dioxide (CO_2). Electrophysiological recording preformed on the sensilla in the LPO of butterfly (Lee et al., 1985) and moth (Bogner et al., 1986; Stange et al., 1995; Guerenstein et al., 2004; Ning et al., 2016) all showed that the LPO sensilla react to CO_2. CO_2 is a ubiquitous source of ecologically relevant information in insect-plant interactions, insect-vertebrate interactions, and insect social behavior (Guerenstein and Hildebrand, 2008). Sensing CO_2 is essential for foraging (Thom et al., 2004), mating (Choi et al., 2018), and oviposition (Myers et al., 1981; Stange, 1997) in many moth species of the Lepidoptera. These studies raised a general question about whether the LPO sensilla in lepidopteran species are sensitive to volatile compounds. Earlier report indicated that the LPO sensilla of *Rhodogastria* respond to cyclopentanone, acetic acid, octanol, limonene, citral, hexanal, butanal, and pentanal (Bogner et al., 1986), and the LPO sensilla in *Pieris brassicae* are responding to terpineol, cyclopentanone, cumol, acetic acid, propionic acid, and butyric acid (Bogner, 1990). According to the findings of these two articles, the labial palps in adult Lepidoptera that are excited by stimulation with CO_2 may also respond to various volatile compounds. However, it is unknown whether these chemical odors elicited responses of labial palps in other species.

Spodoptera frugiperda (Lepidoptera: Noctuidae), also called fall armyworm, is native to America (Sparks, 1979) but has been spread to Africa (Goergen et al., 2016; Nagoshi et al., 2017; Stokstad, 2017), India (Ganiger et al., 2018), and China (Guo et al., 2018a; Li et al., 2019; Sun et al., 2019a,b). *S. frugiperda* has a wide host range of more than 350 species of plants, including corn, rice, wheat, soybean, and cotton (Montezano et al., 2018), and is one of the most damaging crop pests. There have been many latest investigations focusing on the management against this pest, such as genome editing of the receptor for *Bacillus thuringiensis* in *S. frugiperda* (Jin et al., 2019), the potential roles of *Junonia coenia* densovirus in *S. frugiperda* control (Chen et al., 2020), and the positive phototaxis of *S. frugiperda* (Liu et al., 2020). Elevated CO_2 concentration was recently reported to affect the growth and development of *S. frugiperda* (Zhao et al., 2019), providing support for investigating the structure and function of the LPO, the CO_2-sensitive organ. In this study, the distribution and fine structure of sensilla located in the LPO were investigated using scanning electron microscopy. Sensilla in the LPO were divided into two morphological types. Subsequently, we modified the electroantennogram (EAG) setup to function as the electrolabialpalpography (ELPG) to record the responses of labial palps to different concentrations of CO_2 and 29 plant volatiles. Finally, the sensilla that responded to CO_2 in the LPO were identified via the intracellular recording (ICR). The results indicated that there are two types of sensory neurons in the LPO of *S. frugiperda*, one of which could be strongly activated by different concentrations of CO_2, while the other type showed no response to CO_2. Our work established a foundation for further study of the roles of labial palps in insect olfaction-related behaviors. Based on these results, further investigations of the function of labial palps and their biological roles together with responses to CO_2 and volatile ligands identified in this study of *S. frugiperda* are necessary.

MATERIALS AND METHODS

Insects Rearing

The *S. frugiperda* colony was collected in the wild in Yunnan Province, China, in March, 2019, and then maintained at the Institute of Plant Protection, Chinese Academy of Agricultural Sciences, Beijing, China. The larvae were reared on an artificial diet and placed at 27 ± 1°C with a photoperiod of 14:10 h (L:D). Pupae were together kept in a gauze cage before eclosion. Adults were selected by sex and placed in separate test tubes after eclosion and fed 10% sugar solution every day. Adult females and males were used in all experiments.

Light Microscopy and Biometry Measurements

The protruding head of adult *S. frugiperda* was fixed to the rim of a pipette tip by using dental wax and observed under a super-high magnification lens zoom 3D microscope (VHX-2000, Japan). The labial palps were dissected from the head using fine scissors. Scales covering the labial palps were cleared with double-sided tap. Then, the dehydrated and transparent labial palps were positioned on a microscopic slide with a drop of glycerin and a cover slip. Finally, the labial palps were observed and measured using a super-high magnification lens zoom 3D microscope (VHX-2000, Japan). We measured the

length of each segment of labial palps, and the depth and diameter of the LPO.

Scanning Electron Microscopy

The labial palps were removed from 3- to 4-day-old moths and then cleared with double-sided tape to remove the outer scales. In order to study the morphology of the sensilla in LPO, we split the LPO by using fine scissors. Next, these prepared samples were processed by a series of dehydration, drying, and last were sprayed with gold as described by Guo et al. (2018b). In the described steps, the critical point drier was LEICA EM CPD (Germany) and the type of a sputter-coating unit is EIKO IB-3 (Japan). Finally, the samples were investigated using a Hitachi SU8010 scanning electron microscope (Japan) at 10 kV.

Electrolabialpalpography

Taking 3- to 4-day-old adult *S. frugiperda*, the labial palps were carefully cut from the base charily by using fine scissors, and surface scales were removed with double-sided tape. The treated labial palps were used for recording with the base inserted into the conducting gel (Parker Laboratories, United States) and the tip just contacting the conducting gel to ensure that the opening of the LPO, which harbors all the sensilla, was exposed to the air. The conducting gel was painted on the neutral arms of the metal electrode.

For CO_2 stimulus, the mounted labial palp was excited with stimulus delivery in self-regulating stimulus flow controller, which was mainly comprised of a 3/2-way solenoid valve (XP-513, Japan) and two currents of equal flow rate at 0.8 L/min. One current called continuous flow was diverted through bottled synthetic air, and the other current called stimuli flow was diverted through bottled CO_2 at different concentrations. Stimuli were provided for 1 s by controlling the 3/2-way solenoid valve and were delivered through a 14-cm-long metal tube. Commercially available compressed bottled CO_2 gas stimuli were used at concentrations of 0.1, 1, and 10% (the remainder was synthetic air), and synthetic air was used as a control. To make synthetic air CO_2-free, it contained only 21% O_2 and 78% N_2. All above gases in certificated gas cylinders were bought from company (Beijing Shangtonghong Chemical, China). The resulting ELPG amplitudes (negative potential) were recorded and analyzed by using EAG software (Syntech, Germany). The ELPG response values for CO_2 were calculated by subtracting the value of the same labial palp corresponding to the blank control (synthetic air).

For odor stimuli, 10 μl of test solution or solvent was added in to filter paper strips (0.5 cm × 6 cm) inserted in a Pasteur pipette (15 cm long). A flow of purified and humidified air continuously blew toward the labial palp through a metal tube at 0.4 L/min. A stimulus air pulse was added for 200 ms. The intervals between two stimuli were 30 s. The Pasteur pipette connected to the stimulus air controller CS-55 (Syntech, Germany) was used for stimulation. The pre-amplifier was displayed on a computer via a software interface EAGPRO (Syntech, Germany), and action potentials were amplified, digitized, and visualized on a computer screen. The 29 chemical compounds (95% minimum purity compound) used in this study were purchased from Sigma-Aldrich (Germany). These compounds were dissolved in paraffin oil at the concentration of 1 μg/μl. For odor stimuli in ELPG assay, the recording of labial palp to paraffin oil was used as a control. The ELPG response values for odorants were calculated by subtracting the value of the same labial palp corresponding to the paraffin oil.

Intracellular Recording

The 3- to 4-day-old female and male adults after emergence were wedged into a 1 ml plastic pipette tip with the narrow end cut to allow the head and the exposed labial palps to protrude. The protruding head and other organs, including antennae and proboscis, were all immobilized to the edge of the pipette tip with dental wax under a stereomicroscope, just leaving one of the labial palps accessible. The outer scales on the labial palp were removed carefully with double-sided adhesive tape, and then, the labial palp was fixed with dental wax to reveal just the tip of labial palp and the opening of the LPO.

Nerve impulses from single sensory neurons were recorded intracellularly using a sharp quartz electrode. Under a SZX16 microscope (Olympus, Japan), the reference electrode made of a silver wire was inserted into the moth eye, and the recording electrode which containing 0.2 M KAc was inserted vertically into the LPO via a micromanipulator (Leica, Germany). Spikes were recorded when the quartz electrode was inserted into a sensory neuron in sensilla. During the insertion of the recording electrode into the LPO, it was not possible to distinguish the different sensilla under the microscope because they are located inside the LPO and only the opening of LPO was visible. The amplified analog signals of the action potentials were captured and processed using a signal amplifier (Axoclamp 900A, United States) and a digital-to-analog converter (CED MICRO 1401, England). The recorded spikes activity was displayed on a computer screen using the software package Autospike 2 8.01 (Syntech, Germany).

For stimulus delivery, a 5 s CO_2 stimulus flow was provided by a self-regulating stimulus flow controller. A flow of purified and humidified synthetic air (21% O_2, 78% N_2) was continuously blown on the opening of the LPO through a 14-cm-long metal tube by the self-regulating stimulus flow controller at 0.8 L/min. CO_2 stimuli were represented at 0.1, 1, 10%, and synthetic air (21% O_2 and 78% N_2) was used as a control. The response values to specific concentration of CO_2 were calculated using the formula: T − C, where T represents the differences in spike numbers observed between 5 s before and 5 s after CO_2 delivery, and C represents the differences in spike numbers observed between 5 s before and 5 s after control (synthetic air) delivery.

Image Processing and Statistical Analysis

The classification and naming of sensilla in LPO were described in Zhao et al. (2013). ELPG statistics and graphing were

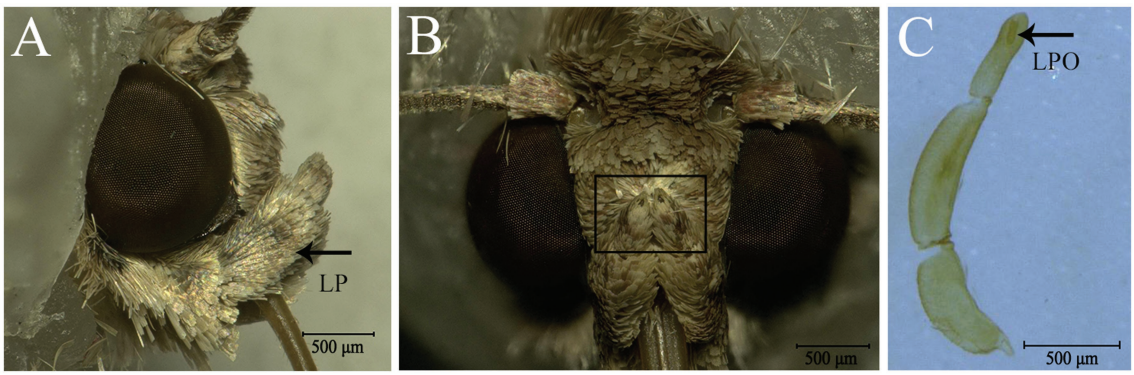

FIGURE 1 | Labial palps (LP) and labial-palp pit organ (LPO) of *Spodoptera frugiperda*. **(A)** Lateral view of the head and the right LP (black arrow); the LPs are covered densely with scales and are located on each side of the proboscis just below the eyes. **(B)** Front view of the head and the LPs. The black boxed area shows the tip of the two LPs and the opening of the LPO. **(C)** Three segments of the LP; the black arrow shows the LPO.

TABLE 1 | The length of each segment of labial palp (LP) and the depth and diameters of LPO of *S. frugiperda*.

	Female	Male	*t*-test
Length of the first LP segment (μm)	688.26 ± 16.30 (23)	663.39 ± 11.03 (23)	$p = 0.213$
Length of the second LP segment (μm)	869.57 ± 17.80 (23)	846.04 ± 11.00 (23)	$p = 0.267$
Length of the third LP segment (μm)	470.78 ± 12.04 (23)	486.43 ± 10.27 (23)	$p = 0.328$
Depth of LPO (μm)	118.35 ± 2.60 (17)	116.22 ± 2.09 (23)	$p = 0.521$
Diameter of LPO opening (μm)	43.08 ± 1.43 (13)	39.15 ± 1.03 (20)	$p = 0.029$
Inner diameter of LPO at half length (μm)	38.77 ± 1.43 (13)	37.53 ± 0.74 (20)	$p = 0.473$
Inner diameter of LPO at the base (μm)	33.69 ± 1.22 (13)	32.80 ± 1.08 (20)	$p = 0.595$

Data in the table are means ± SE. The numbers in parentheses indicate the replicates of measurement.

performed using GraphPad Prism. The measured data of labial palps were analyzed in Microsoft Office Excel 2007. LPO sensilla were measured by LSM Image Browser and analyzed in Microsoft Office Excel 2007. Differences in the response value (or measured data) of females and males were analyzed by *t*-test. Spikes separated from noise were analyzed and evaluated by the computer software Autospike (Syntech, Germany).

RESULTS

Morphological Structure of the Labial Palp and LPO in Adult *S. frugiperda*

Adults of *S. frugiperda* possess a pair of labial palps located on the ventral side of the head that enfold the proboscis (**Figure 1A**). The two labial palps are entirely covered by dense scales and have two small holes at the top (**Figure 1B**). When the scales are removed, each labial palp contains three segments and is tubular (**Figure 1C**). Each segment of labial palps in *S. frugiperda* differs in the morphological structure and length (**Figure 1C**; **Table 1**). The first segment of the labial palp, which is connected to the head, is about 675 μm long, and the second segment is about 857 μm. The third segment is about 478 μm long. An opening near the tip of the third segment extends to a cavity called the LPO (**Figures 1C, 2A**), which is about 117 μm deep and of variable diameter (**Table 1**). In females, the diameter of the LPO opening is 43.08 ± 1.43 μm (mean ± SE, $n = 13$). In males, the diameter of the LPO opening is 39.15 ± 1.03 μm (mean ± SE, $n = 20$). The diameter of the LPO opening in females is significantly longer than in males. The inner diameter of the LPO at the midpoint is approximately 38 μm, and the inner diameter of the LPO at the base is about 33 μm.

Fine Morphological Structure of Sensilla Located in LPO

The LPO is densely packed with approximately 300 sensilla, which comprise hair-shaped sensilla and club-shaped sensilla (**Figure 2C**). The hair-shaped sensilla are slender, and the ends are slightly bent (**Figures 2B,D,E**). Some hair-shaped sensilla have forked tips (**Figure 2B**; blue arrow). The club-shaped sensilla are short and rod-like, and their surfaces have grooves (**Figures 2D,F**). Hair-shaped sensilla and club-shaped sensilla are distributed in separate areas along the vertical axis of the LPO (**Figure 2D**). The length and basal diameter of each sensillum category are shown in **Table 2**. In females, the hair-shaped sensilla are 23.92 ± 0.58 μm long (mean ± SE, $n = 5$) and the basal diameters are 2.74 ± 0.25 μm (mean ± SE, $n = 5$), while the club-shaped sensilla are 13.10 ± 0.54 μm long (mean ± SE, $n = 5$) and the basal diameters are 2.02 ± 0.06 μm long (mean ± SE, $n = 5$). In males, the hair-shaped sensilla are 25.44 ± 0.50 μm long (mean ± SE, $n = 14$) and the basal diameters are 2.88 ± 0.15 μm (mean ± SE, $n = 4$), while the club-shaped sensilla are 12.80 ± 0.27 μm long (mean ± SE, $n = 14$) and the basal diameters are 2.08 ± 0.03 μm (mean ± SE, $n = 14$). The *t*-test results show

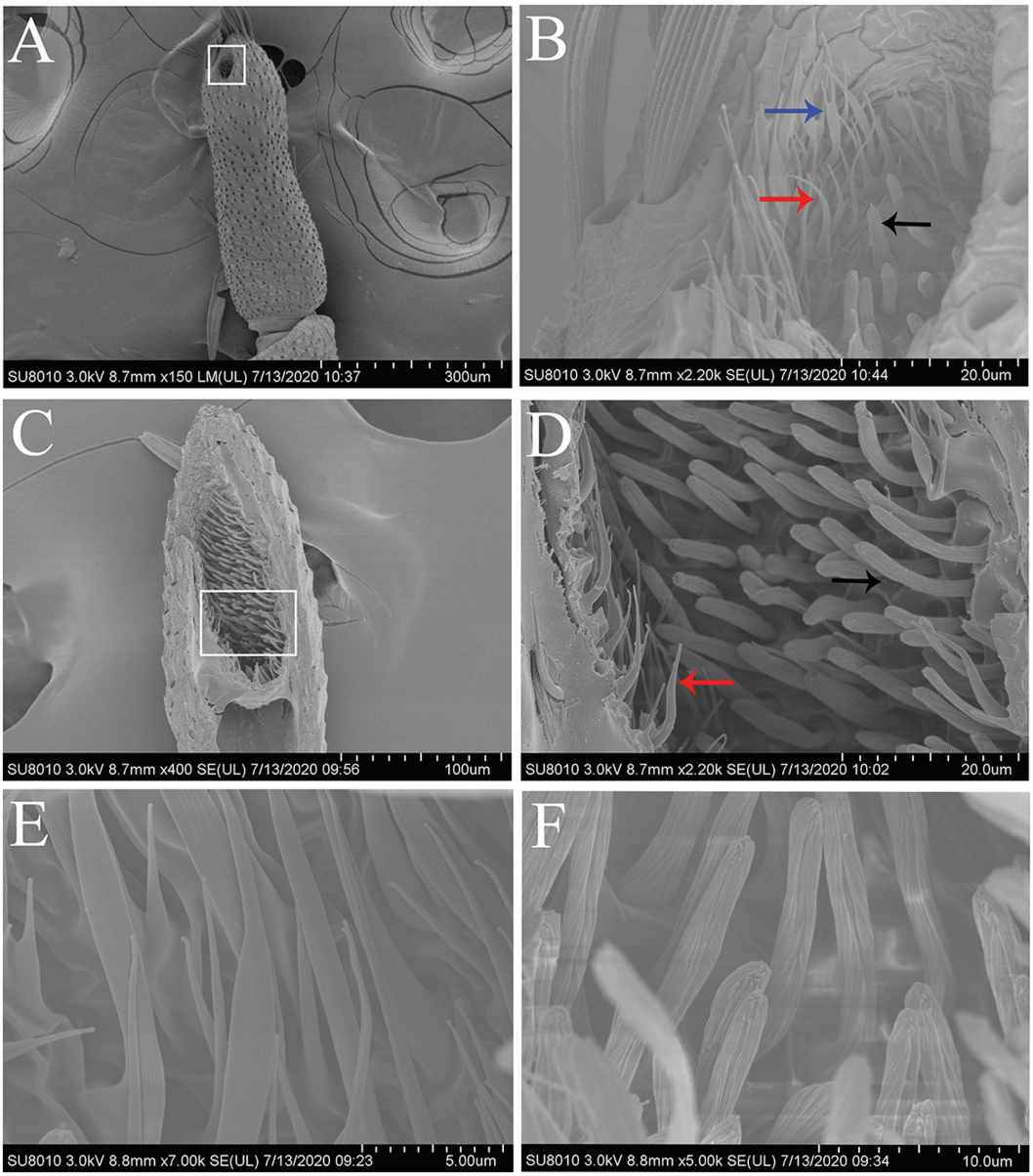

FIGURE 2 | Scanning electron micrographs of the terminal segment of labial palps and the LPO sensilla in *S. frugiperda.* **(A)** The terminal segment of the labial palp showing the opening of the LPO. White boxed area: opening of the LPO. **(B)** Scanning electron micrograph of the sensilla located around the opening of the LPO, which contains hair-shaped sensilla (red and blue arrows) and club-shaped sensilla (black arrow). Two hair-shaped sensilla subtypes were found hair-shaped sensilla (red arrow) and hair-shaped sensilla with forked tips (blue arrow). **(C)** Longitudinal section of the LPO in one labial palp showing two main types of sensilla. **(D)** Enlarged image of white boxed area in **(C)**. The LPO has two types of sensilla, i.e., hair-shaped sensilla (red arrow) and club-shaped sensilla (black arrow). These two types of sensilla are distributed in separate areas along the vertical axis of the LPO. **(E)** Scanning electron micrograph of hair-shaped sensilla. **(F)** Scanning electron micrograph of club-shaped sensilla.

no significant difference in the size of each sensillum type between females and males (**Table 2**).

ELPG Response of Labial Palp to CO_2 and Plant Volatiles

In order to demonstrate the labial palps of *S. frugiperda* also response to odor stimulation besides CO_2 stimulation, we performed ELPG on the female and male labial palps (**Figure 3A**). The labial palp in *S. frugiperda* adults responded obviously to different concentrations of CO_2. The magnitude of response mainly depended on the concentration of CO_2, with the strongest responses to stimulus of 1% CO_2, at about 0.26 ± 0.02 mV (mean ± SE, n = 30), and the weakest responses to the stimulus of 0.1% CO_2, at about 0.18 ± 0.02 mV (mean ± SE, n = 30; **Figure 3B**). In females,

TABLE 2 | The length of LPO sensilla in *S. frugiperda* and their diameter at the base.

	Female	Male	*t*-test
Length of hair-shaped sensilla (μm)	23.92 ± 0.58 (5)	25.44 ± 0.50 (14)	$p = 0.058$
Basal diameter of hair-shaped sensilla (μm)	2.74 ± 0.11 (5)	2.87 ± 0.15 (14)	$p = 0.48$
Length of club-shaped sensilla (μm)	13.10 ± 0.54 (5)	12.79 ± 0.27 (14)	$p = 0.46$
Basal diameter of club-shaped sensilla	2.02 ± 0.06 (5)	2.07 ± 0.03 (14)	$p = 0.37$

Data in the table are means ± SE. The numbers in parentheses indicate the replicates of measurement.

the responses of labial palp to 1% CO_2 are significantly greater than to 0.1% CO_2. There is no significant difference in the responses of labial palp to 1% CO_2 and 10% CO_2, and 0.1% CO_2 and 10% CO_2. In males, the responses of labial palp to 1% CO_2 is significantly greater than to 0.1% CO_2 and is significantly less than to 10% CO_2. There is no significant difference in the responses of labial palp to 0.1% CO_2 and 10% CO_2 (**Figure 3B**). However, The response value of labial palp to the same concentration of CO_2 was not significantly different between females and males (**Figure 3B**).

To verify whether the labial palp, as an olfactory organ, responded to volatile compounds other than CO_2, we also investigated the electrophysiological responses of labial palps to 29 volatile compounds (**Figure 3C**). The labial palps of *S. frugiperda* obviously responded to six compounds: butylamine, heptylamine, heptanal, valeraldehyde, propionic acid, and acetic acid (**Figure 3C**). As with CO_2, responses were not significantly different between females and males.

Recording From LPO Sensilla to CO_2

In order to check the existence of sensilla in the LPO that respond to CO_2, we performed ICR on sensory neurons in LPO sensilla from male and female labial palps. CO_2-sensitive neurons were found in LPO sensilla of adult *S. frugiperda* (**Figure 4**; SN-a). We also found sensory neurons that did not respond to CO_2 in the LPO sensilla (**Figure 4**; SN-b). The sensory neurons that responded to CO_2 were labeled sensory neuron a (SN-a), while those that did not respond to CO_2 were labeled sensory neuron b (SN-b; **Figure 4**). We successfully recorded 11 adults *S. frugiperda* in total, including six females and five males. A total of 22 neurons with unambiguous spikes from eight insects (four females and four males) were analyzed. For SN-a, there was a strong excitatory response to CO_2 stimulus at concentrations of 0.1, 1, and 10% (**Figure 4A**) and the mean activated spikes of these neurons were, respectively, about 93 spikes/5 s, 107 spikes/5 s, and 99 spikes/5 s (**Figure 4B**). Besides, the responses of SN-a were not significantly different between these three concentrations of CO_2.

DISCUSSION

Structure characterization of an olfactory organ and its sensilla are vital to understand how the olfactory organ performs its ecological function. This model has been widely used in the surveys of antennae in lepidopteran insects. In an effort to research the function of another crucial olfactory organ, the labial palp, the fine structure of LPO and LPO sensilla in *S. frugiperda* were investigated in detailed in the present study. For the structure of LPO, we found a significant difference in the diameter of the LPO opening between females and males in *S. frugiperda*. The diameter of the LPO opening in *S. frugiperda* exhibited distinct sexual dimorphism and was much longer in females (43.08 μm) than in males (39.15 μm). In other reported Noctuidae species (Zhao et al., 2013; Dong et al., 2014), the diameter of the LPO opening tends to be the same size in both sexes. The sexual dimorphism of the diameter of the LPO opening is described for the first time in this study, although sexual dimorphism also occurs in the length of labial palps in *Cactoblastis cactorum* (Stange et al., 1995), *Mythimna separata* (Dong et al., 2014), *Carposina sasakii* (Chen and Hua, 2016), and *Plutella xylostella* (Yan et al., 2019). This phenomenon may be related to sex-specific differences in behavior, such as courtship and oviposition. For example, *C. cactorum* probes the surface of a plant with their labial palps before ovipositing, so the length of labial palps in females is much longer than in males (Stange et al., 1995). The differences between the sexes in the diameter of the LPO opening may also be due to the ovipositing behavior of female *S. frugiperda*, though further studies are required to confirm this.

In our study, the densely packed array of LPO sensilla in *S. frugiperda* can be divided into two morphological types: hair-shaped sensilla and club-shaped sensilla, like that in *C. cactorum* (Stange et al., 1995), *Helicoverpa armigera* (Zhao et al., 2013), *M. separata* (Dong et al., 2014), and *C. sasakii* (Chen and Hua, 2016); hair-shaped sensilla in *C. cactorum* and *C. sasakii* have not been described in detail. However, there is only one kind of LPO sensilla in some moth species. For example, in *Rhodogastria* spp. the LPO is densely packed with smooth-walled sensilla of uniform appearance (Bogner et al., 1986), and the LPO in *Plodia interpunctella* also contains a single small trichoid sensillum (Barcaba and Krenn, 2015). The LPO in *Grapholita molesta* (Song et al., 2016) contains three categories of sensilla: hair-shaped sensilla, club-shaped sensilla, and small mastoid sensilla. Although the categories of LPO sensilla are identical, the hair-shaped sensilla and club-shaped sensilla in the LPO of *S. frugiperda* are distributed in separate areas along the vertical axis of LPO, whereas they are situated in the upper half and the lower half of the pit in *H. armigera* (Zhao et al., 2013) and *M. separata* (Dong et al., 2014). This type of distribution of LPO sensilla in *S. frugiperda* is described for the first time. In summary, the differences of LPO sensilla in categories and location may be dependent on the insect species, or related to the behavior of insects and the function of the labial palps.

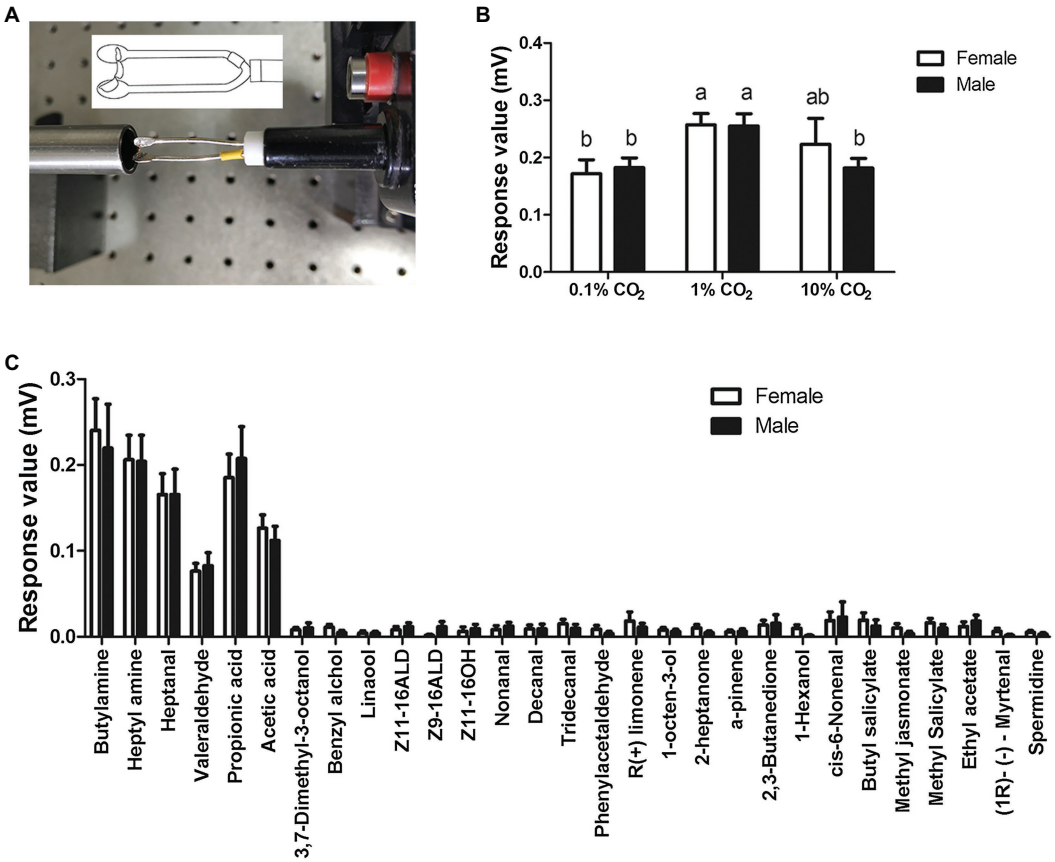

FIGURE 3 | Electrolabialpalpography (ELPG) response of labial palps in *S. frugiperda* to CO_2 and plant volatiles. **(A)** Schematic showing a labial palp mounted on the electrode in the ELPG assay. **(B)** ELPG response of labial palp in *S. frugiperda* to different concentrations of CO_2 including 0.1, 1, and 10%. Data are the mean ± SD (n = 30). **(C)** ELPG responses of labial palp in *S. frugiperda* to 29 plant volatiles. Data are the mean ± SE (n = 15).

Electrolabialpalpography and ICR data in the present investigation support the idea that *S. frugiperda* have CO_2-sensitive neurons in the LPO, as reported in other lepidopteran species (Bogner et al., 1986; Stange et al., 1995; Stange, 1997; Guerenstein et al., 2004; Ning et al., 2016). This suggests that CO_2-detection is a universal function of the LPO in Lepidoptera. Interestingly, we found a kind of sensory neuron that was non-responsive to CO_2 in the LPO of *S. frugiperda*, which has never been reported before. This finding implies that LPO sensilla are not uniform in detecting CO_2 and they may also respond to other odorants. Our electrophysiological recording results strongly support the hypothesis that LPO sensilla can respond to volatile chemicals. The labial palps of *S. frugiperda* obviously responded to six of 29 volatiles tested in our experiment, including butylamine, heptylamine, heptanal, valeraldehyde, propionic acid, and acetic acid. Electrophysiologically active compounds in this study, propionic acid and acetic acid, which are volatiles from host plants, have been reported in other lepidopteran insects (Bogner et al., 1986; Bogner, 1990). In addition, several kinds of odorants and their analogues found to be effective stimuli in *S. frugiperda* also activate CO_2 receptors of antennae in flies and CO_2 receptors of maxillary palps in mosquitoes (Turner and Ray, 2009; Tauxe et al., 2013; Macwilliam et al., 2018). The class of odorants also present in ripe fruits has important ecological significance, as they can modify the CO_2 avoidance behavior, helping the host-seeking behavior of *Drosophila melanogaster* (Turner and Ray, 2009). Hence, we predict that olfactory perception of ecologically relevant volatiles occurs on labial palps of *S. frugiperda*, but its role in behaviors remains to be investigated.

We speculate that the gustatory receptor (GR) genes and ionotropic receptor (IR) genes have pivotal roles in detecting CO_2 and other volatile compounds for *S. frugiperda* LPO. Two GRs, GR21a and GR63a, were identified as the CO_2 receptor genes for the first time in *D. melanogaster* (Jones et al., 2007; Kwon et al., 2007). Later, their homologous genes, GR1, GR2, and GR3, were successively identified as the CO_2 receptors in many mosquito species (Kent et al., 2008; Robertson and Kent, 2009; Coutinho-Abreu et al., 2019). GR1, GR2, and GR3, which are highly expressed in labial palps, have been identified using phylogenetic analysis in several lepidopteran species (Briscoe, 2000; Spaethe and Briscoe, 2004; Liu et al., 2014; Xu and Anderson, 2015; Zhang et al., 2015; Liu et al., 2017), and their functions have been confirmed (Xu and Anderson, 2015; Ning et al., 2016).

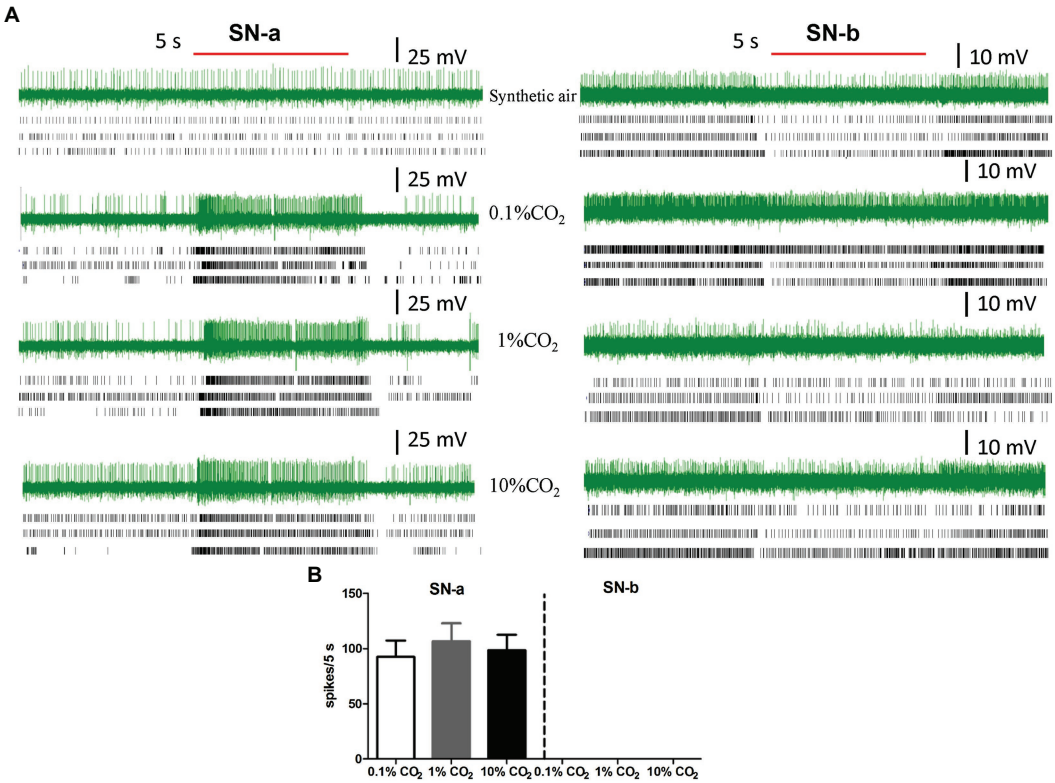

FIGURE 4 | Intracellular recording (ICR) analysis of the sensory neurons housed in LPO sensilla. **(A)** The representative traces of ICRs, three example of rater plots of action potentials of responses of sensory neurons in SN-a and SN-b to synthetic air, 0.1% CO_2, 1% CO_2, and 10% CO_2. The red bold line represents the 5 s stimulation. The letters (SN-a, SN-b) represent the different types of sensory neurons in LPO sensilla. **(B)** Quantification of the mean responses of SN-a and SN-b in LPO sensilla to 0.1% CO_2, 1% CO_2, and 10% CO_2. Data are the mean ± SE (n = 10–16). The response values to specific concentration of CO_2 were calculated using the formula: T − C, where T represents the differences in spike numbers observed between 5 s before and 5 s after CO_2 delivery, and C represents the differences in spike numbers observed between 5 s before and 5 s after control (synthetic air) delivery.

These three GRs are likely required for CO_2 detection in *S. frugiperda*. For volatile compounds detection, the molecular mechanism is generally related to odorant receptors (ORs). However, these six odors, which excited labial palps of *S. frugiperda*, mainly contain acid, aldehyde, and amine. It has been reported that sensing of this class of odors was involved in IRs predominantly (Zhang and Wang, 2020). Moreover, there were indeed IRs identified in labial palps of the lepidopteran *H. armigera* (Guo et al., 2018b). Analogously, IRs might also be the receptor for detecting these six odors in *S. frugiperda*.

Our exploration of ultrastructural characteristics of LPO sensilla and their physiological functions in *S. frugiperda* might be useful not only for obtaining knowledge about the function of labial palps but also for controlling this serious insect pest. Further study is needed to clarify the physiological functions of the two morphological types of sensilla in LPO, hair-shaped sensilla and club-shaped sensilla, and confirm that these two types of LPO sensilla in *S. frugiperda* are separately sensitive to CO_2 and airborne chemicals. Further behavioral studies and molecular investigations of the labial palps are necessary to better understand the ecological significance and molecular basis of olfaction in *S. frugiperda*.

DATA AVAILABILITY STATEMENT

The original contributions presented in the study are included in the article/supplementary material, and further inquiries can be directed to the corresponding author.

AUTHOR CONTRIBUTIONS

JS and GW designed the experiments. QC, XL, SC, BM, and MG performed the experiments. QC and GW wrote the manuscript and analyzed the data. JS and GW revised the manuscript. All authors contributed to the article and approved the submitted version.

FUNDING

This work was supported by the National Natural Science Foundation of China (31861133019 and 31725023).

REFERENCES

Barcaba, T., and Krenn, H. W. (2015). The mouthparts of adult Indian meal moths, *Plodia interpunctella* (Hübner, 1813) (Lepidoptera: Pyralidae). *Entomol. Aust.* 22, 91–105.

Bogner, F. (1990). Sensory physiological investigation of carbon dioxide receptors in Lepidoptera. *J. Insect Physiol.* 36, 951–957. doi: 10.1016/0022-1910(90)90083-R

Bogner, F., Boppré, M., Ernst, K. D., and Boeckh, J. (1986). CO_2 sensitive receptors on labial palps of *Rhodogastria* moths (Lepidoptera: Arctiidae): physiology, fine structure and central projection. *J. Comp. Physiol. A* 158, 741–749. doi: 10.1007/BF01324818

Bohbot, J. D., Sparks, J. T., and Dickens, J. C. (2014). The maxillary palp of *Aedes aegypti*, a model of multisensory integration. *Insect Biochem. Mol. Biol.* 48, 29–39. doi: 10.1016/j.ibmb.2014.02.007

Briscoe, A. D. (2000). Six opsins from the butterfly *Papilio glaucus*: molecular phylogenetic evidence for paralogous origins of red-sensitive visual pigments in insects. *J. Mol. Evol.* 51, 110–121. doi: 10.1007/s002390010071

Chen, J., and Hua, B. (2016). Sexual dimorphism of adult labial palps of the peach fruit moth *Carposina sasakii* Matsumura (Lepidoptera: Carposinidae) with notes on their sensilla. *Acta Zool.* 97, 42–48. doi: 10.1111/azo.12103

Chen, Z. W., Yang, Y. C., Zhang, J. F., Jin, M. H., Xiao, Y. T., Xia, Z. C., et al. (2020). Susceptibility and tissue specificity of *Spodoptera frugiperda* to *Junonia coenia* densovirus. *J. Integr. Agr.* 20, 840–849. doi: 10.1016/S2095-3119(20)63163-X

Choi, K. S., Ahn, S. J., Kim, S. B., Ahn, J. J., Jung, B. N., Go, S. W., et al. (2018). Elevated CO_2 may alter pheromonal communication in *Helicoverpa armigera* (Lepidoptera: Noctuidae). *Physiol. Entomol.* 43, 169–179. doi: 10.1111/phen.12239

Coutinho-Abreu, L. V., Sharma, K., Cui, L., Yan, G., and Ray, A. (2019). Odorant ligands for the CO_2 receptor in two *Anopheles* vectors of malaria. *Sci. Rep.* 9:2549. doi: 10.1038/s41598-019-39099-0

Dong, J., Liu, H., Tang, Q., Liu, Y., Zhao, X., and Wang, G. (2014). Morphology, type and distribution of the labial-palp pit organ and its sensilla in the oriental armyworm, *Mythimna separata* (Lepidoptera: Noctuidae). *Acta Entomol. Sin.* 57, 681–687. doi: 10.16380/j.kcxb.2014.06.012

Faucheux, M. J. (2008). Mouthparts and associated sensilla of a South American moth *Synempora andesae* (Lepidoptera: Neopseustidae). *Rev. Soc. Entomol. Argent.* 67, 21–33. doi: 10.1590/S0373-56802008000100003

Galizia, C. G., and Rossler, W. (2010). Parallel olfactory systems in insects: anatomy and function. *Annu. Rev. Entomol.* 55, 399–420. doi: 10.1146/annurev-ento-112408-085442

Ganiger, P. C., Yeshwanth, H. M., Muralimohan, K., Vinay, N., Kumar, A. R. V., and Chandrashekara, K. (2018). Occurrence of the new invasive pest, fall armyworm, *Spodoptera frugiperda* (JE Smith) (Lepidoptera: Noctuidae), in the maize fields of Karnataka, India. *Curr. Sci.* 115, 621–623. doi: 10.18520/cs/v115/i4/621-623

Goergen, G., Kumar, P. L., Sankung, S. B., Togola, A., and Tamo, M. (2016). First report of outbreaks of the fall armyworm *Spodoptera frugiperda* (J E Smith) (Lepidoptera, Noctuidae), a new alien invasive pest in west and central Africa. *PLoS One* 11:e0165632. doi: 10.1371/journal.pone.0165632

Guerenstein, P. G., Christensen, T. A., and Hildebrand, J. G. (2004). Sensory processing of ambient CO_2 information in the brain of the moth *Manduca sexta*. *J. Comp. Physiol. A* 190, 707–725. doi: 10.1007/s00359-004-0529-0

Guerenstein, P. G., and Hildebrand, J. G. (2008). Roles and effects of environmental carbon dioxide in insect life. *Annu. Rev. Entomol.* 53, 161–178. doi: 10.1146/annurev.ento.53.103106.093402

Guo, J. F., Zhao, J. Z., He, K. L., Zhang, F., and Wang, Z. Y. (2018a). Potential invasion of the crop-devastating insect pest fall armyworm *Spodoptera frugiperda* to China. *Plant Prot.* 44, 1–10. doi: 10.16688/j.zwbh.2018452

Guo, M. B., Chen, Q. Y., Liu, Y., Wang, G. R., and Han, Z. J. (2018b). Chemoreception of mouthparts: sensilla morphology and discovery of chemosensory genes in proboscis and labial palps of adult *Helicoverpa armigera* (Lepidoptera: Noctuidae). *Front. Physiol.* 9:970. doi: 10.3389/fphys.2018.00970

Jin, M. H., Tao, J. H., Li, Q., Cheng, Y., Sun, X. X., Wu, K. M., et al. (2019). Genome editing of the *SfABCC2* gene confers resistance to *Cry1F* toxin from *Bacillus thuringiensis* in *Spodoptera frugiperda*. *J. Integr. Agr.* 20, 815–820. doi: 10.1016/S2095-3119(19)62772-3

Jones, W. D., Cayirlioglu, P., Kadow, I. G., and Vosshall, L. B. (2007). Two chemosensory receptors together mediate carbon dioxide detection in *Drosophila*. *Nature* 445, 86–90. doi: 10.1038/nature05466

Kent, K. S., Harrow, I. D., Quartararo, P., and Hildebrand, J. G. (1986). An accessory olfactory pathway in Lepidoptera: the labial pit organ and its central projections in *Manduca sexta* and certain other sphinx moths and silk moths. *Cell Tissue Res.* 245, 237–245. doi: 10.1007/BF00213927

Kent, L. B., Walden, K. K., and Robertson, H. M. (2008). The Gr family of candidate gustatory and olfactory receptors in the yellow-fever mosquito *Aedes aegypti*. *Chem. Senses* 33, 79–93. doi: 10.1093/chemse/bjm067

Kwon, J. Y., Dahanukar, A., Weiss, L. A., and Carlson, J. R. (2007). The molecular basis of CO_2 reception in *Drosophila*. *Proc. Natl. Acad. Sci.* 104, 3574–3578. doi: 10.1073/pnas.0700079104

Lee, J. K., Selzer, R., and Altner, H. (1985). Lamellated outer dendritic segments of a chemoreceptor within wall-pore sensilla in the labial palp-pit organ of the butterfly, *Pieris rapae* L. (Insecta, Lepidoptera). *Cell Tissue Res.* 240, 333–342. doi: 10.1007/BF00222343

Li, G. P., Ji, T. J., Sun, X. X., Jiang, Y. Y., Wu, K. M., and Feng, H. Q. (2019). Susceptibility evaluation of invaded *Spodoptera frugiperda* population in Yunnan province to five *Bt* toxins. *Plant Prot.* 45, 15–20. doi: 10.16688/j.zwbh.2019201

Liu, N. Y., Xu, W., Papanicolaou, A., Dong, S. L., and Anderson, A. (2014). Identification and characterization of three chemosensory receptor families in the cotton bollworm *Helicoverpa armigera*. *BMC Genomics* 15:597. doi: 10.1186/1471-2164-15-597

Liu, Y. J., Zhang, D. D., Yang, L. Y., Dong, Y. H., Liang, G. M., Donkersley, P., et al. (2020). Analysis of phototactic responses in *Spodoptera frugiperda* using *Helicoverpa armigera* as control. *J. Integr. Agr.* 20, 821–828. doi: 10.1016/S2095-3119(19)62863-7

Liu, Z., Wang, X., Lei, C., and Zhu, F. (2017). Sensory genes identification with head transcriptome of the migratory armyworm *Mythimna separata*. *Sci. Rep.* 7:46033. doi: 10.1038/srep46033

Macwilliam, D., Kowalewski, J., Kumar, A., Pontrello, C., and Ray, A. (2018). Signaling mode of the broad-spectrum conserved CO_2 receptor is one of the important determinants of odor valence in *Drosophila*. *Neuron* 97, 1153.e4–1167.e4. doi: 10.1016/j.neuron.2018.01.028

Montezano, D. G., Specht, A., Sosa-Gómez, D. R., Roque-Specht, V. F., Sousa-Silva, J. C., Paula-Moraes, S. V., et al. (2018). Host plants of *Spodoptera frugiperda* (Lepidoptera: Noctuidae) in the Americas. *Afr. Entomol.* 26, 286–300. doi: 10.4001/003.026.0286

Myers, J. H., Monro, J., and Murray, N. (1981). Egg clumping, host plant selection and population regulation in *Cactoblastis cactorum* (Lepidoptera). *Oecologia* 51, 7–13. doi: 10.1007/BF00344644

Nagoshi, R. N., Koffi, D., Agboka, K., Tounou, K. A., Banerjee, R., Jurat-Fuentes, J. L., et al. (2017). Comparative molecular analyses of invasive fall armyworm in Togo reveal strong similarities to populations from the eastern United States and the Greater Antilles. *PLoS One* 12:e0181982. doi: 10.1371/journal.pone.0181982

Ning, C., Yang, K., Xu, M., Huang, L. Q., and Wang, C. Z. (2016). Functional validation of the carbon dioxide receptor in labial palps of *Helicoverpa armigera* moths. *Insect Biochem. Mol. Biol.* 73, 12–19. doi: 10.1016/j.ibmb.2016.04.002

Robertson, H. M., and Kent, L. B. (2009). Evolution of the gene lineage encoding the carbon dioxide receptor in insects. *J. Insect Sci.* 9:19. doi: 10.1673/031.009.1901

Song, Y. Q., Sun, H. Z., and Wu, J. X. (2016). Ultrastructural characteristics of the proboscis and the labial palp pit organ in the oriental fruit moth, *Grapholita molesta*. *Bull. Insectol.* 69, 59–66.

Spaethe, J., and Briscoe, A. D. (2004). Early duplication and functional diversification of the opsin gene family in insects. *Mol. Biol. Evol.* 21, 1583–1594. doi: 10.1093/molbev/msh162

Sparks, A. N. (1979). A review of the biology of the fall armyworm. *Fla. Entomol.* 62, 82–87. doi: 10.2307/3494083

Stange, G. (1997). Effects of changes in atmospheric carbon dioxide on the location of hosts by the moth, *Cactoblastis cactorum*. *Oecologia* 110, 539–545. doi: 10.1007/s004420050192

Stange, G., Monro, J., Stowe, S., and Osmond, C. B. (1995). The CO_2 sense of the moth *Cactoblastis cactorum* and its probable role in the biological control of the CAM plant *Opuntia stricta*. *Oecologia* 102, 341–352. doi: 10.1007/BF00329801

Stange, G., and Stowe, S. (1999). Carbon-dioxide sensing structures in terrestrial arthropods. *Microsc. Res. Tech.* 47, 416–427. doi: 10.1002/(SICI)1097-0029(19991215)47:6<416::AID-JEMT5>3.0.CO;2-X

Stokstad, E. (2017). New crop pest takes Africa at lightning speed. *Science* 356, 473–474. doi: 10.1126/science.356.6337.473

Sun, X. X., Hu, C. X., Jia, H. R., Wu, Q. L., Shen, X. J., Zhao, S. Y., et al. (2019a). Case study on the first immigration of fall armyworm *Spodoptera frugiperda* invading into China. *J. Integr. Agr.* 20, 664–672. doi: 10.1016/S2095-3119(19)62839-X

Sun, X. X., Zhao, S. Y., Jin, M. H., Zhao, H. Y., Li, G. P., Zhang, H. W., et al. (2019b). Larval spatial distribution pattern and sampling technique of the fall armyworm *Spodoptera frugiperda* in maize fields. *Plant Prot.* 45, 13–18. doi: 10.16688/j.zwbh.2019115

Syed, Z., and Leal, W. S. (2007). Maxillary palps are broad spectrum odorant detectors in *Culex quinquefasciatus*. *Chem. Senses* 32, 727–738. doi: 10.1093/chemse/bjm040

Tauxe, G. M., Macwilliam, D., Boyle, S. M., Guda, T., and Ray, A. (2013). Targeting a dual detector of skin and CO_2 to modify mosquito host seeking. *Cell* 155, 1365–1379. doi: 10.1016/j.cell.2013.11.013

Thom, C., Guerenstein, P. G., Mechaber, W. L., and Hildebrand, J. G. (2004). Floral CO_2 reveals flower profitability to moths. *J. Chem. Ecol.* 30, 1285–1288. doi: 10.1023/B:JOEC.0000030298.77377.7d

Turner, S. L., and Ray, A. (2009). Modification of CO_2 avoidance behaviour in *Drosophila* by inhibitory odorants. *Nature* 461, 277–281. doi: 10.1038/nature08295

Xu, W., and Anderson, A. (2015). Carbon dioxide receptor genes in cotton bollworm *Helicoverpa armigera*. *Sci. Nat.* 102:11. doi: 10.1007/s00114-015-1260-0

Yan, X. Z., Wang, Z. Y., Duan, Y., Feng, X. M., Deng, C. P., Wu, A. H., et al. (2019). Ultrastructure of sensilla on labial palps and the central projection of their sensory neurons in *Plutella xylostella* (Lepidoptera: Plutellidae) adults. *Acta Entomol. Sin.* 62, 205–214. doi: 10.16380/j.kcxb.2019.02.007

Zhang, J., Wang, B., Dong, S., Cao, D., Dong, J., Walker, W. B., et al. (2015). Antennal transcriptome analysis and comparison of chemosensory gene families in two closely related noctuidae moths, *Helicoverpa armigera* and *H. assulta*. *PLoS One* 10:e0117054. doi: 10.1371/journal.pone.0117054

Zhang, X. X., and Wang, G. R. (2020). Advances in research on the identification and function of ionotropic receptors in insects. *Chinese J. Appl. Entomol.* 57, 1046–1055. doi: 10.7679/j.issn.2095-1353.2020.105

Zhao, W. J., He, S. Q., Lu, Z. H., Liu, M. R., Ma, L. Q., Wang, J., et al. (2019). Direct effects of elevated CO_2 concentration on development of fall armyworm *Spodoptera frugiperda* (J. E. Smith). *J. Environ. Ent.* 41, 736–741. doi: 10.3969/j.issn.1674-0858.2019.04.7

Zhao, X. C., Tang, Q. B., Berg, B. G., Liu, Y., Wang, Y. R., Yan, F. M., et al. (2013). Fine structure and primary sensory projections of sensilla located in the labial-palp pit organ of *Helicoverpa armigera* (Insecta). *Cell Tissue Res.* 282, 237–249. doi: 10.1007/BF00319115

Conflict of Interest: The authors declare that the research was conducted in the absence of any commercial or financial relationships that could be construed as a potential conflict of interest.

Publisher's Note: All claims expressed in this article are solely those of the authors and do not necessarily represent those of their affiliated organizations, or those of the publisher, the editors and the reviewers. Any product that may be evaluated in this article, or claim that may be made by its manufacturer, is not guaranteed or endorsed by the publisher.

frontiers in Physiology

REVIEW
published: 09 August 2021
doi: 10.3389/fphys.2021.703768

The Olfactory Chemosensation of Hematophagous Hemipteran Insects

Feng Liu[1,2†], Zhou Chen[1,3†], Zi Ye[1,2] and Nannan Liu[1]*

[1]Department of Entomology and Plant Pathology, Auburn University, Auburn, AL, United States, [2]Department of Biological Sciences, Vanderbilt University, Nashville, TN, United States, [3]Cardiovascular Research Institute, University of California, San Francisco, San Francisco, CA, United States

As one of the most abundant insect orders on earth, most Hemipteran insects are phytophagous, with the few hematophagous exceptions falling into two families: Cimicidae, such as bed bugs, and Reduviidae, such as kissing bugs. Many of these blood-feeding hemipteran insects are known to be realistic or potential disease vectors, presenting both physical and psychological risks for public health. Considerable researches into the interactions between hemipteran insects such as kissing bugs and bed bugs and their human hosts have revealed important information that deepens our understanding of their chemical ecology and olfactory physiology. Sensory mechanisms in the peripheral olfactory system of both insects have now been characterized, with a particular emphasis on their olfactory sensory neurons and odorant receptors. This review summarizes the findings of recent studies of both kissing bugs (including *Rhodnius prolixus* and *Triatoma infestans*) and bed bugs (*Cimex lectularius*), focusing on their chemical ecology and peripheral olfactory systems. Potential chemosensation-based applications for the management of these Hemipteran insect vectors are also discussed.

Keywords: bed bug, kissing bug, host-seeking behavior, peripheral olfactory system, olfaction, push-pull strategies, reverse chemical ecology

OPEN ACCESS

Edited by:
Peng He,
Guizhou University, China

Reviewed by:
Dingze Mang,
Tokyo University of Agriculture and Technology, Japan
Nai-Yong Liu,
Southwest Forestry University, China
Ana Claudia A. Melo,
Federal University of Rio de Janeiro, Brazil
Herbert Venthur,
University of La Frontera, Chile

***Correspondence:**
Nannan Liu
liunann@auburn.edu

†These authors have contributed equally to this work

Specialty section:
This article was submitted to Invertebrate Physiology, a section of the journal Frontiers in Physiology

Received: *30 April 2021*
Accepted: *09 July 2021*
Published: *09 August 2021*

Citation:
Liu F, Chen Z, Ye Z and Liu N (2021) The Olfactory Chemosensation of Hematophagous Hemipteran Insects. Front. Physiol. 12:703768. doi: 10.3389/fphys.2021.703768

INTRODUCTION

The insect order Hemiptera, one of the most abundant insect orders, encompasses a wide range of different species. Although most hemipteran insects feed on plants or other insects, small invertebrates or even sugars (Díaz-Albiter et al., 2016), a few, such as kissing bugs and bed bugs, utilize blood sources from humans and/or animals [for more details, see the review provided in Reinhardt and Siva-Jothy (2007)]. Bed bugs (Cimicidae) have been reported to be resurgent in many developed countries due to the relaxation of monitoring systems, the development of insecticide resistance, and the increase in international travel in recent years (Doggett et al., 2004, 2012; Ter Poorten and Prose, 2005; Romero et al., 2007; Yoon et al., 2008; Haynes and Potter, 2013; Zhu et al., 2013). Kissing bugs, which are members of the *Triatominae* subfamily of the family Reduviidae, are typically found in the southern United States, Mexico, Central America, and South America (Justi et al., 2016; Monteiro et al., 2018).

Both kissing bugs and bed bugs are obligate blood-feeding ectoparasites of multiple hosts, including mammals, birds, and reptiles. For human beings, the major concerns related to these two hemipteran insects lie in their biting nuisance and their potential role as disease vectors. Bites from bed bugs result in the victims experiencing clinical symptoms such as

a wheal-and-flare response, infiltrated papules, vesicles, and/or blisters (Sansom et al., 1992; Alexander, 1994). In addition to the biting nuisance, bacterial infections such as impetigo, ecthyma, cellulitis, and lymphangitis may occur (Burnett et al., 1986). Another concern is the potential vector capacity of bed bugs. A preliminary study suggested that bed bugs probably share the same role as kissing bugs in transmitting *Trypanosoma cruzi*, the flagellate protozoan responsible for American trypanosomiasis, which is better known as Chagas disease. Using mice as their animal model, Salazar et al. (2014) found bed bugs to be a competent vector of *T. cruzi* and that they were able to efficiently and bi-directionally transmit *T. cruzi* to host mice. Most of the bed bugs fed on experimentally infected mice acquired the parasites, and a majority of the previously uninfected mice became infected after cohabitating with the exposed bed bugs in a laboratory environment. *T. cruzi* was also transmitted to mice who were directly exposed to the feces of infected bed bugs. Blakely et al. (2018) found live *T. cruzi* in the gut contents of bed bug adults fed with *T. cruzi*-contaminated blood and this persisted for at least 97 days post-infection in adult bed bugs. More importantly, they also found that nymphal stage bed bugs that were infected with *T. cruzi* maintained the parasite after molting, indicating the capacity for transstadial passage of *T. cruzi* in bed bugs.

As with bed bugs, the reaction to a kissing bug bite depends on the victim's sensitivity toward the substances introduced during the biting process. A typical light reaction to the kissing bug bite is papular lesions with a central punctum or grouped small vesicles; severe symptoms can include giant urticarial-type lesions with swelling at the site of inoculation; hemorrhagic nodular-to-bullous lesions; conjunctivitis, and a generalized morbilliform eruption (Shields and Walsh, 1956; Hemmige et al., 2012). Kissing bugs are known to be the primary vector of the pathogen *T. cruzi* (Stevens et al., 2011; Lidani et al., 2019). Surveys conducted in the United States have indicated that about half of the *Triatominae* species identified were carrying *T. cruzi* (Davis et al., 1943). Two of the epidemiologically important vectors are *Rhodnius prolixus* Stal and *Triatoma infestans* Klug (Coura, 2015). However, unlike the transmission cycle reported for bed bugs, *T. cruzi* is transmitted by kissing bug through various manners, including vector feces, food contamination, blood transfusion, of which oral transmission by food contamination plays the major role (Pereira et al., 2010; Shikanai-Yasuda and Carvalho, 2012).

As both kissing bugs and bed bugs pose a significant risk to humans and are thus a major concern for public health, remarkable progress has been made in recent decades in elucidating their chemical ecology and olfactory physiology. This review focuses on recent advances in: 1) the factors that regulate the host-seeking behavior of bed bugs and kissing bugs; 2) the mechanisms of peripheral chemosensory system in kissing bug and bed bug, including olfactory sensilla, olfactory receptor neurons (ORNs), odorant binding proteins (OBPs) and chemosensory proteins (CSPs), odorant receptors (ORs), ionotropic receptors (IRs), and gustatory receptors (GRs); and 3) perspectives for chemosensation-based applications in the management of kissing bug and bed bugs. This emerging knowledge is expected to make a positive contribution to the control of these blood-feeding insects and thus reduce the potential disease transmissions.

Host-Seeking Behavior of Kissing Bugs and Bed Bugs

Since both kissing bugs and bed bugs rely on human or animal blood sources for survival and reproduction, host localization is a vital part of their daily activities. In the host-seeking process, heat, host odor, and carbon dioxide (CO_2) are important cues for both kissing bugs and bed bugs. Kissing bugs (*R. prolixus* and/or *T. infestans*) were found to be attracted to warm temperature (Wigglesworth and Gillett, 1934; Milne et al., 2009), host-related compounds (Bodin et al., 2009; Milne et al., 2009; Ortiz and Molina, 2010; Ortiz et al., 2011), and CO_2 (Wiesinger, 1956; Nunez, 1982; Guerenstein and Guerin, 2001; Barrozo and Lazzari, 2004; Guerenstein and Lazarri, 2009; Indacochea et al., 2017). Kissing bug nymphs are attracted by CO_2-free traps baited with three host-odor components (ammonia, L-(+)-lactic acid, and hexanoic acid) but not by traps containing either one component alone or two components, suggesting a synergistic effect of host odors in attracting kissing bugs (Guidobaldi and Guerenstein, 2013). Researchers have also found that bed bugs can distinguish temperature differences as low as 1–2°C *via* the thermosensors on their antennae (Sioli, 1937). Heat baited traps attract significantly more bed bugs than unheated traps (Wang et al., 2009; Anderson et al., 2017). CO_2 baited traps are also more attractive for bed bugs than non-CO_2 traps and CO_2 are more effective than heat in trapping assays (Wang et al., 2009). In addition, bed bugs respond to human skin swabs in the absence of all other host cues (DeVries et al., 2019). However, chemical lures baited with specific human odors displayed more complex results, with the trapping efficiency largely depending on the specific compounds incorporated into the lures. For instance, Wang et al. (2009) found that lures baited with two human odors, 1-octen-3-ol, and L-lactic acid, did not attract significantly more bed bugs than non-baited traps, while Anderson et al. (2017) reported that ammonium bicarbonate and a blend of (E)-2-hexenal and (E)-2-octenal at certain concentrations attracted more bed bugs than the untreated control. In another study, Singh et al. (2012) screened twelve chemicals, evaluated the interactions among chemical lures, CO_2, and heat in trapping bed bugs, and revealed a synergistic effect between chemical lures and CO_2 but not heat and CO_2.

Multiple factors have been determined to regulate the host-search activities of both kissing bugs and bed bugs, including food source availability, mating status, and temporal modulation. Studies have shown that starvation plays a critical role in affecting the olfactory responses of kissing bugs (*R. prolixus*) to host odors, with starved *R. prolixus* showing a significant preference for the host-odorant treated arm in a dual-choice olfactometer, while a random distribution was observed in non-starved kissing bugs (Reisenman et al., 2013). Similarly, bed bugs that have been starved for a week were

found to be more active in host-searching than those that had received a blood meal 2 days before testing (Romero et al., 2010). Bed bugs that have received a blood meal are also more likely to aggregate in shelters during the scotophase, while those that have not fed tend to spend more time out of the shelters (Reis and Miller, 2011).

Another factor in determining bed bugs' host-searching activities is mating status. The percentage of females that fed and the amount of blood they ingested were found to be significantly greater in mated females than in unmated females and far more mated than unmated females responded to human odors (DeVries et al., 2019; Saveer et al., 2021). Interestingly, starvation also has a strong impact on the response of mated or unmated female bed bugs to human odors. The response rate of unmated females to skin odor increased with longer starvation periods, while the opposite pattern was observed in mated females (Saveer et al., 2021). Temporal modulation also plays a critical role in determining host-seeking activity. Behavior-related antennal sensitivity is governed by a circadian clock or daily rhythm in multiple insect species, including moths, flies, cockroaches, bed bugs, and kissing bugs (Brady, 1975; Hawkins and Rust, 1977; Van der Goes van Naters et al., 1998; Krishnan et al., 1999; Page and Koelling, 2003; Rosén et al., 2003; Bodin et al., 2008). An endogenous circadian clock has also been found to affect the insect's orientation toward CO_2, but only during the scotophase for both *T. infestans* and *R. prolixus* (Barrozo et al., 2004; Barrozo and Lazzari, 2004; Bodin et al., 2008). In addition, Reisenman (2014) reported that the electroantennogram (EAG) response of starved *R. prolixus* to ammonia (a host odor) was significantly higher than in insects fed only during the night. This modulation of sensory responses at the neural level is believed to trigger host search behavior in starved kissing bugs. In bed bugs, their spontaneous locomotor activity is known to be determined by an inner circadian rhythm, with both adults and nymphs being much more active in the dark than in the light phase (Romero et al., 2010). This is thought to enhance their chance of locating a sleeping human host (Romero et al., 2010).

Mechanism of Peripheral Olfactory System

Kissing bugs and bed bugs, like other insects, sense their chemical environment through their peripheral olfactory system. Their major olfactory appendages are their antennae, where various morphological or functional types of olfactory sensilla are located (**Figures 1A,B**). Olfactory sensory neurons (OSNs) are housed in each olfactory sensillum and OBPs/CSPs are secreted into the sensillum lymph by the accessory cells. Specific or unique olfactory receptors, including ORs, IRs, and CO_2-specific GRs, are expressed on the membrane of these OSNs (**Figure 1C**). Odorants surrounding the antennae pass through the pores on the sensillum surface and potentially bind with the OBPs/CSPs, after which they are delivered to active sites on the olfactory receptors (Brito et al., 2016). When olfactory receptors are activated by specific ligands, the cation channel formed by the olfactory receptors will be open (Nakagawa et al., 2005; Sato et al., 2008), which leads to the depolarization of OSNs and generation of action potentials. The chemical information is then transformed into electrical signals in the OSNs and transmitted along the axons into the antennal lobe in the central nervous system, where chemical information is further processed before the final behavioral decisions are made (Carey and Carlson, 2011; Leal, 2013). While the peripheral olfactory system of kissing bug is comparable with other blood-feeding insects (e.g. mosquito *Anopheles gambiae*) in term of the amount of olfactory sensilla and ORs, bed bugs are found to possess a degenerative olfactory system with much fewer olfactory sensilla and ORs (Levinson et al., 1974; Benoit et al., 2016).

Olfactory Sensilla and Olfactory Receptor Neurons

The olfactory sensilla make up a key structure that plays a critical role in the chemosensation of the insect antennae. Based on their morphological shape, the common bed bug (*C. lectularius*) has three types of olfactory sensilla: D, C, and E (**Table 1**). Of these, the majority are distributed along the distal portion of flagellomere II, with just a few located in the pedicel (Harraca et al., 2010; Liu et al., 2013; Olson et al., 2014). Each different type of sensillum houses a varying number of neurons. Three functional types of D sensilla (Dα, Dβ, Dγ), two types of C sensillum (C1, C2), and two E sensilla (E1, E2) have been identified on flagellomere II. A refined distribution map for each type of sensillum was described by Liu et al. (2017c). Dα, Dβ, Dγ, C1, C2, E1, and E2 have all been identified as olfactory sensilla, while the third type of E sensillum (E3) is thought to be a gustatory sensillum (Singh et al., 1996; Olson et al., 2014). The numbers of olfactory sensilla presenting on the antenna gradually increase as *C. lectularius* progresses from the first nymph instar to the adult stage, but no sexual dimorphism has been observed in either the sensillum number or their distribution along the antenna (Liu et al., 2017c). This is also the case for another bed bug species, the tropical bed bug (*C. hemipterus*), where the number of chemo-sensilla (olfactory and gustatory sensilla) on the antenna again increase from the nymph to the adult stage, with no sexual dimorphism (Mendki et al., 2013). However, the chemo-sensilla are distributed across all four segments of the antennae in the tropical bed bugs, while no chemo-sensilla have been found in either the base or the flagellomere I of the common bed bug antenna (Mendki et al., 2013; Olson et al., 2014). There are also reports of a few chemo-sensilla being seen in the rostrum of the tropical bed bug but not in the common bed bug (Mendki et al., 2013).

In kissing bugs, four morphological types of sensillum have been characterized in the antenna, namely trichoidea, basiconica, coeloconica, and cave organ (**Table 1**; Barrozo et al., 2017). Trichoidea and basiconica are the most common types on flagellomeres I and II, both of which function as chemoreceptors. Two subtypes of trichoidea, multi- and uni-porous, have been identified based on the number of pores on individual sensilla (Guidobaldi et al., 2014). Multi-porous trichoidea sensilla sense odors, whereas uni-porous sensilla (with a single pore at the tip) detect tastants (Mayer, 1968; Taneja and Guerin, 1997;

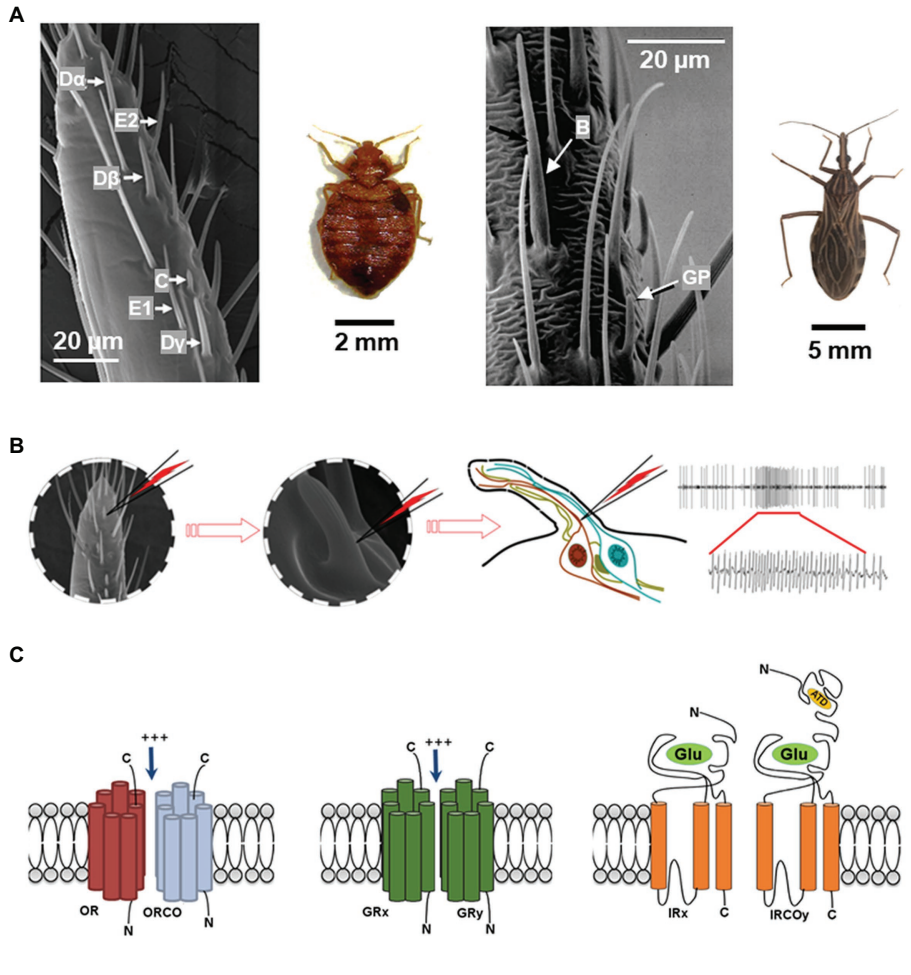

D

Species	OBP/CSP	OR	IR	GR
Rhodnius prolixus	27/19	111	33	31
Cimex lectularius	11/14	49	30	36

FIGURE 1 | Olfactory mechanism of the peripheral olfactory system in bed bugs and kissing bugs. **(A)** Scanning electronic microscope images show six functional types of olfactory sensillum (Dα, Dβ, Dγ, E1, E2, and C) for bed bugs (left; Liu and Liu, 2015) and two types (Basiconica and grooved peg) for kissing bugs (right; adapted from Guerenstein and Guerin, 2001, with the permission from Dr. Guerin). **(B)** The olfactory receptor neurons housed in each olfactory sensillum are responsible for detecting the attractive cues and increasing the firing frequency of the action potentials. Left: one section of a bed bug antennae; middle: a single sensillum is shown at high magnification (x720); right: depiction showing that the recording tungsten electrode is inserted into the shaft of a sensillum to complete the electrical circuit and to extracellularly record the olfactory receptor neuron potentials. **(C)** Schematic diagrams of the structures of three olfactory receptors (OR/ORCO, GR, and IR/IRCO) expressed in the membranes of the neuron dendrites that are the molecular targets for host cues. **(D)** The total number of odorant binding proteins and olfactory receptors (OR/ORCO, GR, and IR/IRCO) identified in the genomes of *C. lectularius* and *R. prolixus*.

Guerenstein and Guerin, 2001; Diehl et al., 2003; Pontes et al., 2014). Sensilla coeloconica are assumed to perform a thermohygrom receptive function in *Triatominae*; basiconica may also perform the same function (Bernard, 1974; Mciver and Siemicki, 1985; Lazzari, 1990). Only one cave-like sense organ has been found on the pedicel segment and electrophysiological evidence supports a thermoreceptive role for this organ (Catalá and Schofield, 1994; Lazzari and Wicklein, 1994).

The distribution of sensory organs on triatomine antennae displays a genus-, sex-, and habitation-biased pattern. For example, the total number of trichoidea sensilla varies dramatically between *Triatoma* (400–800) and *Rhodnius*

TABLE 1 | Types and functions of the antennal sensilla in the common bed bug (Cimicidae) and kissing bug (Triatominae).

Sensillum	Type	Distribution	Number	Number of neurons	Function	References*
Cimicidae (common bed bug)	D	flagellomere II	6	8–19	Chemoreceptors (Olfaction)	[1–8]
	C	flagellomere II	9	4–5	Chemoreceptors (Olfaction)	
	E	Pedicel flagellomere II	34	1–3	Chemoreceptor (Olfaction and gustation)	
Triatominae (kissing bug)	Trichoidea	Pedicel flagellomere I/II	200–800	5–15	Chemoreceptors	[9–24]
	Basiconica	flagellomere I/II	40–130	5–6	Chemoreceptors and thermohygroreceptors	
	Coeloconica	Pedicel flagellomere I/II	5	3	Thermohygroreceptors	
	Cave organ	Pedicel	1	200–300	Thermoreceptors	

[1] Levinson et al., 1974; [2] Steinbrecht and Müller, 1976; [3] Singh et al., 1996; [4] Harraca et al., 2010; [5] Liedtke et al., 2011; [6] Olson et al., 2014; [7] Liu et al., 2014; [8] Liu and Liu, 2015; [9] Wigglesworth and Gillett, 1934; [10] Mayer, 1968; [11] Bernard, 1974; [12] Mciver and Siemicki, 1985; [13] Lazzari, 1990; [14] Catalá and Schofield, 1994; [15] Lazzari and Wicklein, 1994; [16] Catalá, 1997; [17] Taneja and Guerin, 1997; [18] Guerenstein and Guerin, 2001; [19] Carbajal De La Fuente and Catalá, 2002; [20] Diehl et al., 2003; [21] Catalá et al., 2004; [22] Villela et al., 2005; [23] Moreno et al., 2006; [24] Pontes et al., 2014.

(200–500; Catalá and Dujardin, 2001; Carbajal De La Fuente and Catalá, 2002; Catalá et al., 2004, 2005; Esteban et al., 2005; Villela et al., 2005; Moreno et al., 2006; Carbajal De La Fuente et al., 2008; Villacís et al., 2010; May-Concha et al., 2016). *Triatoma* males have trichoidea sensilla that are significantly more thin-walled than those of the females, especially on the pedicel segment (Catalá et al., 2004; Villela et al., 2005; May-Concha et al., 2016), whilst the number of thin-walled trichoidea sensilla in the *Rhodnius* species exhibit no difference between the sexes (Catalá et al., 2004; Villacís et al., 2010). Interestingly, *T. infestans* collected from domestic sites have more thin-walled trichoidea sensilla on the pedicel and more thick-walled trichoidea sensillum on both flagellomere I and II than those collected from sylvan sites (Catalá and Dujardin, 2001; Catalá and Torres, 2001) with the specific mechanism yet to be determined.

Potent sensitivities of the kissing bug olfactory sensillum to host odor plumes and a few unitary aldehyde and acid compounds have been described (Guerenstein and Guerin, 2001), while the bed bug olfactory sensilla are particularly sensitive to several chemical classes of odors in human emanation, especially aldehydes, alcohols, aromatics, and ketones (Liu and Liu, 2015), as well as plant-sourced terpenes and terpenoids (Liu et al., 2014). Similar patterns have also been reported for two mosquitoes, *Culex quinquefasciatus* and *Aedes aegypti* (Liu et al., 2013; Ye et al., 2016; Chen et al., 2018, 2019). As bed bugs possess far fewer olfactory sensilla/OSNs than either kissing bugs or mosquitoes, their capacity for odor discrimination is likely to be inferior. Indeed, a comparison of the distribution of multiple groups of compounds in the odor space of bed bugs, *C. quinquefasciatus* and *A. aegypti* indicates that bed bugs may be less capable of discriminating human-related aldehydes and aromatics and plant-related terpenoids than either *Culex* or *Aedes* mosquitoes (**Figure 2**). These differences in odor-discriminatory capacity probably lie in the much more abundant functional types of olfactory sensilla or OSNs in the antenna of *C. quinquefasciatus* and *A. aegypti* compared to bed bugs. Although as yet there is insufficient data to include kissing bugs in this comparison, it is reasonable to speculate that kissing bugs are likely to be endowed with a much stronger ability for odor discrimination than bed bugs as they have a comparable number of olfactory sensilla to mosquitoes and live in a similarly complex chemical environment.

Odorant-Binding Proteins and Chemosensory Proteins

Odorant-binding proteins (OBPs) and CSPs, low-molecular-weight soluble proteins that are secreted by the accessory cells, are highly concentrated in sensillum lymph. OBPs and CSPs function to transport hydrophobic odorants through the aqueous environment of the sensillum lymph to the ORs' recognition sites. According to the various models that have been proposed, an OR may be activated either by the odorant molecule itself or the OBP(CSP)/odorant complex (Leal, 2013). For instance, knockdown of OBP1 in the southern house mosquito

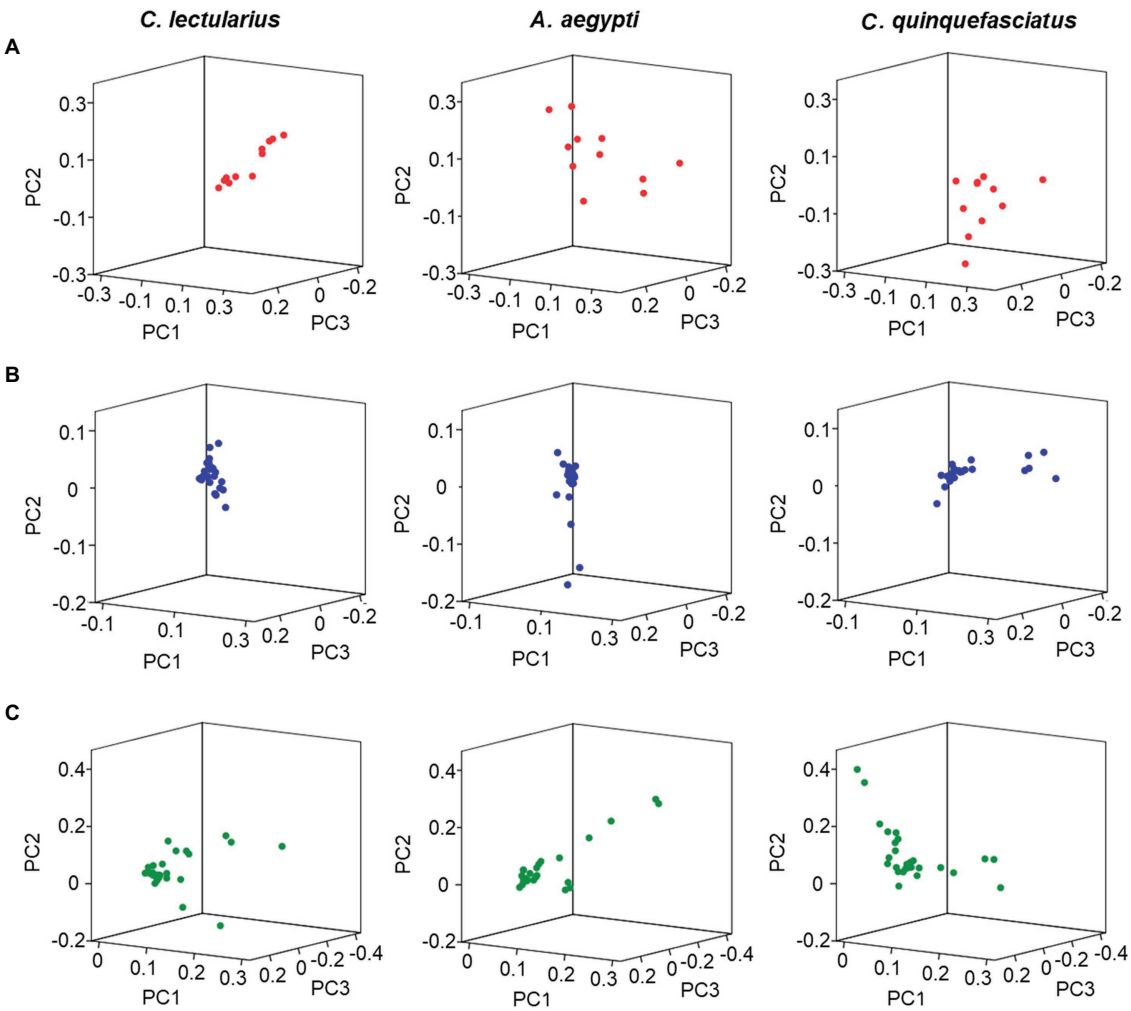

FIGURE 2 | Distribution of odorants in an ORN activity-based odor space. Odor spaces were constructed using the first three principal components of PCA (PAST 3.0, Carey et al., 2010) for the primary sensory responses generated by odorants (Liu et al., 2013, 2014; Liu and Liu, 2015; Ye et al., 2016; Chen et al., 2018, 2019). **(A)** Aldehydes; **(B)** aromatics; **(C)** terpenoids. All odorants from each chemical class are included. The mean inter-odorant distances in three-dimensional space for the set of aldehydes are 0.16 ± 0.01 for *C. lectularius*, 0.34 ± 0.02 for *A. aegypti*, and 0.22 ± 0.01 for *C. quinquefasciatus* (*A. aegypti* vs. *C. lectularius*, $p < 0.001$; *C. quinquefasciatus* vs. *C. lectularius*, $p < 0.001$, *t*-test). The mean inter-odorant distances for aromatics are 0.05 ± 0.00 for *C. lectularius*, 0.10 ± 0.01 for *A. aegypti*, and 0.10 ± 0.01 for *C. quinquefasciatus* (*A. aegypti* vs. *C. lectularius*, $p < 0.001$; *C. quinquefasciatus* vs. *C. lectularius*, $p < 0.001$, *t*-test). The mean inter-odorant distances for terpenoids are 0.11 ± 0.01 for *C. lectularius*, 0.14 ± 0.01 for *A. aegypti*, and 0.16 ± 0.01 for *C. quinquefasciatus* (*A. aegypti* vs. *C. lectularius*, $p < 0.001$; *C. quinquefasciatus* vs. *C. lectularius*, $p < 0.001$, *t*-test).

C. quinquefasciatus results in reduced EAG responses to mosquito oviposition pheromones (Pelletier et al., 2010) and silencing OBP1 leads to a failure to sense indole, a key component of human sweat, in the malaria mosquito *Anopheles gambiae* (Biessmann et al., 2010). In the tsetse fly, silencing the OBPs that interact with 1-octen-3-ol dramatically abolished flies' attraction to 1-octen-3-ol (Diallo et al., 2021), while in brown planthopper, silencing one CSP gene (*NlugCSP8*) induced significant decrease in the behavioral responses to some representative attractants (Waris et al., 2018). With many studies suggesting the essential roles of OBPs and CSPs in the chemosensation of some insect species, there are also opposite discoveries about the odor-transporting role of the OBPs (or CSPs). For example, it is also reported that a fly strain with all *obp* genes deleted still showed robust responses to odors from diverse chemical groups (Xiao et al., 2019), which suggests other functions of OBPs or CSPs beyond odor transportation in the olfactory sensillum. Actually, only a small number of OBPs or CSPs have been found in the olfactory appendages of various insects and some are expressed in non-sensory tissues such as sex pheromone glands of Lepidoptera, venom glands of wasps, and reproductive organs (Dippel et al., 2014; Brito et al., 2016; Sun et al., 2018), which are thus assumed to function as a carrier of internal chemicals other than external compounds (Pelosi et al., 2014). Other potential roles of OBPs or CSPs, such as contributing to the selectivity

of odorant sensation or acting as odorant-degrading enzymes, have also been proposed but remain to be confirmed (Leal, 2013; Larter et al., 2016; Scheuermann and Smith, 2019).

Genome sequencing has contributed greatly to research in this area, which identifies 11 OBPs and 14 CSPs in the common bed bug (*C. lectularius*) and 27 OBPs and 19 CSPs in kissing bugs (*R. prolixus*; **Figure 1D**; Mesquita et al., 2015; Benoit et al., 2016). Transcriptome sequencing of olfactory appendages (antennae or rostrum) in another kissing bug species, *Triatoma brasiliensis*, also identified 27 OBPs and 17 CSPs, most of which have well-supported orthologs in *R. prolixus* (Marchant et al., 2016). Proteomic analysis of the antenna of *R. prolixus* by Oliveira et al. (2017) identified 17 OBPs and 6 CSPs, representing 63 and 31% of all the OBPs and CSPs, respectively, in the genome sequence (Mesquita et al., 2015). Further work by Oliveira et al. (2018) indicated that of the 17 OBP genes identified in the *R. prolixus* adults, although 11 were expressed in all tissues, six were specific to antennae. Of the six antenna-expressing OBPs, two (*RproOBP6* and *RproOBP13*) were expressed in both sexes; two (*RproOBP17* and *RproOBP21*) were female antenna-enriched, and the rest (*RproOBP26* and *RproOBP27*) were male antenna-specific. *RproOBP27* was later confirmed to be involved in the detection of sex pheromones by functional studies (Oliveira et al., 2018). For bed bugs, the functions of OBPs and CSPs have not yet been explored. Given that multiple experimental approaches including RNA interference (Pelletier et al., 2010), CRISPR/Cas9 (Scheuermann and Smith, 2019; Xiao et al., 2019), and competitive binding assays using a fluorescent probe (Brito et al., 2016) have been successfully used to investigate the function of OBPs or CSPs from many other insect species, future studies using similar approaches should yield interesting results about the interactions between bed bug or kissing bug OBPs or CSPs and a wide variety of biologically relevant compounds that have been examined in either electrophysiological or behavioral studies. X-ray crystallography and nuclear magnetic resonance (NMR) are other powerful tools that can provide more details about the unbound or the agonist/antagonist-bound structural complex (Brito et al., 2016), Comparison of the unbound and ligand-bound OBP structures should help identify the amino acid residues involved in ligand binding. All these valuable information will help build our understanding of the mechanisms through which compounds are filtered and transported in the sensillum.

Odorant Receptors

Odorant receptors (ORs) have been extensively studied due to their role in detecting odors from diverse chemical groups (Carey et al., 2010; Joseph and Carlson, 2015; McBride, 2016; Liu et al., 2017a). ORs may evolve from IRs/GRs and are further diversified phylogenetically across different insect taxa (Hansson and Stensmyr, 2011; Missbach et al., 2014; **Figure 3**). However, the odorant receptor co-receptor (Orco) gene is highly conserved across insects (Jones et al., 2005; Leal, 2013). The ORCO protein is considered to play an important role in 1) the localization and stabilization of ORs in the neuron dendritic membranes; and 2) the transient binding and transduction of odorants *via* a heteromeric OR/ORCO complex (Larsson et al., 2004; Benton et al., 2006; see also the review in Stengl and Funk, 2013). Studies on the *Orco* gene of the kissing bug (*RproOrco*) revealed that when it has been silenced by RNA interference, the kissing bug is unable to locate a vertebrate host in a timely manner, leading to decreased blood ingestion, delayed and decreased molt rate, increased mortality rate, and decreased egg-laying (Franco et al., 2016). The expression level of the *RproOrco* gene is regulated by both the kissing bug's feeding status and developmental stage. A significant decrease in *RproOrco* expression has been observed after blood feeding, while an increase follows an imaginal molt (Latorre-Estivalis et al., 2015). In the common bed bug, the *Orco* gene has been found in both olfactory appendages (antennae and legs) and other non-olfactory related tissues (Hansen et al., 2014). Interestingly, phylogenetic analysis has indicated that *R. prolixus* and *C. lectularius Orco* are closely related, with a relatively close evolutionary distance compared to other insect species in different orders (Liu and Liu, 2015).

Whole-genome sequence analyses have revealed 115 and 49 ORs for *R. prolixus* and *C. lectularius*, respectively (**Figures 1D**; Mesquita et al., 2015; Benoit et al., 2016). The striking difference in OR number between these two hemipteran species is thought to be correlated with the complexity of the chemical environment in their respective habitats. The wingless *C. lectularius* lives in relatively closed and limited spaces, indoors or near the host, while the winged *R. prolixus* can fly long distances for host/mate searching (Gringorten and Friend, 1979; Zacharias et al., 2010). This natural selection may result in a comparatively stable chemosensory ecology in *C. lectularius*, which presents rare *OR* gene expansion in the genome compared to *R. prolixus* (Liu et al., 2017a). Benefiting from the availability of the genomic information for these species, the expression patterns for some of the *OR*s in *R. prolixus* have been characterized for different tissues and developmental stages. Using RT-PCR, Latorre-Estivalis et al. (2016) discovered that the *R. prolixus ORs* were expressed in every development stage from embryo to nymph and adult antennae. Most of these *OR*s were found not only in the antennae but also in other tissues such as the rostri, tarsi, tibial pads, and genitalia, suggesting that these appendages may also involve in the chemosensation-mediated behaviors of *R. prolixus*. Similarly, the *ORs* in *C. lectularius* have also been found to be expressed in other structures (e.g. legs) in addition to antennae (Liu and Liu, 2015).

Functional studies aimed at deciphering insect ORs generally use one of the following experimental approaches: 1) *Drosophila* "Empty Neuron" transgenic system, where exogenous OR genes are expressed in certain fly ORNs without the expression of any native ORs (Hallem and Carlson, 2006); 2) neuron-specific calcium imaging, which monitors calcium activity in GCaMP-expressed tissues or organs, mostly in flies and mosquitoes (Silbering and Galizia, 2007); 3) *Xenopus* oocyte expression systems, which are coupled with a two-electrode voltage clamp/patch clamp to detect the receptor current through the ion channels on oocyte membrane (Wang et al.,

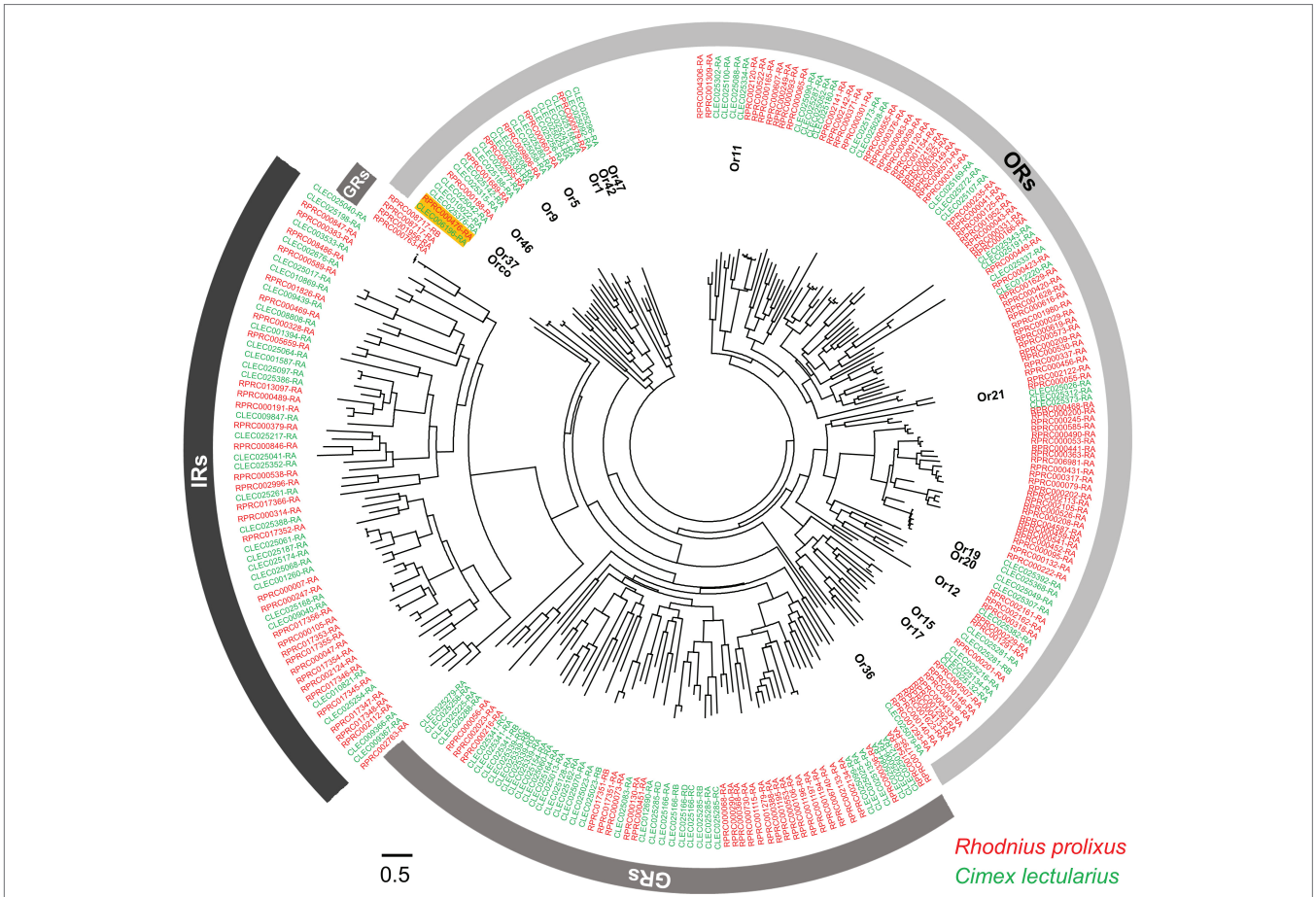

FIGURE 3 | Phylogenetic relationships within the ORs, IRs, and GRs of *R. prolixus* and *C. lectularius*. The dendrogram was computed using FastTree based on a MAFFT alignment of 272 amino acid sequences (VectorBase) from *R. prolixus* (accession number in red color) *and C. lectularius* (accession number in green color). The accession numbers of two *Orco* genes are highlighted. Fifteen ORs of *C. lectularius* that have been tested against around 150 odorants, including human odors and botanical chemical stimuli, are annotated (Liu et al., 2017a).

2010); 4) mammalian cell expression system coupled with patch clamp to measure the receptor current and ion conductance of the channels (Jones et al., 2011); 5) chemical informatics, which utilizes *in silico* modeling to screen large chemical space and identify potential ligands for receptors (Boyle et al., 2013); and 6) gene editing-mediated mutagenesis, which uses gene editing techniques such as clustered regularly interspaced short palindromic repeats/ CRISPR-associated protein 9 (CRISPR/Cas9), Transcription activator-like effector nucleases (TALEN), or zinc-finger nuclease (ZFN) to create mutants and then compares the phenotype changes between the wildtype and mutant insects (McMeniman et al., 2014; Liu et al., 2021). For example, functional studies have been used to investigate the role of four kissing bug ORs in perceiving sex pheromones using a *Xenopus* oocyte expression system coupled with a two-electrode voltage clamp (Franco et al., 2018). Although none of these ORs were identified as sex pheromone receptors, RproOR80 was found to be extremely sensitive to several compounds that turned out to be repellents for kissing bugs (Franco et al., 2018). In the common bed bug, 15 ORs have been successfully expressed in the *Xenopus* oocyte and challenged with a large panel of human odors (Liu et al., 2017a). In general, ORs with strong responses were tuned to aldehydes, ketones, alcohols, and aromatic compounds. Functional tests of these ORs in response to the components of aggregation pheromone also revealed that most of these components were encoded by multiple ORs with various tuning properties (Liu et al., 2017b). In addition, three ORs were identified as potent DEET receptors, even though DEET is not very effective in repelling bed bugs. Interestingly, these DEET-sensitive ORs presented even higher sensitivity to certain botanical terpenes/terpenoids that generally displayed much stronger repellency for bed bugs than DEET (Liu et al., 2017c).

Ionotropic Receptors and Gustatory Receptors

Ionotropic glutamate receptors (iGluRs) are chemosensory receptors that mediate neuronal communication between synapses in both vertebrate and invertebrate nervous systems. They comprise one of the three superfamilies used to classify IRs based on their predicted molecular structures, including an extracellular N-terminus, a cytoplasmic C-terminus, a

bipartite ligand-binding domain, and an ion channel. However, IRs differ from the well-documented kainate, α-amino-3-hydroxy-5-menthyl-isoxazole-4-propionate (AMPA), or N-menthyl-D-aspartate (NMDA) classes of iGluRs as they (1) lack the characteristic glutamate interacting residues but instead have divergent ligand-binding domains; and (2) accumulate in sensory dendrites rather than at synapses (Benton et al., 2009). Phylogenetic studies have revealed that IRs are conserved across bacteria, plants, and animals, which suggests an evolutionarily ancient function in chemosensation (Benton et al., 2009). IRs in coeloconic OSNs are known to be responsible for detecting organic acids, amines, and polyamines (Benton et al., 2009; Ai et al., 2010; Hussain et al., 2016). Like Orco, IR8a, IR25a, and IR76b are highly conserved across different species and are considered to function as co-receptors with other IRs in mediating the olfactory responses to semiochemicals (Croset et al., 2010). For example, in *D. melanogaster*, IR64a and IR8a are physically associated in the OSNs and constitute a functional channel when co-expressed *in vitro* in *Xenopus* oocytes (Ai et al., 2013). In *An. gambiae*, both *IR25a* and *IR76b* are required for the functional expression of *IR41a* and *IR41c* in *Xenopus* oocytes, while IR8a is needed for the expression of *IR75k* in oocytes (Pitts et al., 2017). In addition to its role as a co-receptor, *Drosophila* IR25a has been shown to function as a thermosensor as well as playing a role in establishing the insect's circadian rhythm (Chen et al., 2015), suggesting other potentially important functions of IRs in insect physiology.

In the kissing bug, *R. prolixus,* these three IR co-receptors (IRCO) genes (*IR8a*, *25a*, and *76b*) have been investigated to determine their expression patterns under different physiological and developmental conditions. IRCOs are known to be transcribed in the antennae of all nymph instar development stages and in both male and female kissing bugs (Latorre-Estivalis et al., 2016) and all three of these IRCOs are down-regulated by blood-feeding and up-regulated after the imaginal molt (Latorre-Estivalis et al., 2015), which underlines the plasticity of triatomine olfactory-mediated behaviors. In addition to the IRCOs, the expression patterns for 15 *R. prolixus* IRs in different tissues or sexual conditions have been characterized. Although most (11 out of 15) of these RproIRs were expressed in the antennae of all developmental instars, some exceptions have been reported. For example, no *RproIR75e* expression was observed in embryos and *RproIR20a* was not detected in first instar nymphs; neither *RproIR103* nor *RproIR104* were found in the antennae in either the nymph instars or adults of either sex (Latorre-Estivalis et al., 2016).

Based on the genomic data, 33 and 30 IRs have been annotated in *R. prolixus* and *C. lectularius*, respectively (**Figures 1D**). Functional studies of *Drosophila* IRs have suggested that organic acids and amine compounds are likely to be the primary ligands for IRs (Benton et al., 2009; Ai et al., 2010). Given that the C type sensilla in bed bugs show extreme sensitivity to amine compounds (Liu and Liu, 2015), certain IRs may be expressed in these sensilla. In the kissing bug, *R. prolixus*, ammonia and amines from vertebrate excretion were found to induce an obvious attraction response, suggesting that some factors in the kissing bug olfactory system (e.g. IRs) are actively sensing these compounds and guiding the host-searching behavior (Otálora-Luna and Guerin, 2014). However, as yet none of the IRs from either kissing bugs or bed bugs have been functionally characterized, further studies on these IRs are therefore necessary to clarify the response profiles of IRs in both insects.

In addition to ORs and IRs, GRs are involved in food searching and feeding stimulation. GRs are known to be responsible for detecting CO_2, amines, and polyamines, and compounds in food sources including sugars, bitter tastes, and toxins (Liman et al., 2014; MacWilliam et al., 2018). Based on their genome sequences, there are 36 and 31 GRs in *C. lectularius* and *R. prolixus* (**Figures 1D, 3**), respectively. Among these, no sugar receptors have been identified in either bed bugs (Benoit et al., 2016) or kissing bugs (Mesquita et al., 2015), which explains the lack of phagostimulation by glucose in *C. lectularius* (Romero and Schal, 2014). This lack of sugar receptors has also been documented in other obligate blood-feeders, including tsetse flies (Obiero et al., 2014) and lice (Kirkness et al., 2010). Interestingly, the CO_2 sensory GR subfamily is absent in *R. prolixus*, while the four putative CO_2 sensory GRs that have been identified in bed bugs are phylogenetically conserved with the CO_2 receptors in flies, moths, beetles, and one termite species (Terrapon et al., 2014). Future endeavors to investigate the response profiles of GRs from either kissing bugs or bed bugs would thus advance our understanding of chemoreception in both insects considerably.

Chemosensation-Based Applications

Due to the biting nuisance and risk of potential disease transmission, the effective management of both kissing bugs and bed bugs is one of the basic aims of research in this area and a long-term goal for scientists (Boase and Naylor, 2014; Zermoglio et al., 2015). Various strategies have been applied in the battle to control these two pests, with many based on the widespread use of insecticides. However, the intense application of insecticides leads to strong selection pressure, building up resistance in insect populations and dramatically impairing the efficiency of insecticides. Therefore, new approaches are continually being explored as a matter of urgency. Several promising approaches, such as push-pull or stimulo-deterrent diversionary (SDD) strategies (Cook et al., 2007; **Figure 4A**), are based on the latest research on insect chemosensation. Insects such as bed bugs and kissing bugs can be attracted by host odors (PULL) or repelled by repellents/deterrents (PUSH), while another option is to mask host odors using confusants (MASK). These novel approaches using chemicals, attractants, repellents, and/or confusants are expected to contribute to reducing the vector borne disease transmission.

Chemical Lures

As one of the most important cues released from human skin and breath, CO_2 is highly attractive to most hematophagous insects, including both kissing bugs and bed bugs

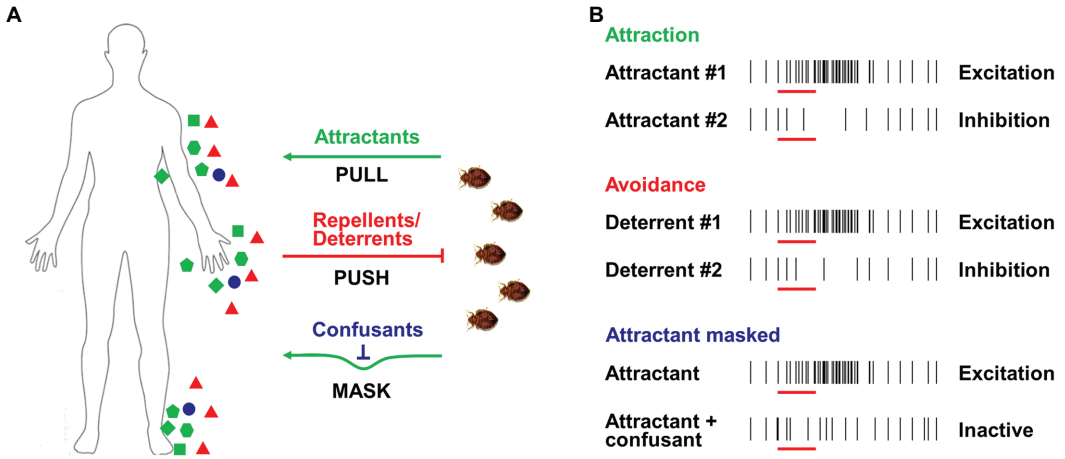

FIGURE 4 | Push-pull strategies and odor-evoked excitation/inhibition activity of ORNs. **(A)** Push-pull or stimulo-deterrent diversionary (SDD) strategies used for insect control; green dots indicate attractants from hosts (PULL), red dots indicate repellents/deterrents (PUSH), and blue dots indicate confusants (MASK). **(B)** Excitation or inhibition activities of ORNs caused by attractants, repellents/deterrents and confusants.

(Barrozo and Lazzari, 2004; Wang et al., 2009; Singh et al., 2013; Indacochea et al., 2017). It is therefore not surprising that CO_2 has been extensively incorporated in many of the bed bug traps that are commercially available as it displays high efficiency in terms of bug catches. Multiple host-related odorants that are generally added to the bait also exert a synergistic effect in attracting kissing bugs or bed bugs. For example, 1-octen-3-ol and nonanal, which are identified in human emanation (Bernier et al., 2000) and bed bug aggregation pheromone (Weeks et al., 2020), display strong activation on OSNs and ORs of bed bugs (Liu and Liu, 2015; Liu et al., 2017a). In laboratory two-choice behavioral assays, 1-octen-3-ol and nonanal have both been shown to attract bed bugs (Singh et al., 2012; **Figure 4B**). When a chemical mixture containing both 1-octen-3-ol and nonanal is combined with CO_2 in a bed bug trap, a synergistic effect has been reported, with increased trap catches (Singh et al., 2012). Since a large number of human odorants have been successively examined in bed bugs using electrophysiological approach and some of them elicit strong neuronal responses in different types of olfactory sensilla (Liu and Liu, 2015), future behavioral studies under laboratory conditions or in the field should identify some promising candidates with potent attraction for bed bugs.

In the kissing bug *T. infestans*, ammonia is reported to activate two types of grooved peg sensilla, making it a strong attractant for *T. infestans* (Taneja and Guerin, 1997). Another study found that a carbon dioxide-free attractant containing three human odorants (ammonia, L-(+)-lactic acid, and hexanoic acid) significantly increased bug catches for both *R. prolixus* and *T. infestans* (Guidobaldi and Guerenstein, 2013). In addition, male *R. prolixus* is attracted by a synthetic female-pheromone blend comprised of ten compounds, which elicit neuronal response from basiconic olfactory sensillum (Bohman et al., 2018). Taken together, these behavioral assays indicate the potential utility of using human odors or pheromone components to boost the performance of chemical lures for both bed bugs and kissing bugs, as well as highlighting the need to explore the potency of other OSNs/receptor-sensitive human odors.

Chemical Repellents/Confusants

Several different mechanisms have been proposed for chemical repellency in insect olfaction. First, certain compounds are known to block the attractant binding sites of OBP(s), resulting in insensitivity or reduced sensitivity to attractants. For example, it has been reported that in the mosquito *An. gambiae,* the synthetic repellent DEET and two natural repellents, 6-menthyl-5-heptene-2-one and eugenyl acetate, occupy the active binding site of OBP1, which is thought to be critical in preventing the transportation of some key attractant odorants (Murphy et al., 2012; Tsitsanou et al., 2012; Affonso et al., 2013). Second, some odorants may cause avoidance behavior by activating or inhibiting the ORN activities in insects (**Figure 4B**). For instance, in the mosquito *C. quinquefasciatus*, DEET is known to activate OR136b, triggering an aversive response (Xu et al., 2014); geraniol has also been shown to inhibit the activity of *Or10a*-ORN and *Or42b*-ORN and induce avoidance behavior in *Drosophila* (Cao et al., 2017). Third, some odorants may block/inhibit (or mask) the excitatory responses elicited by attractive compounds or alter the temporal structure of the insect's ORN response to attractants (**Figure 4B**). Ditzen et al. (2008) reported that DEET significantly blocks the neuronal response of *An. gambiae* to one human odorant (1-octen-3-ol), while Pellegrino et al. (2011) found that DEET appears to scramble the olfactory responses of *D. melanogaster* to some odors, although the precise mechanism is unclear. Bohbot et al. (2011) also suggested that DEET significantly inhibits the function of *Aedes* mosquitos' ORs in response to ligands. Odorants that alter the temporal structure of the ORN response may also affect insect olfaction-mediated behavior. It has been reported that in either mosquito or moth, some mimicking compounds evoke continual firing in the primary compound-sensitive ORN, which disrupts the

normal attractive behavioral response of those insects (Kramer, 1992; Turner et al., 2011).

In the common bed bug, certain ORNs and ORs were found to be directly activated by DEET while DEET also blocked the excitatory responses of ORNs and ORs to some human odors as well as manipulating the temporal dynamic of the odor-evoked neuronal response, which may result in the significant repellency of DEET agaist the bed bugs (Liu et al., 2017c). The same study also identified some components from essential oils, such as (+)-menthone, linalyl acetate and menthyl acetate, which effectively activated multiple ORNs and ORs and elicited very potent repellency against the bed bugs with a corresponding dose threshold of 10–100 fold lower than that of DEET (Liu et al., 2017c). In *R. prolixus*, one male-enriched OR (RproOR80) was functionally sensitized to 4-methylcyclohexanol, which turned out to be a strong repellent for kissing bugs by inducing a significant decrease in residence time to the host and a remarkable reduction in blood intake (Franco et al., 2018). This reverse chemical ecology strategy has also been adopted for identifying compounds with biological significance for other blood-feeding insects (Leal et al., 2008; Choo et al., 2018), agricultural insects (Xu et al., 2021), and mammals (Zhu et al., 2017). All these studies highlight the value of conducting further explorations of novel behaviorally active semiochemicals based on the reverse chemical ecology strategy for better controlling insect pests, such as bed bugs and kissing bugs and terminating the potential disease transmission.

AUTHOR CONTRIBUTIONS

NL, FL, ZC, and YZ: conceived and designed the study, wrote the paper and reviewed the manuscript. All authors contributed to the article and approved the submitted version.

FUNDING

This study was supported by AAES Hatch/Multistate grants ALA08-045 and ALA015-1-10026, and ALA015-1-16009 to NL.

REFERENCES

Affonso, R. D. S., Guimarães, A. P., Oliveira, A. A., Slana, G. B., and França, T. C. (2013). Applications of molecular modeling in the design of new insect repellents targeting the odorant binding protein of *Anopheles gambiae*. *J. Braz. Chem. Soc.* 24, 473–482. doi: 10.1590/S0103-50532013000300015

Ai, M., Blais, S., Park, J. Y., Min, S., Neubert, T. A., and Suh, G. S. (2013). Ionotropic glutamate receptors IR64a and IR8a form a functional odorant receptor complex *in vivo* in *Drosophila*. *J. Neurosci.* 33, 10741–10749. doi: 10.1523/JNEUROSCI.5419-12.2013

Ai, M., Min, S., Grosjean, Y., Leblanc, C., Bell, R., Benton, R., et al. (2010). Acid sensing by the *Drosophila* olfactory system. *Nature* 468, 691–695. doi: 10.1038/nature09537

Alexander, J. O. (ed.) (1994). "Infestation by Hemiptera," in *Arthropods and the human skin*. London: Springer Verlag. 57–74.

Anderson, J. F., Ferrandino, F. J., Vasil, M. P., Bedoukian, R. H., Maher, M., and Mckenzie, K. (2017). Relatively small quantities of CO2, Ammonium Bicarbonate, and a blend of (E)-2-Hexenal Plus (E)-2-Octenal attract bed bugs (Hemiptera: Cimicidae). *J. Med. Entomol.* 54, 362–367. doi: 10.1093/jme/tjw189

Barrozo, R. B., Minoli, S. A., and Lazzari, C. R. (2004). Circadian rhythm of behavioural responsiveness to carbon dioxide in the blood-sucking bug Triatoma infestans (Heteroptera: Reduviidae). *J. Insect Physiol.* 50, 249–254. doi: 10.1016/j.jinsphys.2004.01.001

Barrozo, R. B., and Lazzari, C. R. (2004). Orientation behaviour of the blood-sucking bug *Triatoma infestans* to short-chain fatty acids: synergistic effect of L-lactic acid and carbon dioxide. *Chem. Senses* 29, 833–841. doi: 10.1093/chemse/bjh249

Barrozo, R. B., Reisenman, C. E., Guerenstein, P., Lazzari, C. R., and Lorenzo, M. G. (2017). An inside look at the sensory biology of triatomines. *J. Insect Physiol.* 97, 3–19. doi: 10.1016/j.jinsphys.2016.11.003

Benoit, J. B., Adelman, Z. N., Reinhardt, K., Dolan, A., Poelchau, M., Jennings, E. C., et al. (2016). Unique features of a global human ectoparasite identified through sequencing of the bed bug genome. *Nat. Commn.* 7:10165. doi: 10.1038/ncomms10165

Benton, R., Sachse, S., Michnick, S. W., and Vosshall, L. B. (2006). Atypical membrane topology and heteromeric function of *Drosophila* odorant receptors *in vivo*. *PLoS Biol.* 4:e20. doi: 10.1371/journal.pbio.0040020

Benton, R., Vannice, K. S., Gomez-Diaz, C., and Vosshall, L. B. (2009). Variant ionotropic glutamate receptors as chemosensory receptors in *Drosophila*. *Cell* 136, 149–162. doi: 10.1016/j.cell.2008.12.001

Bernard, J. (1974). *Etude électrophysiologique des récepteurs impliqués dans la orientation vers l'hote et dans l'acte hematophage chez un Hémiptére Triatoma infesfans.* Thesis. Rennes, France: Université de Rennes.

Bernier, U. R., Kline, D. L., Barnard, D. R., Schreck, C. E., and Yost, R. A. (2000). Analysis of human skin emanations by gas chromatography/mass spectrometry. 2. Identification of volatile compounds that are candidate attractants for the yellow fever mosquito (*Aedes aegypti*). *Anal. Chem.* 72, 747–756. doi: 10.1021/ac990963k

Biessmann, H., Andronopoulou, E., Biessmann, M. R., Douris, V., Dimitratos, S. D., Eliopoulos, E., et al. (2010). The *Anopheles gambiae* odorant binding protein 1 (AgamOBP1) mediates indole recognition in the antennae of female mosquitoes. *PLoS One* 5:e9471. doi: 10.1371/journal.pone.0009471

Blakely, B. N., Hanson, S. F., and Romero, A. (2018). Survival and transstadial persistence of Trypanosoma cruzi in the bed bug (Hemiptera: Cimicidae). *J. Med. Entomol.* 55, 742–746. doi: 10.1093/jme/tjx252

Boase, C., and Naylor, R. (2014). *Bed bug management. Urban insect pests: Sustainable management strategies.* London, United Kingdom: CABI Press, 8–22.

Bodin, A., Vinauger, C., and Lazzari, C. R. (2009). State-dependency of host-seeking in *Rhodnius prolixus*: the post-ecdysis time. *J. Insect Physiol.* 55, 574–579. doi: 10.1016/j.jinsphys.2009.02.004

Bodin, A., Barrozo, R. B., Couton, L., and Lazzari, C. R. (2008). Temporal modulation and adaptive control of the behavioural response to odours in *Rhodnius prolixus*. *J. Insect Physiol.* 54, 1343–1348. doi: 10.1016/j.jinsphys.2008.07.004

Bohbot, J. D., Fu, L., Le, T. C., Chauhan, K. R., Cantrell, C. L., and Dickens, J. C. (2011). Multiple activities of insect repellents on odorant receptors in mosquitoes. *Med. Vet. Entomol.* 25, 436–444. doi: 10.1111/j.1365-2915.2011.00949.x

Bohman, B., Weinstein, A. M., Unelius, C. R., and Lorenzo, M. G. (2018). Attraction of Rhodnius prolixus males to a synthetic female-pheromone blend. *Parasit Vectors* 11, 1–7. doi: 10.1186/s13071-018-2997-z

Boyle, S. M., McInally, S., and Ray, A. (2013). Expanding the olfactory code by in silico decoding of odor-receptor chemical space. *elife* 2:e01120. doi: 10.7554/eLife.01120

Brady, J. (1975). Circadian changes in central excitability—the origin of behavioural rhythms in tsetse flies and other animals? *Physiol. Entomol.* 50, 79–95. doi: 10.1111/j.1365-3032.1975.tb00095.x

Brito, N. F., Moreira, M. F., and Melo, A. C. (2016). A look inside odorant-binding proteins in insect chemoreception. *J. Insect Physiol.* 95, 51–65. doi: 10.1016/j.jinsphys.2016.09.008

Burnett, J. W., Calton, G. J., and Morgan, R. J. (1986). Bedbugs. *Cutis* 38:20.

Carbajal De La Fuente, A. L., and Catalá, S. (2002). Relationship between antennal sensilla pattern and habitat in six species of *Triatominae*. *Mem. Inst. Oswaldo Cruz* 97, 1121–1125. doi: 10.1590/S0074-02762002000800010

Carbajal De La Fuente, A. L., Noireau, F., and Catalá, S. S. (2008). Inferences about antennal phenotype: the "*Triatoma maculata* complex," (Hemiptera: Triatominae) is valid? *Acta Trop.* 106, 16–21. doi: 10.1016/j.actatropica.2007.12.010

Carey, A. F., Wang, G., Su, C. Y., Zwiebel, L. J., and Carlson, J. R. (2010). Odorant reception in the malaria mosquito *Anopheles gambiae*. *Nature* 464, 66–71. doi: 10.1038/nature08834

Carey, A. F., and Carlson, J. R. (2011). Insect olfaction from model systems to disease control. *Proc. Natl. Acad. Sci. U. S. A.* 108, 12987–12995. doi: 10.1073/pnas.1103472108

Catalá, S. S. (1997). Antennal sensilla of *Triatominae* (Hemiptera, Reduviidae): a comparative study of five genera. *Int. J. Insect Morphol. Embryol.* 26, 67–73. doi: 10.1016/S0020-7322(97)00014-7

Catalá, S. S., Maida, D. M., Caro-Riano, H., Jaramillo, N., and Moreno, J. (2004). Changes associated with laboratory rearing in antennal sensilla patterns of *Triatoma infestans*, *Rhodnius prolixus*, and *Rhodnius pallescens* (Hemiptera, Reduviidae, Triatominae). *Mem. Inst. Oswaldo Cruz* 99, 25–30. doi: 10.1590/S0074-02762004000100005

Catalá, S., and Dujardin, J. P. (2001). Antennal sensilla patterns indicate geographic and ecotopic variability among *Triatoma infestans* (Hemiptera: Reduviidae) populations. *J. Med. Entomol.* 38, 423–428. doi: 10.1603/0022-2585-38.3.423

Catalá, S., and Schofield, C. (1994). Antennal sensilla of *Rhodnius*. *J. Morphol.* 219, 193–203. doi: 10.1002/jmor.1052190208

Catalá, S., and Torres, M. (2001). Similarity of the patterns of sensilla on the antennae of *Triatoma melanosoma* and *Triatoma infestans*. *Ann. Trop. Med. Parasitol.* 95, 287–295. doi: 10.1080/00034980120051296

Catalá, S., Sachetto, C., Moreno, M., Rosales, R., Salazar-Schettino, P. M., and Gorla, D. (2005). Antennal phenotype of *Triatoma dimidiata* populations and its relationship with species of phyllosoma and protracta complexes. *J. Med. Entomol.* 42, 719–725. doi: 10.1093/jmedent/42.5.719

Cao, L. H., Yang, D., Wu, W., Zeng, X., Jing, B. Y., Li, M. T., et al. (2017). Odor-evoked inhibition of olfactory sensory neurons drives olfactory perception in *Drosophila*. *Nat. Commun.* 8, 1–13. doi: 10.1038/s41467-017-01185-0

Chen, C., Buhl, E., Xu, M., Croset, V., Rees, J. S., Lilley, K. S., et al. (2015). *Drosophila* Ionotropic Receptor 25a mediates circadian clock resetting by temperature. *Nature* 527, 516–520. doi: 10.1038/nature16148

Chen, Z., Liu, F., and Liu, N. (2018). Neuronal responses of antennal olfactory sensilla to insect chemical repellents in the yellow fever mosquito, Aedes aegypti. *J. Chem. Ecol.* 44, 1120–1126. doi: 10.1007/s10886-018-1022-5

Chen, Z., Liu, F., and Liu, N. (2019). Human odour coding in the yellow fever mosquito, *Aedes aegypti*. *Sci. Rep.* 9:13336. doi: 10.1038/s41598-019-49753-2

Choo, Y. M., Xu, P., Hwang, J. K., Zeng, F., Tan, K., Bhagavathy, G., et al. (2018). Reverse chemical ecology approach for the identification of an oviposition attractant for *Culex quinquefasciatus*. *Proc. Natl. Acad. Sci. U. S. A.* 115, 714–719. doi: 10.1073/pnas.1718284115

Cook, S. M., Khan, Z. R., and Pickett, J. A. (2007). The use of push-pull strategies in integrated pest management. *Annu. Rev. Entomol.* 52, 375–400. doi: 10.1146/annurev.ento.52.110405.091407

Coura, J. R. (2015). The main sceneries of Chagas disease transmission. The vectors, blood and oral transmissions-A comprehensive review. *Mem. Inst. Oswaldo Cruz* 110, 277–282. doi: 10.1590/0074-0276140362

Croset, V., Rytz, R., Cummins, S. F., Budd, A., Brawand, D., Kaessmann, H., et al. (2010). Ancient protostome origin of chemosensory ionotropic glutamate receptors and the evolution of insect taste and olfaction. *PLoS Genet.* 6:e1001064. doi: 10.1371/journal.pgen.1001064

Davis, D. J., McGregor, T., and DeShazo, T. (1943). *Triatoma sanguisuga* (LeConte) and *Triatoma ambigua* Neiva as natural carriers of *Trypanosoma cruzi* in Texas. *Public Health Rep.* 58, 353–354. doi: 10.2307/4584383

DeVries, Z. C., Saveer, A. M., Mick, R., and Schal, C. (2019). Bed bug (Hemiptera: Cimicidae) attraction to human odors: validation of a two-choice olfactometer. *J. Med. Entomol.* 56, 362–367. doi: 10.1093/jme/tjy202

Diallo, S., Shahbaaz, M., Makwatta, J. O., Muema, J. M., Masiga, D., Christofells, A., et al. (2021). Antennal enriched odorant binding proteins are required for odor communication in *Glossina f. fuscipes*. *Biomolecules* 11:541. doi: 10.3390/biom11040541

Díaz-Albiter, H. M., Ferreira, T. N., Costa, S. G., Rivas, G. B., Gumiel, M., Cavalcante, D. R., et al. (2016). Everybody loves sugar: first report of plant feeding in triatomines. *Parasit Vectors* 9, 1–8. doi: 10.1186/s13071-016-1401-0

Diehl, P. A., Vlimant, M., Guerenstein, P., and Guerin, P. M. (2003). Ultrastructure and receptor cell responses of the antennal grooved peg sensilla of *Triatoma infestans* (Hemiptera: Reduviidae). *Arthropod Struct. Dev.* 31, 271–285. doi: 10.1016/S1467-8039(03)00004-5

Dippel, S., Oberhofer, G., Kahnt, J., Gerischer, L., Opitz, L., and Schachtner, J. (2014). Tissue-specific transcriptomics, chromosomal localization, and phylogeny of chemosensory and odorant binding proteins from the red flour beetle *Tribolium castaneum* reveal subgroup specificities for olfaction or more general functions. *BMC Genomics* 15, 1–14. doi: 10.1186/1471-2164-15-1141

Ditzen, M., Pellegrino, M., and Vosshall, L. B. (2008). Insect odorant receptors are molecular targets of the insect repellent DEET. *Science* 319, 1838–1842. doi: 10.1126/science.1153121

Doggett, S. L., Dwyer, D. E., Penas, P. F., and Russell, R. C. (2012). Bed bugs: clinical relevance and control options. *Clin. Microbiol. Rev.* 25, 164–192. doi: 10.1128/CMR.05015-11

Doggett, S. L., Geary, M. J., and Russell, R. C. (2004). The resurgence of bed bugs in Australia: with notes on their ecology and control. *Environ. Health* 4, 30–38. doi: 10.1016/j.actatropica.2009.10.014

Esteban, L., Angulo, V. M., Dora Feliciangeli, M., and Catalá, S. (2005). Analysis of antennal sensilla patterns of *Rhodnius prolixus* from Colombia and Venezuela. *Mem. Inst. Oswaldo Cruz* 100, 909–914. doi: 10.1590/S0074-02762005000800014

Franco, T. A., Oliveira, D. S., Moreira, M. F., Leal, W. S., and Melo, A. C. (2016). Silencing the odorant receptor co-receptor RproOrco affects the physiology and behavior of the Chagas disease vector *Rhodnius prolixus*. *Insect Biochem. Mol. Biol.* 69, 82–90. doi: 10.1016/j.ibmb.2015.02.012

Franco, T. A., Xu, P., Brito, N. F., Oliveira, D. S., Wen, X., Moreira, M. F., et al. (2018). Reverse chemical ecology-based approach leading to the accidental discovery of repellents for *Rhodnius prolixus*, a vector of Chagas diseases refractory to DEET. *Insect Biochem. Mol. Biol.* 103, 46–52. doi: 10.1016/j.ibmb.2018.10.004

Gringorten, J. L., and Friend, W. G. (1979). Wing-beat pattern in Rhodnius prolixus Stål (Heteroptera: Reduviidae) during exhaustive flight. *Can. J. Zool.* 57, 391–395. doi: 10.1016/j.jinsphys.2016.09.008

Guerenstein, P. G., and Guerin, P. M. (2001). Olfactory and behavioral responses of the blood-sucking bug *Triatoma infestans* to odours of vertebrate hosts. *J. Exp. Biol.* 204, 585–597. doi: 10.1242/jeb.204.3.585

Guerenstein, P. G., and Lazzari, C. R. (2009). Host-seeking: how triatomines acquire and make use of information to find blood. *Acta Trop.* 110, 148–158. doi: 10.1016/j.actatropica.2008.09.019

Guidobaldi, F., and Guerenstein, P. G. (2013). Evaluation of a CO2-free commercial mosquito attractant to capture triatomines in the laboratory. *J. Vector. Ecol.* 38, 245–250. doi: 10.1111/j.1948-7134.2013.12037.x

Guidobaldi, F., May-Concha, I. J., and Guerenstein, P. G. (2014). Morphology and physiology of the olfactory system of blood-feeding insects. *J. Physiol. Paris* 108, 96–111. doi: 10.1016/j.jphysparis.2014.04.006

Hallem, E. A., and Carlson, J. R. (2006). Coding of odors by a receptor repertoire. *Cell* 125, 143–160. doi: 10.1016/j.cell.2006.01.050

Hansen, I. A., Rodriguez, S. D., Drake, L. L., Price, D. P., Blakely, B. N., Hammond, J. I., et al. (2014). The odorant receptor co-receptor from the bed bug, *Cimex lectularius* L. *PloS One* 9:e113692. doi: 10.1371/journal.pone.0113692

Hansson, B. S., and Stensmyr, M. C. (2011). Evolution of insect olfaction. *Neuron* 72, 698–711. doi: 10.1016/j.neuron.2011.11.003

Harraca, V., Ignell, R., Löfstedt, C., and Ryne, C. (2010). Characterization of the antennal olfactory system of the bed bug (*Cimex lectularius*). *Chem. Senses* 35, 195–204. doi: 10.1093/chemse/bjp096

Hawkins, W. A., and Rust, M. K. (1977). Factors influencing male sexual response in the American cockroach *Periplaneta americana*. *J. Chem. Ecol.* 3, 85–99. doi: 10.1007/BF00988136

Haynes, K. F., and Potter, M. F. (2013). "Recent progress in bed bug management," in *Advanced Technologies for Managing Insect Pests* (New York: Springer), 269–278.

Hemmige, V., Tanowitz, H., and Sethi, A. (2012). Trypanosoma cruzi infection: a review with emphasis on cutaneous manifestations. *Int. J. Dermatol.* 51, 501–508. doi: 10.1111/j.1365-4632.2011.05380.x

Hussain, A., Zhang, M., Üçpunar, H. K., Svensson, T., Quillery, E., Gompel, N., et al. (2016). Ionotropic chemosensory receptors mediate the taste and smell of polyamines. *PLoS Biol.* 14, 1–30. doi: 10.1371/journal.pbio.1002454

Indacochea, A., Gard, C. C., Hansen, I. A., Pierce, J., and Romero, A. (2017). Short-range responses of the kissing bug *Triatoma rubida* (Hemiptera: Reduviidae) to carbon dioxide, moisture, and artificial light. *Insects* 8:E90. doi: 10.3390/insects8030090

Jones, W. D., Nguyen, T. A. T., Kloss, B., Lee, K. J., and Vosshall, L. B. (2005). Functional conservation of an insect odorant receptor gene across 250 million years of evolution. *Curr. Biol.* 15, 119–121. doi: 10.1016/j.cub.2005.02.007

Jones, P. L., Pask, G. M., Rinker, D. C., and Zwiebel, L. J. (2011). Functional agonism of insect odorant receptor ion channels. *Proc. Natl. Acad. Sci. U. S. A.* 108, 8821–8825. doi: 10.1073/pnas.1102425108

Joseph, R. M., and Carlson, J. R. (2015). *Drosophila* chemoreceptors: a molecular interface between the chemical world and the brain. *Trends Genet.* 31, 683–695. doi: 10.1016/j.tig.2015.09.005

Justi, S. A., Galvao, C., and Schrago, C. G. (2016). Geological changes of the Americas and their influence on the diversification of the Neotropical kissing bugs (Hemiptera: Reduviidae: Triatominae). *PLoS Negl. Trop. Dis.* 10:e0004527. doi: 10.1371/journal.pntd.0004527

Kirkness, E. F., Haas, B. J., Sun, W., Braig, H. R., Perotti, M. A., Clark, J. M., et al. (2010). Genome sequences of the human body louse and its primary endosymbiont provide insights into the permanent parasitic lifestyle. *Proc. Natl. Acad. Sci. U. S. A.* 107, 12168–12173. doi: 10.1073/pnas.1003379107

Kramer, E. (1992). Attractivity of pheromone surpassed by time-patterned application of two nonpheromone compounds. *J. Insect Behav.* 5, 83–97. doi: 10.1007/BF01049160

Krishnan, B., Dryer, S. E., and Hardin, P. E. (1999). Circadian rhythms in olfactory responses of *Drosophila melanogaster*. *Nature* 400:375. doi: 10.1038/22566

Larsson, M. C., Domingos, A. I., Jones, W. D., Chiappe, M. E., Amrein, H., and Vosshall, L. B. (2004). Or83b encodes a broadly expressed odorant receptor essential for *Drosophila* olfaction. *Neuron* 43, 703–714. doi: 10.1016/j.neuron.2004.08.019

Larter, N. K., Sun, J. S., and Carlson, J. R. (2016). Organization and function of Drosophila odorant binding proteins. *elife* 5:e20242. doi: 10.7554/eLife.20242

Latorre-Estivalis, J. M., Manuel, J., Omondi, B. A., DeSouza, O., Oliveira, I. H. R., Ignell, R., et al. (2015). Molecular basis of peripheral olfactory plasticity in *Rhodnius prolixus*, a Chagas disease vector. *Front. Ecol. Environ.* 3:74. doi: 10.3389/fevo.2015.00074

Latorre-Estivalis, J. M., de Oliveira, E. S., Esteves, B. B., Guimarães, L. S., Ramos, M. N., and Lorenzo, M. G. (2016). Patterns of expression of odorant receptor genes in a Chagas disease vector. *Insect Biochem. Mol. Biol.* 69, 71–81. doi: 10.1016/j.ibmb.2015.05.002

Lazzari, C. R. (1990). *Fisiologia del comportamiento de Triatoma infestarts (Klug, 1834; Heteroptera: Reduviidae), Orientation térmica*. Thesis University, Buenos Aires, Buenos Aires, Argentina.

Lazzari, C. R., and Wicklein, M. (1994). The cave-like sense organ in the antennae of *Triatominae* bugs. *Mem. Inst. Oswaldo Cruz* 89, 643–648. doi: 10.1590/S0074-02761994000400023

Leal, W. S. (2013). Odorant reception in insects: roles of receptors, binding proteins, and degrading enzymes. *Annu. Rev. Entomol.* 58, 373–391. doi: 10.1146/annurev-ento-120811-153635

Leal, W. S., Barbosa, R. M., Xu, W., Ishida, Y., Syed, Z., Latte, N., et al. (2008). Reverse and conventional chemical ecology approaches for the development of oviposition attractants for *Culex* mosquitoes. *PLoS One* 3:e3045. doi: 10.1371/journal.pone.0003045

Levinson, H. Z., Levinson, A. R., Müller, B., and Steinbrecht, R. A. (1974). Structure of sensilla, olfactory perception, and behaviour of the bed bug, *Cimex lectularius*, in response to its alarm pheromone. *J. Insect Physiol.* 20, 1231–1248. doi: 10.1016/0022-1910(74)90229-7

Lidani, K. C. F., Andrade, F. A., Bavia, L., Damasceno, F. S., Beltrame, M. H., Messias-Reason, I. J., et al. (2019). Chagas disease: from discovery to a worldwide health problem. *Front. Public Health* 7:166. doi: 10.3389/fpubh.2019.00166

Liedtke, H. C., Åbjörnsson, K., Harraca, V., Knudsen, J. T., Wallin, E. A., Hedenström, E., et al. (2011). Alarm pheromones and chemical communication in nymphs of the tropical bed bug *Cimex hemipterus* (Hemiptera: Cimicidae). *PLoS One* 6, 1–7. doi: 10.1371/journal.pone.0018156

Liman, E. R., Zhang, Y. V., and Montell, C. (2014). Peripheral coding of taste. *Neuron* 81, 984–1000. doi: 10.1016/j.neuron.2014.02.022

Liu, F., and Liu, N. (2015). Human odorant reception in the common bed bug, *Cimex lectularius*. *Sci. Rep.* 5, 1–14. doi: 10.1038/srep15558

Liu, F., Chen, L., Appel, A. G., and Liu, N. (2013). Olfactory responses of the antennal trichoid sensilla to chemical repellents in the mosquito. *Culex quinquefasciatus. J. Insect Physiol.* 59, 1169–1177. doi: 10.1016/j.jinsphys.2013.08.016

Liu, F., Chen, Z., and Liu, N. (2017a). Molecular basis of olfactory chemoreception in the common bed bug, *Cimex lectularius*. *Sci. Rep.* 7:45531. doi: 10.1038/srep45531

Liu, F., Haynes, K. F., Appel, A. G., and Liu, N. (2014). Antennal olfactory sensilla responses to insect chemical repellents in the common bed bug, *Cimex lectularius*. *J. Chem. Ecol.* 40, 522–533. doi: 10.1007/s10886-014-0435-z

Liu, F., Xia, X., and Liu, N. (2017b). Molecular basis of N, N-Diethyl-3-Methylbenzamide (DEET) in repelling the common bed bug, *Cimex lectulari*us. *Front. Physiol.* 8:418. doi: 10.3389/fphys.2017.00418

Liu, F., Xiong, C., and Liu, N. (2017c). Chemoreception to aggregation pheromones in the common bed bug, *Cimex lectularius*. *Insect Biochem. Mol. Biol.* 82, 62–73. doi: 10.1016/j.ibmb.2017.01.012

Liu, F., Wang, Q., Xu, P., Andreazza, F., Valbon, W. R., Bandason, E., et al. (2021). A dual-target molecular mechanism of pyrethrum repellency against mosquitoes. *Nat. Commun.* 12, 1–9. doi: 10.1038/s41467-021-22847-0

MacWilliam, D., Kowalewski, J., Kumar, A., Pontrello, C., and Ray, A. (2018). Signaling mode of the broad-spectrum conserved CO_2 receptor is one of the important determinants of odor valence in *Drosophila*. *Neuron* 97, 1153–1167.e4. doi: 10.1016/j.neuron.2018.01.028

Marchant, A., Mougel, F., Jacquin-Joly, E., Costa, J., Almeida, C. E., and Harry, M. (2016). Under-expression of chemosensory genes in domiciliary bugs of the Chagas disease vector *Triatoma brasiliensis*. *PLoS Negl. Trop. Dis.* 10, 1–26. doi: 10.1371/journal.pntd.0005067

May-Concha, I., Guerenstein, P. G., Ramsey, J. M., Rojas, J. C., and Catalá, S. (2016). Antennal phenotype of Mexican haplogroups of the *Triatoma dimidiata* complex, vectors of Chagas disease. *Infect. Genet. Evol.* 40, 73–79. doi: 10.1016/j.meegid.2016.02.027

Mayer, M. S. (1968). Response of single olfactory cell of *Triatoma infestans* to human breath. *Nature* 220, 924–925. doi: 10.1038/220924a0

McBride, C. S. (2016). Genes and odors underlying the recent evolution of mosquito preference for humans. *Curr. Biol.* 26, 41–46. doi: 10.1016/j.cub.2015.11.032

Mciver, S., and Siemicki, R. (1985). Fine structure of antennal putative thermo-/hygrosensilla of adult *Rhodnius prolixus* Stal (Hemiptera: Reduviidae). *J. Morphol.* 183, 15–23. doi: 10.1002/jmor.1051830103

McMeniman, C. J., Corfas, R. A., Matthews, B. J., Ritchie, S. A., and Vosshall, L. B. (2014). Multimodal integration of carbon dioxide and other sensory cues drives mosquito attraction to humans. *Cell* 156, 1060–1071. doi: 10.1016/j.cell.2013.12.044

Mendki, M. J., Prakash, S., Parashar, B. D., and Agarwal, O. P. (2013). Distribution of sensilla on antenna and rostrum in nymphs and adults of *Cimex hemipterus* Fabricius (Hemiptera, Cimicidae). *Dtsch. Entomol. Z.* 60, 213–219. doi: 10.1002/mmnd.201300027

Mesquita, R. D., Vionette-Amaral, R. J., Lowenberger, C., Rivera-Pomar, R., Monteiro, F. A., Minx, P., et al. (2015). Genome of *Rhodnius prolixus*, an insect vector of Chagas disease, reveals unique adaptations to hematophagy and parasite infection. *Proc. Natl. Acad. Sci. U. S. A.* 112, 14936–14941. doi: 10.1073/pnas.1506226112

Milne, M. A., Ross, E. J., Sonenshine, D. E., and Kirsch, P. (2009). Attraction of *Triatoma dimidiata* and *Rhodnius prolixus* (Hemiptera: Reduviidae) to combinations of host cues tested at two distances. *J. Med. Entomol.* 46, 1062–1073. doi: 10.1603/033.046.0513

Missbach, C., Dweck, H. K., Vogel, H., Vilcinskas, A., Stensmyr, M. C., Hansson, B. S., et al. (2014). Evolution of insect olfactory receptors. *elife* 3:e02115. doi: 10.7554/eLife.02115

Moreno, M. L., Gorla, D., and Catalá, S. (2006). Association between antennal phenotype, wing polymorphism and sex in the genus *Mepraia* (Reduviidae: Triatominae). *Infect. Genet. Evol.* 6, 228–234. doi: 10.1016/j.meegid.2005.06.001

Monteiro, F. A., Weirauch, C., Felix, M., Lazoski, C., and Abad-Franch, F. (2018). Evolution, systematics, and biogeography of the Triatominae, vectors of Chagas disease. *Adv. Parasitol.* 99, 265–344. doi: 10.1016/bs.apar.2017.12.002

Murphy, E. J., Booth, J. C., Davrazou, F., Port, A. M., and Jones, D. N. (2012). Interactions of *Anopheles gambiae* odorant binding proteins with a human-derived repellent: implications for the mode of action of DEET. *J. Biol. Chem.* 288, 4475–4485. doi: 10.1074/jbc.M112.436386

Nakagawa, T., Sakurai, T., and Nishioka, T. (2005). Insect sex-pheromone signals mediated by specific combinations of olfactory receptors. *Science* 307, 1638–1642. doi: 10.1126/science.1106267

Nunez, J. A. (1982). Food source orientation and activity in *Rhodnius prolixus* Stal (Hemiptera: Reduviidae) *Bull. Entomol. Res.* 72, 253–262. doi: 10.1017/S0007485300010555

Obiero, G. F., et al. (2014). Odorant and gustatory receptors in the tsetse fly *Glossina morsitans morsitans*. *PLoS Negl. Trop. Dis.* 8:2663. doi: 10.1371/journal.pntd.0002663

Oliveira, D. S., Brito, N. F., Nogueira, F. C. S., Moreira, M. F., Leal, W. S., Soares, M. R., et al. (2017). Proteomic analysis of the kissing bug *Rhodnius prolixus* antenna. *J. Insect Physiol.* 100, 108–118. doi: 10.1016/j.jinsphys.2017.06.004

Oliveira, D. S., Brito, N. F., Franco, T. A., Moreira, M. F., Leal, W. S., and Melo, A. C. (2018). Functional characterization of odorant binding protein 27 (RproOBP27) from *Rhodnius prolixus* antennae. *Front. Physiol.* 9:1175. doi: 10.3389/fphys.2018.01175

Olson, J. F., Moon, R. D., Kells, S. A., and Mesce, K. A. (2014). Morphology, ultrastructure and functional role of antennal sensilla in off-host aggregation by the bed bug, *Cimex lectularius*. *Arthropod Struct. Dev.* 43, 117–122. doi: 10.1016/j.asd.2013.12.004

Ortiz, M. I., and Molina, J. (2010). Preliminary evidence of *Rhodnius prolixus* (Hemiptera: Triatominae) attraction to human skin odour extracts. *Acta Trop.* 113, 174–179. doi: 10.1016/j.actatropica.2009.10.014

Ortiz, M. I., Suárez-Rivillas, A., and Molina, J. (2011). Behavioural responses to human skin extracts and antennal phenotypes of sylvatic first filial generation and long rearing laboratory colony *Rhodnius prolixus*. *Mem. Inst. Oswaldo Cruz* 106, 461–466. doi: 10.1590/S0074-02762011000400013

Otálora-Luna, F., and Guerin, P. M. (2014). Amines from vertebrates guide triatomine bugs to resources. *J. Insect Physiol.* 71, 52–60. doi: 10.1016/j.jinsphys.2014.09.007

Page, T. L., and Koelling, E. (2003). Circadian rhythm in olfactory response in the antennae controlled by the optic lobe in the cockroach. *J. Insect Physiol.* 49, 697–707. doi: 10.1016/S0022-1910(03)00071-4

Pellegrino, M., Steinbach, N., Stensmyr, M. C., Hansson, B. S., and Vosshall, L. B. (2011). A natural polymorphism alters odour and DEET sensitivity in an insect odorant receptor. *Nature* 478, 511–514. doi: 10.1038/nature10438

Pelletier, J., Guidolin, A., Syed, Z., Cornel, A. J., and Leal, W. S. (2010). Knockdown of a mosquito odorant-binding protein involved in the sensitive detection of oviposition attractants. *J. Chem. Ecol.* 36, 245–248. doi: 10.1007/s10886-010-9762-x

Pereira, K. S., Schmidt, F. L., Barbosa, R. L., Guaraldo, A. M., Franco, R. M., Dias, V. L., et al. (2010). *Adv. Food Nutr. Res.* 59, 63–85. doi: 10.1016/S1043-4526(10)59003-X

Pelosi, P., Mastrogiacomo, R., Iovinella, I., Tuccori, E., and Persaud, K. C. (2014). Structure and biotechnological applications of odorant-binding proteins. *Appl. Microbiol. Biotechnol.* 98, 61–70. doi: 10.1007/s00253-013-5383-y

Pitts, R. J., Derryberry, S. L., Zhang, Z., and Zwiebel, L. J. (2017). Variant ionotropic receptors in the malaria vector mosquito *Anopheles gambiae* tuned to amines and carboxylic acids. *Sci. Rep.* 7:40297. doi: 10.1038/srep40297

Pontes, G., Minoli, S., Insaurralde, I. O., de Brito Sanchez, M. G., and Barrozo, R. B. (2014). Bitter stimuli modulate the feeding decision of a blood-sucking insect via two sensory inputs. *J. Exp. Biol.* 217, 3708–3717. doi: 10.1242/jeb.107722

Reinhardt, K., and Siva-Jothy, M. T. (2007). Biology of the bed bugs (Cimicidae). *Annu. Rev. Entomol.* 52, 351–374. doi: 10.1146/annurev.ento.52.040306.133913

Reis, M. D., and Miller, D. M. (2011). Host searching and aggregation activity of recently fed and unfed bed bugs (*Cimex lectularius* L.). *Insects* 2, 186–194. doi: 10.3390/insects2020186

Reisenman, C. E. (2014). Hunger is the best spice: effects of starvation in the antennal responses of the blood-sucking bug *Rhodnius prolixus*. *J. Insect Physiol.* 71, 8–13. doi: 10.1016/j.jinsphys.2014.09.009

Reisenman, C. E., Lee, Y., Gregory, T., and Guerenstein, P. G. (2013). Effects of starvation on the olfactory responses of the blood-sucking bug *Rhodnius prolixus*. *J. Insect Physiol.* 59, 717–721. doi: 10.1016/j.jinsphys.2013.04.003

Romero, A., Potter, M. F., Potter, D. A., and Kenneth, F. (2007). Insecticide resistance in the bed bug: a factor in the pest's sudden resurgence? *J. Med. Entomol.* 44, 175–178. doi: 10.1603/0022-2585(2007)44[175:IRITBB]2.0.CO;2

Romero, A., and Schal, C. (2014). Blood constituents as phagostimulants for the bed bug *Cimex lectularius* L. *J. Exp. Biol.* 217, 552–557. doi: 10.1242/jeb.096727

Romero, A., Potter, M. F., and Haynes, K. F. (2010). Circadian rhythm of spontaneous locomotor activity in the bed bug, *Cimex lectularius* L. *J. Insect Physiol.* 56, 1516–1522. doi: 10.1016/j.jinsphys.2010.04.025

Rosén, W. Q., Han, G. B., and Löfstedt, C. (2003). The circadian rhythm of the sex-pheromone-mediated behavioral response in the turnip moth, *Agrotis segetum*, is not controlled at the peripheral level. *J. Biol. Rhythm.* 18, 402–408. doi: 10.1177/0748730403256869

Salazar, R., Castillo-Neyra, R., Tustin, A. W., Borrini-Mayorí, K., Náquira, C., and Levy, M. Z. (2014). Bed bugs (*Cimex lectularius*) as vectors of *Trypanosoma cruzi*. *Am. J. Trop. Med. Hyg.* 14:0483. doi: 10.4269/ajtmh.14-0483

Sansom, J. E., Reynolds, N. J., and Peachey, R. D. (1992). Delayed reaction to bed bug bites. *Arch. Dermatol.* 128, 272–273. doi: 10.1001/archderm.1992.01680120148027

Sato, K., Pellegrino, M., Nakagawa, T., Nakagawa, T., Vosshall, L. B., and Touhara, K. (2008). Insect olfactory receptors are heteromeric ligand-gated ion channels. *Nature* 452, 1002–1006. doi: 10.1038/nature06850

Saveer, A. M., DeVries, Z. C., Santangelo, R. G., and Schal, C. (2021). Mating and starvation modulate feeding and host-seeking responses in female bed bugs, Cimex lectularius. *Sci. Rep.* 11, 1–11. doi: 10.1038/s41598-021-81271-y

Scheuermann, E. A., and Smith, D. P. (2019). Odor-specific deactivation defects in a *Drosophila* odorant-binding protein mutant. *Genetics* 213, 897–909. doi: 10.1534/genetics.119.302629

Shields, T. L., and Walsh, E. N. (1956). Kissing bug bite. *AMA Arch. Derm. Syphilol.* 74, 14–21. doi: 10.1001/archderm.1956.01550070016004

Shikanai-Yasuda, M. A., and Carvalho, N. B. (2012). Oral transmission of Chagas disease. *Clin. Infect. Dis.* 54, 845–852. doi: 10.1093/cid/cir956

Silbering, A. F., and Galizia, C. G. (2007). Processing of odor mixtures in the Drosophila antennal lobe reveals both global inhibition and glomerulus-specific interactions. *J. Neurosci.* 27, 11966–11977. doi: 10.1523/JNEUROSCI.3099-07.2007

Singh, N., Wang, C., and Cooper, R. (2013). Effect of trap design, chemical lure, carbon dioxide release rate, and source of carbon dioxide on efficacy of bed bug monitors. *J. Econ. Entomol.* 106, 1802–1811. doi: 10.1603/EC13075

Singh, N., Wang, C., Cooper, R., and Liu, C. (2012). Interactions among carbon dioxide, heat, and chemical lures in attracting the bed bug, *Cimex lectularius* L.(Hemiptera: Cimicidae). *Psyche* 2012:273613. doi: 10.1155/2012/273613

Singh, R. N., Singh, K., Prakash, S., Mendki, M. J., and Rao, K. M. (1996). Sensory organs on the body parts of the bed-bug *Cimex hemipterus fabricius* (Hemiptera: Cimicidae) and the anatomy of its central nervous system. *Int. J. Insect Morphol. Embryol.* 25, 183–204. doi: 10.1016/0020-7322(95)00016-X

Sioli, H. (1937). Thermotaxis und Perzeption von W¨armestrahlen bei der Bettwanze (*Cimex lectularius* L.). *Zool. Jahrb. Physiol. Morphol.* 58, 284–296.

Steinbrecht, R. A., and Müller, B. (1976). Fine structure of the antennal receptors of the bed bug, *Cimex lectularius* L. *Tissue Cell* 8, 615–636. doi: 10.1016/0040-8166(76)90035-5

Stengl, M., and Funk, N. W. (2013). The role of the coreceptor Orco in insect olfactory transduction. *J. Comp. Physiol. A.* 199, 897–909. doi: 10.1007/s00359-013-0837-3

Stevens, L., Dorn, P. L., Schmidt, J. O., Klotz, J. H., Lucero, D., and Klotz, S. A. (2011). Kissing bugs. The vectors of Chagas. *Adv. Parasitol.* 75, 169–192. doi: 10.1016/B978-0-12-385863-4.00008-3

Sun, J. S., Xiao, S., and Carlson, J. R. (2018). The diverse small proteins called odorant-binding proteins. *Open Biol.* 8:180208. doi: 10.1098/rsob.180208

Taneja, J., and Guerin, P. M. (1997). Ammonia attracts the haematophaguous bug *Triatoma infestans*: behavioural and neurophysioogical data on nymphs. *J. Comp. Pysiol. A* 181, 21–34. doi: 10.1007/s003590050089

Ter Poorten, M. C., and Prose, N. S. (2005). The return of the common bedbug. *Pediatr. Dermatol.* 22, 183–187. doi: 10.1111/j.1525-1470.2005.22301.x

Terrapon, N., Li, C., Robertson, H., Ji, L., Meng, X., Booth, W., et al. (2014). Molecular traces of alternative social organization in a termite genome. *Nat. Commun.* 5:3636. doi: 10.1038/ncomms4636

Tsitsanou, K. E., Thireou, T., Drakou, C. E., Koussis, K., Keramioti, M. V., Leonidas, D. D., et al. (2012). *Anopheles gambiae* odorant binding protein crystal complex with the synthetic repellent DEET: implications for structure-based design of novel mosquito repellents. *Cell. Mol. Life Sci.* 69, 283–297. doi: 10.1007/s00018-011-0745-z

Turner, S. L., Li, N., Guda, T., Githure, J., Cardé, R. T., and Ray, A. (2011). Ultra-prolonged activation of CO_2-sensing neurons disorients mosquitoes. *Nature* 474, 87–91. doi: 10.1038/nature10081

Van der Goes van Naters, W. M., Den Otter, C. J., and Maes, F. W. (1998). Olfactory sensitivity in tsetse flies: a daily rhythm. *Chem. Senses* 23, 351–357. doi: 10.1093/chemse/23.3.351

Villacís, A. G., Grijalva, M. J., and Catalá, S. S. (2010). Phenotypic variability of *Rhodnius ecuadoriensis* populations at the Ecuadorian central and southern Andean region. *J. Med. Entomol.* 47, 1034–1043. doi: 10.1603/ME10053

Villela, M. M., Catalá, S., Juberg, J., Silva, I. G., and Dias, J. C. P. (2005). Patterns of antenal sensilla of *Panstrongylus megistus* from three Brazilian states. *Mem. Inst. Oswaldo Cruz* 100, 699–702. doi: 10.1590/S0074-02762005000700002

Wang, G., Carey, A. F., Carlson, J. R., and Zwiebel, L. J. (2010). Molecular basis of odor coding in the malaria vector mosquito Anopheles gambiae. *Proc. Natl. Acad. Sci. U. S. A.* 107, 4418–4423. doi: 10.1073/pnas.0913392107

Wang, C., Gibb, T. J., Bennett, G. W., and McKnight, S. (2009). Bed bug (Heteroptera: Cimicidae) attraction to pitfall traps baited with carbon dioxide, heat, and chemical lure. *J. Econ. Entomol.* 102, 1580–1585. doi: 10.1603/029.102.0423

Waris, M. I., Younas, A., Hao, L., Ameen, A., Ali, S., Abdelnabby, H. E., et al. (2018). Silencing of chemosensory protein gene Nlug CSP8 by RNAi induces declining behavioral responses of *Nilaparvata lugens*. *Front. Physiol.* 9:379. doi: 10.3389/fphys.2018.00379

Weeks, E. N. I., Logan, J. G., Birkett, M. A., Caulfield, J. C., Gezan, S. A., Welham, S. J., et al. (2020). Electrophysiologically and behaviourally active semiochemicals identified from bed bug refuge substrate. *Sci. Rep.* 10, 1–14. doi: 10.1038/s41598-020-61368-6

Wiesinger, D. (1956). Die Bedeutung der Umweltfaktoren fiir der Saugakt von *Triatoma infestans*. *Acta Trop.* 13, 97–141.

Wigglesworth, V., and Gillett, J. (1934). The function of the antennae in *Rhodnius prolixus* (Hemiptera) and the mechanism of orientation to the host. *J. Exp. Biol.* 11, 120–139. doi: 10.1242/jeb.11.2.120

Xiao, S., Sun, J. S., and Carlson, J. R. (2019). Robust olfactory responses in the absence of odorant binding proteins. *elife* 8:e51040. doi: 10.7554/eLife.51040

Xu, P., Choo, Y. M., De La Rosa, A., and Leal, W. S. (2014). Mosquito odorant receptor for DEET and methyl jasmonate. *Proc. Natl. Acad. Sci. U. S. A.* 111, 16592–16597. doi: 10.1073/pnas.1417244111

Xu, C., Yang, F., Duan, S., Li, D., Li, L., Wang, M., et al. (2021). Discovery of behaviorally active semiochemicals in *Aenasius bambawalei* using a reverse chemical ecology approach. *Pest Manag. Sci.* 77, 2843–2853. doi: 10.1002/ps.6319

Ye, Z., Liu, F., and Liu, N. (2016). Olfactory responses of southern house mosquito, *Culex quinquefasciatus*, to human odorants. *Chem. Senses* 41, 441–447. doi: 10.1093/chemse/bjv089

Yoon, K. S., Kwon, D. H., Strycharz, J. P., Hollingsworth, C. S., Lee, S. H., and Clark, J. M. (2008). Biochemical and molecular analysis of deltamethrin resistance in the common bed bug (Hemiptera: Cimicidae). *J. Med. Entomol.* 45, 1092–1101. doi: 10.1603/0022-2585(2008)45[1092:BAMAOD]2.0.CO;2

Zacharias, C. A., Pontes, G. B., Lorenzo, M. G., and Manrique, G. (2010). Flight initiation by male Rhodnius prolixus is promoted by female odors. *J. Chem. Ecol.* 36, 449–451. doi: 10.1007/s10886-010-9779-1

Zermoglio, P. F., Martin-Herrou, H., Bignon, Y., and Lazzari, C. R. (2015). *Rhodnius prolixus* smells repellents: behavioural evidence and test of present and potential compounds inducing repellency in Chagas disease vectors. *J. Insect Physiol.* 81, 137–144. doi: 10.1016/j.jinsphys.2015.07.012

Zhu, F., Gujar, H., Gordon, J. R., Haynes, K. F., Potter, M. F., and Palli, S. R. (2013). Bed bugs evolved unique adaptive strategy to resist pyrethroid insecticides. *Sci. Rep.* 3:1456. doi: 10.1038/srep01456

Zhu, J., Arena, S., Spinelli, S., Liu, D., Zhang, G., Wei, R., et al. (2017). Reverse chemical ecology: olfactory proteins from the giant panda and their interactions with putative pheromones and bamboo volatiles. *Proc. Natl. Acad. Sci. U. S. A.* 114, e9802–e9810. doi: 10.1073/pnas.1711437114

Conflict of Interest: The authors declare that the research was conducted in the absence of any commercial or financial relationships that could be construed as a potential conflict of interest.

Publisher's Note: All claims expressed in this article are solely those of the authors and do not necessarily represent those of their affiliated organizations, or those of the publisher, the editors and the reviewers. Any product that may be evaluated in this article, or claim that may be made by its manufacturer, is not guaranteed or endorsed by the publisher.

frontiers in Physiology

ORIGINAL RESEARCH
published: 09 August 2021
doi: 10.3389/fphys.2021.701545

Non-palm Plant Volatile α-Pinene Is Detected by Antenna-Biased Expressed Odorant Receptor 6 in the *Rhynchophorus ferrugineus* (Olivier) (Coleoptera: *Curculionidae*)

Tianliang Ji[1,2], Zhi Xu[1,2], Qingchen Jia[1], Guirong Wang[2] and Youming Hou[1]**

[1] State Key Laboratory of Ecological Pest Control for Fujian and Taiwan Crops, Key Laboratory of Biopesticide and Chemical Biology, Ministry of Education, Fujian Province Key Laboratory of Insect Ecology, College of Plant Protection, Fujian Agriculture and Forestry University, Fuzhou, China, [2] State Key Laboratory for Biology of Plant Diseases and Insect Pests, Institute of Plant Protection, Chinese Academy of Agricultural Sciences, Beijing, China

OPEN ACCESS

Edited by:
Peng He,
Guizhou University, China

Reviewed by:
Huahua Sun,
Duke University, United States
Ke Yang,
Institute of Zoology, Chinese Academy of Sciences (CAS), China
Peng-Fei Lu,
Beijing Forestry University, China

***Correspondence:**
Guirong Wang
wangguirong@caas.cn
Youming Hou
ymhou@fafu.edu.cn

Specialty section:
This article was submitted to Invertebrate Physiology, a section of the journal Frontiers in Physiology

Received: *28 April 2021*
Accepted: *06 July 2021*
Published: *09 August 2021*

Citation:
Ji T, Xu Z, Jia Q, Wang G and Hou Y (2021) Non-palm Plant Volatile α-Pinene Is Detected by Antenna-Biased Expressed Odorant Receptor 6 in the Rhynchophorus ferrugineus (Olivier) (Coleoptera: Curculionidae). Front. Physiol. 12:701545. doi: 10.3389/fphys.2021.701545

The majority of insects rely on a highly complex and precise olfactory system to detect various volatile organic compounds released by host and non-host plants in environments. The odorant receptors (ORs) are considered to play an important role in odor recognition and the molecular basis of ORs, particularly in coleopterans they are relatively poorly understood. The red palm weevil (RPW), *Rhynchophorus ferrugineus* (Olivier) (Coleoptera: *Curculionidae*), is one of the most destructive pests of the global palm industry. Although feeding and egg oviposition behaviors of RPW can be repelled by some non-palm plant volatiles, such as α-pinene, geraniol, or 1-octen-3-ol, there is limited understanding of how RPW recognizes the non-host plant volatiles. In this study, three candidate *RferOrs* were identified from the Rfer-specific clade, and the tissue expression analysis used was mainly expressed in the antennae of both sexes. Functional characterization of *RferOr6*, *RferOr40*, and *RferOr87* was analyzed by using the *Xenopus* oocyte expression system, and the results indicated that *RferOr6*/*RferOrco* was narrowly tuned to α-pinene. The behavioral experiment showed that α-pinene at the concentrations of 10 and 100 μg/μl can cause a significantly repelled behavioral response of RPW. In conclusion, this study reveals that *RferOr6* is an antenna-biased expressed OR used by RPW to detect the volatile compound α-pinene in non-palm plants, and our results provide a foundation for further *in vivo* functional studies of Or6 in RPW, including *in vivo* knockout/knockdown and feeding/ovipositing behavioral studies of RPW and further pest control.

Keywords: odorant receptor, *Xenopus* oocyte, *Rhynchophorus ferrugineus* (Olivier), α-pinene, tissue expression analysis

INTRODUCTION

From bacteria to mammals, most living organisms have evolved a powerful olfactory system with remarkable sensitivities and discriminatory ability to detect and discriminate hundreds of chemicals in the environment (Wuichet and Zhulin, 2010; Hansson and Stensmyr, 2011). Series of insect behaviors, such as host-seeking, mating, communication, and avoidance of predators, were all

mediated by the olfactory systems (Bentley and Day, 1989; Hansson and Stensmyr, 2011; Gadenne et al., 2016; Fleischer et al., 2018). In insect chemoreception, the task of olfactory signals encoding and the process of chemoelectrical transduction are mainly mediated by three primary families of receptors, including the gustatory receptors, ionotropic receptors, and odorant receptors (ORs) (Suh et al., 2014; Wicher, 2015; Robertson, 2019). Among them, ORs are the largest gene families in chemosensory receptors and expressed in the dendritic membrane of odorant receptor neurons, which is the primary means for insects in the discrimination of different odors (Fleischer et al., 2018). ORs can be divided into odorant receptor co-receptor (Orco) and traditional ORs. Orco is a coessential in ORs functioning and highly conserved between insects (Benton et al., 2006; Brand et al., 2018), while ORs vary significantly between different insects with low sequence homology. Functional characterization of ORs is a key step toward understanding the molecular mechanism of chemical signal recognition in the peripheral olfactory system of insects.

Over the past 20 years, with a rapid progress in the sequencing of genomics and transcriptomics of insect olfactory tissues, a large number of complete or partial repertoires of OR genes have been identified from a variety of species, and the numbers of OR genes vary considerably between species (Montagne et al., 2015). However, it was noted that the functional characterization of ORs has been obviously reported based on *Drosophila melanogaster* (Hallem et al., 2004; Kreher et al., 2005; Hallem and Carlson, 2006; Mathew et al., 2013), *Anopheles gambiae* (Carey et al., 2010; Wang et al., 2010), *Spodoptera littoralis* (de Fouchier et al., 2017), and *Helicoverpa armigera* (Guo et al., 2020). Otherwise, ORs related to pheromones as well as certain non-pheromone odorants have been characterized in a number of lepidopteran species, such as *Bombyx mori* (Sakurai et al., 2004; Nakagawa et al., 2005; Grosse-Wilde et al., 2006), *Heliothis virescens* (Grosse-Wilde et al., 2007; Wang et al., 2011), *Ostrinia nubilalis* (Wanner et al., 2010), and *Cydia pomonella* (Gonzalez et al., 2015; Cattaneo et al., 2017; Wan et al., 2019). In contrast, although the identification of OR gene sequences was greatly facilitated in Coleoptera (Mitchell et al., 2020), the identification of ligands significantly lagged behind, leaving most ORs as orphan receptors.

The red palm weevil (RPW), *Rhynchophorus ferrugineus* (Olivier) (Coleoptera: *Curculionidae*), is arguably one of the deadliest pests for palm trees worldwide (Ju et al., 2011; Wang et al., 2015). RPW is a concealed tissue borer that almost always lives inside the trunk of palm trees, the weevil larva is the major infestation stage which feed on the apical growing point of the trunk of palm trees, and the attack is detected only after the palm has been seriously damaged (Butera et al., 2012; Shi et al., 2014). Since RPW spends most of its life span inside the trunks of palm trees except during copulation and oviposition, it is difficult to find and kill them. Traps loaded with aggregation pheromones (e.g., 4-methyl-5-non-anol and 4-methyl-5-non-anone) and supplemented with palm esters (e.g., ethyl acetate, ethyl propionate, ethyl butyrate, and propyl butyrate) and/or fermenting mixtures of plant tissues have been known as the major environment-friendly methods for controlling RPW (Faleiro, 2006; Vacas et al., 2014). Unfortunately, the attractant power of these pheromones seems to be limited in the field. Consequently, it is urgent to develop effective integrated pest management tactics based on pheromone traps. Guarino et al. (2013) have proposed a new idea of combing use of the pheromones to attract the RPW into the traps with repellent compounds that drive the pest away from the nearby palm trees to prevent subsequent attacks. Previous studies pointed out that some of the EAG-active non-plant volatiles, belonging to the isoprenoids, phenylpropanoid derivatives, and fatty acid derivatives, were added to the trap with pheromones, respectively, and the capture number of RPW was obviously reduced in the field (Guarino et al., 2013, 2015). Therefore, these chemicals are potentially used as repellents of RPW in the field. Non-host plant volatile compounds that repel insects could be a valuable tool for pest management, but there is still limited understanding of how insects systematically discriminate host and non-host plant volatiles. Although 76 OR genes were annotated in the RPW antennal transcriptome (Antony et al., 2016), the current knowledge of the olfactory recognition molecular mechanism of non-host plant volatiles still remains unknown. In this study, three full-length open-reading frame (ORF) candidate *RferOrs* were identified from the seven ORs in the Rfer-specific clade. Then, the qRT-PCR expression analysis was used to understand the expression of genes at different tissues. Last, three candidate *RferOrs* were expressed in the *Xenopus* oocyte system and the two-electrode voltage-clamp (TEVC) technique was used to characterize their functions. Our results would provide the basis not only for the OR function characterization of coleopteran insects but also for the OR functions to combine with the reverse chemical ecology approach to develop higher effective repellents to regulate the behavior of RPW.

MATERIALS AND METHODS

Insect Rearing

The *R. ferrugineus* adults used in this study were obtained from the stock population that was originally collected in 2008 from a Canary Island date palm (Phoenix canariensis Hort. ex Chabaud) on the campus of Fujian Agriculture and Forestry University (FAFU), Fujian, China. Later, the colony of *R. ferrugineus* was established at the growth chambers (PRX-250B-30, Haishu Saifu Experimental Instrument Factory, Ningbo, China) and maintained at 27 ± 1°C, 75 ± 5% of relative humidity with 12 h light and 12 h dark scheduled in the laboratory at the College of Plant Protection. Due to its cannibalistic behavior, each larva was reared individually in a plastic bottle (60 mm in diameter and 30 mm in height; Jiafeng Horticultural Products Co., Ltd., Shanghai, China). The adults for breeding were reared together in plastic bottles (65 mm in diameter and 100 mm in height). To get the ideal humidity and keep the air ventilation, we put a moist paper in the bottom and drilled a 5-mm diameter hole at the neck of each bottle. Small pieces (20 cm × 15 cm × 10 cm) of sugarcane were provided as a food resource for the weevils. The bottles and fresh sugarcane were changed every 2 days. In order

to keep high genetic diversity of the laboratory population, new insects were collected seasonally from the field and were mixed with the previous population.

Chemical Compounds

Twenty-nine chemical compounds were selected for this study including five non-palm plant volatiles, 22 palm plant volatiles, and 2 compounds of aggregation pheromone and purchased from Sigma or J&K Scientific Ltd. (**Table 1**). In the following electrophysiological recording experiments to investigate the function of OR genes, these stimulated chemical compounds were followed by the stimulus order.

RNA Extraction and cDNA Synthesis

The total RNA from ten 7–14-day-old male and female antennae was extracted using Trizol. The cDNA was synthesized by the RevertAid First Strand cDNA Synthesis Kit (Fermentas, Vilnius, Lithuania) for the following experiments.

TABLE 1 | All chemical compounds used for the functional characterization of *RferOr6*, *RferOr40,* and *RferOr87*.

Stimuluscompounds	Stimulus order	CAS number	Purity (%)	Company
Non-host plant volatiles				
1-octen-3-ol	1	3391-86-4	98	Sigma
citral	2	5392-40-5	98	Sigma
geraniol	3	106-24-1	99	Sigma
Methyl salicylate	4	119-36-8	98	Sigma
α-pinene	5	80-56-8	97	Sigma
Hosts plant volatiles				
2-methyl-1-butanol	6	137-32-6	98	Sigma
1-butanol	7	71-36-3	99	Sigma
3-methyl-1-butanol	8	123-51-3	98	Sigma
3-Hexanol	9	623-37-0	97	Sigma
2-Hexanol	10	626-93-7	99	Sigma
Citronellol	11	106-22-9	95	Sigma
2,3-Butanediol	12	513-85-9	98	Sigma
3-Hexanone	13	589-38-8	97	Sigma
2-Hexanone	14	591-78-6	98	Sigma
4-Ethylacetophenone	15	937-30-4	97	Sigma
2-Non-anone	16	821-55-6	98	Sigma
Hexanal	17	66-25-1	96	Sigma
Octanal	18	124-13-0	99	Sigma
Phenylacetaldehyde	19	122-78-1	95	Sigma
4-Ethylbenzaldehyde	20	4748-78-1	97	Sigma
Methyl benzoate	21	93-58-3	98	Sigma
Methyl Salicylate	22	119-36-8	98	Sigma
Butyl benzoate	23	136-60-7	98	Sigma
Ethyl benzoate	24	93-58-3	99	Sigma
Ethyl acetate	25	141-78-6	99	Sigma
Octyl acetate	26	112-14-1	99	Sigma
Butyl butyrate	27	109-21-7	98	Sigma
Aggregation pheromone of RPW				
4-Methyl-5-non-anol	28	104170-44-2	99	J&K Scientific Ltd.
4-Methyl-5-non-anone	29	35900-26-6	99	J&K Scientific Ltd.

Sequence and Phylogenetic Analyses of ORs

Twelve *RferOrs* and *RferOrco* from RPW antennal transcriptome (unpublished data) with seven ORs from three beetle species including *Megacyllene caryae* (Mitchell et al., 2012), *Ips typographus* (Yuvaraj et al., 2021), and *Dendroctonus ponderosae* (Andersson et al., 2013) were used to construct the phylogenetic trees. The gene name and accession number in GenBank are listed in **Table 2**. The amino acid sequence data were aligned using ClustalX 2.0 software (Thompson et al., 1994). The transmembrane domains (TMDs) of *RferOrs* were analyzed by using TOPCONS[1]. Phylogenetic trees were constructed by using RAxML version 8 with the maximum likelihood method of the Jones–Taylor–Thornton (JTT) model (Tamura et al., 2013).

Tissue Expression Pattern of *RferOr6*, *RferOr40*, and *RferOr87*

Real-time quantitative PCR (RT-qPCR) was used to evaluate the expression levels of *RferOr6*, *RferOr40,* and *RferOr87* in different tissues of RPW. Total RNA was isolated from 7- to 14-day-old adults of antennae (A), legs (L), head (H), proboscides (P), and body (B) of both sexes, respectively. Tubulin and β-actin were used as reference genes (Antony et al., 2018). The specific primers were designed using Primer Premier 5.0 (PREMIER Biosoft International, CA, United States) and listed in **Supplementary Table 1**. The TransStart Tip Green qPCR SuperMix (TransGen

[1]https://topcons.cbr.su.se

TABLE 2 | Genes used to construct the phylogenetic trees are listed with gene names and accession numbers.

Gene name	Accession number	Gene name	Accession number
RferOrco	A0035283	McOr8	–
RferOr2	MW979235	McOr10	–
RferOr6	MW979236	McOr13	–
RferOr21	MW979237	McOr22	–
RferOr40	MW979238	McOr33	–
RferOr43	MW979239	McOr37	–
RferOr47	MW979240	McOr39	–
RferOr56	MW979241	McOr56	–
RferOr57	MW979242	ItypOrco	QOI12086
RferOr60	MW979243	ItypOr5	GACR01000029
RferOr66	MW979244	ItypOr6	GACR01000018
RferOr67	MW979245	ItypOr11	GACR01000021
RferOr85	MW979246	ItypOr15	GACR01000030
RferOr87	MW979247	DponOrco	XP_019768125
McOrco	–	DponOr8	GABX01000004
McOr2	–	DponOr9	GABX01000059
McOr3	–	DponOr82	–
McOr5	–	DponOr83	XP_019766781

– The accession number has not been deposited in GenBank.

Biotech, Beijing, China) was used for RT-qPCR. The RT-qPCR mix (20 μl) contained 1 μl of cDNA template, 0.6 μl of each primer (10 μM), 10 μl of 2 × TransStart Tip Green qPCR SuperMix, 0.4 μl of Passive Reference Dye (50×), and 7.4 μl of nuclease-free water. The RT-qPCR reactions were performed using the Applied Biosystems 7500 Fast. The real-time PCR system (ABI) was performed under the following conditions: 94°C for 30 s, 40 cycles of 94°C for 5 s, and 60°C for 34 s. The melting curve analysis was followed by the fluorescence measurement with one cycle of 95°C for 15 s, 60°C for 1 min, 95°C for 30 s, and 60°C for 15 s and suggested amplification of a single product. The RT-qPCR experiments were repeated three times using three independently isolated RNA samples. The relative expression level of genes was calculated using the $2^{-\Delta\Delta SM1Ct}$ method (Livak and Schmittgen, 2001). Statistical significance between males and females was analyzed by using Student's *t*-test, and relative expression levels of antennal expression of three candidate genes were compared by using one-way ANOVA with IBM SPSS Statistics 25.0 (IBM Corp., Armonk, New York).

Cloning the Full Length of *RferOr6*, *RferOr40*, and *RferOr87*

According to the tissue expression pattern, we cloned the full-length *RferOr6*, *RferOr40*, *RferOr87*, and *RferOrco* genes of RPW. Primers of ORs were designed using Primer Premier 5.0 and are listed in **Supplementary Table 1**. The ORF of ORs was amplified by using PCR from antennal cDNA. The PCR reaction was performed in 50 μl solution containing 25 μl of 2 × PrimeSTAR mix, 2 μl each of upstream and downstream primers (10 μM), and 19 μl of ddH_2O. The reactions were carried out using a Veriti Thermal Cycler (Applied Biosystems, Carlsbad, CA, United States) under the following conditions: 95°C for 3 min, 35 cycles of 95°C for 30 s, 62°C for 30 s, 72°C for 1.5 min, and 72°C for 10 min (*RferOr6* and *RferOr40*); 95°C for 3 min, 35 cycles of 95°C for 30 s, 61°C for 30 s, 72°C for 1.5 min, and 72°C for 10 min (*RferOr87*); 95°C for 3 min, 35 cycles of 95°C for 30 s, 60°C for 30 s, 72°C for 1.5 min, and 72°C for 10 min (*RferOrco*). PCR amplification products were purified with 1.0% agarose gels, ligated into the pEASY-Blunt vector (TransGen Biotech, Beijing, China), and sequenced by BGI (Beijing, China).

Receptor Expression in *Xenopus* Oocytes and TEVC Recordings

RferOr6, *RferOr40*, *RferOr87*, and *RferOrco* were subcloned into eukaryotic expression vector pT7TS using the ClonExpress II One Step Cloning Kit (Vazyme Biotech Co., Ltd., China). The sequences of the specific primer bearing a Kozak consensus are listed in **Supplementary Table 1**. The constructed pT7TS vectors were linearized by restriction enzymes (*Apa*I and *Not*I) (**Supplementary Table 1**), and cRNAs were synthesized by using the mMESSAGE mMACHINE T7 Ultra Kit (Ambion, Austin, TX). Mature and healthy *Xenopus* oocytes were separated and then treated for 1 h at room temperature with washing buffer (2 mM KCl, 96 mM NaCl, 5 mM HEPES, and 5 mM $MgCl_2$; pH 7.6 adjusted with NaOH) that contained 2 mg/ml of collagenase. Stock solutions (1 M) of all the compounds used for TEVC recordings were prepared in dimethyl sulfoxide (DMSO) and stored at –20°C. Before the experiments, they were diluted in 1 × Ringer's buffer (2 mM KCl, 96 mM NaCl, 5 mM $MgCl_2$, 5 mM HEPES, and 0.8 mM $CaCl_2$, pH 7.6) up to a working concentration of 10^{-4} M. Ringer's buffer (1×) containing 0.1% of DMSO was used as a negative control. For dose–response plots, serial dilutions were made at 10^{-6}, 1×10^{-5}, 10^{-4}, 3×10^{-4}, and 10^{-3} M. Before injection, the cRNA concentration of *RferOrs* and *RferOrco* was diluted to 2 μg/μl, and then, we mixed the candidate *RferOr* with *RferOrco* in the ratio of 1:1. Later, a volume of 27.6 nl of *RferOr*/*RferOrco* mix was microinjected into each mature oocyte. Then, the injected oocytes were cultured for at least 3 days at 18°C in 1 × Ringer's solution supplemented with 5% of dialyzed horse serum, 50 μg/ml of tetracycline, 100 μg/ml of streptomycin, and 550 μg/ml of sodium pyruvate. Using TEVC (Warner Instruments, Hamden, CT, United States) at a holding potential of −80 mV and amplified by an OC-725C oocyte clamp amplifier, the oocytes were exposed to each chemical for 20 s and washed with 1 × Ringer's buffer to bring the current back to baseline before the next stimulus. The data acquisition and analysis were performed with Digidata 1440 A and PCLAMP 10.2 software (Axon Instruments Inc., Union City, CA, United States). The dose–response data were analyzed by using GraphPad Prism 5.0 software.

Behavioral Experiment

Two arms of the Y-tube olfactometer (diameter: 5 cm, main-tube length: 15 cm, arm length: 30 cm, and arm angle: 75°) were used to observe RPW behavioral response to α-pinene. The one arm of the Y-tube olfactometer was connected to the odor source, containing a piece of filter paper with 10 μl of a mix of two components (mix G contains pheromone and α-pinene; ratio of pheromone:α-pinene = 1:1) and the other to the blank, containing a piece of filter paper with 10 μl of pheromone. The air was filtered through activated charcoal, and the entry flow to the olfactometer was 1.2 L/min controlled by using a vacuum pump. RPW was starved overnight, and the experiment was carried out during daytime between 9:00 and 17:00 h at a temperature of 27°C ± 1°C and a humidity of 75 ± 5% (Antony et al., 2021). During the experiment, the Y-tube olfactometer was washed with ethanol and heated every time, and the compound position was changed when every 10 adults were tested. RPW, moving into one-third of the length of one arm and remaining there for at least 30 s, was classified as "making a choice." RPW not entering either arm during 5 min was recorded as "no choice." The data were collected from at least 60 successful "make choice" adults, and the data from "no choice" were excluded and analyzed because we were not sure that RPW was repelled by odor or it did not make a behavioral response at all. Statistical differences were evaluated *via* multiple *t* tests.

RESULTS

Characteristics of the Seven ORs in the Rfer-Specific Clade

We chose the initial candidate *RferOrs* that belong to Group 2 family in beetle species according to previous studies (Antony et al., 2016, 2021; Mitchell et al., 2020). The phylogenetic trees were constructed with four beetle species including *R. ferrugineus* (Rfer, red), *M. caryae* (Mc, pink), *I. typographus* (Ityp, dark), and *D. ponderosae* (Dpon, blue) and analyzed by using the maximum-likelihood method (**Figure 1A**). Orcos were clustered into one branch, and ORs were separated between four species. Seven *RferOrs* were observed as clustered into one branch and obviously showed species specificity. Three of the seven ORs containing a full-length ORF, namely, *RferOr6*, *RferOr40*, and *RferOr87*, encoded proteins of 382, 380, and 376 amino acids, respectively, and predicted to possess 7 TMDs (**Figure 1B**). *RferOr2*, *RferOr21*, *RferOr66*, and *RferOr67* were excluded due to encoded proteins of 261, 312, 158, and 238 amino acids, respectively. The sequences of *RferOr6*, *RferOr40*, and *RferOr87* have been deposited in GenBank under the accession numbers MW979236, MW979238, and MW979247, respectively. Three candidate ORs shared 52.37% amino acid identity, while *RferOrco* shared 92.01% identity with McOrco, ItypOrco, and DponOrco.

Tissue Expression Pattern of *RferOr6, RferOr40*, and *RferOr87* Genes

The RT-qPCR analysis was performed to evaluate the expression levels of three candidate genes in different tissues of male and female RPW (**Figure 2**). It was observed that *RferOr6*, *RferOr40*, and *RferOr87* were significantly highly expressed in antennae than in other tissues, such as heads, proboscides, legs, and body (**Figures 2A–C**). *RferOr6* obviously showed higher expression level in female antennae than male antennae ($P < 0.01$), while *RferOr40* and *RferOr87* showed no significant difference between sexes ($P = 0.57$, $P = 0.25$). *RferOr6* was expressed in the male body but not in the female body, while *RferOr40* and *RferOr87* were not expressed in both male and female bodies. According to the relative expression level of three candidate genes in antennae (**Figure 2D**), *RferOr6* showed the highest expression level, followed by *RferOr87*, and *RferOr40* had the lowest expression level between sexes.

Functional Characterization of Three Candidate RferOrs in the *Xenopus* Oocyte Expression System

To characterize the functions of three candidate *RferOrs*, *RferOr6*, *RferOr40*, and *RferOr87* were co-expressed with *RferOrco* in *Xenopus* oocytes and recorded by using the TEVC system. Twenty-nine compounds (**Table 1**) including non-host plant volatiles, host plant volatiles, and aggregation pheromone compounds were chosen as potential ligands of three candidates of *RferOrs*. The results indicated that *RferOr6*/*RferOrco* was narrowly responded to α-pinene, with responses of about 480 nA (**Figures 3A,B**). In dose–response studies, we assayed the responses of *RferOr6* to a range of α-pinene concentrations (**Figure 3C**), and the EC50 value for α-pinene was 9.447×10^{-5} (**Figure 3D**), while no response has been observed in *RferOr40*/*RferOrco* and *RferOr87*/*RferOrco* (**Figures 3E,F**).

Behavioral Response to α-Pinene of RPW

The results of the Y-tube olfactometer assay showed that with the increased concentration of mix G, an obviously

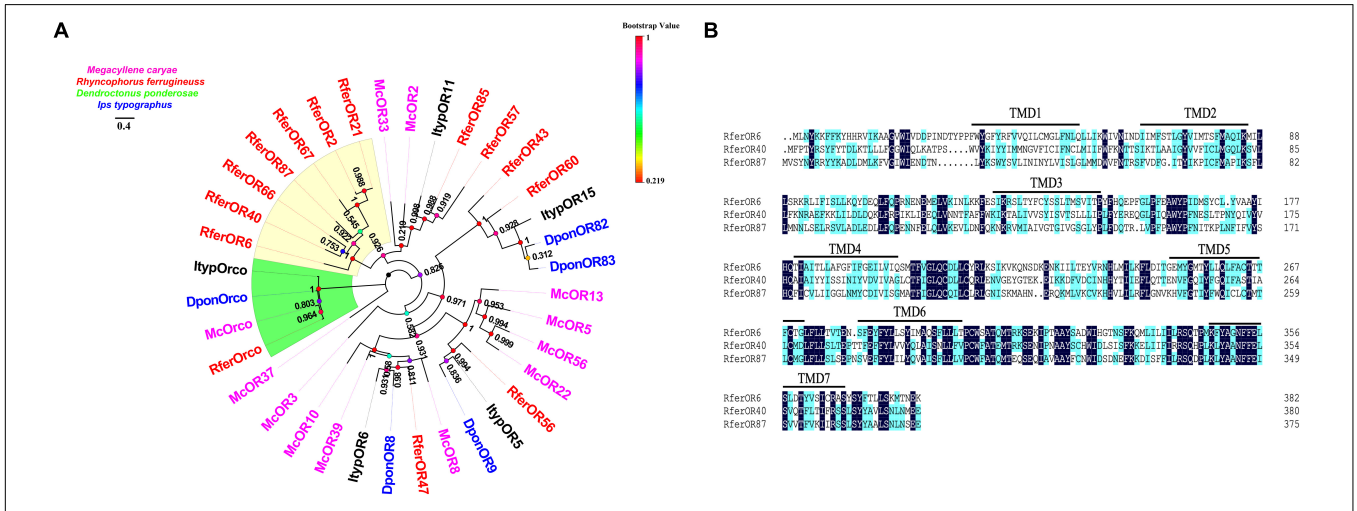

FIGURE 1 | Phylogenetic comparison of odorant receptors (ORs) from four beetle species. **(A)** Maximum likelihood tree of selected OR sequences from *Rhynchophorus ferrugineus* (Rfer, red), *Megacyllene caryae* (Mc, pink), *Ips typographus* (Ityp, dark), and *Dendroctonus ponderosae* (Dpon, blue). Bootstrap based on 1,000 replicates and rooted with the conserved odorant receptor co-receptor (Orco) lineage. *RferOrs* studied in the manuscript are shown in a yellow background. **(B)** Sequences alignment analysis of *RferOr6*, *RferOr40*, and *RferOr87*. The black background indicates the same amino acid sequence of the three genes, and the blue background indicates the same hydrophobicity of the amino acid sequence of the three genes.

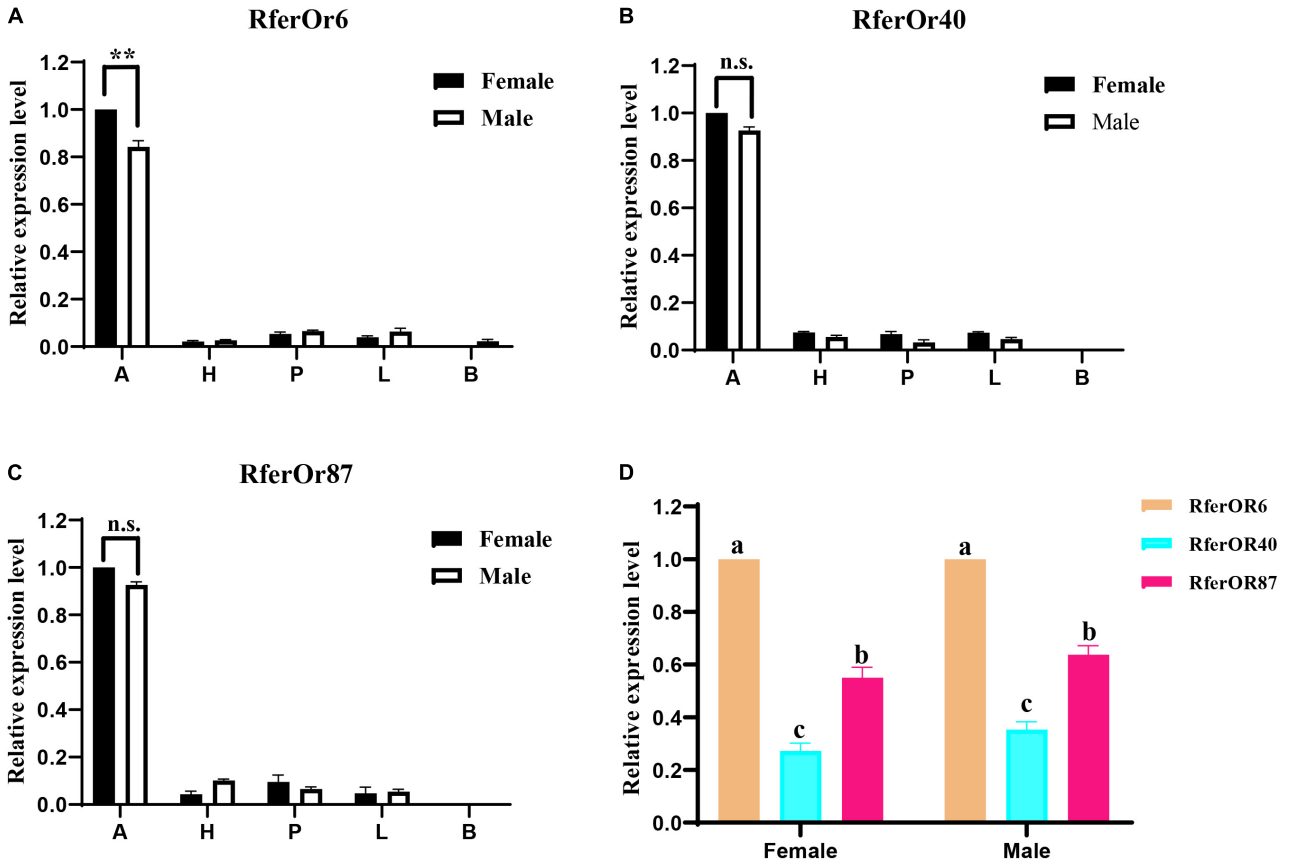

FIGURE 2 | Relative expression levels of three candidate genes in different tissues. **(A)** *RferOr6*. ** indicates the significant difference at the $P < 0.01$ level between sexes (Student's *t*-test, $n = 3$). **(B)** *RferOr40*. n.s indicates no significant difference between sexes (Student's *t*-test, $n = 3$). **(C)** *RferOr87*. n.s indicates no significant difference between sexes (Student's *t*-test, $n = 3$). **(D)** Relative expression levels of antennal expression of *RferOr6*, *RferOr40*, and *RferOr87* (one-way ANOVA). A, antennae; H, heads without antennae and proboscides; P, proboscides; L; legs; B, body. Data represent mean ± SEM.

repelled behavioral response was observed (**Figure 4**). There was no preference between the pheromone and mix G at the concentration of 1 μg/μl ($P = 0.07$), while RPW was repelled by mixed compounds at the concentration of 10 or 100 μg/μl ($P < 0.05$). More than 71% of RPW moved toward the side that contained only pheromone at 100 μg/μl and obviously showed a difference with mix G ($P < 0.01$). A similar lower proportion (62%) was observed at the concentration of 10 μg/μl ($P < 0.05$).

DISCUSSION

Only suitable hosts can obtain sufficient nutrition for growth, development, reproduction, and other series of life activities, while unsuitable hosts can cause insects poisoning and malnutrition (Chapman, 2003). Complex olfactory chemical cues are encoded by a large and divergent repertoire of chemoreceptor proteins, and ORs are considered to play a crucial role in the process of host and non-host plant volatile discrimination (Fleischer et al., 2018). To our knowledge, the functional characterization of ORs is relatively poorly understood in coleopterans. Only several ORs of *M. caryae* (Mitchell et al., 2012), *I. typographus* (Hou et al., 2020; Yuvaraj et al., 2021), and *R. ferrugineus* (Antony et al., 2021) are broadly known for aggregation pheromone receptors of beetles. Besides, two ORs of *I. typographus* specifically responding to host volatiles (Hou et al., 2020) and one OR of *Holotrichia parallela* responding to three volatiles released by the host tree have been reported (Wang et al., 2020). Still, ORs related to the detection of non-host plant volatiles have not been reported. In this study, from seven ORs in the Rfer-specific clade of RPW, we identified that *RferOr6*, *RferOr40*, and *RferOr87* have complete ORF. The tissue expression pattern showed that three *RferOrs* were mainly expressed in antennae and *RferOr6* was highly expressed in female antennae than male antennae. The functional characterization of three candidate *RferOrs* by using the *Xenopus* oocyte expression system showed that *RferOr6* was strongly and narrowly tuned to α-pinene. The behavioral results indicated that 62 and 71% of RPW were attracted to the odor resource without α-pinene at the concentrations of 10 and 100 μg/μl. It means that RPW showed an effective repelled behavioral response to α-pinene at these two concentrations. Meanwhile, previous studies also indicated that feeding and egg oviposition behaviors of RPW can be repelled by α-pinene (Guarino et al., 2013, 2015).

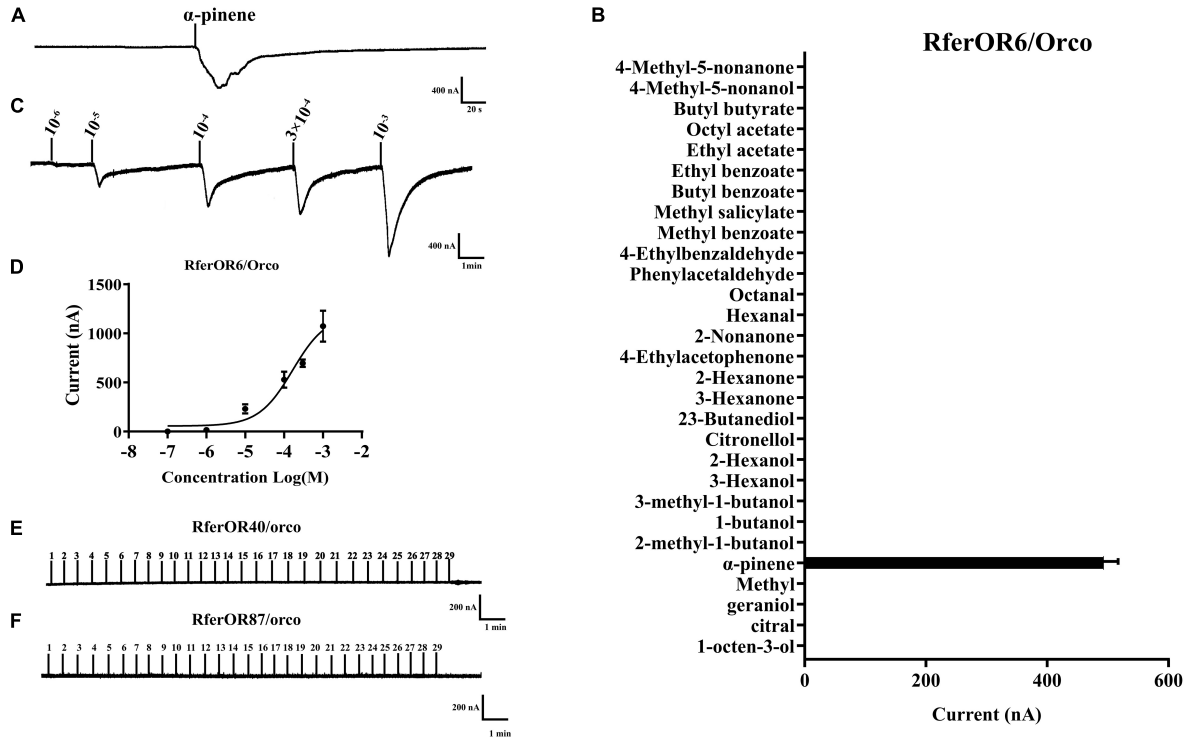

FIGURE 3 | Functional characterization of three candidate genes in *Xenopus* oocytes to stimulation by volatile compounds. **(A)** Inward current responses of *RferOR6*/*RferOrco Xenopus* oocytes in response to 29 tested compounds at the concentration of 10^{-4} M. **(B)** Response profile of *RferOr6*/*RferOrco Xenopus* oocytes. The response value is indicated as means ± SEM (n = 6). **(C)** *RferOr6*/*RferOrco Xenopus* oocytes stimulated with a range of α-pinene concentrations. **(D)** Dose–response curve of *RferOr6*/*RferOrco Xenopus* oocytes stimulated by α-pinene. α-pinene EC50 = 9.447 × 10^{-5} M. Error bars indicate SEM (n = 6). **(E)** Inward current responses of *RferOr40*/*RferOrco Xenopus* oocytes in response to 29 tested compounds at the concentration of 10^{-4} M. **(F)** Inward current responses of RferOr87/*RferOrco Xenopus* oocytes in response to 29 tested compounds at the concentration of 10^{-4} M.

Consequently, our results demonstrated that non-host plant volatile α-pinene may be detected by antenna-biased expressed *RferOr6*, thereby possibly regulating RPW to avoid feeding and egg oviposition on unsuitable hosts.

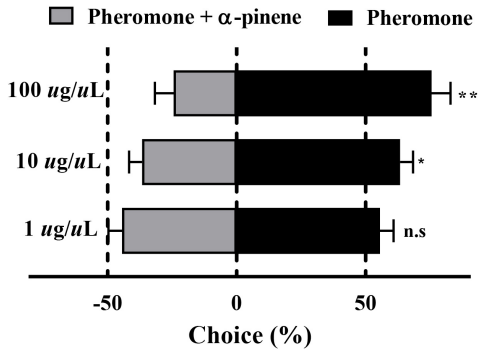

FIGURE 4 | Behavioral response of RPW to α-pinene. The significantly reduced attraction of RPW was elicited by mixed compounds at the concentrations of 10 and 100 μg/μl. No obvious difference was observed at 1 μg/μl. Statistical differences were analyzed by multiple t tests. n.s > 0.05, *P < 0.05, and **P < 0.01. Data indicate the mean ± SEM, N = 60.

A recent phylogenetic analysis included 1,181 ORs from 10 species representing the four coleopteran suborders, and one species of the sister order *Strepsiptera* showed OR Group 7 subfamily, which is highly expanded in coleopterans (Mitchell et al., 2020). Not only aggregation pheromone receptors of *I. typographus* (Hou et al., 2020; Yuvaraj et al., 2021) and *R. ferrugineus* (Antony et al., 2021) but also ORs of *I. typographus* responding to volatiles released by the host trees or the symbiotic fungi (Hou et al., 2020) were presented within this subfamily. Therefore, the functional characterization of ORs in beetles tends to focus on this clade. However, less attention on the lineage-specific expansions and odor specificity may evolve alone with OR-lineage radiations. According to previous studies, targeted *RferOrs* for following the functional characterization are part of an Rfer-specific OR-lineage of RPW, and this lineage belongs to the monophyletic OR Group 2 subfamily in beetles (Mitchell et al., 2012, 2020; Yuvaraj et al., 2021). The phylogenetic tree shows that Orcos were clustered into one branch, which is highly conserved among different insects. Also, ORs vary significantly between four beetles with low sequence homology (**Figure 1A**). Seven *RferOrs* were observed as clustered into one branch and obviously showed species specificity and this suggests that these ORs are related to certain life activities of RPW. Interestingly, previous study suggested that two aggregation pheromone

receptors (i.e., McOr5 and McOr20) of *M. caryae* are scattered in the Group 2 subfamily (Mitchell et al., 2012). In contrary to our initial prediction, we obtained these receptors possibly related to aggregation pheromone compounds of RPW. In this study, the functional results suggested that *RferOr6* was shown to selectively respond to the non-host compound α-pinene. Our findings indicate that ORs from this clad may detect compounds from various biological sources. Hence, the large-scale functional characterization of the OR repertoires of *R. ferrugineus* and additional species is required to further our understanding of the relationships of OR between species.

Actually, the expression pattern of ORs may vary considerably between sexes, developmental stages, or olfactory tissues, and the expression pattern determines their functions to some extent (Alabi et al., 2014). *RferOr6*, *RferOr40*, and *RferOr87* were highly expressed in antennae and *RferOr6* obviously showed the higher expression level in female antennae than male antennae, while *RferOr40* and *RferOr*87 showed no significant difference (**Figure 2**), and thus they function in the detection of volatiles. The *Xenopus* oocyte expression system was widely used to study the connection between ORs and volatiles (Fleischer et al., 2018). When three targeted *RferOrs* were co-expressed with *RferOrco*, *RferOr6* had a very high affinity with an EC_{50} of 9.447×10^{-5}, which indicated that *RferOr6*/*RferOrco* was sensitive to α-pinene. Furthermore, *RferOr6*/*RferOrco* that did not respond to other compounds indicated that *RferOr6*/*RferOrco* had a specific response to α-pinene, whereas no responses have been observed for 29 chemicals from *RferOr40* and *RferOr87*. Therefore, our results demonstrated that *RferOr6* was a functional OR possibly used by RPW to detect compounds in non-palm trees.

In fact, many insects generally show a tendency response to host plant volatiles and non-selectivity or repellency to non-host plant volatiles (Mann et al., 2012; Krause Pham and Ray, 2015). For example, *Cupressus lusitanica* and *Eucalyptus saligna* leaf essential oils are promising insecticides and repellents to be used against insect pests of *Tribolium castaneum*, *Acanthoscelides obtectus*, *Sitotroga cerealella*, and *Sitophilus zeamais* (Bett et al., 2016). Several terpene volatiles [(1R)-(+)-α-pinene, (−)-β-pinene, (R)-(+)-limonene and β-myrcene] released by coniferous trees exhibited significant repellent behavioral responses of Leguminosae pest *Colposcelis signata* (Fan et al., 2020). Previous studies indicated that the behavioral response of insects can be adjusted by detecting non-host-specific compounds (like taxonomically specific compounds) or the different ratios of common plant volatiles in non-host plants with the host plants (Pickett et al., 2012). Given that α-pinene is the compound of coniferous trees with a characteristic odor, several species of conifer-feeding beetles were attracted to the conifer monoterpenes (i.e., α-pinene, β-pinene, myrcene, limonene, camphene, and carene) (Chénier and Philogène, 1989). Considering, α-pinene was not one of the volatile compounds of *Phoenix canariensis* (Vacas et al., 2014), it seems reasonable for α-pinene to exhibit significant repellent to RPW. Since studies on palm volatile profiles are limited to some extent, it is not clear whether α-pinene is a compound of other palm plant volatiles or released only when it is harmed by RPW.

CONCLUSION

RferOr6 is highly expressed in the female antennae and possibly be used by RPW to detect α-pinene to regulate females avoiding feeding and egg oviposition on non-palm trees. 1-Octen-3-ol has been known as a repellent of *Meligethes aeneus* F. (Smart and Blight, 2000) and *Dendroctonus* spp. (Pureswaran and Borden, 2004). Repellent activity of geraniol toward a number of other coleopteran species is also reported (Olivero-Verbel et al., 2010). Unfortunately, the key functional response of ORs to these compounds has not yet been identified. Consequently, it is necessary to characterize more functional ORs related to non-palm plant volatiles and provide a fundamental basis for understanding the RPW olfactory molecular recognition mechanism of host plant volatiles in future studies.

DATA AVAILABILITY STATEMENT

The datasets presented in this study can be found in online repositories. The names of the repository/repositories and accession number(s) can be found below: https://www.ncbi.nlm.nih.gov/, MW979236; https://www.ncbi.nlm.nih.gov/, MW979238; and https://www.ncbi.nlm.nih.gov/, MW979247.

AUTHOR CONTRIBUTIONS

GW and YH designed the experiments and revised the manuscript. TJ, ZX, and QJ performed the experiments. TJ wrote the manuscript and analyzed the data. All authors contributed to the article and approved the submitted version.

FUNDING

We are very grateful for the grant from the National Natural Science Foundation of China (U1705232 and 31872033), the National Key R&D Program of China (2017YFC1200605), and the Fujian Science and Technology Special Project (2017NZ0003-1-6).

SUPPLEMENTARY MATERIAL

The Supplementary Material for this article can be found online at: https://www.frontiersin.org/articles/10.3389/fphys.2021.701545/full#supplementary-material

REFERENCES

Alabi, T., Marion-Poll, F., Danho, M., Mazzucchelli Pauw, E. D., Haubruge, E., and Francis, F. (2014). Identification of taste receptors and proteomic characterization of the antenna and legs of *Tribolium brevicornis*, a stored food product pest. *Insect. Mol. Biol.* 23, 1–12. doi: 10.1111/imb.12056

Andersson, M. N., Grosse-Wilde, E., Keeling, C. I., Bengtsson, J. M., Yuen, M. M., Li, M., et al. (2013). Antennal transcriptome analysis of the chemosensory gene families in the tree killing bark beetles, *Ips typographus* and *Dendroctonus ponderosae* (*Coleoptera*: *Curculionidae*: *Scolytinae*). *BMC Genomics* 14:198. doi: 10.1186/1471-2164-14-198

Antony, B., Johny, J., and Aldosari, S. A. (2018). Silencing the odorant binding protein *RferOBP1768* reduces the strong preference of palm weevil for the major aggregation pheromone compound ferrugineol. *Front. Physiol.* 9:252. doi: 10.3389/fphys.2018.00252

Antony, B., Johny, J., Montagné, N., Jacquin-Joly, E., Capoduro, R., Cali, K., et al. (2021). Pheromone receptor of the globally invasive quarantine pest of the palm tree, the red palm weevil (*Rhynchophorus ferrugineus*). *Mol. Ecol.* 30, 2025–2039. doi: 10.1111/mec.15874

Antony, B., Soffan, A., Jakše, J., Abdelazim, M. M., Aldosari, S. A., Aldawood, A. S., et al. (2016). Identification of the genes involved in odorant reception and detection in the palm weevil *Rhynchophorus ferrugineus*, an important quarantine pest, by antennal transcriptome analysis. *BMC Genomics* 17:69. doi: 10.1186/s12864-016-2362-6

Bentley, M. D., and Day, J. F. (1989). Chemical ecology and behavioral aspects of mosquito oviposition. *Ann. Rev. Entomol.* 34, 401–421. doi: 10.1146/annurev.en.34.010189.002153

Benton, R., Sachse, S., Michnick, S. W., and Vosshall, L. B. (2006). Atypical membrane topology and heteromeric function of *Drosophila* odorant receptors *in vivo*. *PLoS Biol.* 4:e20. doi: 10.1371/journal.pbio.0040020

Bett, P. K., Deng, A. L., Ogendo, J. O., Kariuki, S. T., Kamatenesi-Mugisha, M., Mihale, J. M., et al. (2016). Chemical composition of *Cupressus lusitanica* and *Eucalyptus saligna* leaf essential oils and bioactivity against major insect pests of stored food grains. *Ind. Crop. Prod.* 82, 51–62. doi: 10.1016/j.indcrop.2015.12.009

Brand, P., Robertson, H. M., Lin, W., Pothula, R., Klingeman, W. E., Jurat-Fuentes, J. L., et al. (2018). The origin of the odorant receptor gene family in insects. *Elife* 7:e38340. doi: 10.7554/eLife.38340

Butera, G., Ferraro, C., Colazza, S., Alonzo, G., and Quatrini, P. (2012). The culturable bacterial community of frass produced by larvae of *Rhynchophorus ferrugineus* olivier (*Coleoptera*: *curculionidae*) in the Canary island date palm. *Lett. Appl. Microbiol.* 54, 530–536. doi: 10.1111/j.1472-765X.2012.03238.x

Carey, A. F., Wang, G., Su, C. Y., Zwiebel, L. J., and Carlson, J. R. (2010). Odorant reception in the malaria mosquito *Anopheles gambiae*. *Nature* 464, 66–71. doi: 10.1038/nature08834

Cattaneo, A. M., Gonzalez, F., Bengtsson, J. M., Corey, E. A., Jacquin-Joly, E., Montagne, N., et al. (2017). Candidate pheromone receptors of codling moth *Cydia pomonella* respond to pheromones and kairomones. *Sci. Rep.* 7:41105. doi: 10.1038/srep41105

Chapman, R. F. (2003). Contact chemoreception in feeding by phytophagous insects. *Annu. Rev. Entomol.* 48, 455–484. doi: 10.1146/annurev.ento.48.091801.112629

Chénier, J. V., and Philogène, B. J. (1989). Field responses of certain forest *Coleoptera* to conifer monoterpenes and ethanol. *J. Chem. Ecol.* 15, 1729–1745. doi: 10.1007/BF01012261

de Fouchier, A., Walker, W. B. 3rd, Montagné, N., Steiner, C., Binyameen, M., Schlyter, F., et al. (2017). Functional evolution of Lepidoptera olfactory receptors revealed by deorphanization of a moth repertoire. *Nat. Commun.* 8:15709. doi: 10.1038/ncomms15709

Faleiro, J. R. (2006). A review of the issues and management of the red palm weevil *Rhynchophorus ferrugineus* (*Coleoptera*: *rhynchophoridae*) in coconut and date palm during the last one hundred years. *Int. J. Trop. Insect. Sci.* 26, 135–154. doi: 10.1079/IJT2006113

Fan, R. D., Zhang, Y. K., Bi, J. R., Xu, W., and Zang, L. S. (2020). Electroantennogram and behavioral responses of *Colposcelis signata* adults to non-host plant volatiles. *Chin. J. Biol. Control* 4, 1–10. doi: 10.16409/j.cnki.2095-039x.2021.03.001

Fleischer, J., Pregitzer, P., Breer, H., and Krieger, J. (2018). Access to the odor world: olfactory receptors and their role for signal transduction in insects. *Cell. Mol. Life Sci.* 75, 485–508. doi: 10.1007/s00018-017-2627-5

Gadenne, C., Barrozo, R. B., and Anton, S. (2016). Plasticity in insect olfaction: to smell or not to smell? *Ann. Rev. Entomol.* 61, 317–333. doi: 10.1146/annurev-ento-010715-023523

Gonzalez, F., Bengtsson, J. M., Walker, W. B., Sousa, M. F. R., Cattaneo, A. M., Montagne, N., et al. (2015). A conserved odorant receptor detects the same 1-indanone analogs in a tortricid and a noctuid moth. *Front. Ecol. Evol.* 3:131. doi: 10.3389/fevo.2015.00131

Grosse-Wilde, E., Gohl, T., Bouche, E., Breer, H., and Krieger, J. (2007). Candidate pheromone receptors provide the basis for the response of distinct antennal neurons to pheromonal compounds. *Eur. J. Neurosci.* 25, 2364–2373. doi: 10.1111/j.1460-9568.2007.05512.x

Grosse-Wilde, E., Svatos, A., and Krieger, J. (2006). A pheromone-binding protein mediates the bombykol-induced activation of a pheromone receptor in vitro. *Chem. Senses* 31, 547–555. doi: 10.1093/chemse/bjj059

Guarino, S., Colazza, S., Peri, E., Bue, P. L., Germanà, M. P., Kuznetsova, T., et al. (2015). Behaviour-modifying compounds for management of the red palm weevil (*Rhynchophorus ferrugineus* Oliver). *Pest. Manag. Sci.* 71, 1605–1610. doi: 10.1002/ps.3966

Guarino, S., Peri, E., Bue, P. L., Germanà, M. P., Colazza, S., Anshelevich, L., et al. (2013). Assessment of synthetic chemicals for disruption of *Rhynchophorus ferrugineus* response to attractant-baited traps in an urban environment. *Phytoparasitica* 41, 79–88. doi: 10.1007/s12600-012-0266-9

Guo, M. B., Du, L. X., Chen, Q. Y., Feng, Y. L., Zhang, J., Zhang, X. X., et al. (2020). Odorant receptors for detecting flowering plant cues are functionally conserved across moths and butterflies. *Mol. Biol. Evol.* 38, 1413–1427. doi: 10.1093/molbev/msaa300

Hallem, E. A., and Carlson, J. R. (2006). Coding of odors by a receptor repertoire. *Cell* 125, 143–160. doi: 10.1016/j.cell.2006.01.050

Hallem, E. A., Ho, M. G., and Carlson, J. R. (2004). The molecular basis of odor coding in the *Drosophila* antenna. *Cell* 117, 965–979. doi: 10.1016/j.cell.2004.05.012

Hansson, B. S., and Stensmyr, M. C. (2011). Evolution of insect olfaction. *Neuron* 72, 698–711. doi: 10.1016/j.neuron.2011.11.003

Hou, X. Q., Yuvaraj, J. K., Roberts, R. E., Unelius, C. R., Löfstedt, C., and Andersson, M. N. (2020). Functional evolution of a bark beetle odorant receptor clade detecting monoterpenoids of different ecological origins. *bioRxiv* [preprint]. doi: 10.1101/2020.12.28.424525

Ju, R. T., Wang, F., Wan, F. H., and Li, B. (2011). Effect of host plants on development and reproduction of *Rhynchophorus ferrugineus* (Olivier) (*Coleoptera*: *curculionidae*). *J. Pest Sci.* 84, 33–39. doi: 10.1007/s10340-010-0323-4

Krause Pham, C., and Ray, A. (2015). Conservation of olfactory avoidance in *Drosophila* species and identification of repellents for *Drosophila suzukii*. *Sci. Rep.* 5:11527. doi: 10.1038/srep11527

Kreher, S. A., Kwon, J. Y., and Carlson, J. R. (2005). The molecular basis of odor coding in the *Drosophila* larva. *Neuron* 46, 445–456.

Livak, K. J., and Schmittgen, T. D. (2001). Analysis of relative gene expression data using real-time quantitative PCR and the 2 (-Delta Delta C(T)) method. *Methods* 25, 402–408. doi: 10.1006/meth.2001.1262

Mann, R. S., Tiwari, S., Smoot, J. M., Rouseff, R. L., and Stelinski, L. L. (2012). Repellency and toxicity of plant-based essential oils and their constituents against *Diaphorina citri Kuwayama* (*Hemiptera*: *psyllidae*). *J. Appl. Entomol.* 136, 87–96. doi: 10.1111/j.1439-0418.2010.01592.x

Mathew, D., Martelli, C., Kelley-Swift, E., Brusalis, C., Gershow, M., Samuel, A. D., et al. (2013). Functional diversity among sensory receptors in a *Drosophila* olfactory circuit. *Proc. Natl. Acad. Sci. U. S. A.* 110, 2134–2143.

Mitchell, R. F., Hughes, D. T., Luetje, C. W., Millar, J. G., Soriano-Agatón, F., Hanks, L. M., et al. (2012). Sequencing and characterizing odorant receptors of the cerambycid beetle *Megacyllene caryae*. *Insect Biochem. Mol. Biol.* 42, 499–505. doi: 10.1016/j.ibmb.2012.03.007

Mitchell, R. F., Schneider, T. M., Schwartz, A. M., Andersson, M. N., and McKenna, D. D. (2020). The diversity and evolution of odorant receptors in beetles (*Coleoptera*). *Insect Mol. Biol.* 29, 77–91. doi: 10.1111/imb.12611

Montagne, N., de Fouchier, A., Newcomb, R. D., and Jacquin-Joly, E. (2015). Advances in the identification and characterization of olfactory receptors in

insects. *Prog. Mol. Biol. Transl. Sci.* 130, 55–80. doi: 10.1016/bs.pmbts.2014.11.003

Nakagawa, T., Sakurai, T., Nishioka, T., and Touhara, K. (2005). Insect sex-pheromone signals mediated by specific combinations of olfactory receptors. *Science* 307, 1638–1642.

Olivero-Verbel, L., Nerio, L. S., and Stashenko, E. E. (2010). Bioactivity against *Tribolium castaneum* Herbst (*Coleoptera*: *tenebrionidae*) of *Cymbopogon citratus* and *Eucalyptus citriodora* essential oils grown in Colombia. *Pest. Manag. Sci.* 66, 664–668. doi: 10.1002/ps.1927

Pickett, J. A., Aradottir, G. A., Birkett, M. A., Bruce, T. J. A., Chamberlain, K., Khan, Z. R., et al. (2012). Aspects of insect chemical ecology: exploitation of recognition and detection as tools for deception of pests and beneficial insects. *Physiol. Entomol.* 37, 2–9. doi: 10.1111/j.1365-3032.2011.00828.x

Pureswaran, D. S., and Borden, J. H. (2004). New repellent semiochemicals for three species of *Dendroctonus* (*Coleoptera*: *scolytidae*). *Chemoecology* 14, 67–75. doi: 10.1007/s00049-003-0260-2

Robertson, H. M. (2019). Molecular evolution of the major arthropod chemoreceptor gene families. *Annu. Rev. Entomol.* 64, 227–242. doi: 10.1146/annurev-ento-020117-043322

Sakurai, T., Nakagawa, T., Mitsuno, H., Mori, H., Endo, Y., Tanoue, S., et al. (2004). Identification and functional characterization of a sex pheromone receptor in the silkmoth *Bombyx mori*. *Proc. Natl. Acad. Sci. U. S. A.* 101, 16653–16658. doi: 10.1073/pnas.0407596101

Shi, Z. H., Lin, Y. T., and Hou, Y. M. (2014). Mother-derived trans-generational immune priming in the red palm weevil, *Rhynchophorus ferrugineus* Olivier (*Coleoptera*, *Dryophthoridae*). *Bull. Entomol. Res.* 104, 742–750. doi: 10.1017/S0007485314000583

Smart, L. E., and Blight, M. M. (2000). Response of the pollen beetle, *Meligethes aeneus*, to traps baited with volatiles from oilseed rape, *Brassica napus*. *J. Chem. Ecol.* 26, 1051–1064. doi: 10.1023/A:1005493100165

Suh, E., Bohbot, J., and Zwiebel, L. J. (2014). Peripheral olfactory signaling in insects. *Curr. Opin. Insect. Sci.* 6, 86–92.

Tamura, K., Stecher, G., Peterson, D., Filipski, A., and Kumar, S. (2013). MEGA6: molecular evolutionary genetics analysis version 6.0. *Mol. Biol. Evol.* 30, 2725–2729. doi: 10.1093/molbev/mst197

Thompson, J. D., Higgins, D. G., and Gibson, T. J. (1994). CLUSTAL W: improving the sensitivity of progressive multiple sequence alignment through sequence weighting, positionspecific gap penalties and weight matrix choice. *Nucleic Acids Res.* 22, 4673–4680. doi: 10.1093/nar/22.22.4673

Vacas, S., Abad-Payá, M., Primo, J., and Navarro-Llopis, V. (2014). Identification of pheromone synergists for *Rhynchophorus ferrugineus* trapping systems from Phoenix canariensis palm volatiles. *J. Agr. Food Chem.* 62, 6053–6064. doi: 10.1021/jf502663y

Wan, F. H., Yin, C. L., Tang, R., Chen, M. H., Wu, Q., Huang, C., et al. (2019). A chromosome-level genome assembly of *Cydia pomonella* provides insights into chemical ecology and insecticide resistance. *Nat. Commun.* 10:4237. doi: 10.1038/s41467-019-12175-9

Wang, G., Carey, A. F., Carlson, J. R., and Zwiebel, L. J. (2010). Molecular basis of odor coding in the malaria vector mosquito *Anopheles gambiae*. *Proc. Natl. Acad. Sci. U. S. A.* 107, 4418–4423. doi: 10.1073/pnas.0913392107

Wang, G., Vasquez, G. M., Schal, C., Zwiebel, L. J., and Gould, F. (2011). Functional characterization of pheromone receptors in the tobacco budworm *Heliothis virescens*. *Insect Mol. Biol.* 20, 125–133. doi: 10.1111/j.1365-2583.2010.01045.x

Wang, G. H., Zhang, X., Hou, Y. M., and Tang, B. Z. (2015). Analysis of the population genetic structure of *Rhynchophorus ferrugineus* in Fujian, China, revealed by microsatellite loci and mitochondrial COI sequences. *Entomol. Exp. Appl.* 155, 28–38. doi: 10.1111/eea.12282

Wang, X., Wang, S., Yi, J., Li, Y., Liu, J., Wang, J., et al. (2020). Three host plant volatiles, hexanal, lauric acid, and tetradecane, are detected by an antenna-biased expressed odorant receptor 27 in the dark black chafer *Holotrichia parallela*. *J. Agric. Food Chem.* 68, 7316–7323. doi: 10.1021/acs.jafc.0c00333

Wanner, K. W., Nichols, A. S., Allen, J. E., Bunger, P. L., Garczynski, S. F., Linn, C. E., et al. (2010). Sex pheromone receptor specificity in the European corn borer moth, *Ostrinia nubilalis*. *PLoS One* 5:e8685. doi: 10.1371/journal.pone.0008685

Wicher, D. (2015). Olfactory signaling in insects. *Prog. Mol. Biol. Transl. Sci.* 130, 37–54. doi: 10.1016/bs.pmbts.2014.11.002

Wuichet, K., and Zhulin, I. B. (2010). Origins and diversification of a complex signal transduction system in prokaryotes. *Sci. Signal.* 3:ra50. doi: 10.1126/scisignal.2000724

Yuvaraj, J. K., Roberts, R. E., Sonntag, Y., Hou, X. Q., Grosse-Wilde, E., Machara, A., et al. (2021). Putative ligand binding sites of two functionally characterized bark beetle odorant receptors. *BMC Biol.* 19:16. doi: 10.1186/s12915-020-00946-6

Conflict of Interest: The authors declare that the research was conducted in the absence of any commercial or financial relationships that could be construed as a potential conflict of interest.

Publisher's Note: All claims expressed in this article are solely those of the authors and do not necessarily represent those of their affiliated organizations, or those of the publisher, the editors and the reviewers. Any product that may be evaluated in this article, or claim that may be made by its manufacturer, is not guaranteed or endorsed by the publisher.

frontiers in Physiology

ORIGINAL RESEARCH
published: 12 August 2021
doi: 10.3389/fphys.2021.685012

Anatomical Comparison of Antennal Lobes in Two Sibling *Ectropis* Moths: Emphasis on the Macroglomerular Complex

Jing Liu[1], *Kang He*[2], *Zong-xiu Luo*[1], *Xiao-ming Cai*[1], *Lei Bian*[1], *Zhao-qun Li*[1]* and *Zong-mao Chen*[1]*

[1] Key Laboratory of Tea Biology and Resource Utilization, Ministry of Agriculture, Tea Research Institute, Chinese Academy of Agricultural Science, Hangzhou, China, [2] Institute of Insect Sciences, College of Agriculture and Biotechnology, Zhejiang University, Hangzhou, China

Ectropis obliqua and *Ectropis grisescens* are two sibling moth species of tea plantations in China. The male antennae of both species can detect shared and specific sex pheromone components. Thus, the primary olfactory center, i.e., the antennal lobe (AL), plays a vital role in distinguishing the sex pheromones. To provide evidence for the possible mechanism allowing this distinction, in this study, we compared the macroglomerular complex (MGC) of the AL between the males of the two species by immunostaining using presynaptic antibody and propidium iodide (PI) with antennal backfills, and confocal imaging and digital 3D-reconstruction. The results showed that MGC of both *E. obliqua* and *E. grisescens* contained five glomeruli at invariant positions between the species. However, the volumes of the anterior-lateral glomerulus (ALG) and posterior-ventral (PV) glomerulus differed between the species, possibly related to differences in sensing sex pheromone compounds and their ratios between *E. obliqua* and *E. grisescens*. Our results provide an important basis for the mechanism of mating isolation between these sibling moth species.

Keywords: glomeruli, macroglomerular complex, antennae backfill, antibody staining, *Ectropis obliqua*, *Ectropis grisescens*

OPEN ACCESS

Edited by:
Ya-Nan Zhang,
Huaibei Normal University, China

Reviewed by:
Yihan Xia,
Chalmers University of Technology, Sweden
Xin-Cheng Zhao,
Henan Agricultural University, China

***Correspondence:**
Zong-mao Chen
zmchen2006@163.com
Zhao-qun Li
zqli@tricaas.com

Specialty section:
This article was submitted to Invertebrate Physiology, a section of the journal Frontiers in Physiology

Received: *24 March 2021*
Accepted: *28 June 2021*
Published: *12 August 2021*

Citation:
Liu J, He K, Luo Z-x, Cai X-m, Bian L, Li Z-q and Chen Z-m (2021) Anatomical Comparison of Antennal Lobes in Two Sibling Ectropis Moths: Emphasis on the Macroglomerular Complex. Front. Physiol. 12:685012. doi: 10.3389/fphys.2021.685012

INTRODUCTION

The sophisticated olfactory system of insect species is a key physiological feature involved in behavioral decisions. In insects, olfactory cues are detected by olfactory receptor neurons (ORNs) housed in the antennal sensilla and projected to the antennal lobe (AL). The AL is the primary olfactory center of the brain responsible for integrating complex olfactory information (Homberg et al., 1989; Kuebler et al., 2012). Glomerulus, as the olfactory functional unit, is a subcompartment of the AL and is formed by dense synaptic and recipient dendrites from the ORNs that convey olfactory information from the antenna (Skiri et al., 2005; Yan et al., 2019). The number of glomeruli is species-specific, and their total volume and position are closely related to the complexity of odorant recognition (Berg et al., 2014; Wu et al., 2015).

The macroglomerular complex (MGC) specifically translates sex pheromone information and is a male-specific structure in moth species. Although some species possess a single MGC component (Varela et al., 2009), most moth species have three to four

MGC glomeruli (Hansson et al., 1994; Lee et al., 2006; Namiki et al., 2014; Nirazawa et al., 2017; Jiang et al., 2019; Yan et al., 2019; Dong et al., 2020). Different groups of moth species display different anatomical features. Noctuid species normally possess one large MGC at the entrance of the antennal nerves and smaller satellite glomeruli (Berg et al., 2014). However, in *Bombycinae* species, the cumulus coexists with the toroid in different volume combinations (Namiki et al., 2014).

Sibling moth species generally have the same number of MGC glomeruli. Nevertheless, the position of the MGC glomeruli is slightly different in *Helicoverpa* species (Xu et al., 2016a,b), while the same number and position of MGC glomeruli are present in *Heliothine* species (Vickers and Christensen, 2003). The study of two *Helicoverpa* sibling species, *Helicoverpa armigera* and *H. assulta*, showed that different combinations of certain glomeruli positions and volumes in the MGC could reflect the ratio of the major and minor sex pheromone compartments, which play a vital role in sex pheromone discrimination (Wu et al., 2013).

According to their chemical structures, the sex pheromones emitted from female moths are classified into two main groups: Type I pheromones (75%) are composed of unsaturated compounds with a C10–C18 straight chain and a terminal functional group, such as hydroxyl, acetoxyl, or formyl groups; and Type II pheromones (15%) are composed of unsaturated hydrocarbons and epoxy derivatives with a C17–C23 straight chain. Type I pheromones have been identified from species within various families, such as Crambidae, Tortricidae, and Noctuidae; Type II pheromones are mainly produced by species within highly evolved insect groups, such as Geometridae, Lymantriidae, and Arctiidae moths (Touhara, 2013). However, most studies comparing the AL MGC of sibling moth species have focused on species producing Type I pheromones (Varela et al., 2011). With the rare exception of studies on single species, no anatomical or physiological comparison has been performed for the MGC of species producing Type II pheromones (Namiki et al., 2012).

Ectropis obliqua and *E. grisescens* (Lepidoptera, Geometridae) are two sibling herbivorous pest species of tea plantations. These two species co-occur in the tea plantations of southeast China and share similar sex pheromone components (Luo et al., 2017; Li et al., 2019). The sex pheromone components of *E. grisescens* females were identified as (Z,Z,Z)-3,6,9-octadecatriene (Z3,Z6,Z9-18:H) and (Z,Z)-3,9-cis-6,7-epoxy-octadecadiene (Z3,epo6,Z9-18:H) and those of *E. obliqua* were Z3,Z6,Z9-18:H, Z3,epo6,Z9-18:H, and (Z,Z)-3,9-cis-6,7-epoxy-nonadecadiene (Z3,epo6,Z9-19:H). These sex pheromones of both species are Type II and differences in sex pheromone compounds and their ratios play important roles in the mating isolation of these two sibling species (Touhara, 2013; Luo et al., 2017). Single sensilla recording (SSR) showed the tricoid sensilla type of both species can recognize all three components of the sex pheromones (Liu et al., 2019). However, the population density of the ORNs tuned to the minor component, i.e., Z3,Z6,Z9-18:H, differs between the two species. The reasons for this difference in interspecific sex pheromone recognition and how olfactory information is processed at the primary olfactory center level are still unknown. Therefore, in this study, we compared the anatomy of MGC in *E. obliqua* and *E. grisescens* to determine whether differences in glomeruli number, position, and volume between these two moth species can explain the mechanism of sex pheromone discrimination between them.

MATERIALS AND METHODS

Larvae of male *E. obliqua* were collected from a tea plantation belonging to the Tea Research Institute, Chinese Academy of Agricultural Science, Hangzhou City, Zhejiang Province, China (30.10°N, 120.5°E). Male and female *E. grisescens* larvae were collected from a Yuchacun Tea Co., Ltd. tea plantation in Shaoxing City, Zhejiang Province, China (29.56°N, 120.41°E). After species identification (Li et al., 2019), the larvae were separately reared on fresh tea shoots in a climate-controlled chamber at 25°C, with 60% relative humidity, and a photoperiod of 12:12 h (light:dark). On the second day after eclosion, adults of both species were selected for the experiment.

The presynaptic antibody SYNORF1 (Developmental Studies Hybridoma Bank, University of Iowa, Iowa City, IA, USA) was used for immunostaining to visualize the AL glomerular structure. Eight or nine male moths of both species were anesthetized on ice. Heads were separated from the body and brains were dissected in Ringer's solution. After fixation in 4% paraformaldehyde solution in phosphate-buffered saline (PBS; 0.01M, pH 7.4) overnight at 4°C, the brains were rinsed in PBS four times (20 min per rinse) and pre-incubated in 5% normal goat serum (Sigma Aldrich, St. Louis, MO, USA) in PBS containing 0.5% Triton X-100 (PBST; 0.01 M, pH 7.4) for 3 h at room temperature (20–25°C) to diminish the staining disturbance. Following incubation in the primary antibody SYNORF1 at 1:50 in PBST at 4°C for 7 days, the brains were rinsed in PBS six times (20 min per rinse) and then incubated

TABLE 1 | Specimen thickness of lateral cell cluster (LCCL), medial cell cluster (MCCl), and antennal lobe (AL) in male *Ectropis. grisescens* and *Ectropis obliqua*.

Specimen		MCCL thickness (μm/slices)	LCCL thickness (μm/slices)	AL thickness (μm/slices)	MCCL /AL	LCCL /AL	*n*
Male	Average	49.54/70.29	79.98/116	143.51/198.57	0.35	0.57	7
E. obliqua	SD	10.42/18.39	10.02/15	25.44/26.32	0.08	0.12	
Male	Average	62.91/94.83	101.95/154	170.96/257.67	0.39	0.60	6
E. grisescens	SD	10.88/16.42	24.45/37	38.10/57.19	0.12	0.10	

Data were extracted by ZEN software. n indicated the number of specimens.

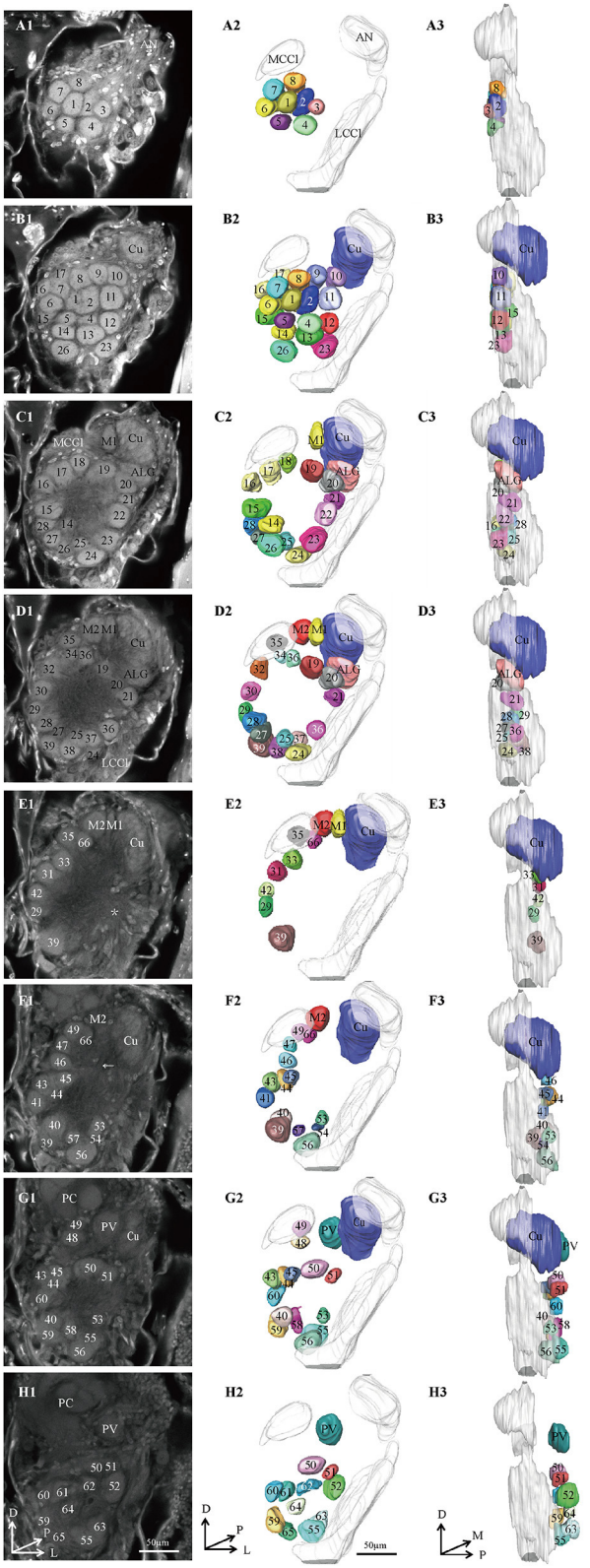

FIGURE 1 | Confocal images and 3D reconstructions of the AL glomeruli of male E. obliqua in a frontal view. **(A1–H1)** confocal images of AL sections at

(Continued)

FIGURE 1 | different depths. The most anterior glomeruli, at 13 μm (A), 22 μm (B), 35 μm (C), 46 μm (D), 56 μm (E), 67 μm (F), 76 μm (G), and 92 μm (H). **(A2–H2)** 3D reconstructions of glomeruli from the confocal images shown in **(A1–H1)** (frontal view). **(A3–H3)** lateral view of the 3D reconstructions shown in **(A2–H2)** AN, antennal nerve; LCCl, lateral cell cluster; MCCl, medial cell cluster; PC, protocerebrum; Cu, cumulus; ALG, anterior-lateral glomerulus; M1, medial glomerulus 1; M2, medial glomerulus 2; PV, posterior-ventral glomerulus. The arrow indicates bundles of MCCl and the star indicates bundles of LCCl. A, anterior; D, dorsal; M, medial. Scale bars 50 μm. Images were drawn by AMIRA 5.3 and further enhanced by adobe illustrator CS 5.

in the secondary antibody, Cy™2-conjugated anti-mouse IgG (H + L) (Cy™2; Jackson Immuno Research, GE Healthcare Bio-Sciences Ltd., West Grove, PA, USA; dilution 1:150 in PBST) at 4°C for 5 days. After this period, the brains were rinsed in PBS six times (20 min per rinse), dehydrated in an ascending ethanol series, and mounted in methyl salicylate.

To mark the olfactory receptor neurons (ORNs) axons, backfills of the antennal nerve were performed using the neuronal tracer neurobiotin (Vector Laboratories, Burlingame, CA, USA). Neurobiotin backfilled antennal nerves were counterstained with propidium iodide (PI; MedChem Express, Monmouth Junction, NJ, USA). The neurobiotin concentration applied (1%) was the same used in similar studies on other insect species (Yan et al., 2019). The insect was fixed in a cone-shaped plastic tube exposing the head and the antennae out of one tip of the tube. Both antennae were cut at the base of the flagellum and the antennal nerve was exposed. The tip of a 2-mm long pipette was filled with the neurobiotin solution; one end of the tip was then sealed with Vaseline. The other end of the pipette tip, which covered the cut end of the antenna, was closed and immobilized with Vaseline. The cut antenna was placed into the pipette ensuring the cut end of the AL was immersed in the neurobiotin tracer solution. Whole preparations were incubated in a dark box with moist paper to avoid desiccation for 24–36 h at 4°C. Then, brains were dissected in Ringer's solution and fixated in 4% paraformaldehyde in PBS (0.1 M, pH 7.4) at 4°C for 1–2 days. For neurobiotin staining, brains were incubated in 2 μg/mL Alexa-488 Streptavidin solution in PBS (pH7.4; Yeason, Shanghai, China) for 1–2 days. Counterstaining was developed using 10 μg/mL PI solution for 30 min at room temperature (20–25°C).

Confocal laser scanning microscopy (LSM 510, META Zeiss, Jena, Germany) was used for AL tomography scanning (objectives: Plan-Neofluar 20 ×/0.5 L) at a step size of 0.3 μm. A 488-nm line of an argon laser was used to excite the Cy™2 antibody or Alexa-488 Streptavidin. The serial optical images were obtained after scanning at a resolution of 512 × 512 pixels. The 3D structure of the AL glomeruli was obtained from reconstructed confocal image stacks by using the AMIRA 5.3 software (Visage Imaging, Fürth, Germany). The volumes of individual glomeruli were measured by the "Tissue Statistics" tool and the quantitative data were imported to Microsoft Excel (Microsoft Corp., Redmond, WA, USA) for further processing.

Male *E. obliqua* and *E. grisescens* were used for presynaptic antibody staining and backfills combined with PI. Only backfills were applied to female *E. grisescens*.

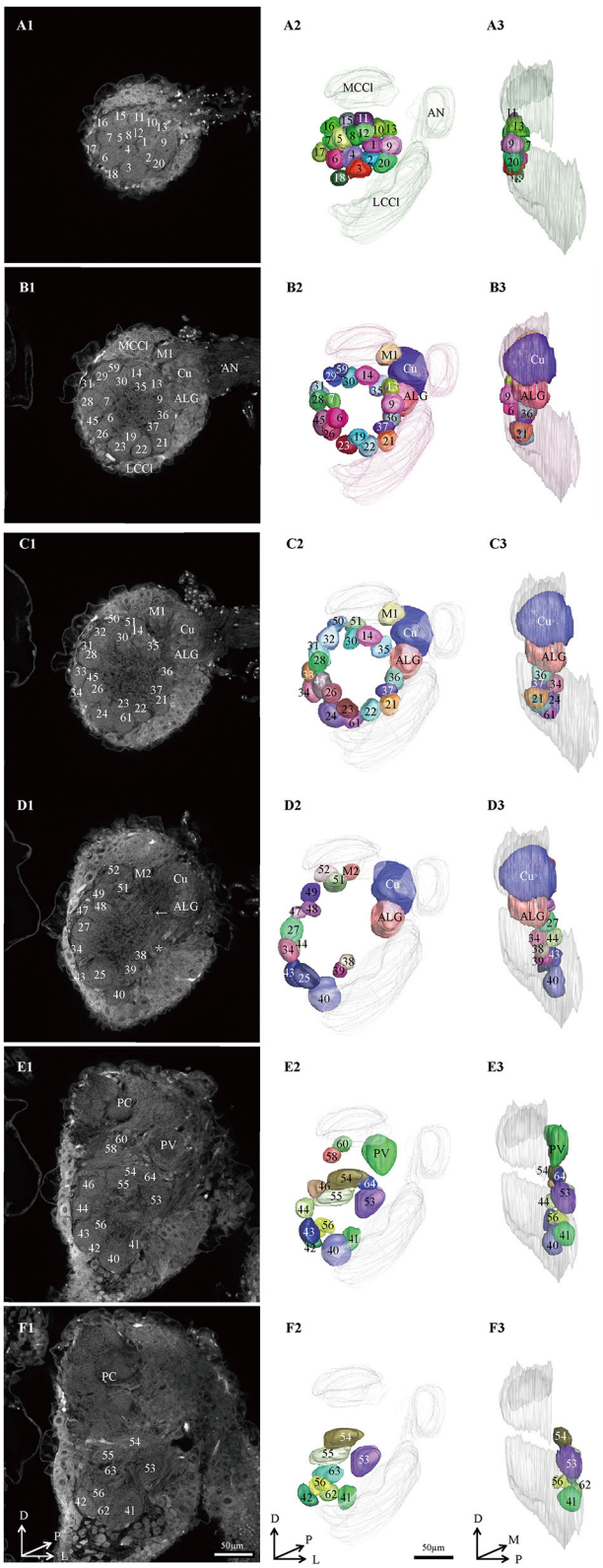

FIGURE 2 | Confocal images and 3D reconstructions of the AL glomeruli of male *E. Grisescens* in a frontal view. **(A1–F1)** confocal images of AL sections *(Continued)*

FIGURE 2 | at different depths. The most anterior glomeruli, at 13 μm (A), 33 μm (B), 46 μm (C), 72 μm (D), 90 μm (E), and 104 μm (F). **(A2–F2)** 3D reconstructions of glomeruli from the confocal images shown in **(A1–F1)** (frontal view). **(A3–F3)** lateral view of the 3D reconstructions shown in **(A2–F2)**. AN, antennal nerve; LCCl, lateral cell cluster; MCCl, medial cell cluster; PC, protocerebrum; Cu, cumulus; ALG, anterior-lateral glomerulus; M1, medial glomerulus 1; M2, medial glomerulus 2; PV, posterior-ventral glomerulus; A, anterior; D, dorsal; M, medial. Scale bars 50 μm. Images were drawn by AMIRA 5.3 and further enhanced by adobe illustrator CS 5.

The glomerular volume data were analyzed by one-away ANOVA and *t*-tests in SigmaPlot.

RESULTS

Histology of the AL of *E. obliqua* and *E. grisescens*

Thirteen AL spheres from the brains of nine male *E. obliqua* and ten AL spheres from the brains of *eight* male *E. grisescens* were reconstructed in this study. In both species, the AL was positioned at the posterior deutocerebrum of the brain, as previously described for other species (Berg et al., 2002; Zhao et al., 2016). The exterior of the AL was similar in both species, except for the larger hemi-lateral sphere. The thickness of the AL was 143.371 ± 25.16 μm and 170.96 ± 38.10 μm in *E. obliqua* and *E. grisescens*, respectively (**Table 1**). One sphere of the AL was composed of many neuropil units of spheroidal shape, called glomerulus. All glomeruli were distributed in a demarcated layer surrounding the hub (**Figures 1**, **2**). The lateral cell cluster (LCCl) and medial cell cluster (MCCl) were stained by both the antibody and PI (**Figures 1**, **2**, **6I,K,L,N**). The LCCl and MCCl were positioned dorsal-medially and lateral-ventrally of the AL, respectively (**Figures 1**, **2**). The average thickness of LCCl was larger than that of MCCl in both *E. obliqua* and *E. grisescens*. Although specimens of MCCl and LCCl were slightly thicker in *E. grisescens*, the ratio to AL thickness displayed no significant difference between the species (**Table 1**).

Identification of Glomeruli of the Whole Antennal Lobe in Male *E. obliqua* and *E. grisescens* and the Dimorphism Between Male and Female *E. grisescens*

In order to identify the male-specific glomeruli of *E. obliqua* and *E. grisescens*, we reconstructed the whole AL sphere of male *E. obliqua* and *E. grisescens* and female *E. grisescens*. The glomerulus of the AL was marked by Arabic numerals in a clockwise direction from anterior to posterior (**Figures 1**, **2**). Four areas were easily recognized by the position and shape of the glomeruli and are described below. Area 1 was the entrance of the antennal nerve and contained a large glomerulus, called cumulus in male *E. obliqua* and *E. grisescens*. Around the cumulus were four smaller satellite glomeruli, and all five glomeruli were larger than the adjacent glomeruli in male *E. gresescens* and *E. obliqua*, therefore, they were primarily identified as the MGC

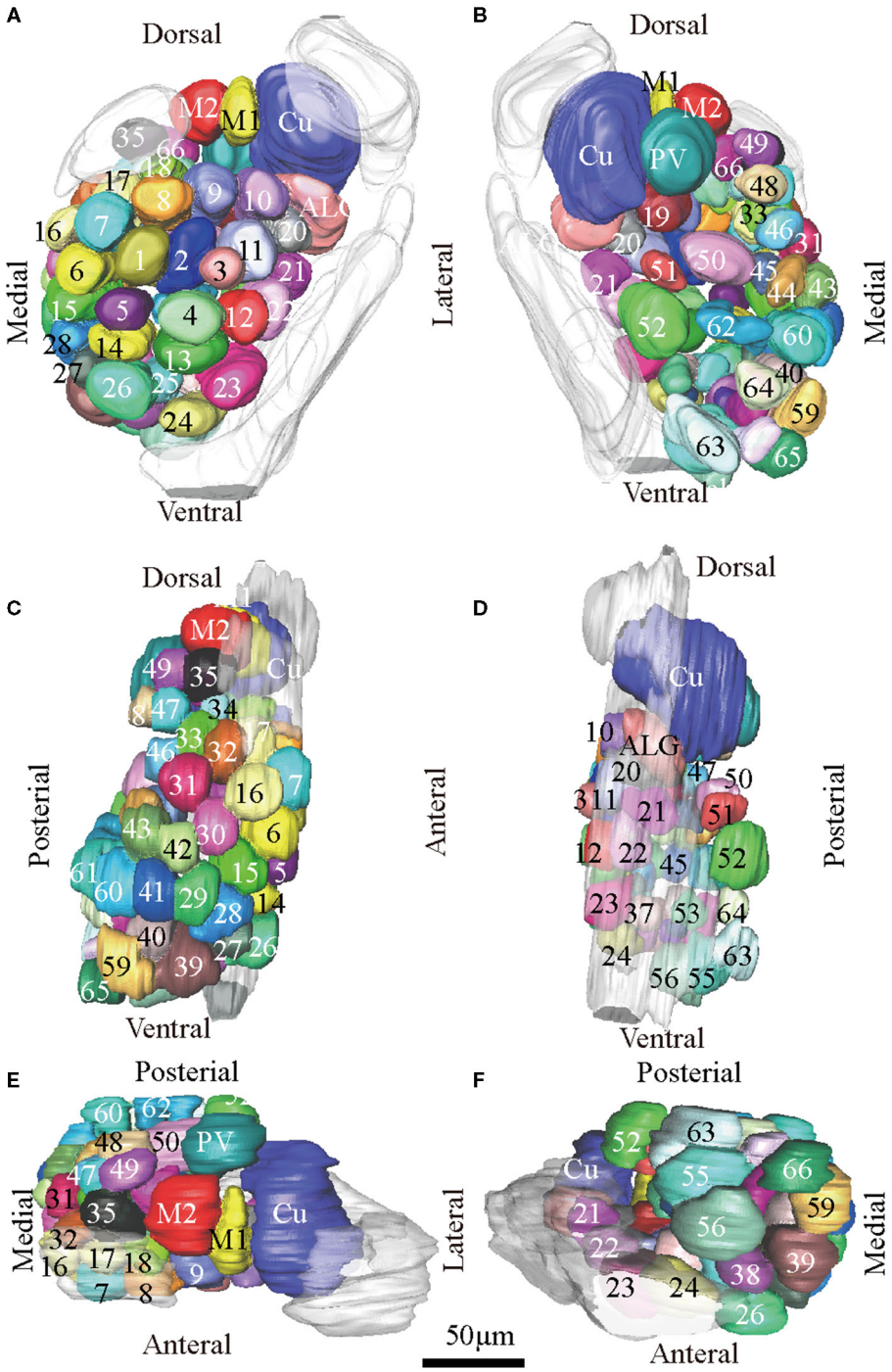

FIGURE 3 | Atlas of the 3D reconstruction of the left AL of male *E. obliqua*. All glomeruli are reconstructed and given a specific number and color. **(A)** anterior view. **(B)** posterior view. **(C)** medial view. **(D)** lateral view. **(E)** dorsal view. **(F)** ventral view. Cu, cumulus; ALG, anterior-lateral glomerulus; M1, medial glomerulus 1; M2, medial glomerulus 2; PV, posterior-ventral glomerulus. Dotted outline indicated MGC area in **(A,B)**. Scale bar is 50 μm (applies to **A–F**). Images were drawn by AMIRA 5.3 and further enhanced by adobe illustrator CS 5.

and landmarked by the antennal nerve and cumulus (**Figures 3**, **4**). Area 2 was the dorsal-medial area landmarked as G35 for *E. obliqua* (**Figure 3**) and G52 for *E. grisescens* (**Figures 4**, **5**). This area was located at the dorsal edge of the AL and adjacent to M2. Area 3 was the ventral area, landmarked as G56, G59 for *E. obliqua* (**Figure 3**), and G40 and G42 for *E. grisescens*

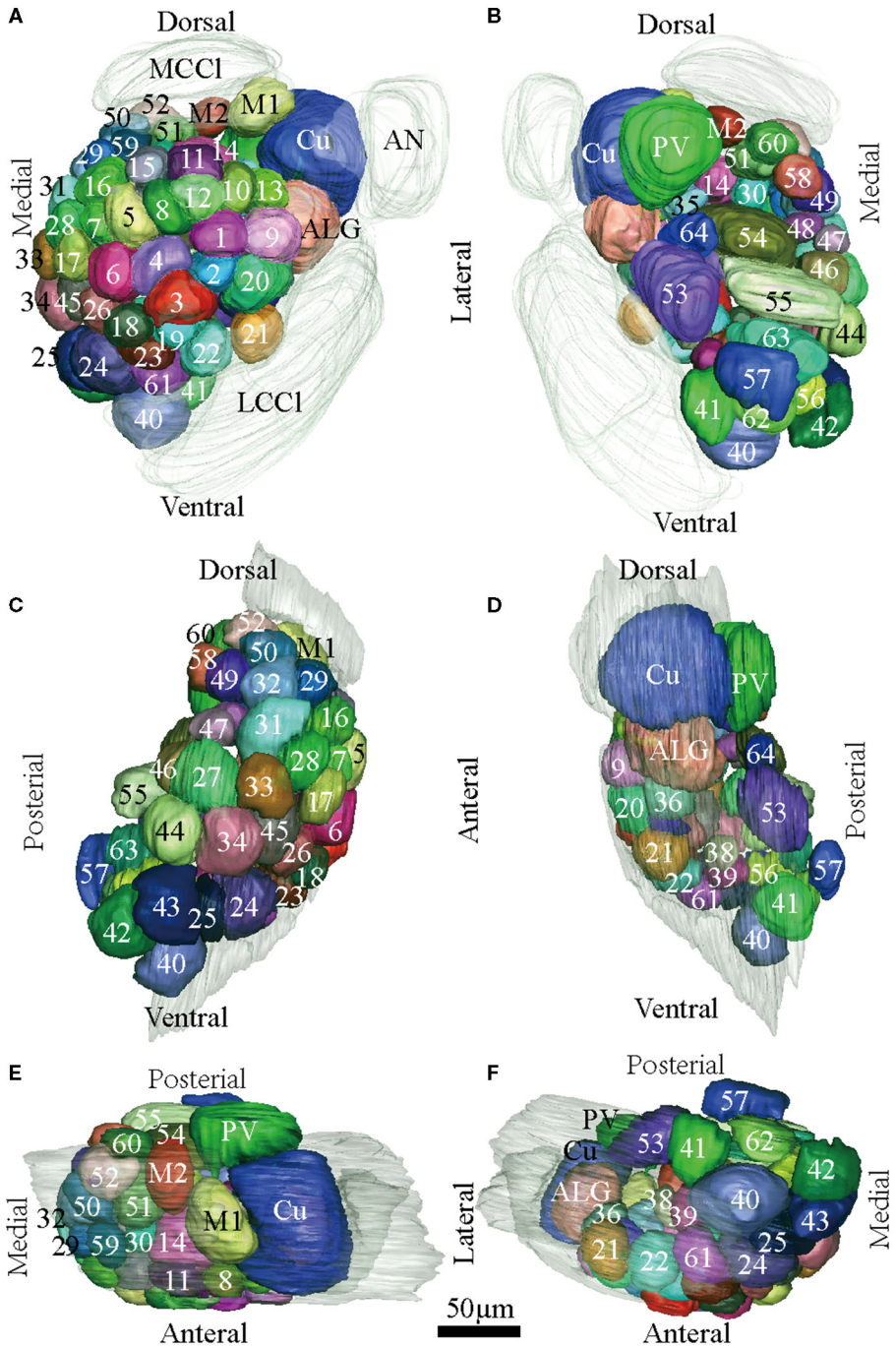

FIGURE 4 | Atlas of the 3D reconstruction of the left AL of male *E. Grisescens*. All glomeruli are reconstructed and given a specific number and color. **(A)** anterior view. **(B)** posterior view. **(C)** medial view. **(D)** lateral view. **(E)** dorsal view. **(F)** ventral view. Cu, cumulus; ALG, anterior-lateral glomerulus; M1, medial glomerulus 1; M2, medial glomerulus 2; PV, posterior-ventral glomerulus. Dotted outline indicated MGC area in **(A,B)**. Scale bar is 50 μm (applies to **A–F**). Images were drawn by adobe illustrator CS 5. Images were drawn by AMIRA 5.3 and further enhanced by adobe illustrator CS 5.

(**Figures 4**, **5**). G59 and G42 were deeper stained by presynaptic antibody and PI, shown at the slices (**Figures 1G1**, **2F1**), and G56 and G40 did not project from the ORNs dendrite (**Figures 6J,M**). Area 4 was the posterior area, landmarked as G50, G51, and G52 for *E. obliqua* (**Figure 3**) and G53, G54, and G64 for *E. grisescens* (**Figures 4**, **5**). This area was situated at the posterior edge of the AL, and G50 and G53 were clavate (Landmarks were shown in **Table 2**). Glomeruli of these four areas were identified

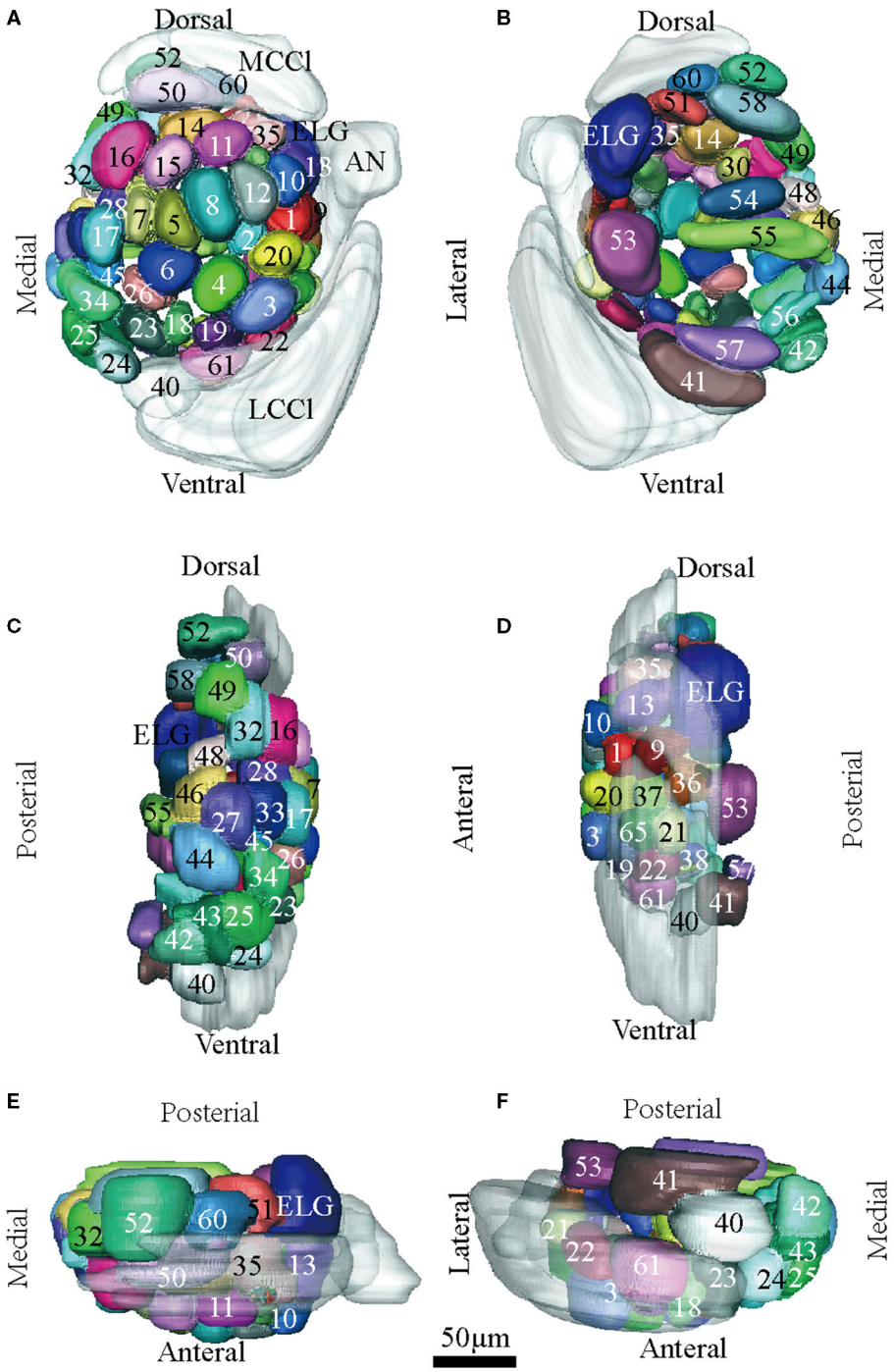

FIGURE 5 | Atlas of the 3D reconstruction of the left AL of female *E. grisescens*. All glomeruli are reconstructed and given a specific number and color. **(A)** anterior view. **(B)** posterior view. **(C)** medial view. **(D)** lateral view. **(E)** dorsal view. **(F)** ventral view. ELG: enlarged glomerulus. Scale bar is 50 μm (applies to **A–F**). Images were drawn by adobe illustrator CS 5. Images were drawn by AMIRA 5.3 and further enhanced by adobe illustrator CS 5.

according to the relative position of the landmarks and the others were recognized according to their relative position to the identified glomeruli.

There was clear dimorphism between female and male *E. grisescens*. The glomeruli number and volume of the female *E. grisescens* AL was smaller than that of males (**Tables 3**, **4**). Only one enlarged glomerulus (ELG) existed at the entrance of the antennal nerve in female *E. grisescens* whose volume was much smaller than the cumulus. The shape of G50 and G58 at the dorsal-medial area of the female AL was clavate (**Figure 5**).

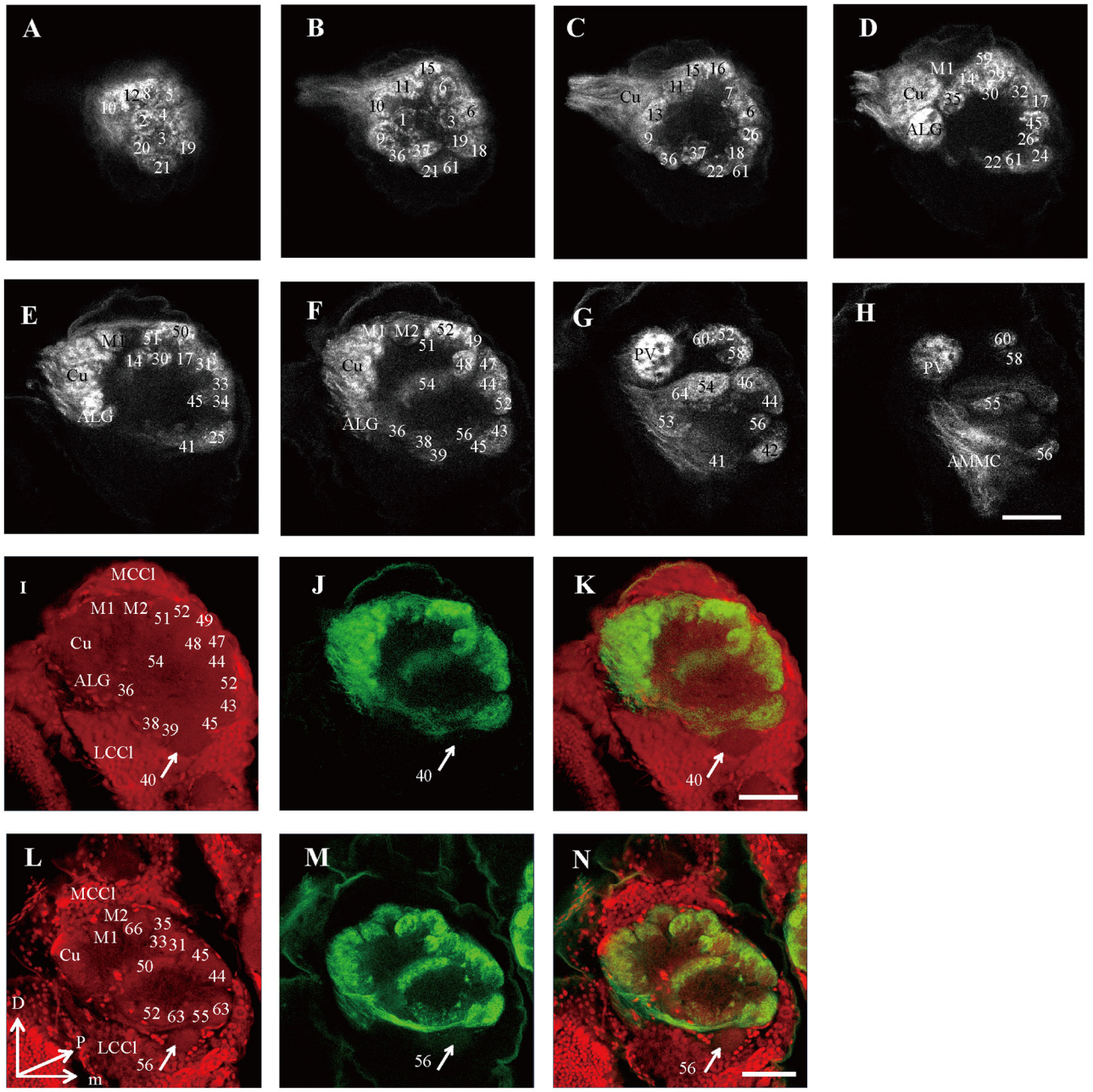

FIGURE 6 | Confocal images showing OSNs projecting into the right AL of male *E. grisescens* and *E. obliqua*. Labeling was obtained by applying antennae backfill with PI co-staining. **(A–H)** confocal sections at different depths of AL showing OSNs innervating in male *E. Grisescens*. The most anterior glomeruli, at 26 μm (A), 37 μm (B), 46 μm (C), 59 μm (D), 72 μm (E), 85 μm (F), 105 μm (G), and 117 μm (H). **(I–K)** showed confocal images 85 μm with co-staining of antennae backfill with PI in male *E. grisescens*. Arrows indicated G40 receives no axons from OSNs. **(L–N)** showed confocal images 85 μm with co-staining of antennae backfill with PI in male *E. obliqua*; Arrows indicated G56 receives no axons from OSNs. LCCl, lateral cell cluster; MCCl, medial cell cluster; Cu, Cumulus; ALG, anterior-lateral glomerulus; M1, medial glomerulus 1; M2, medial glomerulus 2; PV, posterior-ventral glomerulus; D, dorsal; L, lateral; M, medial; V, ventral. Scale bars 50 μm in **(H)** applies to **(A–H)**; in **(K)** applies to **(I–K)**; in **(N)** applies to **(L–N)**. The images were drawn by AMIRA 5.3 and further enhanced by adobe illustrator CS 5.

G17, G21, G22, G24, G25, G27, G30, G32, G38, G39, G40, G42, G43, and G45 were larger in males; however, G50 and G58 were larger in females (**Table 4**). G 29, G31, G48, G59, G62, G63, and G64 were not detected in female *E. grisescens*, and the two other glomeruli, G65 and G66, were absent in male *E. grisescens*.

Most glomeruli in the ventral-medial area of the AL and at the entrance of the antennal nerve of females were smaller than those in males. Therefore, the appearance of the AL sphere in females was almost spherical and that of males was fusiform, in the frontal view (**Figures 4**, **5**).

TABLE 2 | Primary landmarks for identification of Ordinary Glomeruli (OG) in male *E. obliqua* and *E. grisescens* and female *E. grisescens*.

	Landmarks	Specific characteristics of the landmarks	Identified glomeruli according to the relative position of the landmarks
Male and female	Antennal nerve	Largest bundle of the specimen	Cumulus, M1, M2, PV, ALG/ELG
E. grisescens	G52	At the dorsal edge of AL and adjacent to M2	G47, G48, G49, G50, G51, G58, G60
	G54	Clavate at the posterior edge of AL	G46, G27, G44, G34, G33, G31, G32, G28, G45, G17, G6, G26, G23, G18
	G53, G64	At the posterior edge and adjacent to ALG and G54	G9, G20, G21, G22, G36, G37, G38, G39, G61
	G40	LPOG, at anterior-lateral of AL and adjacent to G42	G41, G57, G38, G39
	G42	At posterior-ventral of AL and deeply stained	G43, G25, G24
Male	Antennal nerve	Largest bundle of the specimen	Cumulus, M1, M2, PV, ALG
E. obliqua	G35	At the dorsal edge of AL and adjacent to M2	G31, G46, G47, G34, G66, G48, G49
	G51	Clavate at the posterior edge of AL	G44, G45, G43, G60, G41, G42, G31, G32, G30, G29, G15, G14, G28, G26, G27
	G50, G52	At the posterior edge and adjacent to ALG and G51	G20, G11, G23, G24, G21, G22, G45, G53, G25
	G56	LPOG, at anterior-lateral of AL and adjacent to G65	G55, G63, G45, G53
	G65	At posterior-ventral of AL and deeply stained	G59, G40, G39

Cu, cumulus; ALG, anterior-lateral glomerulus; M1, medial glomerulus 1; M2, medial glomerulus 2; PV, posterior-ventral glomerulus. The landmarks were chosen based on the most obvious glomeruli in terms of position and shape.

TABLE 3 | Comparison of number and volume of the glomerulus in male *E. obliqua*, male *E. grisescens*, and female *E. grisescens*.

Specimen	Total number	Number of glomeruli possessing distinct volumes				Total volume (10^3 μm)	Average volume (10^3 μm)	*n*
		<5 (10^3 μm)	5–10 (10^3 μm)	10–30 (10^3 μm)	40 (10^3 μm)			
Male *E. obliqua*	67	12	36	19	0	552.7	8.25	1
Male *E. grisescens*	64	0	26	35	3	801.72	12.53	4
Female *E. grisescens*	59	5	32	22	0	617.00	10.28	4

n indicated the number of specimens.

Innervation of Olfactory Receptor Neurons Into the Antennal Lobe in *E. obliqua* and *E. grisescens*

Because presynaptic antibody staining applied to *E. grisescens* was not as successful as that applied to *E. obliqua* (**Figure 2**), we applied antennae backfill as an alternative method to confirm the results of *E. grisescens*. Antenna backfill with PI co-staining was used to display the innervating of ORNs. These results showed that OSNs of both *E. obliqua* and *E. grisescens* innervated almost the whole AL, except for G56 of *E. obliqua* and G40 of *E. grisescens* (**Figure 6**).

Comparison of the Macroglomerular Complex Between *E. obliqua* and *E. grisescens*

According to the comparison of glomeruli of female *E. grisescens*, male-specific MGC of *E. grisescens* was identified at the entrance of the AL and was, evidently larger than the other glomeruli (**Figures 1**–**4**). Because no difference was detected in the general morphology of glomeruli between *E. obliqua* and *E. grisescens* in this study, the MGC of *E. obliqua* was defined in the same way as that of *E. grisescens*. In both species, the MGC was composed of five glomeruli, similar to that in other species: cumulus (Cu), anterior-lateral glomerulus (ALG), medial glomerulus 1 (M1), medial glomerulus 2 (M2), and posterior-ventral glomerulus (PV) (**Figures 1**–**4**, **7**). The position of each glomerulus was the same in both species (**Figures 1**–**4**, **7**). The largest glomerulus, Cu, was at the entrance of the antennal nerve and chosen as a landmark of the MGC (**Figures 1**–**4**).

Volume Difference of Macroglomerular Complex Glomeruli Between *E. obliqua* and *E. grisescens*

The volume of each glomerulus within the MGC was calculated for *E. obliqua* and *E. grisescens*. The results revealed that ALG and PV were larger in *E. grisescens* than in *E. obliqua* [ALG: 37,884 ± 3,529 μm^3 ($n = 10$) and 19,010 ± 4,445 μm^3 ($n = 13$), respectively; PV: 42,088 ± 8,815 μm^3 ($n = 10$) and 22,098 ± 2,615 μm^3 ($n = 13$), respectively]. The volumes of other glomeruli were not statistically different between the two species (**Table 5**, **Figure 8**). The volume ratios of Cu to ALG and PV were higher in *E. grisescens* than those in *E. obliqua* (**Figure 8**).

TABLE 4 | Comparison of the OG volume between male and female *E. grisescens*.

	MEG			FEG		
	Average	**SD**	***n***	**Average**	**SD**	***N***
G1	9,319.68	1,990.84	4	10,019.13	3,065.37	4
G2	9,755.57	3,452.96	4	4,873.79	1,359.08	3
G3	12,034.59	4,197.75	4	10,053.35	1,572.98	4
G4	9,314.29	813.44	4	9,592.41	1,756.35	4
G5	10,898.70	4,738.37	4	7,276.96	2,276.79	4
G6	14,293.66	3,961.40	4	10,209.65	626.96	4
G7	8,583.62	609.74	3	7,912.36	2,121.56	4
G8	9,603.40	4,170.71	4	9,698.57	762.03	4
G9	12,738.10	2,768.74	4	9,388.99	4,958.54	4
G10	9,249.31	1,914.87	4	9,039.34	5,637.08	4
G11	10,752.71	1,533.83	4	9,903.65	4,022.17	4
G12	6,720.91	1,715.90	4	7,104.07	1,886.99	4
G13	7,855.77	1,204.40	4	9,810.85	2,770.41	3
G14	13,868.06	4,202.53	4	9,177.46	1,401.56	4
G15	6,875.46	1,143.32	4	9,553.45	2,130.97	4
G16	11,268.65	4,175.97	4	10,830.82	2,926.24	4
G17	10,773.38	4,104.55	4	6,796.03	1,921.72	4
G18	8,475.12	4,840.34	4	8,496.06	2,750.01	4
G19	9,815.03	788.27	4	11,240.36	5,401.28	4
G20	7,125.62	5,742.90	4	10,802.29	2,210.49	4
G21	14,889.89	619.12	4	5,725.85	1,564.62	4
G22	14,976.01	176.27	4	7,084.03	3,445.05	4
G23	9,700.39	2,040.60	4	6,148.79	1,808.32	4
G24	21,438.90	6,290.17	4	6,935.56	1,329.04	4
G25	19,940.78	6,175.03	4	7,586.45	4,110.94	4
G26	11,577.47	3,829.61	4	11,427.15	2,907.94	4
G27	15,152.34	2,686.88	4	9,940.22	5,312.82	4
G28	10,626.33	1,909.44	4	10,095.43	2,693.00	4
G29	7,403.25	1,734.03	2			
G30	9,415.86	2,101.34	3	3,576.23	356.34	2
G31	12,740.29	3,707.55	4			
G32	14,063.10	2,889.18	4	6,168.54	3,441.69	4
G33	10,935.79	3,943.30	4	6,697.45	2,042.14	4
G34	14,024.20	3,148.78	4	9,205.87	944.05	4
G35	9,877.63	328.62	3	8,717.74	2,385.97	4
G36	9,621.80	937.46	4	7,141.27	1,973.17	4
G37	9,080.68	2,410.58	4	5,610.91	3,198.97	4
G38	7,621.70	2,305.69	4	1,957.04	296.32	3
G39	6,751.85	1,662.03	4	2,050.47	865.39	3
G40	33,311.61	4,124.21	4	21,897.09	3,425.65	4
G41	26,594.96	10,767.63	4	25,380.78	3,933.29	4
G42	20,089.42	6,671.27	4	11,174.09	3,517.32	4
G43	24,377.49	7,886.46	4	10,289.70	2,476.03	3
G44	15,524.32	4,766.72	4	10,056.64	1,733.10	4
G45	12,354.68	4,104.04	4	6,083.66	1,962.81	4
G46	10,772.03	4,132.44	4	10,925.79	3,756.51	4
G47	5,832.04	2,502.49	4	4,724.82	1,494.10	4
G48	8,604.37	1,455.06	3			
G49	11,275.30	2,177.53	4	8,236.54	717.53	4
G50	10,675.90	3,140.79	4	13,042.97	1,355.20	4
G51	9,096.62	3,555.25	4	7,094.66	4,112.04	4
G52	11,064.42	1,341.16	4	12,244.61	1,602.26	4
G53	35,535.36	5,474.28	4	29,785.49	9,158.49	4
G54	33,836.40	4,296.80	4	26,240.16	11,483.42	4
G55	28,069.16	4,949.88	4	19,151.33	6,653.85	4
G56	10,993.84	5,471.15	4	7,235.92	1,842.36	4
G57	16,681.20	4,720.03	4	13,483.03	5,753.61	4
G58	8,191.81	2,351.63	4	16,002.94	2,981.00	4
G59	6,435.56	2,212.66	3			
G60	12,550.87	4,236.84	4	9,391.89	3,660.24	4
G61	12,530.05	4,177.33	4	12,225.45	3,424.02	4
G62	14,223.78	2,941.83	3			
G63	18,595.43	5,033.31	4			
G64	8,777.96	5,230.68	2			
G65				5,067.86	1,152.36	4
G66				5,556.99	1,935.64	4
ELG				33,857.05	6,950.06	4

(Continued)

TABLE 4 | Continued

The enlarged glomerulus (ELG) indicated the enlarged glomerulus in female E. grisescens and n indicated the number of specimens.

The MGC proportion, which was calculated as the total volume ratio of MGC to ordinary glomeruli (OG), was smaller in *E. obliqua* than that in *E. grisescens* (0.33 ± 0.03 and 0.37 ± 0.04, respectively; **Figure 9**).

DISCUSSION

The MGC is regarded as the olfactory center of insects for sex pheromone sensing, and it is present in male moths (Galizia et al., 2000; Hansson and Anton, 2000; Zhao et al., 2016). Studies on the coding mechanism of sex pheromone blends in the MGC between sibling species have focused on noctuid moths. Generally, closely related species contain the same number of glomeruli in the MGC. The Cu is the largest glomerulus, and it receives innervation from ORNs tuned to the main pheromone component of each species. The other glomeruli are smaller than Cu and receive information on minor pheromone components or inhibition chemicals (Berg et al., 2014). Differences in the positions of a single glomerulus have been shown between two *Helicoverpa* species, *H. armigera* and *H. assulta* (Xu et al., 2016a,b; Zhao et al., 2016), but not between *Heliothis virescens* and *H. subflexa* (Vickers and Christensen, 2003). In this study, the same number and position of glomeruli were found in the MGC between *E. obliqua* and *E. grisescens* (**Figure 7**), similar to those of *Heliothis* species. However, the volumes of ALG and PV were larger in *E. grisescens* than in *E. obliqua* (**Figure 8**; **Table 5**). The antennae sensilla of both ORNs are reflected in the volume of the corresponding glomerulus, so that species can detect several intra- and interspecies sex pheromone components (Liu et al., 2019). However, the population density of ORNs for sensing the

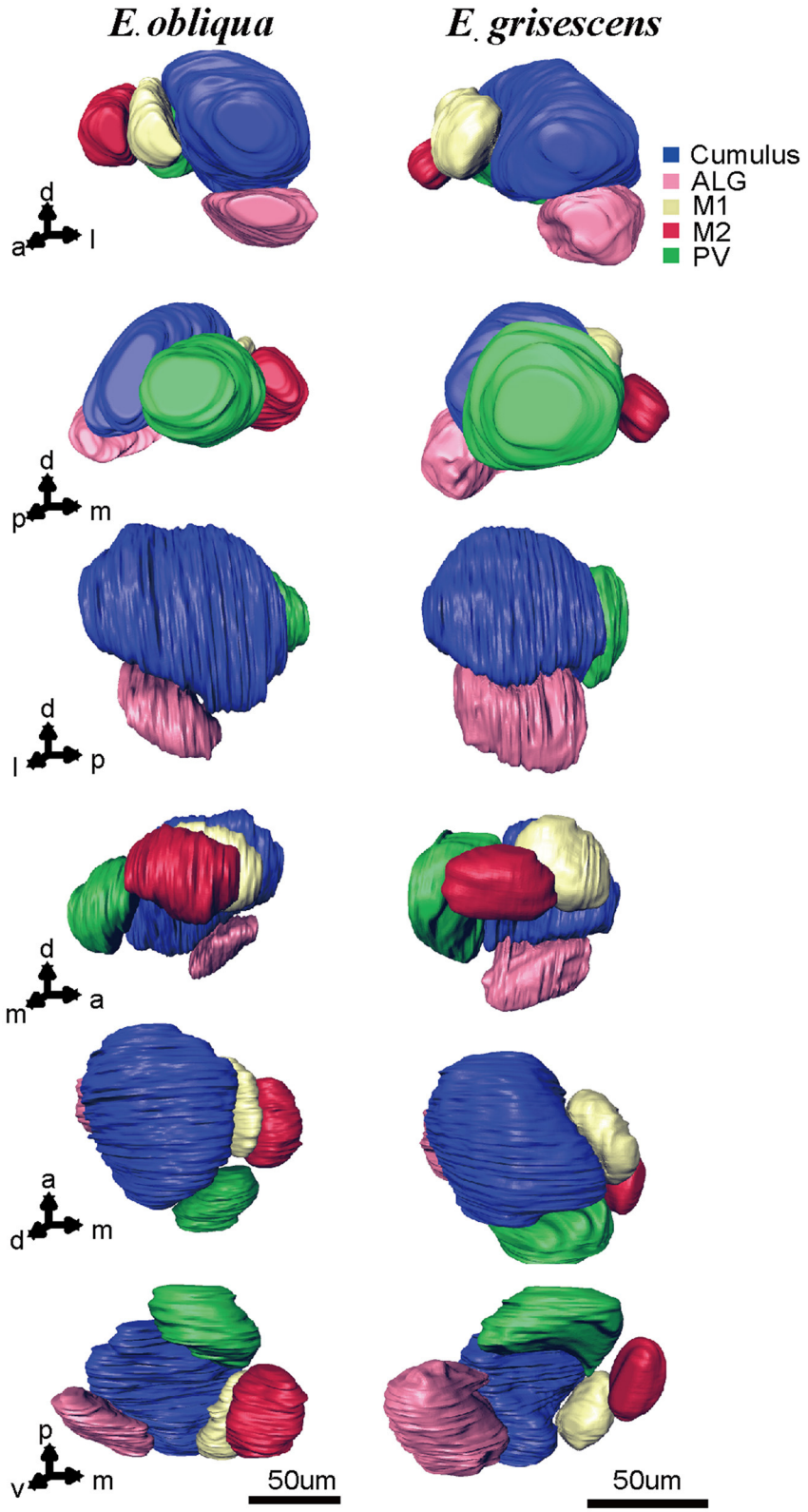

FIGURE 7 | Atlas of the 3D reconstruction of the MGC of male *E. grisescens* and *E. obliqua* exacted from **Figures 3**, **4**. Arrows 1–6 show the anterior view, posterior view, lateral view, medial view, dorsal view, and ventral view, respectively. The colored portions are as follows: Cumulus, blue; ALG, pink; M1, yellow; M2, red; Posterior-ventral glomerulus (PV), green. The images were drawn by AMIRA 5.3 and further enhanced by adobe illustrator CS 5.

TABLE 5 | Comparison of volume of the MGC glomerulus in male *E. obliqua* and *E. grisescens*.

	Male *E. obliqua*			Male *E. grisescens*		
	Volume (μm^3)	**SD**	***n***	**Volume (μm^3)**	**SD**	***n***
Cu	116,899	16,369	10	123,463	7,477	13
ALG	19,010	4,445	10	37,884	3,529	13
M1	16,556	1,390	10	12,956	651	13
M2	17,464	2,882	10	14,259	1,350	13
PV	22,098	2,615	10	42,088	8,815	13

n indicated the number of specimens.

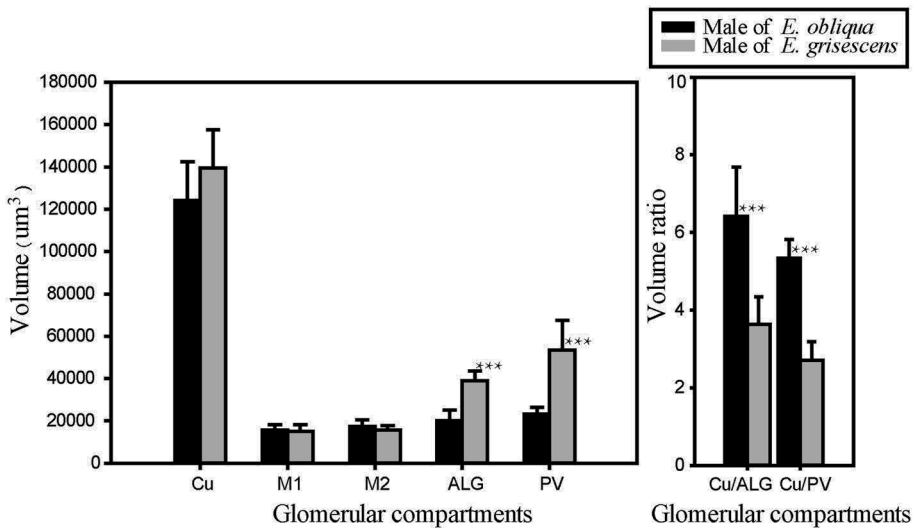

FIGURE 8 | Comparison of MGC volume between male *E. obliqua* and *E. grisescens*. The data is analyzed by one-away ANOVA and *t*-test in SigmaPlot. The plotted values are mean ± SD. $^{***}P \leq 0.001$., *n* is 10 and 13, respectively, in *E. obliqua* and *E. grisescens*. The images were drawn by SigmaPlot Portable and further enhanced by adobe illustrator CS 5.

minor component in the pheromone blends was higher in *E. grisescens* than in *E. obliqua*. Therefore, our results support the premise that the number of ORNs is reflected in the volume of the corresponding glomeruli (Christensen and Hildebrand, 1987; Hansson and Anton, 2000; Masse et al., 2009; Kuebler et al., 2012; Brill et al., 2013), which has proven to be important in peripheral coding in closely related *Helicoverpa* species (Wu et al., 2013, 2015). Therefore, it is reasonable to propose that ALG or PV might be responsible for detecting the minor component Z3, Z6,Z9-18:H in both *E. obliqua* and *E. grisescens*. One of the medial glomeruli (M1 or M2) might be related to the specific component Z3,epo6,Z9-19:H of *E. obliqua*, but functional evidence is needed.

The difference in the ratio of minor to main sex pheromone components might be an important olfactory coding mechanism in closely related species. Noctuid species that are sympatric and synchronic generally contain different main or minor components or different combinations of the same components (Berg et al., 2014). Therefore, differences in the coding for the minor component might not be apparent. In the sibling species *H. armigera* and *Helicoverpa. zea*, both use Z11-16:AL as the main component and Z9-16:AL as the minor component with a ratio of 100:5(20:1) and 98:2, respectively, (Kehat and Dunkelblum, 1990; Fadamiro and Baker, 1997). In both species, the ORNs tuned to Z9-16:AL and received innervation from the ALG glomerulus of the respective MGC (Lee et al., 2006; Xu et al., 2016a,b), similar to the pattern that we observed in *E. obliqua* and *E. grisescens*. Thus, this coding mechanism in closely related species might be a common feature among moth species. No earlier study on these two species has focused on this coding mechanism because *H. armigera* and *H. zea* are not regarded as sympatric species (Cunningham and Zalucki, 2014; Mastrangelo et al., 2014; Anderson et al., 2016).

According to available information on the ALs of moth species, those in the same group contain specific and consistent patterns of MGC arrangement. For example, noctuid moths contain three to four MGC compartments, of which the Cu is the largest (Skiri et al., 2005; Berg et al., 2014; Xu et al., 2016a,b). Bombycid moths display different volume combinations of cumulus to toroid (Namiki et al., 2014). In this study, five glomeruli were found in both species with invariant position and number. These results also showed that the arrangement of MGC compartments in these species is the same as that in noctuid

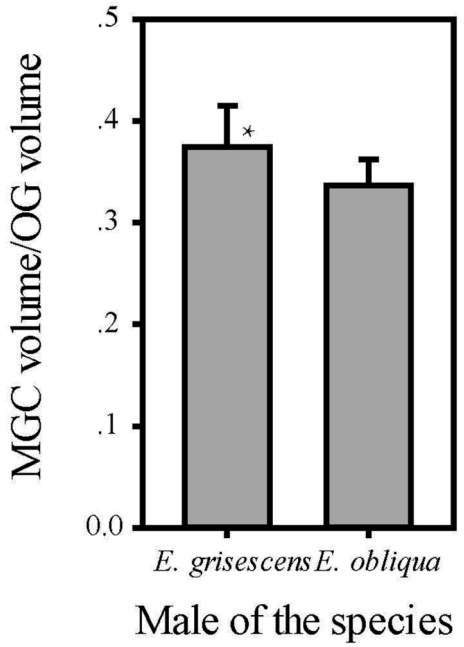

FIGURE 9 | Comparison of ratio of MGC volume to OG between male *E. obliqua* and *E. grisescens*. The data is analyzed by one-away ANOVA. The plotted values are mean ± SD. $P = 0.049$. *indicates significant difference. "*n*" is 7 and 9, respectively, in *E. obliqua* and *E. grisescens*. The images were drawn by SigmaPlot Portable and further enhanced by adobe illustrator CS 5.

TABLE 6 | The MGC glomeruli number in different moth species.

Sex pheromone types	Species	Number of MCGs	References
Type I	*Heliothis virescens*	4	Vickers and Christensen, 2003
	Heliothis subflexa	4	Vickers and Christensen, 2003
	Helicoverpa zea	3	Lee et al., 2006
	Helicoverpa assulta	3	Berg et al., 2002
	Helicoverpa armigera	3	Zhao et al., 2016
	Cydia molesta	1	Varela et al., 2009
	Plutella xylostella	3	Yan et al., 2019
	Mythimna separata	3	Jiang et al., 2019
	Athetis dissimilis	3	Dong et al., 2020
	Agrius convolvuli	3	Nirazawa et al., 2017
	Ernolatia moorei	2	Namiki et al., 2014
	Trilocha varians	2	Namiki et al., 2014
	Manduca sexta	3	Rospars and Hildebrand, 2000
	Rondotia menciana	4	Namiki et al., 2014
	Bombyx mandarina	4	Namiki et al., 2014
	Bombyx mori	4	Namiki et al., 2014
Type II	*Eilema japonica*	4	Namiki et al., 2012
	Ectropis obliqua	5	
	Ectropis grisescens	5	

species, with Cu being the largest glomerulus, which might be consistent among Geometridae species.

This study also showed that MGC to OG proportion was 0.33 ± 0.03 and 0.37 ± 0.04 in *E. obliqua* and *E. grisescens*, respectively (**Figure 9**). The slightly larger MGC in *E. grisescens* than in *E. obliqua* might result from the larger ALG and PV in *E. grisescens*. The MGC proportion was close to that of the diamondback moth, *Plutella xylostella* (0.32), and much higher in both *E. obliqua* and *E. grisescens* than in *H. armigera* (0.12) (Skiri et al., 2005; Zhao et al., 2016; Yan et al., 2019). The significant difference in MGC size might reflect the higher level of specialization in the sex pheromone olfactory processing of both *E. obliqua* and *E. grisescens*.

Except the few species containing only one MGC component (Varela et al., 2009), moth species producing Type I pheromones generally contain three to four glomeruli in their MGC (Hansson et al., 1994; Lee et al., 2006; Namiki et al., 2014; Nirazawa et al., 2017; Yan et al., 2019). It is notable that in both moth species studied here, producing Type II pheromones, five glomeruli were present in their MGC. Another pheromone Type II species, *Eilema japonica,* contains four glomeruli in its MGC (Namiki et al., 2012). The number of glomeruli in the MGC for the known moth species is summarized in **Table 6**. Overall, more glomeruli appear to be present in the MGC of pheromone Type II than in Type I species, suggesting that pheromone Type II species process more complex olfactory information during sex pheromone reception than pheromone Type I species. Given that ORNs, especially the ones tuned to inhibitory chemicals, display broadly innervating destinations in MGC glomeruli (Berg et al., 2014), the pheromone Type II species might be more evolved than pheromone Type I species regarding pheromone reception. However, further studies are needed to confirm this hypothesis.

The presynaptic antibody staining for marking the AL glomeruli of *E. obliqua* and *E. grisescens* was not a suitable technique. The boundaries of certain single glomeruli were not clear when compared to those of other species when the same technique was used. If the contact time between the specimen and the antibody is prolonged, the glomeruli become clearer but the ORNs combined staining (antennae backfilled) failed to stain the glomeruli. The PI staining with the neurobiotin backfilled method seemed to overcome this difficulty (**Figure 6**). However, this method must be combined with antennae backfills, as PI was specifically developed to stain nuclei; by making the fiber lighter, the confocal images become less clear (**Figure 6**). Thus, a new method for specifically staining the AL glomeruli is still necessary for some species. Additionally, antennae backfill marking exhibited an innovative feature of the ORNs. The results showed that ORNs of both *E. obliqua* and *E. grisescens* innervated nearly the whole AL, except for G56 of *E. obliqua* and G40 of *E. grisescens* (**Figure 5**). Therefore, G56 of *E. obliqua* and G40 of *E. grisescens* were predicted as the labial

pit organ glomerulus as found in previous studies, i.e., G38 in *H. armigera* (Zhao et al., 2016) and PV1 in *P. xylostella* (Yan et al., 2019).

DATA AVAILABILITY STATEMENT

The data used to support the findings of this study are available from the corresponding author upon request.

AUTHOR CONTRIBUTIONS

JL, Z-qL, and Z-mC conceived and designed the study and wrote the manuscript. Z-xL, X-mC, and LB provided the insects. JL, X-mC, LB, and KH analyzed and interpreted the data. All authors contributed to the article and approved the submitted version.

FUNDING

This study was funded by the National Key Research & Development (R&D) Plan (2019YFD1002100 and 2016YFD0200900), the National Natural Science Foundation of China (31701795), and the Modern Agricultural Industry Technology System (CARS-23).

ACKNOWLEDGMENTS

We are grateful to Yunqin Li, Center of Electron Microscopy, Zhejiang University and Jiansheng Guo, Department of Pathology, Sir Run Shaw Hospital and Center of Cryo-Electron Microscopy, School of Medicine, Zhejiang University for their assistance in confocal imaging acquisition and 3D structure reconstruction.

REFERENCES

Anderson, C. J., Tay, W. T., Mcgaughran, A., Gordon, K., and Walsh, T. K. (2016). Population structure and gene flow in the global pest, *Helicoverpa armigera*. *Mol. Ecol.* 25, 5296–5311. doi: 10.1111/mec.13841

Berg, B. G., Galizia, G. C., Brandt, R., and Mustaparta, H. (2002). Digital Atlases of the antennal lobe in two species of tobacco budworm moths, the oriental *Helicoverpa assulta* (male) and the American *Heliothis virescens* (male and female). *J. Comp. Neurol.* 446, 123–134. doi: 10.1002/cne.10180

Berg, B. G., Zhao, X. C., and Wang, G. R. (2014). Processing of pheromone information in related species of heliothine moths. *Insects* 5, 742–761. doi: 10.3390/insects5040742

Brill, M. F., Rosenbaum, T., Reus, I., Kleineidam, C. J., Nawrot, M. P., and Rössler, W. (2013). Parallel processing via a dual olfactory pathway in the honeybee. *J. Neurosci.* 33, 2443–2456. doi: 10.1523/JNEUROSCI.4268-12.2013

Christensen, T. A., and Hildebrand, J. G. (1987). Male-specific, sex pheromone-selective projection neurons in the antennal lobes of the moth *Manduca sexta*. *J. Comp. Physiol. A* 160, 553–569. doi: 10.1007/BF00611929

Cunningham, J. P., and Zalucki, M. P. (2014). Understanding heliothine (Lepidoptera: Heliothinae) pests: what is a host plant? *J. Econ. Entomol.* 107, 881–896. doi: 10.1603/EC14036

Dong, J. F., Jiang, N. J., Zhao, X. C., and Tang, R. (2020). Antennal lobe atlas of an emerging corn pest, *Athetis dissimilis*. *Front. Neuroanat.* 14:23. doi: 10.3389/fnana.2020.00023

Fadamiro, H. Y., and Baker, T. C. (1997). *Helicoverpa zea* males (Lepidoptera: Noctuidae) respond to the intermittent fine structure of their sex pheromone plume and an antagonist in a flight tunnel. *Physiol. Entomol.* 22, 316–324. doi: 10.1111/j.1365-3032.1997.tb01175.x

Galizia, C. G., Sachse, S., and Mustaparta, H. (2000). Calcium responses to pheromones and plant odours in the antennal lobe of the male and female moth *Heliothis virescens*. *J. Comp. Physiol. A* 186, 1049–1063. doi: 10.1007/s003590000156

Hansson, B. S., and Anton, S. (2000). Function and morphology of the antennal lobe: new developments. *Annu. Rev. Entomol.* 45, 203–231. doi: 10.1146/annurev.ento.45.1.203

Hansson, B. S., Anton, S., and Christensen, T. A. (1994). Structure and function of antennal lobe neurons in the male turnip moth, *Agrotis segetum* (Lepidoptera: Noctuidae). *J. Comp. Physiol. A* 175, 547–562. doi: 10.1007/BF00199476

Homberg, U., Christensen, T. A., and Hildebrand, J. G. (1989). Structure and function of the deutocerebrum in insects. *Annu. Rev. Entomol.* 34, 477–501. doi: 10.1146/annurev.en.34.010189.002401

Jiang, N. J., Tang, R., Wu, H., Xu, M., Ning, C., Huang, L. Q., et al. (2019). Dissecting sex pheromone communication of *Mythimna separata* (Walker) in North China from receptor molecules and antennal lobes to behavior. *Insect Biochem. Mol. Biol.* 111:103176. doi: 10.1016/j.ibmb.2019.103176

Kehat, M., and Dunkelblum, E. (1990). Behavioral responses of male *Heliothis armigera* (Lepidoptera: Noctuidae) moths in a flight tunnel to combinations of components identified from female sex pheromone glands. *J. Insect Behav.* 3, 75–83. doi: 10.1007/BF01049196

Kuebler, L. S., Schubert, M., Kárpáti, Z., Hansson, B. S., and Olsson, S. B. (2012). Antennal lobe processing correlates to moth olfactory behavior. *J. Neurosci.* 32, 5772–5782. doi: 10.1523/JNEUROSCI.6225-11.2012

Lee, S., Carlsson, M. A., Hansson, B. S., Todd, J. L., and Baker, T. C. (2006). Antennal lobe projection destinations of *Helicoverpa zea* male olfactory receptor neurons responsive to heliothine sex pheromone components. *J. Comp. Physiol. A* 192, 351–363. doi: 10.1007/s00359-005-0071-8

Li, Z. Q., Cai, X. M., Luo, Z. X., Bian, L., Xin, Z. J., Liu, Y., et al. (2019). Geographical distribution of *Ectropis grisescens* (Lepidoptera: Geometridae) and *Ectropis obliqua* in China and description of an efficient identification method. *J. Econ. Entomol.* 112, 277–283. doi: 10.1093/jee/toy358

Liu, J., Li, Z. Q., Luo, Z. X., Cai, X. M., Bian, L., and Chen, Z. M. (2019). Comparison of male antennal morphology and sensilla physiology for sex pheromone olfactory sensing between sibling moth species: *Ectropis grisescens* and *Ectropis obliqua* (Geometridae). *Arch. Insect. Biochem. Physiol.* 101:e21545. doi: 10.1002/arch.21545

Luo, Z. X., Li, Z. Q., Cai, X. M., Bian, L., and Chen, Z. M. (2017). Evidence of Premating isolation between two sibling moths: *Ectropis grisescens* and *Ectropis obliqua* (Lepidoptera: Geometridae). *J. Econ. Entomol.* 110, 2364–2370. doi: 10.1093/jee/tox216

Masse, N. Y., Turner, C. G., and Jefferis, G. S. (2009). Olfactory information processing in Drosophila. *Curr. Biol.* 19, R700–R713. doi: 10.1016/j.cub.2009.06.026

Mastrangelo, T., Paulo, D. F., Bergamo, L. W., Morais, E. G. F., Silva, M., Bezerra-Silva, G., et al. (2014). Detection and genetic diversity of a heliothine invader (Lepidoptera: Noctuidae) from north and northeast of Brazil. *J. Econ. Entomol.* 107, 970–980. doi: 10.1603/EC13403

Namiki, S., Daimon, T., Iwatsuki, C., Shimada, T., and Kanzaki, R. (2014). Antennal lobe organization and pheromone usage in bombycid moths. *Biol. Lett.* 10:20140096. doi: 10.1098/rsbl.2014.0096

Namiki, S., Fujii, T., Ishikawa, Y., and Kanzaki, R. (2012). The brain organization of the lichen moth *Eilema japonica*, which secretes an alkenyl sex pheromone. *NeuroReport* 23, 857–861. doi: 10.1097/WNR.0b013e32835 82007

Nirazawa, T., Fujii, T., Seki, Y., Namiki, S., Kazawa, T., Kanzaki, R., et al. (2017). Morphology and physiology of antennal lobe projection neurons in the hawkmoth *Agrius convolvuli*. *J. Insect Physiol.* 98, 214–222. doi: 10.1016/j.jinsphys.2017.01.010

Rospars, J. P., and Hildebrand, J. G., (2000). Sexually dimorphic and isomorphic glomeruli in the antennal lobes of the sphinx moth *Manduca sexta*. *Chem. Senses*. 25, 119–129. doi: 10.1093/chemse/25.2.119

Skiri, H. T., Rø, H., Berg, B. G., and Mustaparta, H. (2005). Consistent organization of glomeruli in the antennal lobes of related species of heliothine moths. *J. Comp. Neurol.* 491, 367–380. doi: 10.1002/cne.20692

Touhara, K. (2013). *Pheromone Signaling Methods and Protocols*. New York Heidelberg Dordrecht London: Springer, 399.

Varela, N., Avilla, J., Gemeno, C., and Anton, S. (2011). Ordinary glomeruli in the antennal lobe of male and female tortricid moth *Grapholita molesta* (Busck) (Lepidoptera: Tortricidae) process sex pheromone and host-plant volatiles. *J. Exp. Biol.* 214, 637–645. doi: 10.1242/jeb.047316

Varela, N., Couton, L., Gemeno, C., Avilla, J., Rospars, J. P., and Anton, S. (2009). Three-dimensional antennal lobe atlas of the oriental fruit moth, *Cydia molesta* (Busck) (Lepidoptera: Tortricidae): comparison of male and female glomerular organization. *Cell Tissue Res.* 337, 513–526. doi: 10.1007/s00441-009-0839-1

Vickers, N. J., and Christensen, T. A. (2003). Functional divergence of spatially conserved olfactory glomeruli in two related moth species. *Chem. Senses* 28, 325–338. doi: 10.1093/chemse/28.4.325

Wu, H., Hou, C., Huang, L. Q., Yan, F. S., and Wang, C. Z. (2013). Peripheral coding of sex pheromone blends with reverse ratios in two *Helicoverpa* species. *PLoS ONE* 8:e70078. doi: 10.1371/journal.pone.0070078

Wu, H., Xu, M., Hou, C., Huang, L. Q., Dong, J. F., and Wang, C. Z. (2015). Specific olfactory neurons and glomeruli are associated to differences in behavioral responses to pheromone components between two *Helicoverpa* species. *Front. Behav. Neurosci.* 9:206. doi: 10.3389/fnbeh.2015.00206

Xu, M., Dong, J. F., Wu, H., Zhao, X. C., Huang, L. Q., and Wang, C. Z. (2016a). The Inheritance of the pheromone sensory system in two *Helicoverpa* species: dominance of *H. armigera* and possible introgression from *H. assulta*. *Front. Cell. Neurosci.* 10:302. doi: 10.3389/fncel.2016.00302

Xu, M., Guo, H., Hou, C., Wu, H., Huang, L. Q., and Wang, C. Z. (2016b). Olfactory perception and behavioral effects of sex pheromone gland components in *Helicoverpa armigera* and *Helicoverpa assulta*. *Sci. Rep.* 6:22998. doi: 10.1038/srep22998

Yan, X., Wang, Z., Xie, J., Deng, C., Sun, X., and Hao, C. (2019). Glomerular organization of the antennal lobes of the diamondback moth, *Plutella xylostella* L. *Front. Neuroanat.* 13:4. doi: 10.3389/fnana.2019.00004

Zhao, X. C., Chen, Q. Y., Guo, P., Xie, G. Y., Tang, Q. B., Guo, X. R., et al. (2016). Glomerular identification in the antennal lobe of the male moth *Helicoverpa armigera*. *J. Comp. Neurol.* 524, 2993–3013. doi: 10.1002/cne.24003

Conflict of Interest: The authors declare that the research was conducted in the absence of any commercial or financial relationships that could be construed as a potential conflict of interest.

frontiers in Physiology

ORIGINAL RESEARCH
published: 26 August 2021
doi: 10.3389/fphys.2021.732578

Novel Temporal Expression Patterns of EBF-Binding Proteins in Wing Morphs of The Grain Aphid *Sitobion miscanthi*

Siyu Zhang[1,2], Qian Zhang[1], Xin Jiang[1], Qian Li[1], Yaoguo Qin[1], Wenkai Wang[2], Jia Fan[1] and Julian Chen[1]**

[1] State Key Laboratory for Biology of Plant Diseases and Insect Pests, Institute of Plant Protection, Chinese Academy of Agricultural Sciences, Beijing, China, [2] School of Agriculture, Yangtze University, Jingzhou, China

OPEN ACCESS

Edited by:
Joe Hull,
Agricultural Research Service, United States Department of Agriculture, United States

Reviewed by:
Youssef Dewer,
Agricultural Research Center, Egypt
Nathália F. Brito,
Federal University of Rio de Janeiro, Brazil
Amber Afroz,
University of Gujrat, Pakistan

***Correspondence:**
Jia Fan
jfan@ippcaas.cn
Julian Chen
chenjulian@caas.cn

Specialty section:
This article was submitted to Invertebrate Physiology, a section of the journal Frontiers in Physiology

Received: *29 June 2021*
Accepted: *30 July 2021*
Published: *26 August 2021*

Citation:
Zhang S, Zhang Q, Jiang X, Li Q, Qin Y, Wang W, Fan J and Chen J (2021) Novel Temporal Expression Patterns of EBF-Binding Proteins in Wing Morphs of The Grain Aphid Sitobion miscanthi. Front. Physiol. 12:732578. doi: 10.3389/fphys.2021.732578

High chemosensitivity of insects to volatile organic compounds (VOC) stimuli is mediated by odorant binding proteins (OBPs). In aphids, three OBPs (OBP3, OBP7 and OBP9) are E-β-farnesene (EBF)-binding proteins. Winged aphids are generally more sensitive than wingless aphids to VOCs, thus, wing presence is a phenotypic correlate of olfaction sensitivity. Here, we investigate the detailed temporal expression of these EBF-binding proteins and two other *OBPs* (*OBP6* and *OBP10*), in the grain aphid *Sitobion miscanthi* 0 h, 2 h, 1 day, 3 days, 10 days, and 20 days after adult emergence. Both winged and wingless aphids were examined to further uncover phenotypic specification. Then, the expression patterns before and after EBF induction were analyzed. Throughout adulthood, only *OBP7* had significantly higher antennal expression in winged aphids; however, there was no significant difference in the antennal expression of *OBP3* between wing morphs at most time points. Except it was lower in newly emerged winged aphids but increased rapidly to the same level in wingless aphids at 1 day. *OBP9* did not differ in expression between the morphs and was the only OBP that did not exhibit an expression trough at the beginning of the adult stage (0 h). The expression of *OBP9* remained relatively stable and high throughout the adult stage in both phenotypes, showing the highest level among the three EBF-binding proteins. After EBF induction, its expression was further up-regulated in both morphs. Therefore, this protein may be an important molecule for EBF recognition in aphids. *OBP7* strongly responded to EBF but only in winged aphids, suggesting that this protein is important in the more sensitive EBF recognition process of winged aphids. In addition, the antennal expression level of *OBP3* did not respond to EBF induction. These findings revealed a temporal expression pattern of *OBPs* in aphids and showed that figuring out the pattern is critical for correctly selecting morphs and sampling times, which will support the discovery of reliable findings and allow solid conclusions to be drawn. Our findings also inspire on the interaction mode of the three EBF-binding proteins in relation to EBF perception in aphids.

Keywords: *Sitobion miscanthi*, odorant binding protein, expression pattern, temporal expression, E-β-farnesene (EBF), antenna

INTRODUCTION

Odorant binding proteins (OBPs) with high antennal expression levels have been widely identified among insect species since 1981 (Vogt and Riddiford, 1981). The widespread distribution of these proteins, together with their broad affinities for plant volatiles as well as pheromones *in vivo*, suggest critical roles in peripheral signal transmission for foreign olfactory ligands. Compared with other insects, aphids generally express fewer OBPs (between nine and twelve), such as *Acyrthosiphon pisum* with 11 identified genes encoding complete OBPs (Zhou et al., 2010; Biasio et al., 2015), *Aphis gossypii* with nine (Gu et al., 2013), *Myzus persicae* with 11 (Ji et al., 2016), *Sitobion avenae* with twelve (Xue et al., 2016), *Megoura viciae* with 10 (Daniele et al., 2018), and *Aphis glycines* with 11 (Wang et al., 2021). However, at least three OBPs, namely, OBP3 (Qiao et al., 2009), OBP7 (Sun et al., 2012a) and OBP9 (Qin et al., 2020), exhibit properties as E-β-farnesene (EBF)-binding proteins in aphids. The release of alarm pheromone signals enables aphids to escape and defend themselves (Nault et al., 1973; Pickett and Griffiths, 1980). The high proportion of EBF-binding proteins (three out of the nine to twelve OBPs) indicates the importance of alarm pheromones in aphid survival and population expansion.

Spatial expression profiles showed that insect *OBPs* tended to be expressed in chemosensory organs such as antennae, heads and legs (e.g., Vogt and Riddiford, 1981; Sun et al., 2013). Besides, they occur in non-sensory tissues and organs such as the wings (Calvello et al., 2003; Pelosi et al., 2005), reproductive organs (Li et al., 2008; Sun et al., 2012a), mandibular glands (Iovinella et al., 2011) and salivary glands (Zhang et al., 2017) as well. Work on OBPs in aphids has also been widely published, including studies focusing on expression analysis between winged and wingless morphs (e.g., Gu et al., 2013; Xue et al., 2016; Wang et al., 2019, 2021). For example, Wang et al. (2021) conducted a systematic and detailed investigation of *OBP* expression in the antennae, head, wings, legs, cornicles, caudae, and thorax of the soybean aphid *A. glycines* through differential transcriptome analysis and quantitative real-time PCR (RT-qPCR).

The temporal expression profile of aphids has mainly been compared between the nymph and adult stages (e.g., Xue et al., 2016; Wang et al., 2019). The expression profiles revealed higher levels of some *OBPs* in the nymph stage than in adults. However, considering that the body undergoes a substantial transformation from the nymph to adult stage and that the adult stage lasts up to an average of 19 d (Li et al., 2018), a detailed investigation of key time points such as the beginning of the adult stage and several time points during the whole adult stage will hopefully clarify the temporal expression patterns of *OBPs* throughout the adult stage. To date, there has been a lack of research on this topic.

Wing state is a phenotypic correlate of olfaction sensitivity in aphids, with the winged morph displaying greater sensitivity (Pickett, 2009). Winged aphids play more important roles in risk avoidance, migration, and habitat reselection over long distances, whereas wingless aphids are responsible for rapid population expansion after colonization. Therefore, additional investigations of the expression pattern of *OBPs* between the two wing phenotypes will refine the study of temporal expression patterns. In addition, such investigations would help reveal the potential function of OBPs from a novel perspective.

Insect hyperawareness of potential food, mates or danger is mostly due to the highly sensitive insect chemosensory system. Intense responses of OBPs to chemical stimuli have been widely reported (e.g., Pelosi et al., 2005; Siciliano et al., 2014), but how intense the response of OBPs to newly occurring odors is in aphids remains an open question. Before answering this question, we must answer a more fundamental one: under constant conditions, what are the temporal expression patterns of *OBPs* during the aphid adult stage?

In the present study, we carried out a detailed investigation of the temporal expression profile of EBF-binding proteins in the grain aphid *Sitobion miscanthi*, the most widespread and harmful pest and dominant aphid species of wheat in China, at the beginning, middle and end of the adult stage. In China, *S. miscanthi* was wrong using for the Latin name as *S. avenae* (Zhang, 1999; Jiang et al., 2019). The time points employed in the survey were 0, 2 h, 1 day, 3 days, 10 days, and 20 days after the emergence of adults. Furthermore, we collected antennae from both winged and wingless individuals to determine whether wing morph is a phenotypic correlate of *OBP* expression. Finally, the expression of these genes before and after EBF induction was analyzed by carrying out an EBF treatment experiment.

MATERIALS AND METHODS

Aphid Samples

The grain aphid *S. miscanthi* clone was originally collected from wheat in Hebei Province, China, and kept in our laboratory, which is not privately owned or protected. An isogenic colony was started from a single parthenogenetic female and was maintained on wheat (*Triticum aestivum*) in the laboratory at 22 ± 1°C with a 75% relative humidity and 16 h light/8 h dark. Our recent investigation showed an average adult longevity of 19 d in *S. miscanthi* (Li et al., 2018), which indicates that 20 d after adult emergence would be the very end of life.

Sampling

In the present study, we chose 0 h, 2 h (2 h ± 5 min), 1 day (24–36 h), and 3 days (72–84 h) after adult emergence as the beginning of the adult stage, 10 d as the middle of adult stage and 20 d as the end of adult stage to explore the temporal expression patterns of *OBPs* in *S. miscanthi*.

Fourth-instar (the last nymph stage) winged and wingless nymphs were placed in 9-cm-diameter Petri dishes (10 aphids/dish) and fed wheat seedlings grown in 2 ml centrifuge tubes. Antennae at each time points were collected from both wingless and winged aphids. For the EBF treatment experiment, 4th-instar winged and wingless nymphs were placed into 9-cm-diameter Petri dishes (10 aphids/dish) lined with filter paper moistened with water. The nymphs were fed wheat seedlings grown in 2 ml centrifuge tubes. Twenty-four hours after they emerged as adults, 400 ng of EBF (1 μL 400 ng/μL, diluted with *n*-hexane) was applied to a 1 cm square filter paper and quickly placed into the Petri dish. Filter paper (1 cm) with

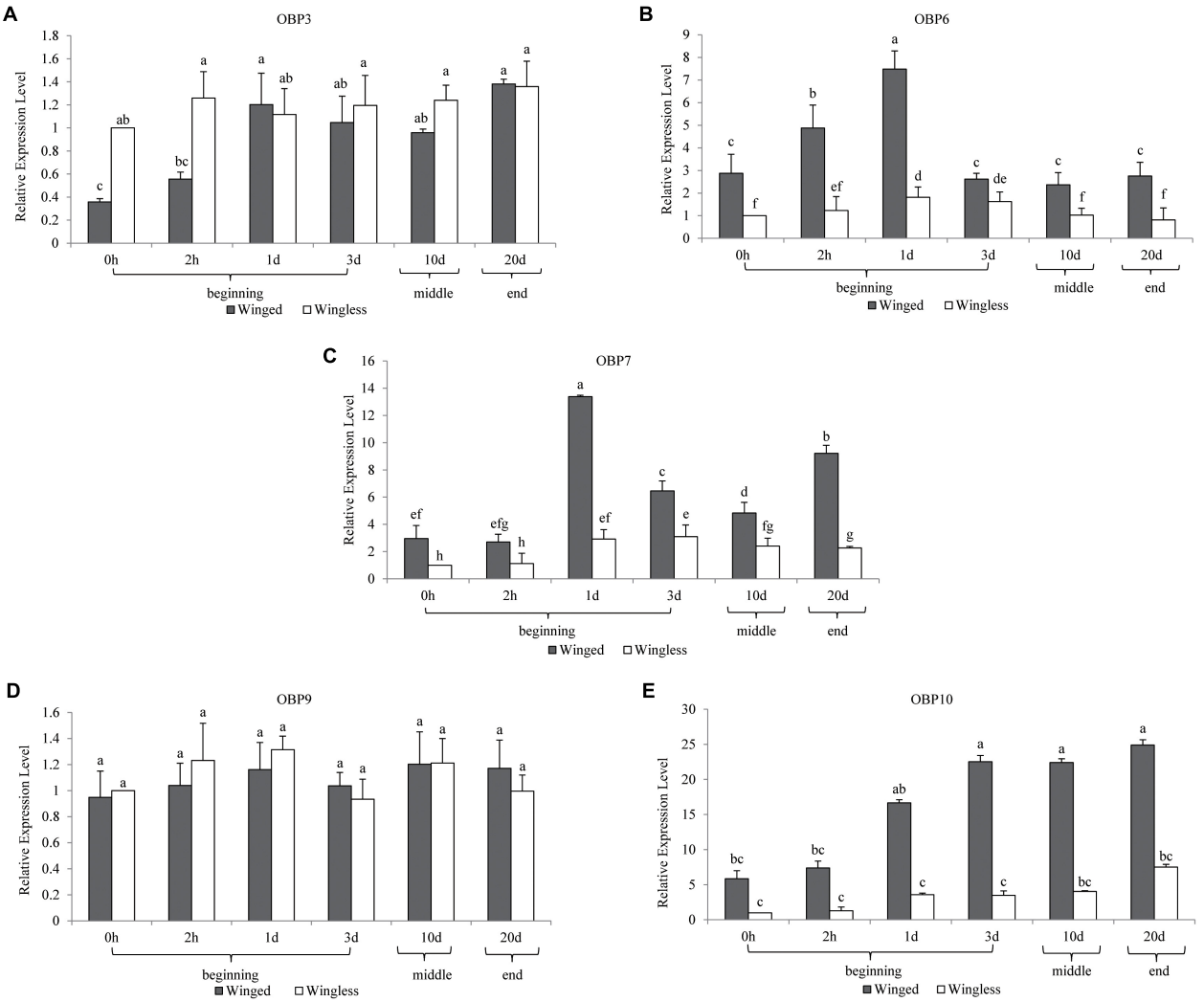

FIGURE 1 | Temporal expression profiles of *OBP3/6/7/9/10* in *S. miscanthi*. Fold changes are relative to the antennal transcript levels of the wingless morph at 0 h after adult emergence. Differences in mean transcript levels were detected using one-way ANOVA, followed by Duncan's multiple range test. Different letters over bars indicate significant differences ($p < 0.05$). Winged, antennae of winged aphid; Wingless, antennae of wingless aphid; Beginning, middle, end, the adult stage after emergence was divided into three parts, namely, beginning (within 3 d), middle (10 d), and end (20 d).

1 μl of n-hexane served as a control. Sampling was performed after 30 min of treatment. Thirty-five pairs of antennae were dissected into 1.5 ml centrifuge tubes in triplicate for each time point as well as EBF treatment and immediately frozen in liquid nitrogen. Antenna samples were ultimately stored at −80°C before total RNA extraction.

Reagents

E-β-farnesene was purchased from Wako Chemical (Osaka, Japan), and n-hexane was purchased from Sigma-Aldrich (St. Louis, MO, United States).

Total RNA Extraction

Total RNA was extracted using total RNA extraction reagent (Tianmo, Beijing, China) following the manufacturer's instructions. The concentration of RNA (OD260/OD280 value) was measured by a Nanodrop 2000 spectrophotometer (DeNovix, Washington, DC, United States). Then, the first strand of cDNA was synthesized using 400 ng of total RNA using the 1st strand cDNA synthesis kit (aidlab, Beijing, China).

Quantitative Real-Time PCR Analysis

The antennal expression levels of *OBP3, OBP6, OBP7, OBP9*, and *OBP10* transcripts at different time points of the adult stage as well as in the EBF treatment experiment were quantified by RT-qPCR. The sequences of primers used for RT-qPCR were designed based on *SaveOBP3* (GenBank accession number KU140607), *SaveOBP6* (KU140610), *SaveOBP7* (KU140611), *SaveOBP9* (KU140613) and *SaveOBP10* (KU140614), which were previously reported by Xue et al. (2016) and are listed in

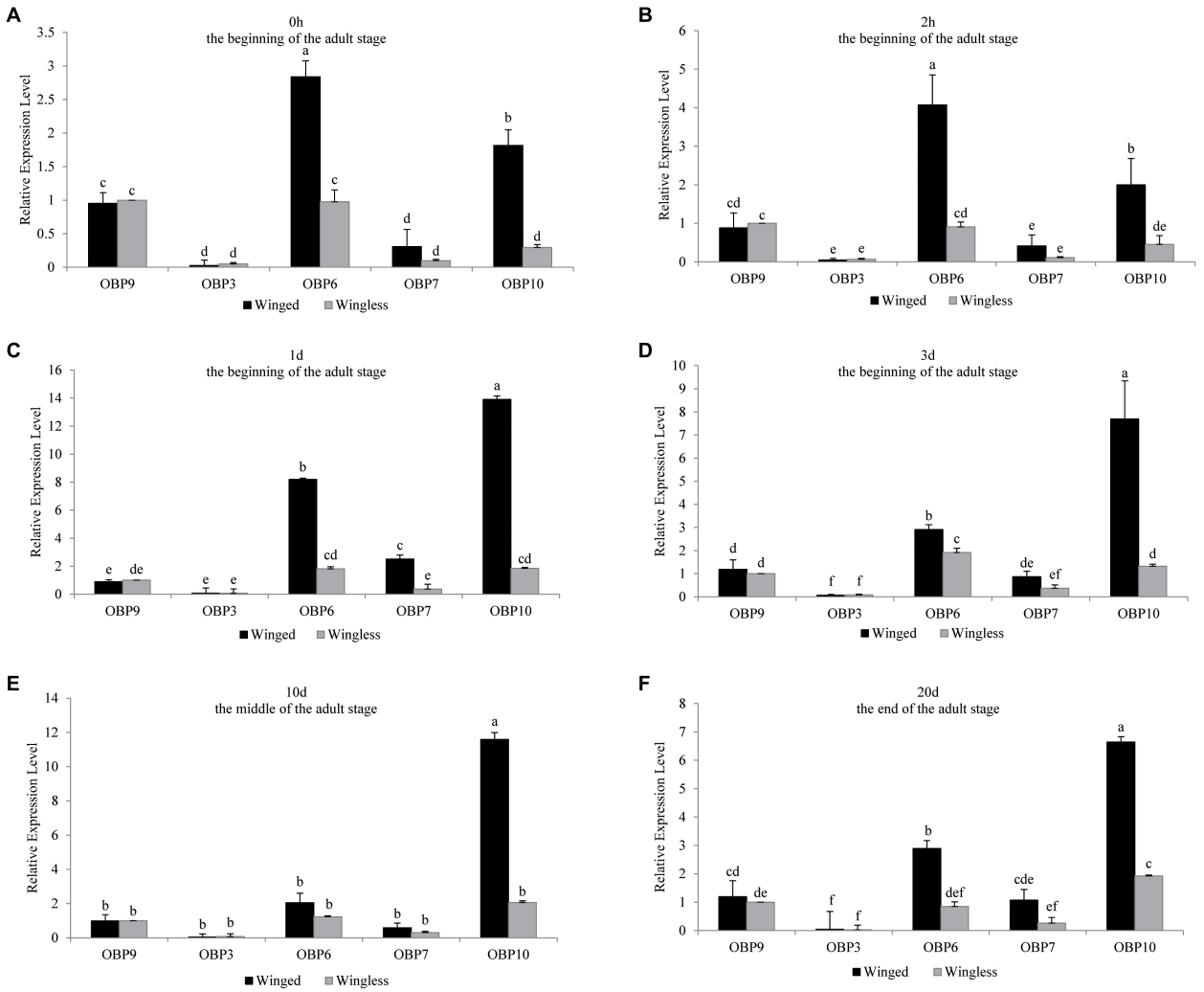

FIGURE 2 | *OBP3/6/7/9/10* expression at each time point (0 h, 1 d, 3 d, 10 d, and 20 d) in *S. miscanthi*. Fold changes are relative to the antennal transcript levels of OBP9 in the wingless morph at the corresponding time point. Differences in mean transcript levels were detected using one-way ANOVA, followed by Duncan's multiple range test. Different letters over bars indicate significant differences ($p < 0.05$). Winged, antennae of winged aphid; Wingless, antennae of wingless aphid; Beginning, middle, end, the adult stage after emergence was divided into three parts, namely, beginning (within 3 d), middle (10 d), and end (20 d).

Supplementary Table 1. The system was established according to the instructions of the SuperReal PreMix Plus Kit (SYBR Green) (Tiangen, Beijing, China). The qPCR reactions were prepared at a total volume of 20 μl with 2 μl of cDNA and 0.5 μl of each primer. qPCR was performed on an ABI 7500 Real-Time PCR System (Applied Biosystems, Carlsbad, CA, United States). The parameters for qPCR amplification were 95°C for 30 s, followed by 40 cycles of 95°C for 15 s and 60°C for 30 s.

To normalize target gene expression and correct for sample-to-sample variation, the relative quantities were calculated based on two internal control genes (Vandesompele et al., 2002), NADH dehydrogenase and dimethyladenosine transferase (DIMT), which were identified from antennal transcriptome data of *S. avenae* (Xue et al., 2016).

The five target genes and two internal control genes were amplified in each sample under the same conditions, and each gene was analyzed using three technical replicates and three biological replicates.

The expression levels of *OBP3, OBP6, OBP7, OBP9* and *OBP10* in the antennae of both winged and wingless aphids at different time points after adult emergence were calculated and statistically analyzed. The temporal expression pattern of each *OBP* among the five time points was analyzed using the value from the antennae of wingless aphids at 0 h as the external reference. The expression of the five *OBPs* at a given time point was relative to the transcript level of *OBP9* in the antennae of wingless aphids at the corresponding time point.

The expression levels of O*BP3, OBP6, OBP7, OBP9*, and *OBP10* in the antennae of winged and wingless aphids before and after EBF induction were quantified relative to the transcript levels of *OBP9* in winged aphids and *OBP9* in wingless aphids, respectively.

Statistical Analysis

Differences in transcript expression at different time points of adult aphid emergence were tested by one-way analysis of variance (ANOVA) followed by Duncan's multiple range test using SPSS version 23.0 software (IBM, Armonk, NY, United States). Differences in antennal transcript expression between winged and wingless aphids were analyzed by two-sample *t*-tests.

RESULTS

Expression Patterns

There was no significant difference in the antennal expression of *OBP3* between winged and wingless aphids at most time points (**Figure 1**). However, at the beginning of the adult stage (0 h), *OBP3* expression in the antennae of the winged type was significantly lower than that in the wingless type, after which it increased to the level observed in the wingless type at 1 day and remained stable in the later adult stage. Meanwhile, the antennal expression of *OBP3* in wingless aphids remained stable after adult emergence (at the $P = 0.05$ level, **Figure 1**). Furthermore, as shown in **Figure 2**, the expression level of *OBP3* in the antennae of both morphs was much lower than that of the other four *OBPs* (*OBP6/7/9/10*, at the $P = 0.05$ level, **Figure 2**).

The antennal expression of *OBP6* in the winged morph was higher than in the wingless morph at all detection time points. However, the expression in both morphs showed a consistent trend over time. It peaked at the same time point (1 d) in the two morphs and then decreased to the level observed at 0 h (at the $P = 0.05$ level, **Figure 1**).

Although the antennal expression of *OBP7* in the wingless morph increased at 1 day and then remained significantly higher than that at 0 h in the later adult stage (at 1 day, 3 days, 10 days, and 20 days, **Figure 1**), it was lower than that in the winged morph at all time points. The antennal expression of *OBP7* in the winged morph increased rapidly after 2 h and reached a peak at 1 day. After that, although it fluctuated, it stayed higher than the expression at 0 h as well as the expression in the wingless morph, as mentioned above (at the $P = 0.05$ level, **Figure 1**).

The expression level of *OBP9* remained stable throughout the whole adult stage, including at the beginning of emergence, and there was no significant difference between the winged and wingless phenotypes (at the $P = 0.05$ level, **Figure 1**).

The antennal expression level of *OBP10* in the wingless morph, which was far lower than that in the winged morph in adulthood (**Figure 1**), showed an upward trend, but there was no statistically significant change during the adult stage. The level in winged aphids was lower at the beginning of adult emergence; it increased rapidly and remained stably high after 2 h and throughout the later adult stage (at the $P = 0.05$ level, **Figure 1**). Moreover, our analysis results showed that among the five tested *OBPs*, *OBP10* showed the highest antennal expression in both winged and wingless antennae after time point "2 h" (at the $P = 0.05$ level, **Figure 2**).

According to the above results, among the three EBF-binding proteins, *OBP3* and *OBP9* were stable and not differentially expressed in the two phenotypes. *OBP7* was highly expressed in winged aphids, showing significant phenotypic specificity. It is also worth noting that in contrast to other *OBPs*, *OBP3* was significantly more highly expressed in the wingless morph at 0 h.

EBF Induction

In wingless aphids, only *OBP9* expression was upregulated after induction by EBF ($P < 0.01$, **Figure 3** and **Supplementary Table 2**). In winged aphids, *OBP9* expression was upregulated by

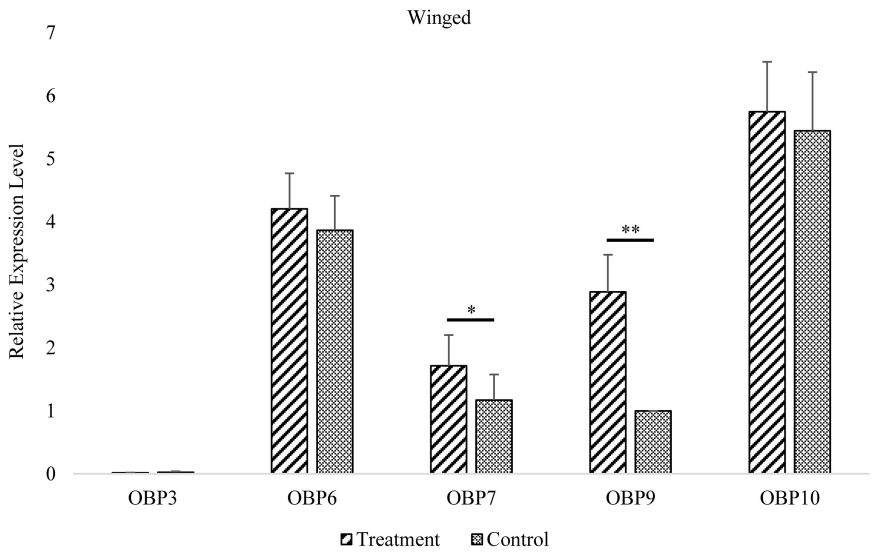

FIGURE 3 | Antennal *OBP3/6/7/9/10* expression in the winged morph before and after EBF induction. Fold changes are relative to the antennal transcript levels of OBP9 in the winged morph before EBF induction. *Significant difference at the $P = 0.05$ level. **Significant difference at the $P = 0.01$ level (two-sample *t*-test). Winged, antennae of winged aphid; Treatment, EBF induction; Control, n-hexane control.

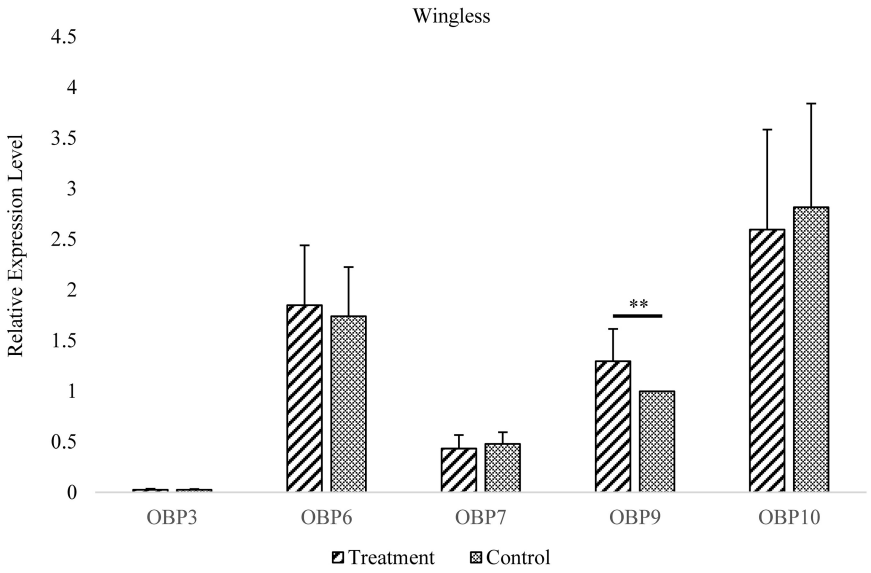

FIGURE 4 | Antennal *OBP3/6/7/9/10* expression in the wingless morph before and after EBF induction. Fold changes are relative to the antennal transcript levels of OBP9 in the wingless morph before EBF induction. **Significant difference at the $P = 0.01$ level (two-sample *t*-test). Wingless, antennae of wingless aphid; Treatment, EBF induction; Control, blank control.

EBF as well ($P < 0.01$, **Figure 4** and **Supplementary Table 2**). In addition, the expression of another EBF-binding protein, *OBP7*, was found to be upregulated by EBF induction ($P < 0.05$, **Figures 3, 4** and **Supplementary Table 2**) as well. Surprisingly, at the expression level, *OBP3*, one of the reported EBF-binding proteins, did not show any change after EBF induction in either wing morph ($P > 0.05$, **Figures 3, 4** and **Supplementary Table 2**). *OBP6* and *OBP10* showed patterns similar to that of *OBP3*, and there was no significant difference between the EBF treatment and control in either morph ($P > 0.05$, **Figures 3, 4** and **Supplementary Table 2**).

DISCUSSION

OBP3 in the pea aphid *A. pisum* was the first reported EBF-binding protein as well as the first OBP reported in aphids (Qiao et al., 2009). Several studies have since reported that OBP7 also shows a specific affinity for EBF in the pea aphid *A. pisum* and peach aphid *M. persicae* (Sun et al., 2012b), grain aphid *S. avenae* (Zhong et al., 2012) and bird cherry oat aphid *Rhopalosiphum padi* (Fan et al., 2017). More recently, OBP9 was reported to have a broad affinity spectrum including EBF (Qin et al., 2020). To date, at least three EBF-binding proteins have been reported, which suggests that peripheral transmission of EBF may be achieved through the interaction of multiple OBPs.

In the present study, in early adulthood, we found two trends of *OBP* expression, namely, stable expression (*OBP3* in the wingless morph, *OBP9* in the winged and wingless morphs, and *OBP10* in the wingless morph, **Figure 1**) and upregulated expression (*OBP3* and *OBP10* in the winged morph and *OBP6* and *OBP7* in the winged and wingless morphs, **Figure 1**), and there was no downregulated expression. By late aphid adulthood, even including the very end of the life cycle (20 d), the expression levels of the five *OBPs* all remained steady. Our investigation revealed complex expression level patterns for different *OBPs* during the aphid adult stage. Therefore, to clarify the expression patterns of aphid *OBPs*, we suggest subdividing the adult stage into different periods and including 0 h as a sampling time point. An additional odorant, i.e., EBF, was able to further stimulate the expression of corresponding *OBPs*, which obviously increased the complexity of the expression patterns.

Interestingly, among the three EBF-binding proteins, only *OBP7* was significantly more highly expressed in the antennae of winged aphids than in wingless aphids. Within the investigated temporal range, the antennal expression levels of this protein were regularly dynamic but remained higher in the winged morph than in the wingless morph at all time points. However, there was a lower but continuously stable expression level in the wingless morph. However, *OBP3* was found to have a novel expression pattern between the wing morphs. There was a significantly lower level of antennal *OBP3* expression in newly emerged winged aphids (at the $P = 0.05$ level), which increased rapidly to the same level as that in the wingless aphids at 1 day and remained steady and equivalent to that level over time. This is in sharp contrast with the patterns observed for *OBP6*, *OBP7*, and *OBP10* (sustained higher expression level in the winged morph, **Figure 1**) and *OBP9* (sustained high expression level in both wing morphs with no significant difference, **Figure 1**). Similar to that of *OBP3*, the expression of *OBP9* showed no phenotypic difference. *OBP9* was the only *OBP* that did not exhibit an expression trough at the beginning of the adult stage (0 h). This *OBP* showed relatively stable and high expression throughout the adult stage

and the highest expression level among the three EBF-binding proteins (**Figure 2**). After EBF induction, the expression of this *OBP* was further upregulated in both morphs (**Figures 3**, **4**). The above results indicated that this protein may be an important molecule for EBF recognition in aphids among two wing morphs. Antennal expression of *OBP7* strongly responded to EBF but only in the winged morph (**Figures 3**, **4**), suggesting that this protein plays an important role in the more sensitive EBF recognition process of winged aphids. In addition, the expression level of *OBP3* in antennae did not respond to EBF induction. It remained at a low level in the antennae of both the winged and wingless phenotypes (**Figures 1–4**). According to previous work showing that *OBP3* is a systemic *OBP* with stronger expression in multiple tissues and organs, such as the cornicles and caudae (Xue et al., 2016; Wang et al., 2021), we speculated that *OBP3* may play a limited role in the olfactory recognition of EBF and may play a carrier role for EBF in EBF storage organs, such as cornicles. The phenotypic specificity of *OBP* expression has been reported in different studies with various results, showing highly complex patterns that are difficult to parse. For example, the expression level of *OBP7* in the winged morph did not increase to a relatively high level until 1 day. Assuming the sampling time is 0 or 2 h or a mixture of samples is sampled at various time points, the results may vary or even seem contradictory. Furthermore, the antennal expression level of *OBP7* in the winged aphids at 0 or 2 h (before the peak at 1 day) was the same as that in the wingless aphids during the whole adult stage after 1 day. Thus, once samples at these two time points were selected, it was not surprising that *OBP7* expression was not significantly different between winged and wingless aphids, as previously reported in some studies (e.g., Xue et al., 2016; Wang et al., 2019). As after emergence, most OBP genes undergo a process of increased expression and then stabilized, and the time to stabilize was about 1–3 days after emergence (**Figure 1**). Our analysis lead to the conclusion that treating the whole adult stage as a single stage in studies on expression levels does not provide sufficient resolution. In general, the repeatable and reliable expression level can be obtained 1–3 days after adult emergence when the OBP expression level is stable.

Similar to that of *OBP7*, the expression of *OBP6* peaked at 1 day in both morphs and then remained steady in the later adult stage, and *OBP10* presented expression patterns similar to that of *OBP7* as well (**Figures 1**, **2**).

In summary, our findings will be helpful for understanding the interaction mode of the three EBF-binding proteins mediating EBF perception in aphids. Obviously, both phenotypes possess a molecular basis (*OBP9*) for ordinary EBF perception by the antennae. Furthermore, *OBP7* may enable greater sensitivity to EBF in winged aphids because of its significantly higher expression level in these aphids than in wingless aphids. Further functional studies are needed to clarify why *OBP3*, which has an EBF affinity, does not respond to EBF induction.

The above findings revealed the detailed temporal expression patterns of *OBPs* in aphids. They showed that figuring out the temporal expression patterns is critical for correctly selecting morphs and sampling times and will help researchers obtain reliable findings and draw solid conclusions.

DATA AVAILABILITY STATEMENT

The original contributions presented in the study are included in the article/**Supplementary Material**, further inquiries can be directed to the corresponding author/s.

AUTHOR CONTRIBUTIONS

JF conceived and designed the study. JF and JC supervised the project. SZ and QZ carried out the laboratory work. SZ, JF, XJ, YQ, and WW performed the RT-qPCR data analysis. SZ, JF, XJ, and QL worked on the statistical analysis and charting. JF and SZ wrote the original manuscript. All authors contributed on polishing and revising the work.

FUNDING

This work was supported by the National Natural Science Foundation of China (31871966), National Key R&D Plan in China (2017YFD0201700), and China's Donation to the CABI Development Fund.

SUPPLEMENTARY MATERIAL

The Supplementary Material for this article can be found online at: https://www.frontiersin.org/articles/10.3389/fphys.2021.732578/full#supplementary-material

REFERENCES

Biasio, F. D., Riviello, L., Bruno, D., Annalisa, G., Congiu, T., Sun, Y. F., et al. (2015). Expression pattern analysis of odorant-binding proteins in the pea aphid *Acyrthosiphon pisum*. *Insect Sci.* 22, 220–234. doi: 10.1111/1744-7917.12118

Calvello, M., Guerra, N., Brandazza, A., D'Ambrosio, C., Scaloni, A., Dani, F. R., et al. (2003). Soluble proteins of chemical communication in the social wasp Polistes dominulus. *Cell. Mol. Life Sci.* 60, 1933–1943. doi: 10.1007/s00018-003-3186-5

Daniele, B., Gerarda, G., Rosanna, S., Andrea, S., Donatella, F., Annalisa, G., et al. (2018). Sensilla morphology and complex expression pattern of odorant binding proteins in the vetch aphid *Megoura viciae* (hemiptera: aphididae). *Front. Physiol.* 9:777. doi: 10.3389/fphys.2018.00777

Fan, J., Xue, W. X., Duan, H. X., Jiang, X., Zhang, Y., Yu, W. J., et al. (2017). Identification of an intraspecific alarm pheromone and two conserved odorant-binding proteins associated with (E)-β-farnesene perception in aphid *Rhopalosiphum padi*. *J. Insect Physiol.* 101, 151–160. doi: 10.1016/j/jinsphys.2017.07.014

Gu, S. H., Wu, K. M., Guo, Y. Y., Field, L. M., Pickett, J. A., Zhang, Y. J., et al. (2013). Identification and expression profiling of odorant binding proteins and chemosensory proteins between two wingless morphs and a winged morph of the cotton aphid Aphis gossypii glover. *PLoS One*. 8:e73524. doi: 10.1371/journal.pone.0073524

Iovinella, I., Dani, F. R., Niccolini, A., Sagona, S., Michelucci, E., Gazzano, A., et al. (2011). Differential expression of odorant-binding proteins in the mandibular glands of the honey bee according to caste and age. *J. Proteome Res.* 10, 3439–3449. doi: 10.1021/pr2000754

Ji, R., Wang, Y., Cheng, Y., Zhang, M., Zhang, H. B., Zhu, L., et al. (2016). Transcriptome analysis of green peach aphid (*Myzus persicae*): insight into developmental regulation and inter-species divergence. *Front. Plant Sci.* 7:1562. doi: 10.3389/fpls.2016.01562

Jiang, X., Zhang, Q., Qin, Y., Yin, H., Zhang, S., Li, Q., et al. (2019). A chromosome-level draft genome of the grain aphid sitobion miscanthi. *GigaScience* 8:8. doi: 10.1093/gigascience/giz101

Li, Q., Fan, J., Sun, J., Wang, M., and Chen, J. (2018). Effect of the secondary symbiont hamiltonella defensa on fitness and relative abundance of buchnera aphidicola of wheat aphid. Sitobion miscanthi. *Front. Microbiol.* 9:582. doi: 10.3389/fmicb.2018.00582

Li, S., Picimbon, J. F., Ji, S., Kan, Y., and Pelosi, P. (2008). Multiple functions of an odorant-binding protein in the mosquito Aedes aegypti. *Biochem. Biophys. Res. Commun.* 372, 464–468. doi: 10.1016/j.bbrc.2008.05.064

Nault, L. R., Edwards, L. J., and Styer, W. E. (1973). Aphid alarm pheromones: secretion and reception. *Environ. Entomol.* 2, 101–105. doi: 10.1093/ee/2.1.101

Pelosi, P., Mariantonietta, C., and Ban, L. (2005). Diversity of odorant-binding proteins and chemosensory proteins in insects. *Chem. Senses* 30:i291. doi: 10.1093/chemse/bjh229

Pickett, J. A. (2009). High-throughput ESI-MS analysis of binding between the *Bombyx mori* pheromone-binding protein BmorPBP1, its pheromone components and some analogues. *Chem. Commun.* 38, 5725–5727. doi: 10.1039/b914294k

Pickett, J. A., and Griffiths, D. C. (1980). Composition of aphid alarm pheromones. *J. Chem. Ecol.* 6, 349–360. doi: 10.1007/BF01402913

Qiao, H. L., Tuccori, E., He, X. L., Gazzano, A., Field, L., Zhou, J. J., et al. (2009). Discrimination of alarm pheromone (E)–β-farnesene by aphid odorant-binding proteins. *Insect Biochem. Mol. Biol.* 39, 414–419. doi: 10.1016/j.ibmb.2009.03.004

Qin, Y. G., Yang, Z. K., Song, D. L., Wang, Q., Gu, S. H., Li, W. H., et al. (2020). Bioactivities of synthetic salicylate-substituted carboxyl (E)-β-Farnesene derivatives as ecofriendly agrochemicals and their binding mechanism with potential targets in aphid olfactory system. *Soc. Chem. Ind.* 76, 2465–2472. doi: 10.1002/ps.5787

Siciliano, P., He, X. L., Woodcock, C., Pickett, J. A., Field, L. M., Birkett, M. A., et al. (2014). Identification of pheromone components and their binding affinity to the odorant binding protein ccapobp83a-2 of the mediterranean fruit fly, ceratitis capitata. *Insect Biochem. Mol. Biol.* 48, 51–62. doi: 10.1016/j.ibmb.2014.02.005

Sun, Y. F., De Biasio, F., Qiao, H. L., Iovinella, I., Yang, S. X., Ling, Y., et al. (2012b). Two odorant-binding proteins mediate the behavioural response of aphids to the alarm pheromone (E)-β-farnesene and structural analogues. *PLoS One* 7:e32759. doi: 10.1371/journal.pone.0032759

Sun, Y. L., Huang, L. Q., Pelosi, P., and Wang, C. Z. (2012a). Expression in antennae and reproductive organs suggests a dual role of an odorant-binding protein in two sibling helicoverpa species. *Plos One* 7:e30040. doi: 10.1371/journal.pone.0030040

Sun, Y. P., Zhao, L. J., Sun, L., Zhang, S. G., and Ban, L. P. (2013). Immunolocalization of odorant-binding proteins on antennal chemosensilla of the peach aphid *Myzus persicae* (Ssulzer). *Chem. Sens.* 38, 129–136. doi: 10.1093/chemse/bjs093

Vandesompele, J., Preter, K. D., Patty, N. F., Poppe, B., and Speleman, F. (2002). Accurate normalization of real-time quantitative RT-PCR data by geometric averaging of multiple internal control genes. *Genome Biol.* 3:34. doi: 10.1186/gb-2002-3-7-research0034

Vogt, R. G., and Riddiford, L. M. (1981). Pheromone binding and inactivation by moth antennae. *Nature* 293, 161–163. doi: 10.1038/293161a0

Wang, L., Bi, Y., Liu, M., Li, W., Liu, M., Di, S. F., et al. (2019). Identification and expression profiles analysis of odorant−binding proteins in soybean aphid. Aphis glycines (hemiptera: aphididae). *Insect Sci.* 27, 1019–1030. doi: 10.1111/1744-7917.12709

Wang, L., Yin, H., Zhu, Z. G., Yang, S., and Fan, J. (2021). A detailed spatial expression analysis of wing phenotypes reveals novel patterns of odorant binding proteins in the soybean aphid. Aphis glycines. *Front. Physiol.* 12:702973. doi: 10.3389/fphys.2021.702973

Xue, W., Jia, F., Zhang, Y., Xu, Q., Han, Z., Sun, J., et al. (2016). Identification and expression analysis of candidate odorant-binding protein and chemosensory protein genes by antennal transcriptome of *sitobion avenae*. *Plos One* 11:e0161839. doi: 10.1371/journal.pone.0161839

Zhang, G. (1999). *Aphids in Agriculture and Forestry of Northwest China. 1st ed*. Beijing: China Environmental Science.

Zhang, Y., Fan, J., Sun, J., Francis, F., and Chen, J. (2017). Transcriptome analysis of the salivary glands of the grain aphid. Sitobion avenae. *Sci. Rep.* 7:15911. doi: 10.1038/s41598-017-16092-z

Zhong, T., Yin, J., Deng, S., Li, K., and Cao, Y. (2012). Fluorescence competition assay for the assessment of green leaf volatiles and trans-β-farnesene bound to three odorant-binding proteins in the wheat aphid *Sitobion avenae* (Fabricius). *J. Insect Physiol.* 58, 771–781. doi: 10.1016/j.jinsphys.2012.01.011

Zhou, J. J., Vieira, F. G., He, X. L., Smadja, C., Liu, R., Rozas, J., et al. (2010). Genome annotation and comparative analyses of the odorant-binding proteins and chemosensory proteins in the pea aphid acyrthosiphon pisum. *Insect Mol. Biol.* 19, 113–122. doi: 10.1111/j.1365-2583.2009.00919.x

Conflict of Interest: The authors declare that the research was conducted in the absence of any commercial or financial relationships that could be construed as a potential conflict of interest.

Publisher's Note: All claims expressed in this article are solely those of the authors and do not necessarily represent those of their affiliated organizations, or those of the publisher, the editors and the reviewers. Any product that may be evaluated in this article, or claim that may be made by its manufacturer, is not guaranteed or endorsed by the publisher.

frontiers in Physiology

ORIGINAL RESEARCH
published: 26 August 2021
doi: 10.3389/fphys.2021.727619

Identification and Characterization of an Antennae-Specific Glutathione S-Transferase From the Indian Meal Moth

Hongmin Liu[1†], *Yin Tang*[2†], *Qinying Wang*[2], *Hongzhong Shi*[1], *Jian Yin*[1*] and *Chengjun Li*[3*]

[1] College of Agronomy, Xinyang Agriculture and Forestry University, Xinyang, China, [2] College of plant protection, Hebei Agricultural University, Baoding, China, [3] Tobacco Research Institute, Henan Academy of Agricultural Sciences, Xuchang, China

Insect glutathione-S-transferases (GSTs) play essential roles in metabolizing endogenous and exogenous compounds. GSTs that are uniquely expressed in antennae are assumed to function as scavengers of pheromones and host volatiles in the odorant detection system. Based on this assumption, antennae-specific GSTs have been identified and functionally characterized in increasing number of insect species. In the present study, 17 putative GSTs were identified from the antennal transcriptomic dataset of the Indian meal moth, *Plodia interpunctella*, a severe stored-grain pest worldwide. Among the GSTs, only PiGSTd1 is antennae-specific according to both Fragments Per Kilobase Million (FPKM) and quantitative real-time PCR (qRT-PCR) analysis. Sequence analysis revealed that PiGSTd1 has a similar identity as many delta GSTs from other moths. Enzyme kinetic assays using 1-chloro-2,4-dinitrobenzene (CDNB) as substrates showed that the recombinant PiGSTd1 gave a K_m of 0.2292 ± 0.01805 mM and a V_{max} of 14.02 ± 0.2545 μmol·mg^{-1}·min^{-1} under the optimal catalytic conditions (35°C and pH = 7.5). Further analysis revealed that the recombinant PiGSTd1 could efficiently degrade the sex pheromone component Z9-12:Ac (75.63 ± 5.52%), as well as aldehyde volatiles, including hexanal (89.10 ± 2.21%), heptanal (63.19 ± 5.36%), (*E*)-2-octenal (73.58 ± 3.92%), (*E*)-2-nonenal (75.81 ± 1.90%), and (*E*)-2-decenal (61.13 ± 5.24%). Taken together, our findings suggest that PiGSTd1 may play essential roles in degrading and inactivating a variety of odorants, especially sex pheromones and host volatiles of *P. interpunctella*.

Keywords: Plodia interpunctella, glutathione S-transferases, pheromone, volatile, semiochemicals, degradation, enzyme

OPEN ACCESS

Edited by:
Yang Liu,
Institute of Plant Protection, Chinese Academy of Agricultural Sciences, China

Reviewed by:
Sufang Zhang,
Chinese Academy of Forestry, China
Youssef Dewer,
Agricultural Research Center, Egypt

***Correspondence:**
Jian Yin
yinjian80@xyafu.edu.cn
Chengjun Li
15937470664@126.com

[†]These authors have contributed equally to this work

Specialty section:
This article was submitted to Invertebrate Physiology, a section of the journal Frontiers in Physiology

Received: *19 June 2021*
Accepted: *20 July 2021*
Published: *26 August 2021*

Citation:
Liu H, Tang Y, Wang Q, Shi H, Yin J and Li C (2021) Identification and Characterization of an Antennae-Specific Glutathione S-Transferase From the Indian Meal Moth. Front. Physiol. 12:727619. doi: 10.3389/fphys.2021.727619

INTRODUCTION

Glutathione S-transferases (GSTs, EC 2.5.1.18) exist ubiquitously in various organisms (Enayati et al., 2005). As a family of multifunctional detoxification enzymes, GSTs play vital roles in metabolizing a wide range of endogenous and exogenous compounds as well as in degrading them into less-toxic metabolites by catalyzing the conjugation of electrophilic molecules with glutathione (GSH) (Singh et al., 2001; Huang et al., 2017). It is widely accepted that GSTs exert their detoxification function *via* two domains: One is the highly conserved N-terminal GSH binding

domain (G-site) and the other is the C-terminal hydrophobic substrate binding domain (H-site) (Enayati et al., 2005). Insect GSTs are classified into the cytosolic, microsomal, and mitochondrial subgroups based on their cellular locations (Hayes et al., 2015). The majority of insect cytosolic GSTs are divided into six subclasses (i.e., delta, epsilon, omega, sigma, theta, and zeta) mainly according to their sequence identities, genomic structures, and biochemical properties (Sheehan et al., 2001; Yu et al., 2008). Among these subclasses, only delta and epsilon are considered insect-specific, while others are found in a variety of invertebrates and vertebrates (Labade et al., 2018).

During the past two decades, an increasing number of studies have focused on the crucial roles of insect GSTs in the detoxification of harmful stimuli, such as phytochemicals and insecticides (Glaser et al., 2013; Liu et al., 2015; Zou et al., 2016). NlGST1-1 from *Nilaparvata lugens* can detoxify various plant metabolites so this planthopper can rapidly adapt to a broader host range (Sun et al., 2013). SlGSTE1 in the gut of *Spodoptera litura* and HaGST-8 from *Helicoverpa armigera* show higher binding activity to insecticides like chlorpyrifos, deltamethrin, malathion, phoxim, and dichloro-diphenyl-trichloroethane (DDT), resulting in insecticide resistance in pests (Xu et al., 2015; Labade et al., 2018). Besides the functions of metabolism and detoxification, antennae-specific GSTs can also function as odorant-degrading enzymes (ODEs) as part of the olfactory system. During the process of odor recognition, antennal GSTs can quickly remove or degrade the odorants from olfactory receptors (ORs) to maintain sensitivity and fidelity of the chemoreceptor (Vogt and Riddiford, 1981; Younus et al., 2014; Durand et al., 2018). BmGSTd4, an antennae-specific GST in the male silk moth, plays a dual role in the detoxification of xenobiotic compounds and the signal termination of sex pheromone signals (Tan et al., 2014). GST-msolf1 from antennal sensilla of *Manduca sexta* can modify (*E*)-2-hexenal, suggesting that the GST is involved in inactivating host plant volatiles (Rogers et al., 1999). Hence, our study on antennae-specific GSTs could deepen understanding of insect olfactory recognition and contribute to the subsequent development of potential pest control strategies.

The Indian meal moth, *Plodia interpunctella* (Lepidoptera: Pyraloidea, Pyralidae), a cosmopolitan stored-product pest, causes severe economic loss yearly (Mohandass et al., 2007). The sex pheromone-based monitoring approach has been proven accurate and efficient in monitoring populations of *P. interpunctella* (Campos and Phillips, 2014). Therefore, revealing the mechanism of pheromone recognition could benefit the development of novel attractants or repellents against this pest. Recently, Jia et al. (2018) have identified a series of odorant-related proteins and chemoreceptors from the antennae of *P. interpunctella* through transcriptomic sequencing. More recently, we reported that antennal-specific carboxylesterases of *P. interpunctella* (PintCXEs) respond to sex pheromone and environmental volatiles (Liu et al., 2019). However, whether GSTs are involved in pheromone recognition remains unknown.

This study aimed to identify GSTs from *P. interpunctella* antennae, analyze their sequences, and evaluate the characteristics of antennae-specific PiGSTs in degrading sex pheromone and host volatiles. Our results will provide fundamental information on the GSTs in the antennae of *P. interpunctella* and pave the way for further research on the semiochemical-based control of this pest.

MATERIALS AND METHODS

Insects and Tissue RNA Collection

P. interpunctella were reared on crushed wheat seeds in the laboratory of the Plant Protection Institute, Hebei Academy of Agricultural and Forestry Sciences, at 28 ± 1°C, 60 ± 5% RH and 14:10 L:D photoperiod (Jia et al., 2018). The last-instar larvae were separated and individually reared in glass vials (diameter 2 cm, height 4.5 cm) until their eclosion. The samples from tissues (antennae, thoraces, abdomens, legs, and wings) were prepared following our previous method (Liu et al., 2019). All samples were immediately frozen in liquid nitrogen and stored at −80°C until further RNA extraction. Total RNA extraction, purity evaluation, and concentration determination were performed as previously reported (Jia et al., 2018).

Identification of GST Genes

The identification of antennal GSTs from *P. interpunctella* was mainly based on previously reported transcriptome datasets (accession number: SRR6002827 and SRR6002828) (Jia et al., 2018). The putative GSTs were preliminarily retrieved from annotations based on the latest database, including non-redundant protein (NR), Gene Ontology (GO), Swiss-Prot, and the Kyoto Encyclopedia of Genes and Genomes (KEGG). Subsequently, all candidates were manually validated using the NCBI BLASTx (http://blast.ncbi.nlm.nih.gov/) with an E-value of $< 10^{-5}$.

Expression of GST Genes Using Quantitative Real-Time PCR (qRT-PCR)

Quantitative real-time PCR tests were conducted on an ABI 7500 (Thermo Fisher Scientific, United States) using Bestar® SybrGreen qPCR mastermix kit (DBI® Bioscience) and using the β-actin gene, which was identified from the antennal transcriptome of *P. interpunctella*, as the reference gene (paired primers: 5′-GTATCAACGGATTTGGTCG-3′ and 5′-CACCTT CCAAGTGAGCAGAT-3′) (Liu et al., 2019). Each reaction was completed in a 20 μL system blend, comprising 10 μL of Bestar SyBr Green qPCR mastermix, 0.2 μM of each primer, 0.4 μL of 50x ROX Reference Dye, 2 μL of cDNA template, and 6.8 μL of RNase-free water at conditions of 1 cycle of 95°C for 2 min, followed by 40 cycles of 95°C for 10 s, 55°C for 34 s, and 72°C for 30 s. Each sample had three independent biological replicates, and each replicate was tested in three technical repeats. All primers are available in **Supplementary Table 1**. The amplification efficiency for each primer pair ranged from 91.6% to 100.3% based on the standard curve analysis. Relative expression of all GST genes was determined using the comparative $2^{-\Delta\Delta Ct}$ method (Livak and Schmittgen, 2001). The heatmaps were created by Heatmapper (http://www.heatmapper.ca/) based on the transformed data of $\log_2 (2^{-\Delta\Delta Ct} + 1)$ values (Babicki et al., 2016).

Bioinformatics Analyses

The GST sequences were characterized by corresponding bioinformatics tools. GST-ORFs were identified using ORF Finder (http://www.ncbi.nlm.nih.gov/gorf/gorf.html). The sequence lengths, molecular weights (MWs), and isoelectric points (pI) were predicted by using ExPASy tools (https://web.expasy.org/compute_pi/) (Gasteiger et al., 2005). The conserved domains were predicted by using the hmmsearch tool from the pfam website (http://pfam.xfam.org/) (Mistry et al., 2021). Identification of conserved motifs of GSTs was conducted with the MEME online program for protein sequence (http://meme.nbcr.net/meme/intro.html) (Bailey et al., 2009) with the optimized parameters being any number of repetitions, a maximum number of 10 motifs, and optimum 6–50 residue length per motif.

Phylogenetic Construction

Deduced amino acid sequences of GST genes from different insects were aligned with the GST sequence identified from the antennae of *P. interpunctella* using ClustalW with default parameters (https://www.genome.jp/tools-bin/clustalw). After sequence alignments, the phylogenetic tree was constructed by MEGA5.0 software using the neighbor-joining method with the following parameters: Poisson model, pairwise deletion, and 1,000 bootstrap replications (Tamura et al., 2011). The dendrogram was further decorated using Evolview software (https://www.evolgenius.info/evolview/). The homologous GST sequences were used to reconstruct a phylogenetic tree from eight species, including *Plutella xylostella* (You et al., 2015), *Cydia pomonella* (Huang et al., 2017), *Bombyx mori* (Yu et al., 2008), *Chilo suppressalis* (Liu et al., 2015), *Acyrthosiphon pisum* (Francis et al., 2001), *Drosophila melanogaster* (Younus et al., 2014), *Anopheles gambiae* (Ding et al., 2003), and *Tribolium castaneum* (Shi et al., 2012). All sequences were obtained from NCBI (https://www.ncbi.nlm.nih.gov/).

Homology Modeling of PiGSTd1

The homology model was constructed by the SWISS-MODEL server (https://swissmodel.expasy.org/interactive). The models of PiGSTd1 were built based on the target-template alignment using ProMod3 (Guex et al., 2009). The QMEAN scoring function was used to assess the global and per-residue model quality (Studer et al., 2020). Then, an automated model BmGSTd1 (PDB ID: 4e8e.1) was selected as the template from PDB database. Pictures of three-dimensional structures were generated with PyMOL (DeLano, 2002). Multisequence alignments were performed using ClustalX 2.1, and the results were presented by GeneDoc software (http://nrbsc.org/gfx/genedoc). The secondary structure was predicted with PSIPRED software (McGuffin et al., 2000).

PiGSTd1 Plasmid Construction, Expression, and Purification

The PiGSTd1 sequence without signal peptide was amplified by PCR using TransStart® FastPfu PCR SuperMix (TransGen Biotech, China). The paired primers were forward 5′-ATGCC GGCTCAAGCCATCAA-3′ and reverse 5′-CTAATCTTTCTTC AGAAATGATGC-3′. The amplification was carried out under the conditions of denaturation at 95°C for 1 min followed by 35 cycles of 95°C for 20 s, 55°C for 20 s, and 72 °C for 1 min, and a final extension at 72°C for 5 min. The PCR products were ligated into a pEASY-Blunt E1 Expression vector (TransGen Biotech, China) and transformed into *Escherichia coli Trans-T1* (Liu et al., 2017). After sequence confirmation by Sangon Biotechnology (Shanghai, China), the positive recombinant plasmids were designated as pEASY-Blunt E1-PiGSTd1.

PiGSTd1 expression and purification were conducted as previously described with a slight modification (Song et al., 2020). Briefly, the recombinant vector (pEASY-Blunt E1-PiGSTd1) was transformed into *E. coli* BL21 (DE3), and the positive clones were isolated for expression. Cultures were started from single colonies, in LB broth with 50 μg/mL ampicillin in a 37°C shaker (220 rpm). When OD of 600 nm reached 0.6, isopropyl β-D-1-thiogalactopyranoside (IPTG) was added to 1 mM. After cultured for 6 h at 25°C and 220 rpm, cells were harvested by centrifugation at 8,000 g at 4°C and suspended in 20 ml of PBS buffer (pH = 7.0).

After ultrasonic cell disintegration, the collected bacteria were centrifuged at 14,000 rpm at 4°C for 20 min. After confirming the expression by 12% SDS–PAGE, the supernatants were loaded on a Ni-chelating affinity column (GE, United States), which had been equilibrated with 20 mM Tris–HCl (pH = 7.9) supplemented with 100 mM NaCl, and eluted with imidazole (50, 100, 150, and 200 mM) in an ascending series. The recombinant PiGSTd1 purity was assayed by SDS–PAGE. Its concentration was determined using Bradford's method with BCA Protein Assay Kits (Legend biotech, Beijing, China). Proteins were stored at −20°C before use.

Kinetic Properties of PGSTd1

The kinetic parameter of PiGSTd1 was determined based on the CDNB (1-chloro-2,4-dinitrobenzene) method (Li et al., 2018). Briefly, 0.4 μg of the purified PiGSTd1 was added into 200 μL acetate–phosphate buffer (pH 7.5) containing 50 mM GSH and a series of CDNB (0, 0.2, 0.4, 0.6, 0.8, 1.0, 1.2, and 1.4 mM) at 35°C in a transparent 96-well plates, and the absorbance at 340 nm in 0–1 min was recorded in a Multiskan Spectrum Microplate Spectrophotometer (BioTek, Shoreline, WA). Heat-inactivated PiGSTd1 was used as the negative control. The *Km* and *Vmax* were calculated by the linear regression of a double reciprocal plot (Balakrishnan et al., 2018). To optimize the reaction pH and temperature of PiGSTd1, the assays were conducted at fixed concentrations of GSH (1 mM) and CDNB (0.5 mM) with varying acetate–phosphate buffer (pH = 5.5, 6.0, 6.5, 7.0, 7.5, 8.0, 8.5 and 9.0) and reaction temperature (20, 25, 30, 35, 40, 50, 55, and 60°C for 30 min). All determinations were performed three times.

Enzymatic Degradation Tests of Recombinant PiGSTd1

A GC-MS (7890A-5975C; Agilent, United States) with a DB-WAX column (30 m × 0.25 mm × 0.25 μm, Agilent) was used to evaluate the degradation activities of PiGSTd1 on the main sex pheromone and environmental volatiles (**Supplementary Table 2**). The degradation assays were

conducted in 1 mL acetate–phosphate buffer (pH = 7.0) containing 2.5 μg purified PiGSTd1, 10 mM GSH, and 20 μg substrates. After reacting for 1 h at 35°C, the reaction mixture was extracted with 1 mL hexane immediately. Subsequently, substrates in the organic phase were qualitatively and quantitatively analyzed on the GC-MS with the chromatographic conditions setting as helium carrier gas at 1 ml·min^{-1}; oven temperature initiated at 50°C (hold 1 min), increased to 120°C at 5°C·min^{-1} (hold 2 min), and subsequently increased to 230°C at 10°C·min^{-1} (hold 5 min). The ionization current and ionization voltage were 100 μA and 70 eV, respectively. All assays were repeated three times with the heat-inactivated PiGSTd1 as the negative control. Degradation data were analyzed by one-way ANOVA (SPSS 19.0 for Windows) with Tukey's test. The least significant difference was set at $P < 0.05$.

RESULTS

Identification and Classification of PiGSTs

From the antennal transcriptome of *P. interpunctella*, we identified a total of 17 sequences encoding putative GSTs, which were designated as PiGSTd1-PiGSTm3. Sequence characteristics (ORFs, MW, and pI) and Blastx results are listed in **Table 1**. Among all PiGSTs, 15 sequences were intact ORFs, while PiGSTo4 and PiGSTd2 were incomplete with truncated 3′-regions. The sequence lengths of the PiGSTs ranged from 149

TABLE 1 | Details of the 17 GSTs identified in *Plodia interpunctella* antennae.

Clade	Gene Name	GenBank accession	Full Length	ORF(aa)	pI	MW(Da)	Blastx annotation (Name/Species)	Accession number	Score	E-value	Identity
Delta	PiGSTd1	MZ410553	Y	245	5.15	27761.04	Glutathione S-transferase delta 1 [*Chilo suppressalis*]	AKS40338.1	379	3E-131	73%
	PiGSTd2	MZ410560	N	237	-	-	Glutathione S-transferase delta 1 [*Aphis gossypii*]	AFM78644.1	444	3E-157	89%
	PiGSTd3	MZ410545	Y	215	6.91	24098.6	Glutathione S-transferase delta [*Antheraea pernyi*]	ACB36909.1	399	3E-140	89%
Epsilon	PiGSTe1	MZ410556	Y	228	6.76	25835.97	Glutathione S-transferase 1 [*Papilio xuthus*]	KPJ03136.1	312	2E-105	63%
	PiGSTe2	MZ410551	Y	217	5.29	24549.23	Glutathione S-transferase GSTD1 [*Helicoverpa armigera*]	AIB07715.1	330	7E-113	73%
Omega	PiGSTo1	MZ410557	Y	256	6.15	29124.28	Glutathione S-transferase [*Plutella xylostella*]	AHW45906.1	436	3E-153	79%
	PiGSTo2	MZ410559	Y	290	8.39	33155.47	Glutathione S-transferase omega 2 [*Bombyx mori*]	ABD36306.1	348	1E-117	56%
	PiGSTo3	MZ410550	Y	242	7.64	27990.27	Glutathione S-transferase omega 3 [*Cnaphalocrocis medinalis*]	AIZ46903.1	365	6E-126	70%
	PiGSTo4	MZ410558	N	241	-	-	Glutathione S-transferase gst [*Trifolium pratense*]	PNX77761.1	376	2E-130	80%
Sigma	PiGSTs1	MZ410548	Y	206	6.34	23737.23	Glutathione S-transferase sigma 4 [*Cnaphalocrocis medinalis*]	AIZ46904.1	277	3E-92	64%
	PiGSTs2	MZ410552	Y	205	6.35	23572.19	Glutathione S-transferase sigma-1 [*Cydia pomonella*]	ARM39007.1	318	2E-108	70%
Theta	PiGSTt1	MZ410547	Y	232	8.8	27123.11	Glutathione S-transferase theta-1 [*Helicoverpa armigera*]	XP_021200219.1	341	1E-116	68%
Zeta	PiGSTz1	MZ410546	Y	215	8.06	24615.57	Glutathione S-transferase zeta-1 [*Cydia pomonella*]	ARM39005.1	432	2E-153	97%
Unclassified	PiGSTu1	MZ410554	Y	234	6.23	26630.45	Glutathione S-transferase 1-1 [*Papilio polytes*]	NP_001298693.1	400	6E-140	79%
Microsomal	PiGSTm1	MZ410561	Y	154	9.55	17032.02	Microsomal glutathione S-transferase [*Antheraea yamamai*]	AII16887.1	214	4E-69	69%
	PiGSTm2	MZ410555	Y	149	9.98	16654.6	Microsomal glutathione S-transferase 1-1 [*Spodoptera litura*]	AIH07603.1	186	6E-58	62%
	PiGSTm3	MZ410549	Y	149	9.77	16357.2	Microsomal glutathione transferase [*Heliothis virescens*]	ADH16761.1	232	3E-76	74%

to 290 amino acid (aa), and their calculated MWs ranged from 16.35 to 33.15 kDa. BLAST$_X$ search of the best hits showed that all PiGST sequences shared relatively high sequence identities (62−97%) with their respective orthologs from other lepidopteran species (**Table 1**).

Phylogenetic Tree Analysis

The phylogenetic tree was reconstructed with 169 GST sequences from nine species, including model insects (e.g., *B. mori* and *D. melanogaster*), typical species in varying families, as well as congeneric Pyraloid moths. Although these GSTs were derived from diverse species, they showed relative conservation in classification. According to their sequence similarities, 17 PiGSTs were distributed into eight branches of the phylogenetic tree: delta (PiGSTd1 to PiGSTd3), epsilon (PiGSTe1 and PiGSTe2), omega (PiGSTo2 to PiGSTo4), sigma (PiGSTs1 and PiGSTs2), theta (PiGSTt1), zeta (PiGSTz1), and unclassified class (PiGSTm1) (**Figure 1**). PiGSTd1 was clustered with CpGSTd2, a well-characterized enzyme involved in odorant degradation for chemosensory perception in *C.*

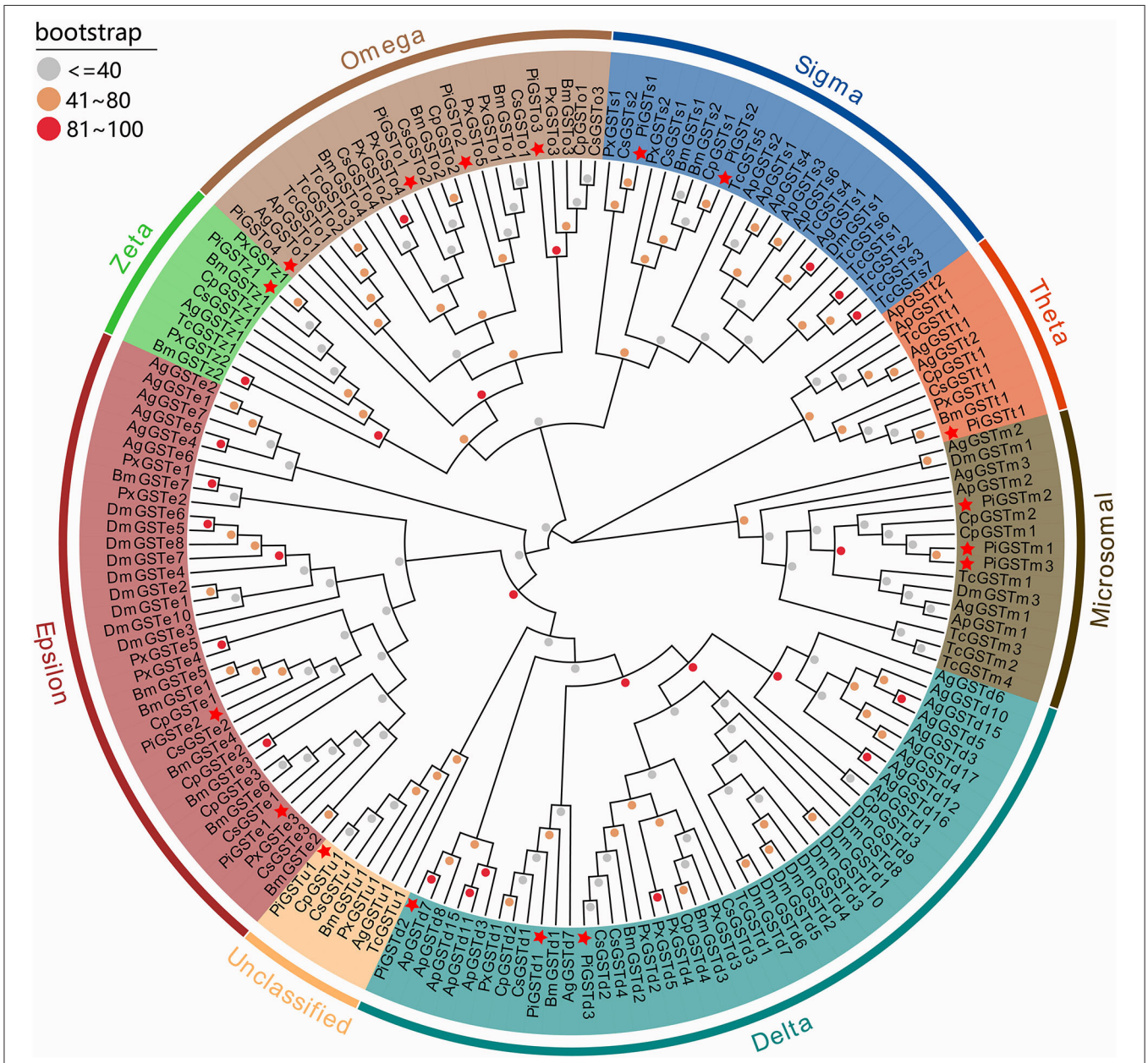

FIGURE 1 | Phylogenetic tree of GSTs from nine insect species. Eight GST branches are distinguished with different background color, and PiGSTs were marked with red stars. Dots with different colors present different bootstrap values: gray, ≤40; orange, 40–80; red, 81–100. Ag, *Anopheles gambiae*; Ap, *Acyrthosiphon pisum*; Bm, *Bombyx mori*; Cs, *Chilo suppressalis*; Cp, *Cydia pomonella*; Dm, *Drosophila melanogaster*; Pi, *Plodia interpunctella*; Px, *Plutella xylostella*; Tc, *Tribolium castaneum*.

pomonella (Huang et al., 2017), indicating it could potentially degrade odorants.

Conserved Domains and Motif Composition Analysis of PiGSTs

The analyses of conserved domains among the PiGSTs revealed two domains of the protein sequences: a fairly conserved N-terminal domain and a more variable C-terminal domain among different subclasses (**Supplementary Figure 1**). Besides, a member of conserved membrane-associated proteins was identified in eicosanoid and glutathione metabolism (MAPGE) from microsomal GSTs (**Supplementary Figure 1**). A schematic representing the structure of all complete PiGSTs sequences was constructed from the MEME motif analysis results. PiGSTs in the same subclass usually shared a similar motif composition and showed highly similar motif distributions, e.g., the clustered PiGST pairs, PiGSTs1-2 and PiGSTe12 (**Figure 2**). Among all motifs, motif 3 and motif 4 were found in all cytosolic GST proteins, while motif 2, motif 6, and motif 9 were exclusively expressed in microsomal GSTs (PiGSTm1-3).

Tissue Expression Profile of PiGSTs

Based on qRT-PCR determination, only PiGSTd1 expression was antennae-specific, and its expression level was significantly higher in males than in females (**Figure 3**), indicating that it has a close association with odorant recognition. In contrast, PiGSTe2 was almost equally expressed in female and male antennae and was also found in the abdomens, but it was not antennae-enriched. PiGSTo2, PiGSTo3, PiGSTm1, PiGSTm2, PiGSTm3, PiGSTs1, PiGSTs2, PiGSTz1, PiGSTe1, PiGSTd3, and PiGSTt1 were abundantly expressed in the abdomens of both sexes (**Figure 3**). Other GST genes were ubiquitously expressed in all tested tissues.

Sequence Analysis of PiGSTd1

According to a multiple alignment of PiGSTd1 with delta GSTs from other moths, PiGSTd1 showed relatively high identities (63.11–68.83%) with HvGSTd1 (AWX68884.1), OfGSTd1 (QIC35737.1), CsGSTd1 (AKS40338.1), SeGSTd1 (ASN63930.1), BmGSTd1 (NP_001037183.1), and PrGSTd1 (APW77568.1) (**Supplementary Figure 3**), indicating high conservation between PiGSTd1 and moth delta GSTs. Additionally, the multiple alignments and homology modeling on the basis of

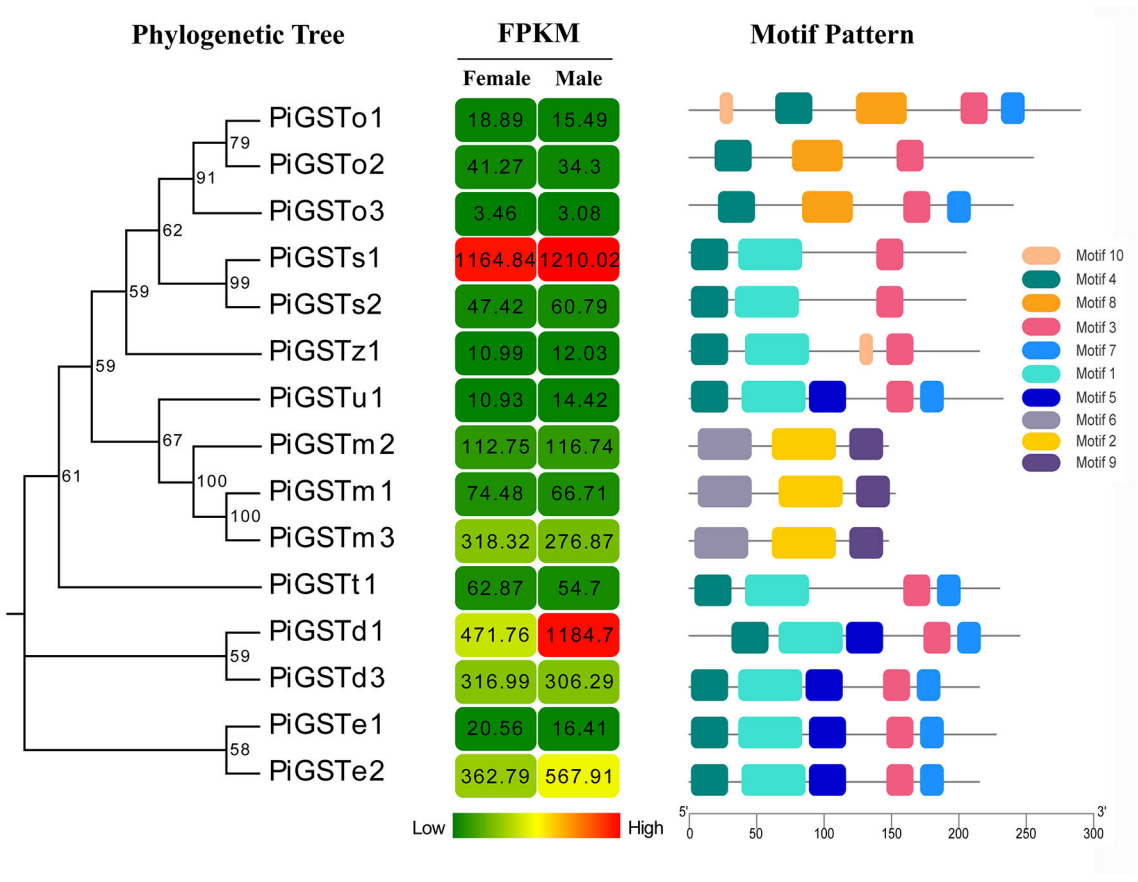

FIGURE 2 | Phylogenetic relationships, FPKM of PiGSTs, and architecture of the conserved motif patterns. The phylogenetic tree was constructed based on the full-length sequences of PiGSTs using MEGA 5.0 software. The sequence information for each motif is provided in **Supplementary Figure 2**. The conserved motifs are displayed in colored boxes, and the length of protein can be estimated using the scale at the bottom.

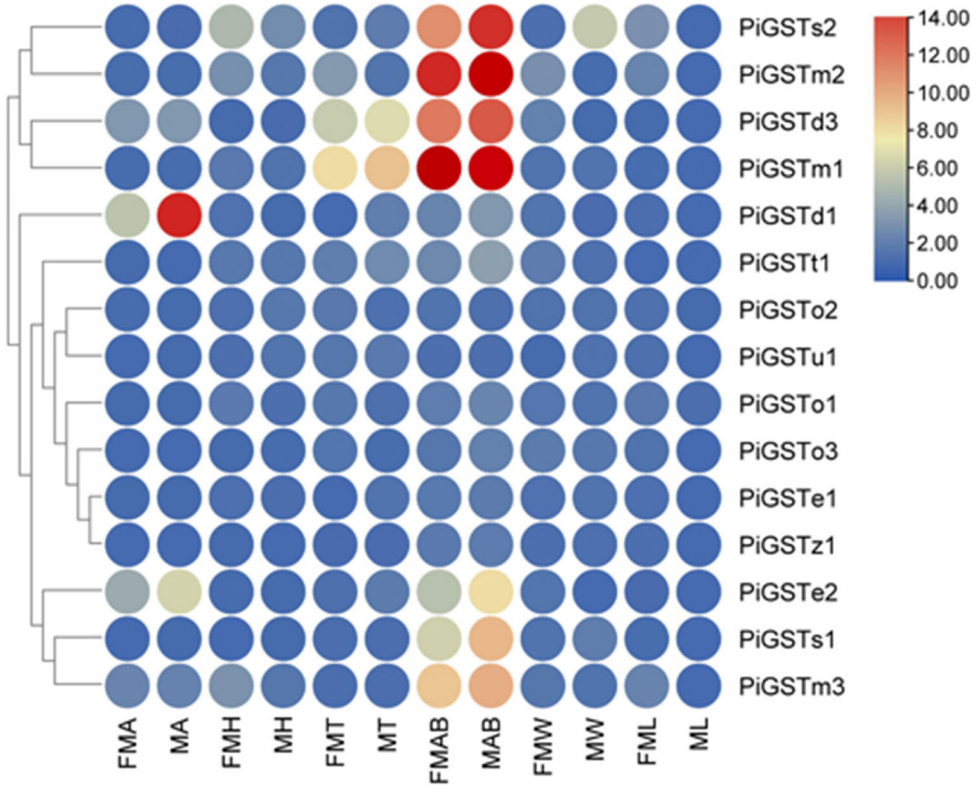

FIGURE 3 | Tissue expression pattern of the PiGST Genes. Levels of gene expression were normalized relative to that in the leg (one-fold). FMA, female antennae; MA, male antennae; FMH, female heads; MH, male heads; FMT, female thoraxes; MT, male thoraxes; FMAB, female abdomens; MAB, male abdomens; FMW, female wings; MW, male wings; FML, female legs; ML, male legs.

BmGSTd1 suggested that PiGSTd1 adopted the classic GST fold and was composed of an *N*-terminal domain, a *C*-terminal domain, and a linker in between (**Figure 4**). In the conserved *N*-terminal domain, a three α-helices and four β-strands motif (βαβαββα) of thioredoxin fold-served as the glutathione binding site (G-site). Ser40 in PiGSTd1 appeared to be responsible for enzyme catalysis.

Enzymatic Properties of PiGSTd1

The entire coding sequence of PiGSTd1 was successfully expressed in *E. coli* strain BL21 through pEASY-Blunt E1 vector. SDS–PAGE showed that Ni^{+}-column-purified PiGSTd1 displayed a single band with a MW of ∼27kDa (**Figure 5A**). Using CDNB and reduced GSH as substrates, the optimized catalytic conditions for PiGSTd1 were 35 °C and pH=7.0 (**Figures 5B,C**). Under these conditions, K_m and V_{max} of recombinant PiGSTd1 were determined as 0.2292 ± 0.01805 mM and 14.02 ± 0.2545 μmol·mg^{-1}·min^{-1}, respectively (**Figure 5D**).

In vitro Degradation Ability of Recombinant PiGSTd1

The ability of recombinant PiGSTd1 to degrade odorants was evaluated by GC-MS. The results showed that PiGSTd1 more efficiently degraded the sex pheromone component Z9-12:Ac (75.63 ± 5.52%) as compared with the pheromone analog Z8-12:Ac (58.47 ± 1.64%), despite only a differently positioned double bond. Besides sex pheromones, PiGSTd1 also displayed high efficiency in degrading various host odorants and environmental volatiles (**Supplementary Table 2**), e.g., α-pinene (68.83 ± 2.37%), hexanal (89.10 ± 2.21%), heptanal (63.19 ± 5.36%), (*E*)-2-octenal (73.58 ± 3.92%), (*E*)-2-nonenal (75.81 ± 1.90%), and (*E*)-2-decenal (61.13 ± 5.24%). The results indicated that PiGSTd1 highly expressed in *P. interpunctella* antennae was involved in degrading sex pheromones and host volatiles.

DISCUSSION

Insect antennal-specific GSTs play important roles in metabolizing a wide range of endogenous and exogenous compounds, including plant secondary compounds, insecticides, and odorant molecules (Huang et al., 2017). Therefore, deciphering the role of insect antennal GSTs will greatly extend our knowledge of the insect olfactory system. In the present study, we identified 17 PiGST genes from the antennal transcriptome of *P. interpunctella*, which is more than the number identified from the antennae of *C. suppressalis* (16 genes) (Liu et al., 2015) and *C. pomonella* (10 genes) (Huang et al.,

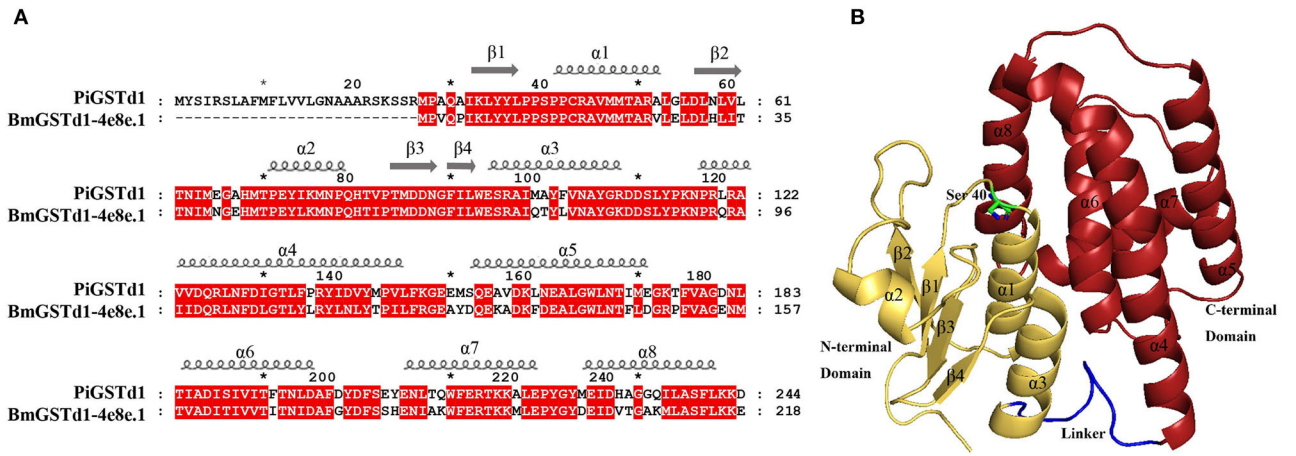

FIGURE 4 | Structural characterization of PiGSTd1. **(A)** Sequence alignment of PiGSTd1 and BmGSTd1 (PDB ID: 4e8e.1). **(B)** Homology model of PiGSTd1. Yellow, red, and blue represent N-terminal domain, C-terminal domain, and linker, respectively. Ser40 in green is proposed to be catalytically essential.

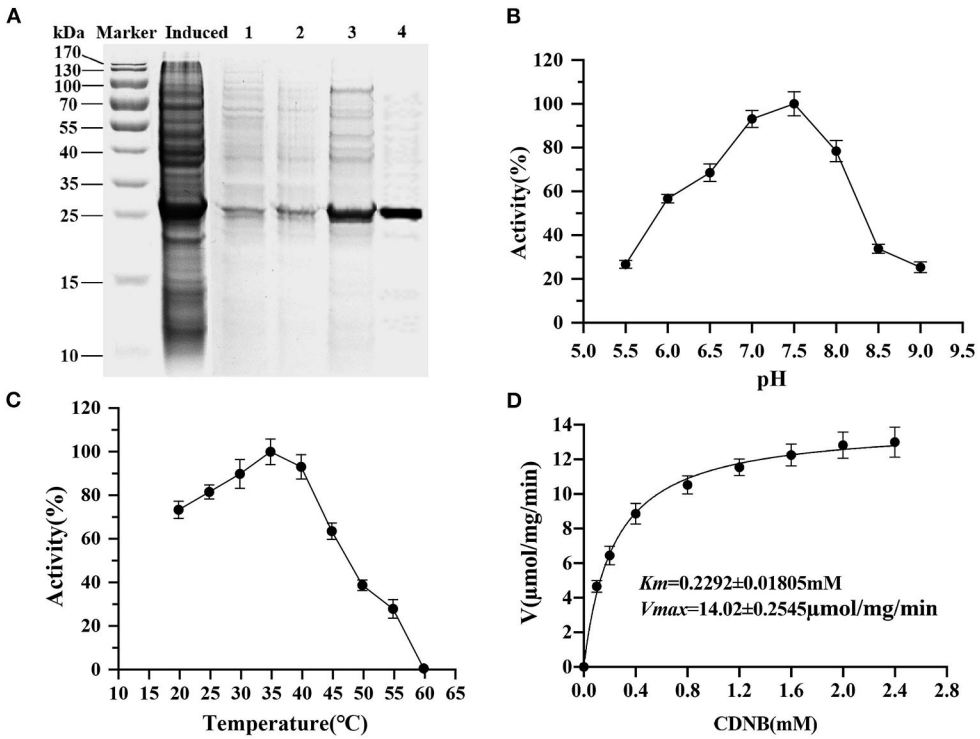

FIGURE 5 | Kinetic properties of recombinant PiGSTd1. **(A)** Purification of recombinant pEasy-Blunt-E1-PiGSTd1. Induced: the crude extracts from the bacterial pellets with 1 mM isopropyl β-D-1-thiogalactopyranoside (IPTG) induction. 1–4: samples eluted with binding buffers containing 50, 100, 150, and 200 mM imidazole, respectively. **(B)** Enzyme kinetic of PiGSTd1 with different CDNB concentrations and a fixed GSH concentration. **(C)** Optimal pH of PiGSTd1 assayed using 100 mM acetate-phosphate buffer at varying pH. **(D)** The catalytic activity of PiGSTd1 was determined by preincubating enzyme solution at different temperatures.

2017), but fewer than the number in other insects, for example, *S. littoralis* (33 genes) (Legeai et al., 2011) and *D. melanogaster* (31 genes) (Younus et al., 2014) (**Supplementary Table 3**). This massive expansion of GSTs in insects is possibly for meeting the requirements of metabolizing odorant molecules and resisting the damages of insecticides and/or plant secondary compounds (Durand et al., 2018). Based on sequence analysis, these 17 PiGSTs were classed into eight subcategories: three delta, two epsilon, four omega, two sigma, one theta, one zeta, three microsomal, and one unclassified (**Figure 1**).

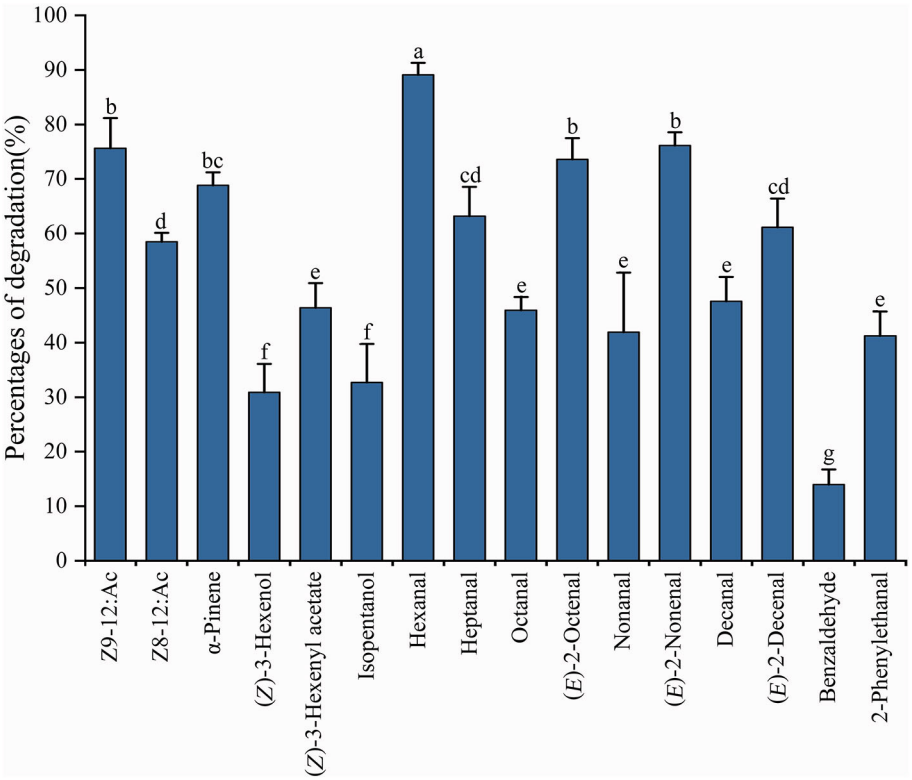

FIGURE 6 | Degradation percentages against various substrates using recombinant PiGSTd1. Columns with different lowercase letters indicate significant differences at the 0.05 level by Tukey's HSD multiple range test.

Insect GSTs play various roles in degrading endogenous and exogenous compounds (Huang et al., 2017; Song et al., 2020). GSTs that metabolize specific substrates are usually expressed specifically in corresponding organs or tissues. For example, GSTs that function as pesticide-degrading enzymes are usually distributed in the insect digestive system, especially the midgut (Xu et al., 2015; Yang et al., 2020). Consequently, odorant-degrading GSTs are presumably antennae-specific. Tissue expression analysis indicated that the majority of PiGSTs genes were highly expressed in the abdomen of both female and male *P. interpunctella* with one exception that PiGSTd1 from a delta subclass showed significant antennae specificity (**Figure 3**). Multiple alignments of amino acid sequences revealed that PiGSTd1 contains conserved residues across antennae-specific GSTs with moths (**Supplementary Figure 3**). PiGSTd1 shares 65.31% identity with GST-msolf1 from *M. sexta*, which is involved in the degradation of aldehyde odorants (Rogers et al., 1999). Our degradation assays also verified that PiGSTd1 is a putative aldehyde scavenger in the odorant recognition pathway. PiGSTd1 showed low similarity (40.16%) to GmolGSTd1 (**Supplementary Figure 3**), which could efficiently degrade sex pheromone component (*Z*)-8-dodecenyl alcohol in antennae of *Grapholita molesta* (75.01%) (Li et al., 2018), suggesting different functions between two GSTs. The results of degradation evaluations are essentially in line with the sequence alignment: PiGSTd1 showed higher degradation efficiency to aldehyde compounds but rather lower efficiency to (*Z*)-3-hexenol (**Figure 6**).

Both FPKM and qRT-PCR results showed that PiGSTd1 expression was significantly higher in male antennae than in female antennae (**Figures 2**, **3**), suggesting that PiGSTd1 is associated with recognizing sex pheromones produced and released from females (Kuwahara et al., 1971). The function of insect GSTds in degrading pheromone has been studied and verified in some moths. For instance, CpomGSTd2 is solely expressed in the antennae of *C. pomonella*, suggesting it is involved in odorant degradation (Huang et al., 2017). Our degradation evaluation showed that purified PiGSTd1 degraded 75.63 ± 5.52% of Z9-12:Ac, the sex pheromone component, in 1-h incubation. However, PiGSTd1 displayed lower degradation activities to Z8-12:Ac (58.47 ± 1.64%), a sex pheromone analog with a differently positioned double bond (**Figure 6**).

Besides degrading sex pheromones, insect delta GSTs also play roles in degrading host volatiles and environmental odorants (Li et al., 2018; Wang et al., 2021a,b). To evaluate the degradation activity of PiGSTd1 to host volatiles, we selected various volatiles from wheat flour or grains as substrates, including alkanals, 2*E*-alkenals, isopentanol, and phenylacetaldehyde (Uechi et al., 2007; Buda et al., 2016), as well as their analogs. Among all tested volatiles, recombinant PiGSTd1 showed best degradation activities to hexanal (89.10 ± 2.21%), (*E*)-2-octenal (73.58 ± 3.92%), and (*E*)-2-nonenal (75.81 ± 1.90%), which could

attract *P. interpunctella* (Uechi et al., 2007; Buda et al., 2016). Unexpectedly, PiGSTd1 showed lower efficiency in degrading common green leaf volatile (*Z*-3-hexenol) and flower fragrance (phenylacetaldehyde), with degradation rates of 30.91 ± 5.17% and 13.97 ± 2.76%, respectively. Presumably, *P. interpunctella* infests processed foods and inhabits indoor areas, resulting in low degradation against green leaf volatiles and flower fragrances. However, how PiGSTd1 affects the olfactory recognition of *P. interpunctella* remains to be investigated *in vivo*.

In conclusion, we identified 17 PiGSTs based on antennal transcriptomic analysis of *P. interpunctella*, analyzed their phylogenetic relationships with GSTs from other moths, and investigated their tissue expression patterns. Furthermore, we cloned and purified the antennae-enriched PiGSTd1 and evaluated its enzymatic properties. The recombinant PiGSTd1 displayed GST activity to CDNB and high degradation efficiency toward pheromones and host volatiles. Thus, our results indicate that PiGSTd1 functions as an odorant degradation enzyme to ensure the sensitivity of the odorant detection system.

DATA AVAILABILITY STATEMENT

The datasets presented in this study can be found in online repositories. The names of the repository/repositories and accession number(s) can be found in the article/**Supplementary Material**.

AUTHOR CONTRIBUTIONS

The research was designed by JY and CL. The experiments were performed by HL, YT and HS. Data were analyzed by YT and QW. HL and YT wrote the manuscript. All authors have read and agreed to the published version of the manuscript.

FUNDING

This work was supported by the Key Discipline Construction Project of Xinyang Agriculture and Forestry University [Grant Number ZDXK201701] and Research and Practice Projects of Higher Education Teaching Reform in Henan Province [Grant Number 2017SJGLX135].

SUPPLEMENTARY MATERIAL

The Supplementary Material for this article can be found online at: https://www.frontiersin.org/articles/10.3389/fphys.2021.727619/full#supplementary-material

REFERENCES

Babicki, S., Arndt, D., Marcu, A., Liang, Y. J., Grant, J. R., Maciejewski, A., et al. (2016). Heatmapper: web-enabled heat mapping for all. *Nucleic Acids Res.* 44, 147–153. doi: 10.1093/nar/gkw419

Bailey, T. L., Boden, M., Buske, F. A., Frith, M., Grant, C. E., Clementi, L., et al. (2009). MEME SUITE: tools for motif discovery and searching. *Nucleic Acids Res.* 37. 202–208. doi: 10.1093/nar/gkp335

Balakrishnan, B., Su, S., Wang, K., Tian, R. Z., and Chen, M. H. (2018). Identification, expression, and regulation of an omega class glutathione S-transferase in *Rhopalosiphum padi* (L.)(Hemiptera: Aphididae) under insecticide stress. *Front. Physiol.* 9:427. doi: 10.3389/fphys.2018.00427

Buda, V., Apšegaite, V., BlaŽyte-Cereškiene, L., Butkiene, R., Nedveckyte, I., and Pečiulyte, D. (2016). Response of moth *Plodia interpunctella* to volatiles of fungus-infected and uninfected wheat grain. *J. Stored Prod. Res.* 69, 152–158. doi: 10.1016/j.jspr.2016.08.001

Campos, M., and Phillips, T. W. (2014). Attract-and-kill and other pheromone-based methods to suppress populations of the Indianmeal moth (Lepidoptera: Pyralidae). *J. Econ. Entomol.* 107, 473–480. doi: 10.1603/EC13451

DeLano, W. L. (2002). *The PyMOL Molecular Graphic System*. Available online at: https://pymol.org/2/ (accessed July 1, 2021)

Ding, Y. C., Ortelli, F., Rossiter, L. C., Hemingway, J., and Ranson, H. (2003). The *Anopheles gambiae* glutathione transferase supergene family: annotation, phylogeny and expression profiles. *BMC Genomics* 4, 1–16. doi: 10.1186/1471-2164-4-35

Durand, N., Pottier, M. A., Siaussat, D., Bozzolan, F., Maïbèche, M., and Chertemps, T. (2018). Glutathione-S-transferases in the olfactory organ of the Noctuid moth *Spodoptera littoralis*, diversity and conservation of chemosensory clades. *Front. Physiol.* 9:1283. doi: 10.3389/fphys.2018.01283

Enayati, A. A., Ranson, H., and Hemingway, J. (2005). Insect glutathione transferases and insecticide resistance. *Insect Mol. Biol.* 14, 3–8. doi: 10.1111/j.1365-2583.2004.00529.x

Francis, F., Haubruge, E., Gaspar, C., and Dierickx, P. J. (2001). Glutathione S-transferases of *Aulacorthum solani* and *Acyrthosiphon pisum*: partial purification and characterization. *Comp. Biochem. Physiol. B, Biochem. Mol. Biol.* 129, 165–171. doi: 10.1016/S1096-4959(01)00329-3

Gasteiger, E., Hoogland, C., Gattiker, A., Duvaud, S', Wilkins, M. R., Appel, R. D., et al. (2005). "Protein identification and analysis tools in the ExPASy server," in *The Proteomics Protocols Handbook*, ed J. M. Walker (Totowa, NJ: Humana Press), 571–607. doi: 10.1385/1-59259-890-0:571

Glaser, N., Gallot, A., Legeai, F., Montagné, N., Poivet, E., Harry, M., et al. (2013). Candidate chemosensory genes in the stemborer *Sesamia nonagrioides*. *Int. J. Biol. Sci.* 9, 481–495. doi: 10.7150/ijbs.6109

Guex, N., Peitsch, M. C., and Schwede, T. (2009). Automated comparative protein structure modeling with SWISS-MODEL and Swiss-PdbViewer: a historical perspective. *Electrophoresis*. 30, S162–S173. doi: 10.1002/elps.200900140

Hayes, J. D., Flanagan, J. U., and Jowsey, I. R. (2015). Glutathione transferases. *Annu. Rev. Pharmacol. Toxicol.* 45, 51–88. doi: 10.1146/annurev.pharmtox.45.120403.095857

Huang, X. L., Fan, D. S., Liu, L., and Feng, J. N. (2017). Identification and characterization of glutathione S-transferase genes in the antennae of codling moth (Lepidoptera: Tortricidae). *Ann. Entomol. Soc. Am.* 110, 409–416. doi: 10.1093/aesa/sax041

Jia, X. J., Zhang, X. F., Liu, H. M., Wang, R. Y., and Zhang, T. (2018). Identification of chemosensory genes from the antennal transcriptome of Indian meal moth *Plodia interpunctella*. *PLos ONE* 13:e0189889. doi: 10.1371/journal.pone.0189889

Kuwahara, Y., Kitamura, C., Takashi, S., Hara, H., Ishii, S., and Fukami, H. (1971). Sex pheromone of the almond moth and the Indian meal moth: *cis*-9, *trans*-12-tetradecadienyl acetate. *Science* 171, 801–802. doi: 10.1126/science.171.3973.801

Labade, C. P., Jadhav, A. R., Ahire, M., S., Zinjarde, S., and, A., et al. (2018). Role of induced glutathione-S-transferase from *Helicoverpa armigera* (Lepidoptera: Noctuidae) HaGST-8 in detoxification of pesticides. *Ecotoxicol. Environ. Saf.* 147, 612–621. doi: 10.1016/j.ecoenv.2017.09.028

Legeai, F., Malpel, S., Montagne, N., Monsempes, C., Cousserans, F., Merlin, C., et al. (2011). An expressed sequence Tag collection from the male antennae of

the Noctuid moth *Spodoptera littoralis*: a resource for olfactory and pheromone detection research. *BMC Genomics* 12:86. doi: 10.1186/1471-2164-12-86

Li, G. W., Chen, X. L., Xu, X. L., and Wu, J. X. (2018). Degradation of sex pheromone and plant volatile components by an antennal glutathione S-transferase in the oriental fruit moth, *Grapholita molesta Busck* (Lepidoptera: Tortricidae). *Arch. Insect Biochem. Physiol.* 99:e21512. doi: 10.1002/arch.21512

Liu, H. M., Lei, X. P., Du, L. X., Yin, J., Shi, H. Z., Zhang, T., et al. (2019). Antennae-specific carboxylesterase genes from Indian meal moth: identification, tissue distribution and the response to semiochemicals. *J. Stored Prod. Res.* 84:101528. doi: 10.1016/j.jspr.2019.101528

Liu, S., Gong, Z. J., Rao, X. J., Li, M. Y., and Li, S. G. (2015). Identification of putative carboxylesterase and glutathione S-transferase Genes from the antennae of the *Chilo suppressalis* (Lepidoptera: Pyralidae). *J. Insect Sci.* 15:103. doi: 10.1093/jisesa/iev082

Liu, S., Zhang, Y. X., Wang, W. L., Zhang, B. X., and Li, S. G. (2017). Identification and characterisation of seventeen glutathione S-transferase genes from the cabbage white butterfly *Pieris rapae*. *Pestic. Biochem. Physiol.* 143, 102–110. doi: 10.1016/j.pestbp.2017.09.001

Livak, K. J., and Schmittgen, T. D. (2001). Analysis of relative gene expression data using real-time quantitative PCR and the $2_{\mathrm{T}}^{-\Delta\Delta\mathrm{C}}$ Method. *Methods* 25, 402–408. doi: 10.1006/meth.2001.1262

McGuffin, L. J., Bryson, K., and Jones, D. T. (2000). The PSIPRED protein structure prediction server. *Bioinformatics* 16, 404–405. doi: 10.1093/bioinformatics/16.4.404

Mistry, J., Chuguransky, S., Williams, L., Qureshi, M., Salazar, G. A., Sonnhammer, E. L. L., et al. (2021). Pfam: the protein families database in 2021. *Nucleic Acids Res.* 49, D412–D419. doi: 10.1093/nar/gkaa913

Mohandass, S., Arthur, F. H., Zhu, K. Y., and Throne, J. E. (2007). Biology and management of *Plodia interpunctella* (Lepidoptera: Pyralidae) in stored products. *J. Stored Prod. Res.* 43, 302–311. doi: 10.1016/j.jspr.2006.08.002

Rogers, M. E., Jani, M. K., and Vogt, R. G. (1999). An olfactory-specific glutathione-S-transferase in the sphinx moth *Manduca sexta*. *J. Exp. Biol.* 202, 1625–1637. doi: 10.1242/jeb.202.12.1625

Sheehan, D., Meade, G., Foley, V. M., and Dowd, C. A. (2001). Structure, function and evolution of glutathione transferases: implications for classification of non-mammalian members of an ancient enzyme superfamily. *Biochem. J.* 360, 1–16. doi: 10.1042/bj3600001

Shi, H. X., Pei, L. H., Gu, S. S., Zhu, S. C., Wang, Y. Y., Zhang, Y., et al. (2012). Glutathione S-transferase (GST) genes in the red flour beetle, *Tribolium castaneum*, and comparative analysis with five additional insects. *Genomics* 100, 327–335. doi: 10.1016/j.ygeno.2012.07.010

Singh, S. P., Coronella, J. A., Beneš, H., Cochrane, B. J., and Zimniak, P. (2001). Catalytic function of *Drosophila melanogaster* glutathione S-transferase DmGSTS1-1 (GST-2) in conjugation of lipid peroxidation end products. *Eur. J. Biochem.* 268, 2912–2923. doi: 10.1046/j.1432-1327.2001.02179.x

Song, X., Pei, L., Zhang, Y., Chen, X., Zhong, Q., Ji, Y., et al. (2020). Functional diversification of three delta–class glutathione S–transferases involved in development and detoxification in *Tribolium castaneum*. *Insect Mol. Biol.* 29, 320–336. doi: 10.1111/imb.12637

Studer, G., Rempfer, C., Waterhouse, A. M., Gumienny, R., Haas, J., and Schwede, T. (2020). QMEANDisCo - distance constraints applied on model quality estimation. *Bioinformatics* 36, 1765–1771. doi: 10.1093/bioinformatics/btz828

Sun, X. Q., Zhang, M. X., Yu, J. Y., Jin, Y., Ling, B., Du, J. P., et al. (2013). Glutathione S-transferase of brown planthoppers (*Nilaparvata lugens*) is essential for their adaptation to gramine-containing host plants. *PLoS ONE* 8:e64026. doi: 10.1371/journal.pone.0064026

Tamura, K., Peterson, D., Peterson, N., Stecher, G., Nei, M., and Kumar, S. (2011). MEGA5: molecular evolutionary genetics analysis using maximum likelihood, evolutionary distance, and maximum parsimony methods. *Mol. Biol. Evol.* 28, 2731–2739. doi: 10.1093/molbev/msr121

Tan, X., Hu, X. M., Zhong, X. W., Chen, Q. M., Xia, Q. Y., and Zhao, P. (2014). Antenna-specific glutathione S-transferase in male silkmoth *Bombyx mori*. *Int. J. Mol. Sci.* 15, 7429–7443. doi: 10.3390/ijms15057429

Uechi, K., Matsuyama, S., and Suzuki, T. (2007). Oviposition attractants for *Plodia interpunctella* (Hübner)(Lepidoptera: Pyralidae) in the volatiles of whole wheat flour. *J. Stored Prod. Res.* 43, 193–201. doi: 10.1016/j.jspr.2006.05.002

Vogt, R. G., and Riddiford, L. M. (1981). Pheromone binding and inactivation by moth antennae. *Nature* 293, 161–163. doi: 10.1038/293161a0

Wang, M. M., He, M., Wang, H., Ma, Y. F., Dewer, Y., Zhang, F., et al. (2021b). A candidate aldehyde oxidase in the antennae of the diamondback moth, *Plutella xylostella* (L.), is potentially involved in the degradation of pheromones, plant-derived volatiles and the detoxification of xenobiotics. *Pestic. Biochem. Physiol.* 171:104726. doi: 10.1016/j.pestbp.2020.104726

Wang, M. M., Long, G. J., Guo, H., Liu, X. Z., Wang, H., Dewer, Y., et al. (2021a). Two carboxylesterase genes in *Plutella xylostella* associated with sex pheromones and plant volatiles degradation. *Pest Manage. Sci.* 77, 2737–2746. doi: 10.1002/ps.6302

Xu, Z. B., Zou, X. P., Zhang, N., Feng, Q. L., and Zheng, S. C. (2015). Detoxification of insecticides, allechemicals and heavy metals by glutathione S-transferase SlGSTE1 in the gut of *Spodoptera litura*. *Insect Sci.* 22, 503–511. doi: 10.1111/1744-7917.12142

Yang, B. J., Lin, X. M., Yu, N., Gao, H. L., Zhang, Y. X., Liu, W., et al. (2020). Contribution of glutathione S-transferases to imidacloprid resistance in *Nilaparvata lugens*. *J. Agric. Food Chem.* 30, 15403–15408. doi: 10.1021/acs.jafc.0c05763

You, Y. C., Xie, M., Ren, N. N., Cheng, X. M., Li, J. Y., Ma, X. L., et al. (2015). Characterization and expression profiling of glutathione S-transferases in the diamondback moth, *Plutella xylostella* (L.). *BMC Genomics* 16:152. doi: 10.1186/s12864-015-1343-5

Younus, F., Chertemps, T., Pearce, S. L., Pandey, G., Bozzolan, F., W., et al. (2014). Identification of candidate odorant degrading gene/enzyme systems in the antennal transcriptome of *Drosophila melanogaster*. *Insect Biochem. Mol. Biol.* 53, 30–43. doi: 10.1016/j.ibmb.2014.07.003

Yu, Q. Y., Lu, C., Li, B., Fang, S. M., Zuo, W. D., Dai, F. Y., et al. (2008). Identification, genomic organization and expression pattern of glutathione S-transferase in the silkworm, *Bombyx mori*. *Insect Biochem. Mol. Biol.* 38, 1158–1164. doi: 10.1016/j.ibmb.2008.08.002

Zou, X. P., Xu, Z. B., Zou, H. W., Liu, J. S., Chen, S. N., Feng, Q. L., et al. (2016). Glutathione S-transferase SlGSTE1 in *Spodoptera litura* may be associated with feeding adaptation of host plants. *Insect Biochem. Mol. Biol.* 70, 32–43. doi: 10.1016/j.ibmb.2015.10.005

Conflict of Interest: The authors declare that the research was conducted in the absence of any commercial or financial relationships that could be construed as a potential conflict of interest.

Publisher's Note: All claims expressed in this article are solely those of the authors and do not necessarily represent those of their affiliated organizations, or those of the publisher, the editors and the reviewers. Any product that may be evaluated in this article, or claim that may be made by its manufacturer, is not guaranteed or endorsed by the publisher.

frontiers in Physiology

ORIGINAL RESEARCH
published: 06 September 2021
doi: 10.3389/fphys.2021.721247

Expression Profiles and Functional Characterization of Chemosensory Protein 15 (HhalCSP15) in the Brown Marmorated Stink Bug *Halyomorpha halys*

*Zehua Wang[1], Fan Yang[1], Ang Sun[1], Shuang Shan[2], Yongjun Zhang[2] and Shanning Wang[1]**

[1]*Beijing Key Laboratory of Environment Friendly Management on Fruit Diseases and Pests in North China, Institute of Plant and Environment Protection, Beijing Academy of Agriculture and Forestry Sciences, Beijing, China,* [2]*State Key Laboratory for Biology of Plant Diseases and Insect Pests, Institute of Plant Protection, Chinese Academy of Agricultural Sciences, Beijing, China*

OPEN ACCESS

Edited by:
Jin Zhang,
Max Planck Institute for Chemical Ecology, Germany

Reviewed by:
Herbert Venthur,
University of La Frontera, Chile
Youssef Dewer,
Agricultural Research Center, Egypt

***Correspondence:**
Shanning Wang
wangshanning@yeah.net

Specialty section:
This article was submitted to Invertebrate Physiology, a section of the journal Frontiers in Physiology

Received: *06 June 2021*
Accepted: *10 August 2021*
Published: *06 September 2021*

Citation:
Wang Z, Yang F, Sun A, Shan S, Zhang Y and Wang S (2021) Expression Profiles and Functional Characterization of Chemosensory Protein 15 (HhalCSP15) in the Brown Marmorated Stink Bug Halyomorpha halys. Front. Physiol. 12:721247. doi: 10.3389/fphys.2021.721247

Chemosensory proteins (CSPs) have been identified in the sensory tissues of various insect species and are believed to be involved in chemical communication in insects. However, the physiological roles of CSPs in *Halyomorpha halys*, a highly invasive insect species, are rarely reported. Here, we focused on one of the antennal CSPs (*HhalCSP15*) and determined whether it was involved in olfactory perception. Reverse transcription PCR (RT-PCR) and quantitative real-time PCR (qRT-PCR) analysis showed that *HhalCSP15* was enriched in nymph and male and female adult antennae, indicating its possible involvement in the chemosensory process. Fluorescence competitive binding assays revealed that three of 43 natural compounds showed binding abilities with HhalCSP15, including β-ionone ($K_i = 11.9 \pm 0.6\,\mu M$), *cis*-3-hexen-1-yl benzoate ($K_i = 10.5 \pm 0.4\,\mu M$), and methyl (2*E*,4*E*,6*Z*)-decatrienoate (*EEZ*-MDT; $K_i = 9.6 \pm 0.8\,\mu M$). Docking analysis supported the experimental affinity for the three ligands. Additionally, the electrophysiological activities of the three ligands were further confirmed using electroantennography (EAG). *EEZ*-MDT is particularly interesting, as it serves as a kairomone when *H. halys* forages for host plants. We therefore conclude that HhalCSP15 might be involved in the detection of host-related volatiles. Our data provide a basis for further investigation of the physiological roles of CSPs in *H. halys*, and extend the olfactory function of CSPs in stink bugs.

Keywords: *Halyomorpha halys*, chemosensory protein, expression profile, fluorescence binding assay, molecular docking, electroantennography

INTRODUCTION

Many insects rely on their sense of smell to locate food sources, search for mating partners, select oviposition sites, and avoid predators (Metcalf and Kogan, 1987; Takken, 1991; Bruce et al., 2005; Ebrahim et al., 2015). The detection of olfactory signals in insects is performed by olfactory receptor neurons located in olfactory sensilla, which are present on the antennae

and other head appendices. Olfactory sensilla are perforated by numerous pores, forming a hollow structure filled with aqueous lymph that harbors the dendritic branches of olfactory receptor neurons and contains abundant small soluble binding proteins (Maida et al., 1993; Steinbrecht, 1997). In the initial stage of olfactory reception, odorants enter the olfactory sensillum cavity through pore canals, and are transported by soluble binding proteins to the olfactory receptor on dendrite membranes (Vogt and Riddiford, 1981; Kaissling, 2009; Leal, 2013).

Odorant binding proteins (OBPs) and chemosensory proteins (CSPs) are the two main types of soluble binding proteins. A large body of evidence from different approaches has extensively documented that OBPs bind to pheromones and odorants, with different degrees of affinity and selectivity for different OBPs (Pelosi et al., 2014; Zhang et al., 2017; Huang et al., 2018; Wang et al., 2020; Rihani et al., 2021). In several instances, it was demonstrated that OBPs are involved not just in detecting olfactory stimuli, but also in modulating stimulus sensitivity in the olfactory system (Xu et al., 2005; Larter et al., 2016; Gonzalez et al., 2020). CSPs may perform functions similar to OBPs in the olfactory system.

Insect CSPs are known as olfactory segment D (OS-D) or A-10 before being named as CSPs because of their high expression in chemosensory organs (McKenna et al., 1994; Pikielny et al., 1994; Angeli et al., 1999). CSPs are smaller than OBPs (100–120 residues) and bear no sequence similarity to OBPs. They present a motif of four conserved cysteines linked by disulfide bridges (Angeli et al., 1999). The three-dimensional (3D) structure of CSP protein is composed of six α-helices that define a hydrophobic cavity (Lartigue et al., 2002). As an olfactory protein, CSPs have been studied in Lepidoptera, Hemiptera, Hymenoptera, and Coleoptera (Gu et al., 2012; Sun et al., 2014; Peng et al., 2017; Fu et al., 2020). CSPs in the alfalfa plant bug *Adelphocoris lineolatus* have been implicated in mediating host recognition (Gu et al., 2012; Sun et al., 2015). However, numerous studies have shown that the expression of CSPs is not restricted to the antennae, and many CSP genes are expressed in other parts of the insect body, with functions different from olfaction. In non-olfactory tissues, they are believed to be involved in development, pheromone delivery, nutrient absorption, insecticide resistance, vision, and immune response (Nomura et al., 1992; Forêt et al., 2007; Maleszka et al., 2007; Bos et al., 2010; Xuan et al., 2015; Pelosi et al., 2017).

The brown marmorated stink bug *Halyomorpha halys* (Stål; Hemiptera: Pentatomidae), which is native to Asia, is an invasive pest that in the last few decades has rapidly spread globally, including in the United States, Canada, and Europe (Hoebeke and Carter, 2003; Wermelinger et al., 2008; Leskey and Nielsen, 2017). In its native and introduced range, *H. halys* feeds on more than 100 crops, and it has become a destructive pest of many crops in the world (Lee et al., 2013; Haye et al., 2015; Kriticos et al., 2017; Leskey and Nielsen, 2017). Being an important invasive pest worldwide, there are many studies examining the chemical ecology of *H. halys* (Khrimian et al., 2014; Harris et al., 2015; Leskey et al., 2015; Weber et al., 2017). In *H. halys*, antennal transcriptomic approaches have already led to the identification of 17 CSP genes (Sun et al., 2020), which now await functional characterization.

In this study, to examine the potential role of one antennal CSP (*HhalCSP15*) in olfaction perception, extensive expression profiling of *HhalCSP15* transcripts was performed using semi-quantitative reverse transcription PCR (RT-PCR) and quantitative real-time PCR (qRT-PCR) methods among different tissues in nymph and male and female adult stages. We further expressed HhalCSP15 *in vitro* and determined its binding affinities for 43 volatiles in fluorescence binding assays. Further, homology modeling and molecular docking were applied for predicting the key amino acids of HhalCSP15 that bind candidate ligands. In addition, electrophysiological activities of HhalCSP15 ligands were confirmed using electroantennography (EAG) recordings.

MATERIALS AND METHODS

Insect Culture, Tissue Collection, Total RNA Isolation, and cDNA Synthesis

Overwintering *H. halys* adults were collected from Beijing Xishan National Forest Park, Beijing, China. The laboratory colony was established in plastic containers (20 cm × 13 cm × 8 cm), which were maintained at 25 ± 1°C, 60 ± 10% relative humidity, and a 16L:8D photoperiod. The adults and nymphs were reared on green beans. Different tissues from third instar nymphs (antennae, mouthparts, heads, thoraxes, abdomens, and legs) and 1- to 3-day-old female and male adults (antennae, mouthparts, heads, thoraxes, abdomens, legs, and wings) were collected. All tissues were immediately frozen in liquid nitrogen and stored at −80°C until RNA isolation.

Total RNA was extracted from different tissues using TRIzol reagent (Invitrogen, Carlsbad, CA, United States) following the manufacturer's protocol. The integrity and quantity of RNA samples were checked using 1.2% agarose gel electrophoresis and a NanoPhotometer N60 (Implen, München, Germany), respectively. cDNA from different tissues was synthesized from 2 μg of RNA using the Fast Quant RT kit with gDNase (Tiangen, Beijing, China) for gene cloning and tissue expression pattern analyses.

Verification of the *HhalCSP15* Sequence by Cloning and Sequencing

Gene-specific primers were designed to clone the open reading frame (ORF) of *HhalCSP15*. PCR was performed using one unit of KOD DNA polymerase (Taihe, Beijing, China) and 200 ng cDNA under the following conditions: denaturation at 94°C for 2 min, followed by 30 cycles of denaturation at 94°C for 20 s, annealing at 55°C for 30 s, and extension at 68°C for 1 min. The final extension step was at 68°C for 5 min. The PCR products were cloned into a pCloneEZ-Blunt vector (Taihe, Beijing, China), and cloned products were sequenced using the M13 primer.

Reverse Transcription PCR

The expression of *HhalCSP15* in different tissues of nymphs and male and female adults was analyzed by RT-PCR using Taq DNA polymerase (Biomed, Beijing, China). Each PCR

volume (25 µl) contained 200 ng of cDNA from different tissues and was used as a template. The following cycling conditions were applied: 94°C for 4 min, and for the subsequent 30 cycles: 94°C for 30 s, 55°C for 30 s, and 72°C for 45 s. The final extension step was at 72°C for 5 min. The elongation factor 1-α (EF-1α, XM_014414739.2) was employed to assess the cDNA integrity for all samples. The amplification products were checked on 1.2% agarose gels. For each gene, one amplification product was sequenced to confirm its identity. The gene-specific primers were designed using Primer 3[1] and are listed in **Supplementary Table S1**.

Quantitative Real-Time PCR

The relative transcript abundance of *HhalCSP15* in the antennae, mouthparts, and legs of nymphs and male and female adults was determined by qRT-PCR. qRT-PCR was conducted using an ABI Prism 7500 System (Applied Biosystems, Carlsbad, CA, United States) and SYBR Green SuperReal PreMix Plus (TianGen, Beijing, China). Each qRT-PCR reaction was conducted in a 20 µl reaction mixture containing 10 µl of 2× SuperReal PreMix Plus, 1 µl (200 ng) of sample cDNA, 0.4 µl of 50× ROX Reference Dye, and 6.1 µl of sterilized ultrapure water. Each qRT-PCR experiment was performed using three biological replicates, and each biological replicate was assessed three times. The ubiquitin conjugation factor E4 A (Ubiquitin, XM_014429239.2) and EF-1α were used as endogenous controls to normalize the target gene expression and correct for any sample-to-sample variation.

The comparative $2^{-\Delta\Delta CT}$ method (Livak and Schmittgen, 2001) was used to calculate the relative transcript levels in each tissue. The primers of the target and reference genes are listed in **Supplementary Table S1**. The specificity of each primer set was validated by melting curve analysis, and the efficiency was calculated by analyzing the standard curves with a 5-fold cDNA dilution series. The comparative analyses of *HhalCSP15* expression among different tissues and developmental stages were conducted with one-way ANOVA, followed by Tukey's honestly significant difference (HSD) test using SPSS Statistics 18.0 (SPSS Inc., Chicago, IL, United States).

Expression and Purification of Recombinant HhalCSP15

HhalCSP15 was PCR-amplified using gene-specific primers (**Supplementary Table S1**). The PCR products were first subcloned into a T vector (Taihe, Beijing, China) and then into the bacterial expression vector pET30a (+; Novagen, Madison, WI, United States) between the NdeI and XhoI sites, and were verified by sequencing. The plasmids containing the correct insert were transformed into BL21 (DE3) competent cells. The protein was expressed in LB at 18°C for 16 h through induction with 1 mM of isopropyl-β-D-thiogalactopyranoside (IPTG). The cultures were harvested by centrifugation and resuspended in a 50 mM Tris buffer (pH 7.4). After sonication and centrifugation, the recombinant proteins, which were mainly present in the supernatant, were purified by a standard Ni column (GE Healthcare, Waukesha, WI, United States). The His-tag was removed using a recombinant enterokinase (Novagen) following the manufacturer's protocol. Purified HhalCSP15 was dialyzed in the Tris buffer, and its concentration was determined by the Bradford method (Bradford, 1976).

Fluorescence Competitive Binding Assays

The binding abilities of HhalCSP15 to 43 volatiles were measured on an F-380 fluorescence spectrophotometer (Tianjin, China) using 10-nm slits and a 1-cm light path. As the fluorescent probe, N-phenyl-1-naphthylamine (1-NPN) was excited at the wavelength of 337 nm, and emission spectra were recorded between 390 and 530 nm. To measure the affinity of 1-NPN to the HhalCSP15 protein, a 2-µM solution of purified protein in 50-mM Tris-HCl at pH 7.4 was titrated with aliquots of 1-mM 1-NPN dissolved in methanol to final concentrations ranging from 2 to 16 µM.

Competitive binding was measured by titration of the solution of both HhalCSP15 protein and 1-NPN at a concentration of 2 µM by adding aliquots of 1-mM methanol solution of ligand to final concentrations of 2–20 µM. Dissociation constants of the competitors were calculated by the equation $K_i = IC_{50}/(1 + [1\text{-NPN}]/K_{1\text{-NPN}})$, where IC_{50} is the concentration of ligands halving the initial fluorescence value of 1-NPN, [1-NPN] is the free concentration of 1-NPN, and $K_{1\text{-NPN}}$ is the dissociation constant of the HhalCSP15/1-NPN complex. The experiments were performed in triplicate, excepting the ligands that did not show significant binding, which were analyzed in single experiments.

3D Structure Modeling and Molecular Docking

A suitable template for 3D modeling was identified using a sequence of similar searches at PSI-BLAST against sequences from the Protein Data Bank.[2] Because of high sequence similarity with the HhalCSP15 protein, the high-resolution structure of a CSP from *Mamestra brassicae* (PDB: 1N8V) was selected for homology modeling using MODELLER 9.25.[3] The structure refinement of the protein model was achieved by energy minimization *via* molecular dynamic simulation (MD) using GROMACSv5.0.7 with AMBER99SB force field (Abraham et al., 2015). A Ramachandran plot was performed to evaluate the rationality of the established 3D model using the online tool PROCHECK.[4] The ligands were 3D optimized in ChemDraw 3D (PerkinElmer, Waltham, MA, United States) and refined with energy minimization. Ligands were docked to the model of HhalCSP15 using Autodock Vina.[5] The best binding modes were selected according to the lowest free binding energy (kcal mol^{-1}). The docked models of proteins interacting with ligands were displayed using PYMOL.[6]

[1]http://primer3.ut.ee/

[2]https://www.rcsb.org/

[3]https://salilab.org/modeller/9.25/release.html

[4]https://saves.mbi.ucla.edu/

[5]http://vina.scripps.edu/

[6]https://pymol.org/2/

Electrophysiological Recordings

The antennal responses of *H. halys* to the three ligands of HhalCSP15 were evaluated using conventional EAG methods as described in previous study (Wang et al., 2020). Briefly, antennae of the third instar nymphs and 1- to 3-day old male and female adults were dissected, and a few terminal segments at the distal end were excised. The treated antennae were attached to electrode holders with electrode gel. Ten microliters of tested chemicals (100 μg/μl, diluted in paraffin oil) were applied to filter paper strips (1.0 cm × 2.0 cm) and inserted into a glass Pasteur pipette as a cartridge. The test cartridge was connected to a stimulus controller (CS-55; Syntech, Kirchzarten, Germany) that generated a 0.5 s stimulus at 30 s intervals, with a constant flow of 10 ml/s. The signals generated by the antennae were recorded using EAG Pro (Syntech). A blank stimulus (solvent control) was presented before testing the compound. For each compound, EAG responses were recorded from eight antennae of different insects. The EAG responses elicited by the test odor stimuli were corrected by subtracting EAG response from the solvent control. The corrected EAG data were statistically analyzed using ANOVA followed by Tukey's HSD test.

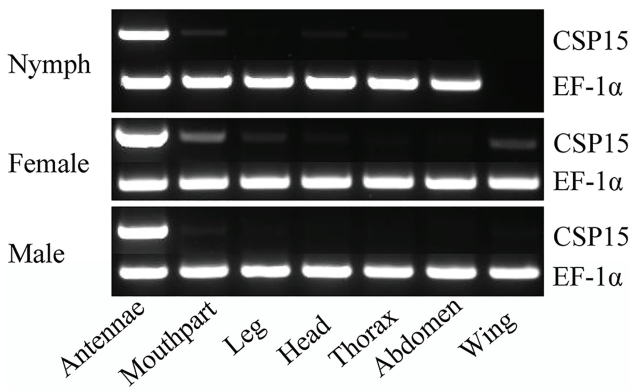

FIGURE 1 | Tissue-specific expression of *HhalCSP15* in different stages (nymph and male and female adult) measured by reverse transcription PCR (RT-PCR). Elongation factor 1-α (EF-1α) was used as a control gene.

RESULTS

Sequence Analysis of *HhalCSP15*

The nucleotide sequence of *HhalCSP15* was verified by molecular cloning and sequencing. Analysis of the *HhalCSP15* sequence revealed full-length ORFs consisting of 366 nucleotides that encode 121 amino acid residues. At its *N*-terminus, HhalCSP15 is predicted to contain a signal peptide consisting of 19 amino acid residues (**Supplementary Figure S1**). The predicted molecular weight of HhalCSP15 protein was 11.91 kDa, and the isoelectric point was 7.76. HhalCSP15 had the typical four-cysteine signature and fit the motif pattern of C1-X6-8-C2-X16-21-C3-X2-C4 of insect CSPs (Zhou et al., 2006).

Expression Profiles of *HhalCSP15*

We used RT-PCR to analyze the tissue-specific expression of the *HhalCSP15* transcript in different nymph and adult tissues. The EF-1α gene was constitutively expressed in all tissues, thereby providing a stable control for the integrity of the cDNA templates (**Figure 1**). *HhalCSP15* was detected specifically in the antennae of nymph and male and female adult, although minor bands were detected in other tissues, such as mouthpart and leg (**Figure 1**).

Quantitative real-time PCR was used to measure the *HhalCSP15* transcript levels in different tissues. The *HhalCSP15* transcript was expressed significantly higher in the antennae than in other tissues; it was approximately 1,803, 3,023, and 2,130 times higher

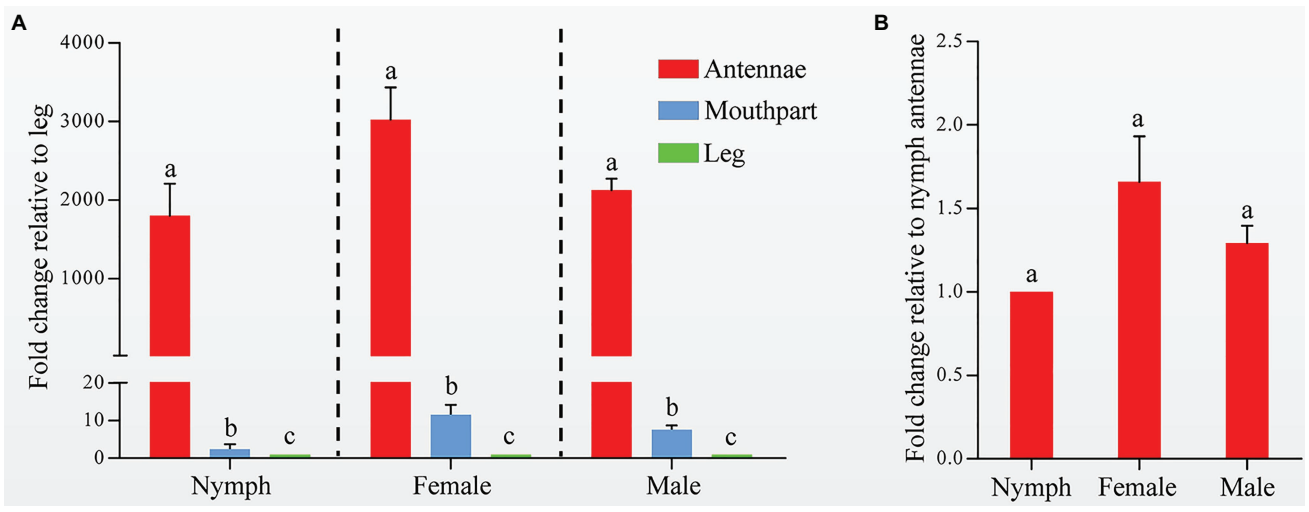

FIGURE 2 | (A) Expression profiles of the *HhalCSP15* gene in different tissues (antennae, mouthpart, and leg) measured by quantitative real-time PCR (qRT-PCR). The fold changes are relative to the transcript levels in the leg. **(B)** Relative transcript levels of the *HhalCSP15* gene in the antennae at different stages. The fold changes are relative to the transcript levels in the antennae of nymph. Reference genes: EF-1α and Ubiquitin. The error bar and different letters represent the SE and significant differences, respectively ($p < 0.05$).

in the antennae than in the leg of nymphs and female and male adults, respectively. The expression of the *HhalCSP15* gene was also detected in the mouthpart at 11.6-, 7.6-, and 2.4-fold higher than the leg of nymphs and female and male adults, respectively (**Figure 2A**). Furthermore, the expression levels were approximately 1.7- and 1.3-fold higher in the female and male adult antennae than in the nymph antennae (**Figure 2B**).

Binding Characteristic of Recombinant HhalCSP15

The specific expression of HhalCSP15 in the antennae of nymphs and adults suggests that HhalCSP15 is potentially involved in peripheral olfactory reception for *H. halys*. To screen the putative ligands for HhalCSP15, we first expressed HhalCSP15 in a bacterial system. The protein was purified by affinity chromatography on Ni columns and was then used for ligand-binding experiments. The size and purity of the recombinant protein were examined by SDS–PAGE (**Figure 3**).

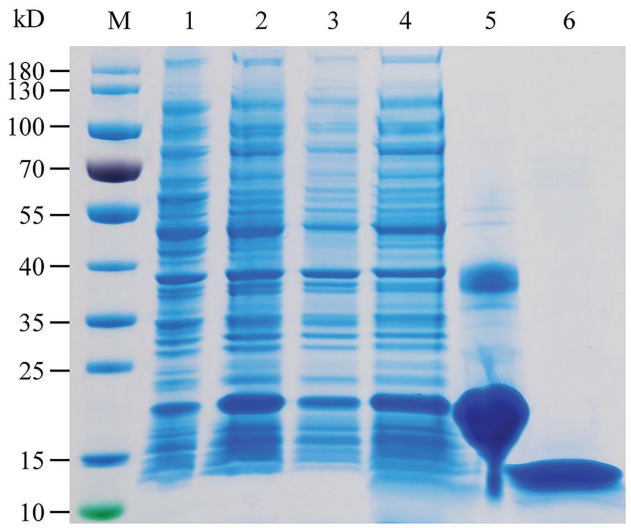

FIGURE 3 | SDS-PAGE analysis of the recombinant HhalCSP15. M: molecular weight markers, 1: cell pellet before induction with IPTG, 2: cell pellet after induction, 3: pellet after sonication, 4: supernatant after sonication, 5: protein purified by affinity chromatography, and 6: purified protein after digestion with enterokinase.

We measured the protein affinity to 43 volatile compounds in competitive binding experiments using 1-NPN as a fluorescent probe. First, the affinity constant was measured for HhalCSP15 to 1-NPN (**Figure 4A**). HhalCSP15 binds reversibly to 1-NPN with a dissociation constant of 9.36 μM, which indicates that 1-NPN is a suitable fluorescent reporter. HhalCSP15 displayed a relatively specific binding spectrum; of the 43 tested odorants, only three compounds showed binding affinities for HhalCSP15: β-ionone, *cis*-3-hexen-1-yl benzoate, and methyl (2*E*,4*E*,6*Z*)-decatrienoate (*EEZ*-MDT), which had binding affinities of 11.9 ± 0.6, 10.5 ± 0.4, and 9.6 ± 0.8 μM, respectively (**Figure 4B**; **Table 1**).

Protein Structure Prediction and Molecular Docking

To support the results of our ligand binding assay and provide insight into the mechanism of HhalCSP15 interaction with ligands, molecular docking of the three ligands with HhalCSP15 was performed. The best model for HhalCSP15 (**Supplementary Figure S2**) was obtained using the crystal structure of the CSP from *M. brassicae* (PDB: 1N8V, 42% identity) as a template. The protein model was subjected to a 50 ns MD simulation to energy minimize and stabilize the protein. The structural stability of the protein was measured by evaluating root mean square deviation (RMSD) and root mean square fluctuation (RMSF; **Supplementary Figure S3**). A Ramachandran plot was employed to estimate the rationality of the predicted protein structure. It revealed that 93.5% of the residues were in the most favored allowed region, 6.5% of the residues were in the additional allowed region, and none were in the disallowed region (**Supplementary Figure S4**), suggesting that the predicted model of HhalCSP15 is reasonable and reliable.

The docking results showed that the ligands tightly bind to the HhalCSP15 pocket with negative energy values (**Table 2**). The 2D and 3D ligand interaction diagram is shown in **Figure 5**.

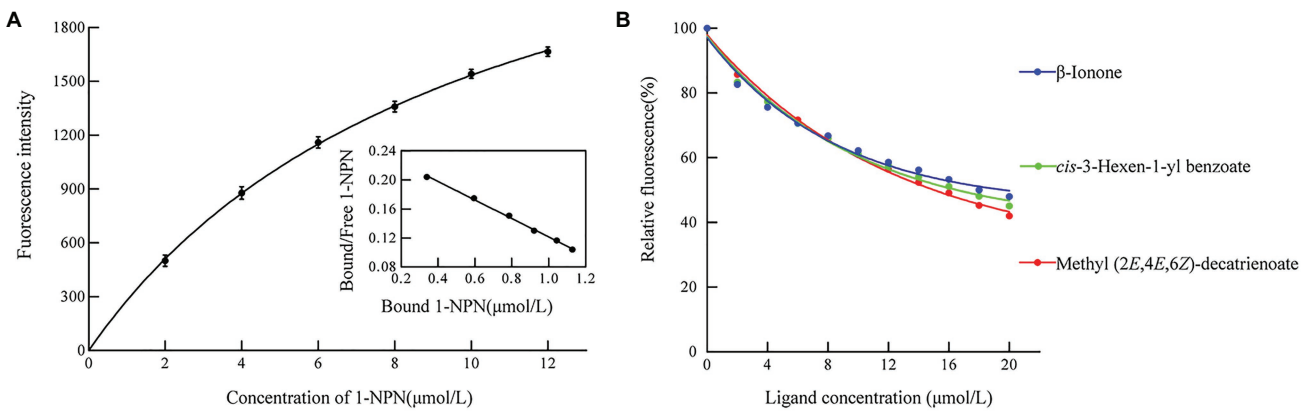

FIGURE 4 | Binding properties of recombinant HhalCSP15. **(A)** Binding curve and Scatchard plot of N-phenyl-1-naphthylamine (1-NPN) to HhalCSP15. **(B)** Binding curves of HhalCSP15 to candidate ligands.

TABLE 1 | Binding affinities of all tested ligands to HhalCSP15.

Ligands	Source	CAS number	Purity (%)	IC_{50} (μM)	K_i (μM)
1-Hexanol	TCI	111–27-3	>98.0	75.8	-
cis-3-Hexen-1-ol	TCI	928–96-1	>97.0	82.4	-
1-Octen-3-ol	TCI	3,391–86-4	>98.0	78.2	-
1-Octanol	TCI	111–87-5	>99.0	72.0	-
Hexanal	TCI	66–25-1	>98.0	78.9	-
Nonanal	TCI	124–19-6	>95.0	81.1	-
n-Octanal	TCI	124–13-0	>98.0	82.2	-
Decanal	TCI	112–31-2	>97.0	61.0	-
trans-2-Hexenal	TCI	6,728–26-3	>97.0	71.8	-
trans-2-Heptenal	TCI	18,829–55-5	>95.0	70.5	-
trans-2-Decenal	TCI	3,913–81-3	>93.0	48.5	-
trans-2-Octenal	TCI	2,548–87-0	>96.0	45.9	-
Benzaldehyde	TCI	100–52-7	>98.0	67.0	-
Octane	TCI	111–65-9	>97.0	79.2	-
Decane	TCI	124–18-5	>99.0	71.7	-
Undecane	TCI	1,120–21-4	>99.0	69.0	-
Dodecane	TCI	112–40-3	>99.0	88.4	-
Tridecane	TCI	629–50-5	>99.0	86.4	-
Methyl salicylate	TCI	119–36–8	>99.0	84.6	-
cis-3-Hexen-1-yl benzoate	TCI	25,152–85-6	>99.0	16.8	10.5 ± 0.8
Methyl benzoate	TCI	93–58-3	>99.0	68.6	-
Isobornyl Acetate	TCI	125–12-2	>99.0	81.3	-
Hexyl butyrate	TCI	2,639–63-6	>98.0	61.9	-
trans-2-Hexenyl acetate	TCI	2,497–18-9	>97.0	75.2	-
Hexyl acetate	TCI	142–92-7	>99.0	83.9	-
cis-3-Hexenyl acetate	TCI	3,681–71-8	>97.0	77.2	-
cis-3-Hexenyl Isovalerate	TCI	35,154–45-1	>98.0	67.1	-
Methyl (2*E*,4*E*,6*Z*)-decatrienoate	Codow	51,544–64-0	>95%	15.3	9.6 ± 0.4
2-Hexanone	TCI	591–78-6	>98.0	85.1	-
4'-Ethylacetophenone	TCI	937–30-4	>97.0	71.0	-
β-Ionone	TCI	14,901–07-6	>95.0	19.0	11.9 ± 0.6
(–)-β-Pinene	TCI	18,172–67-3	≥94.0	70.7	-
Myrcene	Macklin	123–35-3	≥90.0	78.5	-
(+)-Limonene	TCI	5,989–27-5	>95.0	62.8	-
Nerolidol	TCI	7,212–44-4	>97.0	105.0	-
Ocimene	Sigma	13,877–91-3	≥90.0	69.0	-
β-Caryophyllene	TCI	87–44-5	>90.0	141.4	-
Linalool	TCI	78–70-6	>96.0	79.1	-
1,8-Cineole	TCI	470–82-6	>99.0	90.1	-
Citral	TCI	5,392–40-5	>96.0	66.4	-
(–)-Citronellal	TCI	5,949–05-3	>96.0	84.3	-
Eugenol	TCI	97–53-0	>99.0	111.7	-
Phenylacetonitrile	TCI	140–29-4	>98.0	78.4	-

IC_{50}, concentration of ligand halving the initial fluorescence intensity; K_i, dissociation constant; We consider the HhalCSP15 proteins had no binding with the tested ligands if the IC_{50} values > 20 μM and K_i values were not to be calculated and are represented as "-."

TABLE 2 | Docking results for HhalCSP15 with different ligands.

Ligands	Binding energy (Kcal/mol)	Residues involved in hydrogen bond	van der Waals interactions	Hydrophobic interactions
β-Ionone	–7.2	Glu64	Thr7, Tyr10, Asp11, Glu44, Asn67, Ile68, and Phe71	Leu13, Leu45, Ile48, and Ile52
cis-3-Hexen-1-yl benzoate	–6.3	Glu64	Thr7, Tyr10, Asp11, Val15, Leu45, Ile48, Ile52, and Asn67	Leu13, Ile68, and Phe71
Methyl (2*E*,4*E*,6*Z*)-decatrienoate	–6.3	Glu64	Thr7, Asp11, Glu44, Ile48, Leu49, Ile52, Asn67, Ile68, and Phe71	Tyr10 and Leu45

The results indicated that different residues from the binding pocket participated in the recognition of distinct ligands. The HhalCSP15 amino acid residue Glu64 forms a hydrogen bond with all three compounds. Apart from hydrogen bond formation, the compounds exhibited van der Waals as well as hydrophobic interactions with HhalCSP15 (**Figure 5**; **Table 2**).

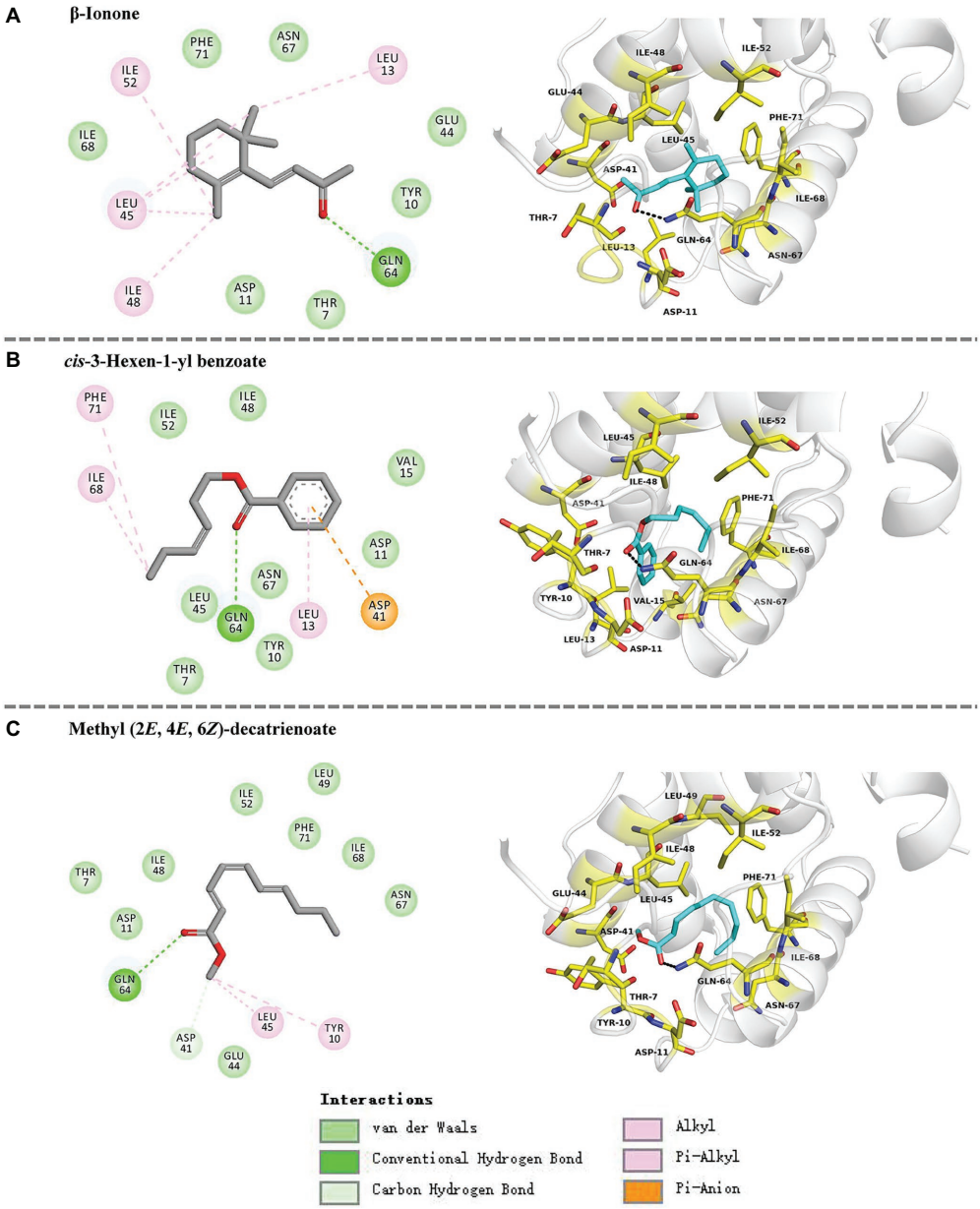

FIGURE 5 | Molecular docking of HhalCSP15 with **(A)** β-ionone, **(B)** *cis*-3-hexen-1-yl benzoate, and **(C)** methyl (*2E,4E,6Z*)-decatrienoate.

Electrophysiological Activities of Putative Ligands of HhalCSP15

To determine whether the HhalCSP15 ligands have biological activity, we measured the electrophysiological responses of nymph and adult *H. halys* to these three volatiles using EAG recordings. The results indicated that all three volatiles elicited electrophysiological responses in the antennae of both nymphs and adults (**Figure 6**). Adult *H. halys* showed significantly greater responses than nymphs. *Cis*-3-hexen-1-yl benzoate and β-ionone elicited significantly greater responses in females compared with males and nymphs. *EEZ*-MDT stimulated significantly greater EAG responses in adults compared with nymphs, but there was no significant difference between the sexes of adults. Of note, *cis*-3-hexen-1-yl benzoate elicited the highest EAG response among all ligands in both nymphs and adults (**Figure 6**).

DISCUSSION

Insect CSPs exhibit broad expression profiles both in chemosensory organs and non-chemosensory organs. In *H. halys* antennal transcriptome, 17 CSPs were identified and half of them had diverse expression patterns (Sun et al., 2020). In southern green stink bug *Nezara viridula*, 13 CSP genes were identified from

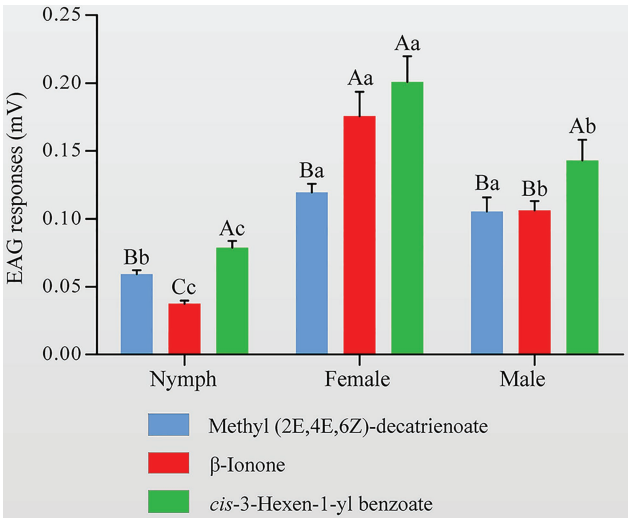

FIGURE 6 | Electroantennography (EAG) activity of *Halyomorpha halys* antennae to different ligands of HhalCSP15. Different uppercase letters indicate significant differences among different chemicals, and different lowercase letters indicate significant differences among nymphs, females, and males ($p < 0.05$).

antennae and mouthpart transcriptome, and only four genes were primarily expressed in antennae (Wu et al., 2019). The broad and diverse expression patterns of stink bug CSPs are consistent with their possible multiple roles in chemoreception, development, and other processes. HhalCSP15 is orthologous with NvirCSP4 (GenBank: QCZ25118.1, 81% identity) and both of them are specifically expressed in antennae, which suggests their conserved roles in olfactory perception. *NvirCSP4* was expressed roughly equally in both male and female antennae (Wu et al., 2019). Our data also reveal that no obvious difference was observed in expression levels of *HhalCSP15* between male and female antennae. In addition, *HhalCSP15* was also specifically expressed in nymph antennae. Thus, it is conceivable that HhalCSP15 is involved in the detection of odorants eliciting common stink bug behaviors, such as host location or intraspecific communication.

In fluorescent binding assays, 43 volatile compounds, including plant volatiles and *H. halys* volatiles, were selected as candidate ligands. Ligand-binding experiments demonstrated that HhalCSP15 has highly selective binding to volatile compounds. Some specific amino acids located in the hydrophobic cavities may be involved in the process of ligand binding in HhalCSP15 (Tomaselli et al., 2006). For example, in CSPsg4, I76 and W83 are involved in oleamide binding (Tomaselli et al., 2006); in CSP2, Y11 plays a key role in the binding of (*E*)-3,8-dimethyl-1,4,7-nonatriene (Li et al., 2021). Molecular docking analyses indicate favorable interactions between HhalCSP15 and its ligands. Glu64 forms a hydrogen bond with all ligands and could actively participate in forming the binding site of HhalCSP15. However, the specific binding sites that mediate the interactions between HhalCSP15 and ligands need to be investigated in future site-directed mutagenesis experiments.

β-Ionone and *cis*-3-hexen-1-yl benzoate are widely distributed in plants (Fraser et al., 2003; Simkin et al., 2004; Wei et al., 2011; Baldermann et al., 2012; Suckling et al., 2012). The binding experiments showed that the two compounds have strong binding abilities with HhalCSP15 and elicit an EAG response in both nymph and adult *H. halys* antennae. *EEZ*-MDT, which was identified as a binding ligand of HhalCSP15, is the aggregation pheromone of *Plautia stali*, which attracts stink bugs and is used as a lure in traps to monitor *H. halys* (Sugie et al., 1996; Aldrich et al., 2007; Morrison et al., 2017). *H. halys* does not emit *EEZ*-MDT though it may use *EEZ*-MDT as an indirect clue when searching for food plants (Funayama, 2008; Weber et al., 2017). These data further support a potential role of HhalCSP15 in *H. halys* host location. It was also found that HhalCSP15 could not bind with selected *H. halys*-derived volatiles, such as tridecane and *(E)*-2-decenal. *(E)*-2-decenal is an alarm pheromone in *H. halys* (Harris et al., 2015), and at least five *H. halys* OBPs showed high binding activities to it (Zhong et al., 2018). Thus, these findings also indicate that HhalCSP15 is not a pheromone binding protein of the stink bug and unlikely participates in the intraspecific communication for *H. halys*. However, gene editing and behavioral assays need to be further performed to verify the roles of this protein in the olfactory system of *H. halys*.

In conclusion, we report the antenna-specific expression as well as ligand binding capability of the CSP HhalCSP15 from *H. halys*, providing evidence for the possible olfactory roles of CSPs in the host-finding behavior of stink bugs. Although our results indicate that β-ionone and *cis*-3-hexen-1-yl benzoate are potential bioactive volatiles, further studies are necessary to confirm their behavioral activity as well as their possible applications for regulating the olfactory behavior of *H. halys*.

DATA AVAILABILITY STATEMENT

The original contributions presented in the study are included in the article/**Supplementary Material**, further inquiries can be directed to the corresponding author.

AUTHOR CONTRIBUTIONS

SW conceived and designed the research and wrote the manuscript. SW and ZW conducted all the experiments. ZW, AS, and FY analyzed the data. SS and YZ revised the manuscript. All authors contributed to the article and approved the submitted version.

FUNDING

This work was supported by the National Natural Science Foundation of China (31801740) and the Promotion and Innovation of Beijing Academy of Agriculture and Forestry Sciences (KJCX201910).

SUPPLEMENTARY MATERIAL

The Supplementary Material for this article can be found online at: https://www.frontiersin.org/articles/10.3389/fphys.2021.721247/full#supplementary-material

REFERENCES

Abraham, M. J., Murtola, T., Schulz, R., Pall, S., Smith, J. C., Hess, B., et al. (2015). GROMACS: high performance molecular simulations through multi-level parallelism from laptops to supercomputers. *SoftwareX* 1, 19–25. doi: 10.1016/j.softx.2015.06.001

Aldrich, J. R., Khrimian, A., and Camp, M. J. (2007). Methyl 2,4,6-decatrienoates attract stink bugs and tachinid parasitoids. *J. Chem. Ecol.* 33:801. doi: 10.1007/s10886-007-9270-9

Angeli, S., Ceron, F., Scaloni, A., Monti, M., Monteforti, G., Minnocci, A., et al. (1999). Purification, structural characterization, cloning and immunocytochemical localization of chemoreception proteins from *Schistocerca gregaria*. *Eur. J. Biochem.* 262, 745–754. doi: 10.1046/j.1432-1327.1999.00438.x

Baldermann, S., Kato, M., Fleischmann, P., and Watanabe, N. (2012). Biosynthesis of α- and β-ionone, prominent scent compounds, in flowers of *Osmanthus fragrans*. *Acta Biochim. Pol.* 59, 79–81. doi: 10.18388/abp.2012_2176

Bos, J. I., Prince, D., Pitino, M., Maffei, M. E., Win, J., and Hogenhout, S. A. (2010). A functional genomics approach identifies candidate effectors from the aphid species *Myzus persicae* (green peach aphid). *PLoS Genet.* 6:e1001216. doi: 10.1371/journal.pgen.1001216

Bradford, M. M. (1976). A rapid and sensitive method for the quantitation of microgram quantities of protein utilizing the principle of protein-dye binding. *Anal. Biochem.* 72, 248–254. doi: 10.1016/0003-2697(76)90527-3

Bruce, T. J., Wadhams, L. J., and Woodcock, C. M. (2005). Insect host location: a volatile situation. *Trends Plant Sci.* 10, 269–274. doi: 10.1016/j.tplants.2005.04.003

Ebrahim, S. A., Dweck, H. K., Stökl, J., Hofferberth, J. E., Trona, F., Weniger, K., et al. (2015). *Drosophila* avoids parasitoids by sensing their semiochemicals via a dedicated olfactory circuit. *PLoS Biol.* 13:e1002318. doi: 10.1371/journal.pbio.1002318

Forêt, S., Wanner, K. W., and Maleszka, R. (2007). Chemosensory proteins in the honey bee: insights from the annotated genome, comparative analyses and expressional profiling. *Insect Biochem. Mol. Biol.* 37, 19–28. doi: 10.1016/j.ibmb.2006.09.009

Fraser, A. M., Mechaber, W. L., and Hildebrand, J. G. (2003). Electroantennographic and behavioral responses of the sphinx moth *Manduca sexta* to host plant headspace volatiles. *J. Chem. Ecol.* 29, 1813–1833. doi: 10.1023/A:1024898127549

Fu, S., Li, F., Yan, X., and Hao, C. (2020). Expression profiles and binding properties of the chemosensory protein PxylCSP11 from the diamondback moth, *Plutella xylostella* (Lepidoptera: Plutellidae). *J. Insect Sci.* 20:17. doi: 10.1093/jisesa/ieaa107

Funayama, K. (2008). Seasonal fluctuations and physiological status of *Halyomorpha halys* (Stål) (Heteroptera: Pentatomidae) adults captured in traps baited with synthetic aggregation pheromone of *Plautia crossota stali* Scott (Heteroptera: Pentatomidae). *Jpn. J. Appl. Entomol. Zool.* 52, 69–75. doi: 10.1303/jjaez.2008.69

Gonzalez, D., Rihani, K., Neiers, F., Poirier, N., Fraichard, S., Gotthard, G., et al. (2020). The *Drosophila* odorant-binding protein 28a is involved in the detection of the floral odour ß-ionone. *Cell. Mol. Life Sci.* 77, 2565–2577. doi: 10.1007/s00018-019-03300-4

Gu, S. H., Wang, S. Y., Zhang, X. Y., Ji, P., Liu, J. T., Wang, G. R., et al. (2012). Functional characterizations of chemosensory proteins of the alfalfa plant bug *Adelphocoris lineolatus* indicate their involvement in host recognition. *PLoS One* 7:e42871. doi: 10.1371/journal.pone.0042871

Harris, C., Abubeker, S., Yu, M., Leskey, T., and Zhang, A. (2015). Semiochemical production and laboratory behavior response of the brown marmorated stink bug, *Halyomorpha Halys*. *PLoS One* 10:e0140876. doi: 10.1371/journal.pone.0140876

Haye, T., Gariepy, T., Hoelmer, K., Rossi, J. P., Streito, J. C., Tassus, X., et al. (2015). Range expansion of the invasive brown marmorated stinkbug, *Halyomorpha halys*: an increasing threat to field, fruit and vegetable crops worldwide. *J. Pest. Sci.* 88, 665–673. doi: 10.1007/s10340-015-0670-2

Hoebeke, E., and Carter, M. E. (2003). *Halyomorpha halys* (Stål) (Heteroptera: Pentatomidae): a polyphagous plant pest from Asia newly detected in North America. *Proc. Entomol. Soc. Wash.* 105, 225–237.

Huang, G. Z., Liu, J. T., Zhou, J. J., Wang, Q., Dong, J. Z., Zhang, Y. J., et al. (2018). Expressional and functional comparisons of two general odorant binding proteins in *Agrotis ipsilon*. *Insect Biochem. Mol. Biol.* 98, 34–47. doi: 10.1016/j.ibmb.2018.05.003

Kaissling, K. E. (2009). Olfactory perireceptor and receptor events in moths: a kinetic model revised. *J. Comp. Physiol. A.* 195, 895–922. doi: 10.1007/s00359-009-0461-4

Khrimian, A., Zhang, A., Weber, D. C., Ho, H. Y., Aldrich, J. R., Vermillion, K. E., et al. (2014). Discovery of the aggregation pheromone of the brown marmorated stink bug (*Halyomorpha halys*) through the creation of stereoisomeric libraries of 1-bisabolen-3-ols. *J. Nat. Prod.* 77, 1708–1717. doi: 10.1021/np5003753

Kriticos, D. J., Kean, J. M., Phillips, C. B., Senay, S. D., Acosta, H., and Haye, T. (2017). The potential global distribution of the brown marmorated stink bug, *Halyomorpha halys*, a critical threat to plant biosecurity. *J. Pest. Sci.* 90, 1033–1043. doi: 10.1007/s10340-017-0869-5

Larter, N. K., Sun, J. S., and Carlson, J. R. (2016). Organization and function of *Drosophila* odorant binding proteins. *eLife* 15:e20242. doi: 10.7554/eLife.20242

Lartigue, A., Campanacci, V., Roussel, A., Larsson, A. M., Jones, T. A., Tegoni, M., et al. (2002). X-ray structure and ligand binding study of a moth chemosensory protein. *J. Biol. Chem.* 277, 32094–32098. doi: 10.1074/jbc.M204371200

Leal, W. S. (2013). Odorant reception in insects: roles of receptors, binding proteins, and degrading enzymes. *Annu. Rev. Entomol.* 58, 373–391. doi: 10.1146/annurev-ento-120811-153635

Lee, D. H., Short, B. D., Joseph, S. V., Bergh, J. C., and Leskey, T. C. (2013). Review of the biology, ecology, and management of *Halyomorpha halys* (Hemiptera: Pentatomidae) in China, Japan, and the Republic of Korea. *Environ. Entomol.* 42, 627–641. doi: 10.1603/EN13006

Leskey, T. C., Agnello, A., Bergh, J. C., Dively, G. P., Hamilton, G. C., Jentsch, P., et al. (2015). Attraction of the invasive *Halyomorpha halys* (Hemiptera: Pentatomidae) to traps baited with semiochemical stimuli across the United States. *Environ. Entomol.* 44, 746–756. doi: 10.1093/ee/nvv049

Leskey, T., and Nielsen, A. (2017). Impact of the invasive brown marmorated stink bug in North America and Europe: history, biology, ecology, and management. *Annu. Rev. Entomol.* 7, 599–618. doi: 10.1146/annurev-ento-020117-043226

Li, F., Dewer, Y., Li, D., Qu, C., and Luo, C. (2021). Functional and evolutionary characterization of chemosensory protein CSP2 in the whitefly, *Bemisia tabaci*. *Pest Manag. Sci.* 77, 378–388. doi: 10.1002/ps.6027

Livak, K. J., and Schmittgen, T. D. (2001). Analysis of relative gene expression data using real-time quantitative PCR and the 2(-Delta Delta C(T)) method. *Methods* 25, 402–408. doi: 10.1006/meth.2001.1262

Maida, R., Steinbrecht, A., Ziegelberger, G., and Pelosi, P. (1993). The pheromone binding protein of *Bombyx mori*: purification, characterization and immunocytochemical localization. *Insect Biochem. Mol. Biol.* 23, 243–253. doi: 10.1016/0965-1748(93)90005-D

Maleszka, J., Forêt, S., Saint, R., and Maleszka, R. (2007). RNAi-induced phenotypes suggest a novel role for a chemosensory protein CSP5 in the development of embryonic integument in the honeybee (*Apis mellifera*). *Dev. Genes Evol.* 217, 189–196. doi: 10.1007/s00427-006-0127-y

McKenna, M. P., Hekmat-Scafe, D. S., Gaines, P., and Carlson, J. R. (1994). Putative *Drosophila* pheromone-binding proteins expressed in a subregion of the olfactory system. *J. Biol. Chem.* 269, 16340–16347. doi: 10.1016/S0021-9258(17)34013-9

Metcalf, R. L., and Kogan, M. (1987). Plant volatiles as insect attractants. *Crit. Rev. Plant Sci.* 5, 251–301. doi: 10.1080/07352688709382242

Morrison, W. R., Park, C. G., Seo, B. Y., Park, Y. L., Kim, H. G., Rice, K. B., et al. (2017). Attraction of the invasive *Halyomorpha halys* in its native Asian range to traps baited with semiochemical stimuli. *J. Pest. Sci.* 90, 1205–1217. doi: 10.1007/s10340-016-0816-x

Nomura, A., Kawasaki, K., Kubo, T., and Natori, S. (1992). Purification and localization of p10, a novel protein that increases in nymphal regenerating legs of *Periplaneta americana* (American cockroach). *Int. J. Dev. Biol.* 36, 391–398.

Pelosi, P., Iovinella, I., Felicioli, A., and Dani, F. R. (2014). Soluble proteins of chemical communication: an overview across arthropods. *Front. Physiol.* 5:320. doi: 10.3389/fphys.2014.00320

Pelosi, P., Iovinella, I., Zhu, J., Wang, G., and Dani, F. R. (2017). Beyond chemoreception: diverse tasks of soluble olfactory proteins in insects. *Biol. Rev. Camb. Philos. Soc.* 93, 184–200. doi: 10.1111/brv.12339

Peng, Y., Wang, S. N., Li, K. M., Liu, J. T., Zheng, Y., Shan, S., et al. (2017). Identification of odorant binding proteins and chemosensory proteins in *Microplitis mediator* as well as functional characterization of chemosensory protein 3. *PLoS One* 12:e0180775. doi: 10.1371/journal.pone.0180775

Pikielny, C. W., Hasan, G., Rouyer, F., and Rosbash, M. (1994). Members of a family of *Drosophila* putative odorant-binding proteins are expressed in different subsets of olfactory hairs. *Neuron* 12, 35–49. doi: 10.1016/0896-6273(94)90150-3

Rihani, K., Ferveur, J. F., and Briand, L. (2021). The 40-year mystery of insect odorant-binding proteins. *Biomol. Ther.* 11:509. doi: 10.3390/biom11040509

Simkin, A. J., Schwartz, S. H., Auldridge, M., Taylor, M. G., and Klee, H. J. (2004). The tomato carotenoid cleavage dioxygenase 1 genes contribute to the formation of the flavor volatiles β-ionone, pseudoionone, and geranylacetone. *Plant J.* 40, 882–892. doi: 10.1111/j.1365-313X.2004.02263.x

Steinbrecht, R. A. (1997). Pore structures in insect olfactory sensilla: a review of data and concepts. *Int. J. Insect Morphol. Embryol.* 26, 229–245. doi: 10.1016/S0020-7322(97)00024-X

Suckling, D. M., Twidle, A. M., Gibb, A. R., Manning, L. M., Mitchell, V. J., Sullivan, T. E., et al. (2012). Volatiles from apple trees infested with light brown apple moth larvae attract the parasitoid *Dolichogenidia tasmanica*. *J. Agric. Food Chem.* 60, 9562–9566. doi: 10.1021/jf302874g

Sugie, H., Yoshida, M., Kawasaki, K., Noguchi, H., Moriya, S., Takagi, K., et al. (1996). Identification of the aggregation pheromone of the brown-winged green bug, *Plautia stali* Scott (Heteroptera: Pentatomidae). *Appl. Entomol. Zool.* 31, 427–431. doi: 10.1303/aez.31.427

Sun, H., Guan, L., Feng, H., Yin, J., Cao, Y., Xi, J., et al. (2014). Functional characterization of chemosensory proteins in the scarab beetle, *Holotrichia oblita* Faldermann (Coleoptera: Scarabaeida). *PLoS One* 9:e107059. doi: 10.1371/journal.pone.0107059

Sun, D., Huang, Y., Qin, Z., Zhan, H., Zhang, J., Liu, Y., et al. (2020). Identification of candidate olfactory genes in the antennal transcriptome of the stink bug *Halyomorpha halys*. *Front. Physiol.* 11:876. doi: 10.3389/fphys.2020.00876

Sun, L., Zhou, J. J., Gu, S. H., Xiao, H. J., Guo, Y. Y., Liu, Z. W., et al. (2015). Chemosensillum immunolocalization and ligand specificity of chemosensory proteins in the alfalfa plant bug *Adelphocoris lineolatus* (Goeze). *Sci. Rep.* 5:8073. doi: 10.1038/srep08073

Takken, W. (1991). The role of olfaction in host-seeking of mosquitoes: a review. *Int. J. Trop. Insect Sci.* 12, 287–295. doi: 10.1017/S1742758400020816

Tomaselli, S., Crescenzi, O., Sanfelice, D., Ab, E., Wechselberger, R., Angeli, S., et al. (2006). Solution structure of a chemosensory protein from the desert locust *Schistocerca gregaria*. *Biochemistry* 45, 10606–10613. doi: 10.1021/bi060998w

Vogt, R. G., and Riddiford, L. M. (1981). Pheromone binding and inactivation by moth antennae. *Nature* 293, 161–163. doi: 10.1038/293161a0

Wang, S. N., Shan, S., Yu, G. Y., Wang, H., Dhiloo, K. H., Khashaveh, A., et al. (2020). Identification of odorant-binding proteins and functional analysis of antenna-specific AplaOBP1 in the emerald ash borer, *Agrilus planipennis*. *J. Pest. Sci.* 93, 853–865. doi: 10.1007/s10340-019-01188-4

Weber, D. C., Morrison, W. R., Khrimian, A., Rice, K. B., Leskey, T. C., Rodriguez-Saona, C., et al. (2017). Chemical ecology of *Halyomorpha halys*: discoveries and applications. *J. Pest. Sci.* 90, 989–1008. doi: 10.1007/s10340-017-0876-6

Wei, S., Hannoufa, A., Soroka, J., Xu, N., Li, X., Zebarjadi, A., et al. (2011). Enhanced β-ionone emission in *Arabidopsis* over-expressing AtCCD1 reduces feeding damage *in vivo* by the crucifer flea beetle. *Environ. Entomol.* 40, 1622–1630. doi: 10.1603/EN11088

Wermelinger, B., Wyniger, D., and Forster, B. (2008). First records of an invasive bug in Europe: *Halyomorpha halys* Stål (Heteroptera: Pentatomidae), a new pest on woody ornamentals and fruit trees? *Mitt. Schweiz. Entomol. Ges.* 81, 1–8.

Wu, Z. Z., Cui, Y., Qu, M. Q., Lin, J. H., Chen, M. S., Bin, S. Y., et al. (2019). Candidate genes coding for odorant binding proteins and chemosensory proteins identified from dissected antennae and mouthparts of the southern green stink bug *Nezara viridula*. *Comp. Biochem. Physiol. Part D Genomics Proteomics* 31:100594. doi: 10.1016/j.cbd.2019.100594

Xu, P., Atkinson, R., Jones, D. N., and Smith, D. P. (2005). *Drosophila* OBP LUSH is required for activity of pheromone-sensitive neurons. *Neuron* 45, 193–200. doi: 10.1016/j.neuron.2004.12.031

Xuan, N., Guo, X., Xie, H.-Y., Lou, Q.-N., Lu, X.-B., Liu, G. X., et al. (2015). Increased expression of CSP and CYP genes in adult silkworm females exposed to avermectins. *Insect Sci.* 22, 203–219. doi: 10.1111/1744-7917.12116

Zhang, R., Wang, B., Grossi, G., Falabella, P., Liu, Y., Yan, S., et al. (2017). Molecular basis of alarm pheromone detection in *Aphids*. *Curr. Biol.* 27, 55–61. doi: 10.1016/j.cub.2016.10.013

Zhong, Y. Z., Tang, R., Zhang, J. P., Yang, S. Y., Chen, G. H., He, K. L., et al. (2018). Behavioral evidence and olfactory reception of a single alarm pheromone component in *Halyomorpha halys*. *Front. Physiol.* 9:1610. doi: 10.3389/fphys.2018.01610

Zhou, J. J., Kan, Y., Antoniw, J., Pickett, J. A., and Field, L. M. (2006). Genome and EST analyses and expression of a gene family with putative functions in insect chemoreception. *Chem. Senses* 31, 453–465. doi: 10.1093/chemse/bjj050

Conflict of Interest: The authors declare that the research was conducted in the absence of any commercial or financial relationships that could be construed as a potential conflict of interest.

Publisher's Note: All claims expressed in this article are solely those of the authors and do not necessarily represent those of their affiliated organizations, or those of the publisher, the editors and the reviewers. Any product that may be evaluated in this article, or claim that may be made by its manufacturer, is not guaranteed or endorsed by the publisher.

frontiers in Physiology

ORIGINAL RESEARCH
published: 10 September 2021
doi: 10.3389/fphys.2021.674023

Identification of Candidate Carboxylesterases Associated With Odorant Degradation in *Holotrichia parallela* Antennae Based on Transcriptome Analysis

Jiankun Yi[1,2†], Shang Wang[1†], Zhun Wang[1,3], Xiao Wang[1], Gongfeng Li[1], Xinxin Zhang[1], Yu Pan[1], Shiwen Zhao[1], Juhong Zhang[1], Jing-Jiang Zhou[1,4], Jun Wang[1] and Jinghui Xi[1*]*

[1]College of Plant Science, Jilin University, Changchun, China, [2]School of Life Science, Huizhou University, Huizhou, China, [3]Changchun Customs Technology Center, Changchun, China, [4]Rothamsted Research, University of Hertfordshire, Harpenden, United Kingdom

Insects rely on their olfactory systems in antennae to recognize sex pheromones and plant volatiles in surrounding environments. Some carboxylesterases (CXEs) are odorant-degrading enzymes (ODEs), degrading odorant signals to protect the olfactory neurons against continuous excitation. However, there is no report about CXEs in *Holotrichia parallela*, one of the most major agricultural underground pests in China. In the present study, 20 candidate *CXEs* were identified based on transcriptome analysis of female and male antennae. Sequence alignments and phylogenetic analysis were performed to investigate the characterization of these candidate *CXEs*. The expression profiles of *CXEs* were compared by RT-qPCR analysis between olfactory and non-olfactory tissues of both genders. *HparCXE4, 11, 16, 17, 18, 19,* and *20* were antenna-biased expressed genes, suggesting their possible roles as ODEs. *HparCXE6, 10, 11, 13,* and *16* showed significantly higher expression profiles in male antennae, whereas *HparCXE18* was expressed more in female antennae. This study highlighted candidate CXE genes linked to odorant degradation in antennae, and provided a useful resource for further work on the *H. parallela* olfactory mechanism and selection of target genes for integrative control of *H. parallela*.

Keywords: *Holotrichia parallela*, antennal transcriptome, odorant-degrading enzyme, carboxylesterase, antenna-biased expression profile

OPEN ACCESS

Edited by:
Joe Hull,
United States Department of Agriculture, United States

Reviewed by:
Jacob Corcoran,
Biological Control of Insects Research Laboratory (USDA-ARS), United States
William Benjamin Walker III,
United States Department of Agriculture (USDA-ARS), United States

***Correspondence:**
Jinghui Xi
jhxi1965@jlu.edu.cn
Jun Wang
wang_jun@jlu.edu.cn

†These authors have contributed equally to this work and share first authorship

Specialty section:
This article was submitted to Invertebrate Physiology, a section of the journal Frontiers in Physiology

Received: *28 February 2021*
Accepted: *01 July 2021*
Published: *10 September 2021*

Citation:
Yi J, Wang S, Wang Z, Wang X, Li G, Zhang X, Pan Y, Zhao S, Zhang J, Zhou J-J, Wang J and Xi J (2021) Identification of Candidate Carboxylesterases Associated With Odorant Degradation in Holotrichia parallela Antennae Based on Transcriptome Analysis. Front. Physiol. 12:674023. doi: 10.3389/fphys.2021.674023

INTRODUCTION

The insect olfactory system resides mainly in antennae and plays an integral role in mediating insect behaviors related to survival and reproduction, including locating host plants, mate partners, and oviposition sites (Younus et al., 2014; Zhang et al., 2017a). These complex olfactory behaviors rely on a series of proteins for transporting and recognizing odorant molecules, including binding proteins i.e., odorant-binding proteins (OBPs); chemosensory proteins (CSPs), chemoreceptors (i.e., olfactory receptors, ORs; ionotropic receptors, IRs), and sensory neuron membrane proteins (SNMPs; Zhou, 2010; Leal, 2013; Yi et al., 2018). However, when the

odorant molecules successfully activate receptors, they must be inactivated and removed rapidly by odorant-degrading enzymes (ODEs), allowing recovery of sensitivity of the olfactory system and starting the next new potential responses (Leal, 2013; Younus et al., 2014). So far, a variety of antennal-specific and-abundant ODEs have been functionally characterized, including carboxylesterases (CXEs), cytochrome P450s (CYPs), glutathione S-transferases (GSTs), UDP-glycosyltransferases (UGTs), and alcohol dehydrogenases (ADHs), etc. (Leal, 2013; Younus et al., 2014; Zhang et al., 2017a).

CXEs belong to the α/β-fold hydrolase superfamily and include proteins implicated in neuro/developmental functions and secreted catalytically active enzymes, suggesting that they have relatively specific functions in hormone and pheromone processing and intracellular enzymic activities (Younus et al., 2014). Most esterases implicated in insecticide detoxification and metabolic resistances are intracellular enzymes, with a few secreted enzymes (Claudianos et al., 2006). CXEs commonly contain a conserved catalytic triad (Ser-His-Glu) and specifically catalyze the hydrolysis of ester bonds in various substrates (Oakeshott et al., 2005). Many insect CXEs have been identified and functionally characterized for their involvement in sex pheromone and odorant degradation to date (Sun et al., 2017). The first pheromone-degrading enzyme ApolPDE, specifically distributed in the male antennae of the moth *Antheraea polyphemus* belongs to the insect CXE family (Vogt and Riddiford, 1981). ApolPDE was later cloned and functionally characterized, and was shown to degrade the sex pheromone E6Z11-16:Ac (Vogt and Riddiford, 1981; Ishida and Leal, 2005). In the Coleoptera *Popilia japonica*, male-specific antennal esterase PjapPDE could rapidly inactivate the sex pheromone (*R*)-japonilure (Ishida and Leal, 2008). In the cotton leafworm *Spodoptera littoralis*, two esterases SlCXE7 and SlCXE10 were found to be involved in ester odorant hydrolysis, not only for sex pheromone components, Z9E11-14:Ac and Z9E12-14:Ac but also for host plant volatile (Z)-3-hexenyl acetate (Durand et al., 2010a, 2011). Among the three antennae-enriched esterases from *Spodoptera exigua*, SexiCXE4 and SexiCXE14 displayed higher degradation activities not only for ester sex pheromones, but also for ester plant volatiles (He et al., 2014a,b), while SexiCXE10 preferred to hydrolyze plant volatiles (He et al., 2015).

Holotrichia parallela (Motschulsky; Coleoptera: Scarabaeidae) is an economically important pest of many agricultural crops in China (Ju et al., 2012; Wang et al., 2017). Both adults and larvae could cause damage. The adults feed on the leaves, flowers, and fruits of crops, while the larvae attack the roots and other underground parts of crops, resulting in low-quality products and even plant death (Luo et al., 2009; Ju et al., 2012). Recent studies on the olfactory proteins of *H. parallela* have focused on the identification and functional characteristics of olfactory binding proteins (OBPs and CSPs; Ju et al., 2012, 2018; Fang et al., 2016), chemoreceptor proteins (ORs, IRs, and GRs; Yi et al., 2018), and microRNA (Wang et al., 2017), as well as electrophysiology and behavior bioassays (Zhou et al., 2009; Ju et al., 2017). In addition to the above studies, the morphology and distribution of antennal sensilla are also described by electron microscopy (Yi et al., 2019). Until now, very little is known about the antennal ODEs of *H. parallela*. The sex pheromone blend of *H. parallela* were also identified as two components (*L*)-isoleucine methyl ester and (*R*)-(-)-linalool (Leal et al., 1992, 1993). The previous studies have shown that males and females of *H. parallela* exhibited behavioral preferences for sex pheromones (Zhou et al., 2009) and ester plant volatiles such as (E)-2-hexenyl acetate and (Z)-3-hexenyl acetate (Ju et al., 2017). Since the sex pheromones and many odorants attracting *H. parallela* are ester molecules, it is meaningful to investigate the role of CEXs in the process of odorant degradation, and to further explore the olfactory recognition mechanism of *H. parallela*. In fact, previous studies have showed that a lot of male antennae-specific or -enriched CEXs could degrade sex pheromone components (Vogt and Riddiford, 1981; Ishida and Leal, 2005; Chertemps et al., 2012) and/or odorants (He et al., 2014a,b, 2015).

Our objective in this study was to identify candidate CXEs related to odorant degradation using male and female antennal transcriptomes and explore their putative functions. The candidate *CXEs* were identified and phylogenetic characteristics were also analyzed. In addition, the tissue expression patterns of the identified *H. parallela CXEs* were investigated in olfactory tissues (antennae) and non-olfactory tissues (heads, thoraxes, abdomens, legs, and wings) and their potential functions were predicted and discussed.

MATERIALS AND METHODS

Insect Rearing and Extraction of Total RNA

The insects *H. parallela* were obtained from the Institute of Plant Protection, Chinese Academy of Agricultural Sciences, Beijing, China. They were reared in plastic containers (100 × 50 cm) with damp soil (20% moisture) at 25°C, 80% RH, and on a 12-hL:12-hD photoperiod and supplied with fresh elm, *Ulmus parvifolia* Jacquin, leaves until RNA extraction (Yi et al., 2018). Various tissues, including antennae, heads, thoraxes, abdomens, legs, and wings, were dissected separately and immediately thrown in liquid nitrogen. These tissue samples were frozen at −80°C until use. Total RNAs of all tissues were extracted using TRIzol Reagent (Invitrogen, Carlsbad, CA, United States) according to the manufacturer's protocol. The RNA integrity and purity were examined by 1.2% agarose electrophoresis and with a NanoDrop™ spectrophotometer (Thermo Fisher Scientific, Waltham, MA, United States).

Construction of cDNA Library, Sequencing, and Assembly

Fifty male or female antennae were used for the RNA extraction and transcriptome analysis. The poly (A) mRNA was separated from 20 μg of total RNA and purified with Oligo d(T) magnetic beads, and fragmented into short fragments by fragmentation buffer. The first-strand of cDNA was synthesized using a random hexamer primer with these mRNA fragments as templates. Next, the second-strand of cDNA was synthesized by adding DNA polymerase I, dNTPs, and RNase H and purified with

a QIAquick PCR purification kit (Qiagen, Hilden, Germany), resolved with EB (ethidium bromide) buffer for end reparation and single nucleotide A (adenine) addition to the 3' end of the cDNA. Next, the short fragments were connected with sequencing adapters. After that, fragment sizes were assessed by agarose gel electrophoresis, and the appropriate fragments were subjected to PCR amplification and sequencing (Illumina HiSeq™ 2000, San Diego, CA, United States) by the Beijing Genomics Institute (BGI) sequencing company (Shenzhen, China). After sequencing, image deconvolution and quality value calculations were performed using the Illumina GA pipeline 1.3 (Huang et al., 2012). Then, the low quality reads (with >50% of nucleotides for which the Phred Quality Score Q was less than or equal to 5) were filtered out to generate clean reads. Transcriptome *de novo* assembly was carried out with short reads assembling program – Trinity (version 20130225;[1] Grabherr et al., 2011). Firstly, clean reads with a certain length of overlap were combined to form longer contiguous sequences (contigs). Then the clean reads were mapped back to contigs; with paired-end approaches it was able to detect contigs from the same transcript as well as the distances between these contigs. Next, Trinity connected the contigs, and sequences that could not be extended were obtained. These result sequences of Trinity were defined as 'unigenes' by the BGI Company (Shenzhen, China; Xiao et al., 2015; Xie et al., 2015).

Functional Annotation for Transcriptome Data

The unigenes were firstly aligned to protein databases using BLASTx, including those from the database of Nr, COG,[2] Swiss-Prot,[3] and the KEGG[4] with a cut-off E-value of $<10^{-5}$, and they were also aligned to the Nt database using BLASTn with a cut-off E-value of $<10^{-5}$. With Nr annotation, Blast2GO (v2.5.0) was used to obtain gene ontology (GO) annotation of the unigenes. After getting GO annotation for every unigene, Web Gene Ontology Annotation Plot software was used to complete GO functional classification for all unigenes. With the KEGG database, the metabolic pathway annotation for unigenes was also performed. The above detailed steps are similar to a previous study (Huang et al., 2012).

Identification of Candidate CXE Genes

Candidate CXE genes were chosen from the transcriptome data. Further, all candidate CXEs were manually checked by the BLASTx program at the National Center for Biotechnology Information (NCBI). The open reading frames (ORFs) of candidate *CXE* genes were predicted using the ORFfinder program.[5] Then, the theoretical pI and Mw of deduced CXE proteins were calculated using the ExPASy tool with average resolution.[6] Next, the putative N-terminal signal peptides of deduced CXE proteins were predicted using the SignalP 5.0 server, and the organism group was set to Eukarya.[7] Multiple sequence alignment of identified CXE sequences was generated using the online Clustal Omega program.[8]

Phylogenetic Analysis of Candidate CXE Genes

The amino acid sequences for constructing phylogenetic trees were obtained from Coleoptera, Lepidoptera, Hymenoptera, and Diptera species, including *Tribolium castaneum* (Tcas), *Leptinotarsa decemlineata* (Ldec), *Bombyx mori* (Bmor), *A. polyphemus* (Apol), *S. littoralis* (Slit), *S. exigua* (Sexi), *Spodoptera litura* (Slitu), *Drosophila melanogaster* (Dmel), *Anopheles gambiae* (Agam), and *Apis mellifera* (Amel). Their accession numbers from Genbank are listed in **Supplementary Table 2**. The amino acid sequences were aligned using ClustalX 2.0 software.[9] The unrooted neighbor-joining (NJ) trees of candidate CXEs with full-length ORFs were constructed using the MEGA 7.0 software with the p-distance model.[10] Gaps/missing data were treated as partial deletion with a site coverage cut-off = 95%. Node support was assessed using a bootstrapping procedure based on 1,000 replicates. Some CXEs functionally characterized as ODEs or restrictively expressed in olfactory sensilla were marked with black dots in the phylogenetic trees from species *A. polyphemus* (Apol-PDE and Apol-ODE; Ishida and Leal, 2002, 2005), *D. melanogaster* (DmelEst6, DmelJHE and DmelJHEdup; Chertemps et al., 2012, Steiner et al., 2017, Hopkins et al., 2019), *S. exigua* (SexiCXE4, 10, 14; He et al., 2014a,b, 2015), *S. littoralis* (SlitCXE7, SlitCXE10 and Slit-EST; Durand et al., 2010a, 2011, Merlin et al., 2007), *Sesamia nonagrioides* (Snon-EST; Merlin et al., 2007), and *P. japonica* (Pjap-PDE; Ishida and Leal, 2008). The generated phylogenetic trees were colored and arranged using Figtree 1.42 software[11] (Yi et al., 2018). CXEs were mainly divided into secreted enzyme, intracellular enzyme, and neuro-signaling enzyme clades according to the classification system of CXEs described previously (Durand et al., 2010b).

Tissue Expression Profiles by RT-qPCR

Fifty male or female antennae and ten male or female heads, thoraxes, abdomens, legs, and wings were used as a biological sample for the RNA isolation and qPCR analysis. RT-qPCR was performed on a StepOne Plus Real-time PCR System (Applied Biosystems, Foster City, CA, United States) using SYBR Premix ExTaq II (Tli RNaseH Plus; Takara, Dalian, China). Candidate GAPDH, actin, and 18 s rRNA were selected to evaluate the suitability as internal reference genes, and GAPDH had the most stable expression. So GAPDH was chosen as the reference gene for qPCR analysis. Primers of 20 *CXEs* and the reference gene (*GAPDH*) were designed using the Primer Premier 5 software, and are listed in

[1]http://trinityrnaseq.github.io/
[2]http://clovr.org/docs/clusters-of-orthologous-groups-cogs/
[3]http://www.ebi.ac.uk/uniprot
[4]http://www.genome.jp/kegg/
[5]https://www.ncbi.nlm.nih.gov/orffinder/
[6]http://web.expasy.org/compute_pi/
[7]http://www.cbs.dtu.dk/services/SignalP/
[8]https://www.ebi.ac.uk/Tools/msa/clustalo/
[9]http://www.clustal.org/clustal2/
[10]http://www.megasoftware.net/
[11]http://tree.bio.ed.ac.uk/software/figtree/

Supplementary Table 3. The primer efficiencies of each gene were calculated and the primers with efficiency values ranging from 0.95 to 1.05 were selected for further experiments. RT-qPCR was performed under the following conditions: 30 s at 95°C, 40 cycles of 5 s at 95°C, 10 s at 55°C, and 34 s at 72°C. This program was followed by a melting temperature analysis: 95°C for 15 s, 60°C for 1 min, increasing 0.3°C per min, and 95°C for 15 s. Each reaction was run in triplicate from three biological replicates. The expression levels of these genes were calculated using the $2^{-\Delta\Delta Ct}$ method.

Statistic Analysis

Significant differences were analyzed by *t*-test (between sexes) and one-way ANOVA (between different tissues), followed by Tukey's HSD multiple comparisons test using SPSS software version 13.0. Expression profiles were created using the software Prism 6.0 (GraphPad Software, CA, United States; Yi et al., 2019). The significant differences between sexes were marked with asterisks (*, $p < 0.05$; **, $p < 0.01$, NS, no differences). The expression levels among different tissues of each gender followed by the different lowercase or uppercase letters were significantly different.

RESULTS

Annotation Results of *H. parallela* Antennal Transcriptome

Using the Illumina HiSeq2000 sequencing platform, 34,706 unigenes in total were obtained in the antennal transcriptomes and analyzed by searching against Nr (NCBI non-redundant protein sequences), Nt (NCBI non-redundant nucleotide database), Swiss-Prot, KEGG, COG (Cluster of Orthologous Groups of proteins), and GO databases. As to the results, significant matches were found against 18,312 (52.76%) unigenes in the Nr database, 8,524 (24.56%) unigenes in the Nt database, 14,071 (40.54%) unigenes in the Swiss-Prot database, 6,879 (19.82%) unigenes in the KEGG database, 6,508 (18.75%) unigenes in the COG database, and 8,919 (25.70%) unigenes in the GO database. A total of 19,025 (54.82%) unigenes were successfully annotated in at least one database, while 15,681 (45.18%) unigenes had no matching sequences in any of these databases (**Table 1**). The sequencing data were available at the NCBI Sequence Read Archive database with accession number SRP233063.

TABLE 1 | Annotations of *H. parallela* unigenes in public databases.

Protein database	Number of unigene hit	Percentage (%)
Nr	18,312	52.76
Nt	8,524	24.56
Swiss-Prot	14,071	40.54
KEGG	6,879	19.82
COG	6,508	18.75
GO	8,919	25.70
Total	19,025	54.82

Identification of Candidate CXEs

In order to explore the role of CXEs in the process of odorant signal inactivation, it is necessary to identify candidate *CXEs* related to odorant degradation by blasting against the Nr database. A total of 20 candidate *CXEs* were identified with complete ORFs. The length of deduced HparCXEs was between 535 and 854 amino acid residues (**Table 2**). The predicted theoretical isoelectric point (pI) of HparCXEs was from 4.29 to 9.09 with the predicted molecular weight (Mw) of 60.6 kDa to 98.4 kDa. Furthermore, all HparCXEs except for HparCXE1, 11, and 16 were predicted to have the putative N-terminal signal peptide (SP), indicating that they could be secretory proteins. Multiple sequence alignments of candidate HparCXEs showed that they had the conserved pentapeptide motif of insect CXEs, Gly-X-Ser-X-Gly ("X" represents any residue) of typical CXE proteins except for HparCXE5, 9, and 20 (**Figure 1**). In addition, conserved oxyanion hole-forming residues (Gly, Gly, and Ala) were also found, which were thought to stabilize the transition states of the hydrolysis reaction (Durand et al., 2010b). The oxyanion hole-forming residues of four HparCXEs (HparCXE2, 3, 7, and 15) and nine HparCXEs (HparCXE1, 4, 5, 8, 11, 14, 16, 17, and 18) consisted of "G-G-A" and "G-G-G," respectively (**Figure 1**). Additionally, the HparCXEs possessed the three conserved catalytic residues: serine (S), glutamate (E), and histidine (H), except HparCXE9 and 20 (lacking S), HparCXE7 (lacking E) and 19 (lacking E and H).

Phylogenetic Analysis of Candidate CXEs

In order to identify the phylogenetic relationships between CXEs of *H. parallela* and those of other insect species, the NJ tree of *H. parallela* CXEs was constructed together with CXEs from several Coleoptera, Lepidoptera, and Diptera species (**Figure 2**). The phylogenetic analysis grouped all 20 HparCXEs into three families: the secreted enzyme family (clade II, III, V-VII: 8 HparCXEs), the intracellular enzyme family (clade I, IV: 10 HparCXEs), and the catalytically inactive, neuro-signaling family (VIII-XI: 2 HparCXEs). HparCXE1, 7, 8, 11, and 12 were clustered into the α-esterase clade in the intracellular enzyme family, well known for their involvement in detoxification of insecticide/xenobiotics and digestion of food esters (Durand et al., 2010b). This clade included some functionally characterized ODEs, such as SlitCXE10 from *S. littoralis* (Durand et al., 2010a) and SexiCXE10 from *S. exigua* (He et al., 2015). HparCXE13 shared a close relationship with juvenile hormone esterases (JHEs) of other species in the secreted enzyme family clade, with more than 90% bootstrapping support with JHEs of other species. In this clade, DmelJHE and DmelJHEdup have been functionally characterized and have high degrading activities against ester plant volatiles (Steiner et al., 2017; Hopkins et al., 2019). HparCXE6, 9, and 10 were clustered into the cuticular/antennal esterase clade in the secreted enzyme family. HparCXE2, 4, 15, and 17 were clustered into the β and pheromone esterase clade in the secreted enzyme family, together with three functionally characterized ODEs, Apol-PDE (Ishida and Leal, 2005), Pjap-PDE (Ishida and Leal, 2008), and DmelEst6 (Chertemps et al., 2012). HparCXE3, 5, 14, 16,

TABLE 2 | Molecular characteristics and access numbers of candidate carboxylesterases.

Gene name	Access number	ORF (aa)	Mw(kDa)	PI	SP	Female FPKM	Male FPKM
HparCXE1	MN256341	554	61.82	4.29	No	7.9681	11.4349
HparCXE2	KY849880	548	61.27	5.75	Yes	149.4849	182.5306
HparCXE3	MN256342	548	62.06	6.15	Yes	65.5346	60.5936
HparCXE4	KY849884	548	61.21	5.23	Yes	257.6295	272.8335
HparCXE5	MN256343	556	62.33	6.54	Yes	1141.8355	1387.434
HparCXE6	MN256344	558	62.88	6.37	Yes	11.5945	11.6575
HparCXE7	MN256345	540	60.85	5.18	Yes	14.7613	13.5931
HparCXE8	MK863374	562	63.05	5.48	Yes	10.6951	3.9505
HparCXE9	MN256346	571	64.12	6.05	Yes	63.3226	68.1454
HparCXE10	MN256347	560	63.79	6.68	Yes	78.2333	102.1316
HparCXE11	MN256348	535	60.58	6.15	No	29.0704	40.4632
HparCXE12	MN256349	547	61.12	4.87	Yes	61.6074	78.2758
HparCXE13	MK863373	606	68.87	6.52	Yes	3.9849	16.0031
HparCXE14	MN256350	568	64.33	7.05	Yes	5.1524	4.14
HparCXE15	MN256351	568	63.89	5.84	Yes	25.9026	25.7384
HparCXE16	MN256352	555	62.74	5.28	No	47.4856	49.5223
HparCXE17	KY849897	547	60.75	5.32	Yes	29.709	21.3717
HparCXE18	MN256353	574	64.65	9.09	No	2935.9639	2625.5904
HparCXE19	MN256354	604	69.34	8.87	Yes	76.4188	57.648
HparCXE20	MN256355	854	98.36	6.32	Yes	6.4155	3.6196

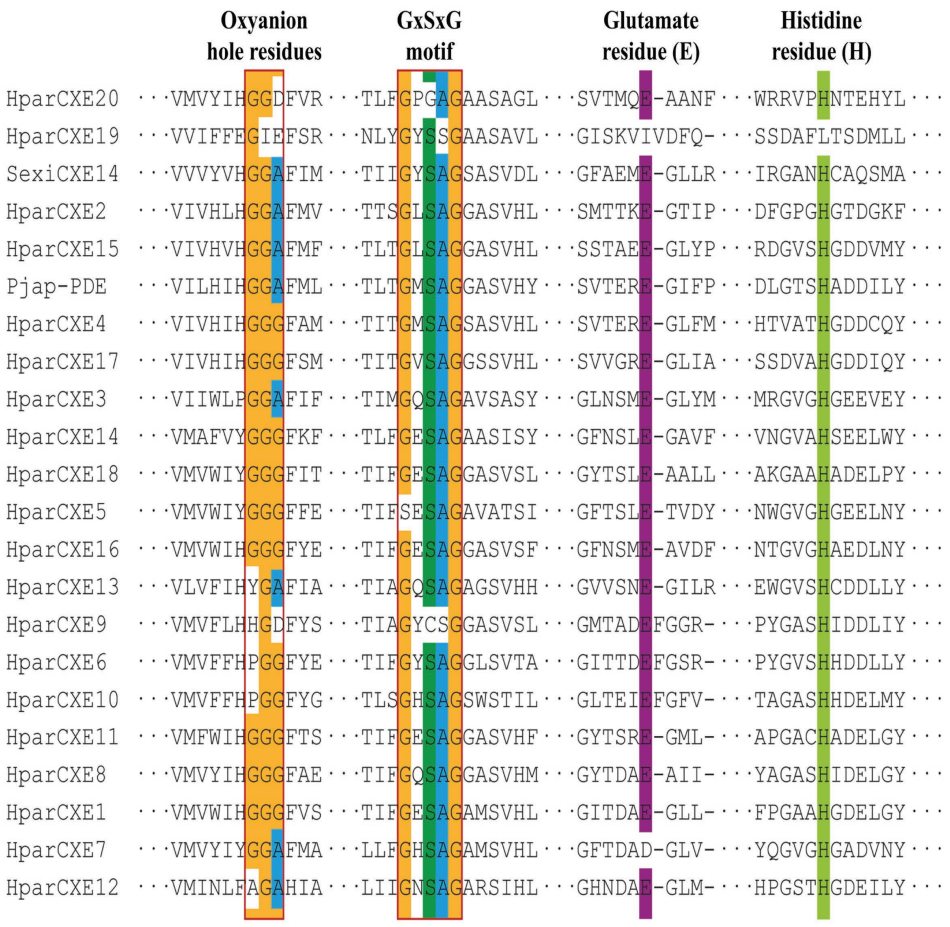

FIGURE 1 | Alignments of amino acid sequences of carboxylesterases (CXEs) from *Holotrichia parallela* and other insect species. The reference amino acid sequences are from *S. exigua* (Sexi) and *Popilia japonica* (Pjap). Amino acids not shown here are represented by three sequential dots. The Gly-X-Ser-X-Gly motif and the oxyanion hole-forming residues (Gly, Gly Ala) are boxed.

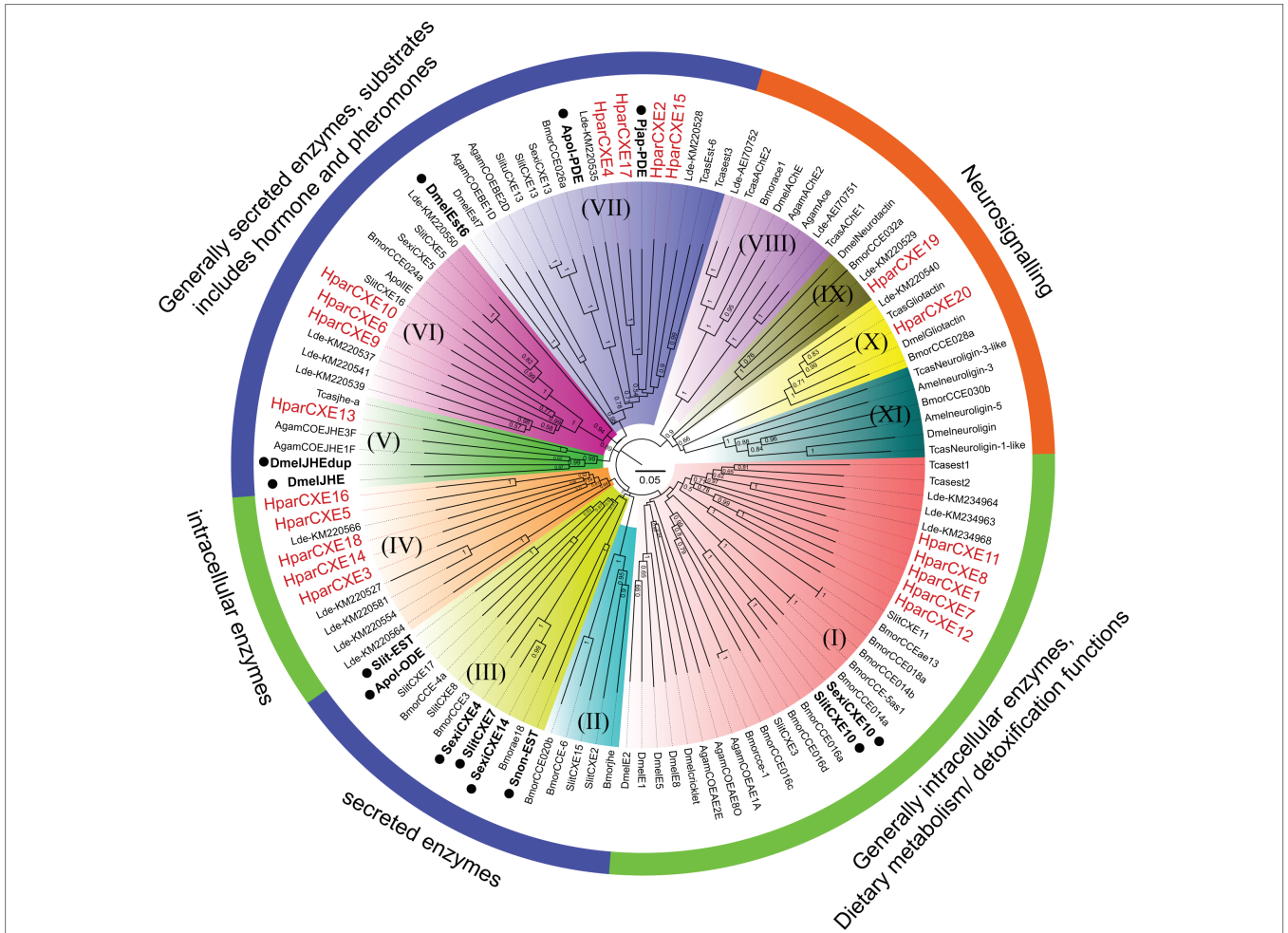

FIGURE 2 | Phylogenetic analysis of candidate CXEs between *H. parallela* and other species *from Coleoptera, Lepidoptera, Hymenoptera,* and *Diptera*. The neighbor-joining (NJ) trees were constructed using MEGA7.0 software with the p-distance model. All nodes have bootstrap support based on 1,000 replicates. CXEs are divided into secreted enzymes, intracellular enzymes, and neuro-signaling enzymes. (I) α-esterase clade. (II) Lepidopteran juvenile hormone esterases. (III) Mitochondrial, cytosolic, and secreted esterases. (IV) Coleopteran xenobiotic metabolizing enzymes. (V) Juvenile hormone esterase clade. (VI) Cuticular/antennal esterases. (VII) β and pheromone esterase clade. (VIII) AchE calde. (IX) Neurotactins. (X) Gliotactins. (XI) Neuroligins. Scale bar represents the 0.05 amino acid substitutions per site. Some CXEs functionally characterized as odorant-degrading enzymes or restrictively expressed in olfactory sensilla were marked with black dots.

and 18 belonged to coleopteran xenobiotic metabolizing enzymes in the intracellular enzyme family. Only HparCXE19 and HparCXE20 were clustered into the neuro-signaling enzyme family (**Figure 2**).

Tissue Expression Analysis for CXEs

Tissue expression profiles of all 20 *CXEs* were determined by RT-qPCR analysis (**Figure 3**). Five putative *HparCXEs* (*HparCXE6, 10, 11, 13,* and *16*) were significantly expressed higher in the male antennae than in the female antennae, whereas only one *HparCXE* (*HparCXE18*) showed significantly higher expression in the female antennae than in the male antennae. *HparCXE4, 11, 16, 17, 18, 19,* and *20* were expressed higher in both male and female antennae than in other tissues, whereas other *HparCXEs* were widely distributed in heads, thoraxes, abdomens, legs, and wings. *HparCXE5, 6, 14,* and *15* were expressed at a higher level in legs than in other tissues in both sexes. *HparCXE1* and *HparCXE12* had higher expression levels in both female and male wings and legs than in other tissues. *HparCXE9* was significantly expressed in both male and female heads.

DISCUSSION

H. parallela is one of the most important underground pests, and can eat leaves of crops by adults and roots by larvae, resulting in substantial yield losses (Ju et al., 2014; Yi et al., 2018). Chemical pesticides have always been the main control measure, but their use leads to the emergence of pest resistance (Wang et al., 2017). Olfaction is the main way of chemical communication between insects and the surrounding

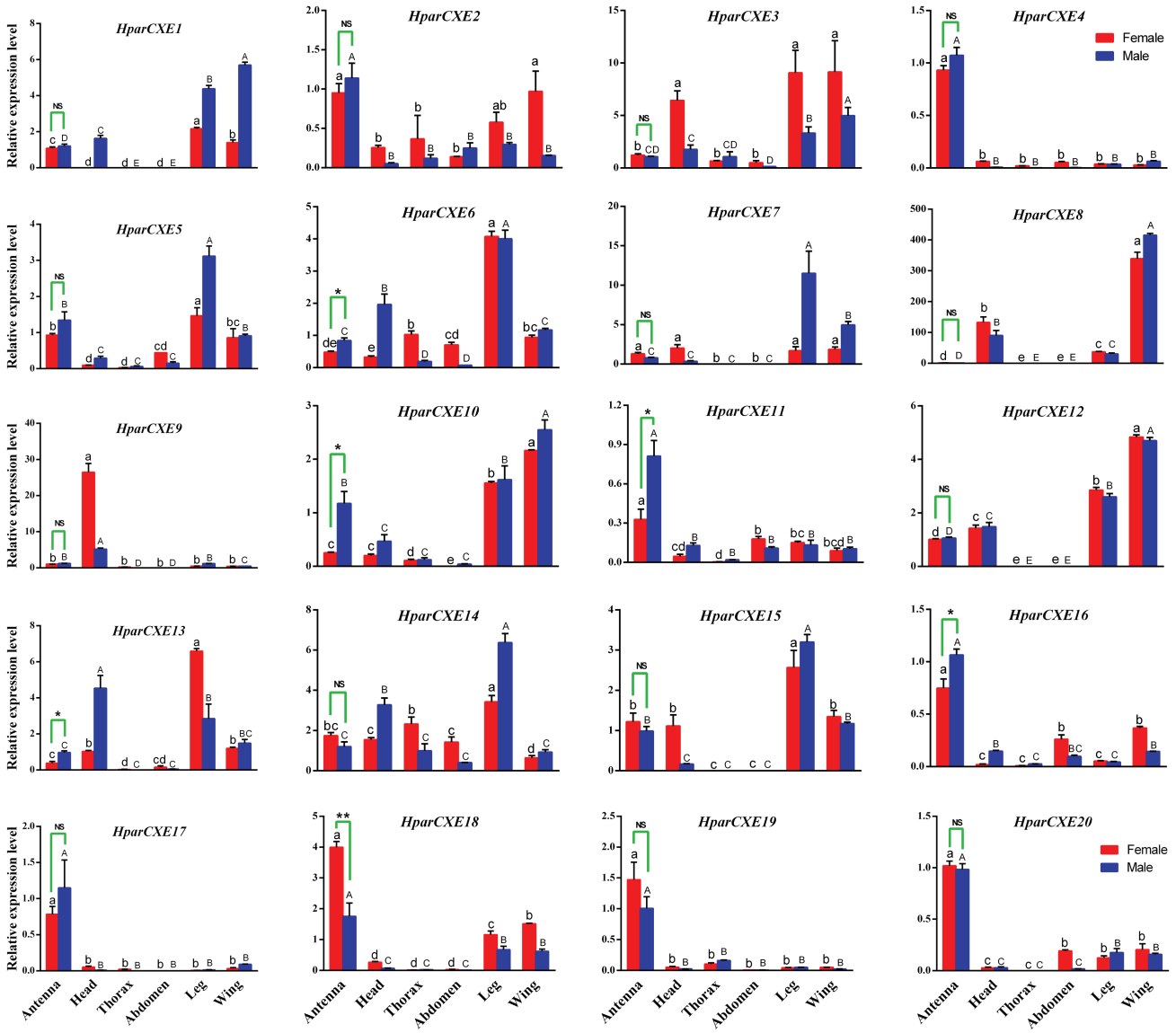

FIGURE 3 | Real-time quantitative PCR validation of CXE expression levels between different sexes and tissues. Different asterisks indicate significant differences between male and female antennae (*t*-test, *, $p < 0.05$; **, $p < 0.01$; NS, no statistical significance). The uppercase and lowercase letters represent the significant differences among different male and female tissues, respectively, using one-way ANOVA.

environment (Leal, 2013). Identification of ODEs involved in the termination of odorant signals will help us further explore the olfaction mechanism of *H. parallela* and provide target genes for integrative control of *H. parallela*.

This study identified for the first time 20 antennal CXEs. Bioinformatics analysis showed they are members of the alpha/beta hydrolase fold esterase family (Huang et al., 2016). Previous studies have suggested that similar to CXEs of almost insects, HparCXEs also have three conserved motifs (**Figure 1**): GXSXG, E, and H residues (in the GxxHxxD/E motif; Durand et al., 2010a). The S (in GXSXG), E, and H (in GxxHxxD/E) residues are the most conserved because they collectively comprise the catalytic triad (Zhu et al., 2017). As stated in previous studies, CXEs of some moths with the same conserved residues had the function of degrading odorants (Zhang et al., 2017b).

In the phylogenetic analysis, HparCXE2, 4, 15, and 17 were strongly associated with the β and pheromone esterases clade (**Figure 2**) in which some have been confirmed to degrade pheromones and/or plant volatiles (like Apol-PDE for the acetate sex pheromone E6Z11-16:Ac and Pjap-PDE for the female sex pheromone (R)-japonilure; Ishida and Leal, 2005, 2008). This clade also contained DmelEst6, a male antennae-enriched CEX from *D. melanogaster* (Diptera), which has a high degradation activity against the female sex pheromone cis-vaccenyl acetate (Chertemps et al., 2012). HparCXE13 was in the clade of JHEs, required for JH degradation, and pheromone or food ester

degradation (Oakeshott et al., 2005; Durand et al., 2010b). In this same clade, DmelJHE in *D. melanogaster* shows higher activity with methyl decanoate and some other esters, like propyl propionate and octyl butyrate (Hopkins et al., 2019). Additionally, DmelJHEdup was shown to be an active antennal ODE against certain food acetates, including isoamyl acetate, ethyl butyrate, and ethyl propionate by physiological and behavioral experiments (Steiner et al., 2017). These results suggest that HparCXE13 may participate in ester odorant inactivation like DmelJHE and DmelJHEdup. In addition, HparCXE1, 7, 8, 11, and 12 were grouped in the α-esterase clade. In this clade, SlitCXE10 in *S. littoralis* was highly active to plant volatiles and two sex pheromone components (Z9E11-14:Ac and Z9E12-14:Ac; Durand et al., 2010b). SexiCXE10 in *S. exigua* had high activity specifically for ester plant volatiles with 7–10 carbon atoms, but no activity for sex pheromone components (He et al., 2015). Therefore, HparCXE1, 7, 8, 11, and 12 were strongly suggested as putative ODEs, and may play important roles in the detection of ester host plants and/or ester sex pheromone components of *H. parallela*. Taken together, the phylogenetic analysis showed that different HparCXEs could be involved in the different degradation process of sex pheromones, host plant volatiles, and/or other xenobiotics.

The RT-qPCR experiments were performed in order to identify the antennal-specific or antennal-biased CXEs that may be involved in odorant degradation in the antennae (**Figure 3**). *HparCXE4, 11, 16, 17, 18, 19,* and *20* were expressed more in antennae than in other non-olfactory tissues. Just like *jhedup*, a CEX in Drosophila, which detected food odorants and showed a predominant expression in the antennae rather than other body parts, like legs (Steiner et al., 2017). These antennae-biased expression profiles in *H. parallela* antennae suggested that these seven *HparCXEs* could play important roles in olfaction of *H. parallela* (Huang et al., 2016; Zhang et al., 2017a). *HparCXE18* presented higher expression levels in female antennae, whereas *HparCXE6, 10, 11, 13,* and *16* showed significantly higher expressions in male antennae, suggesting that the former were more related to the degradation of host plant volatiles, while the latter were more likely to participate in the degradation of sex pheromones (Yi et al., 2018). Previous studies have reported that some male antennae-specific or -enriched CEXs were shown to participate in the termination of female sex pheromones, like Esterase-6 in *Drosophila melanogaster* (Diptera; Chertemps et al., 2012) and ApolPDE in *A. polyphemus* (Lepidoptera; Vogt and Riddiford, 1981; Ishida and Leal, 2005). *HparCXE6, 10, 12,* and *15* were expressed more in legs or wings than in antennae (**Figure 3**), suggesting that they might not perform as ODEs, but might be involved in other physiological processes (He et al., 2014a, Zhang et al., 2017b).

The results presented here provided candidate CXEs related to odorant degradation. They need further functional verification to characterize the respective physiological roles of CXEs between sexes and in olfactory tissues. This study will provide insights in understanding the olfactory mechanism of *H. parallela* antennae and candidate target genes for integrative control of *H. parallela*.

DATA AVAILABILITY STATEMENT

The datasets presented in this study can be found in online repositories. The names of the repository/repositories and accession number(s) can be found at: https://www.ncbi.nlm.nih.gov/, PRJNA591176.

AUTHOR CONTRIBUTIONS

JX, JW, and JZ designed the experiment. JY performed the transcriptome experiments, organized data, and wrote this manuscript. SW performed the sequence alignments and RT-qPCR experiments. GL and ZW operated these instruments and participated in the statistical analysis. XW, XZ, YP, and SZ reared the insects and prepared the experimental samples. JJZ discussed and corrected the final manuscript. All authors contributed to the article and approved the submitted version.

FUNDING

This work was supported by the project of disciplinary crossing and integration from Jilin University (JLUXKJC2020107) and the National Key Research and Development Program of China (Grant no. 2018YFD0201000 and 2017YFD0200600), and was also supported by the Professorial and Doctoral Scientific Research Foundation of Huizhou University (2020JB069).

ACKNOWLEDGMENTS

We appreciate JJ Scientific Consultant Ltd. for editing and proofreading.

SUPPLEMENTARY MATERIAL

The Supplementary Material for this article can be found online at: https://www.frontiersin.org/articles/10.3389/fphys.2021.674023/full#supplementary-material

REFERENCES

Chertemps, T., Francois, A., Durand, N., Rosell, G., Dekker, T., Lucas, P., et al. (2012). A carboxylesterase, Esterase-6, modulates sensory physiological and behavioural response dynamics to pheromone in *drosophila*. *BMC Biol.* 10:56. doi: 10.1186/1741-7007-10-56

Claudianos, C., Ranson, H., Johnson, R. M., Biswas, S., Schuler, M. A., Berenbaum, M. R., et al. (2006). A deficit of detoxification enzymes: pesticide sensitivity and environmental response in the honeybee. *Insect Mol. Boil.* 15, 615–636. doi: 10.1111/j.1365-2583.2006.00672.x

Durand, N., Carot-Sans, G., Bozzolan, F., Rosell, G., Siaussat, D., Debernard, S., et al. (2011). Degradation of pheromone and plant volatile components by

a same odorant-degrading enzyme in the cotton leafworm, *Spodoptera littoralis*. *PLoS One* 6:e29147. doi: 10.1371/journal.pone.0029147

Durand, N., Carot-Sans, G., Chertemps, T., Bozzolan, F., Party, V., Renou, M., et al. (2010a). Characterization of an antennal carboxylesterase from the pest moth *Spodoptera littoralis* degrading a host plant odorant. *PLoS One* 5:e15026. doi: 10.1371/journal.pone.0015026

Durand, N., Carot-Sans, G., Chertemps, T., Montagné, N., Jacquin-Joly, E., Debernard, S., et al. (2010b). A diversity of putative carboxylesterases are expressed in the antennae of the noctuid moth *Spodoptera littoralis*. *Insect Mol. Biol.* 19, 87–97. doi: 10.1111/j.1365-2583.2009.00939.x

Fang, C. C., Zhang, X. X., Liu, D. D., Li, K. B., Zhang, S., Cao, Y. Z., et al. (2016). Cloning and functional analysis of an odorant-binding protein HparOBP15a gene from *Holotrichia parallela* (Coleoptera: Melolonthidae). *Acta Entomol. Sin.* 59, 260–268. doi: 10.16380/j.kcxb.2016.03.002

Grabherr, M. G., Haas, B. J., Yassour, M., Levin, J. Z., Thompson, D. A., Amit, I., et al. (2011). Full-length transcriptome assembly from RNA-Seq data without a reference genome. *Nat. Biotechnol.* 29, 644–652. doi: 10.1038/nbt.1883

He, P., Zhang, Y. N., Li, Z. Q., Yang, K., Zhu, J. Y., Liu, S. J., et al. (2014a). An antennae nriched carboxylesterase from *Spodoptera exigua* displays degradation activity in both plant volatiles and female sex pheromones. *Insect Mol. Biol.* 23, 475–486. doi: 10.1111/imb.12095

He, P., Zhang, J., Li, Z. Q., Zhang, Y. N., Yang, K., and Dong, S. L. (2014b). Functional characterization of an antennal esterase from the noctuid moth, *Spodoptera exigua*. *Arch. Insect Biochem. Physiol.* 86, 85–99. doi: 10.1002/arch.21164

He, P., Zhang, Y. N., Yang, K., Li, Z. Q., and Dong, S. L. (2015). An antenna-biased carboxylesterase is specifically active to plant volatiles in *Spodoptera exigua*. *Pestic. Biochem. Physiol.* 123, 93–100. doi: 10.1016/j.pestbp.2015.03.009

Hopkins, D. H., Rane, R. V., Younus, F., Coppin, C. W., Pandey, G., Jackson, C. J., et al. (2019). The molecular basis for the neofunctionalization of the juvenile hormone esterase duplication in drosophila. *Insect Biochem. Mol. Biol.* 106, 10–18. doi: 10.1016/j.ibmb.2019.01.001

Huang, X., Liu, L., Su, X., and Feng, J. (2016). Identification of biotransformation enzymes in the antennae of codling moth *Cydia pomonella*. *Gene* 580, 73–79. doi: 10.1016/j.gene.2016.01.008

Huang, Q., Sun, P., Zhou, X., and Lei, C. (2012). Characterization of head transcriptome and analysis of gene expression involved in caste differentiation and aggression in *Odontotermes formosanus* (Shiraki). *PLoS One* 7:e50383. doi: 10.1371/journal.pone.0050383

Ishida, Y., and Leal, W. S. (2002). Cloning of putative odorant degrading enzyme and integumental esterase cDNAs from the wild silkmoth, *Antheraea polyphemus*. *Insect Biochem. Mol. Biol.* 32, 1775–1780. doi: 10.1016/S0965-1748(02)00136-4

Ishida, Y., and Leal, W. S. (2005). Rapid inactivation of a moth pheromone. *Proc. Natl. Acad. Sci. U. S. A.* 102, 14075–14079. doi: 10.1073/pnas.0505340102

Ishida, Y., and Leal, W. S. (2008). Chiral discrimination of the Japanese beetle sex pheromone and a behavioral antagonist by a pheromone-degrading enzyme. *Proc. Natl. Acad. Sci. U. S. A.* 105, 9076–9080. doi: 10.1073/pnas.0802610105

Ju, Q., Guo, X. Q., Li, X., Jian, G. X. G., Ni, W. L., and Qu, M. J. (2017). Plant volatiles increase sex pheromone attraction of *Holotrichia parallela* (Coleoptera: Scarabaeoidea). *J. Chem. Ecol.* 43, 236–242. doi: 10.1007/s10886-017-0823-2

Ju, Q., Li, X., Guo, X. Q., Du, L., Shi, C. R., and Qu, M. J. (2018). Two odorant-binding proteins of the dark black chafer (*Holotrichia parallela*) display preferential binding to biologically active host plant volatiles. *Front. Physiol.* 9:769. doi: 10.3389/fphys.2018.00769

Ju, Q., Li, X., Jiang, X. J., Qu, M. J., Guo, X. Q., Han, Z. J., et al. (2014). Transcriptome and tissue-specific expression analysis of OBP and CSP genes in the dark black chafer. *Arch. Insect Biochem. Physiol.* 87, 177–200. doi: 10.1002/arch.21188

Ju, Q., Qu, M. J., Wang, Y., Jiang, X. J., Li, X., Dong, S. L., et al. (2012). Molecular and biochemical characterization of two odorant-binding proteins from dark black chafer, *Holotrichia parallela*. *Genome* 55, 537–546. doi: 10.1139/g2012-042

Leal, W. S. (2013). Odorant reception in insects: roles of receptors, binding proteins, and degrading enzymes. *Annu. Rev. Entomol.* 58, 373–391. doi: 10.1146/annurev-ento-120811-153635

Leal, W. S., Matsuyama, S., Kuwahara, Y., Wakamura, S., and Hasegawa, M. (1992). An amino acid derivative as the sex pheromone of a scarab beetle. *Naturwissenschaften* 79, 184–185. doi: 10.1007/BF01134440

Leal, W. S., Sawada, M., Matsuyama, S., Kuwahara, Y., and Hasegawa, M. (1993). Unusual periodicity of sex pheromone production in the large black chafer *Holotrichia parallela*. *J. Chem. Ecol.* 7, 1381–1391. doi: 10.1007/BF00984883

Luo, Z. X., Li, K. B., Cao, Y. Z., Yin, J., Zhang, J., Zhang, J. T., et al. (2009). Investigations on soil-inhabiting pests in peanut fields in Henan. *Plant Prot.* 35, 104–108. doi: 10.3969/j.issn.0529-1542.2009.02.025

Merlin, C., Rosell, G., Carot-Sans, G., François, M. C., Bozzolan, F., Pelletier, J., et al. (2007). Antennal esterase cDNAs from two pest moths, *Spodoptera littoralis* and *Sesamia nonagrioides*, potentially involved in odourant degradation. *Insect Mol. Biol.* 16, 73–81. doi: 10.1111/j.1365-2583.2006.00702.x

Oakeshott, J. G., Claudianos, C., Campbell, P. M., Newcomb, R. D., and Russell, R. J. (2005). "Biochemical genetics and genomics of insect esterases," in *Comprehensive Molecular Insect Science*. eds. L. I. Gilbert, K. Iatrou and S. S. Gill (London: Elsevier), 309–381.

Steiner, C., Bozzolan, F., Montagné, N., Maïbèche, M., and Chertemps, T. (2017). Neofunctionalization of "juvenile hormone esterase duplication" in drosophila as an odorant-degrading enzyme towards food odorants. *Sci. Rep.* 7:12629. doi: 10.1038/s41598-017-13015-w

Sun, L., Wang, Q., Wang, Q., Zhang, Y., Tang, M., Guo, H., et al. (2017). Identification and expression patterns of putative diversified carboxylesterases in the tea geometrid *Ectropis obliqua* Prout. *Front. Physiol.* 8:1085. doi: 10.3389/fphys.2017.01085

Vogt, R. G., and Riddiford, L. M. (1981). Pheromone binding and inactivation by moth antennae. *Nature* 293, 161–163. doi: 10.1038/293161a0

Wang, S., Yi, J. K., Yang, S., Liu, Y., Zhang, J. H., and Xi, J. H. (2017). Identification and characterization of microRNAs expressed in antennae of *Holotrichia parallela* Motschulsky and their possible roles in olfactory regulation. *Arch. Insect Biochem. Physiol.* 94:e21369. doi: 10.1002/arch.21369

Xiao, X., Ma, J., Sun, Y., and Yao, Y. (2015). A method for the further assembly of targeted unigenes in a transcriptome after assembly by trinity. *Front. Plant Sci.* 6:843. doi: 10.3389/fpls.2015.00843

Xie, Q., Niu, J., Xu, X., Xu, L., Zhang, Y., Fan, B., et al. (2015). *De novo* assembly of the Japanese lawngrass (Zoysia japonica Steud.) root transcriptome and identification of candidate unigenes related to early responses under salt stress. *Front. Plant Sci.* 6:610. doi: 10.3389/fpls.2015.00610

Yi, J. K., Yang, S., Wang, S., Wang, J., Zhang, X. X., Liu, Y., et al. (2018). Identification of candidate chemosensory receptors in the antennal transcriptome of the large black chafer *Holotrichia parallela* Motschulsky (Coleoptera: Scarabaeidae). *Comp. Biochem. Physiol. D.* 28, 63–71. doi: 10.1016/j.cbd.2018.06.005

Yi, J., Zhang, X., Pan, Y., Wang, X., Wang, S., Yang, S., et al. (2019). Antennal morphology and ultrastructure of *Holotrichia parallela* (Coleoptera: Scarabaeidae). *J. Entomol. Sci.* 54, 378–389. doi: 10.18474/JES18-101

Younus, F., Chertemps, T., Pearce, S. L., Pandey, G., Bozzolan, F., Coppin, C. W., et al. (2014). Identification of candidate odorant degrading gene/enzyme systems in the antennal transcriptome of *Drosophila melanogaster*. *Insect Biochem. Mol. Biol.* 53, 30–43. doi: 10.1016/j.ibmb.2014.07.003

Zhang, Y. N., Li, Z. Q., Zhu, X. Y., Qian, J. L., Dong, Z. P., Xu, L., et al. (2017b). Identification and tissue distribution of carboxylesterase (CXE) genes in, *Athetis lepigone*, (Lepidoptera: Noctuidae) by RNA-seq. *J. Asia Pac. Entomol.* 20, 1150–1155. doi: 10.1016/j.aspen.2017.08.016

Zhang, Y. X., Wang, W. L., Li, M. Y., Li, S. G., and Liu, S. (2017a). Identification of putative carboxylesterase and aldehyde oxidase genes from the antennae of the rice leaf folder, *Cnaphalocrocis medinalis*, (Lepidoptera: Pyralidae). *J. Asia Pac. Entomol.* 20, 907–913. doi: 10.1016/j.aspen.2017.06.001

Zhou, J. J. (2010). Odorant-binding proteins in insects. *Vitam. Horm.* 83, 241–272. doi: 10.1016/S0083-6729(10)83010-9

Zhou, L. M., Ju, Q., Qu, M. J., Zhao, Z. Q., Dong, S. L., Han, Z. J., et al. (2009). EAG and behavioral responses of the large black chafer, *Holotrichia parallela* (Coleoptera: Scarabaeidae) to its sex pheromone. *Acta Entomol. Sin.* 52, 121–125. doi: 10.3321/j.issn:0454-6296.2009.02.001

Zhu, L., Yin, T. Y., Sun, D., Liu, W., Zhu, F., Lei, C. L., et al. (2017). Juvenile hormone regulates the differential expression of putative, juvenile hormone esterases, *via*, methoprene-tolerant, in non-diapause-destined and diapause-

destined adult female beetle. *Gene* 627, 373–378. doi: 10.1016/j.gene.2017.06.061

Conflict of Interest: The authors declare that the research was conducted in the absence of any commercial or financial relationships that could be construed as a potential conflict of interest.

Publisher's Note: All claims expressed in this article are solely those of the authors and do not necessarily represent those of their affiliated organizations, or those of the publisher, the editors and the reviewers. Any product that may be evaluated in this article, or claim that may be made by its manufacturer, is not guaranteed or endorsed by the publisher.

frontiers in Physiology

ORIGINAL RESEARCH
published: 04 October 2021
doi: 10.3389/fphys.2021.717698

Identification of Candidate Olfactory Genes in *Scolytus schevyrewi* Based on Transcriptomic Analysis

*Xiaofeng Zhu[1], Bingqiang Xu[1], Zhenjie Qin[2], Abudukyoum Kader[1], Bo Song[1], Haoyu Chen[1], Yang Liu[2] and Wei Liu[3]**

[1] Key Laboratory of Integrated Pest Management on Crops in Northwestern Oasis, Ministry of Agriculture and Rural Affairs, Institute of Plant Protection, Xinjiang Academy of Agricultural Sciences, Urumqi, China, [2] State Key Laboratory for Biology of Plant Diseases and Insect Pests, Institute of Plant Protection, Chinese Academy of Agricultural Sciences, Beijing, China, [3] Guangdong Laboratory for Lingnan Modern Agriculture (Shenzhen Branch), Genome Analysis Laboratory of the Ministry of Agriculture and Rural Affairs, Agricultural Genomics Institute at Shenzhen, Chinese Academy of Agricultural Sciences, Shenzhen, China

The bark beetle, *Scolytus schevyrewi (S. schevyrewi)*, is an economically important pest in China that causes serious damage to the fruit industry, particularly, in Xinjiang Province. Chemical signals play an important role in the behavior of most insects, accordingly, ecofriendly traps can be used to monitor and control the target pests in agriculture. In order to lay a foundation for future research on chemical communication mechanisms at the molecular level, we generate antennal transcriptome databases for male and female *S. schevyrewi* using RNA sequencing (RNA-seq) analysis. By assembling and analyzing the adult male and female antennal transcriptomes, we identified 47 odorant receptors (ORs), 22 ionotropic receptors (IRs), 22 odorant-binding proteins (OBPs), and 11 chemosensory proteins (CSPs). Furthermore, expression levels of all the candidate OBPs and CSPs were validated in different tissues of male and female adults by semiquantitative reverse transcription PCR (RT-PCR). *ScosOBP2* and *ScosOBP18* were highly expressed in female antennae. *ScosCSP2*, *ScosCSP3*, and *ScosCSP5* were specifically expressed in the antennae of both males and females. These results provide new potential molecular targets to inform and improve future management strategies of *S. schevyrewi*.

Keywords: *Scolytus schevyrewi*, transcriptome, olfactory genes, expression analysis, antennae

OPEN ACCESS

Edited by:
Kayvan Etebari, The University of Queensland, Australia

Reviewed by:
Youssef Dewer, Agricultural Research Center, Egypt
Matan Shelomi, National Taiwan University, Taiwan
William Benjamin Walker III, United States Department of Agriculture (USDA-ARS), United States
Daniele Silva De Oliveira, Federal University of Rio de Janeiro, Brazil

****Correspondence:***
Wei Liu
liuwei11@caas.cn

Specialty section:
This article was submitted to Invertebrate Physiology, a section of the journal Frontiers in Physiology

Received: *31 May 2021*
Accepted: *30 August 2021*
Published: *04 October 2021*

Citation:
Zhu X, Xu B, Qin Z, Kader A, Song B, Chen H, Liu Y and Liu W (2021) Identification of Candidate Olfactory Genes in Scolytus schevyrewi Based on Transcriptomic Analysis. Front. Physiol. 12:717698. doi: 10.3389/fphys.2021.717698

INTRODUCTION

Olfaction serves to detect environmental chemical information necessary for insect behavior such as finding food sources, mates, and oviposition sites (Hanson, 1999; Clyne et al., 2000). Insects have a sophisticated olfactory system that begins with the reception of odorants at the peripheral chemosensory system. Insect olfaction is dependent on olfactory receptor neurons (ORNs) in sensilla (Leal, 2013) distributed mainly in antennae and also in maxillary palps or labial palps (Stoker et al., 1990). The research of molecular mechanisms of olfactory reception in insects has predominantly been in the model organism *Drosophila melanogaster*. These studies have shown diverse olfactory genes encoding proteins, such as odorant receptors (ORs), ionotropic receptors (IRs), odorant-binding proteins (OBPs), and chemosensory proteins (CSPs), involved in different chemical signal transduction processes (Benton et al., 2009; Wilson, 2013; Xiao et al., 2019).

Odorant receptors play a critical role in recognizing thousands of odorant molecules in the insect olfactory system. Insect ORs were first identified in *Drosophila* which has the characteristic feature

of a seven-transmembrane domain (TMD) structure that is unrelated to the ORs in vertebrates (Clyne et al., 1999; Benton et al., 2006). Every ORN can express a single or two OR genes (Vosshall and Hanson, 2011). Specificity of OR relies on the ligand-banding ORs (Dobritsa et al., 2003; Elmore et al., 2003; Hallem et al., 2004), while Orco functions as an obligatory chaperon for the Orco-OR complex (Larsson et al., 2004; Benton et al., 2006; Stengl, 2017).

Evolved from the ionotropic glutamate receptor superfamily, IRs have been shown to be involved in odor reception. They are expressed in the sensory neurons that respond to many distinct odors, such as acids, amines, and other chemicals that cannot be recognized by ORs (Benton et al., 2006). Aside from olfaction, IRs serve various functions, such as cool sensation (Ni et al., 2015), hygrosensation (Knecht et al., 2016), circadian clock (Chen et al., 2015), and detection of carbon dioxide (CO_2) (Breugel et al., 2018).

In addition to ORs and IRs, other multigene families encode proteins that also play critical roles in olfaction. OBPs are small soluble proteins secreted in the sensillar lymph. They are characterized by an N-terminal signal peptide sequence and a set of six conserved cysteine residues that form three disulfide bridges (Pelosi et al., 2005, 2006). Studies of defective mutants and wild-type counterparts of OBP76a (also known as LUSH) in *Drosophila* have shown that this protein has a key role in the perception of alcohol and 11-cis vaccenyl acetate (Kim et al., 1998; Xu et al., 2005; Gomez-Diaz et al., 2013). OBPs have also been reported as a pheromone-binding protein in *Lepidoptera* (Jing et al., 2019). Some OBPs operate similar to LUSH in response to pheromones. *In vivo* studies have shown that OBPs significantly affect pheromone perception in moths. Knocking out these OBPs significantly reduced electrophysiological responses to pheromones in several species, such as *Helicoverpa armigera* (Ye et al., 2017), *Spodoptera litura* (Liu et al., 2012; Zhu et al., 2016a), and *Chilio suppressalis* (Dong et al., 2017).

Chemosensory proteins are also small soluble proteins but are shorter in amino acid sequence length than that of OBPs, and CSPs share the same structure of having four conserved cysteines forming two disulfide bridges (Pelosi et al., 2005, 2006; Honson et al., 2015). As semiochemical carriers, some CSPs are involved in chemodetection (Pelosi et al., 2018; Li et al., 2021) because CSPs are abundant in the lymph of chemosensory hairs (Angeli et al., 1999; Jacquin-Joly et al., 2001; Monteforti et al., 2002; Sun et al., 2014). Some of them already have been reported to function such as OBPs, e.g., CSP3 of the honeybee, which specially binds some components of brood pheromone (Briand et al., 2002).

Bark beetles (Coleoptera; Curculionidae; Scolytinae) feed on woods and several of them pose serious threats to forestry, e.g., *Ips typographus* (Wermelinger, 2004), *Dendroctonus ponderosae* (Andersson et al., 2013). Since their host-finding relies on chemical communication, e.g., aggregation behavior based on male-produced pheromone (Schlyter et al., 1987), pheromone-based technique could be used for the detection and control of this pest. In order to develop this technique efficiently, one way is to exploit olfactory genes that are critical for successful mate and host finding. Transcriptomic and genomics studies have been performed for searching olfactory genes in bark beetles (Andersson et al., 2013, 2019; Mitchell et al., 2019), and functional studies were limited to only seven ORs (Hou et al., 2021; Yuvaraj et al., 2021). *Scolytus schevyrewi* (*S. schevyrewi*) (Cleoptera: Scolylidae) is one of the most destructive insect pests of fruit trees in China. It has a wide host range and has been reported to attack several families of trees in Xinjiang province (Li et al., 1995). Several studies have focused on the identification and field bioassay of chemical attractants in the bark beetle (Fan et al., 2014). In order to provide a molecular basis for gene targets for putative chemical lures of this pest, we performed Illumina Hiseq 2000 sequencing of the transcriptome of adult male and female antennae samples.

MATERIALS AND METHODS

Insect Rearing and Tissue Collection

Scolytus schevyrewi larvae were reared on the branches of their host plants (Armeniaca vulgaris) collected from Baren County, Xinjiang province, China (39.0°N, 75.8°E) and maintained in the lab under the following conditions of 26.5°C, a cycle of 14-h light:10-h dark, and 65% relative humidity. Pupae were placed on a branch and the emerged adults were collected every day. Two-day-old adults were used to collect male and female antennae, heads (without antennae), thorax, abdomen, legs, and wings using the fine-tip forceps, immediately frozen in liquid nitrogen and stored at−80°C until RNA isolation.

RNA Extraction

Total RNA from different tissues of *S. schevyrewi* was obtained using TRIzol reagent (Invitrogen, Carlsbad, California, USA) following the instruction of manufacturer. The total RNA from each pair of antennae, legs, and wings were separately obtained from each adult, totaling 300 males and 300 females. Heads (without antennae), thoraxes, and abdomens were separately collected from 20 to 30 adult males and 20 to 30 females. Total RNA was dissolved in RNase-free water, and RNA integrity was verified by gel electrophoresis. RNA concentration and purity were determined on the Nanodrop ND-2000 spectrophotometer (NanoDrop products, Wilmington, DE, USA).

cDNA Library Construction and Sequencing

A total of 1 μg of total RNA of each sample of male and female antennae were used to construct two separate cDNA libraries, one for each sex. Paired-end reads of 100 bp were sequenced using the Illumina HiSeq 2000 platform to obtain library-sequencing information at Beijing Genome Institute (Shenzhen, China). The detailed protocols for cDNA library construction and sequencing applied have been described in the previous studies (Cao et al., 2014; Zhang et al., 2015). The raw data were uploaded to the NCBI SRA database (Accession: PRJNA732801, https://www.ncbi.nlm.nih.gov/sra).

Assembly

Low-quality reads were filtered out, low-quality nucleotides at each end were trimmed, and 3′ adaptors and poly-A/T

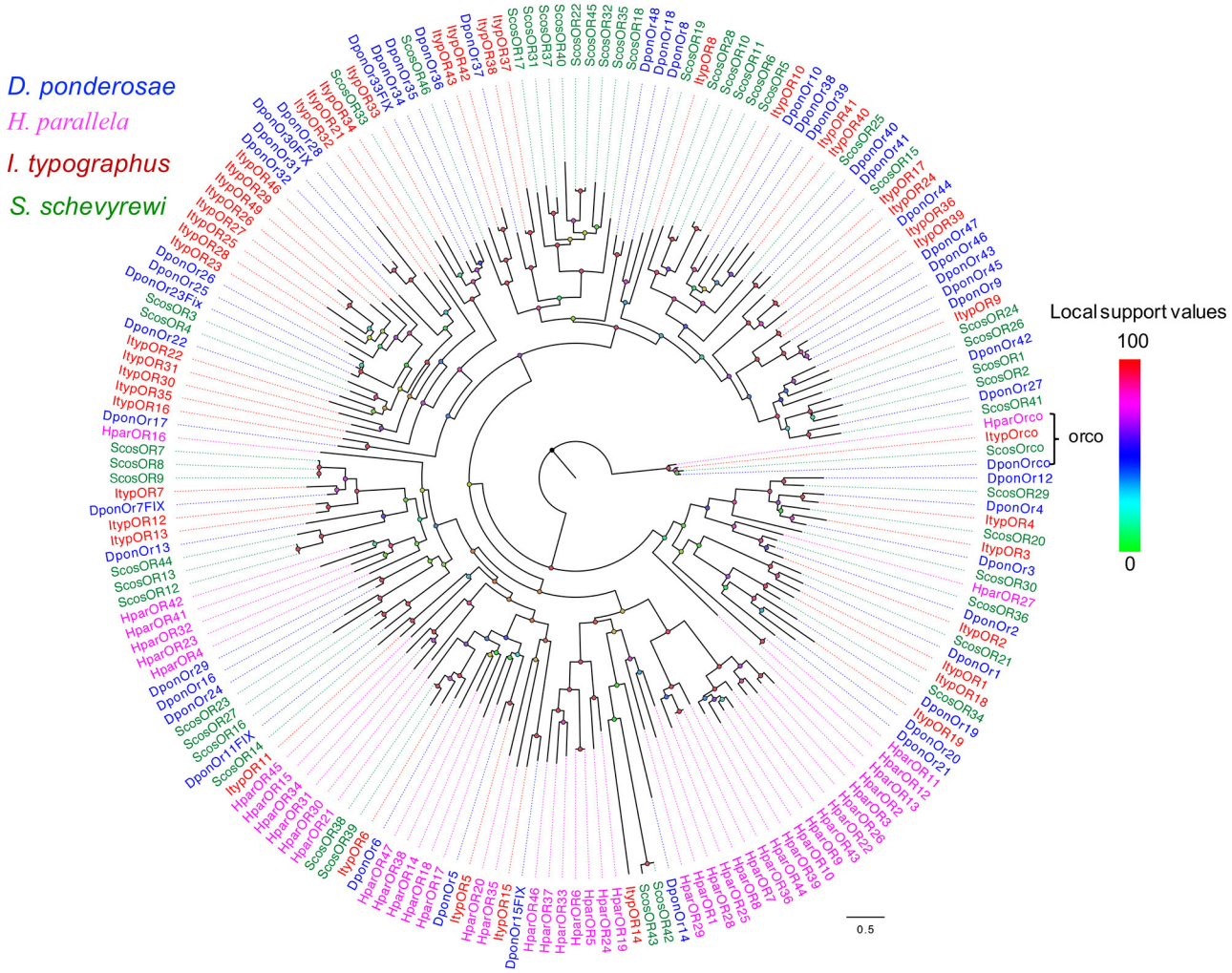

FIGURE 1 | Phylogenetic tree of candidate ScosORs with known Coleoptera odorant receptors sequences. Dpon, *D. ponderosae*; Hpar, *H. parallela*; Ityp, *I. typographus*; Scos, *S. schevyrewi*.

were removed from the raw reads to generate the clean reads. Subsequently, the clean reads were used to form a *de novo* assembly using the Trinity platform (v2.1.0) with default parameters (Grabherr et al., 2011). The Trinity outputs were then clustered by TIGR gene indices clustering tools (TGICL) to generate the final unigene dataset (Pertea et al., 2003).

Identification of Olfactory Genes

Unigenes were annotated using blastx against NCBI nonredundant (nr) sequences with e <1e^{-5}. The blast results were then imported into the Blast2Go (version 3.1) with default parameters (Conesa et al., 2005). OR, IR, OBP, and CSP genes of the candidates were selected according to the nr sequence annotation results in the remote server from the lab. All candidate olfactory genes were manually checked using the blastx program against the nr sequence database. The open-reading frames (ORFs) of the putative olfactory genes were predicted using the ExPASy (Expert Protein Analysis System) translate tool (https://web.expasy.org/translate/). The TMDs of ORs and IRs were predicted using TMHMM server version 2.0 (http://www.cbs.dtu.dk/services/TMHMM). Putative N-terminal signal peptides of OBPs and CSPs were predicted using the SignalP 4.0 server (http://www.cbs.dtu.dk/services/SignalP-4.0/) with default parameters.

Phylogenetic Analysis

Olfactory genes from *S. schevyrewi, Ips typographus, Dendroctonus ponderosae* (Andersson et al., 2013), and *Holotrichia parallela* (Yi et al., 2018) were selected for the phylogenetic analysis. Sequence information was listed in **Supplementary Table 2**. Amino acid sequences were aligned by MAFFT (https://www.ebi.ac.uk/Tools/msa/mafft/). Phylogenetic trees of olfactory genes were constructed using RAxML version 8 with the Jones-Taylor-Thornton amino acid substitution model. Node support was assessed using a bootstrap method based on

TABLE 1 | Unigenes of candidate odorant receptors.

Unigene reference	Gene name	Length (bp)	ORF(aa)	Blastx best hit (Reference/Name/Species)	*E*-value	Full length	TMD
CL839.Contig1_All	ScosOR1	735	244	XP_019765879.1 PREDICTED: odorant receptor 94a-like [Dendroctonus ponderosae]	1.00E-129	No	3
CL839.Contig2_All	ScosOR2	1,143	380	XP_019765879.1 PREDICTED: odorant receptor 94a-like [Dendroctonus ponderosae]	2.00E-144	Yes	6
CL1001.Contig1_All	ScosOR3	1,251	416	XP_019754377.1 PREDICTED: putative odorant receptor 92a [Dendroctonus ponderosae]	5.00E-92	No	6
CL1001.Contig2_All	ScosOR4	1,365	454	XP_019762540.1 PREDICTED: odorant receptor 49b-like [Dendroctonus ponderosae]	4.00E-92	No	7
CL1025.Contig1_All	ScosOR5	1,173	390	XP_019765587.1 PREDICTED: odorant receptor Or2-like [Dendroctonus ponderosae]	5.00E-57	No	5
CL1025.Contig2_All	ScosOR6	996	331	XP_019765587.1 PREDICTED: odorant receptor Or2-like [Dendroctonus ponderosae]	3.00E-45	No	4
CL1127.Contig1_All	ScosOR7	1,131	376	XP_019762033.1 PREDICTED: odorant receptor 4-like isoform X2 [Dendroctonus ponderosae]	4.00E-133	Yes	5
CL1127.Contig2_All	ScosOR8	1,155	384	XP_019762033.1 PREDICTED: odorant receptor 4-like isoform X2 [Dendroctonus ponderosae]	2.00E-144	Yes	6
CL1127.Contig4_All	ScosOR9	1,149	382	XP_019762033.1 PREDICTED: odorant receptor 4-like isoform X2 [Dendroctonus ponderosae]	5.00E-144	Yes	6
CL1283.Contig1_All	ScosOR10	1,188	395	XP_019755291.1 PREDICTED: odorant receptor 47b-like [Dendroctonus ponderosae]	4.00E-63	No	4
CL1283.Contig2_All	ScosOR11	774	257	AKK25156.1 odorant receptor 15 [Dendroctonus ponderosae]	3.00E-64	No	4
CL1562.Contig1_All	ScosOR12	891	296	XP_018564120.1 PREDICTED: odorant receptor 85b-like [Anoplophora glabripennis]	6.00E-19	No	6
CL1562.Contig2_All	ScosOR13	1,156	384	XP_018564120.1 PREDICTED: odorant receptor 85b-like [Anoplophora glabripennis]	2.00E-33	No	7
CL2075.Contig3_All	ScosOR14	1,455	484	ALR72569.1 odorant receptor OR26 [Colaphellus bowringi]	2.00E-57	No	7
CL2243.Contig2_All	ScosOR15	1,191	396	XP_019754447.1 PREDICTED: odorant receptor 49b-like [Dendroctonus ponderosae]	9.00E-59	No	7
CL2311.Contig1_All	ScosOR16	1,137	378	XP_019770928.1 PREDICTED: odorant receptor 94a-like [Dendroctonus ponderosae]	6.00E-127	Yes	7
CL2593.Contig1_All	ScosOR17	1,173	390	AKK25156.1 odorant receptor 15 [Dendroctonus ponderosae]	1.00E-20	No	5
CL2643.Contig2_All	ScosOR18	1,176	391	XP_019874691.1 PREDICTED: odorant receptor 67c-like [Aethina tumida]	3.00E-27	No	6
CL2759.Contig1_All	ScosOR19	377	125	XP_019768086.1 PREDICTED: odorant receptor Or2-like [Dendroctonus ponderosae]	1.00E-29	No	2
CL2885.Contig1_All	ScosOR20	1,206	401	XP_019771895.1 PREDICTED: odorant receptor 67c-like, partial [Dendroctonus ponderosae]	3.00E-106	Yes	7
CL3312.Contig1_All	ScosOR21	1,176	391	XP_018567969.1 PREDICTED: odorant receptor Or2-like [Anoplophora glabripennis]	4.00E-54	Yes	6
Unigene7_All	ScosOR22	1,179	392	XP_019772797.1 PREDICTED: odorant receptor Or2-like [Dendroctonus ponderosae]	3.00E-18	No	7
Unigene529_All	ScosOR23	367	122	AKK25157.1 odorant receptor 17, partial [Dendroctonus ponderosae]	6.00E-15	No	2
Unigene2373_All	ScosOR24	1,167	388	XP_019761187.1 PREDICTED: odorant receptor Or2-like [Dendroctonus ponderosae]	8.00E-75	Yes	4
Unigene2403_All	ScosOR25	1,179	424	XP_019753281.1 PREDICTED: odorant receptor 47b-like [Dendroctonus ponderosae]	5.00E-92	Yes	6
Unigene3424_All	ScosOR26	1,170	389	XP_019761187.1 PREDICTED: odorant receptor Or2-like [Dendroctonus ponderosae]	4.00E-199	Yes	6
Unigene3466_All	ScosOR27	1,134	377	XP_019770928.1 PREDICTED: odorant receptor 94a-like [Dendroctonus ponderosae]	1.00E-138	No	7
Unigene3624_All	ScosOR28	1,179	392	AKK25156.1 odorant receptor 15 [Dendroctonus ponderosae]	9.00E-72	No	5

(Continued)

TABLE 1 | Continued

Unigene reference	Gene name	Length (bp)	ORF(aa)	Blastx best hit (Reference/Name/Species)	*E*-value	Full length	TMD
Unigene3644_All	ScosOR29	1,176	391	XP_019756949.1 PREDICTED: odorant receptor 67c-like isoform X2 [Dendroctonus ponderosae]	3.00E-119	Yes	7
Unigene4009_All	ScosOR30	1,185	394	XP_018571501.1 PREDICTED: odorant receptor 67c-like [Anoplophora glabripennis]	1.00E-49	No	6
Unigene6079_All	ScosOR31	1,122	373	XP_019765855.1 PREDICTED: odorant receptor 49b-like [Dendroctonus ponderosae]	1.00E-23	No	3
Unigene7306_All	ScosOR32	1,188	395	XP_019765855.1 PREDICTED: odorant receptor 49b-like [Dendroctonus ponderosae]	1.00E-26	No	6
Unigene8744_All	ScosOR33	372	123	XP_019771464.1 PREDICTED: odorant receptor 46a-like isoform X3 [Dendroctonus	3.00E-31	No	0
Unigene9796_All	ScosOR34	1,160	385	XP_019755672.1 PREDICTED: odorant receptor 4 [Dendroctonus ponderosae]	7.00E-133	Yes	6
Unigene10776_All	ScosOR35	1,158	385	XP_019759347.1 PREDICTED: odorant receptor 30a-like [Dendroctonus ponderosae]	8.00E-24	No	6
Unigene12156_All	ScosOrco	1,467	488	AOO35283.1 olfactory co-receptor [Rhynchophorus ferrugineus]	0.00E+00	Yes	7
Unigene12163_All	ScosOR36	1,184	393	XP_015836240.1 PREDICTED: odorant receptor 49b [Tribolium castaneum]	1.00E-114	No	6
Unigene12204_All	ScosOR37	1,134	378	XP_019874691.1 PREDICTED: odorant receptor 67c-like [Aethina tumida]	2.00E-24	No	5
CL90.Contig6_All	ScosOR38	1,236	411	XP_019768012.1 PREDICTED: odorant receptor 83a-like isoform X2 [Dendroctonus ponderosae]	2.00E-170	No	6
CL90.Contig22_All	ScosOR39	927	308	XP_019768012.1 PREDICTED: odorant receptor 83a-like isoform X2 [Dendroctonus]	7.00E-82	No	2
CL90.Contig22_All	ScosOR39	927	308	XP_019768012.1 PREDICTED: odorant receptor 83a-like isoform X2 [Dendroctonus]	7.00E-82	No	2
Unigene17267_All	ScosOR40	1,041	346	AKK25154.1 odorant receptor 7, partial [Dendroctonus ponderosae]	9.00E-08	No	2
Unigene18514_All	ScosOR41	370	123	XP_019765855.1 PREDICTED: odorant receptor 49b-like [Dendroctonus ponderosae]	1.00E-37	No	1
CL110.Contig4_All	ScosOR42	900	299	EFA01416.1 odorant receptor 283 [Tribolium castaneum]	1.00E-06	No	4
CL110.Contig8_All	ScosOR43	825	273	EFA01423.1 odorant receptor 293 [Tribolium castaneum]	4.60E+00	No	4
CL548.Contig1_All	ScosOR44	1,161	386	XP_015837918.1 PREDICTED: putative odorant receptor 85d [Tribolium castaneum]	7.00E-26	No	7
CL584.Contig4_All	ScosOR45	1,179	392	XP_019772797.1 PREDICTED: odorant receptor Or2-like [Dendroctonus ponderosae]	2.00E-18	No	8
CL733.Contig1_All	ScosOR46	1,176	391	XP_019765855.1 PREDICTED: odorant receptor 49b-like [Dendroctonus ponderosae]	6.00E-25	No	4

1,000 replicates. The trees were visualized, and color-coded in FigTree 1.4.3. For ORs, the tree was rooted in the Orco lineage.

Expression Analysis of the Candidate OBPs and CSPs by Semiquantitative Reverse Transcription PCR (RT-PCR)

Reverse transcription-PCR was performed to verify the expression patterns of OBPs and CSPs of *S. schevyrewi*. Total RNA from male and female antennae, heads (without antennae), thoraxes, legs, abdomens, and wings were used to synthesize cDNA by RevertAid First Strand cDNA Synthesis Kit (Thermo Scientific, Waltham, MA, USA). Gene-specific primers were designed using Primer 5 and synthesized by Sangon Biotech Co., Ltd. (Shanghai, China) (**Supplementary Table 1**). PCR was performed with the Veriti Thermal Cycler (Applied Biosystems, Carlsbad, CA, USA) under the following conditions: 95°C for 3 min, 25 cycles at 95°C for 30 s, 55°C for 30 s, 72°C for 30 s, and 72°C for 10 min. PCR amplification products were run on a 2% agarose gel. Because it is difficult to acquire massive amounts of RNA from antennae samples of *S. schevyrewi*, only two technical repeats were performed for each gene. Uncropped gel images were uploaded as supplements (**Supplementary Figure 2**).

RESULTS

Transcriptome Assembly

The transcriptomes of male and female *S. schevyrewi* antennae were separately sequenced by the Illumina HiSeq 2000 platform.

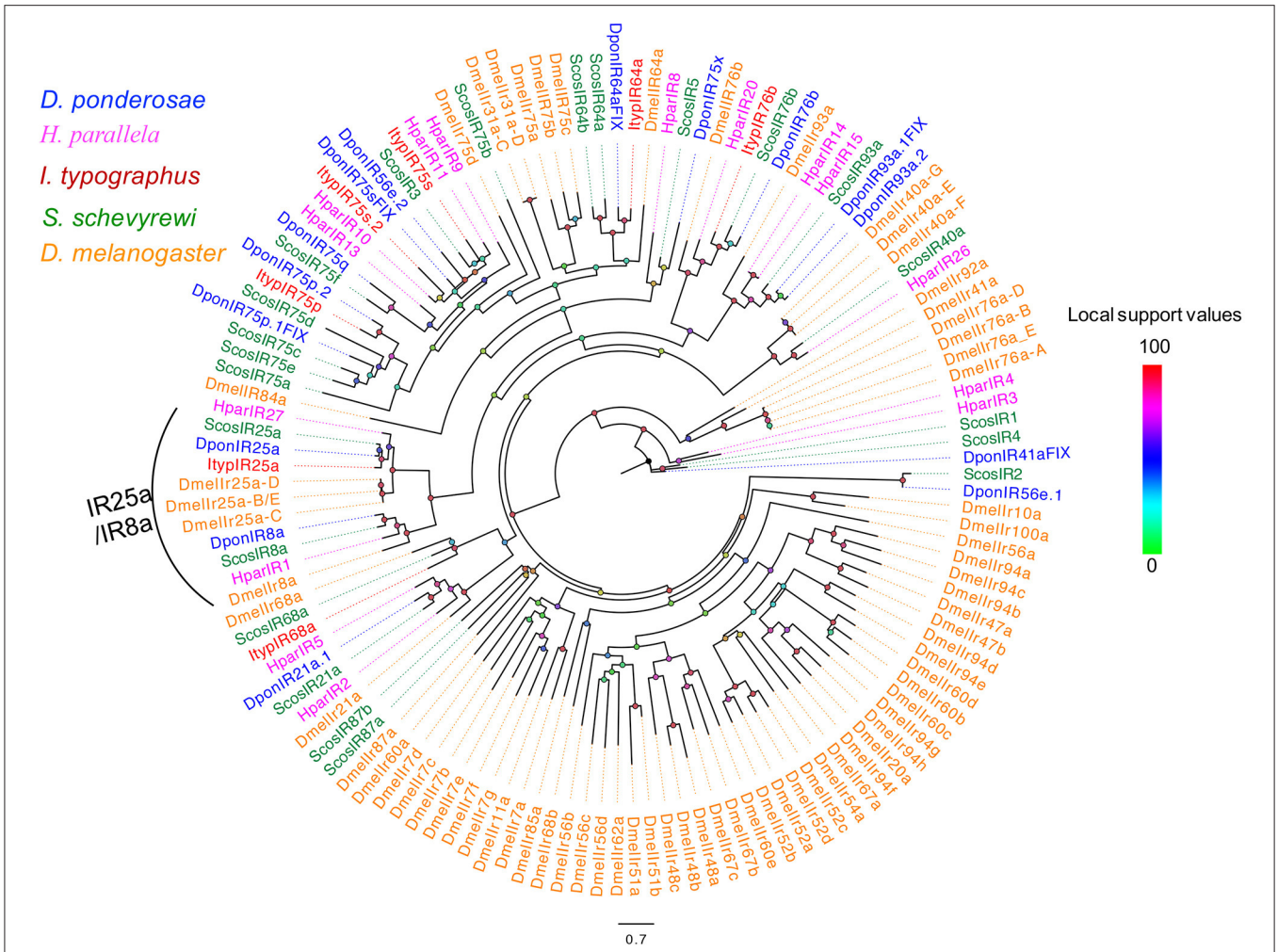

FIGURE 2 | Phylogenetic tree of candidate ScosIRs with ionotropic receptor sequences from other insects. Tcas, *T. castaneum*; Dpon, *D. ponderosae*; Hpar, *H. parallela*; Ityp, *I. typographus*; Dmel, *D. melanogaster*; Scos, *S. schevyrewi*.

Then after filtering, 26,804,894 and 29,176,485 clean reads with 98.60 and 98.55% Q20 scores were generated for male and female samples, respectively. The clean reads were assembled subsequently and generated 40,666 and 36,216 unigenes, respectively. After merging and clustering, a final transcript dataset was revealed with 34,098 unigenes consisting of 14,071 clusters and 20,027 distinct singletons. The dataset was 46.7∼57.4 Mb in size and with unigenes having a mean length of 1,684 bp and N50 of 3,179 bp.

Gene Identification and Functional Annotation

The functional annotations of the unigenes were performed mainly based on the blastx results against the nr sequence database. We matched 22,815 (66.9%) unigenes to known proteins by blastx. Among those annotated genes, 16,725 (73.3%) unigenes showed strong homology (*e*-values lower than $1e^{-45}$), while 6,090 (26.7%) unigenes showed poor matches with *e*-values between $1e^{-15}$ and $1e^{-5}$. The similarity analysis showed that 11,514 (50.5%) unigenes had more than 60% similarity with known proteins. Most of the annotated unigenes were matched to *Tribolium castaneum* (67.3%), followed by *D. ponderosae* (13.7%) and others species (19.0%).

Gene ontology (GO) annotations of the entire set of unigenes were performed using the Blast2GO pipeline based on the blastx searches against nr sequences. A total of 12,720 unigenes were assigned various GO terms. In the molecular function category, genes involved in the binding activity and catalytic activity were most abundant. In the cellular component category, genes involved in cell, cell part, macromolecular, membrane, organelle, and organelle part were enriched. In the biological process category, genes involved in the cellular process, metabolic process and single-organism process were the most represented.

Identification of Candidate Odorant Receptors

The candidate ORs were identified by keyword search of the blastx annotations. We identified 47 putative OR genes. Thirteen

TABLE 2 | Unigene of candidate ionotropic receptors.

Unigene reference	Gene name	Length (bp)	ORF(aa)	Blastx best hit (Reference/Name/Species)	*E*-value	Full length	TMD
Unigene10667_All	ScosIR1	1,497	498	XP_019865961.1 PREDICTED: LOW QUALITY PROTEIN: glutamate receptor 2-like [Aethina tumida]	4.00E-102	No	2
CL3060.Contig1_All	ScosIR2	927	308	ABD36125.1 glutamate receptor Gr2 [Bombyx mori]	2.00E-101	No	7
CL146.Contig15_All	ScosIR3	1,836	611	ALR72541.1 ionotropic receptor IR2 [Colaphellus bowringi]	5.00E-172	No	5
Unigene2622_All	ScosIR4	1,803	600	XP_019865961.1 PREDICTED: LOW QUALITY PROTEIN: glutamate receptor 2-like [Aethina tumida]	5.00E-108	No	4
Unigene14518_All	ScosIR5	319	106	XP_018563257.1 PREDICTED: glutamate receptor ionotropic, NMDA 2D-like [Anoplophora glabripennis]	5.00E-62	No	1
CL296.Contig4_All	ScosIR8a	2,649	882	XP_019770830.1 PREDICTED: ionotropic receptor 25a [Dendroctonus ponderosae]	0.00E+00	No	3
Unigene4531_All	ScosIR21a	2,370	789	XP_019753472.1 PREDICTED: ionotropic receptor 21a [Dendroctonus ponderosae]	0.00E+00	No	3
CL3341.Contig1_All	ScosIR25a	2,796	931	XP_019763174.1 PREDICTED: ionotropic receptor 25a [Dendroctonus ponderosae]	0	No	3
Unigene6808_All	ScosIR40a	539	179	XP_019764671.1 PREDICTED: glutamate receptor ionotropic, delta-2-like [Dendroctonus ponderosae]	2.00E-97	No	0
CL16.Contig22_All	ScosIR64a	1,860	619	XP_019770931.1 PREDICTED: glutamate receptor-like [Dendroctonus ponderosae]	5.00E-164	No	3
Unigene8833_All	ScosIR64b	1,863	620	XP_019770931.1 PREDICTED: glutamate receptor-like [Dendroctonus ponderosae]	7.00E-173	No	0
Unigene11157_All	ScosIR68a	357	118	XP_015839172.1 PREDICTED: glutamate receptor ionotropic, kainate 5 [Tribolium castaneum]	1.00E-27	No	1
Unigene5334_All	ScosIR75a	540	180	XP_021192228.1 glutamate receptor ionotropic, delta-1-like isoform X2 [Helicoverpa armigera]	1.00E-22	No	3
Unigene11324_All	ScosIR75b	1,533	510	XP_015836653.1 PREDICTED: glutamate receptor 2-like [Tribolium castaneum]	2.00E-72	No	4
CL266.Contig1_All	ScosIR75c	1,854	617	AKC58589.1 chemosensory ionotropic receptor 75q, partial [Anomala corpulenta]	3.00E-85	No	3
Unigene2679_All	ScosIR75d	390	129	APC94258.1 ionotropic receptor 2, partial [Pyrrhalta maculicollis]	6.00E-06	No	1
Unigene6978_All	ScosIR75e	1,893	630	XP_018572783.1 PREDICTED: glutamate receptor 1-like [Anoplophora glabripennis]	4.00E-77	No	3
CL1275.Contig2_All	ScosIR75f	1,626	541	XP_018572783.1 PREDICTED: glutamate receptor 1-like [Anoplophora glabripennis]	4.00E-92	No	3
Unigene11968_All	ScosIR76b	1,668	555	XP_019762016.1 PREDICTED: LOW QUALITY PROTEIN: glutamate receptor ionotropic, kainate 1-like [Dendroctonus ponderosae]	0.00E+00	Yes	5
Unigene2912_All	ScosIR87a	352	117	XP_017770100.1 PREDICTED: glutamate receptor ionotropic, NMDA 2B-like isoform [Nicrophorus vespilloides]	1.00E-101	No	0
Unigene1422_All	ScosIR87b	1,848	615	OWR45511.1 putative chemosensory ionotropic receptor IR68a [Danaus plexippus]	2.00E-054	No	5
Unigene874_All	ScosIR93a	2,598	865	XP_018576793.1 PREDICTED: glutamate receptor ionotropic, delta-1 isoform X2	0.00E+00	No	1

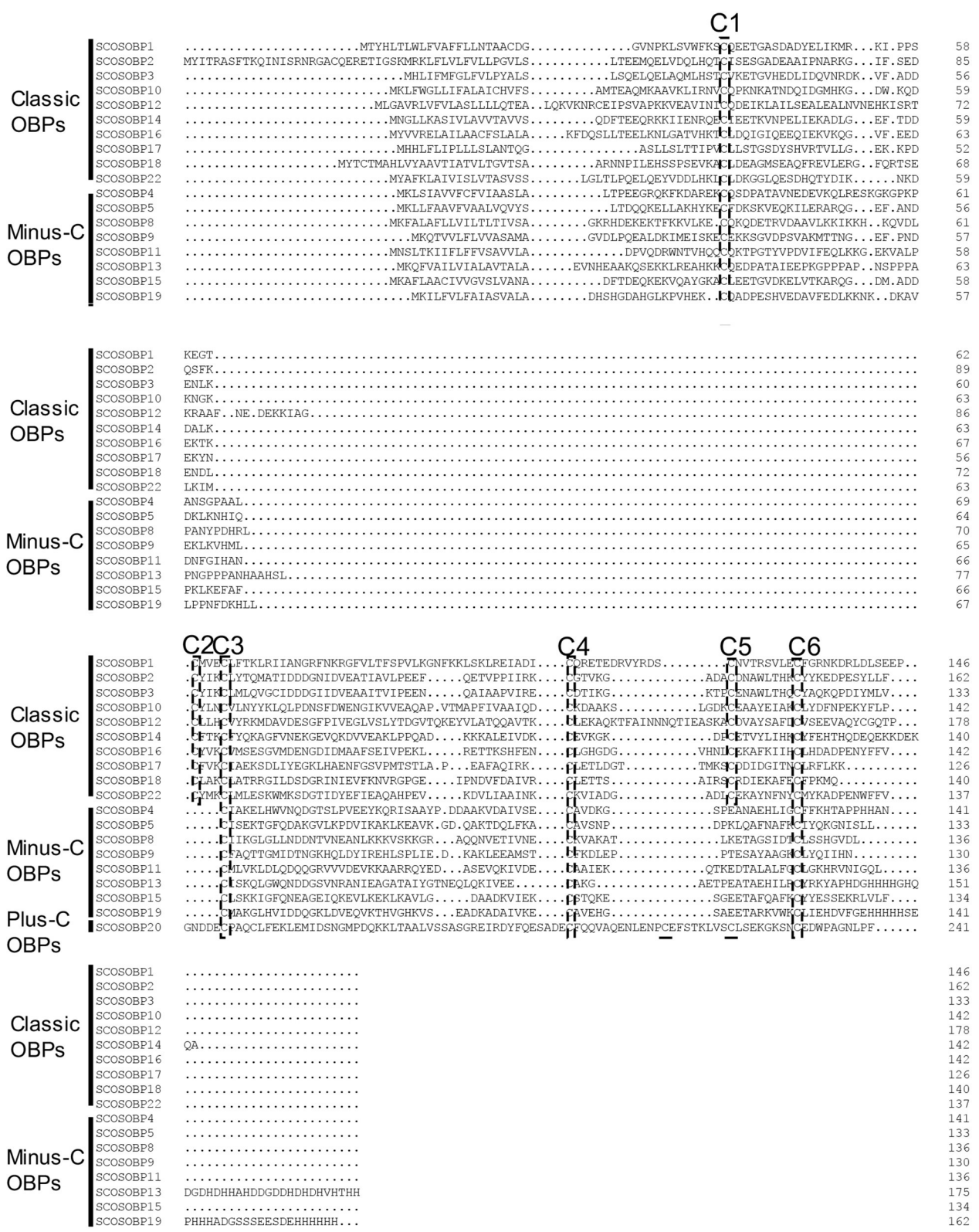

FIGURE 3 | Sequence alignment of candidate ScosOBPs. The six conserved cysteine residues are marked as C1–C6.

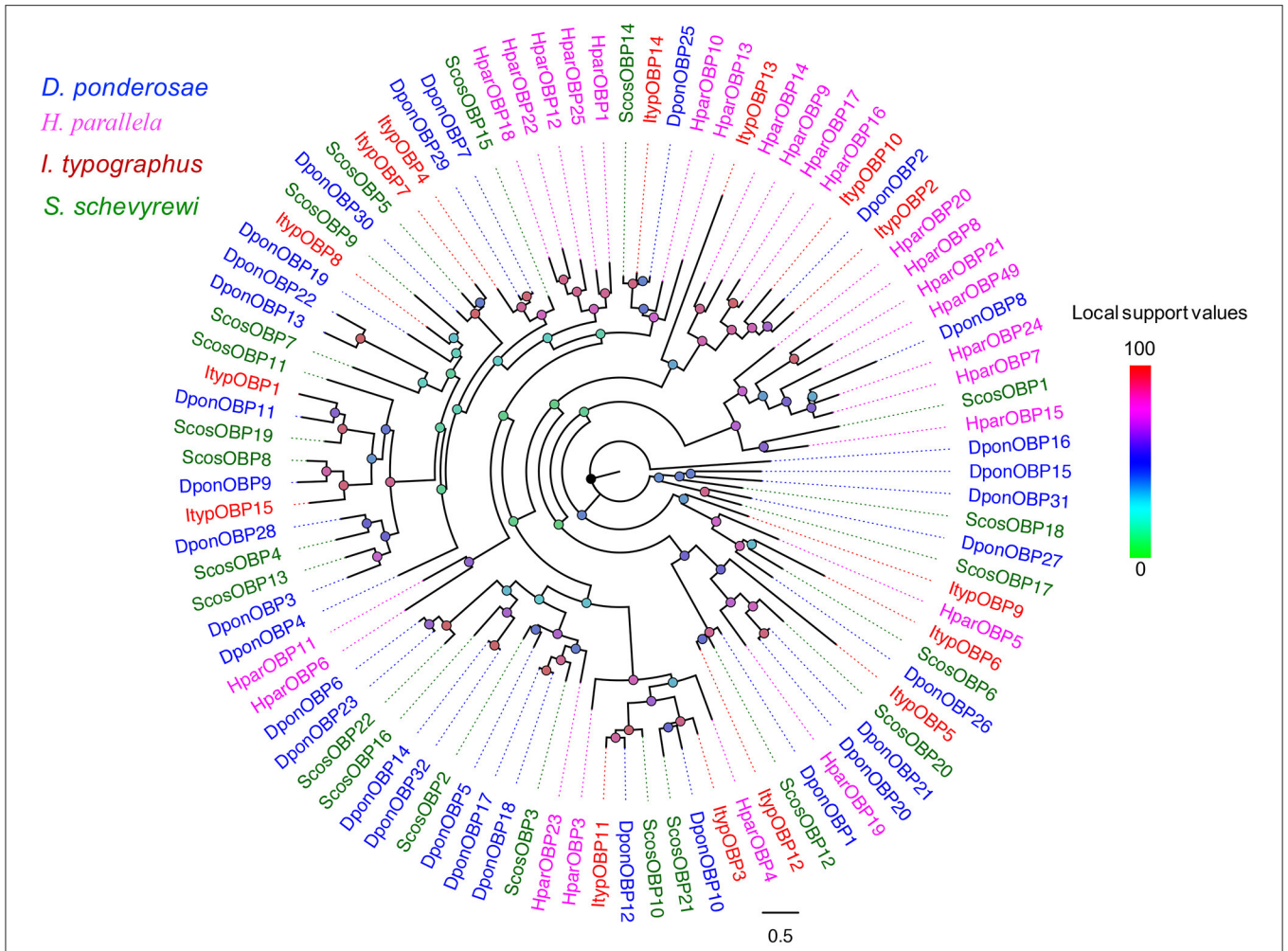

FIGURE 4 | Phylogenetic tree of candidate ScosOBPs with known Coleoptera odorant-binding proteins sequences. Tcas, *T. castaneum*; Dpon, *D. ponderosae*; Hpar, *H. parallela*; Ityp, *I. typographus*; Scos, *S. schevyrewi*.

of them were full-length putative OR genes ranging from 1,100 to 1,400 bp with complete ORFs and 5 to 7 TMDs, which are characteristics of typical insect ORs. This includes the full-length ScosOrco gene encoding 488 amino acids. Seven of the predicted incomplete ORs were shorter in length and contained a deduced protein longer than 300 amino acids. Four of the predicted incomplete ORs were even shorter than 200 amino acids.

The blastx results indicated that the identities of the most predicted ORs shared with known insect ORs were very low, ranging from 24 to 49%. Nine predicted ORs (ScosOR1, ScosOR27, ScosOR7, ScosOR38, ScosOR39, ScosOR2, ScosOR8, ScosOR9, and ScosOR34) had greater identity (52–62%) with the OR from *D. ponderosae*. ScosOrco had 88% identity with the Orco from *Rhynchophorus ferrugineus*. Phylogenetic analysis was performed with ORs from *D. ponderosae*, *I. typographus*, *H. parallela*, and *S. schevyrewi* (**Figure 1**). A branch for Orco was identified in the phylogenetic tree. Two expanded branches in this species relative to others in the comparison were also identified. One branch consisted of ScosOR5, ScosOR6, ScosOR10, ScosOR11, ScosOR25, and ScosOR28 and the other consisted of ScosOR17, ScosOR18, Scos22, Scos31, Scos32, Scos37, Scos40, and Scos45. Most of the branches in the tree were supported by high-local support values and few branches were not reliable.

Information on unigene reference, length, and best blastx hit of all 47 ORs are listed in **Table 1**.

Identification of Candidate Ionotropic Receptors

Bioinformatics analysis identified 22 putative IRs in the *S. schevyrewi* transcriptome. Only ScosIR76b was a full-length sequence with 555 amino acids and five TMDs; the other IRs were incomplete due to the lack of the 5′ or 3′ terminus.

The blastx results showed that more than half of the predicted IRs (ScosIR1, ScosIR75a, ScosIR75b, ScosIR75c,

TABLE 3 | Unigene of candidate odorant binding proteins.

Unigene reference	Genename	Length (bp)	ORF(aa)	Blastx best hit	*E*-value	Full length	Signal peptide
CL1164.Contig1_All	ScosOBP1	441	146	ALR72497.1 odorant binding protein 9 [Colaphellus bowringi]	6.00E-24	No	Yes
CL2073.Contig1_All	ScosOBP2	489	162	AAQ96921.1 odorant-binding protein RpalOBP4', partial [Rhynchophorus palmarum]	6.00E-48	Yes	Yes
CL2693.Contig1_All	ScosOBP3	402	133	AKK25145.1 odorant binding protein 21 [Dendroctonus ponderosae]	4.00E-39	No	Yes
CL3244.Contig1_All	ScosOBP4	426	141	ALM64971.1 odorant binding protein 13 [Dendroctonus armandi]	2.00E-32	Yes	Yes
CL3634.Contig1_All	ScosOBP5	402	133	ALM64972.1 odorant binding protein 14 [Dendroctonus armandi]	9.00E-44	No	Yes
CL3848.Contig1_All	ScosOBP6	489	162	APG79364.1 pheromone binding protein 3 [Cyrtotrachelus buqueti]	1.00E-27	No	Yes
Unigene1743_All	ScosOBP7	358	119	ARU83754.1 odorant binding protein 3 [Anoplophora glabripennis]	9.00E-09	No	Yes
Unigene1760_All	ScosOBP8	411	136	AGI05185.1 odorant-binding protein 9 [Dendroctonus ponderosae]	2.00E-42	Yes	Yes
Unigene1792_All	ScosOBP9	393	130	AQY18983.1 odorant-binding protein [Galeruca daurica]	8.00E-18	Yes	Yes
Unigene4680_All	ScosOBP10	429	142	AKK25140.1 odorant binding protein 16 [Dendroctonus ponderosae]	3.00E-64	Yes	Yes
Unigene5401_All	ScosOBP11	411	136	AKK25135.1 odorant binding protein 9, partial [Dendroctonus ponderosae]	8.00E-44	Yes	Yes
Unigene6017_All	ScosOBP12	537	178	ARH65471.1 odorant binding protein 16 [Anoplophora glabripennis]	9.00E-69	No	Yes
Unigene7865_All	ScosOBP13	531	176	AMK48596.1 odorant-binding protein, partial [Rhynchophorus ferrugineus]	7.00E-24	No	Yes
Unigene9055_All	ScosOBP14	429	142	AHE13793.1 odorant binding protein [Lissorhoptrus oryzophilus]	2.00E-75	Yes	Yes
Unigene9643_All	ScosOBP15	405	134	AHE13799.1 odorant binding protein [Lissorhoptrus oryzophilus]	9.00E-40	Yes	Yes
Unigene9992_All	ScosOBP16	429	142	AHE13800.1 odorant binding protein, partial [Lissorhoptrus oryzophilus]	6.00E-50	Yes	Yes
Unigene10379_All	ScosOBP17	381	126	ALM64968.1 odorant binding protein 6 [Dendroctonus armandi]	7.00E-22	No	Yes
Unigene11422_All	ScosOBP18	423	140	ALM64970.1 odorant binding protein 8 [Dendroctonus armandi]	3.00E-09	No	Yes
Unigene11547_All	ScosOBP19	489	162	AGI05181.1 odorant-binding protein 11 [Dendroctonus ponderosae]	1.00E-18	Yes	Yes
Unigene12124_All	ScosOBP20	726	241	AGI05159.1 odorant-binding protein 21 [Dendroctonus ponderosae]	1.00E-43	Yes	Yes
Unigene17771_All	ScosOBP21	242	80	ANE37553.1 odorant binding protein 9 [Rhynchophorus ferrugineus]	1.00E-24	No	Yes
CL142.Contig2_All	ScosOBP22	414	137	AFI45061.1 odorant-binding protein [Dendroctonus ponderosae]	8.00E-60	Yes	Yes

ScosIR75d, ScosIR75e, ScosIR75f, ScosIR3, ScosIR4, ScosIR64a, ScosIR64b, and ScosIR87b) shared low identity (24–49%) with known insect IRs. A total of 10 predicted IRs (ScosIR68a, ScosIR93a, ScosIR76b, ScosIR2, ScosIR21a, ScosIR8a, ScosIR40a, ScosIR87a, ScosIR25a, and ScosIR5) had greater identity (54–95%) with known insect IRs, most of which were from *D. ponderosae*. Candidate genes with high identity (87%) to DponIR25a were deemed IR 25a homologs. A phylogenetic tree was constructed based on the IR sequences from *D. ponderosae*, *I. typographus*, *H. parallela*, and *S. schevyrewi* (**Figure 2**). ScosIR8a and ScosIR25a were identified as putative IR8a and IR25a homlogs due to the IR8a/IR25a branch.

Information on unigene reference, length, and best blastx hit of all 22 IRs are listed in **Table 2**.

Identification of Odorant-Binding Proteins

In the *S. schevyrewi* antennal transcriptome, 22 different sequences encoding putative OBPs were identified. More than half of them (ScosOBP2, ScosOBP4, ScosOBP8, ScosOBP9,

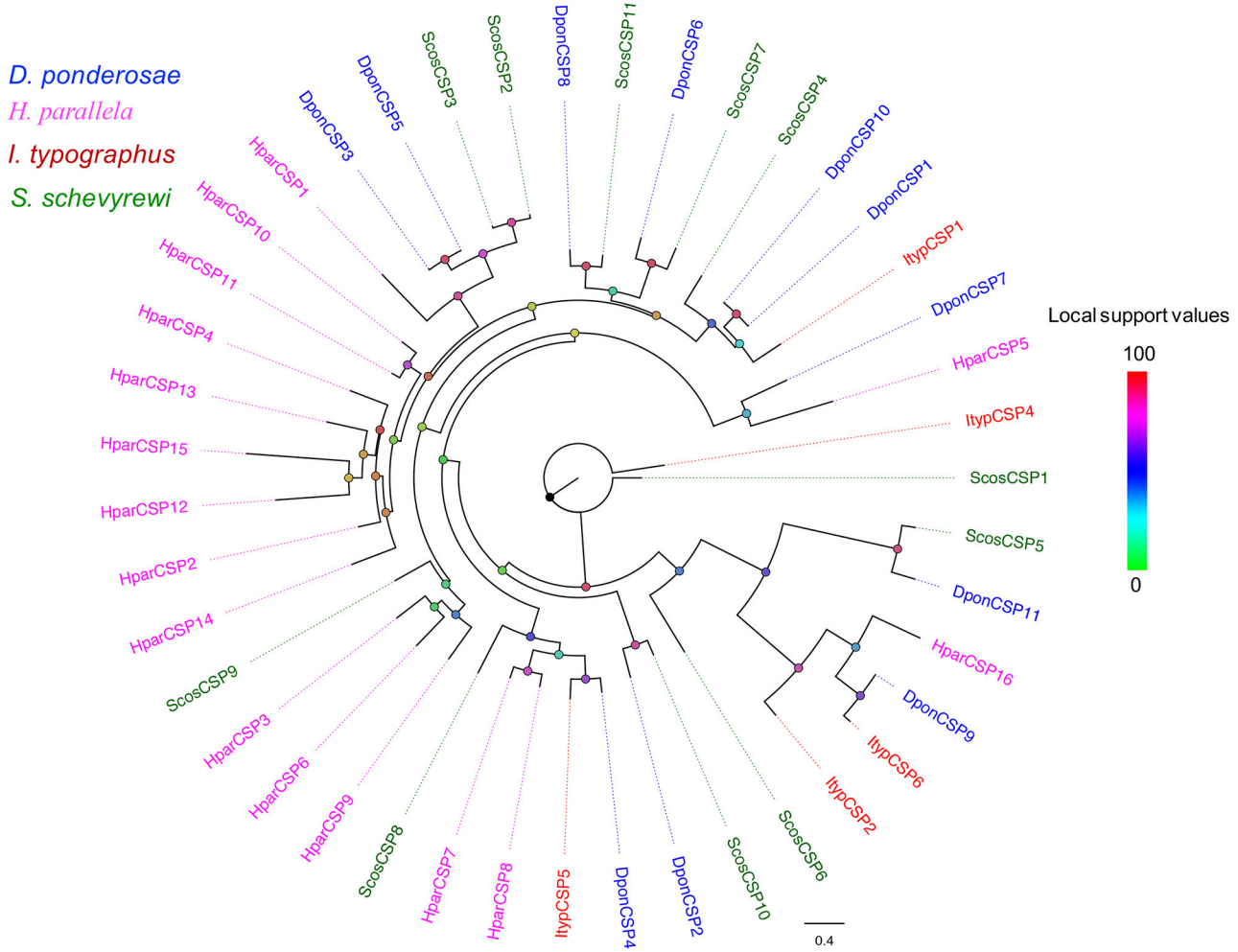

FIGURE 5 | Phylogenetic tree of candidate ScosCSPs with known Coleoptera chemosensory proteins sequences. Tcas, *T. castaneum*; Dpon, *D. ponderosae*; Hpar, *H. parallela*; Ityp, *I. typographus*; Scos, *S. schevyrewi*.

ScosOBP10, ScosOBP11, ScosOBP14, ScosOBP15, ScosOBP16, ScosOBP19, ScosOBP20, and ScosOBP22) were identified as full-length sequences. The lengths of all full-length ScosOPBs ranged from 130 to 241 amino acids.

Nearly, half of the predicted OBPs (ScosOBP7, ScosOBP18, ScosOBP9, ScosOBP1, ScosOBP20, ScosOBP19, ScosOBP17, ScosOBP4, ScosOBP4, ScosOBP6, and ScosOBP8) shared relatively low identity with known insect OBPs (31–49%). A total of 12 predicted OBPs (ScosOBP13, ScosOBP15, ScosOBP11, ScosOBP16, ScosOBP21, ScosOBP5, ScosOBP2, ScosOBP3, ScosOBP22, ScosOBP12, ScosOBP10, and ScosOBP14) had greater identity (51–83%) with known OBPs, a majority of which were *D. ponderosae* OBPs. Sequence alignment showed that 10 OBPs (ScosOBP1, 2, 3, 10, 12, 14, 16, 17, 18, and 22) matched in amino acid sequence to the sequence structure of classic OBPs, and eight OBPs (ScosOBP4, 5, 8, 9, 11, 13, 15, and 19) matched the sequence structure of Minus-C OBPs (**Figure 3**). Other OBPs were not analyzed by sequence alignment due to their limited sequence lengths. In the phylogenetic analysis of OBPs of different coleopterans, ScosOBPs were found across various branches and generally formed small subgroups together with OBPs from other coleopterans (**Figure 4**). No species-specific branch was discovered.

Information on unigene reference, length, and best blastx hit of all 22 OBPs are listed in **Table 3**.

Identification of Putative Chemosensory-Binding Proteins

A total of 11 putative CSPs were identified from the *S. schevyrewi* antennal transcriptome. Seven of them had full-length ORFs and nine of them had the predicted signal peptide. All of them shared the typical structure of a CSP except ScosCSP3 and ScosCSP10 because these two lacked the signal peptide.

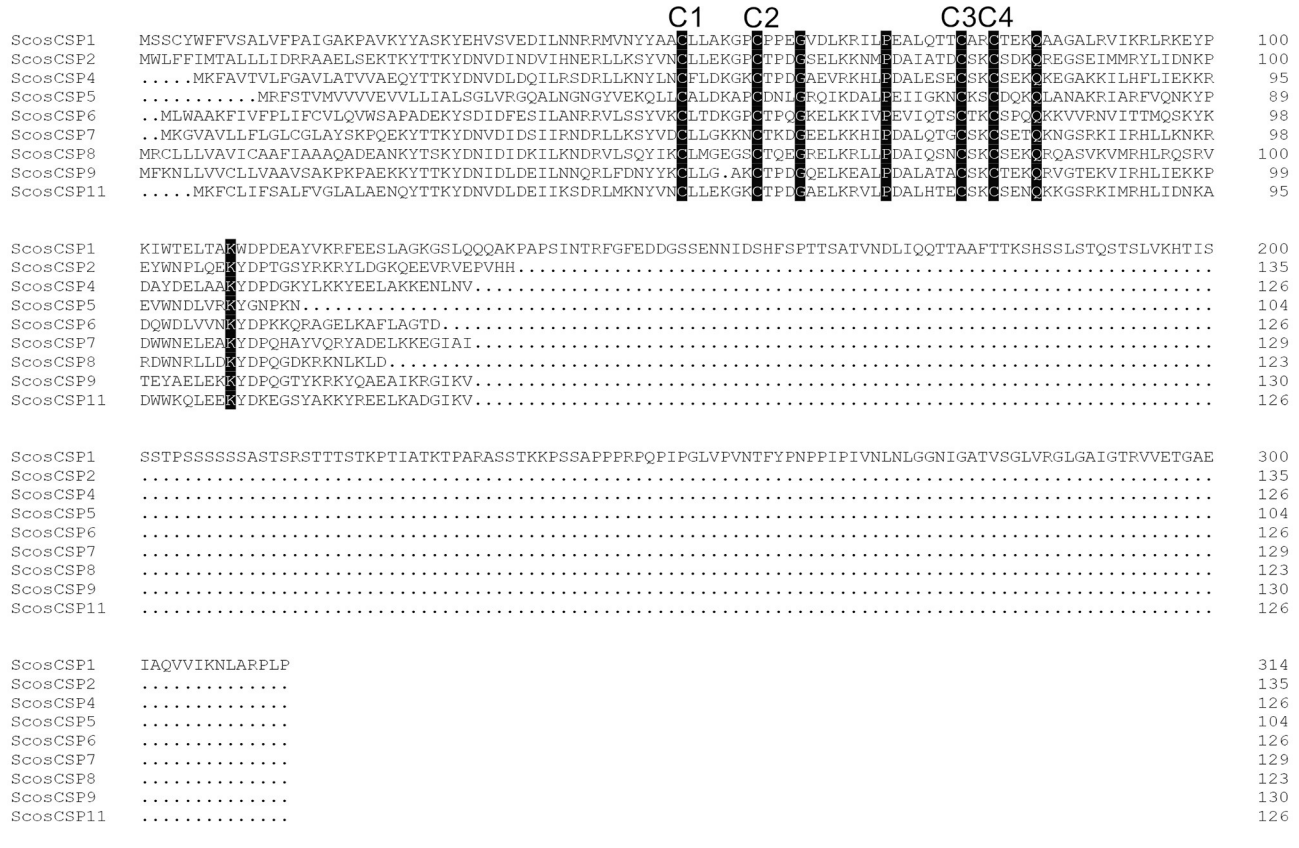

FIGURE 6 | Sequence alignment of candidate ScosCSPs. The four conserved cysteine residues are marked as C1–C4. Additional residues that conserved in this species were also marked.

All of the predicted CSPs shared relatively high identity (57–100%) with known insect CSPs. The phylogenetic analysis of the CSPs in different beetles showed that most of the ScosCSPs were clustered with orthologs of *D. ponderosae*, *I. typographus*, and *H. parallela* in a separate clade (**Figure 5**). Only ScosCSP2 and ScosCSP3 formed a small subgroup.

Information on sequence alignment, unigene reference, length, and best blastx hit of all 11 CSPs are shown in **Figure 6** and **Table 4**.

Tissue- and Sex-Specific Expression of Candidate ScosOBP and ScosCSP Genes

The expression patterns of ScosOBPs and ScosCSPs were analyzed by RT-PCR and are shown in **Figures 7**, **8**. ScosOBP1, 2, 3, 7, 9, 10, 16, 17, 18, 20, and 22 were highly expressed or specifically expressed in the antennae and head tissues. Among them, ScosOBP2 and OBP18 expressed at higher levels in female antennae than in male antennae. ScosOBP4, 5, 6, 11, 12, 13, 15, 16, and 19 were generally expressed in multiple tissues. Among them, ScosOBP12 and ScosOBP19 expressions were stronger in the female than in the male antennae. ScosOBP8 and ScosOBP21 were not detected by RT-PCR possibly because their expression levels were too low to detect.

ScosCSP2, ScosCSP3, and ScosCSP5 were specifically expressed in the male and female antennae. Other ScosCSPs were expressed in multiple tissues. Among them, ScosCSP1 was not detected in male antennae and ScosCSP10 was not detected in the antennae of both the sexes. Potentially due to undetectable expression levels, ScosCSP6, ScosCSP8, and ScosCSP9 were not detected by RT-PCR.

DISCUSSION

The genes reported in our study provide additional knowledge on the pool of identified olfactory genes in coleopterans. Compared with a large number of studies on Lepidopteran species, the current understanding of olfactory genes in Coleoptera is mainly sourced from a few reported studies on *T. castaneum* (Engsontia et al., 2008), *Megacyllene caryae* (Mitchell et al., 2012), *I. typographus*, and *D. ponderosae* (Andersson et al., 2013), *Leptinotarsa decemlineata* (Liu et al., 2015), *H. parallela* (Yi et al., 2018), *Rhynchophorus ferrugineus* (Antony et al., 2016; Gonzalez et al., 2021), etc. *S. schevyrewi* belongs to the genus of bark beetles and shares similar biology with the related species that are destructive forest pests, such as *I. typographus* and *D. ponderosae.* Aggregation behaviors are critical for bark beetle survival and rely on chemical communication (Byers, 1989). The genes we

TABLE 4 | Unigene of candidate chemosensory binding proteins.

Unigene reference	Gene name	Length (bp)	ORF(aa)	Blastx best hit	*E*-value	Full length	Signal peptide
CL2121.Contig1_All	ScosCSP1	948	315	XP_008193776.1 PREDICTED: chemosensory protein 6 isoform X1 [Tribolium castaneum]	3.00E-51	No	Yes
CL3677.Contig1_All	ScosCSP2	408	135	AFI45003.1 chemosensory protein [Dendroctonus ponderosae]	6.00E-65	Yes	Yes
CL3677.Contig2_All	ScosCSP3	207	68	ALR72526.1 chemosensory protein 12 [Colaphellus bowringi]	3.00E-35	No	No
Unigene2372_All	ScosCSP4	381	126	AHE13802.1 chemosensory protein 6 [Lissorhoptrus oryzophilus]	1.00E-45	Yes	Yes
Unigene3205_All	ScosCSP5	315	104	AGI05163.1 chemosensory protein 11 [Dendroctonus ponderosae]	4.00E-46	No	Yes
Unigene3958_All	ScosCSP6	381	126	AGZ04932.1 chemosensory protein 4 [Laodelphax striatella]	3.00E-86	Yes	Yes
Unigene4248_All	ScosCSP7	390	180	AGI05162.1 chemosensory protein 6 [Dendroctonus ponderosae]	1.00E-58	Yes	Yes
Unigene5446_All	ScosCSP8	372	123	AGZ04930.1 chemosensory protein 2 [Laodelphax striatella]	5.00E-56	Yes	Yes
Unigene5467_All	ScosCSP9	393	130	AGZ04940.1 chemosensory protein 12 [Laodelphax striatella]	7.00E-78	Yes	Yes
Unigene5845_All	ScosCSP10	333	110	AGI05172.1 chemosensory protein 2 [Dendroctonus ponderosae]	1.00E-52	No	No
Unigene12055_All	ScosCSP11	381	126	AHE13803.1 chemosensory protein 8 [Lissorhoptrus oryzophilus]	9.00E-67	Yes	Yes

identified might contribute to aggregation behavior and provide molecular targets for novel pest management techniques.

We identified a total of 47 OR genes in the *S. schevyrewi* antennae transcriptome. In another coleopteran, 265 candidate OR genes were annotated in the *T. castaneum* genome (Richards, 2008), which is much more than the known number of OR genes reported by other beetles. The numbers of ORs in *M. caryae* (Mitchell et al., 2012), *I. typographus* (Andersson et al., 2013), *D. ponderosae* (Andersson et al., 2013), and *H. parallela* (Yi et al., 2018) range from 43 to 57. The number of ScosORs identified in this study is consistent with that identified in these reports. Most of the predicted ORs in *S. schevyrewi* share greater identity with ORs of *D. ponderosae*, another bark beetle, indicating that these two species may be able to share the same ecological environments and detect similar semiochemicals. Functional studies in OR from bark beetles were relatively limited to only seven ORs (Hou et al., 2021; Yuvaraj et al., 2021). ItypOR46 and ItypOR49 were responsive to single enantiomers of the common bark beetle pheromone compounds ipsenol and ipsdienol, respectively (Yuvaraj et al., 2021). The other five ItypORs were responsive to monoterpenoids of different ecological origins (Hou et al., 2021). Future studies should be focused on deorphinized ScosORs with similar functions to provide potential molecular targets for detection and control methods.

We identified, in total, 22 IR genes in the *S. schevyrewi* antennae transcriptome. ScosIR8a and ScosIR25a were identified as coreceptors. The numbers of IR genes in *I. typographus*, *D. ponderosae*, and *H. parallela* (Yi et al., 2018) are 7, 15, and 27, respectively (Andersson et al., 2013; Yi et al., 2018). The number of ScosIRs identified in this study is considerable compared with the numbers reported in the previous studies. More than half of the predicted IRs shared relatively low identity with other coleopteran IRs. These IRs with low identity were probably not conserved in Coleoptera, and they might serve diverse functions in *S. schevyrewi*.

Within the *S. schevyrewi* antennae transcriptome, a total of 22 OBPs were predicted. Genome annotation indicated that 46 OBPs were identified in *T. castaneum* (Richards, 2008). Fewer OBPs were found in other coleopteran antennae transcriptomes. In *D. ponderosae*, *I. typographus*, and *H. parallela,* respectively, 31, 15, and 25 OBPs were annotated (Andersson et al., 2013; Ju et al., 2014). Our number of ScosOBPs is consistent with the numbers stated in these reports.

A total of 11 CSPs were identified in the *S. schevyrewi* antennae transcriptome. In the *T. castaneum* genome, a total of 40 CSPs were identified (Richards, 2008). Other coleopterans have fewer CSPs in their antennae transcriptomes; in *D. ponderosae*, *I. typographus*, and *H. parallela*, 11, 6, and 16 were annotated, respectively (Andersson et al., 2013; Ju et al., 2014). Our recorded number of ScosCSPs is comparable with these reports. The high level of sequence conservation (57–100%) indicates the function of CSPs is likely conserved among coleopterans.

All ScosOBPs and ScosCSPs contain a typical OBP and CSP motif, respectively. ScosOBP1, 2, 3, 10, 12, 14, 16, 17, 18, and 22 generally possessed the "classic" OBP motif C_1-X_{22-44}-C_2-X_3-C_3-X_{21-42}-C_4-X_{8-12}-C_5-X_8-C_6 of coleopteran insects (Xu et al., 2009). ScosOBP4, 5, 8, 9, 11, 13, 15, and 19 generally contained the "minus-C" OBP motif C_1-X_{30-32}-C_2-X_{38}-C_3-X_{16-18}-C_4 (Ju et al., 2014). The cysteine-spacing pattern of ScosOBP20 followed

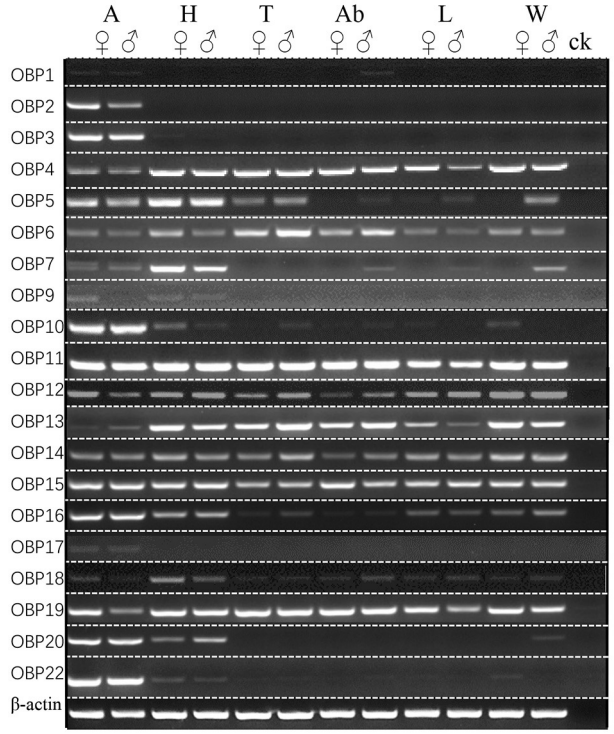

FIGURE 7 | Sex- and tissue-specific expression of candidate ScosOBPs. A, antennae; H, head; T, thorax; Ab, abdomen; L, leg; W, wing; ck, control [ultra-pure water (germ-free)].

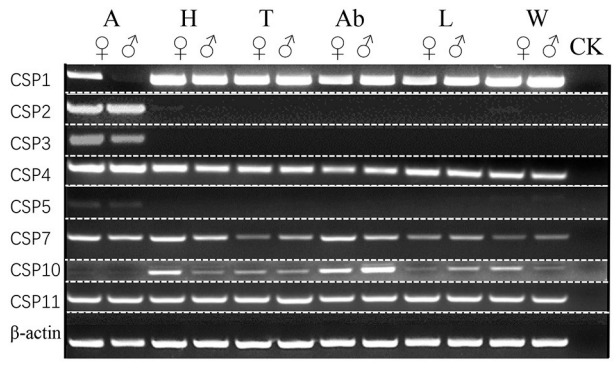

FIGURE 8 | Sex- and tissue-specific expression of candidate ScosCSPs. A, antennae; H, head; T, thorax; Ab, abdomen; L, leg; W, wing; ck, control [ultra-pure water (germ-free)].

the "plus-C" OBP motif C_1-X_{24-28}-C_2-X_3-C_3-X_{43}-C_4-X_{13-15}-C_{4a}-X_9-C_5-X_8-C_{6p}-X_9-C_{6a} from *D. melanogaster* and *Anopheles gambiae* (Zhou et al., 2008). All the CSPs were conserved in having the motif C_1-X_6-C_2-X_{18}-C_3-X_2-C_4 (Xu et al., 2009).

Scolytinae beetles respond to volatiles that emanate from both the host and non-host plants (Zhang and Schlyter, 2004; Erbilgin et al., 2007; Andersson et al., 2010). However, most individuals locate target trees by relying on an important signal called an aggregation pheromone released by beetles that have already attacked a tree (Andersson et al., 2013). Thus, olfactory signals and proteins serve critical roles in insect behavior. In this study, ScosOBP1, 2, 3, 7, 9, 10, 16, 17, 18, 20, and 22 might be important in odor perception because they were only expressed in the antennae and head, especially, ScosOBP2 and ScosOBP18. These two may be the key proteins in female olfactory behavior based on the specificity of protein expression we observed. ScosCSP2, ScosCSP3, and ScosCSP5 might also be important in olfaction due to their antennae-specific expression. Other ScosOBPs and ScosCSPs might not be involved in odor reception. Studies have shown a multitude of other roles that insect OBPs and CSPs have in Pelosi et al. (2018) releasing semiochemicals in pheromone glands (Benton, 2007), regeneration and development (Cheng et al., 2015), anti-inflammatory action (Isawa et al., 2002), nutrition (Zhu et al., 2016b), carrying visual pigments (Wang et al., 2007), and insecticide resistance (Bautista et al., 2015).

DATA AVAILABILITY STATEMENT

The datasets presented in this study can be found in online repositories. The names of the repository/repositories and accession number(s) can be found at: https://www.ncbi.nlm.nih.gov/bioproject/PRJNA732801.

AUTHOR CONTRIBUTIONS

XZ and WL designed the research, analyzed the data, and wrote the paper. YL gave a lot of adivces and help to revise the paper. AK, BS, and HC provided biological samples. XZ, BX, and ZQ performed the experiment. All authors contributed to the article and approved the submitted version.

FUNDING

This study was funded by the National Natural Science Foundation of China (Grant No. 31660518) and the earmarked fund of the Xinjiang apricot Industrial technology (Grant No. XJCYTX-03).

ACKNOWLEDGMENTS

We thank Sai Zhang and Yilu Feng for rearing the experimental larvae for the study.

SUPPLEMENTARY MATERIAL

The Supplementary Material for this article can be found online at: https://www.frontiersin.org/articles/10.3389/fphys.2021.717698/full#supplementary-material

Supplementary Figure 1 | GO classification analysis of unigenes in all-unigene. GO functions are shown in the X-axis. The right Y-axis shows the number of genes that have the GO function, and the left Y-axis shows the percentage.

Supplementary Figure 2 | Uncropped gel images of candidate ScosOBPs and candidate ScosCSPs. A, antennae; H, head; T, thorax; Ab, abdomen; L, leg; W, wing; ck, control [ultra-pure water (germ free)].

Supplementary Figure 3 | Uncropped gel images for candidate ScosOBPs and ScosCSPs.

Supplementary Table 1 | Forward and reverse primer sequence used in RT-PCR.

Supplementary Table 2 | Sequence information.

REFERENCES

Andersson, M. N., Grosse-Wilde, E., Keeling, C. I., Bengtsson, J. M., Yuen, M., Li, M., et al. (2013). Antennal transcriptome analysis of the chemosensory gene families in the tree killing bark beetles, *Ips typographus* and *Dendroctonus ponderosae* (Coleoptera: Curculionidae: Scolytinae). *BMC Genom*. 14:198. doi: 10.1186/1471-2164-14-198

Andersson, M. N., Keeling, C., and Mitchell, R. F. (2019). Genomic content of chemosensory genes correlates with host range in wood-boring beetles (*Dendroctonus ponderosae*, *Agrilus planipennis* and *Anoplophora glabripennis*). *BMC Genom*. 20:690. doi: 10.1186/s12864-019-6054-x

Andersson, M. N., Larsson, M. C., BlaŽenec, M., Jakuš, R., Zhang, Q. H., and Schlyter, F. (2010). Peripheral modulation of pheromone response by inhibitory host compound in a beetle. *J. Exp. Biol.* 213, 3332–3339. doi: 10.1242/jeb.044396

Angeli, S., Ceron, F., Scaloni, A., Monti, M., Monteforti, G., Minnocci, A., et al. (1999). Purification, structural characterization, cloning and immunocytochemical localization of chemoreception proteins from *Schistoceraca gregaria*. *Eur. J. Biochem.* 262, 745–754. doi: 10.1046/j.1432-1327.1999.00438.x

Antony, B., Soffan, A., Jakse, J., Mahmoud, M. M., Aldosari, S. A., and Aldawood, A. S. (2016). Identification of the genes involved in odorant reception and detection in the palm weevil Rhynchophorus ferrugineus, an important quarantine pest, by antennal transcriptome analysis. *BMC Genom*. 17:69. doi: 10.1186/s12864-016-2362-6

Bautista, M. A., Bhandary, B., Wijeratne, A. J., Michel, A. P., Hoy, C. W., and Mittapalli, O. (2015). Evidence for trade-offs in detoxification and chemosensation gene signatures in *Plutella xylostella*. *Pest. Manag. Sci*. 71, 423–432. doi: 10.1002/ps.3822

Benton, R. (2007). Sensitivity and specificity in *Drosophila* pheromone perception. *Trends.Neurosci.* 30, 512–519. doi: 10.1016/j.tins.2007.07.004

Benton, R., Sachse, S., Michnick, S. W., and Vosshall, L. B. (2006). A typical memobrane topology and heteromeric function of Drosophila odorant receptors *in vivo*. *PLoS. Biol.* 4:e20. doi: 10.1371/journal.pbio.0040020

Benton, R., Vannice, K. S., Gomez-Diaz, C., and Vosshall, L. B. (2009). Variant ionotropic glutamate receptors as chemosensory receptors in *Drosophila*. *Cell*. 136, 149–162. doi: 10.1016/j.cell.2008.12.001

Breugel, F. V., Huda, A., and Dickinson, M. H. (2018). Distinct activity-gated pathways mediate attraction and aversion to CO2 in *Drosophila*. *Nature* 564, 420–424. doi: 10.1038/s41586-018-0732-8

Briand, L., Swasdipan, N., Nespoulous, C., Bézirard, V., Blon, F., Huet, J. C., et al. (2002). Characterization of a chemosensory protein (ASP3c) from honeybee (*Apis mellifera* L.) as a brood pheromone carrier. *Eur. J. Biochem.* 269, 4586–4596. doi: 10.1046/j.1432-1033.2002.03156.x

Byers, J. (1989). Chemical ecology of bark beetles. *Experientia*. 45, 271–283.

Cao, D., Liu, Y., Wei, J., Liao, X., Walker, W. B., Li, J., et al. (2014). Identification of Candidate olfactory genes in Chilo suppressalis by antennal transcriptome analysis. *Int. J. Biol. Sci*. 10, 846–860. doi: 10.7150/ijbs.9297

Chen, C. H., Buhl, E., Xu, M., Croset, V., Rees, J. S., Lilley, K. S., et al. (2015). *Drosophila* ionotropic receptor 25a mediates circadian clock resetting by temperature. *Nature* 527, 516–520. doi: 10.1038/nature16148

Cheng, D. F., Lu, Y. Y., Zeng, L., Liang, G. W., and He, X. F. (2015). Si-CSP9 regulates the integument and moulting process of larvae in the red imported fire ant, *Solenopsis invicta*. *Sci. Rep*. 5:9245. doi: 10.1038/srep09245

Clyne, P. J., Warr, C. G., and Carlson, J. R. (2000). Candidate taste receptors in *Drosophila*. *Science* 287, 1830–1834. doi: 10.1126/science.287.5459.1830

Clyne, P. J., Warr, C. G., Marc, R. F., Lessing, D., Kim, J. Y., and Carlson, J. R. (1999). A novel family of divergent seven-transmembrane proteins: candidate odorant receptors in *Drosophila*. *Neuron* 22, 327–338. doi: 10.1016/S0896-6273(00)81093-4

Conesa, A., Götz, S., García-Gómez, J. M., Terol, J., Talón, M., and Robles, M. (2005). Blast2GO: a universal tool for annotation, visualization and analysis in functional genomics research. *Bioinformatics.* 21: 3674–3676. doi: 10.1093/bioinformatics/bti610

Dobritsa, A. A., van der Goes van Naters, W., Warr, C. G., Steinbrecht, R. A., and Carlson, J. R. (2003). Integrating the molecular and cellular basis of odor codling in the *Drosophila* antenna. *Neuron* 37, 827–841. doi: 10.1016/S0896-6273(03)00094-1

Dong, X. T., Liao, H., Zhu, G. H., Khuhro, S. A., Ye, Z. F., Yan, Q., et al. (2017). CRISPR/Cas9-mediated PBP1 and PBP3 mutagenesis induced significant reduction in electrophysiological response to sex pheromones in male *chilo suppressalis*. *Insect. Sci.* 26, 388–399. doi: 10.1111/1744-7917.12544

Elmore, T., Ignell, R., Carlson, J., and Smith, D. (2003). Targeted mutation of a *Drosophila* odor receptor defines receptor requirement in a novel class of sensillum. *J. Neurosci*. 23, 9906–9912. doi: 10.1523/JNEUROSCI.23-30-09906.2003

Engsontia, P., Sanderson, A. P., Matthew, C., Walden, K., Robertson, H. M., and Browna, S. (2008). The red flour beetle's large nose: An expanded odorant receptor gene family in *Tribolium castaneum*. *Insect. Biochem. Mol. Biol.* 38, 387–397. doi: 10.1016/j.ibmb.2007.10.005

Erbilgin, N., Mori, R. I., Sun, J. H., Stein, J. D., Owen, D. R., and Merrill, L. D. (2007). Response to host volatiles by native and introduced populations of *Dendroctonus valens* (Coleoptera: Curculionidae, Scolytinae) in North America and China. *J. Chem. Ecol.* 33, 131–146. doi: 10.1007/s10886-006-9200-2

Fan, L. H., Niu, H. L., Zhang, J. T., Liu, J. L., Yang, M. H., and Zong, S. X. (2014). Extraction and identification of aggregation pheromone components of *Scolytus schevyrewi* Semenov(Coleoptera: Scolytidae) and trapping test. *Acta Ecol. Sinica* 35, 892–899. doi: 10.5846/stxb201311032656

Gomez-Diaz, C., Reina, J. H., Cambillau, C., Benton, R. (2013). Ligands for pheromone-sensing neurons are not conformatinally activated odorant binding proteins. *PLoS Biology*. 11:e1001546. doi: 10.1371/journal.pbio.1001546

Gonzalez, F., Johny, J., Walker, I. I. I. W. B., Guan, Q. T., Mfarrej, S., and Jakse, J. (2021). Antennal transcriptome sequencing and identification of candidate chemoreceptor proteins from an invasive pest, the American plam weevil, *Rhynchophorus palmarus*. *Sci. Rep.* 11:8334. doi: 10.1038/s41598-021-87348-y

Grabherr, M. C., Haas, B. J., Yassour, M., Levin, J. Z., Tompson, D. A., Amit, I., et al. (2011). Full-length transcriptome assembly from RNA-Seq data without a reference genome. *Nat. Biothchnol.* 29, 644–652. doi: 10.1038/nbt.1883

Hallem, E. A., Ho, M. G., and Carlson, J. R. (2004). The molecular basis of odor coding in the Drosophila antenna. *Cell* 117, 965–979. doi: 10.1016/j.cell.2004.05.012

Hanson, B. S., (1999). *Insect Olfaction*. New York, NY: Springer.

Honson, N., Gong, Y., Plettner, E. (2015). "Structure and function of insect odorant and pheromone-binding proteins (OBPs and PBPs) and chemosensory-specific proteins (CSPs)," in *Chemical Ecology and Phytochemistry of Forest Ecosystems*, ed J. T. Romeo (Oxford: Elsevier Ltd.), 227–268. doi: 10.1016/S0079-9920(05)80010-3

Hou, X. Q., Yuvaraj, K. J., Roberts, R. E., Zhang, D. D., Uneilius, C. R., Löfstedt, C., et al. (2021). Functional evolution of a bark beetle odorant receptor clade detecting monoterpenoids of different ecological origins. *Mol. Biol. Evol.* msab218. doi: 10.1093/molbev/msab218

Isawa, H., Yuda, M., Orito, Y., and Chinzei, Y. (2002). A mosquito salivary protein inhibits activation of the plasma contact system by binding to factor XII and high molecular weight kininogen. *J. Biol. Chem.* 277, 27651–27658. doi: 10.1074/jbc.m203505200

Jacquin-Joly, E., Vogt, R. G., François, M. C., and Nagnan-Le Meillour, P. (2001). Functional and expression pattern analysis of chemosensory proteins expressed in antennae and pheromonal gland of *Mamestra brassicae*. *Chem. Senses* 26, 833–844. doi: 10.1093/chemse/26.7.833

Jing, D., Zhang, T., Bai, S., Prabu, S., He, K., Dewer, Y., et al. (2019). GOBP1 plays a key role in sex pheromones and plant volatiles recognition in yellow peach moth, conogethes punctiferalis (Lepidoptera: Crambidae). *Insects* 10:302. doi: 10.3390/insects10090302

Ju, Q., Li, X., Jiang, J. X., Qu, M. J., Guo, X. Q., Han, Z. J., et al. (2014). Transcriptome ranscriptome and tissue-specific expression analysis of obp and csp genes in the dark black chafer. *Arch. Insect. Biochem.* 87, 177–200. doi: 10.1002/arch.21188

Kim, M. S., Repp, A., and Smith, D. P. (1998). LUSH odorant binding protein mediates chemosensory responses to alcohols in *Drosophila melanogaster*. *Genetics* 150, 711–721. doi: 10.1093/genetics/150.2.711

Knecht, Z. A., Silbering, A. F., Ni, L. N., Klein, M., Budelli, G., Bell, R., et al. (2016). Distinct combinations of variant ionotropic glutamate receptors mediate thermosensation and hygrosensation in *Drosophila*. *Elife* 5:e17879. doi: 10.1101/056267

Larsson, M. C., Domingos, A. I., Jones, W. D., Chiappe, M. E., Amrein, H., and Vosshall, L. B. (2004). Or83b encodes a broadly expressed odorant receptor essential for *Drosophila* olfaction. *Neuron* 43, 703–714. doi: 10.1016/j.neuron.2004.08.019

Leal, W. S. (2013). Odorant reception in insects: roles of receptors, binding proteins, and degrading enzymes. *Annu. Rev. Entomol.* 58, 373–391. doi: 10.1146/annurev-ento-120811-153635

Li, F., Dewer, Y., Li, D., Qu, C., and Luo, C. (2021). Functional and evolutionary characterization of chemosensory protein CSP2 in the whitefly, Bemisia tabaci. *Pest. Manag. Sci.* 77, 378–388. doi: 10.1002/ps.6027

Li, J. L., Zhang, T., Li, X. T., and Ma, S. K. (1995). Studies on the bionomics of *Scolytus seulensis* Murayama and its control. *Plant Protection* 21, 8–10. doi: 10.1016/j.aspen.2008.04.001

Liu, S. J., Liu, N. Y., He, P., Li, Z. Q., Dong, S. L., and Mu, L. F. (2012). Molecular characterization, expression patterns, and ligand-binding properties of two OBP genes from *Orthaga achatina*(Butler) (Lepidoptera: Pyralidae). *Arch. Insect. Biochem.* 80, 123–139. doi: 10.1002/arch.21036

Liu, Y., Sun, L. J., Cao, D. P., Walker, W. B., Zhang, Y. Q., and Wang, G. R. (2015). Identification of candidate olfactory genes in *Leptinotarsa decemlineata* by antennal transcriptome analysis. *Font. Ecol. Evol.* 19:60. doi: 10.3389/fevo.2015.00060

Mitchell, R. F., Hughes, D. T., Luetje, C. W., Millar, J. G., Soriano-Agatónc, F., Hanks, L. M., et al. (2012). Sequencing and characterizing odorant receptors of the cerambycid beetle *Megacyllene caryae*. *Insect Biochem. Mol. Biol.* 42, 499–505. doi: 10.1016/j.ibmb.2012.03.007

Mitchell, R. F., Schneider, T. M., Schwartz, A. M., Andersson, M. N., and McKenna, D. D. (2019). The diversity and evolution of odorant receptors in beetles (Coleoptera). *Insect Mol. Biol.* 29, 77–91. doi: 10.1111/imb.12611

Monteforti, G., Angeli, S., Petacchi, R., and Minnocci, A. (2002). Ultrastructural characterization of antennal sensilla and immunocytochemical localization of a chemosensory protein in *Carausius morosus* Brünner (Phasmida: Phasmatidae). *Arthropod Struct. Dev.* 30, 195–205. doi: 10.1016/S1467-8039(01)00036-6

Ni, L., Klein, M., Svec, K., Budelli, G., Chang, E. C., Ferrer, A. J. et al. (2015). The Ionotropic Receptors IR21a and IR25a mediate cool sensing in Drosophila. *Elife*. 5. doi: 10.7554/eLife.13254

Pelosi, P., Calvello, M., and Ban, L. P. (2005). Diversity of odorant binding protein and chemosensory proteins in insects. *Chem. Senses* 30, 1291–1292. doi: 10.1093/chemse/bjh229

Pelosi, P., Iovinella, I., Zhu, J., Wang, G. R., and Dani, F. R. (2018). Beyond chemoreception: diverse tasks of soluble olfactory proteins in insects. *Bio. Rev.* 93, 184-200. doi: 10.1111/brv.12339

Pelosi, P., Zhou, J. J., Ban, L. P., and Calvello, M. (2006). Solube proteins in insect chemical communication. *Cell. Mol. Life. Sci.* 63, 1658–1676. doi: 10.1007/s00018-005-5607-0

Pertea, G., Huang, X. Q., Liang, F., Antonescu, V., Razvan, S. R., Svetlana, K. S., et al. (2003). TIGR Gene Indices clustering tools (TGICL): a software system for fast clustering of large EST datasets. *Bioinformatics* 19, 651–652. doi: 10.1093/bioinformatics/btg034

Richards, S. (2008). The genome of the model beetle and pest *Tribolium castaneum*. *Nature* 452, 949–955. doi: 10.5167/uzh-2931

Schlyter, F., Birgersson, G., Byers, J. A., Löfqvist, J., and Bergström, G. (1987). Field response of spruce bark beetle, Ips typographus, to aggregation pheromo candidates. *J. Chem. Ecol.* 13:701–716.

Stengl, M. (2017). Chemosensory transduction in arthropods," in *Oxford Handbooks Online. The Oxford Handbook of Invertebrate Neurobiology*, ed J. H. Byrne (Oxford University Press), 1–42. doi: 10.1093/oxfordhb/9780190456757.013.15

Stoker, R. F., Lienhard, M. C., Borst,. A., and Fischbach, K. F. (1990). Neuronal architecture of the antennal lobe in Drosophila melanogaster. *Cell. Tissue Res.* 262, 9–34.

Sun, H. Y., Guan, L., Feng, H. L., Yin, J., Cao, Y. Z., Xi, J. H., et al. (2014). Functional characterization of chemosensory proteins in the scarab beetle, holotrichia oblita faldermann (Coleoptera: Scarabaeida). *PLoS ONE* 9:e107059. doi: 10.1371/journal.pone.0107059

Vosshall, L. B., and Hanson, B. S. (2011). A unified nomenclature system for the insect olfactory coreceptor. *Chem. Senses* 36, 497–498. doi: 10.1093/chemse/bjr022

Wang, T., Jiao, Y., and Montell, C. (2007). Dissection of the pathway required for generation of vitamin A and for *Drosophila* phototransduction. *J. Cell. Biol.* 177, 305–316. doi: 10.1083/jcb.200610081

Wermelinger, B. (2004). Ecology and management of the spruce bark beetle Ips typographus-a review of recent research. *For. Ecol. Manag.* 202, 67–82. doi: 10.1016/j.foreco.2004.07.018

Wilson, R. I. (2013). Early olfactory processing in Drosophila: mechanisms and principles. *Annu. Rev. Neurosci.* 36, 217–241. doi: 10.1146/annurev-neuro-062111-150533

Xiao, S., Sun, J. S., and Carlson, J. R. (2019). Robust olfactory responses in the absence of odorant binding proteins. *Elife: e*51040. doi: 10.7554/eLife.51040

Xu, P. X., Atkinson, R., Jones, D. N. M., and Smith, D. P. (2005). Drosophila OBP LUSH is required for activity of pheromone-sensitive neurons. *Neuron* 45, 192–200. doi: 10.1016/j.neuron.2004.12.031

Xu, Y. L., He, P., Zhang, L., Fang, S. Q., Dong, S. L., Zhang, Y. J., et al. (2009). Large-scale identification of odorant-binding proteins and chemosensory proteins from expressed sequence tags in insects. *BMC. Genom.* 10:632. doi: 10.1186/1471-2164-10-632

Ye, Z. F., Liu, X. L., Han, Q., Liao, H., Dong, X. T., Zhu, G. H., et al. (2017). Functional characterization of PBP1 gene in *Helicoverpa armigera* (Lepidoptera: Noctuidae). *Sci. Rep.* 7:8769. doi: 10.1038/s41598-017-08769-2

Yi, J. K., Yang, S., Wang, S., Wang, J., Zhang, X. X., and Liu, Y. (2018). Identification of candidate chemosensory receptors in the antennal transcriptome of the large black chafer *Holotrichia parallela* Motschulsky (Coleoptera: Scarabaeidae). *Comp. Biochem. Phys. D* 28, 63–71. doi: 10.1016/j.cbd.2018.06.005

Yuvaraj, J. K., Roberts, R. E., Sonntag, Y., Hou, X. Q., Grosse-Wilde, E., Machara, A., et al. (2021). Putative ligand binding sites of two functionally characterized bark beetle odorant receptors. *BMC Biol.* 19:16. doi: 10.1186/s12915-020-00946-6

Zhang, J., Wang, B., Dong, S. L., Cao, D. P., Dong, J. F., Walker, W. B., et al. (2015). Antennal transcriptome analysis and comparison of chemosensory gene families in two closely related noctuidae moths, helicoverpa armigera and H. assulta. *PloS ONE* 10. doi: 10.1371/journal.pone.0117054

Zhang, Q. H., and Schlyter, F. (2004). Olfactory recognition and behavioural avoidance of angiosperm nonhost volatiles by conifer-inhabiting bark beetles. *Agr. Forest. Entomol.* 6, 1–19. doi: 10.1111/j.1461-9555.2004.00202.x

Zhou, J. J., He, X. L., Pickett, J. A., and Field, L. M. (2008). Identification of odorant-binding proteins of the yellow fever mosquito *Aedes aegypti*: genome annotation and comparative analyses. *Insect Mol. Biol.* 17, 147–163. doi: 10.1111/j.1365-2583.2007.00789.x

Zhu, G. H., Xu, J., Cui, Z., Dong, X. T., Ye, Z. F., Niu, D. J., et al. (2016a). Functional characterization of SlitPBP3 in *Spodoptera litura* by CRISPR/Cas9 mediated

genome editing. *Insect Biochem. Mol. Biol.* 75, 1–9. doi: 10.1016/j.ibmb.2016.05.006

Zhu, J., Iovinella, I., Dani, F. R., Liu, Y. L., Huang, L. Q., Liu, Y., et al. (2016b). Conserved chemosensory proteins in the proboscis and eyes of Lepidoptera. *Int. J. Biol. Sci.* 12, 1394–1404. doi: 10.7150/ijbs.16517

Conflict of Interest: The authors declare that the research was conducted in the absence of any commercial or financial relationships that could be construed as a potential conflict of interest.

Publisher's Note: All claims expressed in this article are solely those of the authors and do not necessarily represent those of their affiliated organizations, or those of the publisher, the editors and the reviewers. Any product that may be evaluated in this article, or claim that may be made by its manufacturer, is not guaranteed or endorsed by the publisher.

frontiers in Physiology

ORIGINAL RESEARCH
published: 28 October 2021
doi: 10.3389/fphys.2021.712593

An Expanded Survey of the Moth PBP/GOBP Clade in *Bombyx mori*: New Insight into Expression and Functional Roles

Xia Guo[1†], *Ning Xuan*[1†], *Guoxia Liu*[1†], *Hongyan Xie*[1], *Qinian Lou*[2], *Philippe Arnaud*[3], *Bernard Offmann*[3] *and Jean-François Picimbon*[1,4*]

[1] *Biotechnology Research Center, Shandong Academy of Agricultural Sciences, Jinan, China,* [2] *Shandong Silkworm Institute, Shandong Academy of Agricultural Sciences, Yantai, China,* [3] *Protein Engineering and Functionality Unit, UMR CNRS 6286, University of Nantes, Nantes, France,* [4] *School of Bioengineering, QILU University of Technology, Jinan, China*

OPEN ACCESS

Edited by:
Joe Hull, Agricultural Research Service, United States Department of Agriculture (USDA), United States

Reviewed by:
Karen Rihani, Max Planck Institute for Chemical Ecology, Germany
William Benjamin Walker III, Temperate Tree Fruit and Vegetable Research Unit, Agricultural Research Service, United States Department of Agriculture (USDA-ARS), United States

***Correspondence:**
Jean-François Picimbon
jfpicimbon@gmail.com

[†]*These authors have contributed equally to this work and share first authorship*

Specialty section:
This article was submitted to Invertebrate Physiology, a section of the journal Frontiers in Physiology

Received: *20 May 2021*
Accepted: *13 September 2021*
Published: *28 October 2021*

Citation:
Guo X, Xuan N, Liu G, Xie H, Lou Q, Arnaud P, Offmann B and Picimbon J-F (2021) An Expanded Survey of the Moth PBP/GOBP Clade in Bombyx mori: New Insight into Expression and Functional Roles. Front. Physiol. 12:712593. doi: 10.3389/fphys.2021.712593

We studied the expression profile and ontogeny (from the egg stage through the larval stages and pupal stages, to the elderly adult age) of four OBPs from the silkworm moth *Bombyx mori*. We first showed that male responsiveness to female sex pheromone in the silkworm moth *B. mori* does not depend on age variation; whereas the expression of BmorPBP1, BmorPBP2, BmorGOBP1, and BmorGOBP2 varies with age. The expression profile analysis revealed that the studied OBPs are expressed in non-olfactory tissues at different developmental stages. In addition, we tested the effect of insecticide exposure on the expression of the four OBPs studied. Exposure to a toxic macrolide insecticide endectocide molecule (abamectin) led to the modulated expression of all four genes in different tissues. The higher expression of OBPs was detected in metabolic tissues, such as the thorax, gut, and fat body. All these data strongly suggest some alternative functions for these proteins other than olfaction. Finally, we carried out ligand docking studies and reported that PBP1 and GOBP2 have the capacity of binding vitamin K1 and multiple different vitamins.

Keywords: insect, Lepidoptera, silkworm, pheromone binding protein, general odorant binding protein, ontogeny, abamectin, vitamin

INTRODUCTION

In insects, the solubilization of pheromone and plant odor molecules before interacting with olfactory receptor neurons (ORNs) is strongly believed to be a *sine qua non* because of the anatomy of the antennal *sensillum* or sensory hair, i.e., the microunit involved in odor detection. In each antennal hair sensillum, an aqueous barrier (sensory lymph) clearly separates each ORN from the pores in the cuticular walls that govern the entry of environmental odor molecules (Picimbon, 2002). The need for the absorption of odor molecules at the surface of the olfactory organ to trap and concentrate the stimuli molecules close to the olfactory receptor (OR) has become the main concept in insect neurobiology, principally in the silkworm moth *Bombyx mori,* where the first sex pheromone (Bombykol) was identified (Butenandt et al., 1959).

Following the discovery of a soluble pheromone-binding protein (PBP) in the antennal sensory lymph of the giant silk moth *Antheraea polyphemus*, it has been postulated that sex pheromone molecules need to interact with PBP in order to activate OR and ORN (Vogt and Riddiford, 1981). The extremely high PBP protein concentration in the sensillum lymph surrounding OR

and ORN, pH and pheromone-induced conformational changes in the structure of PBP, PBP-pheromone ligand interaction kinetics and specific mechanisms underlying odor ligand release, resolution of the X-ray crystal structure of *B. mori* PBP1 (BmorPBP1) with the bombykol molecule integrated into the central core of the protein, as well as the notion of supramolecular pheromone-PBP complexes activating OR and PBP-OR co-expression are all in support of a function that is fine-tuned through interaction with sex pheromone molecules and odor chemosensing (Wojtasek and Leal, 1999; Plettner et al., 2000; Sandler et al., 2000; Horst et al., 2001; Lautenschlager et al., 2007; Gong Y. et al., 2009; Krieger et al., 2009). Accordingly, numerous kinetic models with PBP-based sex pheromone deactivation and/or pheromone transport in the moth antennae have been proposed (Vogt et al., 1985; Kaissling, 1998, 2009, 2019; Vogt, 2003, 2005; Gong Y. et al., 2009; Terrado et al., 2019, 2020).

Pheromone-binding proteins and general odorant-binding proteins are very well-recognized members of the larger odorant binding protein gene family, which has been shown to be represented in most insect lineages and species (Picimbon, 2003; Li et al., 2008; He et al., 2011; Iovinella et al., 2011; Donnell, 2014; Ozaki, 2019). Pheromone-binding proteins (PBPs) and general odorant-binding proteins (GOBPs) are particularly notable because (1) they comprise a Lepidoptera-specific clade within the larger insect OBP gene family; (2) they comprise a single gene cluster that arose through early gene duplication; and (3) they are the original genes identified that establish the OBP gene family (Vogt et al., 1989, 1991a,b, 2002; Picimbon, 2003, 2005, 2019; Abraham et al., 2005; Vogt, 2005).

When PBPs and GOBPs were first identified, a major criterion of interest was their antennal specificity: the proteins were localized to the extracellular space of olfactory sensilla and demonstrated to interact with specific pheromone molecules (Vogt et al., 1989; Steinbrecht et al., 1995; Plettner et al., 2000; Zhang et al., 2001; Nardi et al., 2003; Wang et al., 2003; Zhou et al., 2009). The noctuid *PBP/GOBP* clade was maintained despite sex pheromone divergence, speciation, and species recognition (Picimbon and Gadenne, 2002; Picimbon, 2003; Abraham et al., 2005; Allison and Cardé, 2016). It was, however, the antennal specificity that argued strongly that the proteins were involved in olfactory functions and, therefore, had some major role entirely strictly tuned to the detection of odor molecules. Originally, PBP and GOBP in adult moths were considered to be absent from the thorax, midgut, fat body, and metabolic tissues but abundant in the antennae and legs; this also included proteins/genes of the current study, namely, "PBP1, PBP2, GOBP1, and GOBP2" of the silkworm moth, *B. mori* (BmorPBP1, BmorPBP2, BmorGOBP1, and BmorGOBP2; Vogt et al., 1991a,b; Krieger et al., 1996; Sandler et al., 2000; Forstner et al., 2006; Gong D. et al., 2009; Zhou et al., 2009; Li et al., 2012; Xuan et al., 2014; Picimbon, 2019). In addition, while the larval expression of GOBP2 was restricted to large sensilla basiconica, sensilla styloconica, or other gustatory chemosensilla from maxillary palps and antenna (Vogt et al., 2002), the adult expression of BmorGOBP2 was shown to be associated with the female moth pheromone gland (Xuan et al., 2014), strongly suggesting multiple functions for this protein. Gel digestion of SDS-PAGE-separated proteins and liquid chromatography coupled to tandem mass spectrometry (Nano-LC/MS/MS) analysis showed the presence of GOBP2 with many other OBPs (OBP6, OBP56d, PBP-related protein 3, sericotropin, and protein B1) in a library of more than 9,000 peptides from the *Bombyx* pheromone gland (Xuan et al., 2014), urging us to use molecular biology and quantitative real-time PCR as an alternative/complementary approach of biochemistry and immunoblotting to focus on the PBP/GOBP clade. The occurrence of GOBP2s and other OBPs not only in insects but also in the kingdom of bacteria emphasizes their involvement in various additional non-olfactory tasks (Liu and Picimbon, 2017; Picimbon, 2019). Moth PBPs and GOBPs display about 30–79% identity with "pheromone/odorant binding proteins" from *Acinetobacter baumannii* and *Macrococcus caseolyticus* (OIE61716, RKO12089, RKO12629, RKO12557, RKO12708, RKO12709, WP_170831700; Genetic locus: LYIE01000111, RBVL01000056, RBVL01000061, RBVL01000065, and RBVL01000098). Therefore, it could be that non-olfactory function is a very general feature of the OBP protein gene family. Many members of the OBP family have since been shown to be expressed not only in the antennae and legs but also in many various metabolic organs, including the thorax, midgut, and fat body (Li et al., 2008; Ribeiro et al., 2014; Sun et al., 2018; Rihani et al., 2021).

We report further on these studies in relation to multifunction and OBP genes. First, we assay the sex pheromone responsiveness to make an inference based on temporal analyses of PBP/GOBP expression. Then, we report on our entire study in relation to the temporal and tissue-specific expression of four OBPs, two pheromone-binding proteins (PBPs), PBP1 and PBP2, and two general odorant-binding proteins (GOBPs), GOBP1 and GOBP2, of the domesticated silkworm moth *B. mori*. Contrary to the strong widespread belief that these proteins in the moth PBP/GOBP clade are expressed exclusively in adult (predominantly male) antennae and used exclusively for pheromone binding and sex recognition, we show data that the respective genes, and in many cases also the proteins, are expressed in multiple larval, pharate adult, and adult tissues as well as in non-sensory tissues of young adult males subjected to immersion into a specific anthelminthic/insecticide (abamectin, Avermectin B1) solution. This "abamectin" experiment is crucial to cover the gene expression of PBPs and GOBPs in the thorax, gut, and fat body as well as some age- and chemical stress-dependent conditions. Due to such unusual findings, we also carry out ligand docking studies and report that BmorPBP1 and BmorGOBP2 have the capacity to bind vitamin K1 and multiple different vitamins, respectively.

MATERIALS AND METHODS

Bombyx mori Rearing and Tissue Dissection

Original collections of silkworms were made from Qingsong × Haoyue crossbreeds (Yantai, Zhifu, Shandong Province) maintained from the egg stage and throughout larval

development in growth chambers at 23°C with 70% relative humidity and a photoperiod of 15-h light: 9-h dark. The larvae were reared on a layer of mulberry leaves until spinning prior to being sexed and transferred to laboratory conditions. Fifth-instar larvae were used for tissue collection. In the laboratory (Jinan, Shandong Sheng), male and female "cocoons" were maintained at room temperature. The pupae were kept separately in two batches (males and females) in two different rooms, both held at 25°C and 15 h light: 9 h dark. Female pupae were used for tissue extraction (antennae, fat body, gut, head, legs, pheromone gland, epidermis, cuticle, thorax, and wings) at five different stages of the adult development, e.g., 1- to 5-days before emergence, E-1 to E-5, following Vogt et al. (1993), Dedos and Fugo (2001) and Picimbon et al. (2001). For the antennae and legs, cuticle deposition, which was initiated in the early stages, was observed under a microscope as a change in the external structure. On E-5, the moth tissues had a soft yellowish-white appearance/coloration and no cutinized layer (Picimbon et al., 2001). On E-4 (abdominal cuticle deposition), E-3 (eye pigmentation), and E-2 (formation of legs), the coloration and rigidity of the nymph body changed to nearly reach the adult form (imago stage: E-1, antenna, and wing pigmentation).

At the adult stage, the males and females were also kept separately. When the adults eclosed, no newly born (D0) male and female were paired. Therefore, all data related to unmated status. Males and females were dissected for antennae, head, legs, wings, thorax, the abdomen, and, in females, the pheromone gland at precise age after emergence. Epidermis, gut, and fat body tissues were extirpated from the abdomen. The anterior, median, and posterior legs were also collected separately. All the legs were cut off at the femur-tibia (tarsal segments) articulation. Compound eyes were removed from the cephalic capsule. We also collected eggs laid by 8-day-old virgin females and unlaid eggs in the female abdomen (ovarian tissue) that were kept separately. Hemolymph and meconium were aspirated with a micropipette after pressure on the abdomen and diluted in water. The cocoons were cut into small pieces and heated in a boiling water bath for several hours before collecting protein samples. Antennae were harvested at the same time each day during the hours of light (Ichikawa, 1998; Ichikawa and Ito, 1999). All the organs and tissues were frozen and stored at −80°C until protein or RNA extraction.

In a mixed cocoon population, both silkworm adult males and females became active even under light conditions as soon as they have emerged from the cocoons. The females stayed nearby the cocoons, rising wings, and expelling ovipositor and pheromone gland that, soon enough, will draw the males to their vicinity. Newly emerged males fanned their wings and walked immediately to *Bombyx* females ready for mating. The expected adult lifespan of the Qingson x Haoyue strain is ∼10–15-days, with mating activities significantly decreasing after 7–9-days. Unmated females lay eggs after 7–9-days as described by Osanai (1978).

Olfactometer Behavioral Studies

In the pheromone response tests, adult males of different ages (1- to 8-day-old) were placed individually in an I-shaped tube olfactometer connected to a separated glass chamber housing one young (1-day-old) virgin female in a calling posture. The same female was used to test a series of 10 males. Thirty-forty males were tested for each category. We tested 9-day-old males, we noted pheromone responsiveness but we did not consider the result for statistical analysis (sample size $n = 10$). Old males d16–18 were also assayed but exhibited no activity ($n = 10$). The characteristics of the female adopting a calling posture were wing vibrations, intense pulses of abdominal movements, and pheromone gland extrusions at the abdominal tip (Ichikawa, 1998). The source chamber was covered to exclude visual stimuli. In the open I-track olfactometer tube (20-cm long with a diameter of 3 cm), humidified and pre-cleaned air was constantly blown at a total flow of 2.5 l/min (air pump vacuum cleaner AG 1605; Beijing-Keep Science Analysis & Technology, Co. Ltd.). Tests were conducted at room temperature (25°C) during the light period (photophase) of the silkworms. The females also sustained calling behavior and pheromone production during photophase (Ichikawa and Ito, 1999). The male was introduced in the upper part of the olfactometer once the female flapped wings, lifted abdomens, and expelled the sex pheromone gland every several seconds. Male behavioral responses were evaluated using two criteria: (1) time reaction (Tr: the male left the upper part of the tube, crossing the arbitrary point in the reaction zone, 18 cm away from the odor source) and (2) time to reach the female odor source (Ts: the male reached the other extremity of the tube, touching the zone connected to the calling female). The behavior score test lasted for 2 min. The data were statistically analyzed using a Mann-Whitney U test at $p < 0.001$.

Quantitative Real-Time PCR (qRT-PCR)

For the measurement of gene expression in adult tissues, complementary DNAs were synthesized from antennal RNA (1 μg) using M-MuLV transcriptase (Fermentas, Waltham, MA, United States). The qRT-PCR was carried out using a StepOnePlus ABI7500 (Thermo Fisher Scientific, Waltham, MA, United States) system. The thermocycler program had an initial denaturing step of 2 min at 95°C followed by 40 cycles of 5 at 95, 20 at 60, 30 at 72, and 15 s at 95°C. A melting curve analysis was performed by monitoring fluorescence (SYBR Green I; Takara Bio Inc., Shiga, Japan) at 60°C for 1 min as suggested by the instructions of the manufacturer. Using 60 insects per age, three mRNA samples were collected (yielding three separate cDNA samples). Each sample taken for RNA extraction and cDNA synthesis corresponded to 20 moths equivalents.

Each of the three resulting reaction samples was run in triplicates. Specific primers were designed to yield amplicons of about 130–200 bps: BmorPBP1 (#X94987) sense 5′-tttgccaagaaacatggagc-3′, antisense 5′-tgtggatttcagctttgaagc-3′; BmorPBP2 (#AM403100) sense 5′-ggaaaagctcacgagtttgc-3′, antisense 5′-gaccttcagtgttctttcgca-3′. The BmorGOBP1 (#X94988) and BmorGOBP2 (#X94989) primers were same as those used for one-step RT-PCR. Controls used cyclophilin A and actin primers described in *One-Step Reverse transcriptase PCR (RT-PCR)*. Primers to additional sensory and non-sensory genes, such as *antennal oxydase-1* (AOX1), *antennal esterase-1* (AE41), *JH esterase* (JHE), *cytosolic juvenile hormone-binding*

protein (cJHBP), *hemolymph JHBP* (hJHBP), *ecdysone receptor variant B1* (EcR-B1), *pheromone olfactory receptor-1* (OR1), and *cytochrome P450* (CYP306A1 and CYP4M9) were as follows: BmorAOX1 (NM_001110342, 5′-gatctgaccgtattcaaagc-3′, 5′-gcaaagtcttcttccacgtt-3′), BmorAE41 (NM_001130880, 5′-tttggccgtttgaaatcagc-3′, 5′-gcttgctttccatgttggaa-3′), BmorJHE (AF287267, 5′-tccataatggaggtgaaagc-3′, 5′-tgctcatggacgtcagtaat-3′), BmorcJHBP (NM_001044203, 5′-gtctgaagtatgttgaggct-3′, 5′-aaagtcagtagaccgttcca-3′), BmorhJHBP (NM_00143609, 5′-actaaagcgaagacggtgc-3′, 5′-tgtagccatacctgacagc-3′), BmorEcR-B1 (NM_001173375, 5′-aggtatctttcggagaagct-3′, 5′-ccaagtctgcgttactcttt-3′), BmorOR1 (NM_001043410, 5′-tcgcttcataacggtaatgc-3′, 5′-ccataaggatccgaaaatgc-3′), BmorCYP306A1 (NM_00111275, 5′-aaatacaggaggaaggatgc-3′, 5′-ccacggactagaacttcaat-3′), and BmorCYP4M9 (NM_001079666, 5′-aatgggccgtattttaagc-3′, 5′-ggtcaaacacaagaggatct-3′).

All the qRT-PCR products were sequenced to attest to the specificity of the amplicon. Gene expression levels were calculated relative to the *actin* gene using the 2[−ΔΔC(T)] method and following Livak and Schmittgen (2001) and Xuan et al. (2015). In using the 2[−ΔΔC(T)] method, it was mandatory to use a single set of primers and compare specific gene expression with actin across different age or tissue samples (Step 1). The final quantitative real time-PCR data were statistically analyzed by one-way ANOVA with the SPSS software. In Step 2, we compared the average value of the specific gene expression to that of PBP1 (calibrated to 1) across different ages and antennal samples to see or monitor the peak of PBP or GOBP expression in the same experiment (see **Supplementary Figure 1**). For comparison of tissues after insecticide exposure, we analyzed each gene separately. Expression in the antennae was calibrated to 1 (Step 2, **Figure 5C**) to see or monitor the peak of PBP/GOBP expression in a specific tissue after chemical stress.

One-Step Reverse Transcriptase PCR (RT-PCR)

For the measurement of gene expression in the egg, larva, and pupa tissue samples, total RNAs from all the various tissues were isolated using the Trizol™ method (Invitrogen, Waltham, MA, United States). RNA quality was assessed by optical density measurements (Eppendorf BioPhotometer; Eppendorf, Hamburg, Germany) and electrophoresis on agarose gel (1 μg). The total RNAs were then used as templates in specific one-step-reverse transcription PCR experiments (Takara Bio Inc., Shiga, Japan). For the samples taken for RNA extraction and one-step RT-PCR, three 1.5-ml Eppis tubes full of eggs and about 50 larvae and fifty pupae (per pre-eclosion stage) were required.

The RT-PCRs were performed on total RNA sample (100 ng) in a TaKaRa PCR Thermal Cycler Dice (Takara Bio Inc., Shiga, Japan) under optimal conditions: reaction cycles at 50°C for 30 min, 94°C for 2 min, 40 cycles of 94°C for 30 s, 60°C for 30 s, and 72°C for 40 s. Test primers were: BmorPBP1 (#X94987) sense 5′-gagatgacgctaacagatgc-3′, antisense 5′-ttcagctttgaagcaggtcg-3′; BmorPBP2 (#AM403100) sense: 5′-gcaatcctgtgcatgtccaa-3′, antisense 5′-agacctctgccattaagagc-3′; BmorGOBP1 (#X94988) sense 5′-caagttcgaacacagagagc-3′, antisense 5′-gcgtccttgaaacattcagc-3′; BmorGOBP2 (#X94989) sense 5′-taagacccttgaggaatgcc-3′, antisense 5′-ttttctcagctagaacttgcc-3′. *Cyclophilin A* and *actin3* genes from *B. mori* were both amplified alongside the test genes to calibrate for both experimental variability and RNA integrity. Control CypA and Actin primers were: CypA (#NM_001043836) sense 5′-cgagaatttcacccttaagc-3′, antisense 5′-catgccttcaacaacattcc-3; Actin (#X04507) sense 5′-gacatggagaagatttggc-3′, antisense 5′-agtcattcgtcagataacgg-3′. The one-step RT-PCR products were analyzed on 1% agarose gel, visualized using ethidium bromide staining, gel-purified (TIANgel Midi purification kit; Tiangen, Sichuan, China), and cloned into a pGEM-T Easy vector (TransGen Biotech, Beijing, China) before they were sequenced on an ABI3700 sequencer instrument using an RR Dye Deoxy terminator cycle sequencing kit (PerkinElmer, Waltham, MA, United States) and specific primers.

Protein Analysis

Biochemical studies were preliminarily conducted on fractions of soluble proteins extracted from eggs, gut, head, mouthparts, epidermis, silk gland, and tail-end spine, as well as thoracic and abdominal legs from fifth instar silkworm larvae. There were not enough proteins to perform SDS-PAGE and immunoblotting, even in concentrated samples. Subsequently, highly concentrated protein samples were used from calling virgin 4-day-old female adult tissues (fat body, eggs, gut, head without antennae, legs, epidermis, thorax, and wings). In further experiments, anterior, median, and posterior legs were dissected from a pool of fifty 5-, 6-, 7-, 8-, and 9-day-old unmated females, providing 1 mg/ml of various age-dependent leg protein samples. Proteins were also extracted from the anterior, median, and posterior legs of fifty 8-day-old males from another pool of silkworms. In this pool of silkworms, the tarsi and femur/tibia of males were dissected at the same time as those of females (8-day-old). From these insects, the antennae, head, eyes, cephalic capsule, sex pheromone gland, hemolymph, and meconium were also collected.

In the preparation of protein samples, tissues were freeze-dried in liquid nitrogen and crushed to powder with mortar and pestle in a specific protein extraction buffer (20 mM Tris-HCl, pH 7.4, containing 100 mM of phenylmethylsulfonyl fluoride, PMSF). The tissue homogenates were centrifuged (Neofuge 15R; HealForce, Shanghai, China) at 12,000 g for 10 min at 4°C to collect the protein supernatant. The protein concentration in the supernatant was measured by Bradford assay. Using larval tissues, the following protein concentrations (in μg/μl) were determined: anterior legs (2.99), median legs (5.24), posterior legs (3.95), gut (3.4), head (2.71), mouth (3.55), the epidermis (5.07), silk gland (0.49), and tail (1.37). Tissue-specific ∼16 kDa protein bands were observed, but no labeling was found in the first attempts to immunoblot. The relevance of this was linked to the approximate molecular weight of PBPs/GOBPs, i.e., 15.89–17.17 kDa (without the signal peptide).

Using adult tissues, the following protein concentrations (in μg/μl) were determined: wings (1.08), legs (1.95), head (1.46), thorax (5.25), the abdominal epidermis (6.83), fat body

including eggs (14.66), and gut (3.03). The protein solution was then concentrated by lyophilization (Labconco, Kansas City, MO, United States). After freeze-drying, the protein powder corresponding to 1-, 5-, 10-, 20- and 40-fold concentrated samples were resuspended in 20 µl of a 5x SDS (denaturing)-loading sample buffer, boiled, and loaded onto a 15% acrylamide gel under denaturing conditions. SDS-PAGE was run at 120 V for 2.5 h. All tissue samples that allowed for visualization of a protein band in the zone corresponding to the 14–24 kDa markers (14–100 kDa Blue Plus® II Protein Marker; TransGen Biotech Company, Beijing, China) were selected for immunoblotting.

Immunoblotting was performed to check for the detection of BmorPBP1, BmorGOBP1, and BmorGOBP2 in concentrated protein samples of various tissues. No antibody was available for the detection of BmorPBP2. Accordingly, four aliquots per tissue were prepared for protein analysis and immunodetection. Polyclonal antibodies against these proteins were from Maida et al. (2005). Sodium dodecyl sulfate-polyacrylamide gel electrophoresis SDS-PAGE and Western blotting were performed with traditional biochemical methods. After the SDS-PAGE, proteins were transferred to pure nitrocellulose blotting membranes (Pall Corporation, Port Washington, NY, United States) using a system from Beijing Junyi-Dongfang Electrophoresis Equipment Co. Ltd. (Beijing, China), as described in Xuan et al. (2014). Protein was detected using an HRP-DAB chromogenic substrate detection system (Tiangen, Sichuan, China) as described by the protocol of the manufacturer. Blocking was done in TBST (10 mM Tris-HCl, 0.15 M NaCl, 0.05% Tween-20) overnight at 4°C. Primary and secondary antibody sera were used at dilutions of 1:2,000 and 1:10,000, respectively. Unbound antibodies were washed off, leaving only signals corresponding to antibodies bound to the protein. The specificity of antibody cross-reactivity with electrophoresed bands was confirmed by the position of molecular mass markers (visualization of both the 14–24 kDa marker and sample proteins on the same gel or Western blot; prestained Blue Plus® II Protein Marker, 14–100 kDa, TransGen Biotech Company, Beijing, China).

Application of Abamectin and Measurement of OBP Expression Levels

To examine how moth tissues and the *PBP/GOBP* clade respond to chemical stress (insecticide), 4-day-old male adult silkworm *B. mori* were dipped in abamectin (China Agricultural University Biological Technology Co., Beijing, China) diluted in water following the method described in Xuan et al. (2015). Xuan et al. (2015) established that *B. mori* responds to abamectin with an array of "chemosensory protein" genes. Precise conditions for the insect treatments with the specific insecticide and controls were as described by Xuan et al. (2015) for the induction of "CSP" genes. The abamectin concentration was 4.2 ppm. The biological reason for this concentration was to overcome the slow penetration of insect cuticles by avermectins B1a and B1b (Clark et al., 1994). This abamectin concentration (4.2 ppm) compares with the reported low LC50 values with sublethal effects on insects (Batiha et al., 2020). The dipping duration was 10 s. This dose- and time-treatment was linked to the upregulation of detoxification genes such as *CYP4G25*, *CYP6AE21*, *CYP6B29*, *CYP15C1,* and *CYP333A2* (Xuan et al., 2015). Three replications (3x $n = 10$) were maintained for both abamectin exposure and control in real-time PCR as described by Xuan et al. (2015). The fourth batch of D4 adult males ($n = 40$) was maintained for electrophoresis, immunodetection, and protein data. As in the study of "*CSPs*," the dipping method was chosen to optimize the deposition of chemical insecticide molecules on the epidermis and more precisely assess gene expression simultaneously in multiple tissues (see **Figures 4**, **5** and **Supplementary Figures 3**–**5**).

In total, about 100 silkworms were cut into pieces using scissors and forceps about 6 h after the dipping experiment (Xuan et al., 2015). On the basis of tissue distribution and ontogeny of the PBP/GOBP clade in the silkworm moth, the main olfactory sense organs and metabolic tissues were dissected for gene expression data. In three replications for both abamectin exposure and control, antennae, head, legs, thorax, gut, and fat body were dissected and immediately frozen in liquid nitrogen. RNA/cDNA samples were prepared as described under quantitative real-time PCR. In the fourth batch, epidermis and wings were added to the analysis but did not show any PBP/GOBP signals.

Protein samples from the antennae, head, legs, thorax, gut, fat body, epidermis, and wings of D4 adult virgin males treated with insecticide or control were prepared as described under protein analysis. Protein samples (1 mg/ml) for each tissue in the control and treated groups of D4 silkworms were analyzed by SDS-PAGE and Western blot using BmorPBP1, BmorGOBP1, and BmorGOBP2 antibodies as described before.

The qRT-PCR method was used to more precisely address *PBP/GOBP* gene expression and other gene protein families in response to chemical stress comparing sensory (antennae, head, and legs) and metabolic tissues (gut, thorax, and fat body). For qRT-PCR, messenger RNA samples were used to quantify *PBP1*, *PBP2*, *GOBP1*, *GOBP2*, *CYP306A1*, *CYP4M9*, *AOX1*, *AE41*, *JHE*, *cJHBP*, *hJHBP*, *EcR-B1*, and *OR1* gene expression in response to abamectin chemical as described in Xuan et al. (2015).

Structural Modeling and Ligand Docking

The 3D models for BmorPBP1 (1DQE_mono2; X-ray, pH 8.4, resolution 1.8 Å) and BmorGOBP2 (2WCH; X-ray, pH 8.5, resolution 1.7 Å) were built using Modeler in Linux (Sali, 2020). For each of the two targets, structural models displayed 100% homology with templates from the Protein Data Bank (Sandler et al., 2000; Zhou et al., 2009). Docking and binding mode prediction of pheromone and non-pheromone ligands on PBP1 and GOBP2 were done with PyMOL and Vina (AutoDock Vina 4.2; Seeliger and de Groot, 2010; Trott and Olson, 2010) on "flexible protein": 100 conformations for each protein were generated with Rosetta stimulating flexibility (Loshbaugh and Kortemme, 2020). Relative affinity in Kcal/mol corresponded to the best energy score of the most populated cluster using a contact-based ligand clustering approach for the identification

of "active" compounds in *in-silico* screening (Mantsyzov et al., 2012). The root-mean-square deviation (RMSD) among ligand positions was < 2 Å.

First, we checked for the position of the bombykol molecule on the model to validate the method as performed by Klusák et al. (2003). For PBP1, the bombykol position is such that the hydroxyl group of the pheromone interacts with Ser56. For GOBP2, the bombykol position is such that the hydroxyl group of the pheromone falls close to Arg110 and Glu98 (Sandler et al., 2000; Zhou et al., 2009). We measured $\Delta G = -7.4$ Kcal/mol for bombykol bound to PBP1 using Linux (see **Supplementary Figure 6**). This is consistent with actual *in vitro* ligand binding studies: $\Delta G = -8.1$ Kcal/mol (Sandler et al., 2000; Campanacci et al., 2001; Leal et al., 2005; Mansurova et al., 2009; **Supplementary Figure 6**; Zenodo dataset). However, we measured a much lower relative affinity for bombykol bound to GOBP2 using Linux. The interaction of GOBP2 with bombykol could be due to the presence of water molecules in the protein binding site in the ligand-binding study *in vitro* (Zhou et al., 2009). The presence of a water molecule in the vicinity of Arg110 and Glu98 is favorable to the interaction of bombykol with GOBP2 (*In vitro*/Kd: 7.71E-06 ± 3.61E-06 vs. Linux/Kd: 4.27E-05 ± 4.38E-06 without water molecule in the vicinity of Arg110 and Glu98). So, in our docking experiments, bombykol achieved much more higher affinity for BmorPBP1 than for BmorGOBP2, which provides a greater degree of confidence in our modeling analyses based on bombykol for PBP1. We then used the same approach to measure the ability of non-semiochemical ligands to displace the bombykol molecule and integrate fully into the functional binding site of the protein (see **Figures 6**, **7** and **Supplementary Figures 6–8** and **Tables 1**, **2** and **Supplementary Tables 2**, **3**). Docking experiments were conducted using both BmorPBP1 and BmorGOBP2 as protein structures tested for binding non-semiochemical ligands such as vitamins (A, B1, B2, B3, B5, B6, C, D2, E, H, K1, K2, and K3), juvenoids (juvenile hormones I, JH II, JH III, and methoprene), regulatory neurotransmitters (acetylcholine and octopamine), methylxanthine drugs active on the nervous system and degraded by cytochromes (such as caffeine), insecticides (imidacloprid, pyrethrin II, and malathion), and several esters of carboxylic fatty acids important for various primary metabolic pathways, such as those of glucose and chemical energy (ethyl carbamate or urethane, dimethyl malonate, propionate, and succinate; **Supplementary Figure 7**).

Given all the ligands tested, many molecules representing all major chemical classes were subject to protein structure-ligand interaction by systematic docking (**Supplementary Figure 7**). For each "non-semiochemical" ligand, the interaction was measured with scoring of poses, motifs, accuracy metrics, model performances, and binding energy (ΔG in Kcal/mol) in protein docking for BmorPBP1 and BmorGOBP2 (**Supplementary Tables 2**, **3**), identifying vitamins as potentially active "non-semiochemical" ligands for PBP1. The relative binding value was determined by docking using flexible protein in Linux. Linux yielded molecular protein models with a large hydrophobic pocket as observed in the X-ray structure (PDB: 1DQE). In addition, a qualitative analysis of the residues involved in the interaction with ergocalciferol, and vitamins A, E, K1, K2, and riboflavin were performed using the LigPlot+ software (Laskowski and Swindells, 2011).

TABLE 1 | Binding energy scores of the interaction of BmorPBP1 and BmorGOBP2 protein structures with "non-semiochemical" ligands in docking experiments (Linux).

"Non-semiochemical" ligand	ΔG (Kcal/mol) BmorPBP1	ΔG (Kcal/mol) BmorGOBP2
Ergocalciferol	−11.8	−9.5
Vitamin K2	−11.8	−10.8
Vitamin K1	−11.5	−9.1
Vitamin E	−11.3	−6.6
Vitamin A	−10.9	−9.5
Riboflavin	−10.1	−6.2
Pyrethrin II	−9.5	−7.5
Vitamin K3	−9.6	−8.6
Juvenile hormone I	−9.4	−8.1
Methoprene	−9.1	−8.2
Juvenile hormone II	−9.0	−7.9
Juvenile hormone III	−8.9	−8.1
Imidacloprid	−7.8	−7.2
Thiamine	−7.0	−6.9
Biotin	−6.7	−6.1
Caffeine	−6.2	−6.1
Malathion	−6.1	−4.0
Dimethylmalonate	−5.6	−5.6
Pyridoxine	−6.2	−5.5
Nicotinamide	−6.1	−5.2
Nicotinic acid	−6.0	−5.1
Octopamine	−5.9	−5.7
Panthothenic acid	−5.9	−5.4
Ascorbic acid	−5.6	−5.1
Succinate	−4.8	−4.5
Acetylcholine	−4.7	−4.0
Ethyl carbamate	−3.6	−3.3
Propionate	−4.0	−3.3

Those in red show predicted high affinity of PBP1 for vitamin compounds.

RESULTS

Age Variations of Male Pheromone Responsiveness in *B. mori*

Under our laboratory conditions (23°C, 70% relative humidity, 15-h light: 9-h dark), pheromone detection with young silkmoth resulted in the initiation of mating immediately after emergence.

By I-tube behavioral tests, we observed a consistent behavioral response through days 7–9 of adult male life. Time to react (Tr) and time to reach the source (Ts) were on average at about 11.29 ± 8.75 and 37.7 ± 31.38 s in 1- to 8-day-old males (n = 30–40; **Figure 1**). A few 9-day-old males tested were able to respond to pheromone (n = 10; Tr: 10.33 ± 6.51, Ts: 31.67 ± 20.55). The late-stage males (∼D16–18) showed no response in the behavior test. They showed symptoms of disease, i.e., bluish-gray melatonin spots on the body starting on the abdomen.

TABLE 2 | Main interactions (amino acid residues) between vitamin K1 and BmorPBP1 (pdb: 1DQE).

Index	Residue	Amino Acid	Distance (Å)	Ligand Atom	Protein Atom
1	12B	Phe	3.36	2,105	187
2	12B	Phe	3.48	2,109	185
3	12B	Phe	3.45	2,103	188
4	12B	Phe	3.65	2,111	182
5	36B	Phe	3.47	2,106	562
6	36B	Phe	3.65	2,104	563
7	37B	Trp	3.08	2,108	584
8	52B	Ile	3.94	2,105	817
9	52B	Ile	3.87	2,104	819
10	68B	Leu	3.77	2,124	1061
11	68B	Leu	3.57	2,118	1062
12	73B	Ala	3.72	2,118	1133
13	76B	Phe	3.59	2,114	1180
14	90B	Leu	3.95	2,115	1387
15	90B	Leu	3.51	2,117	1385
16	91B	Ile	3.91	2,118	1405
17	118B	Phe	3.59	2,102	1796
18	118B	Phe	3.59	2,119	1799
19	135B	Val	3.82	2,106	2067

B means hydrophobic interactions. Amino acid Ser56 side chain (polar charges) conjugates with menadione (PyMOL and Autodock/Vina; Seeliger and de Groot, 2010).

Expression of PBP and GOBP Genes in Aging *B. mori*

A real-time qPCR analysis of the expression profiling of the *BmorPBP1*, *BmorPBP2*, *BmorGOBP1,* and *BmorGOBP2* genes in the antennae across the whole adult lifetime of the silkworm showed that *PBP* and *GOBP* expression varied with age (**Figure 2**).

Analyzing *OBP* expression across ages compared with d1, expression peaks were noted for *PBP1*, *PBP2*, and *GOBP2* in 7-day-old males (**Figure 2A**), while different peaks of expression were observed in females (**Figure 2B**). Compared with d1, *PBP1*, *PBP2*, *GOBP1,* and *GOBP2* expression was reduced in d2 and d3 males (**Figure 2A**), while only *PBP1* and *GOBP1* expression was reduced in 2- and 3-day-old females (**Figure 2B**).

The expression of both *PBP* and *GOBP* was found to increase with age in both males and females (**Figures 2A,B**). *PBP* and *GOBP* expression increased in late-stage adults, but the females showed more gene changes than the males (D16–D18; **Figures 2A,B**). *PBP1*, *GOBP1,* and *GOBP2* expression increased in late-stage adult males. The four genes were induced over aging in the late-stage adult females (**Figures 2A,B**).

Analyzing the gene expression ratio for each day using *PBP1* as a reference showed about a 100-fold increase on Days 2 and 3 in *GOBP1* and *GOBP2* expression in the males but not in the females (**Supplementary Figure 1**). The *PBP1-PBP2* expression ratio was seen to change to 1:9 on Day 9 in males on the basis of gene expression using *PBP1* = 1 (**Supplementary Figure 1A**). *GOBP* gene expression peaked on Day 7 in the females (**Supplementary Figure 1B**).

Expression of PBP and GOBP Proteins in Legs of Aging *B. mori* Females

Behavioral analysis showed no age-dependent variations in the responsiveness of males to the female sex pheromone in the silkworm moth *B. mori* (see **Figure 1**). However, an RNA analysis showed age-dependent changes in the variance of *BmorPBP1*, *BmorPBP2*, *BmorGOBP1,* and *BmorGOBP2* expression in the antennae in both sexes (see **Figure 2**). To check for non-pheromone functions in the moth PBP/GOBP clade, we set out to determine which tissues other than the antennae express PBP and/or GOBP proteins.

We used a large repertoire of sensory and metabolic tissues from the adult stage. We examined 4-day-old *Bombyx* female tissues (eggs, epidermis, fat body, gut, legs, thorax, wings, and head without antennae) from 1 to 5, 10, 20, and 40 mg/ml of protein concentration and checked for the presence of PBP and/or GOBP in each concentrated protein sample by SDS-PAGE and Western blot, and using a specific antibody (**Supplementary Figures 2A,B**). Protein bands corresponding to 14–16 kDa soluble proteins were detected in particular in the (x20) leg samples (**Supplementary Figure 2A**). No cross-reactivity with the BmorGOBP1 antibody was observed (**Supplementary Figure 2B**); however, cross-reactivity with the BmorPBP1 antibody identified 14–16 kDa proteins in the head (lacking antennae) and leg tissue samples (**Supplementary Figure 2B**).

Young (4-day-old) female leg samples with a very high concentration of protein (20 mg/ml) showed a signal when incubated with either the PBP1 or the GOBP2 antibody (**Supplementary Figure 2**). We then conducted a Western blot to investigate the abundance of the BmorPBP1, BmorGOBP1, and BmorGOBP2 proteins in leg tissues from females of different ages with only 1 mg/ml of protein concentration (**Figure 3**). Total protein concentration and SDS-PAGE (no apparent differences) were used as two loading controls (**Figure 3A**). We found that the BmorGOBP1 antibody labeled all the different female leg samples from D5 to D8. Interestingly, the GOBP1 immunoreactivity of the adult silkworm legs increased in an age-dependent manner. The BmorGOBP1 antibody more strongly labeled 14–16 kDa proteins in particular in posterior legs of the 9-day-old virgin females (see D9; **Figure 3A**). The PBP1 labeling resulted in a much weaker signal in the D8–D9 female (posterior) legs. No labeling or GOBP2 protein was evident in the legs of Days 5–9 female adults using samples with a low concentration of protein (1 mg/ml; **Figure 3A**). In another experiment, we used 1 mg/ml femur/tibia and tarsi samples in order to compare PBP/GOBP expression between the two sexes and different parts of the legs from unmated D8 female *Bombyx* (**Figure 3B**). The labeling of PBP/GOBP in the antennae was used as a control (**Figure 3B**). No labeling was found for GOBP1 in the antenna and leg samples (**Figure 3B**). We found weak labeling for PBP1 and GOBP2 in the male legs, but BmorPBP1 and BmorGOBP2 strongly labeled the leg tarsi from aging (8-day-old) females (**Figure 3B**). Therefore,

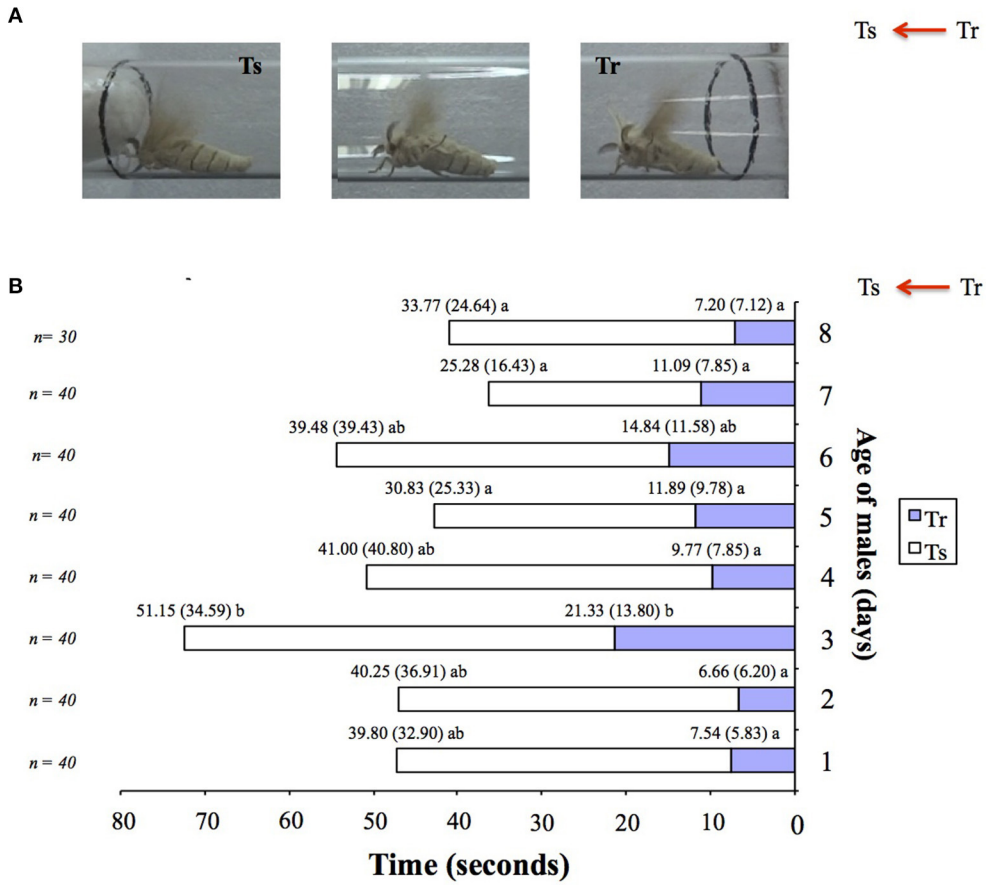

FIGURE 1 | Age-related variations in pheromone responsiveness of male moths in *Bombyx mori*. **(A)** Behavioral responses of adult virgin male silkworm moths in an I-olfactometer to one calling Day 1 virgin conspecific female (odor source). Two-time responses (in s) are recorded: 1° Tr (time to react), 2° Ts (time to reach the source). **(B)** Behavioral responsiveness of 1-day-old (Day 1) to 8-day-old (Day 8) adult virgin male silkworm moths in the I-olfactometer (**A**) to one calling Day 1 virgin conspecific female (odor source). 0 was noted as the time when the males entered the upper part of the I-olfactometer. Average values and standard deviations (in brackets) are indicated atop the bars. Different letters indicate significant statistical differences at $p < 0.001$ by Mann–Whitney U test. n, number of males tested per age category.

our results from age-related changes in protein expression and immunoblots in the female silkworm moth *B. mori* are such that tarsi may turn GOBP1 off when PBP1 and GOBP2 are turned on D8. It may be that the expressions of GOBP1 and PBP1/GOBP2 are inversely related, suggesting a potential reciprocal regulation of transcription and/or translation in sex-, tissue-, and age-dependent manner (see **Figures 2**, **3**).

However, the immunoblots showed that the expression of PBP/GOBP proteins was not specific to antenna and leg appendages (see **Supplementary Figure 3**). When performing other immunoblots using various male and female tissues, we found some immunoreactive signals for BmorPBP1 in the eyes, cephalic capsule, and whole insect head (brain and epidermis of the scalp, head without antenna). The heads of moths of both sexes expressed the BmorPBP1 protein (**Supplementary Figure 3**), while the BmorGOBP1 protein was found in the meconium (metabolic waste products from the pupal stage; **Supplementary Figure 3**).

Expression of PBP and GOBP Genes in Non-sensory/Metabolic Tissues Across Different Developmental Stages of the Silkworm *B. mori*

By SDS-PAGE/immunoblot and using protein samples of various adult tissues, the expression of PBP and GOBP was found to be not restricted to the antennae (see **Figure 3** and **Supplementary Figures 2**, **3**). The expression was evident in the tarsi of aging females seeking oviposition (Days 8–9; **Figure 3**). Protein expression data for Day 8 adults also showed rather convincing evidence for the presence of PBP1 in male (traces) and female heads without antenna and more abundant expression in cephalic capsules and in compound eyes, although no quantitative statements were possible because of lack of a loading control other than Coomassie Blue staining (**Supplementary Figure 3**). However, traces of GOBP were also detected in the meconium excreted by silkworm adults, suggesting a role

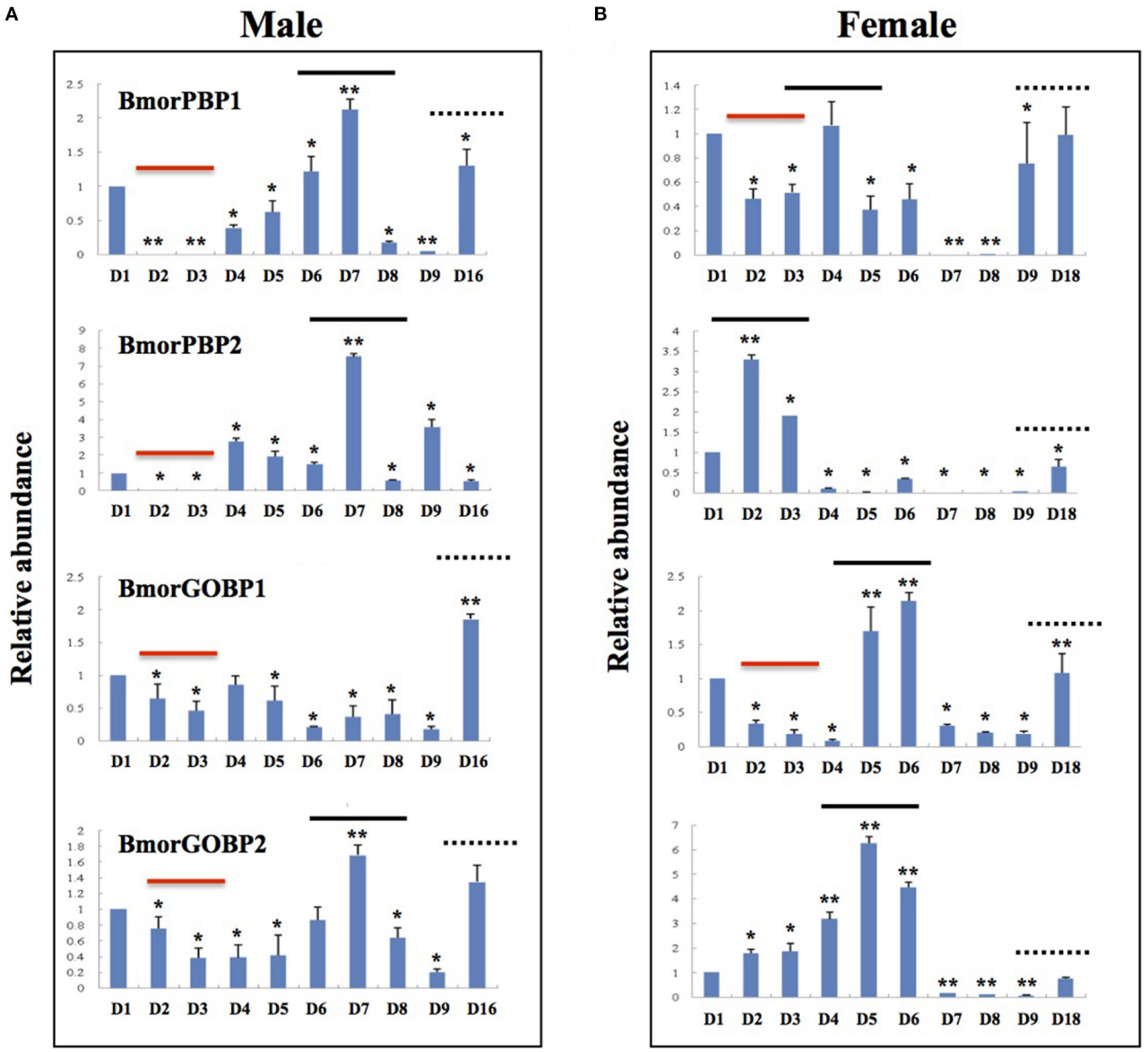

FIGURE 2 | Age-related variations in the expression of *PBP1*, *PBP2*, *GOBP1,* and *GOBP2* genes in adult antennae of *Bombyx mori*. Quantitative real-time PCR (qRT-PCR) analysis of antennal expression levels of *BmorPBP1*, *BmorPBP2*, *BmorGOBP1,* and *BmorGOBP2* in different age groups of adult silkworm moths. Age variation of *PBP/GOBP* expression in **(A)** males and **(B)** females. Antennal gene expression levels in D1 (1-day-old) moths were used as reference (=1). The bold lines show age-dependent changes in *PBP/GOBP* gene expression levels in both sexes. The dotted lines show the upregulation of gene expression in the antennae of elderly moths (D9–D16/18). The red line shows the downregulation of gene expression in the antennae of young moths (D2–D3). The bars show means ± standard deviation ($n = 9$). *significant statistical differences at *alpha* = 0.05 by one-way ANOVA. **significant statistical differences at *alpha* = 0.01 (ANOVA).

in metabolic processes associated with insect development (**Supplementary Figure 3**). To investigate in detail the ontogeny of *PBP*/*GOBP* expression in *B. mori*, we used molecular biology methods and performed a much more comprehensive and specific detection of RNA transcripts to examine the expression profiles of *PBP1*, *PBP2*, *GOBP1,* and *GOBP2* from eggs to most of all the tissues developed in fifth instar larvae and E-5 through E-1 pupae (**Figure 4** and **Supplementary Figure 4**).

Amplification of the two control genes (*actin3* and *cyclophilin A*) indicated the overall RNA integrity of the samples assayed. Semi-quantitative one-step RT-PCR amplification revealed the presence of transcripts for *PBP1*, *PBP2,* and *GOBP1* in the eggs. No PCR products were detected in the eggs for *CYP306A1*, *CYP4M9*, *EcRB1, JHE,* and *OR1* (**Figure 4A**). In the larvae, amplicons for *BmorGOBP1* expression were readily detectable not only in the mouthparts, gut, silk gland, and tail spine but also in both the thoracic and abdominal prolegs, although in

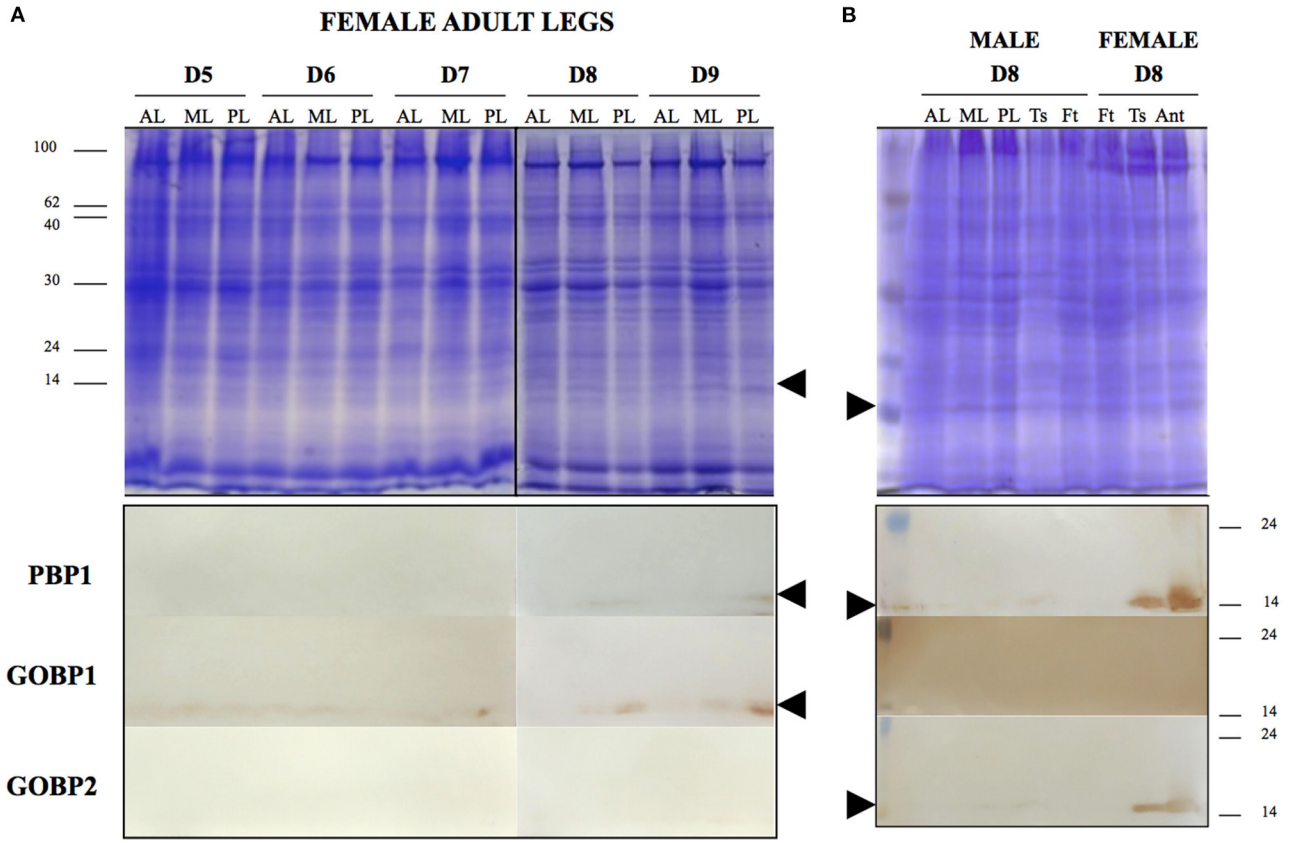

FIGURE 3 | Age-related variations in the expression of PBP/GOBP protein in adult legs of *Bombyx mori*. **(A)** Gel electrophoretic separation (top) and immunoblots (below) of leg soluble protein samples in different age groups of female adult silkworms. AL, anterior legs; ML, median legs; PL, posterior legs. Age groups of female silkworm moths are from Day 5 (5-day-old, calling) to Day 9 (9-day-old, laying eggs). Below shows the results of female leg proteins exposed to BmorPBP1, BmorGOBP1, and BmorGOBP2 antibodies for immunodetection. The arrow tips show the position of PBP/GOBP-immunoreactive proteins (~16 kDa) in D7–D9 legs of mulberry adult female silkworm moth *B. mori*. **(B)** Gel electrophoretic separation (top) and immunoblots (below) of leg protein samples in the D8 group of male and female adult silkworms. For comparison between male and female, soluble proteins from the three pairs of legs (AL, anterior legs; ML, median legs; and PL, posterior legs) and different parts of the leg (Ts, tarsi and Ft, femur tibia) are exposed to BmorPBP1, BmorGOBP1, and BmorGOBP2 antibodies, respectively. The arrow tips show the position of PBP/GOBP-immunoreactive proteins (~16 kDa) in D8 leg tarsi of mulberry female silkworm *B. mori*. The same immunoreactive proteins are detected in the female antennal samples used as control (Ant).

lower amounts (**Figure 4A**). In the silk gland, *BmorGOBP1*-amplicons were noted in both the secretory section (rich in fibroin) and the storage sac (containing the gel-like unspun silk). *BmorGOBP2*-amplicons were found associated with the mouthparts, but *BmorPBP1*-amplicons were detected in all the larval tissues examined, including more particularly the gut and the prolegs (**Figure 4A**). Correlatively, the expression of ecdysone-related genes, such as *CYP306A1*, *CYP4M9*, and *EcRB1*, was found to be expressed in the prolegs and the silk gland of *Bombyx* larvae, while the *OR1* and *JH esterase* genes were silent (**Figure 4A**).

In addition, we detected PCR products for *BmorPBP1* in many various tissues, including not only the antennae but also the head (epidermis and brain) and legs across various pupal stages (**Figure 4B**). PCR products for *BmorPBP2* were found to be particularly high in the antennae and in the gut, head, legs, silk gland, thorax, and wings of E-4 and E-3 pupae (**Figure 4B**). *BmorGOBP1*-PCR products were particularly high starting at the E-4 pupal stage in many and various tissues (**Figure 4B**). Analyzing tissues from the pupae, the expression of *BmorGOBP2* was found to be not restricted to the antennae but also in the head and legs, in particular, 2-days before emergence (**Figure 4B**).

High levels of *BmorPBP1* expression were detected in the adult stage on the first-day post-emergence (Day 1). However, *BmorPBP1* expression on Day 1 was not restricted to the antennae, it was also detected in the head, legs, and epidermis (**Supplementary Figure 4**). Similarly, PCR products for *BmorGOBP2* expression in older adults (Day 9) were also found in various tissues, including the gut, head, legs, epidermis, and wings (**Supplementary Figure 4**). In the immature pupal stage (E-5, when tissues are colorless and soft), no PCR products or amplicons for *BmorPBP1* expression were detected. However, amplicons for *BmorGOBP1*, *BmorGOBP2,* and *BmorPBP2* expressions were detected rather ubiquitously in all the tissues

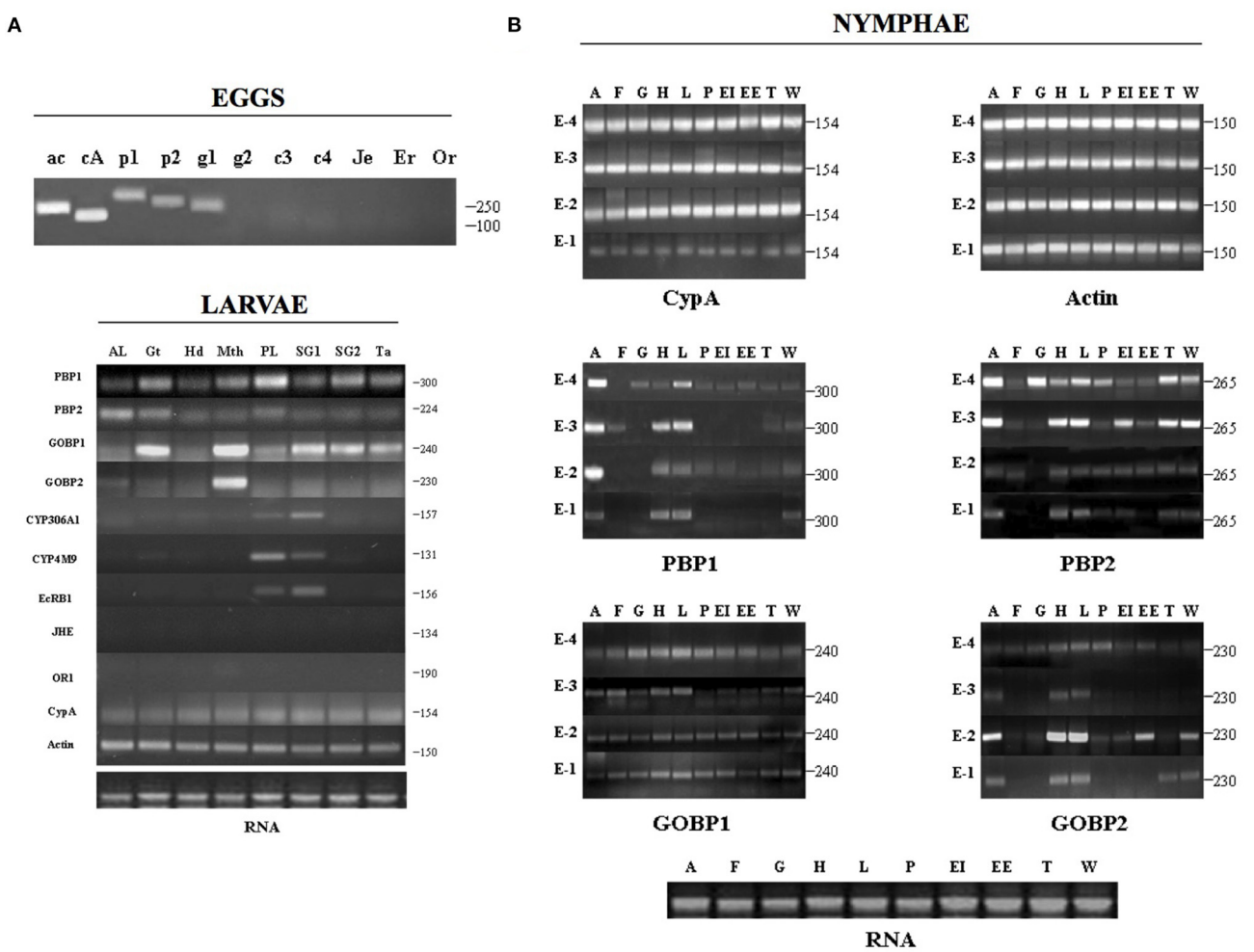

FIGURE 4 | Ontogeny of *PBP/GOBP* expression. Expression of *BmorPBP1, BmorPBP2, BmorGOBP1, and BmorGOBP2* across 19 distinct tissues in *Bombyx mori* development. **(A)** Gene expression profiling in eggs (embryo) and fifth-instar larval tissues (AL, anterior -thoracic- legs; Gt, gut; Hd, head; Mth, mouth parts; PL, prolegs; SG1, silk gland (secretory section); SG2, silk gland (storage sac); Ta, dorsal tail end spine) of the silkworm moth. Eggs/ac: *actin*, cA: *CypA* (*cyclophilin A*), p1: *BmorPBP1*, p2: *BmorPBP2*, g1: *BmorGOBP1*, g2: *BmorGOBP2*, c3: *CYP306A1*, c4: *CYP4M9*, Je: *JHE*, Er: *EcR-B1*, Or: *OR1*. RNA: RNA control of larval tissue samples (1 μg/lane). The numbers indicate the length in bps of specific RT-PCR products. *Actin* and *cyclophilin A* are used as housekeeping control genes that are expected to express equally across the different tissues. **(B)** Gene expression profiling in late pupal stages (E-4 to E-1) of the silkworm. Using primers for *actin* and *cyclophilin A* (reference genes) shows an amplicon of expected length in similar amounts in all the tissue samples tested [A: antennae, F: fat body, G: gut, H: head (without antennae), L: legs, P: pheromone gland, EI: internal envelope (epidermis), EE: external envelope (cuticle), T: thorax, W: wings]. The numbers indicate the length in bps of specific RT-PCR products for *BmorPBP1*, *BmorPBP2*, *BmorGOBP1,* and *BmorGOBP2*, showing that RNA signals peaked not only in the antennae but also in many various metabolic tissues from E-4 to E-1. RNA: total RNA control of pupal tissue samples (E-1 to E-4: 1 μg/lane).

investigated (**Supplementary Figure 4**), strongly suggesting a function related to early pupal development and tissue formation for these genes.

A BLASTn analysis in Silkbase (brain, early embryo of strain p50T, early embryo of strain N4, fat body, internal genitalia, midgut, anterior silk gland, middle silk gland, and epidermis) confirmed that transcripts encoding PBP1, PBP2, GOBP1, and GOBP2 are not restricted to the adult tissue, but found in different stages of the development, including embryo (**Supplementary Table 1**). By the BLASTn analysis in Silkbase, *BmorPBP1* expression was detected in the brain tissue and early embryo of the two *B. mori* strains (p50T and N4; **Supplementary Table 1**). *BmorPBP2* gene expression was detected not only in the brain and early embryo of p50T and N4 but also in the internal genitalia, similar to *BmorGOBP1* (**Supplementary Table 1**). However, *BmorGOBP1* expression was also detected in the anterior silk gland (**Supplementary Table 1**). *BmorGOBP2* expression was detected in the brain and early embryo RNA seq libraries, similar to *BmorPBP1* (**Supplementary Table 1**), strongly suggesting non-pheromone and/or non-olfactory functions for all the four OBP protein genes.

Expression of PBP/GOBP Genes in Response to Insecticide Exposure

We then applied a toxic macrolide insecticide endectocide molecule (abamectin) to check for the involvement of OBPs in insect defense following Xuan et al. (2015). Accordingly, RNA transcripts and the protein expression of *BmorPBP1*, *BmorPBP2*, *BmorGOBP1,* and *BmorGOBP2* were assessed in a comparative study of sensory and metabolic tissues from D4 silkworm males using qRT-PCR and immunoblot (**Figure 5**).

By immunoblot and using a group of tissues from 4-day-old *Bombyx* males, we found high expression levels and abundance of BmorPBP1 in the antennae (**Figure 5A**). However, in this immunoblot experiment, analyzing two different sets of samples (treated vs. control), we found that BmorPBP1 protein expression was not restricted solely to the antennae, and BmorPBP1 signals were also found in other tissues, such as fat body, head, and thorax, particularly in the group of males treated with the abamectin insecticide (**Figure 5A**), showing the increased synthesis of BmorPBP1 in metabolic tissues in response to chemical stress. However, in the blots (**Figure 5A**), it appeared that there was also a signal in the control samples for PBP1 in the head and thorax. Therefore, it cannot be said that the presence of PBP in these tissues is attributed only to stress response.

The qRT-PCR results showed that poisoning the tissues of male silkworm moths with an insecticide, such as abamectin, showed that abamectin exposure modulated the expression of all four genes examined depending upon tissue and gene (**Figure 5B**). For example, PBP1 and GOBP2 showed decreased expression in the antennae, but PBP2 showed increased expression. Similarly, PBP1/2 showed decreased expression in the head, but GOBP1 showed increased expression. In the legs, PBP2, GOBP1, and GOBP2 showed severely decreased expression, but PBP1 rather showed increased expression. So, it is not always the case for the four genes that the expression was decreased (**Figure 5B**). However, in some instances, as shown in **Figure 5B**, an increase in the expression is apparent.

Abamectin insecticide exposure led to the increased expression of the *BmorPBP1*, *BmorPBP2*, *BmorGOBP1,* and *BmorGOBP2* genes in various metabolic tissues, such as the thorax and fat body (**Figure 5B**). The exposure also led to the increased expression of *BmorPBP2* in the gut (**Figure 5B**). Similarly, abamectin promoted the increased expression of *BmorPBP1* in other tissues including not only the legs but also the gut, thorax, and fat body (**Figure 5B**). *BmorPBP2* gene expression was increased by a factor of 4 in the gut, while the two *B. mori GOBP* genes, *BmorGOBP1* and *BmorGOBP2*, were upregulated in the thorax and fat body, two organs for intermediary metabolism in the insect, by a factor of 4 to 16 in response to abamectin exposure (**Figure 5B**).

Intriguingly, applying abamectin by dipping the moth in the insecticide solution did not change the expression levels of the gene encoding olfactory pheromone receptor (*OR1*; low detection levels). However, exposure to abamectin upregulated not only the *PBP* and *GOBP* genes but also 20-hydroxyecdysone-related genes and cytochrome oxidase genes responsible for moth metabolism in the fat body (**Figure 5B**). In contrast, abamectin had no effect on the antennal expression of *cJHBP* or *OR1*. *PBP/GOBP* was stimulated along with *CYP306A1*, *CYP4M9*, *EcR-B1*, *AOX*, *AE*, *JHE,* and *hJHBP* in response to insecticide exposure (**Figure 5B**). *BmorPBP1* and *BmorGOBP2* expression increased by up to 50–300 times higher in metabolic tissues, such as the gut, thorax, and fat body, in response to abamectin exposure (**Figure 5C**), strongly suggesting a metabolic function for genes of the *PBP/GOBP* clade in moths.

Docking of Non-semiochemical Ligands on PBP and GOBP Structures

To justify the tissue-developmental profiles (see **Figures 2–5** and **Supplementary Figures 1–5**, **Supplementary Table 1**), we tested 28 different non-semiochemical ligands, including insecticides, juvenoids, caffeine, esters of carboxylic fatty acids, and multiple vitamins in docking of BmorPBP1 and BmorGOBP2 binding sites using Linux for 3D modeling and AutoDock Vina (see **Figures 6**, **7** and **Supplementary Figures 6–8**, **Tables 1**, **2** and **Supplementary Tables 2**, **3**, Zenodo dataset). First, we showed that the position of the bombykol molecule on the model was similar to that observed on the crystal structure. This was attested by a measurement of the binding energy values (in Kcal/mol). The binding energy values obtained with Linux were very close to those obtained with X-ray, e.g., for the measurement of bombykol bound to PBP1: $\Delta G = -7.4$ vs. -8.1 Kcal/mol (Sandler et al., 2000; Campanacci et al., 2001; Leal et al., 2005; Mansurova et al., 2009; **Supplementary Figure 6**; Zenodo dataset). The binding affinity of bombykol with PBP1 was much higher than that measured for bombykol-GOBP2 (only 4.3 in the absence of water; **Supplementary Figures 6**, **8** and **Supplementary Table 3**; Zenodo dataset).

Among the different models, our docking study showed that the PBP1 binding pocket could interact directly with K1 (distance < 4 Å, $\Delta G = -11.5$ Kcal/mol), and that K1 could be accommodated into the PBP1 binding pocket in the same seating U-shaped configuration compared with bombykol (**Figures 6**, **7** and **Supplementary Figure 6** and **Tables 1**, **2**, Zenodo dataset). Furthermore, the binding of K1 was very similar to the binding of bombykol in BmorPBP1 (**Figures 6**, **7** and **Table 2**). In contrast, BmorGOBP2 showed a different binding site for multiple various non-semiochemicals, such as vitamins (**Supplementary Figure 8**). Except for vitamin K2, relative energy values (ΔG) were < -10 Kcal/mol for most of all the ligands tested with BmorGOBP2 (**Supplementary Figures 7**, **8** and **Table 1**). The best affinity value was obtained when the ligand molecule (A, E, ergocalciferol, K2, or pyrethrin II) fell inside the central hydrophobic pocket of the protein, but this rarely happened with BmorGOBP2 (**Supplementary Figure 8** and **Supplementary Table 3**, Zenodo dataset).

DISCUSSION

We have analyzed the behavioral responsiveness of the adult silkworm moth *B. mori* together with the tissue/development profiling of four odorant-binding proteins (referred to as BmorPBP1, BmorPBP2, BmorGOBP1, and BmorGOBP2) that

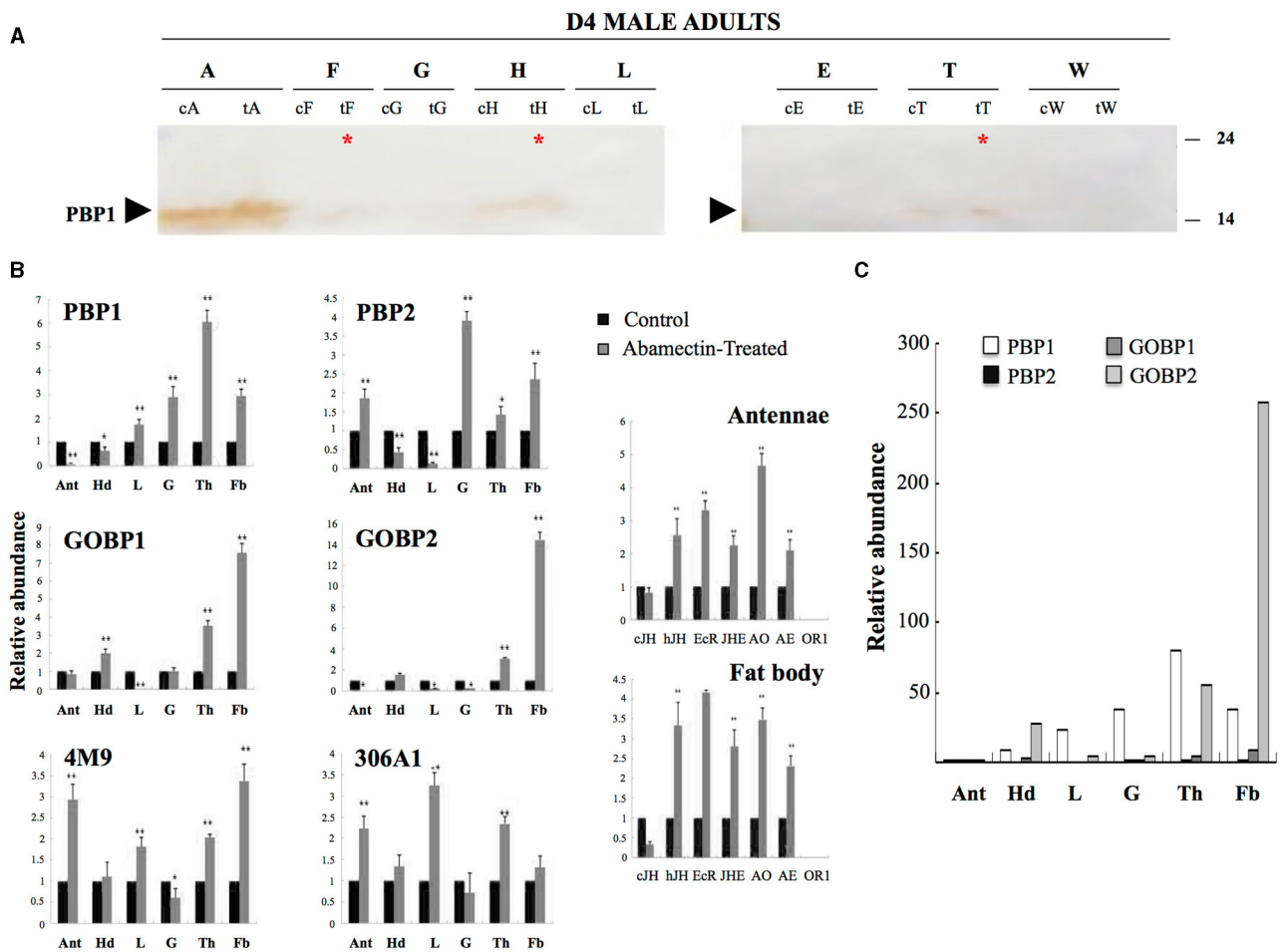

FIGURE 5 | Induction of *PBP/GOBP* expression by abamectin. Tissue-specific regulation of *PBP/GOBP* in male adult *Bombyx mori* treated with insecticide. **(A)** Effects of abamectin insecticide on BmorPBP1 protein expression. Immunoblots of protein samples (1 mg/ml) from 4-day-old male adult tissues probed with antibodies against BmorPBP1. c, control; t, treated. The arrow tip indicates the position of PBP1 on the blot membrane. The asterisk shows PBP1 signals in various metabolic tissues in response to abamectin exposure, although in much lower amounts compared with the antennae (cA, tA). Antennae (A), fat body (F), gut (G), head without antennae (H), legs (L), epidermis (E), thorax (T), and wings (W). The arrow tip indicates the position of 16 kDa proteins on the gel. The numbers aside give the positions of protein molecular weight markers. **(B)** Quantitative real-time PCR (qRT-PCR) analysis of antennal (Ant), head (Hd), legs (L), gut (G), thorax (Th), and fat body (Fb) expression levels of *BmorPBP1*, *BmorPBP2*, *BmorGOBP1*, *BmorGOBP2*, *CYP4M9* (cytochrome P450 4M9), and *CYP306A1* (cytochrome P450 306A1) in the control (saline) and abamectin-treated groups of male adult silkworm moths. Control levels are used as reference (=1). On the right: qRT-PCR analysis of antennae/fat body expression levels of *cJHBP*, *hJHBP*, *EcR-B1*, *JHE*, *AOX1*, *AE41,* and *OR1*. CypA: cyclophilin A, cJH: cytosolic juvenile hormone binding protein (cJHBP), hJH: hemolymphatic JHBP, EcR: ecdysone receptor variant B1 (EcR-B1), JHE: JH esterase, AO: antennal oxydase-1 (AOX1), AE: antennal esterase-1 (AE41), OR1: pheromone/olfactory receptor-1. The bars show means ± standard deviation ($n = 9$). The single asterisk *significant statistical differences at $alpha = 0.05$ by one-way ANOVA. The double asterisk **significant statistical differences at $alpha = 0.01$ (ANOVA). **(C)** Comparative *BmorPBP1, BmorPBP2, BmorGOBP1,* and *BmorGOBP2* gene expression profiles across different tissues in response to insecticide exposure in male adult silkworm moths. Focus on the x-fold increase in gene expression from RNA samples (gut, thorax, and fat body) in the same experiment than 5B (Step 1). Quantitative real-time PCR results with means ($n = 9$) of metabolic tissues compared with antennae (Ant) used as reference (Step 2: Ant expression = 1). Upregulation of PBP/GOBP expression in metabolic tissues after insecticide abamectin treatment.

represent the derived PBP/GOBP clade of Lepidoptera. The OBPs we studied are well-known, e.g., BmorPBP1 and BmorGOBP2, exclusively defined by their affinity to bombykol (Sandler et al., 2000; Zhou et al., 2009). However, the four main points in our study are new and innovative with a marked impact on research as follows: (1) the four OBPs exhibit an age-dependent expression that is independent of pheromone release/detection, suggesting roles outside of the olfactory paradigm, (2) the expression of moth PBPs and GOBPs in non-olfactory tissues in different developmental stages points to an alternative role of these proteins, (3) their expression can be induced under specific physiological conditions (chemical stress) by an insecticide, perhaps indicating that the alternative function is related to insecticide resistance, and (4) their ability to bind non-semiochemical ligands, such as vitamin compounds, is in agreement with the expression of *OBP* genes in bacteria and a great variety of metabolic organs and tissues during insect development.

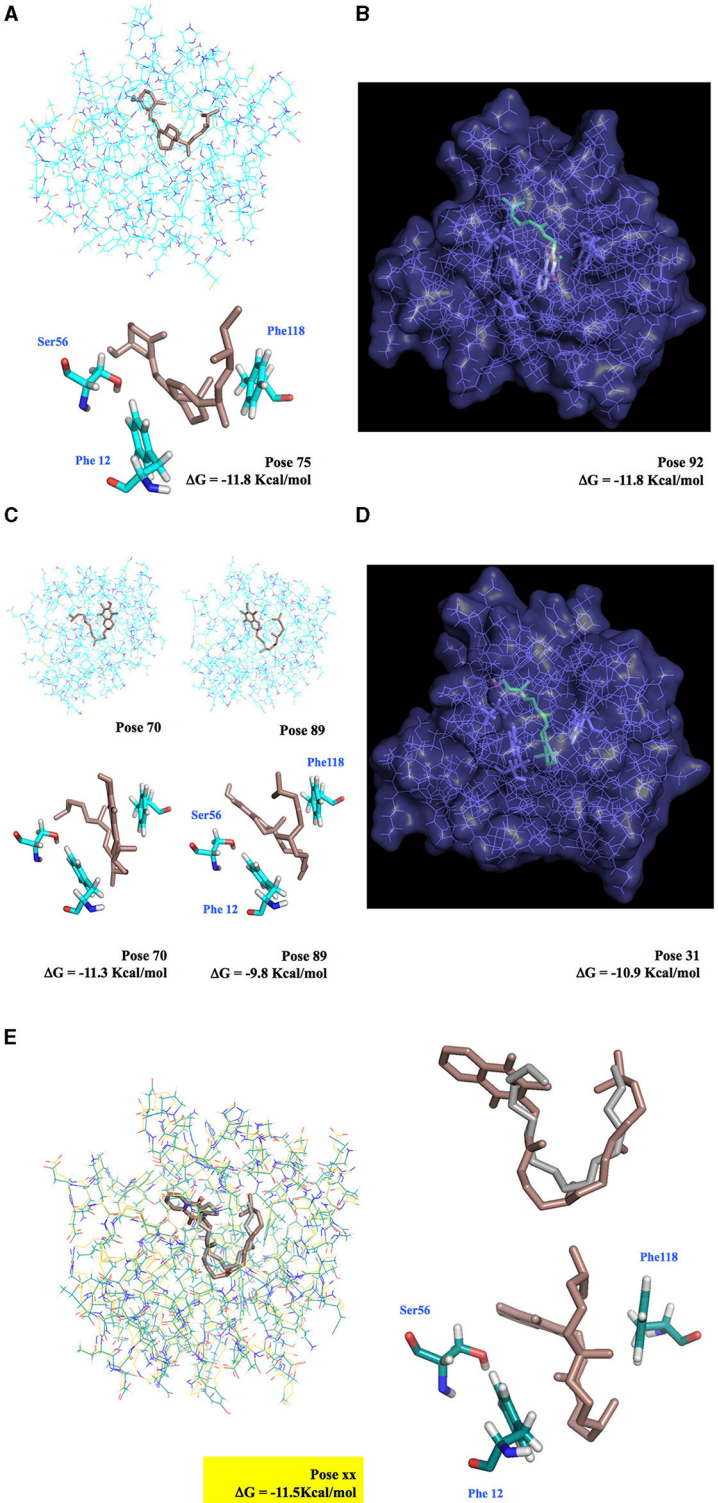

FIGURE 6 | Docking simulation of vitamin molecules integrated into BmorPBP1 binding pocket. **(A)** Ergocalciferol-BmorPBP1 protein complex. **(B)** Cutaway view of the interaction of BmorPBP1 with vitamin K2. **(C)** Vitamin E-BmorPBP1 protein complex in two binding modes. **(D)** Cutaway view of the interaction of BmorPBP1 with vitamin A. **(E)** Interaction of BmorPBP1 with vitamin K1 (docking Vina, in brown) and bombykol (X-ray structure, in gray). Vitamin K1 completely overlaps with bombykol. Vitamin K1 attached to Ser56, Phe12, and Phe118 folds in the same position compared with bombykol in the PBP binding site. ΔG shows the relative binding affinity value for vitamin compounds to PBP1. Docking pose shows scored matching or "best-fit" of fragment atoms from vitamin compound and BmorPBP1 in a multiple-grid arrangement.

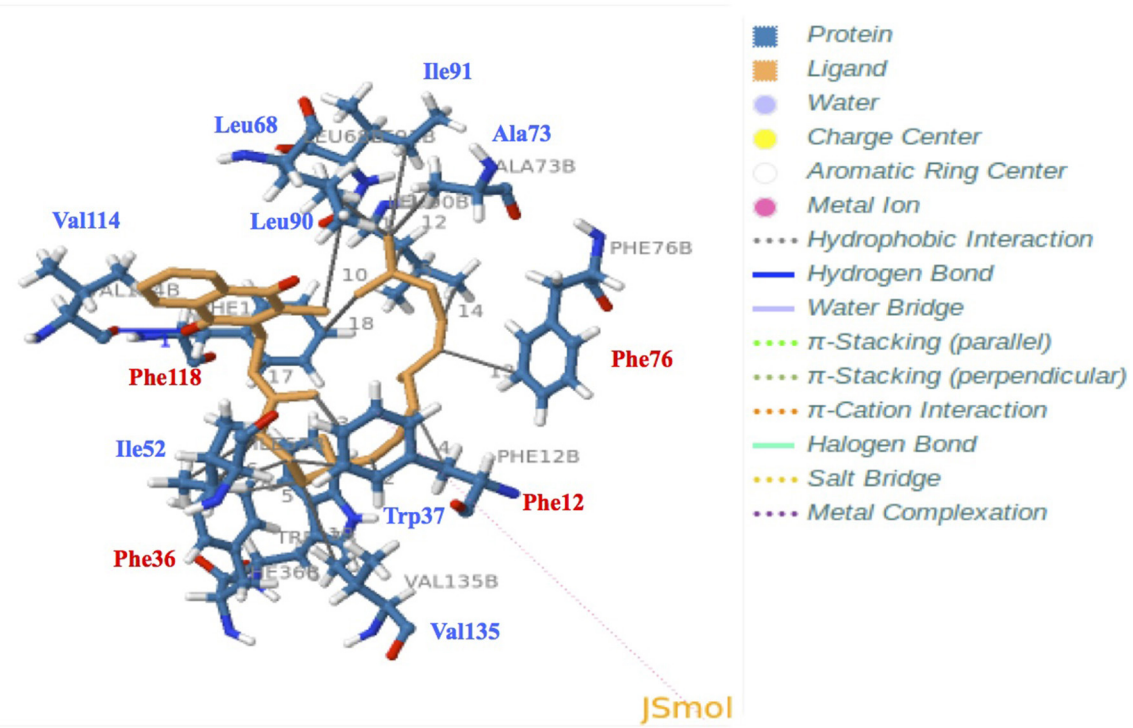

FIGURE 7 | Docking and 3D analysis of BmorPBP1 internal cavity bound to vitamin K1 ligand molecule. Hydrophobic interactions: Phe12, Trp37, Ile52, Leu68, Ala73, Phe76, Leu90, Ile91, Phe118, and Val135. Hydrogen bonds: Index 1, Residue 114B, amino acid: Valine, distances H–A: 3.04 Å, distances D–A: 3.68 Å, donor angle: 124.05°, donor atom: 2,131 [O_3], acceptor atom: 1,742 [O_2]. The predicted vitamin K1-BmorPBP1 complex is visualized with JSMol (modality of Jmol: An Open-Source Java Viewer for Chemical Structures in 3D).

First, by analyzing age-related behavioral responses of the male silkworm *B. mori* and *PBP/GOBP* gene expression in the male antennae by relative RNA abundance and quantitative real time-PCR, we note a reduction in the accumulation of PBP and GOBP RNA in the young males, a linear increase from D4 to D7 for *PBP1/GOBP2* and *BmorPBP1*, *BmorPBP2*, *BmorGOBP1,* and *BmorGOBP2* expressions in time or age. This corresponds to previously reported observations on *B. mori* of no or reduced sex pheromone communication, mating activity, and reproduction (Biram et al., 2005). D2–D3 age-related *PBP/GOBP* expression changes in the males are not associated with the decline in physical responsiveness or the neural discrimination of sex pheromone components (see **Figures 1**, **2**). Then, we observe increased *PBP/GOBP* gene expression in the antennae of aging adult silkworm moths (see **Figure 2** and **Supplementary Figure 1**), which could be directly linked to age-related behaviors and the activation of specific response control elements.

Interestingly, many response control elements are found upstream of the four *OBP* genes studied here. Although alternative promoters and/or regulatory DNA sequences could appear in more distant regions, these sequences may help to explain the *OBP* expression patterns observed in our study (see **Figure 2** and **Supplementary Figure 1**). The mechanisms underlying the *PBP1-PBP2* vs. *GOBP1-GOBP2* expression, in particular, should be investigated with caution. The *PBP1*, *PBP2*, *GOBP1,* and *GOBP2* genes are localized in the same genomic DNA regions 7K−9K at the tip of chromosome 19 (Bm_Scaf100). In the silkworm, *PBP1* and *PBP2* are tandem genes (only separated by 859 bps), while *GOBP1* and *GOBP2* are separated by 115,673 bps and not so closely linked on the genetic map of the silk moth *B. mori* (KAIKObase; Liu and Picimbon, 2017).

In the *B. mori* genome, we find a signal transducer and activator of transcription (JF267349), a sericin promoter region (HQ702379), and multiple transposable elements (Bm1-450bp, BMC1, Hope, gypsy-Ty3-like Kabuki, LTR Yamato, Manga, Mariner, Minichikuri, microsatellite repeats, non-LTR_TREST-W, Rikishi marker, Suju*Minghu, Tama and TREST1) in front of the *PBP1/PBP2* (contig35963), *GOBP1* (contig35949) and/or *GOBP2* (contig35962) genes. Coincidentally, the expression profile of the *GOBP* genes differs in the sexes. The antennal expression of *PBP1* and *PBP2* is constant throughout early adult male life (i.e., D1-D8), whereas the expression of *PBP/GOBP* is only synchronous after D5 in the females (see **Figure 2** and **Supplementary Figure 1**). This might indicate the occurrence of sex-specific regulation of *PBP/GOBP* clade expression, in particular, in the antennae of aging moths.

This view is supported further by the observation that *BmorPBP1*, *BmorPBP2*, *BmorGOBP1,* and *BmorGOBP2* are highly expressed in late-stage *B. mori* adults (about 2-week-old;

Figure 2). The increased accumulations on Day 16/18 in the antennae when the insects are becoming more sensitive to chemical or microbial toxin infection perhaps mean that PBPs and GOBPs give rise to a specific phenotype (longevity). A high expression of these OBPs in late age moths might have phenotypic consequences, in particular, on lifespan. There are numerous gene expression hallmarks of cellular aging, such as dysregulation of immune system genes and signaling in eukaryotes from yeast to humans (Frenk and Houseley, 2018). However, the high expression levels of the *PBP* and *GOBP* genes in late-stage adult moths may coincide with the moth aging process, particularly in the absence of mating. The absence of mating can affect the endocrine system, female and male moth fitness, and senescence (Truman and Riddiford, 1971). The adult lifetime among many various silkworm strains is known to be genetically controlled (Choi et al., 2013). Therefore, it could be that the *PBP/GOBP* clade plays a crucial part in lifespan-related genes controlling neuronal plasticity, moth aging, and/or senescence in a *B. mori* strain, such as Qingsong x Haoyue (Münch et al., 2008; Jarriault et al., 2009; Jindra et al., 2013). Our results suggest genetic interactions between *PBPs*/*GOBPs* and other kinds of genes involved in phenotypic plasticity, resistance, and longevity in insects. Aging beyond the main reproductory period might be particularly relevant to seek additional matings and/or more suitable oviposition sites, especially in long-lived species of moths. The ability of female spruce budworms (Tortricidae, *Choristoneura*) to discriminate cues from host plants for oviposition is very bad in virgins, but changes markedly following mating (Wallace et al., 2004). Additionally, it is known that *OBP* expression levels can be significantly affected by mating in both sexes (Boni Campanini et al., 2017). Therefore, the expression peak of *OBPs* on D4–D7 and D9–D16/18 may be due to the activation of common promoter regulatory regions for "late" mating activity and/or oviposition behavior, although promoter complexity may decrease from immediate newly emerged early to late elderly senescence genes. Promoter regions and transposable elements responsible for the specific expression of senescence genes have been identified in various organisms (Noh and Amasino, 1999; Andrenacci et al., 2020). It would be interesting to identify which promoters (or retroposons) in front of *PBP*/*GOBP* genes are involved in aging silkworm moths. When "late" expression is synchronized for the four genes in the *PBP*/*GOBP* clade in females, but not in males (see **Figure 2** and **Supplementary Figure 1**), there are usually sex-specific functions and gene regulatory processes expected for the clade in the antennal tissues of aging moths.

Very interestingly, we find sex- and age-dependent regulation of *PBP*/*GOBP* gene expression not only in the antennae but also in the legs from the silkworm moth (see **Figure 3**). This provides additional insights into sex-, age- and tissue-dependent regulation of genes within this OBP clade of Lepidopterans (see **Figures 2**, **3** and **Supplementary Figures 1**, **2**). The expression of PBPs and GOBPs in the moth legs is an interesting result, but not surprising, for two reasons: (1) as the antennae and legs are appendages of a particular segment and have similar embryonic origins and (2) many other OBPs are known to be expressed in the legs of insects (Starostina et al., 2009; Yin et al., 2012; Sun et al., 2013, 2017; Ohta et al., 2015; Li et al., 2017, 2020; Guo et al., 2018; Huang et al., 2018; Zhang et al., 2018; Ozaki, 2019). Some insects have sensory hairs on the legs, particularly the tarsi and tibia of pairs of hind legs. It is possible that the OBPs expressed in the legs are implicated more in taste detection than in pheromone detection (Ozaki et al., 2011). However, not only the differential expression of PBP1/GOBP2 vs. GOBP1 but also the increased expression of OBPs in the legs of aging female silkmoths are a very surprising result (see **Figure 3**). This observation allows debating about PBP/GOBP clade and a function narrowly tuned to moth sex pheromone. In *B. mori*, females have four to seven times more tarsal sensilla than males (Takai et al., 2018). The males engage in orientation and locomotion behaviors during or close to mating that involves the legs and would require any sensilla on the legs to be protected from pheromone overdoses, but 8-day-old female silkworms need to engage in an oviposition behavior to lay eggs on the most suitable plant leaves and cocoons. The ontogenies of adult male and female silkworms with regard to the expression of the PBP/GOBP clade were not keyed to pheromone exchanges, mating behavior, and reproduction. We show what happens if males and females are reared separately and if an individual ages without mating in both sexes. It is known that pheromone and mating activities start immediately after eclosion and are terminated after 8–10-days in the adult life cycle of silkworm *B. mori* maintained in laboratory conditions. Females start to lay eggs without mating on day 8 in the same laboratory conditions (Ando et al., 1996; Matsumoto et al., 2002; Blomquist et al., 2012). Therefore, we find a correlation between oviposition behavior and OBP expression in the legs of silkworm moths. There is a difference in pre-oviposition (D5-D7) vs. post-oviposition (D8–D9; see **Figure 3**), suggesting an age-dependent increase in the activation of key regulatory elements in the front of *PBP/GOBP* genes in the legs of the moths. This difference was apparent not only for PBP1 but also for GOBP1. GOBP1 showed presence in all ages but significantly increased in the posterior legs of D8–D9 females (see **Figure 3**). The expression of PBP and GOBP in the tarsi of 8-day-old virgin females could suggest a taste gustatory function involved in host plant recognition for oviposition of the silkworm (**Figure 3**), as described for OBP11 in the alfalfa plant bug *Adelphocoris lineolatus* and specific taste receptors in the papilionid swallowtail butterfly *Pachlioptera aristolochiae* (Ozaki et al., 2011; Sun et al., 2016).

However, here, we observe the presence of BmorPBP1, BmorGOBP1, and BmorGOBP2 proteins not only in the forelegs but also in the cephalic capsule, compound eyes, and meconium of D8 adult silkworm moth *B. mori* (see **Supplementary Figures 2**, **3**). Therefore, it is not only the antennae/legs appendages but also neurons in the brain and retina that seem to express the *PBP/GOBP* clade. Meconium is what remains from the gut following the process of metamorphosis from the pupal to adult digestive tract. So theoretically, there could be a lot of different molecules, such as PBP and GOBP, related to the physiology of this process. Accordingly, we have analyzed the ontogeny of *BmorPBP1, BmorPBP2, BmorGOBP1,* and *BmorGOBP2* gene expressions

through all the various stages of *Bombyx* development from egg to late instar larvae and pupae. We report about the induction of gene expression in the *PBP/GOBP* clade much before the appearance of adult rigid organs (see **Figure 4** and **Supplementary Figure 4**). We find *PBP1, PBP2,* and *GOBP1* expression in eggs (embryo; see **Figure 4A** and **Supplementary Table 1**) as found for *OBPs* in many various insect species, including particularly egg noctuid moths (Amenya et al., 2011; Sun et al., 2012). We find a low-abundance *GOBP2* sequence in *B. mori* eggs by analyzing the EST contain the NCBI library or database (HX266954). Therefore, the *PBP/GOBP* clade is not only expressed in adults but also in eggs (embryo), and this seems to be a marked expression throughout many different species of moths. We also found *BmorPBP1, BmorPBP2, BmorGOBP1,* and *BmorGOBP2* expression in numerous larval tissues, which is in good agreement with EST resource in NCBI where numerous hits for the two *GOBP* sequences can be found in tags of silkworm larvae libraries (*GOBP1*: FY38063-FY755241, *GOBP2*: FY741717-FY57625; see KAIKObase, Shimomura et al., 2009). Like EST-RNA sequences, RT-PCR products for *PBP1*, *PBP2*, *GOBP1,* and *GOBP2* genes do not necessarily signify the presence of the respective proteins, but they certainly signify the induction of the respective genes not only in the egg but also in many tissues of the larvae of the silkworm moth (see **Figure 4**). In the fifth instar larvae (feeding stage) of the silkworm *B. mori*, we find the induction of the *GOBP1* and *GOBP2* expression to be mainly associated with the mouthparts, confirming the studies of Vogt et al. (2002). However, our results show that *GOBP1* expression is not restricted to chemosensory sensilla surrounding the mouth, but that *GOBP1* RNA transcripts are also particularly abundant in the secretory section (rich in fibroin) and the storage sac (unspun silk) of the moth silk gland (see **Figure 4A**). This is in agreement with the BLASTn analysis of *B. mori* tissues in Silkbase. Based on BLASTn data of Silkbase (**Supplementary Table 1**), we emphasize the presence of PBP and GOBP RNA sequences in tissues other than the brain or early embryo, for example, internal genitalia and anterior silk gland but no epidermis or middle silk gland, which we detected using RT-PCR (see **Figure 4** and **Supplementary Figure 4**). BmorPBP1 and BmorGOBP1 clones are also found in the anterior silk gland of the wild silkmoth *Bombyx mandarina* (A_BomaASGc47494 and A_BomaASGc16510). Therefore, although it should be remembered that the presence of RT-PCR products or even intact mRNA sequences in these tissues does not necessarily imply the presence of functional proteins, the activation of response control elements and detection of transcripts imply PBP/GOBP protein synthesis in tissues as diverse as brain, antennae, legs, gut, epidermis, and silk gland in the silkworm moth *B. mori* (see **Figure 4** and **Supplementary Figure 4**, **Supplementary Table 1**). High expression levels during whole insect development from the egg (embryo) to late instar larvae, pupae, and adults in a high number of tissues from the brain to silk gland strongly suggest for PBPs and GOBPs some alternate functions to pheromone/odor detection.

The non-antennal specific expression of PBP1, PBP2, GOBP1, and GOBP2 across a number of "non-sensory" tissues raises questions regarding the assigned olfactory role of these proteins (**Supplementary Figure 5**). Because our data indicate a broader expression profile for the PBP/GOBP clade (**Supplementary Figure 5**), we posit a new hypothesis in which OBPs are pleiotropic carrier proteins that function in diverse physiological processes, such as CNS function, development, metabolism, and immunity.

Interestingly, high-throughput RNA sequencing (RNA-Seq) of larval transcriptomes in the silkworm challenged by the fungus *Beauveria bassiana* failed to identify PBPs and GOBPs during the early response to infection (Hou et al., 2014). This could indicate that different methods have different sensitivity analyses and/or that PBPs and GOBPs are expressed under specific physiological conditions, i.e., downregulated for fungal infection. Therefore, we checked for evidence of variations in *BmorPBP1*, *BmorPBP2*, *BmorGOBP1,* and *BmorGOBP2* expressions in response to chemical stress/abamectin exposure using specific qRT-PCR and following Xuan et al. (2015). There could be multi levels of insecticide resistance in insects, enrolling more genes than the one typically involved in immunological responses under chemical stress conditions, including not only cytochrome P450s, carboxylesterases, and acetylcholinesterase but also small soluble binding proteins, such as "CSPs" (Mamidala et al., 2012; David et al., 2014; Xuan et al., 2015; Einhorn and Imler, 2019). Like THP12 (12 kDa *Tenebrio* hemolymph protein precursor), numerous OBPs are described as immune proteins in the insect hemolymph involved with microbial toxin infection (Graham et al., 2003; Levy et al., 2004; Song et al., 2006; Contreras et al., 2013; Behrens et al., 2014; Hou et al., 2014; Einhorn and Imler, 2019). In particular, antennal binding protein (ABP)-7 is known to be upregulated in the plasma of silkworm larvae in an innate immune response to bacterial stress/*Bacillus* exposure (Song et al., 2006). More recently, symbiotic bacteria, such as the obligate mutualist *Wigglesworthia,* have been shown to induce OBP synthesis in insect gut to maintain hematopoiesis and regulate symbiont-mediated immunological pathways, such as melanotic response in tsetse flies (Benoit et al., 2017; Rihani et al., 2021). These studies are in line with our results from using the pesticide active substance abamectin on several sensory and metabolic tissues from *B. mori* (see **Figure 5** and **Supplementary Figure 5**). Abamectin (avermectins B1a/B1b) is not used in the rearing of the silkworm. It has been chosen because of its insecticide activity in the context of targeting muscles and neurons, i.e., various internal tissues [potentiating gamma-aminobutyric acid (GABA) effects on gated chloride channels], and because it is closely related to macrocyclic lactones produced by soil bacteria. *B. mori* males were chosen because we challenged the moth PBP/GOBP function exclusively tuned to sex pheromone responsiveness (see **Figures 1–4** and **Supplementary Figures 1–4**, **Supplementary Table 1**). Here, we demonstrate the induction of *PBP/GOBP* genes by the natural product abamectin (see **Figure 5**), which could be a very important result for insect pest control. If the OBPs are knocked out, it could be that the moths, pupae, or larvae become much more susceptible to abamectin, which is used as an insecticide. This is a new line of research for OBP knockout, insect physiology, and potential application for pest control.

Very interestingly, the increased expression of genes in the moth *PBP/GOBP* clade, in response to abamectin exposure, is found to be tissue-specific, as found for "*CSPs*" and *cytochrome P450* "*CYPs*" (see **Figure 5**; Xuan et al., 2015). Similar to *CSPs* and *CYPs*, the increased expression of *PBP* and *GOBP* genes after insecticide exposure mainly occurred in tissues with high metabolic rate, such as the gut, thorax (prothoracic glands), and fat body (see **Figure 5** and **Supplementary Figure 5**; Xuan et al., 2015). We also find that the *BmorPBP1* and *BmorGOBP2* genes have significant hits (85–87%) in the EST database from the midgut of another bombycid species, *Trilocha varians* (TrvaMGcomp3213 and TrvaMGcomp652766; silkbase.ab.a.u-tokyo.ac.jp), which is very congruent with our qRT-PCR data. The immunoblot comparisons for the same tissues are not always compatible with those revealed by the analysis of the RNA transcripts in PCR or Expressed Sequence Tags. Transcript levels by themselves are not sufficient to predict protein levels because of various regulatory cellular processes, i.e., RNA and protein synthesis and turnover. There could be a delay (> 6 h) for high effects of abamectin at the protein level (see **Figure 5A**), which could be detected further by LC/MS/MS. This would, perhaps, reveal additional OBPs induced by the insecticide. Here, the sequences of immunoreactive bands were not confirmed by LC/MS/MS analysis, but the expression of PBP/GOBP outside the olfactory system was confirmed by molecular biology analysis. We did not use immunoblot and protein data as a tool to measure the PBP/GOBP protein copy number per tissue. We checked for the presence of proteins in the PBP/GOBP clade outside the antennal olfactory system in response to insecticide exposure. We performed quantitative real-time PCR to assess relative RNA copy numbers per tissue, therefore showing an interesting link between *OBP* expression and metabolic tissues, such as the gut, thorax (ecdysteroids), and fat body (see **Figure 5B**). Both qRT-PCR and immunoblot experiments show PBP/GOBP expression outside the olfactory system, which is not a so surprising result. BmorPBP1 rather enhances the sensitivity, but not the selectivity, of pheromone detection (Shiota et al., 2018). Robust olfactory responses are observed in the absence of OBPs (Xiao et al., 2019). The pheromone specificity of PBPs has been revisited in the giant silk moth *A. polyphemus* (Saturniid) and the cabbage moth *Mamestra brassicae* (Noctuid). Using a fluorescence binding assay and several fatty acid ligand molecules brings into doubt the first overwhelmingly held belief that PBP is only tuned to a specific cognate sex pheromone compound (Campanacci et al., 2001; Lautenschlager et al., 2007). Then, an increasing number of *OBP* genes are reported to be expressed in many fluids and tissues as various as tarsi, legs, hemocytes, salivary gland, pheromone gland, prothoracic gland, fat body, gut, epidermis, testis, and wings in a lot of insect species (Li et al., 2008; Okamoto et al., 2008; Xuan et al., 2014; Song et al., 2016; Benoit et al., 2017; Sun et al., 2018; Einhorn and Imler, 2019; Picimbon, 2019; Zhang et al., 2020; Rihani et al., 2021). Some OBP proteins even help in the hemolymph transport of juvenile hormone or JH (Kim et al., 2017). Not only the developmental profiling but also the response to abamectin exposure, fat body, gut, and thorax expression for *PBP/GOBP* clade, and expression co-fluctuation with metabolic and endocrine genes (see **Figures 2–5** and **Supplementary Figures 1–5**) argue for a compact alternative to the traditional olfaction expression, a function far from any olfactory component or semiochemical substance for this clade of moth protein genes or even for the whole insect OBP protein gene family.

Prior to initiating behavioral studies with mutants, we sought to more extensively assess the role of insecticide exposure in *PBP/GOBP* expression. A first hypothesis would be that abamectin exposure leads to induction because PBP/GOBP binds this compound in an innate immune response to chemical insecticide. This is rather very unlikely because the large size of abamectin ($C_{95}H_{142}O_{28}$) is not appropriate to accommodate the OBP binding site (Sandler et al., 2000; Zhou et al., 2009). In addition, this would not explain the induction of *PBPs* and *GOBPs* in the absence of abamectin at many different stages of moth development. There could be multiple sources of induction of *OBP* gene expressions, such as lipid and hormonal signaling pathways that are activated during development and/or abamectin insecticide stress (see **Figures 4**, **5** and **Supplementary Figure 5**). We leaped from gene expression profiling of tissues and developmental stages to a more functional interpretation of PBP and GOBP using the molecular docking modeling approach to assess possible candidates for "non-chemosensory" ligands. Besides insecticides, hormones, and fatty acids, vitamins were chosen, because insects need high content of these nutrients for multiple physiological functions, from cell growth to immune response (Krivosheina, 2008; Salem et al., 2014; Basset et al., 2017). Vitamin K1 was chosen because its structure (and conformation) is very similar to that of Bombykol. Accordingly, our molecular docking results in Linux, PyMOL, and Autodock/Vina suggest a specific binding site and critical amino acid residues (Ser56, Phe12, and Phe118) for binding of a non-semiochemical ligand, such as vitamin phylloquinone K1 in BmorPBP1 (see **Figures 6**, **7** and **Supplementary Figures 6–8**, **Tables 1**, **2** and **Supplementary Tables 2**, **3**, Zenodo dataset). The biological relevance of *in silico* binding of vitamin K and other compounds needs to be investigated further. Just because it can bind (< 4 Å distance between K1 and PBP1 binding site, same configuration with bombykol, U-shape, and the same critical residues in the protein core, Ser56, Phe12, and Phe118 to anchor the ligand, interaction with vitamin > interaction with bombykol, ΔG: -11.5 vs. -7.4 Kcal/mol) does not necessarily mean it does bind and trigger specific physiological responses. However, the structural data presented here (see **Figures 6**, **7** and **Supplementary Figures 6–8**, **Tables 1**, **2** and **Supplementary Tables 2**, **3**, Zenodo dataset) strongly agree with the broad expression of *PBPs* and *GOBPs* in both time and space, expression in eggs, embryo, and aging moths, and expression under insecticide stress, in the physiological data also presented here (see **Figures 1–5** and **Supplementary Figures 1–5**, **Supplementary Table 1**). The structure and expression results of OBPs in this study compare with previous studies where only structural and binding data were reported without a link to physiology. Our study was more rigorous in examining spatio/temporal expression

patterns for OBP/PBP/GOBP-encoding genes. Although the new hypothesis needs to be ultimately proved by additional *in vitro* binding and X-ray studies, our ontogeny, protein/gene expression, and docking data help us to propose that OBPs, such as PBPs and GOBPs, retain a function tuned to "non-semiochemical" ligands, which will remain to be found addressing specifically transport and binding properties of micronutrients and vitamins rather than pheromones and general odorants in future functional analyses of the moth PBP/GOBP clade.

None of the numerous studies on moths have tested the hypothesis that PBPs and GOBPs are regulatory molecules for the binding of non-semiochemicals. This also applies to all various functional analyses and binding studies conducted on OBPs. Based on our extensive physiological study on the silkworm moth *B. mori*, PBP/GOBP in metabolic processes becomes a strong research hypothesis. Like PBP, GOBP is detected in the brain and the earliest stage during insect development, i.e., early embryo, perhaps suggesting a function in neuroplasticity and/or neurogenesis for these proteins. *PBP/GOBP* expression is also detected in the silk gland and gut of wild silk moth species (*B. mandarina* and *T. varians*). Therefore, the function of PBP/GOBP in the metabolic system (changes in growth and nutrient profiles) does not seem to have been altered by thousands of years of domestication, although comparisons are needed to be made with closely related non-domesticated species of the same genus to make a clear claim. If the *B. mori PBP/GOBP* gene set was knocked out, perhaps by CRISPR-based editing, it would be interesting to see what physiological effects might arise, such as non-responsive males to pheromonal stimulation or, as suggested by our molecular docking, potential vitamin deficiencies.

CONCLUSIONS

We comprehensively analyzed the expression profile of the PBP/GOBP gene set in *B. mori* in response to age, development, tissue specificity, and insecticide exposure. Amazingly enough, 20 years after the structure, this is the first complete survey of the tissue and ontogeny expression of PBP/GOBP in silkworms. Here, we carry out the study around the theme "physiological regulation," and we investigate this theme using multiple experiments, analyzing this clade at different developmental stages in males and females, and using both molecular and biochemical approaches.

The expression of *Bombyx* PBPs and GOBPs in leg tarsi of aged adult females, as well as in tissues as diverse as an early embryo, brain, and silk gland raises questions regarding the currently accepted paradigm of their functionality that is restricted to male-specific pheromone detection. When the OBPs become extremely well-known, at several levels, but focusing only on interaction with semiochemicals, the induction of PBPs and GOBPs in metabolic tissues in response to abamectin insecticide exposure adds new interest to these two classes of binding proteins that appear to be much more versatile than believed so far. The age-, mating-, development- and tissue-dependent expressions of OBPs have been studied in many insect species; thus, structure in relation with physiology is something expected. The amount of tissues covered, as well as specific physiological conditions (exposure to insecticide), maybe just descriptive, but the description strongly indicates non-olfactory functions for OBPs. The role of PBPs and GOBPs was tuned to olfaction. By docking, we report that vitamins could be selective and potent ligands for PBP/GOBP, which would be in agreement with the PBP/GOBP gene expression profiling revealed here in our study.

DATA AVAILABILITY STATEMENT

The original contributions presented in the study are included in the article/**Supplementary Material**, further inquiries can be directed to the corresponding author. Docking data are linked to Zenodo Dataset doi: 10.5281/zenodo.5597323, https://zenodo.org/record/5597323#.YXhGxXxxfIU.

AUTHOR CONTRIBUTIONS

JFP conceived and designed the study, dissected all the organs and tissues, prepared the RNA samples, analyzed and interpreted the data, analyzed the complete set of data, and wrote the manuscript. QL reared the silkworms. JFP and GL coordinated the insects and lab works. JFP and XG conceived and carried out behavioral assays, prepared the protein samples from all the tissues, performed the biochemical analyses, and did the biochemical work on infected tissues. XG, NX, GL, HX, and JFP did the molecular biology work (one-step RT-PCR and real-time PCR) and performed real-time PCR on moth tissues infected by abamectin. XG, NX, GL, HX, and JFP ran the insecticide test on *Bombyx* tissues. PA and BO planned and performed the docking experiments and conceived and presented the docking results. PA, BO, and JFP interpreted the docking results. All the authors approved the final version of the manuscript.

FUNDING

This study was supported by the Natural Sciences Foundation of Shandong Province (ZR2011CM046) and Overseas Talent, Taishan Scholar (JFP, No. tshw20091015).

ACKNOWLEDGMENTS

We thank A-J Wang for helping us with silkworm rearing in Yantai. We also thank J. Krieger and H. Breer for gifting *B. mori* PBP1, GOBP1, and GOBP2 antibodies. Heartfelt thanks to Prof. Dr. H. Breer (Hohenheim University, Germany) for the precious advice and comments on the earliest version of the manuscript. Also heartfelt thanks to the editor and four reviewers (#reviewers 2 and 4) for the most helpful comments and consideration on the final version of the manuscript to Frontiers in Physiology.

SUPPLEMENTARY MATERIAL

The Supplementary Material for this article can be found online at: https://www.frontiersin.org/articles/10.3389/fphys.2021.712593/full#supplementary-material

Supplementary Figure 1 | Comparative *BmorPBP1, BmorPBP2, BmorGOBP1,* and *BmorGOBP2* gene expression profiles across different age groups in **(A)** male and **(B)** female adult silkworm moths. Focus on OBP ratio and x-fold increase in gene expression from RNA samples (D2–D9) in the same experiment as **Figure 2** (Step 1). qRT-PCR results with means ($n = 9$) of *PBP2*, *GOBP1,* and *GOBP2* compared with *PBP1* used as reference (Step 2: *PBP1* expression = 1). PBP/GOBP expression aging differences between males and females.

Supplementary Figure 2 | Detection of BmorPBP1 and BmorGOBP2 proteins in legs of female *Bombyx mori* adults. **(A)** Gel electrophoretic separation of highly concentrated protein samples (5–20 mg/ml) from the fat body (Fb), egg, gut (G), head without antennae (Hd), legs (L), epidermis (Ei), thorax (Th), and wings (Wg) of 4-day-old female adult silkworms. **(B)** Immunoblots of 4-day-old female tissues probed with BmorPBP1, BmorGOBP1, and BmorGOBP2 antibodies. The numbers (kDa) aside from the gels or the blots give the position of protein molecular weight markers (MK). The arrow indicates the position of immunoreactive ∼16 kDa proteins in the head and leg samples. The asterisk (*) shows PBP/GOBP signals in the leg samples and the PBP1 signal in the head (without antennae) samples.

Supplementary Figure 3 | Immunoblots of 11 tissues of 8-day-old adult silkworms probed with BmorPBP1, BmorGOBP1, and BmorGOBP2 antibodies. Co, cocoon; G, gut; Hm, hemolymph; Mc, meconium; PG, pheromone gland; iE, internal (unlaid) eggs; eE, external (laid) eggs; mH, male head (without antennae); fH, female head (without antennae); Cp, cephalic capsule; Ey, compound eyes. The numbers aside the blots give the positions of protein molecular weight markers (kDa). The arrow tip indicates the position of immunoreactive ∼16 kDa proteins for PBP1 and GOBP1. The asterisk (*) shows PBP/GOBP signals in the male head (without antennae), female head (without antennae), cephalic capsule, compound eyes, and meconium of adult silkworms.

Supplementary Figure 4 | Expression profiling of *BmorPBP1*, *BmorPBP2*, *BmorGOBP1,* and *BmorGOBP2* genes across 9 distinct tissues in early pupae (E-5) and adult (D1/D9) moths. A, antennae; F, fat body; G, gut; H, head (without antennae); L, legs; P, pheromone gland; Ei, internal envelope (epidermis); T, thorax; W, wings. E-5, 5-days before emergence (no rigid organs); D1, 1-day-old female adult *B. mori*; D9, 9-day-old female adult *B. mori*. The numbers indicate the length in bps of specific RT-PCR products (*CypA*, *Actin*, *PBP1*, *PBP2*, *GOBP1,* and *GOBP2*). *Actin* and *CypA* (*cyclophilin A*) are used as housekeeping control genes that are expected to express equally across the different tissues. RNA control of tissue samples (1 μg/lane) is shown below. *PBP/GOBP* gene expression profiles in specific tissues are age-dependent. The arrow tip indicates (1) *PBP1* expression in the antennae, head, legs, and epidermis of D1; (2) *PBP2* expression in the antennae, head, legs, thorax, and wings of E-5, (3) *GOBP1* expression in most of all the tissues of D1; and (4) *GOBP2* expression in the antennae, gut, head, legs, epidermis, and wings of D9.

Supplementary Figure 5 | Tissue expression profiling of moth *PBP/GOBP*. *B. mori PBP/GOBP* gene expression profiling during the silkworm development from eggs to adults under **(A)** normal conditions and **(B)** following exposure to abamectin insecticide. Data are from **Figures 2**–**5**, **Supplementary Figures 1**–**4**, and **Supplementary Table 1**. Specific gene expression is shown by color code: red (PBP1), blue (PBP2), green (GOBP1), and orange (GOBP2). Upregulation in the expression levels of *PBP/GOBP* genes is indicated by a larger circle. Downregulation is indicated by a triangle oriented down. Ant, antennae; Ep, epidermis; FB, fat body; G, gut; Lg, legs; HPL, hair-pencils; Th, thorax; Wg, wings.

Supplementary Figure 6 | Configuration and position of bombykol in protein binding site. **(A)** PBP1. **(B)** GOBP2. In blue: linux (theoretical), in red: X-ray (experimental).

Supplementary Figure 7 | A repertoire of "non-sensory" chemical structures tested in docking experiments for preferred orientation and interaction when bound to BmorPBP1 and BmorGOBP2 binding sites. **(A)** Vitamins (A–K3). **(B)** Insecticides (neonicotinoids, organophosphates, and pyrethrins). **(C)** Juvenoids (JH and mimetics). **(D)** Caffeine (alkaloid methylxanthines). **(E)** Esters of carboxylic fatty acids (short chains).

Supplementary Figure 8 | Docking simulation of vitamin and insecticide pyrethrin molecules bound to BmorGOBP2. Vitamin K2 (pose 1): motif 1, total_Nb 14, Val de Ene (ΔG) = −11.1 Kcal/mol; Vitamin K2 (pose 96): Motif 1, Total_Nb 24, Val de Ene (ΔG) = −10.8 Kcal/mol; vitamin A (pose 18): Motif 1, Total_Nb 32, Val de Ene (ΔG) = −9.5 Kcal/mol; vitamin A (pose 95): motif 1, total_Nb 4, Val de Ene (ΔG) = −10.2 Kcal/mol; vitamin K1 (pose 40): motif 1, total_Nb 1, Val de Ene (ΔG) = −9.1 Kcal/mol; vitamin K1 (pose 18): motif 6, total_Nb 4, Val de Ene (ΔG) = −7.3 Kcal/mol; ergocalciferol (pose 97): motif 1, total_Nb 0, Val de Ene (ΔG) = −9.5 Kcal/mol; ergocalciferol (pose 47): motif 9, total_Nb 35, Val de Ene (ΔG) = −6.5 Kcal/mol; vitamin E (pose 97): motif 1, total_Nb 0, Val de Ene (ΔG) = −10.6 Kcal/mol; vitamin E (pose 66): motif 7, total_Nb 14, Val de Ene (ΔG) = −6.6 Kcal/mol; pyrethrin II (pose 43): motif 1, total_Nb 0, Val de Ene (ΔG) = −9.9 Kcal/mol; pyrethrin II (pose 0): motif 2, total_Nb 23, Val de Ene (ΔG) = −7.5 Kcal/mol. ΔG shows the relative binding affinity value for vitamin compound to BmorGOBP2 protein. Docking pose shows scored matching or "best-fit" of fragment atoms from vitamin and BmorGOBP2 in a multiple-grid arrangment.

Supplementary Table 1 | BLASTn analysis of *B. mori* tissues (strain p50T) in silkbase. Silkbase.ab.a.u-tokyo.ac.jp; Br, brain; EE, early embryo; FB, fat body; IG, internal genitalia; Mg, midgut; ASG, anterior silk gland; MSG, middle silk gland; Ep, epidermis; N4EE, early embryo (strain N4). E value 0.0-7e-28.

Supplementary Table 2 | Docking parameters for each "non-semiochemical" ligand in BmorPBP1 binding site (Linux). = indicates the same ligand position compared with the geometry adopted by the optimized Bombykol position. ≠ indicates a different position. Sym: symmetrical position. Results are ranked by best binding energy (ΔG) value calculated using the experimentally observed best conformation for each ligand. Ergocalciferol, vitamins K2, K1, E, A, and riboflavin (vitamin B2) are the best ligands (predicted high binding affinity) for the BmorPBP1 binding site (in a conformation similar or symmetrical to that of Bombykol).

Supplementary Table 3 | Docking parameters for each "non-semiochemical" ligand in the BmorGOBP2 binding site (Linux). ≠ indicates a different position compared with the optimized Bombykol position. * indicates that the statistical difference between the position of vitamin K and the position of bombykol in BmorGOBP2 is low. Results are ranked by best binding energy (ΔG) value calculated using the experimentally observed best conformation for each ligand. Vitamin K is the best ligand (predicted high binding affinity in docking experiment) for the BmorGOBP2 binding site (in a position different than the geometry adopted by bombykol).

REFERENCES

Abraham, D., Löfstedt, C., and Picimbon, J. F. (2005). Molecular characterization and evolution of pheromone binding protein genes in *Agrotis* moths. *Insect Biochem. Mol. Biol.* 35, 1100–1111. doi: 10.1016/j.ibmb.2005.05.002

Allison, J. D., and Cardé, R. T. (2016). *Pheromone Communication in Moths: Evolution, Behavior, and Application, 1st Edn*. Oakland, CA: University of California Press.

Amenya, D. A., Chou, W., Li, J., Yan, G., Gershon, P. D., James, A. A., et al. (2011). Proteomics reveals novel components of the *Anopheles gambiae* eggshells. *J. Insect Physiol.* 56, 1414–1419. doi: 10.1016/j.jinsphys.2010.04.013

Ando, T., Kasuga, K., Yajima, Y., Kataoka, H., and Suzuki, A. (1996). Termination of sex pheromone production in mated females of the silkworm moth. *Arch. Insect Biochem. Physiol.* 31, 207–218.

Andrenacci, D., Cavaliere, V., and Lattanzi, G. (2020). The role of transposable elements activity in aging and their possible involvement in laminopathic diseases. *Ageing Res. Rev.* 57:100995. doi: 10.1016/j.arr.2019.100995

Basset, G. J., Latimer, S., Fatihi, A., Soubeyrand, E., and Block, A. (2017). Phylloquinone (Vitamin K1): occurrence, biosynthesis and functions. *Mini Rev. Med. Chem.* 17, 1028–1038. doi: 10.2174/1389557516666160623082714

Batiha, G. E. S., Alqahtani, A., Ilesanmi, O. B., Saati, A. A., El-Mleeh, A., Hetta, H. F., et al. (2020). Avermectin derivatives, pharmacokinetics,

therapeutic and toxic dosages, mechanism of action, and their biological effects. *Pharmaceuticals* 13:196. doi: 10.3390/ph13080196

Behrens, S., Peuß, R., Milutinovic, B., Eggert, H., Esser, D., Rosenstiel, P., et al. (2014). Infection routes matter in population-specific responses of the red flour beetle to the entomopathogen *Bacillus thuringiensis*. *BMC Genomics* 15:445. doi: 10.1186/1471-2164-15-445

Benoit, J. B., Vigneron, A., Broderick, N. A., Wu, Y., Sun, J. S., Carlson, J. R., et al. (2017). Symbiont-induced odorant-binding proteins mediate insect host hematopoiesis. *Elife* 6:e19535. doi: 10.7554/eLife.19535

Biram, S. N. M., Tribhuwan, S., Kalappa, H. K., and Beera, S. (2005). Mating behaviour in mulberry silkworm, *Bombyx mori* (L.). *Int. J. Indust. Entomol.* 10, 87–94. Available online at: https://agris.fao.org/agris-search/search.do?recordID=KR2006015832

Blomquist, G. J., Jurenka, R., Schal, C., and Tittiger, C. (2012). Chapter 12 - Pheromone production: biochemistry and molecular biology. *Insect Endocrinol.* 2012, 523–567. doi: 10.1016/B978-0-12-384749-2.10012-3

Boni Campanini, E., Congrains, C., Torres, F. R., and de Brito, R. A. (2017). Odorant-binding proteins expression patterns in recently diverged species of *Anastrepha* fruit flies. *Sci. Rep.* 7:2194. doi: 10.1038/s41598-017-02371-2

Butenandt, A., Beckmann, R., Stamm, D., and Hecker, E. (1959). Uber den sexuallockstoff des Seidenspinner *Bombyx mori*. Reindarstellung und Konstitution. *Z. Naturforsch.* 14b, 283–284.

Campanacci, V., Krieger, J., Bette, S., Sturgis, J. N., Lartigue, A., Cambillau, C., et al. (2001). Revisiting the specificity of *Mamestra brassicae* and *Antheraea polyphemus* pheromone-binding proteins with a fluorescence binding assay. *J. Biol. Chem.* 8, 20078–20084. doi: 10.1074/jbc.M100713200

Choi, K. H., Goo, T. W., Kim, S. R., Kim, S. W., Kang, S. W., and Kang, P. D. (2013). Investigation of lifespan related genes of the silkmoth, *Bombyx mori* L. *J. Ser. Entomol. Sci.* 51, 211–217. doi: 10.7852/jses.2013.51.2.211

Clark, J. M., Scott, J. G., Campos, F., and Bloomquist, J. R. (1994). Resistance to avermectins: extent, mechanisms, and management implications. *Annu. Rev. Entomol.* 40, 1–30. doi: 10.1146/annurev.en.40.010195.000245

Contreras, E., Rausell, C., and Real, M. D. (2013). Proteome response of *Tribolium castaneum* larvae to *Bacillus thuringiensis* toxin producing strains. *PLoS ONE* 8:e55330. doi: 10.1371/journal.pone.0055330

David, J. P., Faucon, F., Chandor-Proust, A., Poupardin, R., Asam Riaz, M., Bonin, A., et al. (2014). Comparative analysis of response to selection with three insecticides in the dengue mosquito *Aedes aegypti* using mRNA sequencing. *BMC Genomics* 15:174. doi: 10.1186/1471-2164-15-174

Dedos, S. G., and Fugo, H. (2001). Acceleration of pupal-adult development by Fenoxycard in the silkworm, *Bombyx mori*. *Zool. Sci.* 18, 771–777. doi: 10.2108/zsj.18.771

Donnell, D. M. (2014). Analysis of odorant-binding protein gene family members in the polyembryonic wasp, *Copidosoma floridanum*: evidence for caste bias and host interaction. *J. Insect Physiol.* 60, 127–135. doi: 10.1016/j.jinsphys.2013.12.002

Einhorn, E., and Imler, J. L. (2019). "Insect immunity: from systemic to chemosensory organs protection," in *Olfactory Concepts of Insect Control-Alternative to Insecticides*, Vol. 2, ed J. F. Picimbon (Cham: Springer Nature Switzerland AG), 205–229.

Forstner, M., Gohl, T., Breer, H., and Krieger, J. (2006). Candidate pheromone binding proteins of the silkmoth *Bombyx mori*. *Invertebr. Neurosci.* 6, 177–187. doi: 10.1007/s10158-006-0032-0

Frenk, S., and Houseley, J. (2018). Gene expression hallmarks of cellular ageing. *Biogerontology* 19, 546–567. doi: 10.1007/s10522-018-9750-z

Gong, D., Zhang, H., Zhao, P., Xia, Q., and Xiang, Z. (2009). The odorant binding protein gene family from the genome of silkworm, *Bombyx mori*. *BMC Genomics* 10:332. doi: 10.1186/1471-2164-10-332

Gong, Y., Pace, T. C. S., Castillo, C., Bohne, C., O'Neill, M. A., and Plettner, E. (2009). Ligand-interaction kinetics of the pheromone-binding protein from the gypsy moth, *L. dispar*: insights into the mechanism of binding and release. *Chem. Biol.* 16, 162–172. doi: 10.1016/j.chembiol.2009.01.005

Graham, L. A., Brewer, D., Lajoie, G., and Davies, P. L. (2003). Characterization of a subfamily of beetle odorant-binding protein found in hemolymph. *Mol. Cell. Prot.* 2, 541–549. doi: 10.1074/mcp.M300018-MCP200

Guo, W., Ren, D., Zhao, L., Jiang, F., Song, J., Wang, X., et al. (2018). Identification of odorant-binding proteins (OBPs) and functional analysis of phase-related OBPs in the migratory locust. *Front. Physiol.* 9:984. doi: 10.3389/fphys.2018.00984

He, P., Zhang, J., Liu, N. Y., Zhang, Y. N., Yang, K., and Dong, S. L. (2011). Distinct expression profiles and different functions of odorant binding proteins in *Nilaparvata lugens* Stål. *PLoS ONE* 6:e28921. doi: 10.1371/journal.pone.0028921

Horst, R., Damberger, F., Luginbuhl, P., Guntert, P., Peng, G., Nikonova, L., et al. (2001). NMR structure reveals intramolecular regulation mechanism for pheromone binding and release. *Proc. Natl. Acad. Sci. U.S.A.* 98, 14374–14379. doi: 10.1073/pnas.251532998

Hou, C., Qin, G., Liu, T., Geng, T., Gao, K., Pan, Z., et al. (2014). Transcriptome analysis of silkworm, *Bombyx mori*, during early response to *Beauveria bassiana* challenges. *PLoS ONE* 9:e91189. doi: 10.1371/journal.pone.0091189

Huang, G. Z., Liu, J. T., Zhou, J. J., Wang, Q., Dong, J. Z., Zhang, Y. J., et al. (2018). Expressional and functional comparisons of two general odorant binding proteins in *Agrotis ipsilon*. *Insect Biochem. Mol. Biol.* 98, 34–47. doi: 10.1016/j.ibmb.2018.05.003

Ichikawa, T. (1998). Activity patterns of neurosecretory cells releasing pheromonotropic neuropeptides in the moth *Bombyx mori*. *Proc. Natl. Acad. Sci. U.S.A.* 95, 4055–4060. doi: 10.1073/pnas.95.7.4055

Ichikawa, T., and Ito, K. (1999). Calling behavior modulates heartbeat reversal rhythm in the silkmoth *Bombyx mori*. *Zool. Sci.* 16, 203–209. doi: 10.2108/zsj.16.203

Iovinella, I., Dani, F. R., Niccolini, A., Sagona, S., Michelucci, E., Gazzano, A., et al. (2011). Differential expression of odorant-binding proteins in the mandibular glands of the honey bee according to caste and age. *J. Prot. Res.* 10, 3439–3449. doi: 10.1021/pr2000754

Jarriault, D., Barrozo, R. B., de Carvalho Pinto, C. J., Greiner, B., Dufour, M. C., Massante-Roca, I., et al. (2009). Age-dependent plasticity of sex pheromone response in the moth *Agrotis ipsilon*: combined effects of octopamine and juvenile hormone. *Horm. Behav.* 56, 185–191. doi: 10.1016/j.yhbeh.2009.04.005

Jindra, M., Palli, S. R., and Riddiford, L. M. (2013). The Juvenile Hormone signaling pathway in insect development. *Annu. Rev. Entomol.* 58, 181–204. doi: 10.1146/annurev-ento-120811-153700

Jmol: An Open-Source Java Viewer for Chemical Structures in 3D. Available online at: jmol.sourceforge.net

Kaissling, K. E. (1998). Pheromone deactivation catalyzed by receptor molecules: a quantitative kinetic model. *Chem. Senses* 23, 385–395. doi: 10.1093/chemse/23.4.385

Kaissling, K. E. (2009). Olfactory perireceptor and receptor events in moths: a kinetic model revised. *J. Comp. Physiol. A Neuroethol. Sens. Neural Behav. Physiol.* 195, 895–922. doi: 10.1007/s00359-009-0461-4

Kaissling, K. E. (2019). "Responses of insect olfactory neurons to single pheromone molecules," in *Olfactory Concepts of Insect Control-Alternative to Insecticides*, Vol. 2, ed J. F. Picimbon (Cham: Springer Nature Switzerland AG), 1–27.

Kim, I. H., Pham, V., Jablonka, W., Goodman, W. G., Ribeiro, J. M. C., and Andersen, J. F. (2017). A mosquito hemoplymph odorant-binding protein family member specifically binds juvenile hormone. *J. Biol. Chem.* 292, 15329–15339. doi: 10.1074/jbc.M117.802009

Klusák, V., Havlas, Z., Rulísek, L., Vondrásek, J., and Svatos, A. (2003). Sexual attraction in the silkworm moth: nature of binding of bombykol in pheromone binding protein – an *ab initio* study. *Chem. Biol.* 10, 331–340. doi: 10.1016/S1074-5521(03)00074-7

Krieger, J., Gondesen, I., Forstner, M., Gohl, T., Dewer, Y., and Breer, H. (2009). HR11 and HR13 receptor-expressing neurons are housed together in pheromone-responsive sensilla trichodea of male *Heliothis virescens*. *Chem. Senses* 34, 469–477. doi: 10.1093/chemse/bjp012

Krieger, J., von Nickisch-Roseneck, E. V., Mameli, M., Pelosi, P., and Breer, H. (1996). Binding proteins from the antennae of *Bombyx mori*. *Insect Biochem. Mol. Biol.* 26, 297–307. doi: 10.1016/0965-1748(95)00096-8

Krivosheina, M. G. (2008). On insect feeding on cyanobacteria. *Paleontol. J.* 42, 596–599. doi: 10.1134/S003103010806004X

Laskowski, R. A., and Swindells, M. B. (2011). LigPlot+: multiple ligand-protein interaction diagrams for drug discovery. *J. Chem. Inf. Model.* 51, 2778–2786. doi: 10.1021/ci200227u

Lautenschlager, C., Leal, W. S., and Clardy, J. (2007). *Bombyx mori* pheromone-binding protein binding non-pheromone ligands: implications for pheromone recognition. *Structure* 15, 1148–1154. doi: 10.1016/j.str.2007.07.013

Leal, W. S., Chen, A. M., Ishida, Y., Chiang, V. P., Erickson, M. L., Morgan, T. I., et al. (2005). Kinetics and molecular properties of pheromone binding and release. *Proc. Natl. Acad. Sci. U.S.A.* 102, 5386–5391. doi: 10.1073/pnas.0501447102

Levy, F., Bulet, P., and Ehret-Sabatier, L. (2004). Proteomic analysis of the systemic immune response of *Drosophila*. *Mol. Cell. Prot.* 3, 156–166. doi: 10.1074/mcp.M300114-MCP200

Li, L., Zhou, Y. T., Tan, Y., Zhou, X. R., and Pang, B. P. (2017). Identification of odorant-binding protein genes in *Galeruca daurica* (Coleoptera: Chrysomelidae) and analysis of their expression profiles. *Bull. Entomol. Res.* 107, 550–561. doi: 10.1017/S0007485317000402

Li, S., Picimbon, J. F., Ji, S., Kan, Y., Chuanling, Q., Zhou, J. J., et al. (2008). Multiple functions of an odorant-binding protein in the mosquito *Aedes aegypti*. *Biochem. Biophys. Res. Commun.* 372, 464–468. doi: 10.1016/j.bbrc.2008.05.064

Li, Y., Wang, G., Tian, J., Liu, H., Yang, H., Yi, Y., et al. (2012). Transcriptome analysis of the silkworm (*Bombyx mori*) by high-throughput RNA sequencing. *PLoS ONE* 7:e47313. doi: 10.1371/journal.pone.0043713

Li, Z., Zhang, Y., An, X., Wang, Q., Khashaveh, A., Gu, S., et al. (2020). Identification of leg chemosensory genes and sensilla in the *Apolygus lucorum*. *Front. Physiol.* 11:276. doi: 10.3389/fphys.2020.00276

Liu, G. X., and Picimbon, J. F. (2017). Bacterial origin of insect chemosensory odor binding proteins. *Gene Transl. Bioinform.* 3:e1548. doi: 10.14800/gtb.1548

Livak, K. J., and Schmittgen, T. D. (2001). Analysis of relative gene expression data using real-time quantitative PCR and the 2(-ΔΔC(T)) method. *Methods* 25, 402–408. doi: 10.1006/meth.2001.1262

Loshbaugh, A. L., and Kortemme, T. (2020). Comparison of Rosetta flexible-backbone computational protein design methods on binding interactions. *Proteins Struct. Funct. Bioinf.* 88, 206–226. doi: 10.1002/prot.25790

Maida, R., Mameli, M., Müller, B., Krieger, J., and Steinbrecht, R. A. (2005). The expression pattern of four odorant-binding proteins in male and female silk moths, *Bombyx mori*. *J. Neurocytol.* 34, 149–163. doi: 10.1007/s11068-005-5054-8

Mamidala, P., Wijeratne, A., Wijeratne, S., Kornacker, K., Sudhamalla, B., Rivera-Vega, L. J., et al. (2012). RNA-*seq* and molecular docking reveal multi-level pesticide resistance in the bed bug. *BMC Genomics* 13, 6–23. doi: 10.1186/1471-2164-13-6

Mansurova, M., Klusák, V., Nešněrová, P., Muck, A., Doubský, J., and Svatoš, A. (2009). Design and synthesis of bombykol analogues for probing pheromone-binding protein-ligand interactions. *Tetrahedron* 65, 1069–1076. doi: 10.1016/j.tet.2008.10.106

Mantsyzov, A. B., Bouvier, G., Evrard-Todeschi, N., and Bertho, G. (2012). Contact-based ligand-clustering approach for the identification of active compounds in virtual screening. *Adv. Appl. Bioinform. Chem.* 5, 61–79. doi: 10.2147/AABC.S30881

Matsumoto, S., Fónagy, A., Yamamoto, M., Wang, F., Yokoyama, N., Esumi, Y., et al. (2002). Chemical characterization of cytoplasmic lipid droplets in the pheromone-producing cells of the silkmoth, *Bombyx mori*. *Insect Biochem. Mol. Biol.* 32, 1447–1455. doi: 10.1016/S0965-1748(02)00065-6

Münch, D., Amdam, G. V., and Wolschin, F. (2008). Ageing in a eusocial insect: molecular and physiological characteristics of life span plasticity in the honeybee. *Funct. Ecol.* 22, 407–421. doi: 10.1111/j.1365-2435.2008.01419.x

Nardi, J. B., Miller, L. A., Walden, K. K. O., Rovelstad, S., Wang, L., Frye, J. C., et al. (2003). Expression patterns of odorant-binding proteins in antennae of the moth *Manduca sexta*. *Cell Tissue Res.* 313, 321–333. doi: 10.1007/s00441-003-0766-5

Noh, Y. S., and Amasino, R. M. (1999). Identification of a promoter region responsible for the senescence-specific expression of SAG12. *Plant Mol. Biol.* 41, 181–194. doi: 10.1023/A:1006342412688

Ohta, S., Seto, Y., Tamura, K., Ishikawa, Y., and Matsuo, T. (2015). Comprehensive identification of odorant-binding protein genes in the seed fly, *Delia platura* (Diptera: Anthomyiidae). *Appl. Entomol. Zool.* 50, 457–463. doi: 10.1007/s13355-015-0353-8

Okamoto, S., Futahashi, R., Kojima, T., Mita, K., and Fujiwara, H. (2008). Catalogue of epidermal genes: genes expressed in the epidermis during larval molt of the silkworm *Bombyx mori*. *BMC Genomics* 9:396. doi: 10.1186/1471-2164-9-396

Osanai, M. (1978). Longevity and body weight loss of silkworm moth, *Bombyx mori*, varied by different temperature treatments. *Exp. Gerontol.* 13, 375–388. doi: 10.1016/0531-5565(78)90048-7

Ozaki, K., Ryuda, M., Yamada, A., Utoguchi, A., Ishimoto, H., Calas, D., et al. (2011). A gustatory receptor involved in host plant recognition for oviposition of a swallowtail butterfly. *Nat. Commun.* 2:542. doi: 10.1038/ncomms1548

Ozaki, M. (2019). "Odorant binding proteins in taste system: putative roles in taste sensation and behavior," in *Olfactory Concepts of Insect Control-Alternative to Insecticides*, Vol. 2, ed J. F. Picimbon (Cham: Springer Nature Switzerland AG), 187–204.

Picimbon, J. F. (2002). Chemosensory perireceptors of insects. *Med. Sci.* 11, 1089–1094. doi: 10.1051/medsci/200211111089

Picimbon, J. F. (2003). "Biochemistry and evolution of CSP and OBP proteins," in *Insect Pheromone Biochemistry and Molecular Biology, The Biosynthesis and Detection of Pheromones and Plant Volatiles*, eds G. J. Blomquist and R. G. Vogt (London; San Diego, CA: Academic Press), 539–566.

Picimbon, J. F. (2005). "Synthesis of odorant reception-suppressing agents, Odorant-Binding Proteins (OBPs) and Chemosensory Proteins (CSPs): molecular targets for pest management," in *Biopesticides of Plant Origin,* eds C. Regnault-Roger, B. Philogène, and C. Vincent (Paris; Hampshire; Secaucus, NJ: Intercept-Lavoisier), 245–266.

Picimbon, J. F. (2019). "Evolution of protein physical structures in insect chemosensory systems," in *Olfactory Concepts of Insect Control-Alternative to Insecticides*, Vol. 2, ed J. F. Picimbon (Cham: Springer Nature Switzerland AG), 231–263.

Picimbon, J. F., Dietrich, K., Krieger, J., and Breer, H. (2001). Identity and expression pattern of chemosensory proteins in *Heliothis virescens* (Lepidoptera, Noctuidae). *Insect Biochem. Mol. Biol.* 31, 1173–1181. doi: 10.1016/S0965-1748(01)00063-7

Picimbon, J. F., and Gadenne, C. (2002). Evolution of noctuid pheromone binding proteins: identification of PBP in the black cutworm moth, *Agrotis ipsilon*. *Insect Biochem. Mol. Biol.* 32, 839–846. doi: 10.1016/S0965-1748(01)00172-2

Plettner, E., Lazar, J., Prestwich, E. G., and Prestwich, G. D. (2000). Discrimination of pheromone enantiomers by two pheromone binding proteins from the gypsy moth *Lymantria dispar*. *Biochemistry* 39, 8953–8962. doi: 10.1021/bi000461x

Ribeiro, J. M., Genta, F. A., Sorgine, M. H., Logullo, R., Mesquita, R. D., Paiva-Silva, G. O., et al. (2014). An insight into the transcriptome of the digestive tract of the bloodsucking bug, *Rhodnius prolixus*. *PLoS Negl. Trop. Dis.* 8:e2594. doi: 10.1371/journal.pntd.0002594

Rihani, K., Ferveur, J. F., and Briand, L. (2021). The 40-year mystery of insect odorant-binding proteins. *Biomolecules* 11:509. doi: 10.3390/biom11040509

Salem, H., Bauer, E., Strauss, A. S., Vogel, H., Marz, M., and Kaltenpoth, M. (2014). Vitamin supplementation by gut symbionts ensures metabolic homeostasis in an insect host. *Proc. Biol. Sci.* 281:20141838. doi: 10.1098/rspb.2014.1838

Sali, A. (2020). MODELLER A program for protein structure modeling. *Release* 9.25, r11894. Available online at: https://salilab.org/modeller

Sandler, B. H., Nikonova, L., Leal, W. S., and Clardy, J. (2000). Sexual attraction in the silkworm moth: structure of the pheromone-binding-protein-bombykol complex. *Chem. Biol.* 7, 143–151. doi: 10.1016/S1074-5521(00)00078-8

Seeliger, D., and de Groot, B. L. (2010). Ligand docking and binding site analysis with PyMOL and Autodock/Vina. *J. Comput. Aided Mol. Des.* 24, 417–422. doi: 10.1007/s10822-010-9352-6

Shimomura, M., Minami, H., Suetsugu, Y., Ohyanagi, H., Satoh, C., Antonio, B., et al. (2009). KAIKObase: an integrated silkworm genome database and data mining tool. *BMC Genomics* 10:486. doi: 10.1186/1471-2164-10-486

Shiota, Y., Sakurai, T., Daimon, T., Mitsuno, H., Fujii, T., Matsuyama, S., et al. (2018). *In vivo* functional characterisation of pheromone binding protein-1 in the silkmoth, *Bombyx mori*. *Sci. Rep.* 8:13529. doi: 10.1038/s41598-018-31978-2

Song, K. H., Jung, S. J., Seo, Y. R., Kang, S. W., and Han, S. S. (2006). Identification of up-regulated proteins in the hemolymph of immunized *Bombyx mori* larvae. *Comp. Biochem. Physiol. Part D Genomics Proteomics* 1, 260–266. doi: 10.1016/j.cbd.2006.01.001

Song, L. M., Jiang, X., Wang, X. M., Li, J. D., Zhu, F., Tu, X. B., et al. (2016). Male tarsi specific odorant-binding proteins in the diving beetle *Cybister japonicus* sharp. *Sci. Rep.* 6:31848. doi: 10.1038/srep31848

Starostina, E., Xu, A., Lin, H., and Pikielny, C. W. (2009). A *Drosophila* protein family implicated in pheromone perception is related to Tay-Sachs GM2-Activator protein. *J. Biol. Chem.* 284, 586–594. doi: 10.1074/jbc.M806474200

Steinbrecht, R. A., Laue, M., and Ziegelberger, G. (1995). Immunolocalization of pheromone-binding protein and general odorant-binding protein in olfactory sensilla of the silk moths *Antheraea* and *Bombyx*. *Cell Tissue Res.* 282, 203–217. doi: 10.1007/BF00319112

Sun, J. S., Xiao, S., and Carlson, J. R. (2018). The diverse small proteins called odorant-binding proteins. *Open Biol.* 8:180208. doi: 10.1098/rsob.180208

Sun, L., Wang, Q., Wang, Q., Dong, K., Xiao, Y., and Zhang, Y. J. (2017). Identification and characterization of odorant binding proteins in the forelegs of *Adelphocoris lineolatus* (Goeze). *Front. Physiol.* 8:735. doi: 10.3389/fphys.2017.00735

Sun, L., Wei, Y., Zhang, D. D., Ma, X. Y., Xiao, Y., Zhang, Y. N., et al. (2016). The mouthparts enriched odorant binding protein 11 of the alfalfa plant bug *Adelphocoris lineolatus* displays a preferential binding behavior to host plant secondary metabolites. *Front. Physiol.* 7:201. doi: 10.3389/fphys.2016.00201

Sun, M., Liu, Y., and Wang, G. (2013). Expression patterns and binding properties of three pheromone binding proteins in the diamondback moth, *Plutella xyllotella*. *J. Insect Physiol.* 59, 46–55. doi: 10.1016/j.jinsphys.2012.10.020

Sun, Y. L., Huan, L. Q., Pelosi, P., and Wang, C. Z. (2012). Expression in antennae and reproductive organs suggests a dual role of an odorant-binding protein in two cibling *Helicoverpa* species. *PLoS ONE* 7:e30040. doi: 10.1371/journal.pone.0030040

Takai, H., Asaoka, K., Ishizuna, F., Kiuchi, T., Katsuma, S., and Shimada, T. (2018). Morphological and electrophysiological differences in tarsal chemosensilla between the wild silkmoth *Bombyx mandarina* and the domesticated species *Bombyx mori*. *Arthropod Struct. Dev.* 47, 238–247. doi: 10.1016/j.asd.2018.03.001

Terrado, M., Okon, M., McIntosh, L. P., and Plettner, E. (2020). Ligand- and pH-induced structural transition of gypsy moth *Lymantria dispar* pheromone-binding protein 1 (LdisPBP1). *Biochemistry* 59, 3411–3426. doi: 10.1021/acs.biochem.0c00592

Terrado, M., Pinnelli, G. R., Sanes, J., and Plettner, E. (2019). "Binding interactions, structure-activity relationships and blend effects in pheromone and host olfactory detection of herbivorous Lepidoptera," in *Olfactory Concepts of Insect Control-Alternative to Insecticides*, Vol. 2, ed J. F. Picimbon (Cham: Springer Nature Switzerland AG), 265–310.

Trott, O., and Olson, A. J. (2010). AutoDock Vina: improving the speed and accuracy of docking with a new scoring function, efficient optimization and multithreading. *J. Comput. Chem.* 31, 455–461. doi: 10.1002/jcc.21334

Truman, J. W., and Riddiford, L. M. (1971). Role of the *corpora cardiaca* in the behavior of saturniid moths. II. Oviposition. *Biol. Bull.* 140, 8–14. doi: 10.2307/1540022

Vogt, R. G. (2003). "Biochemical diversity of odor detection: OBPs, ODEs and SNMPs," in *Insect Pheromone Biochemistry and Molecular Biology*, eds G. J. Blomquist and R. G. Vogt (New York, NY: Academic Press), 391–445.

Vogt, R. G. (2005). "Molecular basis of pheromone detection in insects," in *Comprehensive Insect Physiology, Biochemistry, Pharmacology and Molecular Biology*, Vol. 3, *Endocrinology*, eds L. I. Gilbert, K. Iatrou, and S. Gill (London: Elsevier), 753–804.

Vogt, R. G., Köhne, A. C., Dubnau, J. T., and Prestwich, G. D. (1989). Expression of pheromone binding proteins during antennal development in the gypsy moth *Lymantria dispar*. *J. Neurosci.* 9, 3332–3346. doi: 10.1523/JNEUROSCI.09-09-03332.1989

Vogt, R. G., Prestwich, G. D., and Lerner, M. R. (1991b). Odorant-binding protein subfamilies associate with distinct classes of olfactory receptor neurons in insects. *J. Neurobiol.* 24, 581–596.

Vogt, R. G., and Riddiford, L. M. (1981). Pheromone binding and inactivation by moth antennae. *Nature* 293, 161–163. doi: 10.1038/293161a0

Vogt, R. G., Riddiford, L. M., and Prestwich, G. D. (1985). Kinetic properties of a sex pheromone-degrading enzyme: the sensillar esterase of *Antheraea polyphemus*. *Proc. Natl. Acad. Sci. U.S.A.* 82, 8827–8831. doi: 10.1073/pnas.82.24.8827

Vogt, R. G., Rogers, M. E., Franco, M. D., and Sun, M. (2002). A comparative study of odorantbinding protein genes: differential expression of the PBP1-GOBP2 gene cluster in *Manduca sexta* (Lepidoptera) and the organization of OBP genes in *Drosophila melanogaster* (Diptera). *J. Exp. Biol.* 205, 719–744. doi: 10.1242/jeb.205.6.719

Vogt, R. G., Rybczynski, R., Cruz, M., and Lerner, M. R. (1993). Ecdysteroid regulation of olfactory proteins in the developing antenna of the tobacco hawk moth, *Manduca sexta*. *J. Neurobiol.* 24, 581–597. doi: 10.1002/neu.480240505

Vogt, R. G., Rybczynski, R., and Lerner, M. R. (1991a). Molecular cloning and sequencing of general odorant-binding proteins GOBP1 and GOBP2 from the tobacco hawk moth *Manduca sexta*: comparisons with other insect OBPs and their signal peptides. *J. Neurosci.* 11, 2972–2984. doi: 10.1523/JNEUROSCI.11-10-02972.1991

Wallace, E. K., Albert, P. J., and McNeil, J. N. (2004). Oviposition behavior of the eastern spruce budworm, *Choristoneura fumiferana* (Clemens) (Lepidoptera: Tortricidae). *J. Insect Behav.* 17, 245–254. doi: 10.1023/B:JOIR.0000028565.41613.1a

Wang, G. R., Wu, K. M., and Guo, Y. Y. (2003). Cloning, expression and immunocytochemical localization of a general odorant-binding protein gene from *Helicoverpa armigera* (Hübner). *Insect Biochem. Mol. Biol.* 33, 115–124. doi: 10.1016/S0965-1748(02)00182-0

Wojtasek, H., and Leal, W. S. (1999). Conformational change in the pheromone-binding protein from *Bombyx mori* induced by pH and by interaction with membranes. *J. Biol. Chem.* 274, 30950–30956. doi: 10.1074/jbc.274.43.30950

Xiao, S., Sun, J. S., and Carlson, J. R. (2019). Robust olfactory responses in the absence of odrant binding proteins. *Elife* 8:51040. doi: 10.7554/eLife.51040.020

Xuan, N., Bu, X., Liu, Y. Y., Yang, X., Liu, G. X., Fan, Z. X., et al. (2014). Molecular evidence of RNA editing in *Bombyx* chemosensory protein family. *PLoS ONE* 9:e86932. doi: 10.1371/journal.pone.0086932

Xuan, N., Guo, X., Xie, H. Y., Lou, Q. N., Lu, X. B., Liu, G. X., et al. (2015). Increased expression of CSP and CYP genes in adult silkworm females exposed to avermectins. *Insect Sci.* 22, 203–219. doi: 10.1111/1744-7917.12116

Yin, J., Feng, H., Sun, H., Xi, J., Cao, Y., and Li, K. (2012). Functional analysis of general odorant binding protein 2 from the meadow moth, *Loxostege sticticalis* L. *(Lepidoptera: Pyralidae). PLoS ONE* 7:e33589. doi: 10.1371/journal.pone.0033589

Zhang, S., Maida, R., and Steinbrecht, R. A. (2001). Immunolocalization of odorant-binding proteins in noctuid moths (Insecta, Lepidoptera). *Chem. Senses* 26, 885–896. doi: 10.1093/chemse/26.7.885

Zhang, Y. C., Gao, S. S., Xue, S., Zhang, K. P., Wang, J. S., and Li, B. (2020). Odorant-binding proteins contribute to the defense of the red flour beetle, *Tribolium castaneum*, against essential oil of *Artemisia vulgaris*. *Front. Physiol.* 11:819. doi: 10.3389/fphys.2020.00819

Zhang, Y. L., Fu, X. B., Cui, H. C., Zhao, L., Yu, J. Z., and Li, H. L. (2018). Functional characteristics, electrophysiological and antennal immunolocalization of general odorant-binding protein 2 in tea geometrid, *Ectropis obliqua*. *Int. J. Mol. Sci.* 19:875. doi: 10.3390/ijms19030875

Zhou, J. J., Robertson, G., He, X., Dufour, S., Hooper, A. M., Pickett, J. A., et al. (2009). Characterisation of *Bombyx mori* odorant-binding proteins reveals that a general odorant-binding protein discriminates between sex pheromone components. *J. Mol. Biol.* 389, 529–545. doi: 10.1016/j.jmb.2009.04.015

Conflict of Interest: The authors declare that the research was conducted in the absence of any commercial or financial relationships that could be construed as a potential conflict of interest.

Advantages of publishing in Frontiers

OPEN ACCESS
Articles are free to read for greatest visibility and readership

FAST PUBLICATION
Around 90 days from submission to decision

HIGH QUALITY PEER-REVIEW
Rigorous, collaborative, and constructive peer-review

TRANSPARENT PEER-REVIEW
Editors and reviewers acknowledged by name on published articles

Frontiers
Avenue du Tribunal-Fédéral 34
1005 Lausanne | Switzerland

Visit us: www.frontiersin.org
Contact us: frontiersin.org/about/contact

REPRODUCIBILITY OF RESEARCH
Support open data and methods to enhance research reproducibility

DIGITAL PUBLISHING
Articles designed for optimal readership across devices

FOLLOW US
@frontiersin

IMPACT METRICS
Advanced article metrics track visibility across digital media

EXTENSIVE PROMOTION
Marketing and promotion of impactful research

LOOP RESEARCH NETWORK
Our network increases your article's readership